UNIVERSITY OF LONDON THESIS

Degree PhD Year 2006 Name of Author THORPE
Joanna Lucy

COPYRIGHT

This is a thesis accepted for a Higher Degree of the University of London. It is an unpublished typescript and the copyright is held by the author. All persons consulting the thesis must read and abide by the Copyright Declaration below.

COPYRIGHT DECLARATION

I recognise that the copyright of the above-described thesis rests with the author and that no quotation from it or information derived from it may be published without the prior written consent of the author.

LOAN

Theses may not be lent to individuals, but the University Library may lend a copy to approved libraries within the United Kingdom, for consultation solely on the premises of those libraries. Application should be made to: The Theses Section, University of London Library, Senate House, Malet Street, London WC1E 7HU.

REPRODUCTION

University of London theses may not be reproduced without explicit written permission from the University of London Library. Enquiries should be addressed to the Theses Section of the Library. Regulations concerning reproduction vary according to the date of acceptance of the thesis and are listed below as guidelines.

A. Before 1962. Permission granted only upon the prior written consent of the author. (The University Library will provide addresses where possible).

B. 1962 - 1974. In many cases the author has agreed to permit copying upon completion of a Copyright Declaration.

C. 1975 - 1988. Most theses may be copied upon completion of a Copyright Declaration.

D. 1989 onwards. Most theses may be copied.

This thesis comes within category D.

☐ This copy has been deposited in the Library of UCL

☐ This copy has been deposited in the University of London Library, Senate House, Malet Street, London WC1E 7HU.

Records of late Quaternary climatic change from Tswaing crater lake, South Africa, and the Central Kenya Rift

Thesis submitted for the degree of Doctor of Philosophy,
University of London,
by

Joanna Lucy Thorpe

Department of Geography,
University College London,
August 2006

ProQuest LLC
789 East Eisenhower Parkway
P.O. Box 1346
Ann Arbor, MI 48106-1346

I, , confirm that the work presented in this thesis is my own. Where information has been derived from other sources, I confirm that this has been indicated in the thesis.

Abstract

The relative influence of precessionally-driven changes in direct insolation and changes in boundary conditions associated with glacial-interglacial cycles on climatic conditions at low latitudes remains uncertain. This thesis presents records of late Quaternary climatic change from Tswaing crater lake in South Africa and from the Naivasha and Nakuru-Elmenteita basins in the Central Kenya Rift, with the aim of increasing our understanding of the nature and causes of climatic change at low latitudes in Africa.

The sedimentary sequence from Tswaing crater lake provides some of the longest terrestrial records of palaeoclimatic change in southern Africa, but the confidence associated with these records is limited by chronological uncertainty. This thesis presents five new $^{230}Th/^{234}U$ dates from the lower, previously undated section of the sequence, which are used to construct a new age-depth model for the sediments. When viewed in light of this chronology, new sedimentological, geochemical, and diatom assemblage records from the sequence indicate that boundary conditions associated with glacial-interglacial cycles determined climatic conditions at the site over the last ~150 kyr, and that the obliquity of the earth's axis may have affected conditions between ~150 and ~350 kyr B.P.

Diatomite beds deposited in the Naivasha and Nakuru-Elmenteita basins at the time of the last interglacial document a period in which deep, dilute lakes existed in the Central Kenya Rift. $\delta^{18}O_{diatom}$ records from these $^{40}Ar/^{39}Ar$-dated beds are used to reconstruct palaeohydrological conditions during this lake-level highstand. The records indicate that lake levels in both basins responded to increases in precipitation driven by peaks in March and September insolation on the equator, and by increased tropical sea-surface temperatures. It is therefore concluded that precipitation in the Central Kenya Rift was influenced by both precessionally-driven changes in insolation and global boundary conditions during this period.

Acknowledgements

I would like to thank my supervisor, Dr. Anson Mackay (UCL), for all his help and support over the course of this project. I would also like to thank Prof. Tim Partridge (Climatology Research Unit, University of the Witwatersrand) for many useful discussions, providing me with additional data, organising a field trip to Tswaing, and for his hospitality while I was in South Africa. I am grateful to Dr. Hedi Oberhänsli (GFZ, Potsdam) for allowing me to work on the cores from Tswaing, and for her help and advice during my visits to Potsdam. I would also like to thank Dr. Martin Trauth (University of Potsdam) for giving me the opportunity to work on the diatomite profiles in the Central Kenya Rift, and for organising a field trip to Kenya.

Prof. Melanie Leng (NIGL, Keyworth) provided invaluable help and advice on the use of stable isotopes as palaeoenvironmental proxies, and her comments improved many chapters of this thesis. I am also grateful to Prof. Sarah Metcalfe (University of Nottingham) and Dr. Jonathan Holmes (UCL) for their help and advice, and for insightful comments on parts of this thesis. I would also like to thank Dr. Mark Maslin (UCL) for suggesting that I work on the material from Kenya, and for his help in doing so. Prof. John Birks (University of Bergen) provided useful advice about age-depth modelling, and Dr. Angela Lamb (NIGL, Keyworth) provided help and advice when I visited NIGL.

I would also like to thank Dr. Andreas Bergner (University of Potsdam) for many useful discussions about the diatomite profiles in Kenya, and for providing me with sedimentological and diatom assemblage data from the profile in the Nakuru-Elmenteita basin. I am also grateful to Iris Kristen (GFZ, Potsdam) for her help and hospitality while I was in Potsdam, and for useful discussions about the project, as well as for providing new radiocarbon dates on the sediments from Tswaing crater lake.

Dr. Mabs Gilmour, Dr. Louise Thomas, and Dr. Peter van Calsteren (Uranium Series Dating Facility, the Open University) provided invaluable advice about $^{230}Th/^{234}U$ dating during my stay at the Open University. Dr. Mabs Gilmour and Dr. Louise

Thomas also helped me to prepare and analyse many samples, as well as analysing some for me. I am grateful to Jo Greene, Hilary Sloane, and Carol Arrowsmith (NIGL, Keyworth) for analysing my stable isotope samples. Kevin Reeves (UCL) allowed me to use the SEM in the Institute of Archaeology and Jennifer Huggett (Natural History Museum) carried out the XRD analysis. Prof. Alan Deino (Berkeley Geochronology Center) carried out the $^{40}Ar/^{39}Ar$ dating of the diatomite profile in the Nakuru-Elmenteita basin.

I would also like to thank everyone at the ECRC for their help and encouragement. Dr. Patrick Rioual helped with diatom identification, and Dr. David Morley taught me how to prepare diatom samples for oxygen isotope analysis. Janet Hope, Tula Maxted, and Ian Patmore also provided much help in the laboratory.

Funding was provided by a NERC Ph.D. studentship (NER/S/A/2002/10423), and by grants from the NERC Isotope Geoscience Facilities Steering Committee for $^{230}Th/^{234}U$ dating at the Open University Uranium Series Dating Facility (IP/793/1103), and for $\delta^{18}O_{diatom}$ analysis at NIGL (IP/816/0504).

Finally, I would like to thank Paul for putting up with me through it all.

Table of contents

List of figures

List of tables

Chapter 1: Introduction

Changes in insolation caused by variations in the earth's orbital configuration have driven climatic change during the Quaternary period (Croll, 1890; Milankovitch, 1920; Milankovitch, 1941). Insolation can either affect climate in a given region directly, by affecting factors such as the intensity of monsoonal circulation, or indirectly, by causing large-scale responses in the climate system (*e.g.* Hays *et al.*, 1976; Kutzbach, 1981). The most significant response of the climate system to variations in insolation during the Quaternary has been the change in boundary conditions associated with glacial-interglacial cycles (Köppen and Wegener, 1924; Milankovitch, 1941; Hays *et al.*, 1976). The relative influence of changes in direct insolation and changes in boundary conditions associated with glacial-interglacial cycles on climatic conditions remains uncertain in many parts of the world, however, and understanding the effects of these forcing factors is therefore an important challenge for Quaternary scientists.

The potential effects of direct insolation on climate in a given region can be assessed using knowledge of the climate system, because the amount of insolation received at a given latitude can be calculated using the laws of celestial mechanics (*e.g.* Kutzbach and Street-Perrott, 1985). The amount of insolation received over the course of a year does not change significantly, and variations in the seasonality of insolation therefore have the most significant effect on climatic conditions. This parameter influences the seasonal heating of the earth's surface, and can therefore affect variables such as sea-ice extent and the intensity of monsoonal circulation (*e.g.* Kutzbach, 1981; Waelbroeck *et al.*, 1995; Kim *et al.*, 1998). At low latitudes, the seasonal distribution of insolation is largely determined by the precession of the equinoxes, but at mid- and high-latitudes, the obliquity of the earth's axis also has a significant effect (Milankovitch, 1941; Berger and Loutre, 1991).

Glacial-interglacial cycles have traditionally been thought to be forced by changes in summer insolation at high northern latitudes, but a number of alternative explanations have recently been proposed (*e.g.* Köppen and Wegener, 1924; Milankovitch, 1941; Hays *et al.*, 1976; Clement *et al.*, 1999; Raymo and Nisancioglu, 2003; Kukla and

Gavin, 2005). The changes in boundary conditions associated with these cycles include changes in ice-sheet and sea-ice extent, surface albedo, sea level, oceanic circulation, and the atmospheric concentration of greenhouse gases and aerosols; all of which have the potential to affect climatic conditions on large spatial scales (*e.g.* Petit *et al.*, 1981; Smythe *et al.*, 1985; Barnola *et al.*, 1987; Boyle and Keigwin, 1987; Shackleton, 1987; Berger *et al.*, 1993; Petit *et al.*, 1999; EPICA community members, 2004).

At mid- and high-latitudes, changes in boundary conditions associated with glacial-interglacial cycles are the dominant control on climatic conditions, although it has been suggested that changes in direct insolation can also be influential (*e.g.* Kim *et al.*, 1998; Vandergoes *et al.*, 2005). The factors that influence climatic conditions at low latitudes are considerably less certain, however. In many tropical and subtropical regions, including parts of South America and northern Africa, direct insolation appears to be the primary influence on hydrological conditions (*e.g.* Rossignol-Strick, 1983; Pokras and Mix, 1985; Baker *et al.*, 2001a,b; Wang *et al.*, 2004; Cruz *et al.*, 2005), although there is also evidence that changes in global boundary conditions have affected precipitation in these areas (*e.g.* deMenocal *et al.*, 1993; Ledru *et al.*, 2005). Records from southern Africa, in contrast, suggest that global boundary conditions have had a more significant influence on hydrological conditions than direct insolation, at least since the last glacial maximum (LGM) (cf. Gasse, 2000; Baker, 2002; Barker and Gasse, 2003). There is evidence that this anomalous situation may have only existed over the last ~50 kyr, and that precipitation was determined by direct insolation before this period (Partridge *et al.*, 1997), but it is difficult to test this proposal due to a lack of long palaeoclimatic records from southern Africa.

It is evident that long, accurately-dated palaeoclimatic records from tropical and subtropical regions, particularly southern Africa, are required to increase our understanding of the factors that control climatic change at low latitudes. This information is particularly important in light of the proposal that climatic change at low latitudes could affect climate on a global scale (*e.g.* Chappellaz *et al.*, 1993; Sirocko *et al.*, 1996; Clement *et al.*, 1999; Schneider *et al.*, 1999; Lea *et al.*, 2000; Kukla and Gavin, 2005). This study therefore presents new palaeoclimatic records from Tswaing crater lake in South Africa (25°S, 28°E) and from the Naivasha and

Nakuru-Elmenteita basins in the Central Kenya Rift (CKR) (0°S, 36°E) (Fig. 1.1), with the aim of increasing our understanding of the relative influences of direct insolation and global boundary conditions on climatic change in equatorial and southern Africa.

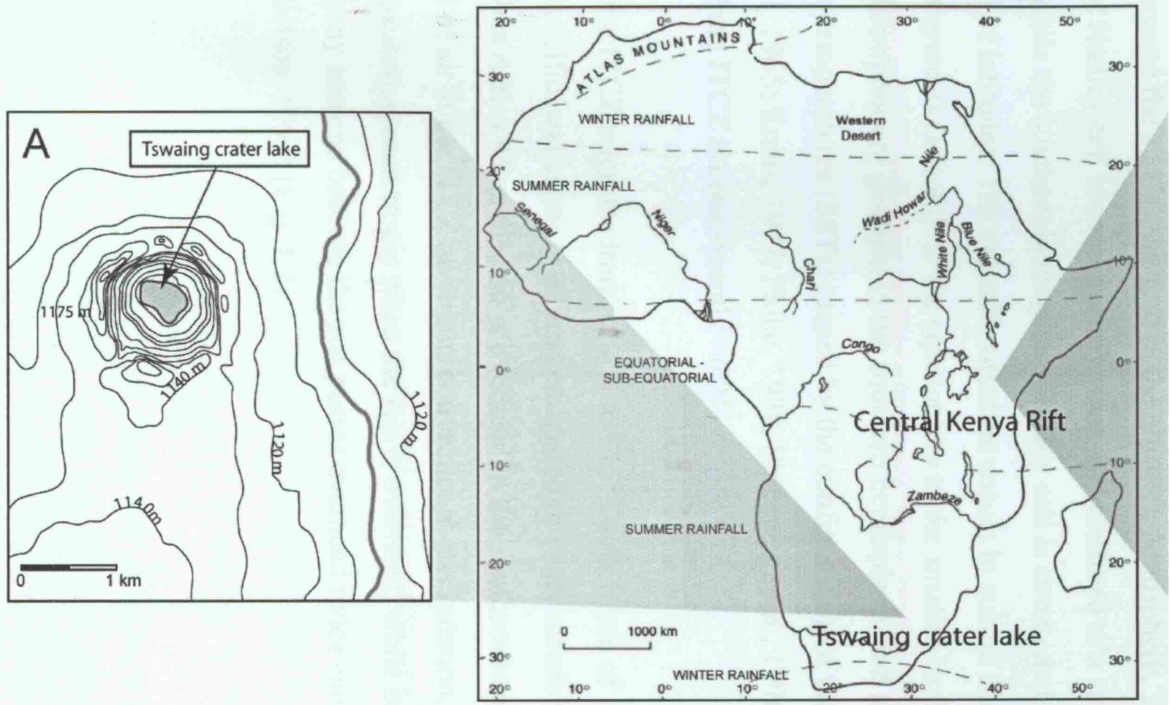

Figure 1.1: Map of Africa showing the location of the sites used in this study, with enlarged maps of (A) Tswaing crater lake in South Africa, and (B) the Naivasha and Nakuru-Elmenteita basins in the Central Kenya Rift. Partly based on a map from Gasse (2000) and a map created by A. Bergner (University of Potsdam).

1.1 Modern African climate

In order to assess the causes of climatic change in the tropics and subtropics of Africa, it is important to understand the climate systems that currently affect these regions. A brief description of atmospheric circulation over Africa is therefore presented in this section. The climatic settings of southern and East Africa are discussed in more detail in chapters 5 and 7, respectively.

When considered in terms of mean meridional circulation, tropical and subtropical climate is dominated by the Hadley cells, which rise in the areas of surface convergence that make up the Inter-tropical Convergence Zone (ITCZ), and subside in subtropical anticyclones. In boreal summer, the ITCZ is located north of the equator, because the sun is overhead in the northern hemisphere. The northern hemisphere Hadley cell is consequently weak and confined to a small range of latitudes, while the southern hemisphere Hadley cell is strong and extends across a wide range of latitudes. The opposite situation occurs in austral summer, but the ITCZ does not migrate as far south of the equator due to the smaller land area and larger meridional temperature gradient in the southern hemisphere, and an asymmetry in sea-surface temperatures (SSTs) caused by the configuration of the continents (Woldstedt, 1965; Kraus, 1977; Flohn, 1978; Philander *et al.*, 1996). The average position of the ITCZ is consequently ~6°N.

In Africa, the ITCZ migrates from ~20°N to ~15°S over much of the continent, but the lower specific heat capacity of land compared to water means that it remains at ~8°N in West Africa when the sun is overhead in the southern hemisphere (Fig. 1.2). The ascent of air at the ITCZ generates convectional precipitation, and rainfall is therefore greatest at each tropic when the sun is overhead, while equatorial regions have two rainy seasons because the sun passes overhead twice each year (Hastenrath, 1991; Nicholson, 1996) (Fig. 1.2).

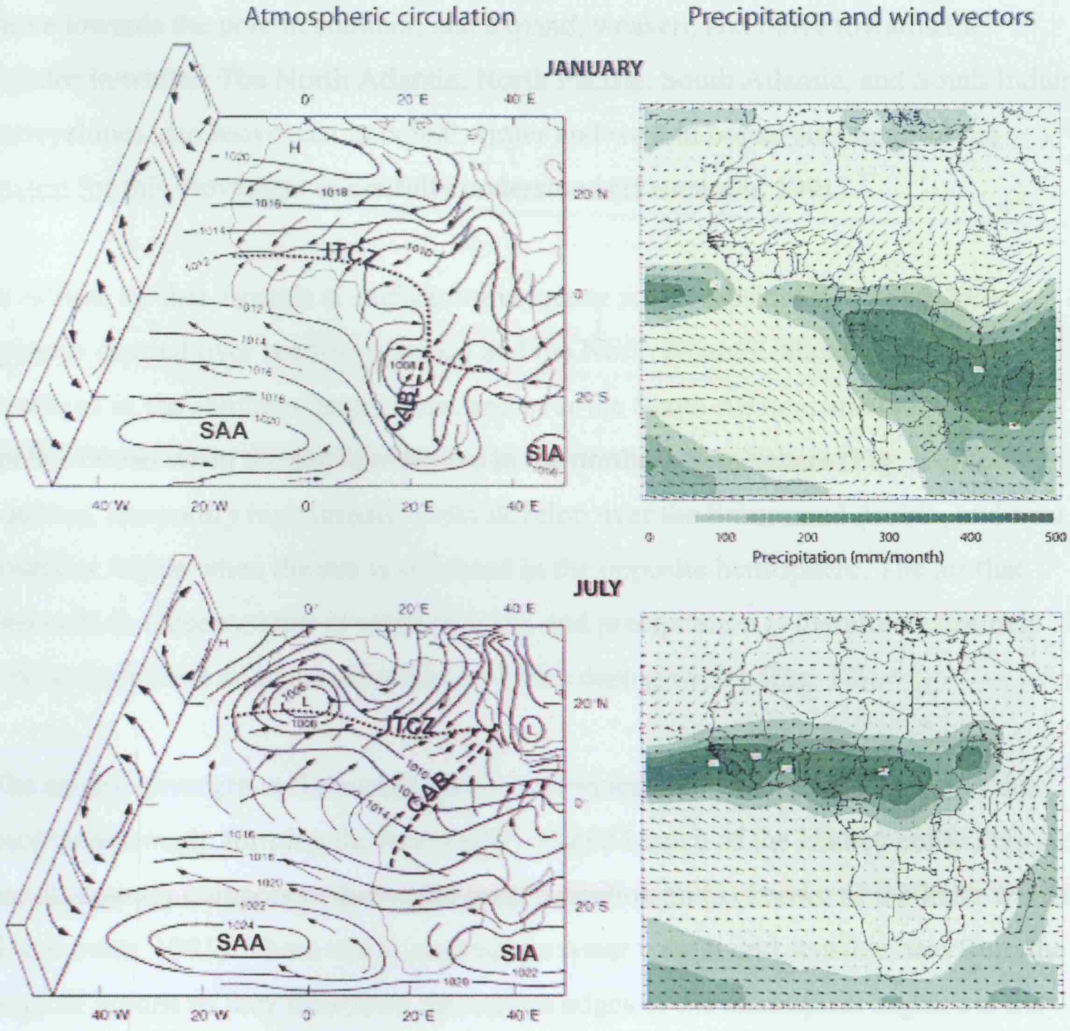

Figure 1.2: Atmospheric circulation and monthly precipitation and wind vectors for the 925 hPa pressure level over Africa in January and July. ITCZ is the Inter-tropical Convergence Zone, CAB is the Congo Air Boundary, SAA is the South Atlantic Anticyclone, SIA is the South Indian Anticyclone. Atmospheric circulation diagrams are modified from Nicholson (1996). Climatological maps were created at http://iridl.ldeo.columbia.edu. Precipitation data are based on satellite estimates over oceans (1979 to present) and rain gauge data over land (1961-1990), and wind vectors are based on observations (1961-1990) (NCEP, Climate Prediction Center USA, from http://iridl.ldeo.columbia.edu).

Air that ascends within the equatorial trough subsides at the top of the Hadley cells, forming semi-permanent anticyclones over the North Pacific and North Atlantic in the northern hemisphere, and over the South Atlantic, South Pacific, and southern Indian

Ocean in the southern hemisphere (Hastenrath, 1991). These cells strengthen and move towards the pole in summer, and expand, weaken, and move towards the equator in winter. The North Atlantic, North Pacific, South Atlantic, and South Indian anticyclones also move east in boreal winter and west in boreal summer, but the reason for this movement is not fully understood (Hastenrath, 1991).

In Africa, air that ascends at surface convergence zones subsides in anti-cyclonic systems centred over northwest Africa and the North Atlantic when the sun is overhead in the southern hemisphere, and over the South Atlantic and the southern Indian Ocean when the sun is overhead in the northern hemisphere (Fig. 1.2). In addition, temporary high pressure cells develop over the Sahara and Arabia, and over southern Africa when the sun is overhead in the opposite hemisphere. The air that descends in these systems is warm and dry, and precipitation is therefore extremely low in the Sahara and parts of southern Africa during winter (Fig. 1.2).

The air that diverges at the surface in the subtropical anticyclones converges at the equatorial trough, forming the lower tropospheric branch of the Hadley cells. This air has an easterly component due to the earth's rotation and is known as the trade winds (Hastenrath, 1991). These winds accumulate water vapour and sensible heat from the tropical oceans as they flow from the eastern edges of the subtropical highs, but they remain stable due to the subsidence of warm, dry air aloft. The release of latent and sensible heat from the trade winds is therefore concentrated in the equatorial trough. This phenomenon increases the intensity of the Hadley cells, leading to a positive feedback that is partly responsible for the intensity of tropical circulation (Kraus, 1959; Lindzen and Nigam, 1987).

In Africa, surface convergence draws the trade winds onto the continent from the east (Fig. 1.2). The north-easterly trades mainly flow over continental regions and are therefore dry, but one branch crosses the Indian Ocean and brings rain to equatorial East Africa (Nicholson, 1996). In contrast, the south-easterly trades cross the southern Indian Ocean and are therefore relatively moist (Ogallo, 1988). These winds are associated with the East African low level jet, which develops over the western Indian Ocean during boreal summer and flows to the coast of East Africa, before changing direction at the equator and becoming part of the south-westerly Asian monsoon

winds (Findlater, 1977; Hastenrath, 1991). In East Africa, the trades blow parallel to the coast, which induces subsidence. They therefore bring relatively little rain to this region, except when the sun is overhead and on-shore winds are forced to rise by topographic features and coastal friction (Nicholson, 1996). In northern and central Africa, surface convergence also draws air onto the continent from the Atlantic Ocean. This air is humid and brings rain to western Africa throughout the year. It can also penetrate deep into the continent, generating precipitation in East Africa (Nicholson, 1996). A secondary convergence zone, known as the Congo Air Boundary (CAB), forms where this air mass converges with the trade winds from the east (Nicholson, 1996) (Fig. 1.2).

It is evident from this discussion that monsoonal circulation forms an integral part of atmospheric circulation in tropical and subtropical Africa, as it does in most low-latitude regions (cf. Hastenrath, 1991). Monsoonal circulation is defined by a summer precipitation maximum and a seasonal reversal of wind direction, and is driven by a pressure gradient between land and the surrounding oceans (Hastenrath, 1991). In summer, when the sun is overhead, landmasses heat up more quickly than the surrounding oceans, creating surface convergence and convectional precipitation over continents, and generating surface divergence and low precipitation over the oceans. The opposite situation prevails in winter, as the landmasses cool more rapidly than the surrounding oceans. The strength of the circulation depends on the sensible heating of the landmass by insolation, and on the latent heat released by condensation during convection. In North Africa, the easterly trades and the westerly winds from the Atlantic Ocean that bring moisture into the region in boreal summer therefore form the North African monsoon. Similarly, the easterly trade winds that bring moisture into southern Africa in austral summer form the South Africa monsoon.

The highest latitudes of the African continent are influenced by the circum-polar westerlies. The waves in these winds generate divergence aloft, which causes air to ascend and therefore generates precipitation in cyclonic systems. In winter, the westerlies expand towards the equator due to the increase in the meridional temperature gradient, bringing cyclonic precipitation to latitudes north of ~20-23°N in boreal winter, and to latitudes south of ~26-33°S in austral winter (Fig. 1.2) (Deacon and Lancaster, 1988; Hoelzmann *et al.*, 2004). The westerlies are stronger and more

zonal in the southern hemisphere than in the northern hemisphere due to the larger meridional temperature gradient and the absence of land at sub-polar latitudes in the southern hemisphere (Flohn, 1967). The high latitudes of the African continent therefore experience a Mediterranean climate, with warm, dry summers caused by anti-cyclonic conditions, and cool, wet winters caused by the expansion of the circum-polar westerlies.

1.2 Past climatic change in tropical and subtropical regions

A number of forcing factors could potentially influence climatic conditions in tropical and subtropical regions on orbital timescales. These factors will be outlined briefly in the following section, before considering some of the palaeoclimatic evidence that is available, particularly from Africa, to distinguish between these potential causes of climatic change. The discussion will focus on hydrological change, because hydrological conditions are believed to have changed more significantly than temperature in tropical and subtropical regions, and because hydrological change at low latitudes has the potential to affect climate on a global scale (*e.g.* Street-Perrott, 1993; Leuschner and Sirocko, 2003). The causes of climatic change on millennial timescales are not considered, because they are often different from those that act on orbital timescales, and they do not form the focus of this study (*e.g.* McIntyre and Molfino, 1996; Curry and Oppo, 1997; Leuschner and Sirocko, 2000; Peterson *et al.*, 2000; Wang *et al.*, 2005).

1.2.1 Mechanisms of climatic change

1.2.1.1 Direct insolation forcing

Precipitation at tropical and subtropical latitudes is primarily generated by the monsoonal circulation that develops in response to solar heating of the land surface (section 1.1). The insolation received at these latitudes in summer affects both the strength of surface convergence and the magnitude of the land-ocean pressure gradient, and thus determines the strength of monsoonal circulation. It has therefore been suggested that direct insolation may be the primary influence on precipitation in these regions (Kutzbach, 1981; Kutzbach and Otto-Bliesner, 1982; Kutzbach and Guetter, 1984a,b; Kutzbach and Street-Perrott, 1985).

In a slight variation on this model, it has also been suggested that the strength of insolation at low latitudes affects the latitudinal migration of the ITCZ, with stronger summer insolation in a given hemisphere causing the ITCZ to migrate further towards the pole of that hemisphere (*e.g.* de Noblet *et al.*, 1996; Mayle *et al.*, 2000; Haug *et al.*, 2001; Wang *et al.*, 2004). Climate simulations confirm that this may have been the case over land, due to its low specific heat capacity (de Noblet *et al.*, 1996), but indicate that it was probably not the case over the oceans (Chiang *et al.*, 2003). In another variation on the model proposed by Kutzbach (1981), Meehl *et al.* (2003) proposed that insolation influences precipitation in tropical regions by determining the amount of evaporation from oceans in the relatively cloud-free subtropics, which in turn determines the amount of energy released during convection, and thus affects the intensity of tropical circulation.

The amount of insolation received at low latitudes at a given time of year is primarily determined by the precession of the equinoxes, which determines the direction of the earth's axis relative to the sun during perihelion and aphelion, and therefore affects the seasonal distribution of insolation. This parameter causes insolation to vary with periods of 19 and 23 kyr, and to vary in anti-phase in the northern and southern hemispheres (Fig. 1.3) (cf. Berger and Loutre, 1991). The amplitude of these changes in insolation is modulated by the eccentricity of the earth's orbit, which determines the distance between the earth and the sun at perihelion and aphelion. This parameter varies with periods of 100 and 412 kyr, but has a much less significant influence on the seasonality of insolation than the precession of the equinoxes. Thus, changes in precipitation would be expected to occur with frequencies of 19 and 23 kyr, and to be of equal magnitude but opposite direction in the northern and southern hemispheres if the strength of insolation determined precipitation at low latitudes (Fig. 1.3). The same logic applies in equatorial regions, but precipitation would be expected to peak approximately every 11.5 kyr, because the sun passes overhead twice each year (Fig. 1.3).

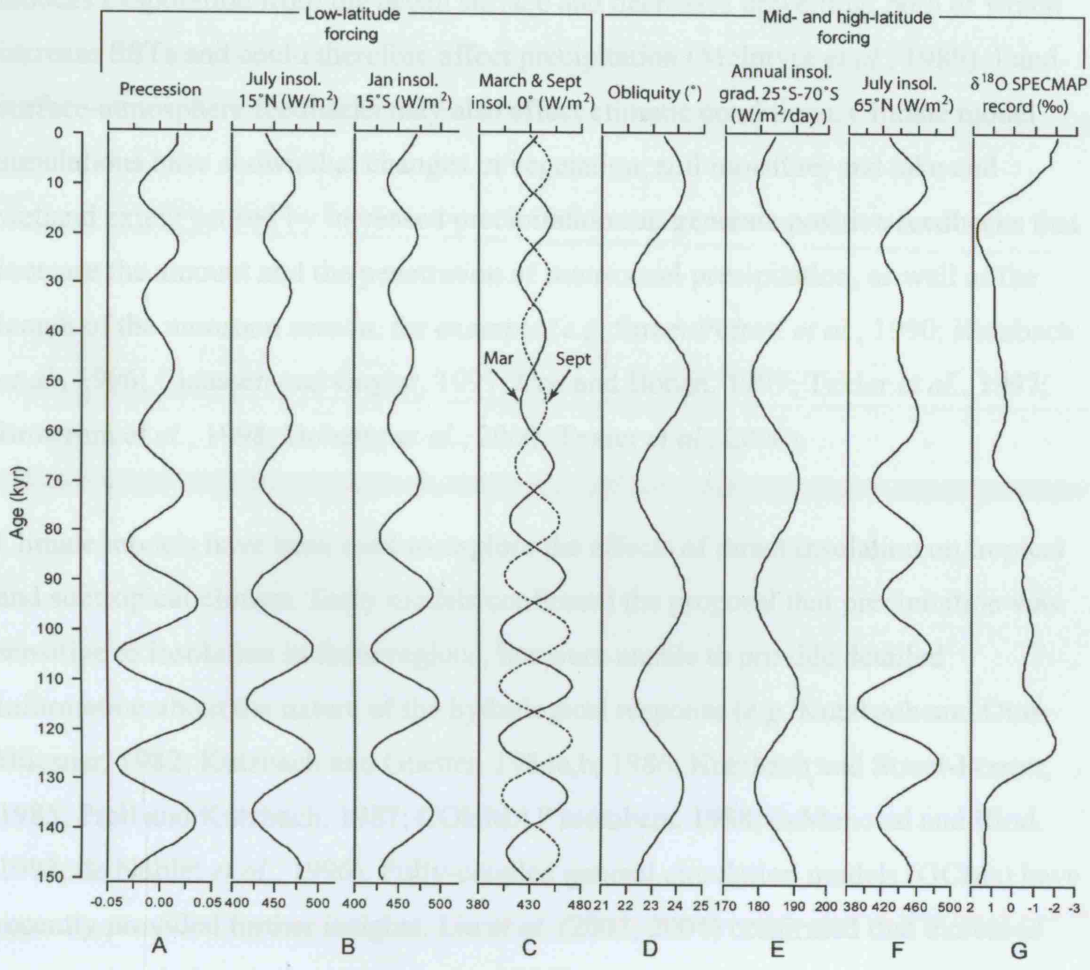

Figure 1.3: Potential forcing factors of climatic change in tropical and subtropical Africa over the last 150 kyr, showing (A) the precession of the earth's equinoxes, (B) daily July insolation at 15°N and daily January insolation at 15°S, (C) daily March and September insolation on the equator, (D) the obliquity of the earth's axis (Berger and Loutre, 1991), (E) the mean annual insolation gradient between 25°S and 70°S in W/m^2/day (calculated using Laskar *et al.*, 2004), (F) daily July insolation at 65°N, which is often considered to force glacial-interglacial cycles (Berger and Loutre, 1991), and (G) the SPECMAP $\delta^{18}O$ record, which is primarily a proxy for ice volume (Imbrie *et al.*, 1984).

This model is complicated by the fact that changes in the climate system caused by direct insolation may cause climatic feedbacks. It has been suggested, for example, that an increase in the strength of the westerly winds associated with the North African monsoon reduces the strength of the easterly trade winds, which in turn

reduces evaporation from the ocean surface and decreases upwelling; both of which increase SSTs and could therefore affect precipitation (McIntyre *et al.*, 1989). Land surface-atmosphere feedbacks may also affect climatic conditions. Climate model simulations have shown that changes in vegetation, soil moisture, and lake and wetland extent caused by increased precipitation can generate positive feedbacks that increase the amount and the penetration of monsoonal precipitation, as well as the length of the monsoon season, for example (*e.g.* Street-Perrott *et al.*, 1990; Kutzbach *et al.*, 1996; Claussen and Gayler, 1997; Coe and Bonan, 1997; Texier *et al.*, 1997; Bröstrom *et al.*, 1998; Doherty *et al.*, 2000; Texier *et al.*, 2000).

Climate models have been used to explore the effects of direct insolation on tropical and subtropical climate. Early models confirmed the proposal that precipitation was sensitive to insolation in these regions, but were unable to provide detailed information about the nature of the hydrological response (*e.g.* Kutzbach and Otto-Bliesner, 1982; Kutzbach and Guetter, 1984a,b, 1986; Kutzbach and Street-Perrott, 1985; Prell and Kutzbach, 1987; COHMAP members, 1988; deMenocal and Rind, 1993; de Noblet *et al.*, 1996). Fully-coupled general circulation models (GCMs) have recently provided further insights. Liu *et al.* (2003, 2004) confirmed that increased summer insolation during the early- to mid-Holocene increased precipitation in the monsoonal regions of Asia, North Africa and North America, and that reduced summer insolation decreased precipitation in southern Africa and South America. They also showed, however, that oceanic and atmospheric feedbacks had a significant influence on precipitation at this time. In North Africa, an increase in the SST gradient in the northern tropical Atlantic caused by factors such as increased equatorial upwelling led to the ITCZ migrating further north (Kutzbach and Liu, 1997; Liu *et al.*, 2004). In southern Africa, high SSTs in the southern Atlantic and Indian Oceans driven by factors such as high spring insolation and a decrease in the strength of the subtropical highs acted to increase precipitation, even though total precipitation decreased in response to lower summer insolation (Liu *et al.*, 2004). Similarly, in southern East Africa, feedbacks such as an increase in the strength of the Asian winter monsoon acted to increase precipitation by increasing the strength of on-shore winds in austral summer, despite an overall decrease in precipitation (Liu *et al.*, 2003).

1.2.1.2 Remote insolation forcing

The climate systems of the low latitudes are linked to those of the mid- and high-latitudes by both atmospheric and oceanic circulation, and insolation received at remote locations could therefore affect climate in tropical and subtropical regions. The seasonal distribution of insolation at mid- and high-latitudes is affected by the obliquity of the earth's axis, which varies with a period of 41 kyr, and connections with these latitudes could thus cause climatic change at this frequency in low-latitude regions (Fig. 1.3). Clemens and Prell (2003) suggested, for example, that the strength of the Asian monsoon was affected by the seasonality of insolation over the southern Indian Ocean, which is partly determined by obliquity, because this parameter affects the amount of water vapour available to release latent heat in the monsoon low.

The insolation received at mid- and high-latitudes also affects the gradient of summer and mean annual insolation from low to high latitudes (Fig. 1.3). This gradient has a significant effect on the meridional temperature gradient (cf. Raymo and Nisancioglu, 2003; Liu and Herbert, 2004; Loutre *et al.*, 2004), and could thus affect climatic conditions at low latitudes by affecting the strength of meridional circulation (cf. Rind, 1998, 2000).

Prell and Kutzbach (1987) explored the effects of high- and low-latitude insolation on monsoonal climates by performing sensitivity experiments with an atmospheric GCM. They changed either the date of perihelion or the obliquity of the earth's axis while holding the other variable constant, and demonstrated that, although both variables affected precipitation in the northern tropics, the date of perihelion had a greater effect on precipitation than the obliquity of the earth's axis. Tuenter *et al.* (2003) explored the same question using a fully coupled GCM of intermediate complexity. They confirmed that the amount and the penetration of monsoonal precipitation in northern Africa were influenced by precessionally-driven changes in insolation and, to a lesser extent, by changes in insolation at higher latitudes. In particular, they found that increased summer insolation at high latitudes increased the moisture content of air converging over North Africa and increased the strength of on-shore winds by increasing convergence over Asia. In contrast, they found that the amount and the extent of monsoonal precipitation in the southern African tropics were only influenced by direct, precessionally-driven changes in insolation.

1.2.1.3 Global boundary conditions

The shifts between glacial and interglacial states involve significant changes in boundary conditions, including ice-sheet and sea-ice extent, the atmospheric concentrations of greenhouse gases and dust, surface albedo, sea level, and oceanic circulation (*e.g.* Petit *et al.*, 1981; Smythe *et al.*, 1985; Barnola *et al.*, 1987; Boyle and Keigwin, 1987; Shackleton, 1987; Berger *et al.*, 1993; Petit *et al.*, 1999; EPICA community members, 2004) (Fig. 1.3). These factors are referred to in this thesis as "boundary conditions", and they have the potential to affect climate in tropical and subtropical regions in a number of ways (Street and Grove, 1976).

The increase in ice-sheet and sea-ice extent during glacial periods would have increased the meridional temperature gradient. This change may have increased the intensity of atmospheric circulation and displaced climatic belts towards the equator (cf. Penck, 1914; COHMAP members, 1988; Rind, 1998, 2000). Consequently, the Hadley cells were probably stronger and more compressed during glacials, which would have increased the strength of trade winds, subtropical anticyclones, and equatorial convergence, and limited the latitudinal migration of the ITCZ (Hess, 1959; Flohn, 1964; van Zinderen Bakker, 1976; Nicholson and Flohn, 1980). In theory, these changes would have increased precipitation at the ITCZ, but also reduced the area that received precipitation from this system and increased the strength of subsidence in the subtropics (cf. van Zinderen Bakker, 1976; Lindzen and Nigam, 1987).

These effects would have been greater in the northern hemisphere than the southern hemisphere, due to the proportionally larger increase in ice-sheet volume in the northern hemisphere. Consequently, the hemispheric difference in meridional temperature gradients was probably lower during glacials, and the average location of the ITCZ may have therefore been further south than it is today (section 1.1) (Woldstedt, 1965; Flohn, 1967; Newell, 1973; Street and Grove, 1976; Lancaster, 1979; Chiang *et al.*, 2003). It is therefore possible that areas at the southern edge of the region currently influenced by tropical precipitation received more precipitation during glacial periods (cf. van Zinderen Bakker, 1967).

The increase in the meridional temperature gradient during glacials would have also increased the intensity and zonality of the circum-polar westerlies, and may have caused them to shift towards the equator, particularly in the northern hemisphere (cf. Penck, 1914; COHMAP members, 1988; Rind, 1998, 2000). These changes may have increased precipitation at the northern and southern extremes of the African continent during glacial periods, and may have also increased the latitudinal extent of the regions influenced by the mid-latitude westerlies (van Zinderen Bakker, 1967, 1976; Street and Grove, 1976; Nicholson and Flohn, 1980; Tyson, 1986; Cockcroft *et al.*, 1987).

The decrease in SSTs, including tropical SSTs, during glacial periods (*e.g.* Rind and Peteet, 1985; Guilderson *et al.*, 1994; Bard *et al.*, 1997; Beck *et al.*, 1997; Schneider *et al.*, 1997; Kirst *et al.*, 1999; Mix *et al.*, 1999) may have also affected climatic conditions in Africa. Lower SSTs would have reduced evaporation into air masses travelling inland and increased the stability of the lower atmosphere, and could have thus reduced precipitation on the continent (*e.g.* Rind, 1998; Bush and Philander, 1998; Ganopolski *et al.*, 1998; Clement *et al.*, 2004). The decrease in SSTs may have also affected the position of the ITCZ, possibly limiting its latitudinal migration (Biasutti *et al.*, 2003).

Lower atmospheric temperatures during glacials may have affected the amount of precipitation in tropical and subtropical regions by reducing convergence over landmasses, and by decreasing evaporation from tropical oceans (cf. Farrera *et al.*, 1999). A fall in atmospheric temperatures would have also decreased evaporation from water bodies, which would have acted to increase moisture availability independently of changes in precipitation.

These changes in boundary conditions may have caused further climatic change through feedback processes. Increased trade-wind strength may have increased the response of tropical SSTs to glacial boundary conditions by increasing evaporation from the ocean surface and stimulating further upwelling at the equator and on continental edges, for example (Bush and Philander, 1998; Ganopolski *et al.*, 1998). An expansion of the circum-Antarctic vortex and associated ocean fronts may have also reduced the amount of "Agulhas leakage" around the southern tip of Africa,

which could have affected SSTs in this area (*e.g.* Prell *et al.*, 1980; Kuhn and Diekmann, 2002; Peeters *et al.*, 2004).

Climate models have been used to explore the effects of glacial boundary conditions on tropical and subtropical climate, but the accuracy of many of these simulations is limited by their use of the SSTs reconstructed by CLIMAP (1981), which appear to over-estimate tropical SSTs during the LGM (*e.g.* Kutzbach and Guetter, 1986; deMenocal and Rind, 1993; Braconnot *et al.*, 2000). More recent models of climatic change in the tropics and subtropics have used revised or computed estimates of SSTs, however, and should therefore provide a more accurate indication of climatic conditions during glacials. Hostetler and Mix (1999) suggested that precipitation was lower in areas near and downwind of low SSTs during the LGM, particularly in the Amazon basin, parts of central Africa, and in Madagascar, but that it was higher in the Andes, northern Mexico, and parts of East Africa. The PMIP simulations of climate during the LGM that used computed SSTs, as opposed to the CLIMAP reconstructions, suggest that the tropics were generally dry during this period, but that precipitation may have been higher than today in Indonesia, northern Australia, and parts of South America and southern Africa (cf. Pinot *et al.*, 1999).

Fully coupled ocean-atmosphere GCMs offer the most advanced means of simulating climatic conditions, although these models are often low-resolution. Bush and Philander (1998) and Ganopolski *et al.* (1998) used such models to simulate global climate during the LGM, and found that precipitation was lower in most parts of the tropics, but that winter precipitation may have increased slightly in the southern hemisphere. Shin *et al.* (2003) performed a similar experiment, and showed that precipitation associated with the ITCZ decreased during the LGM, despite an increase in the strength of the Hadley circulation, but that precipitation increased between 20° and 30° due to an increase in cyclone formation in the mid-latitude westerlies.

Finally, Clement *et al.* (2004) made an explicit attempt to distinguish the effects of changes in boundary conditions associated with glacial-interglacial cycles from the effects of precessionally-driven changes in insolation using an atmospheric GCM coupled to a mixed-layer ocean. They showed that glacial boundary conditions were associated with lower mean annual precipitation in the northern hemisphere tropics

due to a reduction in the intensity of the Hadley cell, but with increased mean annual precipitation over land between 9°S and 30°S, due to a southward shift of the ITCZ. They also found, however, that lower SSTs acted to reduce precipitation in the southern tropics and that, consequently, precipitation did not increase in southern Africa under glacial boundary conditions. The experiments also confirmed that precessionally-driven changes in summer insolation influenced precipitation in the tropics and subtropics. Unfortunately, the effects of changes in insolation were not modelled under glacial boundary conditions, however, making it difficult to assess the relative influence of boundary conditions and changes in insolation on climatic conditions.

Obviously, the forcing factors described in this section acted simultaneously, and are not independent of one another. These considerations often make it difficult to determine the influence of individual factors on climatic conditions. In some cases, forcing factors appear to have been additive, with the direct effects of direct insolation dampened by glacial boundary conditions, for example (Prell and van Campo, 1986; Prell and Kutzbach, 1987; deMenocal *et al.*, 1993), but it has also been proposed that either insolation or global boundary conditions were the only influence on climatic conditions at certain times in the past (*e.g.* Partridge *et al.*, 1997).

1.2.2 Palaeoclimatic change in tropical and subtropical Africa

Some of the evidence for palaeoclimatic change on orbital timescales in tropical and subtropical Africa is outlined in this section in order to demonstrate our current understanding of the factors that have affected climatic conditions in this region. All radiocarbon dates have been converted to calibrated calendar years (using Calib version 5.0.1 (Stuiver and Reimer, 1993) where necessary), unless otherwise stated. The location of the terrestrial sites mentioned in the text is shown in Figure 1.4.

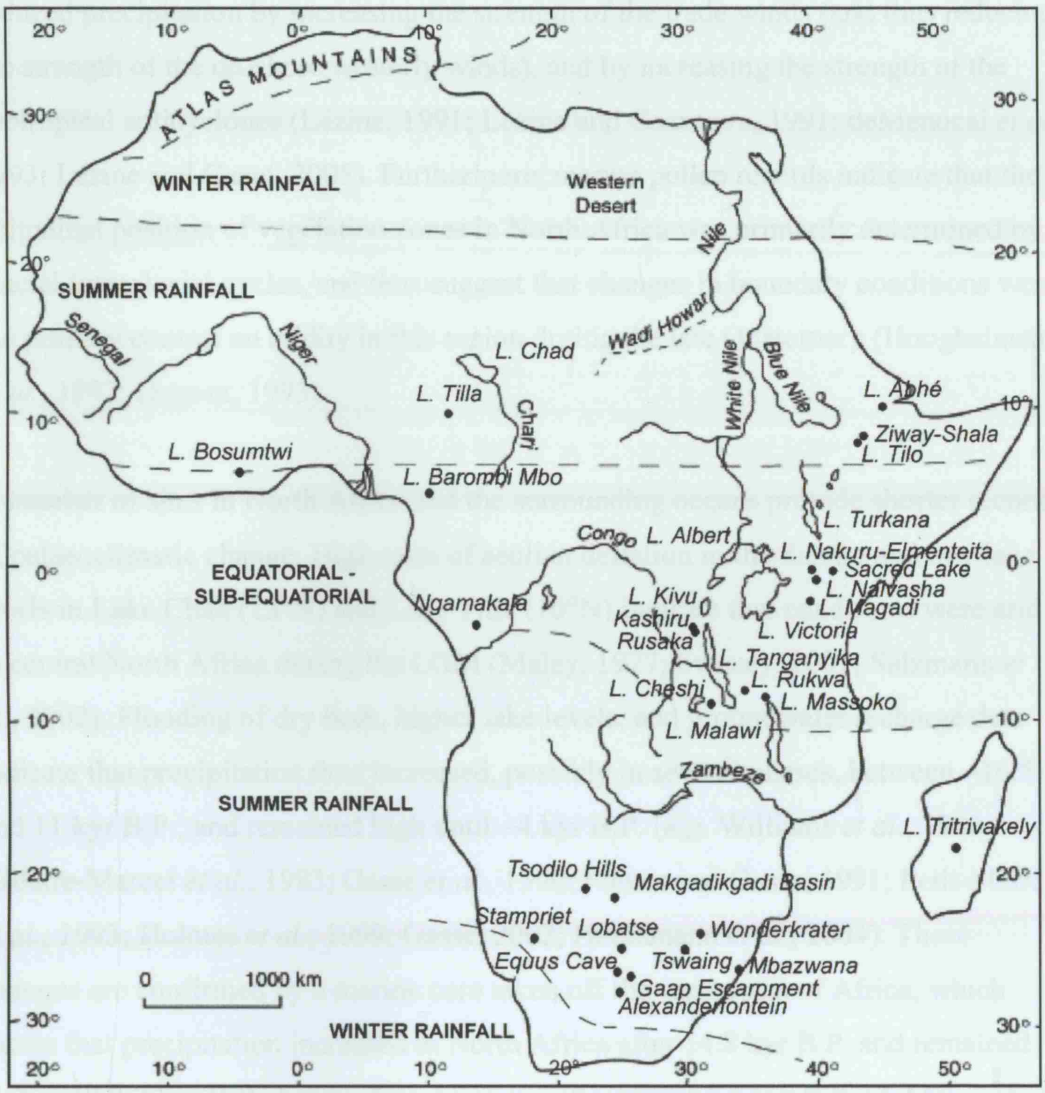

Figure 1.4: Location of terrestrial sites mentioned in the text. Modified from Gasse (2000).

The longest records of palaeoclimatic change in North Africa are from marine cores. Some of these records provide strong evidence that precessionally-driven changes in insolation have affected precipitation in this region. A 260 kyr-record from the equatorial Atlantic suggests that aridity increased every 23 kyr in the region between the equator and ~15°N, indicating that periods of high precipitation corresponded with peaks in summer insolation, for example (Pokras and Mix, 1987). Other marine records suggest that global boundary conditions have affected climate in North Africa, however. A 900 kyr-record of aeolian material from a core in the equatorial Atlantic and pollen records from cores off northwest Africa suggest that, although summer insolation acted to increase precipitation in North Africa, glacial conditions also

reduced precipitation by increasing the strength of the trade winds (and thus reducing the strength of the on-shore westerly winds), and by increasing the strength of the subtropical anticyclones (Lézine, 1991; Lézine and Casanova, 1991; deMenocal *et al.*, 1993; Lézine and Cazet, 2005). Furthermore, marine pollen records indicate that the latitudinal position of vegetation zones in North Africa was primarily determined by glacial-interglacial cycles, and thus suggest that changes in boundary conditions were the primary control on aridity in this region during the late Quaternary (Hoogheimstra *et al.*, 1992; Dupont, 1993).

A number of sites in North Africa and the surrounding oceans provide shorter records of palaeoclimatic change. High rates of aeolian deflation in the Sahara and low lake levels in Lake Chad (13°N) and Lake Tilla (10°N) indicate that conditions were arid in central North Africa during the LGM (Maley, 1977; Swezey, 2001; Salzmann *et al.*, 2002). Flooding of dry beds, higher lake levels, and groundwater recharge data indicate that precipitation then increased, possibly in several phases, between ~16.5 and 11 kyr B.P., and remained high until ~4 kyr B.P. (*e.g.* Williams *et al.*, 1980; Hillaire-Marcel *et al.*, 1983; Gasse *et al.*, 1990; Fontes and Gasse, 1991; Petit-Maire *et al.*, 1993; Holmes *et al.*, 1999; Gasse, 2002; Hoelzmann *et al.*, 2004). These changes are confirmed by a marine core taken off the west coast of Africa, which shows that precipitation increased in North Africa after 14.8 kyr B.P. and remained high until 8.2 kyr B.P., before decreasing significantly at 5.5 kyr B.P. (deMenocal *et al.*, 2000). This pattern of change is in line with that expected from changes in summer insolation in the northern hemisphere, and thus suggests that direct insolation has had a significant effect on precipitation in North Africa since the LGM (Fig. 1.3) (deMenocal *et al.*, 2000).

A similar pattern emerges from sites in the Horn of Africa. Lake Abhé in the central Afar region (11°N) provides one of the longest terrestrial records in Africa, covering the last 70 kyr (Gasse, 1977; Gasse *et al.*, 1980). This record indicates that lake levels were low at ~36 kyr B.P. and during the LGM, when summer insolation was low, and high at ~30 kyr B.P. and ~10 kyr B.P., when summer insolation was high (Fig. 1.3). Similarly, lake levels in the Ziway-Shalla basin were high at ~30 kyr B.P., but fell and remained low until ~14.5 kyr B.P. (Street, 1979). Lake levels then increased and remained relatively high until ~5 kyr B.P., with the exception of a significant

regression centred on 8.5 kyr B.P. and a shorter one at 6.7 kyr B.P. (Gasse, 1977; Street, 1979; Gillespie *et al.*, 1983). These patterns of change are supported by records from lakes in the Main Ethiopian Rift such as Lake Tilo (7°N), which indicate that lake levels rose at ~11 kyr B.P. and remained high until ~5.5 kyr B.P., when they decreased and generally remained low until the present day (Chalié and Gasse, 2002; Lamb *et al.*, 2000, 2004). Lake Turkana (4°N) was also deep during the early- to mid-Holocene and decreased in depth after ~5 kyr B.P., but there is no evidence for an increase in lake level between 40 and 12 kyr B.P., which suggests that precipitation at this site did not increase in response to the peak in summer insolation at ~32 kyr B.P. (Butzer *et al.*, 1972; Owen *et al.*, 1982; Johnson, 1996).

In West Africa, seismic reflection data from Lake Bosumtwi (6°N) suggest that lake levels were low ~108, ~86, ~65 and ~16.8 kyr B.P., and during the late Holocene (Brooks *et al.*, 2005). Brooks *et al.* (2005) attributed these changes to events in the North Atlantic, but their timing and frequency suggests that they were probably caused by precessionally-driven changes in insolation. Sediment cores from the lake indicate that moisture availability decreased between ~29 and ~11.5 kyr B.P. (although it fluctuated several times during this period), and was high during the early Holocene (Talbot *et al.*, 1984; Talbot and Johansson, 1992). Pollen records from Lake Barombi Mbo (4°N) show a similar pattern, indicating that conditions were dry during the LGM, and that lake levels fluctuated after this period, before increasing and remaining high until 3 kyr B.P. (Maley and Brenac, 1998). This pattern is in broad agreement with that expected from forcing by summer insolation. Furthermore, records from both lakes suggest that conditions may have been relatively wet at ~28 kyr B.P., which could represent a response to the peak in summer insolation at ~32 kyr B.P. (Giresse *et al.*, 1991; Talbot and Johansson, 1992; Maley and Brenac, 1998). Cores from the Niger River Delta, which reflect climatic conditions between ~10°N and ~20°N in western Africa, confirm these patterns, indicating that runoff increased after 14.5 kyr B.P. and remained high until 7.1 kyr B.P. (Lézine *et al.*, 2005). These records do not show evidence for an increase in moisture availability at 32 kyr B.P., however, which again suggests that the peak in summer insolation at this time may not have had a significant effect on precipitation in all parts of North Africa (Lézine and Cazet, 2005).

The northern tropics of Africa therefore appear to have experienced climatic changes that are in line with those expected from changes in northern hemisphere summer insolation, at least since the LGM. The climatic shifts are more rapid than would be expected from gradual changes in insolation, however, and may therefore represent non-linear responses of the climate system to insolation forcing through processes such as SST and surface-albedo feedbacks (Claussen *et al.*, 1999; deMenocal *et al.*, 2000). Evidence from longer records suggests that changes in boundary conditions related to glacial-interglacial cycles, particularly the strength of the trade winds, also affected climatic conditions in North Africa, but their influence remains uncertain.

In equatorial Africa, the longest well-dated records of climatic change are from the Naivasha basin (1°S) (Richardson and Dussinger, 1986; Trauth *et al.*, 2001, 2003). These records indicate that Lake Naivasha increased in volume in response to peaks in both September and March insolation on the equator, providing strong evidence for the link between precessionally-driven changes in insolation and tropical precipitation. A mineral magnetic record from Sacred Lake in Kenya (0°) that covers the last ~110 kyr also indicates that precessionally-driven changes in insolation determined precipitation in East Africa, because the record varies with a periodicity of ~11.5 kyr (Olago *et al.*, 2000). The longest and most significant highstands in the Naivasha Basin, at ~135 kyr B.P. and during the early Holocene, correspond with the onset of interglacial periods, however, which suggests that changes in boundary conditions also affected precipitation in equatorial East Africa (Richardson and Dussinger, 1986; Trauth *et al.*, 2001, 2003). This proposal is supported by evidence of extreme highstands in lakes in the East African Rift Valley during, or close to the time of, the last interglacial (Butzer *et al.*, 1969; Hillaire-Marcel *et al.*, 1986; Sturchio *et al.*, 1993; Trauth *et al.*, 2001, 2003).

Shorter records from equatorial Africa indicate that climatic conditions in this region have changed in a similar manner to those in northern Africa since the LGM, although some records indicate that moisture availability remained high during the late Holocene. Lakes Nakuru and Elmenteita (0°) in the CKR were low during the LGM, but increased in volume between ~15 and ~6 kyr B.P., in line with records from the northern tropics (Richardson and Dussinger, 1986). Similarly, Lake Kivu (2°S), which lies west of Lake Victoria, increased in depth at ~11.5 kyr B.P. and remained high

until ~4.5 kyr B.P. (Haberyan and Hecky, 1987). Lakes Albert (1°N) and Victoria (0-2.5°S) were low or dry during the LGM, rose briefly between ~16 and ~15 kyr B.P., and then increased significantly after ~15 kyr B.P. (Talbot and Livingstone; 1989; Johnson, 1996; Beuning *et al.*, 1997; Talbot and Laerdal, 2000; Stager *et al.*, 2002). Lake Victoria remained high during the late Holocene, but evidence of sediment erosion suggests that Lake Albert may have dried out at 3.7 kyr B.P. (Beuning *et al.*, 1997; Talbot and Laerdal, 2000). The reason that the pattern of climatic change in this region since the LGM is similar to that in northern Africa remains uncertain. It is possible that the similarity can partly be explained by changes in SST and their influence on moisture transport into the region (cf. Barker and Gasse, 2003), but this explanation does not account for the decrease in lake levels observed at many sites during the late Holocene.

Records from a marine core in the eastern Atlantic suggest that precipitation in western and central equatorial Africa increased at ~17 kyr B.P., peaked during the early Holocene, and decreased over the mid- to late-Holocene; a pattern that is similar to that in equatorial East Africa and the northern tropics (Schefuβ *et al.*, 2005). Schefuβ *et al.* (2005) attributed these changes to variations in the strength of the south-easterly trade winds, which affected the strength of on-shore, moisture-bearing westerly winds. The strength of the trade winds appears, in turn, to have been determined by the gradient of SSTs between the tropical and subtropical South Atlantic (Schefuβ *et al.*, 2005).

In summary, long-term records from equatorial East Africa suggest that precessionally-driven changes in equatorial insolation have influenced climatic conditions in this region, but the magnitude of the lake-level highstands observed in some East African lakes close to the time of the last interglacial and during the early Holocene suggests that boundary conditions associated with glacial-interglacial cycles have also affected precipitation in this area. The similarity of many palaeoclimatic records from equatorial Africa to those from the northern tropics during the period since the LGM complicates this picture, however, as neither changes in direct insolation nor changes in boundary conditions associated with glacial-interglacial conditions can completely explain this pattern of change.

A number of new records have recently improved our understanding of the nature of climatic change in the southern African tropics. One of the longest records from this region is a 100-kyr record from Lake Tanganyika (4-8°S) (Scholz *et al.*, 2003). Scholz *et al.* (2003) proposed that this record indicates climatic change in phase with changes at high northern latitudes, but the 11 kyr periodicity evident in the bulk density record hints at precessional forcing. Records from Lake Massoko (9°S) and Kashiru swamp (4°S) also suggest that precessional forcing may have been important before the LGM, as they indicate that precipitation was relatively high ~45-40 kyr B.P., close to the time of a peak in austral summer insolation (Fig. 1.3) (Bonnefille *et al.*, 1990; Bonnefille and Chalié, 2000; Barker *et al.*, 2003).

Records of climatic conditions since the LGM suggest that the pattern of change in the southern tropics was similar to that in northern and equatorial regions, however, with relatively arid conditions during the LGM and an increase in moisture availability during the late glacial and early Holocene. Lakes Rukwa (8°S) and Cheshi (9°S) were low during the LGM and increased in depth between ~14 and ~6 kyr B.P. (Stager, 1988; Barker *et al.*, 2002). Similarly, the level of Lake Massoko (9°S) was low during the LGM, increased during the late glacial, and generally remained high until ~4.5 kyr B.P. (Barker *et al.*, 2000, 2003). Sites in the Burundi highlands (2-4°S), including Rusaka swamp (3.5°S), indicate that precipitation was low during the LGM, but that it increased significantly at ~15 kyr B.P. and remained high until the end of the Holocene (Bonnefille *et al.*, 1995; Bonnefille and Chalié, 2000). Records from West Africa are more equivocal, but provide some support for the suggestion that moisture availability was low during the LGM. A record from Ngamakala (4°S) suggests that precipitation was low during the LGM, but that humidity remained relatively high in lowland coastal regions due to fogs that formed over coastal upwelling zones, for example (Elenga *et al.*, 1994).

Records from Lake Malawi (9.5°S-14.5°S) were initially thought to indicate high lake levels between 32.5 and 11.5 kyr B.P., and between 7 kyr B.P. and the present, which suggested that austral summer insolation determined precipitation at this site (Fig. 1.3) (Finney and Johnson, 1991; Finney *et al.*, 1996). This led to the suggestion of a climatic "hinge" between Lake Tanganyika and Lake Malawi (at ~9-10°S), south of which southern hemisphere insolation determined precipitation. More recent records

of biogenic silica accumulation rates, diatom assemblage composition, and organic matter composition suggest, however, that Lake Malawi was low during the LGM and increased in depth after ~17 kyr B.P. The lake then remained at intermediate levels until ~4.5 kyr B.P. (with the exception of a regression at ~11 kyr B.P.), when lake levels may have risen slightly (Gasse *et al.*, 2002; Johnson *et al.*, 2002, 2004; Filippi and Talbot, 2004). This reconstruction is in closer agreement with other records from the region, although the apparent increase in lake levels at ~4.5 kyr B.P. suggests that southern hemisphere insolation may have influenced precipitation during the late Holocene (Gasse *et al.*, 2002; Johnson *et al.*, 2004).

Climatic change since the LGM in the region of Africa between the equator and ~9°S therefore appears to have been similar to that in equatorial and northern areas, suggesting that the same factors determined climatic change in all three regions. Changes in boundary conditions such as SSTs could have affected climatic conditions throughout this area, and may thus have been responsible for the changes observed, possibly in association with land surface-atmosphere feedbacks (cf. Barker and Gasse, 2003). As in equatorial regions, this explanation does not account for the observation that some lakes remained deep during the late Holocene, while others decreased in depth, however. In addition, the evidence that a peak in austral summer insolation at ~45 kyr B.P. may have increased precipitation at some sites in the region, and that the level of Lake Malawi may have increased in response to a peak in summer insolation during the late Holocene, suggests that southern hemisphere insolation could have also influenced climatic conditions in this region.

Unfortunately, there are few long records from the region south of Lake Malawi. A 190-kyr marine pollen record from a site off the west coast of central Africa (6.5°S) suggests that conditions in the region east and southeast of the coring station were cold and dry during glacials, and warm and wet during interglacials (Jahns, 1996). There is also evidence that precessionally-driven changes in northern hemisphere insolation influenced SSTs, atmospheric temperatures, and precipitation in this region during marine isotope stage (MIS) 5, however, possibly through the influence of the North African monsoon on the strength of the trade winds (Schneider *et al.*, 1995, 1996; Jahns, 1996). In contrast, records from Lake Tritrivakely in Madagascar (19°S) and from Tswaing crater lake in South Africa (25°S) suggest that precessionally-

driven changes in southern hemisphere insolation have affected precipitation in southern Africa and the surrounding islands (Partridge *et al.*, 1997, 1999; Gasse and van Campo, 1998, 2001). The records from Lake Tritrivakely cover the last 150 kyr, but they are not directly dated beyond 41 kyr B.P. (Gasse and van Campo, 1998, 2001). The longest and most extreme highstands of the lake correspond with peaks in austral summer insolation, but high levels of evaporation during summer and low rainfall during winter appear to have out-weighed increases in precipitation during some periods of high insolation, including the LGM, resulting in arid conditions (Gasse and van Campo, 1998, 2001). The records from Tswaing crater lake suggest that the intensity of austral summer insolation controlled the amount of precipitation at the site between ~200 and ~50 kyr B.P., after which regional or global boundary conditions appear to have dominated climatic conditions (Partridge *et al.*, 1997, 1999) (sections 1.3.1 and 5.2).

There are also a number of short and discontinuous palaeoclimatic records from tropical and subtropical regions south of Lake Malawi, but these records do not provide a coherent picture of climatic change, and only a few will therefore be mentioned here. Luminescence dating of sand dunes in the Kalahari basin suggests that, on average, conditions were arid between ~35 and 8 kyr B.P., and wetter after 8 kyr B.P. (Munyikwa, 2005). It has been shown, for example, that there were major phases of dune building in the southern Kalahari (~26°S) at 30-23 and 16-10 kyr B.P., but that there has only been localized dune activation since this time (Stokes *et al.*, 1997a,b; Thomas *et al.*, 1997). The $\delta^{13}C$ record from a stalagmite in Lobatse II Cave in Botswana (25°S) also suggests that conditions were dry during the LGM, because the abundance of C_4 vegetation increased before this period, and the speleothem stopped growing at ~21 kyr B.P. (Holmgren *et al.*, 1995).

Other records indicate that moisture availability was high in southern Africa during parts of the last glacial, and possibly during the LGM, however. A palaeolake completely filled the Makgadikgadi basin in southern Botswana (21°S), which covers an area of ~80,000 km^2, at some point during the last glacial, and partly filled it twice between 32 and 27 kyr B.P., for example (Thomas and Shaw, 1991; Shaw *et al.*, 1997). Records of lake level and dune construction in the Tsodilo Hills (19°S) suggest that moisture availability was high 40-36, 27-22, and 19-12 kyr B.P., although it is not

clear whether lake levels fell during the LGM (Brook *et al.*, 1992; Thomas *et al.*, 2003). Further south, the record of tufa formation at the Gaap Escarpment (~27°S) suggests that moisture availability was generally higher than at present 45-9 and 3.6-0.5 kyr B.P. (Butzer *et al.*, 1978; Beaumont and Vogel, 1993; Brook *et al.*, 1998). High lake levels in basins such as the Alexandersfontein Pan (29°S) and Mbazwana (27°S) also suggest that conditions were wet during parts of the last glacial, although the highstand at Alexandersfontein may be older than the age of ~23-15 ^{14}C kyr B.P. originally assigned to it (Butzer *et al.*, 1973; Butzer, 1984; Maud *et al.*, 1993). The picture of climatic change in southern Africa therefore remains uncertain, with no equivocal evidence even as to whether conditions were wetter or drier than today during the LGM in many parts of the region.

Finally, it is important to note that the mid-latitude westerlies may have brought precipitation to subtropical regions in the past. In northern Africa, the gradient of the isotope composition of fossil groundwater from west to east across the Sahara indicates that areas north of ~16°N received more precipitation from the mid-latitude westerlies during wet phases of the last glacial than they do today (Sonntag *et al.*, 1978; Sultan *et al.*, 1997; Edmunds *et al.*, 2004). In southern Africa, evidence from terrestrial sites suggests that the westerlies brought more precipitation to the region that is currently influenced by these systems during the LGM than they do at present (cf. Beaumont, 1986; Cowling *et al.*, 1999; Meadows and Baxter, 1999; Parkington *et al.*, 2000). A record of aridity in southwestern Africa based on grain-size analysis of a marine core from the Walvis Ridge (19°S) suggests that an equator-ward shift of the westerlies during glacials may have also increased moisture availability in areas north of the region that currently receives precipitation from these winds (Stuut *et al.*, 2002). In contrast, pollen records from cores taken off the coast of Namibia suggest that although vegetation associated with a winter rainfall regime grew as far north as 19°S on the west coast of southern Africa during the LGM, conditions were generally arid between 21 and 17.5 kyr B.P., and thus that a northward shift of the westerlies did not increase overall moisture availability in this region (Shi and Dupont, 1997; Shi *et al.*, 1998, 2000; Dupont and Wyputta, 2003). The influence of the mid-latitude westerlies on climatic conditions in southern Africa therefore remains uncertain.

1.2.3 Palaeoclimatic change in other tropical and subtropical regions

This study is primarily concerned with climatic change in tropical and subtropical Africa, but some of the longest and most accurately dated records of climatic change in tropical and subtropical regions are from other continents. The most informative of these records are mentioned here, with the aim of shedding light on processes that may have operated in Africa, but these findings cannot be applied directly to Africa, due to the different climatic settings of individual tropical and subtropical regions.

A number of records have provided insights into the nature and causes of climatic change in tropical and subtropical South America. In the northern hemisphere, records indicate that precipitation increased in phase with summer insolation. Records from Haiti (18°N) (Hodell *et al.*, 1991) and northern Guatemala (17°N) (Hillesheim *et al.*, 2005) indicate that the peak in boreal summer insolation during the early Holocene increased precipitation by increasing the intensity of convection and/or causing a northward shift of the ITCZ, for example. Similarly, records from the Cariaco basin (10°N) indicate that runoff increased during the early Holocene due to a northward shift of the ITCZ caused by increasing summer insolation (Haug *et al.*, 2001). On longer timescales, a record of productivity from Lake Pata (0°16'N) indicates that precessionally-driven changes in insolation have affected lake levels at this site since 170 kyr B.P. (Bush *et al.*, 2002).

Records from the southern tropics of South America also indicate that precipitation has responded to changes in summer insolation. A series of speleothem and travertine deposits from northeastern Brazil (10°S) that covers the last 210 kyr indicates that precipitation increased when the ITCZ shifted southwards in response to peaks in summer insolation (Wang *et al.*, 2004). Similarly, isotope records from a speleothem in southern Brazil (27°S) show that peaks in austral summer insolation over the last 116 kyr caused a southward shift of the ITCZ, and possibly an increase in precipitation (Cruz *et al.*, 2005). Shorter records of precipitation from the Bolivian altiplano and parts of Amazonia also indicate that the intensity of austral summer insolation has influenced precipitation by affecting either the southern limit of the ITCZ (Martin *et al.*, 1997; Mayle *et al.*, 2000; Tapia *et al.*, 2003), or the strength of

the moisture-bearing north-easterly trade winds and convective activity at the ITCZ (Cross *et al.*, 2000; Seltzer *et al.*, 2000; Baker *et al.*, 2001a,b).

There is, however, also evidence that changes in global boundary conditions associated with glacial-interglacial cycles have influenced climatic conditions in South America. A record of lake extent from Panama (7°N) indicates that the average location of the ITCZ shifted south during the last glacial in response to an increase in the meridional temperature gradient in the northern hemisphere (Bush, 2002). In the southern hemisphere, the speleothem record from southern Brazil suggests that precipitation may have increased slightly during glacials due to a southward shift of the ITCZ, although direct insolation remains the dominant signal (Cruz *et al.*, 2005). The record of moisture availability from Salar de Uyuni in the Bolivian altiplano (20°S) suggests that factors such as SST-gradients over the North Atlantic affected precipitation at this site before 50 kyr B.P. (Fritz *et al.*, 2004). Finally, a record of arboreal pollen abundance from Colônia in the Atlantic rainforest region of Brazil (24°S) indicates that climatic conditions in this region were primarily determined by changes in global boundary conditions over the last ~100 kyr (Ledru *et al.*, 2005).

Two well-dated, highly-resolved terrestrial records of the intensity of tropical precipitation have also been produced from China, adding to the wealth of data relating to the strength of the Asian monsoon from the marine environment (*e.g.* Prell and van Campo, 1986; Clemens and Prell, 1990; Anderson and Prell, 1993; Sirocko *et al.*, 1993; Morley and Heusser, 1997; Schulz *et al.*, 1998; Budziak *et al.*, 2000; Clemens and Prell, 2003). These records, from stalagmites in Hulu Cave (32°N) and Dongge Cave (25°N), indicate that precessionally-driven variations in summer insolation were the primary cause of changes in the intensity of the Asian and East Asian monsoons over the last 160 kyr, but also demonstrate that precipitation has responded to gradual changes in insolation in a non-linear manner, with abrupt transitions at the start and end of the last interglacial, for example (Wang *et al.*, 2001; Yuan *et al.*, 2004; Wang *et al.*, 2005).

1.3 Aims and outline of this study

It is evident from the discussion above that precessionally-driven changes in insolation have been the primary cause of climatic change in many tropical and subtropical regions during the late Quaternary. There is evidence that changes in boundary conditions associated with glacial-interglacial cycles have also influenced climatic conditions at low latitudes, but these changes often appear to play a secondary role. The causes of climatic change in equatorial and southern Africa remain uncertain, however, largely due to a lack of long palaeoclimatic records from these regions.

This study aims to add to our understanding of the nature and causes of climatic change south of the equator in Africa by producing palaeoclimatic records from Tswaing crater lake in South Africa (25°24'S, 28°04'E), and from the Naivasha and Nakuru-Elmenteita basins in the CKR (0°4'S, 36°1'E) (Fig. 1.3). These sites have particular potential to contribute to our understanding of climatic change because Tswaing crater lake lies at the southern limit of the region influenced by tropical circulation and should therefore be sensitive to changes in the latitudinal position of this system, while the CKR lies close to the equator and is therefore likely to have been influenced by tropical circulation throughout the late Quaternary. Consequently, comparisons of palaeoclimatic records from these sites may provide insights into the causes of climatic change that could not be obtained by considering either site alone.

A brief introduction to these sites will be provided in the following sections, together with a brief summary of the work that has previously been carried out at the sites, and a description of the ways in which this study aims to add to this work. The structure of this thesis will then be outlined. Full background information for the two sites is provided in chapters 3 and 7.

1.3.1 Tswaing crater lake

Tswaing is a crater that lies 40 km northwest of Pretoria, on the interior plateau of South Africa, at an altitude of 1045 m. It is almost circular, with a diameter of 1.13 km, and the highest section of the rim lies 60 m above the plain that surrounds it and 119 m above the crater floor (Fig. 1.5). The crater is thought to have been formed by

meteorite impact ~220 kyr B.P., and appears to have held a lake since its formation (Reimold *et al.*, 1991, 1992; Partridge *et al.*, 1991; Storzer *et al.*, 1993, 1999; Koeberl *et al.*, 1994).

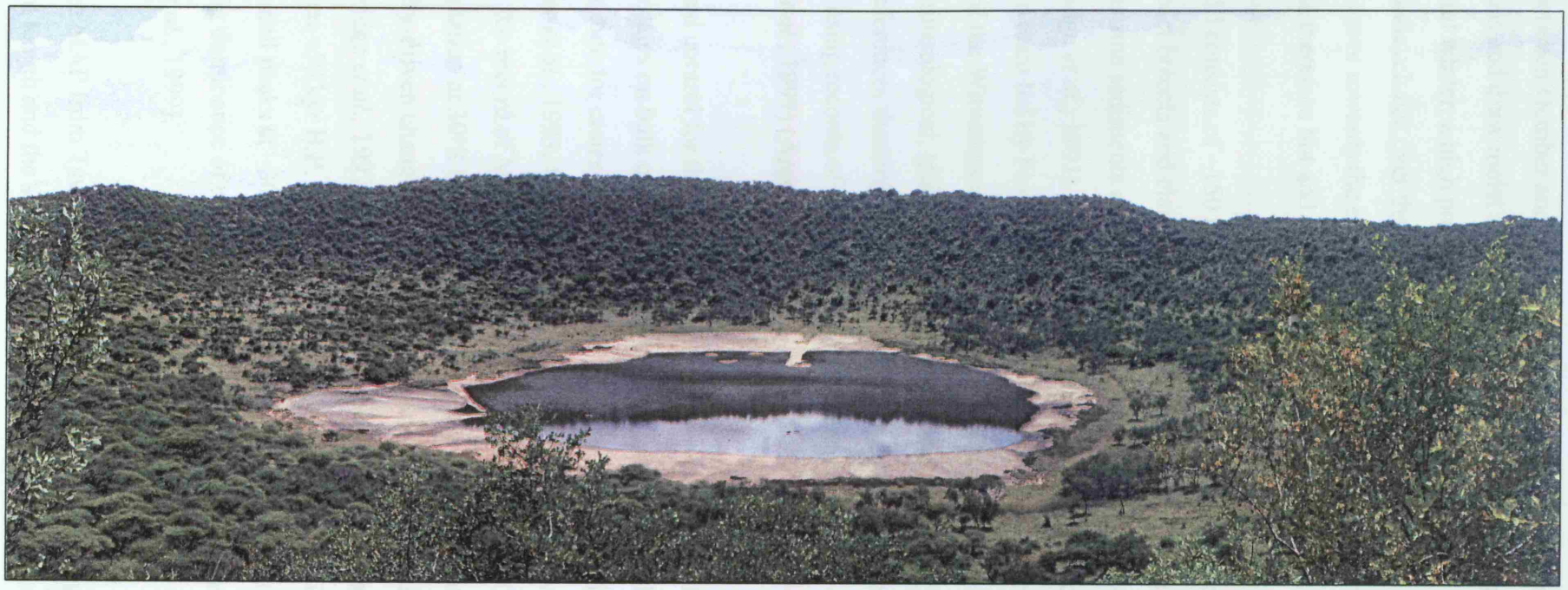

Figure 1.5: Photograph of Tswaing crater lake, South Africa, taken from the southeast edge of the rim, facing northeast. Photographs taken by the author in February 2005.

The site lies in the summer rainfall zone of southern Africa, receiving around 80% of its rainfall between October and March, as the ITCZ and CAB reach their southern-most locations and draw moist air into southern Africa from the Indian Ocean (Fig. 1.2). In austral winter, a high pressure cell develops over southern Africa and the permanent anticyclones over the South Atlantic and the southern Indian Ocean expand and move towards the equator, bringing dry, stable air to the region (Fig. 1.2). Summers are therefore hot and wet, while winters are cool and dry.

The crater-fill consists of ~150 m of sediments, of which the lower 60 m consist of suevitic impact breccia and clastic sediments, and the upper 90 m consist of fine-grained lacustrine sediments and coarse mass-flow deposits derived from the crater walls (Partridge *et al.*, 1991). A core of this material was obtained from the site in 1988/89 by a team led by Prof. T. C. Partridge (Climatology Research Unit, University of the Witwatersrand). The lacustrine sediments were subjected to low-resolution mineralogical, grain-size, pollen, and diatom analysis (Partridge *et al.*, 1999, and references therein), and a record of mean annual precipitation (MAP) was constructed using records of the carbonate content and grain size of the sediments (Partridge *et al.*, 1997) (Appendix A).

Chronological control for the sedimentary sequence was provided by seven radiocarbon dates on bulk organic material in the upper 18 m of the sequence, and a fission-track date for crater formation of 220 ± 52 kyr B.P. (Partridge *et al.*, 1993, 1997; Storzer *et al.*, 1993, 1999; Koeberl *et al.*, 1994). When viewed in light of this chronology, the record of MAP indicates that precipitation varied in phase with summer insolation at 30°S between ~50 and 200 kyr B.P., and thus suggests that precessionally-driven changes in insolation determined precipitation during this period (Partridge *et al.*, 1997). The relationship between rainfall and insolation breaks down between ~50 kyr B.P. and the present, however, when precipitation remains low apart from small peaks at ~30 kyr B.P. and after 5 kyr B.P. This shift was attributed to the increasing dominance of regional or global climatic conditions after ~50 kyr B.P. (Partridge *et al.*, 1999).

The record of MAP from Tswaing crater lake has proved to be highly influential due to its unusual length and the scarcity of palaeoclimatic records from southern Africa

(*e.g.* Battarbee *et al.*, 2004). The confidence that can be placed in its accuracy is limited by a number of factors, however. The chronological control of the sequence is poor, as the fission-track date for crater formation (which has errors of ±24%) provides the only form of age control below 18 m. The records of pollen and diatom assemblage composition from the core are also affected by poor preservation, which limits the extent to which they can be used to validate the record of MAP (Scott, 1999; Metcalfe, 1999). Finally, the low resolution of the records from the core (samples were obtained at intervals of 0.5 to 1 m) limits their temporal resolution to a maximum of ~2 kyr.

Two new cores of lacustrine sediments were obtained from Tswaing crater lake in 2001/02, as part of a collaborative project involving Prof. T. C. Partridge (Climatology Research Unit, University of the Witwatersrand), Dr. H. Oberhänsli (GFZ, Potsdam), and University College London. This study aims to use these cores to add to our understanding of palaeoclimatic change at Tswaing crater lake by improving the chronological control of the sedimentary sequence, and by producing higher-resolution, multi-proxy records of palaeoclimatic change.

1.3.2 Central Kenya Rift

Lake Naivasha (0°55'S, 36°20'E) lies 1890 m a.s.l. in the CKR, and Lakes Nakuru (0°22'S, 36°05'E) and Elmenteita (0°20'S, 36°10'E) lie immediately to the north, at 1758 and 1776 m a.s.l., respectively (Fig. 1.1). The lakes lie between the shoulders of the rift valley, which are formed by the Kinangop Plateau and the Aberdare Range to the east, and by the Mau Escarpment to the west (Richardson and Richardson, 1972) (Fig. 1.1). Exposed lake sediments and strandlines show that Lakes Nakuru and Elmenteita formed a single lake, known as Palaeolake Nakuru-Elmenteita, during the late Pleistocene and the early Holocene, but there is no evidence that this lake was ever connected to Lake Naivasha (Washbourn, 1967; Washbourn-Kamau, 1970, 1971; Dühnforth *et al.*, in prep.).

The CKR lies between the influences of the humid Congo air mass to the west, and the trade wind circulation over the Indian Ocean to the east (Nicholson, 1996). The exposed flanks of the rift generate orographic precipitation from these air masses, and therefore receive high levels of precipitation for much of the year (Nicholson, 1996;

Leroux, 2001). The valley floor, in contrast, lies in the rain-shadow of the rift shoulders, and most precipitation in this region is therefore generated by local convection, which is strongest four to six weeks after the ITCZ passes overhead, in April-May and October-November (Rodhe and Virji, 1976; Vincent *et al.*, 1979; Nicholson, 1996; KMD, 2000).

During the early Holocene, Lake Naivasha overflowed to the south and cut the Ol Njorowa Gorge by headward erosion, thereby exposing a 60m-thick section of lacustrine sediments, diatomite beds, lava flows, and tuffs that were deposited between 60 and 320 kyr B.P. (Washbourn-Kamau, 1977; Trauth *et al.*, 2001). Trauth *et al.* (2001, 2003) identified six highstands of Lake Naivasha in this sequence, based on sediment composition, the degree of volcanic glass alteration, the presence of authigenic mineral phases, and the composition of diatom assemblages. $^{40}Ar/^{39}Ar$ dating of the deposits showed that each highstand coincided with a peak in either September or March insolation on the equator, and it was therefore concluded that insolation was the primary influence on precipitation in the Naivasha basin during the late Pleistocene (Trauth *et al.*, 2001, 2003).

The longest and deepest highstand in the sequence, which was centred on ~135 kyr B.P., straddles two peaks in insolation. Trauth *et al.* (2003) suggested that the magnitude and length of this lake-level highstand could probably be attributed to high SSTs in the Indian Ocean during the last interglacial. This suggestion is supported by the high levels of other lakes in East Africa at this time (Butzer *et al.*, 1969; Hillaire-Marcel *et al.*, 1986; Sturchio *et al.*, 1993). Bergner and Trauth (2004) produced sedimentological and diatom assemblage records from the diatomite bed that was deposited during this highstand, but their records were low resolution and led to conflicting reconstructions of lake-level change. Consequently, these records were unable to demonstrate whether precessionally-driven changes in insolation influenced palaeohydrological conditions during the highstand or, contrarily, whether interglacial boundary conditions were the dominant control.

The oxygen isotope composition of diatom silica ($\delta^{18}O_{diatom}$) offers an ideal means of obtaining additional information about palaeohydrological change during the lake-level highstand centred on ~135 kyr B.P., because clean diatom samples can often be

obtained from small quantities of diatomite. This study therefore presents $\delta^{18}O_{diatom}$ records from the diatomite bed deposited in Lake Naivasha during this lake-level highstand, and from a diatomite bed deposited in Palaeolake Nakuru-Elmenteita at approximately the same time. The bed deposited in Lake Naivasha is exposed at the Ol Njorowa Gorge (Fig. 1.6a), and the bed deposited in Palaeolake Nakuru-Elmenteita is exposed at Soysambu (Fig. 1.6b). These records are used to assess the relative influence of precessionally-driven changes in insolation and changes in boundary conditions associated with the last interglacial on climatic conditions in the CKR, and to thereby provide additional information about the nature and causes of palaeoclimatic change in equatorial East Africa.

1.3.3 Outline of the thesis

Chapter 2 provides the theoretical background necessary to interpret the stable isotope and sedimentological data presented in this thesis. This information is presented in a separate chapter because stable isotope and sedimentological data form the basis of much of the study, and are discussed in several different chapters (chapters 3, 5, 6 and 7). The information necessary to interpret the $^{230}Th/^{234}U$ data presented in chapter 4 and the records of diatom assemblage composition and siliceous microfossil concentrations presented in chapter 6 is provided in these chapters.

In chapter 3, stable isotope analysis is used to explore the processes that operate at Tswaing crater lake today, in order to allow palaeoclimatic records from the site to be interpreted as accurately as possible. In particular, the $\delta^{18}O$ and $\delta^{2}H$ values of water samples are used, in conjunction with geochemical data provided by others, to shed light on the hydrological setting of the lake. The $\delta^{13}C$ values of dissolved inorganic carbon (DIC) are used to explore the processes that affect the inorganic carbon cycle at the site, and the $\delta^{13}C$ and C/N values of organic matter are used to shed light on the composition of organic matter in the lake and its catchment.

Chapter 4 describes the new sediment cores from Tswaing crater lake, and presents five new $^{230}Th/^{234}U$ dates on carbonates from the lower, previously undated section of the sedimentary sequence. These dates are used, together with three new radiocarbon dates provided by I. Kristen (GFZ, Potsdam), and seven radiocarbon dates from the core obtained in 1988/89, to construct a new age-depth model for the sequence.

In chapter 5, sedimentological (%LOI 550°C and %LOI 950°C) and geochemical ($\delta^{18}O_{calcite}$, $\delta^{13}C_{calcite}$, $\delta^{13}C_{organic}$, and C/N ratios of bulk organic matter) records from the sedimentary sequence at Tswaing are used to reconstruct palaeoenvironmental conditions. These reconstructions are used, in light of the age-depth model presented in chapter 4, to explore the nature and causes of palaeoclimatic change at the site. The records presented in this chapter contain a number of discrepancies, and chapter 6 therefore presents short records of diatom assemblage composition and siliceous microfossil concentrations (from between 34.40 and 54.80 m) that are used to resolve

these issues, and to thereby increase the confidence associated with the palaeoclimatic reconstructions from the site.

Chapter 7 presents $\delta^{18}O_{diatom}$ records from the diatomite beds deposited in the Naivasha and Nakuru-Elmenteita basins during a period of high lake levels close to the time of the last interglacial. These records are used, with support from low-resolution sedimentological and diatom assemblage records produced by A. Bergner (University of Potsdam) (Bergner and Trauth, 2004; Bergner, pers. comm.), to reconstruct palaeohydrological conditions in the two lakes at this time. This information, in turn, is used to explore the nature and causes of climatic change in the CKR.

In chapter 8, the results from both sites are summarised, and the palaeoclimatic records are considered in light of other records from tropical and subtropical Africa, with the aim of adding to our knowledge of the nature and causes of orbital-scale climatic change in Africa during the late Quaternary.

Chapter 2: Theoretical background

This chapter provides the theoretical background necessary to interpret the stable isotope and sedimentological data presented in this study. Stable isotope analysis is the study of the ratios of stable isotopes of an element in a given material. These ratios are expressed as the per mil (‰) deviation of the absolute ratio of two isotopes in a sample from the absolute ratio of the same isotopes in a standard material, which is known as delta (δ) notation:

$$\delta(‰) = \left[\frac{(R_{sample} - R_{standard})}{R_{standard}}\right] \times 1000 \qquad (2.1)$$

where R is the measured ratio of the given isotopes in the sample or a standard material. Stable isotopes are fractionated because certain thermodynamic properties of molecules depend on their mass. This phenomenon allows environmental processes to be reconstructed based on the stable isotope composition of different materials. In order to use stable isotope analysis to explore these processes, it is necessary, however, to have a thorough understanding of the factors that determine the stable isotope composition of the material being studied.

Section 2.1 outlines the factors that influence the stable isotope composition of a number of modern materials, in order to allow the interpretation of the modern environmental data presented in chapters 3 and 7, and as background to the following sections. Section 2.2 outlines the factors that control the abundance and isotope composition ($\delta^{18}O$ and $\delta^{13}C$) of carbonates in lake sediments, and section 2.3 outlines the factors that influence the abundance and composition ($\delta^{13}C$ and C/N ratios) of bulk organic material in such sediments. This information provides the background necessary to interpret the sedimentological and geochemical records presented in chapter 5. Finally, section 2.4 outlines the factors that control $\delta^{18}O_{diatom}$ in order to allow the interpretation of the $\delta^{18}O_{diatom}$ records presented in chapter 7.

2.1 Modern materials

The factors that control the $\delta^{18}O$ and $\delta^{2}H$ of precipitation and lake water, the $\delta^{13}C$ of DIC, and the $\delta^{13}C$ and C/N ratios of organic material are outlined in the following sections.

2.1.1 $\delta^{18}O$ and $\delta^{2}H$ of precipitation

The isotope composition of meteoric precipitation is primarily determined by the fractionation of water during evaporation from the oceans and condensation to form precipitation. Isotopes are fractionated during both these processes because the hydrogen bonds between molecules of water containing heavy isotopes are slightly stronger than those between molecules containing light isotopes. This difference means that the vapour pressure of water molecules is inversely proportional to their mass, and that water molecules that contain light isotopes therefore evaporate more readily, and condense less readily, than those that contain heavy isotopes. At thermodynamic equilibrium, the extent of this fractionation for a given isotope is described by an equilibrium fractionation factor (α), which decreases as temperature increases. During evaporation, isotopes are also fractionated by a kinetic isotope effect that results from the fact that molecules that contain heavy isotopes diffuse through air more slowly than molecules that contain light isotopes (Craig and Gordon, 1965) (section 2.1.2).

Water vapour that evaporates from the oceans is isotopically lighter (*i.e.* has lower $\delta^{18}O$ and $\delta^{2}H$ values) than the water from which it evaporates, as a result of both the equilibrium and kinetic fractionation effects described above. The actual composition depends on the isotope composition of the ocean water, SSTs, and the relative humidity of the atmosphere. Most water vapour evaporates from the tropical and sub-tropical oceans and is cooled by adiabatic expansion or radiative heat-loss as it moves away from these regions until the air mass becomes saturated and cloud formation begins.

Water that condenses from an air mass as it cools is isotopically heavier than the vapour from which it condenses, due to the equilibrium fractionation effect outlined above. If the air mass is isolated from other moisture sources and condensate is

removed as precipitation, the water vapour left after each condensation event becomes progressively lighter, as does the water condensing from the air mass in each event. This process can be described by the Rayleigh distillation equation:

$$\frac{R}{R_0} = f^{(\alpha-1)} \qquad (2.2)$$

where R_0 is the isotope ratio of the vapour before condensation begins, R is the isotope ratio of the vapour remaining after a given amount of condensation, f is the fraction of the vapour remaining, and α is the equilibrium isotope fractionation factor between liquid and vapour phases (Dansgaard, 1964; Craig and Gordon, 1965; Broecker and Oversby, 1971). Under these conditions, the isotope composition of precipitation is thus related to the degree of rainout from an air mass.

As raindrops fall, they re-equilibrate with atmospheric water vapour. The extent of this equilibration depends on the relative humidity of the atmosphere, the distance between the cloud base and the ground, and the size of the raindrops (Bolin, 1959; Friedman *et al.*, 1962). In general, the isotope composition of precipitation at ground level therefore approaches isotope equilibrium with local water vapour, the composition of which is also related to the degree of rainout at a given location (Sonntag *et al*, 1983; Araguás-Araguás *et al.*, 2000).

In most cases, this highly simplified model describes the isotope composition of precipitation relatively well. The evaporation of rain drops in the atmosphere alters their isotope composition and thus disrupts the relationship between their isotope composition and the rainout history of the air-mass, however. The formation of solid precipitation (snow and hail) is also more complex than the model described above suggests, because the fractionation of isotopes is greater during the formation of solid precipitation than liquid precipitation, kinetic isotope fractionation occurs at low temperatures, and snow and hail do not equilibrate with atmospheric moisture as they fall (Jouzel and Merlivet, 1984).

In simple terms, the isotope composition of precipitation at a given location therefore depends on: the isotope composition of the ocean from which it evaporates; the

temperature and relative humidity at which it evaporates; the degree of rainout of the air mass from which it condenses and of the atmospheric water vapour with which it re-equilibrates; and any evaporation that occurs as it falls (Dansgaard, 1964). Each of these factors has a significant influence on the isotope composition of precipitation falling in a given storm, but some can be ignored when considering the composition of precipitation on annual timescales, because they effectively remain constant. In particular, most water vapour evaporates from the tropical and subtropical oceans, where the isotope composition and temperature of water and the relative humidity of the atmosphere remain relatively constant. In addition, the degree of rainout from an air mass is broadly determined by the temperature difference between the source and the site of precipitation, which is largely determined by the latter (Dansgaard, 1964).

As a consequence of these observations, the average isotope composition of precipitation at a given location is often related to the temperature at the site of precipitation (Dansgaard, 1964). Dansgaard (1964) quantified this relationship at mid- and high-latitude coastal stations, showing that:

$$\delta^{18}O_{ppt}(‰) = 0.695T(°C) - 13.6 \qquad (2.3)$$

where $\delta^{18}O_{ppt}$ is the mean annual $\delta^{18}O$ of precipitation falling at a given site, and T is the mean annual temperature at that site in degrees Celsius (Dansgaard, 1964). Rozanski *et al.* (1992) extended this relationship by considering more stations and longer time periods, and found that the relationship between $\delta^{18}O_{ppt}$ and surface air temperature ranged from +0.9‰/°C at high latitudes to almost 0‰/°C in tropical regions on annual timescales, and that it was +0.63‰/°C on inter-annual timescales in Europe. Surface temperatures generally decrease with increasing altitude and latitude, resulting in lower isotope values of precipitation. These relationships are known as the "altitude" and "latitude" effects (Dansgaard, 1954).

A number factors disrupt the relationship between the average isotope composition of precipitation and average surface air temperature, however. Vertical movements along air-mass trajectories can mean that the $\delta^{18}O$ and $\delta^{2}H$ of precipitation at inland stations is lower than expected from surface temperatures, as these movements result in the

progressive loss of heavy isotopes without a proportional decrease in surface temperatures (Dansgaard, 1964; Rozanski *et al.*, 1982, 1993). The addition of isotopically-light water that has evaporated from large water bodies to an air mass can also decrease the isotope values of precipitation at interior locations (Dansgaard, 1964). These processes may contribute to the "continental effect", which describes the observation that precipitation at inland stations tends to have lower isotope values than expected according to equation 2.3 (Dansgaard, 1964).

Precipitation that falls during heavy storms also tends to be isotopically lighter than precipitation that falls in light storms ("the amount effect") because a higher proportion of vapour in an air mass condenses during heavy precipitation events (equation 2.2), and because evaporation and re-equilibration of falling raindrops is lower for larger, faster-falling raindrops (Dansgaard, 1964). This effect is particularly important in the tropics, because annual temperature variations are low and rain often forms in deep, convectional storms that involve significant uplift and cooling (*e.g.* Araguás-Araguás *et al.*, 1998, 2000).

On long timescales, the isotope values of precipitation may also be affected by changes in the location or the composition of the source of precipitation. During the last glacial, the $\delta^{18}O$ of ocean water was ~1.5‰ higher than today, for example (Shackleton, 1987).

It is important to note that the $\delta^{18}O$ and $\delta^{2}H$ values of meteoric water are closely related, because both oxygen and hydrogen isotopes are fractionated during the processes that determine the isotope composition of precipitation (Friedman, 1953). Craig (1961) showed that the $\delta^{18}O$ and $\delta^{2}H$ values of meteoric water are related by the following equation (Craig, 1961):

$$\delta^{2}H = 8\,\delta^{18}O + 10 \qquad (2.4)$$

which is known as the global meteoric water line (GMWL) (Fig. 2.1). The gradient of this line is related to the ratio of the equilibrium fractionation factors of ^{18}O and ^{2}H (Dansgaard, 1964). The intercept of the GMWL (10) is known as the deuterium excess parameter, and is caused by kinetic isotope fractionation during evaporation

from the ocean at relative humidities less than 100%, which increases the fractionation of oxygen isotopes relative to the fractionation of hydrogen isotopes (section 2.1.2) (Dansgaard, 1964).

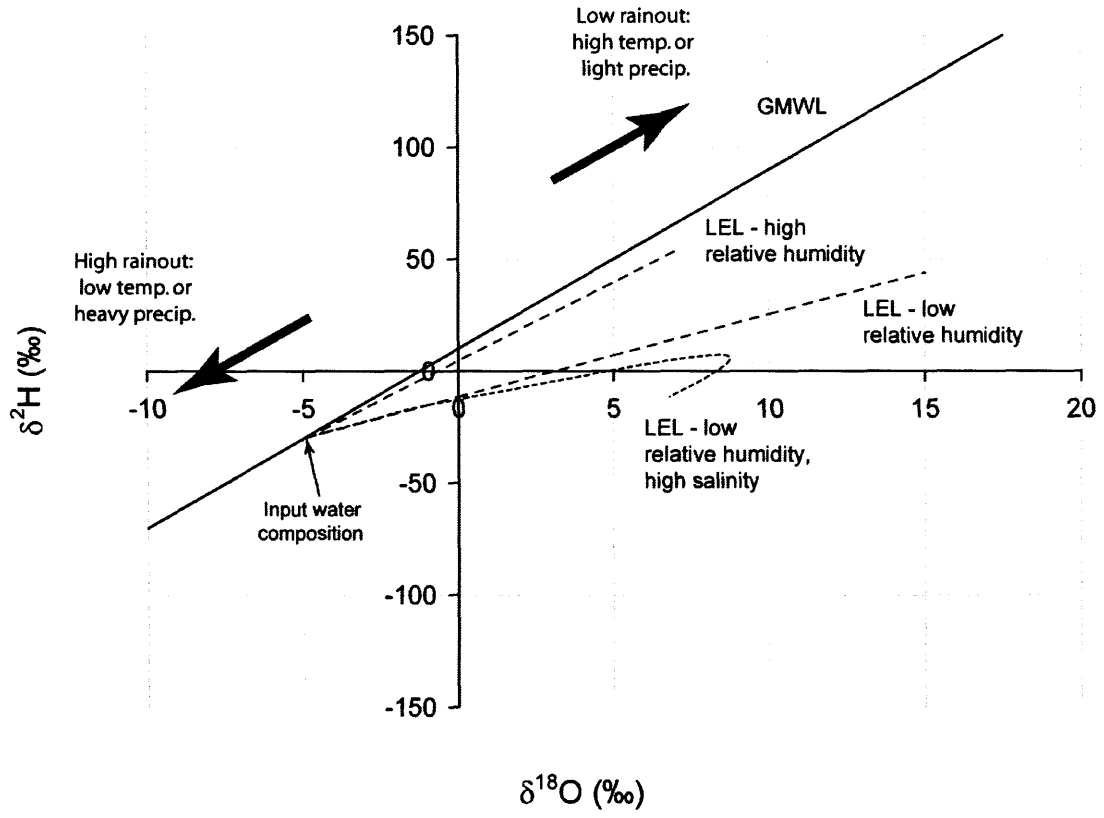

Figure 2.1: Schematic illustration of the relationship between the $\delta^{18}O$ and $\delta^{2}H$ values of meteoric water (GMWL), showing the effects of evaporation on the isotope composition of a water body at low and high relative humidities, and on the isotope composition of a highly saline water body at low relative humidity (initial composition of the water body: $\delta^{18}O = -5‰$, $\delta^{2}H = -30‰$).

The GMWL actually represents an average of many local meteoric water lines (LMWLs), as the relationship between the $\delta^{18}O$ and $\delta^{2}H$ of meteoric waters varies in different geographical regions. The deuterium excess of these lines depends on the extent of kinetic fractionation at the point of evaporation over the ocean, which is primarily determined by atmospheric humidity (Dansgaard, 1964; Gat and Carmi, 1970). This parameter can vary seasonally, affecting the slope of the LMWL. The slope of LMWLs is also affected by seasonal variation in the evaporation of

raindrops, with slopes less than 8 tending to prevail where evaporation affects the composition of precipitation that falls in summer or in light rain storms (and thus has relatively high $\delta^{18}O$ and $\delta^{2}H$) (Friedman *et al.*, 1962; Ehhalt *et al.*, 1963; Gat, 1980). The slope of a LMWL can also deviate significantly from the GMWL if the source of precipitation varies seasonally, resulting in precipitation with different isotope- and deuterium excess-values falling at different times of year (Araguás-Araguás *et al.*, 2000; IAEA/WMO, 2001).

2.1.2 $\delta^{18}O$ and $\delta^{2}H$ of lake water

The $\delta^{18}O$ and $\delta^{2}H$ composition of lake water is determined by the isotope composition and volume of lake-water inputs, and by the extent to which evaporation alters the composition of these inputs after they enter the water body. Lake-water inputs are usually derived from precipitation in the basin, but a number of processes can alter the isotope composition and the amount of precipitation before it enters a lake, on a range of timescales.

On annual timescales, the average isotope composition of lake-water inputs may be affected by evaporation of precipitation before it enters the lake, or by "selection" of precipitation with different isotope compositions (Gat and Tzur, 1967; Gat, 1971). Evaporation can increase the isotope value of precipitation after interception by vegetation (the "canopy effect"), during over-land flow, in streams, rivers and lakes, and during passage through the soil or vadose zone (cf. Darling *et al.*, 2006). Selection of precipitation with a certain composition can occur if high rates of evapotranspiration result in a disproportionately low proportion of the precipitation that falls in summer entering a water body (cf. Ito, 2001). Similarly, precipitation that falls during light storms may be "lost" through evaporation, which can influence the average isotope composition of lake-water inputs if storm intensity varies seasonally, or if the isotope composition of precipitation is determined by the amount effect (Gat, 1971). It has been shown, however, that these processes usually have a small effect (<1‰ in $\delta^{18}O$) on the average composition of lake-water inputs (Gat and Tzur, 1967; Darling *et al.*, 2006). In most cases, the mean annual isotope composition of lake-water inputs therefore tends to reflect the mean annual isotope composition of precipitation.

On seasonal timescales, the composition of lake-water inputs also depends on the extent to which precipitation is mixed in the groundwater system before being discharged into the lake (cf. Darling *et al.*, 2006). Where most water is supplied to a water body through direct precipitation or runoff, the composition of inputs will vary according to variations in the composition of precipitation. If water enters the groundwater system before being discharged into rivers or lakes, it is usually well-mixed during its passage through the unsaturated zone and/or in the aquifer. Consequently, shallow groundwater reservoirs tend to "average out" short-term variations in the amount and composition of precipitation (cf. Darling *et al.*, 2006). It should be noted, however, that if groundwater is recharged in areas far from the local catchment or by surface water that has been affected by evaporation, or if it is held in the aquifer for long periods of time or affected by geothermal processes, its composition may differ significantly from that of local precipitation (Gat, 1971).

Once lake-water inputs enter a water body, evaporation may alter their composition. The effect of evaporation on lake water composition can be understood using a simplified version of the model developed by Craig and Gordon (1965). As water evaporates, isotopes are fractionated due to the equilibrium fractionation associated with the liquid-vapour transition (section 2.1.1). After molecules have left the water surface, they diffuse through a boundary layer above the water's surface, and enter the atmosphere. This process causes kinetic isotope fractionation because molecules that contain heavy isotopes diffuse through air more slowly than those that contain light isotopes, and its influence increases as the relative humidity of the atmosphere decreases (section 2.1.1) (Vogt, 1976; Merlivat, 1978). Finally, water vapour from the atmosphere enters the saturated layer above the water's surface and may condense into the water body. The effect of this process depends on the relative humidity of the atmosphere and on the isotope composition of atmospheric water vapour.

The kinetic fractionation associated with diffusion affects the $\delta^{18}O$ and $\delta^{2}H$ of water vapour to a similar extent, but the equilibrium fractionation associated with the phase transition between liquid and vapour is an order of magnitude greater for $^{2}H/^{1}H$ than for $^{18}O/^{16}O$. Kinetic effects therefore have a proportionally larger effect on the fractionation of $^{18}O/^{16}O$ than on the fractionation of $^{2}H/^{1}H$ during evaporation (which explains the deuterium excess parameter of the GMWL). This observation means that,

relative to the rate expected without kinetic effects, the $\delta^{18}O$ value of an evaporating water body increases faster than the $\delta^{2}H$ value. Water bodies that have undergone significant evaporation therefore plot to the right of the GMWL, on local evaporation lines (LELs) (Craig *et al.*, 1963; Ehhalt *et al.*, 1963) (Fig. 2.1). The slope of these lines is primarily determined by the relative humidity of the atmosphere, as this determines the relative influence of kinetic isotope fractionation. In completely dry air, the kinetic effect is at its most significant, and thus the LEL deviates significantly from the GMWL (the gradient of which depends only on the equilibrium fractionation factors), with a gradient of 3.7. When relative humidity is high, the influence of the kinetic enrichment factor is low, and thus the gradient of the LEL approaches that of the GMWL (Fig. 2.1). The displacement of water along a given line depends on the extent to which evaporation has enriched the water body in heavy isotopes (Gonfiantani, 1986).

If evaporation significantly increases the salinity of a water body, the fractionation of isotopes during evaporation may change (Gonfiantani, 1986). High salinity decreases the thermodynamic activity of water, which reduces its saturated vapour concentration and thus effectively increases the relative humidity of the layer through which molecules diffuse after evaporating. This change reduces the relative influence of the kinetic fractionation effect, and therefore reduces the extent to which evaporation enriches a water body in heavy isotopes (Gonfiantani, 1986). Furthermore, water molecules that are bound in the hydration sphere of an ion are, in most cases, enriched in ^{18}O and ^{2}H relative to free water, which effectively decreases the isotope value of the water body (Gonfiantani, 1986). A further, but usually minor, effect of increasing salinity is that water of crystallisation may be removed from the water body when salts precipitate. This process can act to increase or decrease the isotope values of the water body, depending on the salts involved (Gonfiantani, 1986). Overall, these effects reduce the degree of isotope enrichment during evaporation at high salinities, and mean that LELs may reverse (developing a hook or "U-turn") as evaporation proceeds (Gonfiantani, 1986) (Fig. 2.1).

The extent to which evaporation affects the isotope composition of lake water is determined by the proportion of lake-water inputs that are lost through evaporation, which can be expressed as the ratio of inputs to evaporative outputs (I/E ratio) (Gat,

1971). This ratio is influenced by the lake's residence time, as this parameter affects the extent to which lake water is exposed to evaporation. Lakes with relatively short residence times are not exposed to significant evaporation, and their isotope composition therefore tends to reflect the composition of lake-water inputs (cf. Leng and Marshall, 2004). If the residence time is less than one year, the isotope composition of lake water may reflect short-term variations in the composition or amount of lake-water inputs, because the lake is not large enough to "average out" these short-term variations (Gat, 1971; Leng and Marshall, 2004). The composition of surface water in stratified lakes may also reflect these short-term changes, even if the lake has a relatively long residence time, because the epilimnion is effectively isolated from the hypolimnion when the lake is stratified. In contrast, the composition of well-mixed lakes with residence times longer than 1 year (but not long enough for evaporation to significantly affect their composition) is less variable, and may reflect the mean annual composition of inputs to the lake (Gat, 1971; Leng and Marshall, 2004).

Lakes with long residence times (hydrologically closed or large lakes) are potentially exposed to evaporation for long periods, and their composition is therefore often influenced by this process. The extent of the influence is determined by the I/E ratio, which is affected by both climatic conditions and characteristics of the lake such as surface-area to volume ratio and residence time (cf. Gat, 1995). Changes in I/E ratio usually have a greater effect on lake-water composition than variations in the composition or amount of lake-water inputs in lakes with long residence times, and the I/E ratio therefore tends to be the primary control on the composition of these water bodies (cf. Leng and Marshall, 2004). The sensitivity of lake-water composition to changes in the I/E ratio is affected by the residence time (and thus volume) of the lake, as the effects of changes in the I/E ratio are buffered in large lakes with very long residence times (cf. Gat, 1995). At hydrological steady-state, the isotope composition of lake water reaches a steady-state value that is determined by the I/E ratio, humidity, and the isotope composition of lake-water inputs and atmospheric moisture (cf. Gat, 1995). In the special case of hydrologically closed lakes, the I/E ratio at steady-state is 1, and the steady-state composition of these lakes is therefore independent of lake volume (cf. Gat, 1995).

2.1.3 $\delta^{13}C_{DIC}$ of lake water

The $\delta^{13}C$ of DIC ($\delta^{13}C_{DIC}$) in lake water is determined by the $\delta^{13}C$ of inorganic carbon that enters the lake, and by factors that influence $\delta^{13}C_{DIC}$ within the lake (Fig. 2.2).

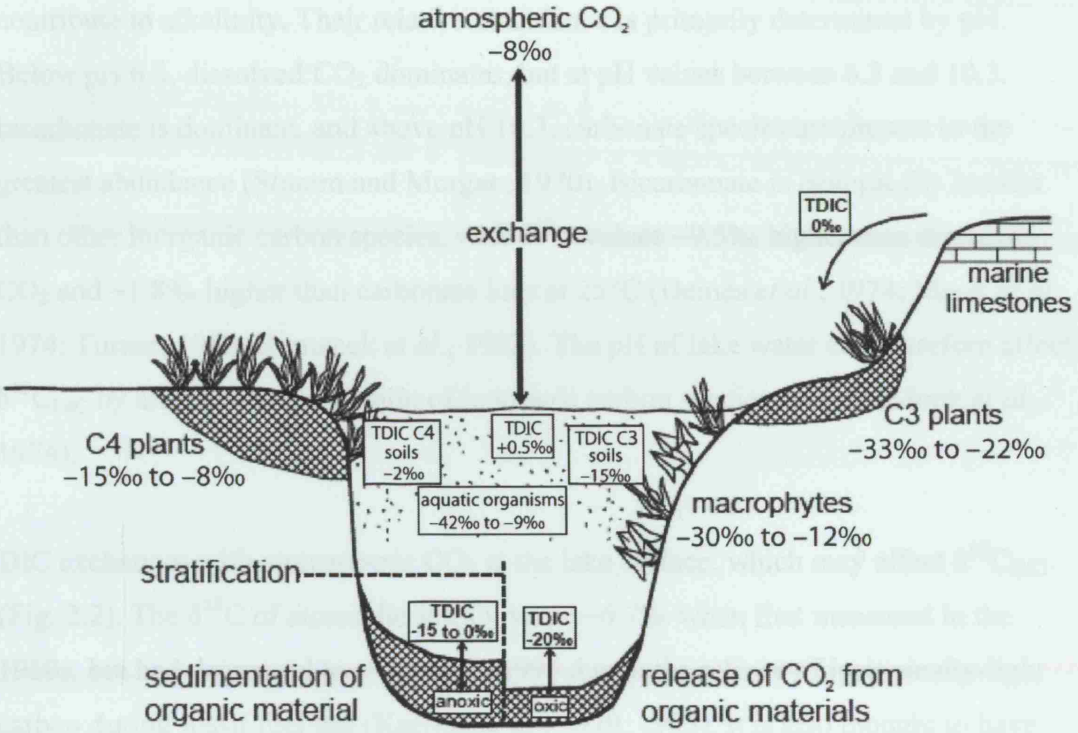

Figure 2.2: Schematic illustration of the factors that control the $\delta^{13}C$ of organic matter and dissolved inorganic carbon (DIC) in lacustrine environments. Modified from Leng and Marshall, (2004).

DIC may enter a lake in runoff, stream flow, and groundwater. The $\delta^{13}C_{DIC}$ of this water is usually low (often between –10‰ and –15‰) because it contains CO_2 released into the soil by plant root respiration and, to a lesser extent, the decomposition of organic material, which is isotopically light (Park and Epstein, 1960, 1961; Deines, 1980) (section 2.1.4.1) (Fig. 2.2). Water entering a lake may also react with marine carbonates in the basin, which have $\delta^{13}C$ values between –2 and +3‰ (Keith and Weber, 1964) (Fig. 2.2). The extent to which this process alters $\delta^{13}C_{DIC}$ depends on the amount and $\delta^{13}C$ of the carbonates, as well as the amount of dissolved CO_2 available to react with the rock. The reaction of water with silicates in the basin does not alter $\delta^{13}C_{DIC}$ directly, but increases the pH and alkalinity of the

water, which may affect $\delta^{13}C_{DIC}$ by changing the proportion of inorganic carbon species present (see below).

Within-lake processes also influence $\delta^{13}C_{DIC}$. Dissolved inorganic carbon is made up of four species: CO_2 (aq), H_2CO_3, HCO_3^-, and CO_3^{2-}, of which the latter two contribute to alkalinity. Their relative abundance is primarily determined by pH. Below pH 6.3, dissolved CO_2 dominates, but at pH values between 6.3 and 10.3, bicarbonate is dominant, and above pH 10.3, carbonate species are present in the greatest abundance (Stumm and Morgan, 1970). Bicarbonate is isotopically heavier than other inorganic carbon species, with $\delta^{13}C$ values ~9.5‰ higher than dissolved CO_2 and ~1.8‰ higher than carbonate ions at 25°C (Deines *et al.*, 1974; Mook *et al.*, 1974; Turner, 1982; Romanek *et al.*, 1992). The pH of lake water can therefore affect $\delta^{13}C_{DIC}$ by altering the proportion of inorganic carbon species present (Mook *et al.*, 1974).

DIC exchanges with atmospheric CO_2 at the lake surface, which may affect $\delta^{13}C_{DIC}$ (Fig. 2.2). The $\delta^{13}C$ of atmospheric CO_2 was ~−6.7‰ when first measured in the 1950s, but had decreased to ~−8.0‰ in 1995 due to the release of isotopically-light carbon during fossil fuel use (Keeling *et al.*, 1979, 1995). It is also thought to have been ~0.3‰ lower during the last glacial than during the Holocene (Leuenberger *et al.*, 1992). The process of dissolving in water reduces the $\delta^{13}C$ of CO_2 by ~1.1‰, and bicarbonate in equilibrium with atmospheric CO_2 today thus has a $\delta^{13}C$ value of ~+0.5‰ (Vogel *et al.*, 1970; Mook *et al.*, 1974; Turner, 1982). The extent to which a water body equilibrates with atmospheric CO_2 depends on its residence time. If this time is sufficiently long, the $\delta^{13}C_{DIC}$ of lake water may approach a steady-state value determined by this process (Li and Ku, 1997).

Photosynthesis affects $\delta^{13}C_{DIC}$ because it preferentially removes ^{12}C from the DIC reservoir and thus increases the $\delta^{13}C$ of the remaining DIC (Park and Epstein, 1960; McKenzie, 1985) (section 2.1.4.1). Evaporative concentration of lake water can also increase $\delta^{13}C_{DIC}$ by causing outgassing of CO_2, which is isotopically light relative to other species of inorganic carbon (Talbot and Kelts, 1990; Cole *et al.*, 1994; Mees *et al.*, 1998). The effect of this process is particularly large if outgassing leads to non-equilibrium isotope fractionation (Stiller *et al.*, 1985). This situation is most likely to

occur in eutrophic water bodies, where pCO_2 in the lake water is much larger than pCO_2 in the atmosphere. The effect of outgassing on $\delta^{13}C_{DIC}$ may also be enhanced by increasing salinity and temperature, which decrease the solubility of CO_2, and by increasing pH, which decreases the proportion of carbonate species in the form of CO_2 (cf. Eugster and Jones, 1979).

$\delta^{13}C_{DIC}$ can also be altered by the release of isotopically-light CO_2 during the oxidation of organic matter, either in the water column or in lake sediments (Fig. 2.2). CO_2 from this source can reduce $\delta^{13}C_{DIC}$ to values as low as –20‰ if the lake water is oxygenated and productivity is high (Williams and Gordon, 1970; Leng and Marshall, 2004) (Fig. 2.2). If the lake is stratified, the hypolimnion may become anoxic, which reduces the rate at which isotopically-light CO_2 is released, and thus increases $\delta^{13}C_{DIC}$. Dissolution of carbonate minerals in lake sediments may also affect $\delta^{13}C_{DIC}$ in acidic lakes, as the isotope composition of DIC produced during this process reflects the composition of the carbonate from which it is derived (cf. Irwin *et al.*, 1977; Ogrinc, 2002).

Decomposition of organic matter via methanogenesis can also affect the $\delta^{13}C_{DIC}$ of lake water (Rosenfeld and Silverman, 1959; Bottinga 1969). Rates of methanogenesis are highest in warm, anoxic, low-sulphate environments where the supply of organic material is high, as these conditions increase the rate of anaerobic decomposition but limit the rate of sulphate reduction (*e.g.* Lovely and Klug, 1986; Whiticar *et al.*, 1986). Methanogenesis can occur through carbon dioxide reduction or acetate fermentation (cf. Klass, 1984). Carbon dioxide reduction involves reduction of carbon dioxide or bicarbonate to produce methane and water, and acetate fermentation releases methane and carbon dioxide. Carbon dioxide reduction is energetically more favourable than acetate fermentation, but acetate formation is often the dominant form of methanogenesis in lakes due to the limited supply of CO_2 (Whiticar *et al.*, 1986; Talbot and Kelts, 1990). Both pathways can increase $\delta^{13}C_{DIC}$, as carbon dioxide reduction preferentially uses isotopically-light CO_2, leaving the remaining DIC enriched in ^{13}C, and the CO_2 produced by acetate fermentation is isotopically heavy (often ~10‰ heavier than the organic material from which it is derived) (Stiller and Magaritz, 1974; Whiticar *et al.*, 1986). The methane produced by both reactions has extremely low $\delta^{13}C$ (between ~–110‰ and –60‰ for carbon dioxide reduction and

~−70‰ and −50‰ for acetate fermentation), and if this gas is oxidised within the lake, isotopically-light CO_2 is produced, reducing $\delta^{13}C_{DIC}$ (Barker and Fritz, 1981; Devol *et al.*, 1984). This process is unusual, however, as methane is normally lost from lakes by ebullition or sulphate reduction.

2.1.4 $\delta^{13}C$ and C/N ratios of organic matter

2.1.4.1 $\delta^{13}C$ of organic matter

The $\delta^{13}C$ of photosynthetic organisms depends on the $\delta^{13}C$ of the inorganic carbon used during photosynthesis, and on the photosynthetic pathway used to assimilate this carbon. Terrestrial plants and emergent vegetation use atmospheric CO_2, which currently has a $\delta^{13}C$ value of −8.0‰ (section 2.1.3), as their source of inorganic carbon, while aquatic organisms use dissolved inorganic carbon, which has highly variable $\delta^{13}C$ values, as their source.

The photosynthetic pathway used to assimilate inorganic carbon affects the $\delta^{13}C$ of plant tissue because the enzymes that fix carbon fractionate against ^{13}C, and the degree of fractionation is specific to each enzyme (Park and Epstein, 1960). C_3 photosynthesis, which is used by most trees, shrubs, high altitude grasses and aquatic plants, uses the enzyme ribulose-1,5-bisphosphate carboxylase (RuBisCO). This enzyme produces sugars that are ~20-25‰ lighter than the source of inorganic carbon, and the $\delta^{13}C$ values of C_3 plants that use atmospheric CO_2 during photosynthesis are therefore usually between −22‰ and −33‰ (O'Leary, 1981) (Fig. 2.3). C_4 photosynthesis, which is primarily used by low-altitude grasses in regions with high growing season temperatures, uses the enzyme phosphoenolpyruvate carboxylase (PEP carboxylase) to fix carbon. This enzyme uses bicarbonate as its source of inorganic carbon, and produces sugars that are 4-5‰ lighter than this source. Together, these effects mean that the $\delta^{13}C$ values of C_4 plant tissues tend to range from −8‰ to −15‰ (Reibach and Benedict, 1977) (Fig. 2.3). Crassulacean Acid Metabolism (CAM), which is mostly used by succulents, uses both RuBisCO and PEP carboxylase to fix carbon. The photosynthetic products of this pathway therefore tend to have $\delta^{13}C$ values between those of C_3 and C_4 plants, usually ranging from −4‰ to −20‰ (O'Leary, 1988).

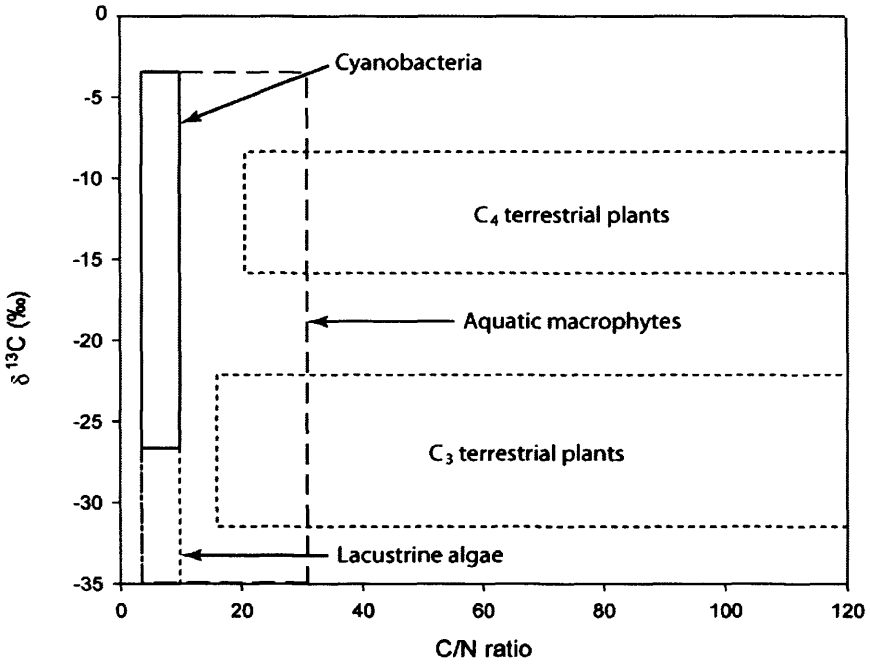

Figure 2.3: Approximate ranges of $\delta^{13}C$ values and C/N ratios associated with terrestrial C_3 and C_4 plants and aquatic organisms (based primarily on Tyson, 1995).

The efficiency of C_3 photosynthesis is reduced by photorespiration, in which RuBisCO produces a glycolate and a glycerate from oxygen. C_4 photosynthesis avoids this problem because it involves a mechanism that actively concentrates CO_2 around RuBisCO. This adaptation allows C_4 plants to assimilate carbon dioxide with less loss of water, and C_4 plants therefore have a higher water-use efficiency than C_3 plants. Consequently, plants that use C_4 photosynthesis are usually favoured when atmospheric carbon dioxide levels are low, or when temperatures are high during the growing season (Osmond *et al.*, 1982; cf. Boom *et al.*, 2002), although their abundance can also be influenced by fire intensity (Wooller *et al.*, 2000). In the tropics, there is evidence that lower atmospheric CO_2 concentrations during glacial periods favoured the expansion of C_4 grasses (*e.g.* Street-Perrott *et al.*, 1997). This is not the case in southern Africa, however, where changes in temperature and precipitation appear to have determined the distribution of C_3 and C_4 vegetation (cf. Scott, 2002). Today, C_3 grasses are most abundant in the winter rainfall region and on the high-altitude eastern escarpment of southern Africa (section 3.2), where growing season temperatures are low (either due to winter rainfall or high altitude) (Vogel,

1978). C_4 grasses, in contrast, are most abundant in the summer rainfall region, where growth occurs during the warm summer season (Vogel, 1978). Pollen and phytolith records and carbon isotope evidence (from soils, hyrax dung, stalagmites, fossil tooth enamel, and fossil bones) from southern Africa indicate that C_3 plants dominated vegetation in the winter rainfall region of southern Africa throughout the late Quaternary, but that C_3 grasses became more abundant at many sites in the summer rainfall region during glacials due to lower growing season temperatures and possibly increased winter rainfall (*e.g.* Vogel, 1983; Talma and Vogel, 1992; Scott and Vogel, 2000).

Most aquatic organisms preferentially use dissolved CO_2 as their source of carbon during photosynthesis, but some aquatic plants and cyanobacteria can also use bicarbonate ions (Miller and Colman, 1980; Allen and Spence, 1981; Kaplan *et al.*, 1982; Boston *et al.*, 1989). Bicarbonate is isotopically heavier than dissolved CO_2, and the $\delta^{13}C$ values of organisms that use bicarbonate as their source of carbon therefore tend to be higher than those of organisms that use dissolved CO_2 (Iversen, 1929; Smith and Walker, 1980; Allen and Spence, 1981; Lucas, 1983; Maberly and Spence, 1983). The tendency of aquatic organisms to use bicarbonate as a source of DIC increases as the concentration of dissolved CO_2 decreases, and low CO_2 availability can thus increase the average $\delta^{13}C$ values of aquatic organisms through this effect. The $\delta^{13}C$ values of both dissolved CO_2 and bicarbonate are influenced by a range of factors (section 2.1.3), and the $\delta^{13}C$ of aquatic organisms can therefore vary significantly according to the isotope composition of DIC (Figs. 2.2 and 2.3).

The $\delta^{13}C$ values of aquatic organisms are also affected by the fact that carbon limitation reduces the extent to which photosynthesis fractionates against ^{13}C (increasing the $\delta^{13}C$ values of the organic material produced). Carbon limitation can be caused by a range of factors, including increased evaporative concentration, pH, salinity, and productivity, and lower atmospheric pCO_2 during glacial periods (*e.g.* Park and Epstein, 1960; McKenzie, 1985; Hollander and McKenzie, 1991; Laws *et al.*, 1995; Street-Perrott *et al.*, 1997; Huang *et al.*, 1999). The availability of carbon can also be limited by the rate of diffusion through the boundary layer of organisms; an effect that is known to increase the $\delta^{13}C$ values of both submerged macrophytes and benthic algae (Hecky and Hesslein, 1995).

Most aquatic plants use C_3 photosynthesis, and therefore tend to produce tissues with $\delta^{13}C$ values ~20-25‰ lighter than their source of inorganic carbon, although some macrophytes use C_4 photosynthesis (cf. Hecky and Hesslein, 1995). Cyanobacteria also use RuBisCO to fix carbon, but the form of the enzyme used by these organisms only fractionates carbon by ~16-22‰ (Guy *et al.*, 1993; Sakata *et al.*, 1997; Popp *et al.*, 1998). The $\delta^{13}C$ of cyanobacteria using a specific source of inorganic carbon will consequently tend to be higher than the $\delta^{13}C$ of aquatic plants using the same source. In fact, cyanobacteria often use bicarbonate as a source of inorganic carbon (reflecting their preference for neutral to alkaline conditions), and their $\delta^{13}C$ values therefore often range between ~−10‰ and −20‰ (Badger, 1985; Sakata *et al.*, 1997), although they can reach values as high as −3‰ and as low as −27‰ (Tyson, 1995) (Fig. 2.3).

The $\delta^{13}C$ of organic matter may change during decomposition due to the selective degradation of compounds with different isotope values (Benner *et al.*, 1987). Lehmann *et al.* (2002) demonstrated that decomposition of organic material decreased $\delta^{13}C$ by ~1.6‰ under both oxic and anoxic conditions, for example. Most studies indicate that this effect is not large enough to mask changes in the $\delta^{13}C$ of the original material, however (*e.g.* Williams and Gordon, 1970; Meyers and Eadie, 1993).

2.1.4.2 C/N ratios of organic matter

Non-vascular plants and bacteria contain little carbon-rich cellulose or lignin and relatively large quantities of nitrogen-rich proteins and nucleic acids, and consequently tend to have low ratios of atomic carbon to atomic nitrogen (C/N) (cf. Meyers, 1994; Tyson, 1995; Raven *et al.*, 2004) (Fig. 2.3). In general, algae have C/N ratios between 4 and 10 and, in particular, diatoms have C/N ratios between 5 and 8 (Lerman, 1979; Tyson, 1995). Vascular plants, in contrast, contain relatively large amounts of cellulose and lignin, and thus tend to have high C/N ratios. Terrestrial and emergent plants tend to have C/N ratios greater than ~20, and can have values greater than 200 (Tyson, 1995; Meyers and Teranes, 2001; Raven *et al.*, 2004) (Fig. 2.3). There are significant exceptions to these general cases, however. Green algae such as *Botryococcus braunii* can have bulk C/N ratios as high as 36, due to hydrocarbon synthesis (cf. Street-Perrott *et al.*, 1997), and freshwater macrophytes tend to have C/N ratios between 12 and 30 (Tyson, 1995), for example.

Decomposition can change the C/N ratio of organic matter through selective degradation of specific compounds. The C/N ratio of algal material often increases during decomposition, as nitrogen-rich proteins are decomposed preferentially, while the C/N ratio of terrestrial material can decrease due to immobilisation of N-rich compounds and remineralisation of carbon by microbes (Fenchel *et al.*, 1998; Meyers and Lallier-Vergès, 1999; Lehmann *et al.*, 2002). Bacterial growth in organic matter during decomposition can also reduce its average C/N ratio (Müller, 1977; Lehmann *et al.*, 2002). These changes rarely outweigh the influence of plant type on C/N ratios, however (Meyers and Teranes, 2001).

2.2 Carbonates in lacustrine sediments

The factors that influence the amount of carbonate in lacustrine sediments and the stable isotope composition of these carbonates are outlined in the following sections in order to provide the background necessary to interpret records of percentage weight-loss on ignition (%LOI) at 950°C, $\delta^{18}O_{calcite}$, and $\delta^{13}C_{calcite}$.

2.2.1 Carbonate abundance

Carbonates that form in lakes can be classified as either biogenic carbonates, which are formed by organisms such as molluscs and charophytes, or inorganic precipitate (although the latter may be induced by biological processes) (Jones and Bowser, 1978). Biogenic carbonates will not be discussed here, as they were not analysed in this study. Inorganic carbonate precipitation can either occur in the water column (endogenic carbonate) or in lake sediments (authigenic carbonate) (Jones and Bowser, 1978; Last, 2002), and is controlled by the concentration of suitable cations and carbonate or bicarbonate ions, as well as the pCO_2, pH, pressure, and temperature of the environment (Stumm and Morgan, 1970; Kelts and Hsü, 1978). In addition, the presence of materials such as phosphate and organic films may inhibit carbonate precipitation (Kelts and Hsü, 1978)

Photosynthesis is often the primary cause of endogenic carbonate precipitation. The draw-down of CO_2 reduces pCO_2 and increases lake-water pH; both of which reduce the solubility of calcium carbonate (Mengard, 1968; Brunskill, 1969; Kelts and Hsü, 1978). This form of biologically-induced carbonate precipitation can occur throughout

the year, but in temperate lakes it often occurs in summer or after lake turnover, when productivity reaches maximum levels (Kelts and Hsü, 1978).

Carbonate precipitation can also be induced by physical processes. Increasing temperature may cause carbonate to precipitate because the solubility of carbonate decreases as temperature increases, and because higher temperatures reduce the solubility of CO_2, which decreases pCO_2 and increases the pH of lake water. This effect can induce carbonate precipitation in summer, when atmospheric temperatures are high, and during lake turn-over, when the temperature of water in the hypolimnion increases as it is brought to the surface (Kelts and Hsü, 1978). Evaporation can also cause super-saturation with respect to carbonates by increasing the concentration of ions in lake water. This process is commonly thought to induce carbonate precipitation in saline lakes, and is associated with specific paths of brine evolution (Eugster and Hardie, 1978).

Finally, the mixing of water bodies with different chemical compositions can lead to super-saturation with respect to carbonate and thus induce carbonate precipitation. This form of precipitation occurs if a water body with a high $Ca^{2+}/HCO_3^- + CO_3^{2-}$ ratio mixes with water with a low $Ca^{2+}/HCO_3^- + CO_3^{2-}$ ratio, for example (Müller *et al.*, 1972; *e.g.* Barkan *et al.*, 2001). Shapley *et al.* (2005) demonstrated that the mass accumulation rate of endogenic carbonate in Evans Lake, Montana, was controlled by this process, as the input of Ca^{2+}-rich groundwater to the alkaline lake determined the rate of carbonate precipitation.

Authigenic carbonates either precipitate from pore water or result from the diagenesis of other carbonates (cf. Talbot and Kelts, 1990). In lacustrine environments, authigenic carbonates often precipitate in response to the anaerobic decomposition of organic matter, as this process can increase the carbonate alkalinity of pore water. Sulphate reduction and acetate fermentation increase pore-water alkalinity when coupled with metal cation reduction, which buffers pH change (Talbot and Kelts, 1990). Carbon dioxide reduction induces carbonate precipitation by reducing pCO_2 and increasing the pH of pore water (Talbot and Kelts, 1986, 1990). As mentioned above, low levels of sulphate and a limited supply of CO_2 mean that acetate fermentation is often the most significant path of anaerobic decomposition in

lacustrine sediments. Consequently, this process is often responsible for authigenic carbonate precipitation (as long as it is accompanied by metal cation reduction) (Lovely and Klug, 1986; Whiticar *et al.*, 1986; Talbot and Kelts, 1990).

The amount of carbonate present in lake sediments is also influenced by the amount removed by dissolution, either in the water column or after deposition (Kelts and Hsü, 1978). The most common reasons for under-saturation with respect to carbonate are low pH and high pCO_2 (which are usually related), but low temperature and high pressure (which also increase pCO_2) also increase carbonate solubility (Stumm and Morgan, 1970). In lakes, the water of the hypolimnion is often under-saturated with respect to carbonate because CO_2 produced by the oxidation of organic matter increases pCO_2 and decreases pH, and because temperatures are at their lowest (Kelts and Hsü, 1978). Carbonate dissolution can also occur in lake sediments in response to the anaerobic decomposition of organic material by sulphate reduction and acetate fermentation, as these processes decrease the pH of pore water if they are not buffered by metal cation reduction (see above) (Morse *et al.*, 1985; Morse and Mackenzie, 1990).

Finally, detrital carbonates may enter lake sediments from the catchment, but the quantity of such material is usually only significant if the lake has river or stream inputs, or if it lies in a carbonate-rich geology (cf. Leng and Marshall, 2004). It is sometimes possible to detect the presence of detrital carbonate using scanning electron microscope (SEM) or X-ray diffraction (XRD) analysis, but it is not possible to separate this material from endogenic carbonate, and its presence therefore invalidates the use of stable isotope analysis of lacustrine carbonates to reconstruct lake-water composition.

2.2.2 $\delta^{18}O$ of endogenic carbonate

The $\delta^{18}O$ of carbonate that precipitates in thermodynamic equilibrium with water is determined by the isotope composition of the dissolved inorganic carbon species from which it precipitates, and the temperature at which it forms. In practise, the $\delta^{18}O$ of carbon species reflects the $\delta^{18}O$ of the water with which they equilibrate, however, because the vast majority of oxygen atoms in the DIC-water system are from water molecules (cf. Zeebe, 1999).

The relationship between the $\delta^{18}O$ of low-Mg calcite that precipitates in thermodynamic equilibrium with water and the $\delta^{18}O$ and temperature of the water from which it forms has been determined using a number of different methods (*e.g.* Epstein *et al.*, 1953; O'Neil *et al.*, 1969; Kim and O'Neil, 1997). One of the most recently published expressions describing this relationship is:

$$T(°C) = 13.8 - 4.58(\delta^{18}O_{calcite} - \delta^{18}O_{water}) + 0.08(\delta^{18}O_{calcite} - \delta^{18}O_{water})^2 \quad (2.5)$$

where $\delta^{18}O_{calcite}$ is the isotope composition of CO_2 produced from calcite at 25°C (relative to Vienna Pee Dee Belemnite (VPDB)), $\delta^{18}O_{water}$ is the isotope composition of CO_2 in equilibrium at 25°C with the water from which the calcite precipitated (relative to Vienna Standard Mean Oceanic Water (VSMOW)), and T is the temperature at which the calcite precipitated in degrees Celsius (Leng and Marshall (2004), based on Kim and O'Neil, (1997)). This expression indicates that the $\delta^{18}O$ of carbonate decreases by ~0.23‰ for every 1°C increase in water temperature (Craig, 1965).

The mean annual $\delta^{18}O$ of precipitation increases by ~0.6‰ for every 1°C increase in temperature at many mid- and high-latitude locations, although it is important to note that this relationship varies in both time and space (section 2.1.1) (Dansgaard, 1964; Rozanski *et al.*, 1992). Thus, if calcite precipitates from lake water with a $\delta^{18}O$ value that is determined by the $\delta^{18}O$ value of precipitation, $\delta^{18}O_{calcite}$ will increase by ~0.37‰ for every 1°C increase in temperature at the site (assuming no change in the $\delta^{18}O$ or temperature of the source of precipitation) (Stuiver, 1968, 1970). The $\delta^{18}O$ of lake water is often affected by evaporation, however, and in lakes with long residence times, changes in this variable usually overwhelm changes in the $\delta^{18}O$ of carbonate caused by variations in the $\delta^{18}O$ of precipitation or temperature (section 2.1.2) (cf. Leng and Marshall, 2004).

It is also worth noting that the different species of inorganic carbon (CO_2 (aq), H_2CO_3, HCO_3^-, and CO_3^{2-}) have different equilibrium oxygen isotope fractionation with water, and thus that changes in pH that affect the relative abundance of these species will affect the $\delta^{18}O$ of carbonate that precipitates from the water (Usdowski *et al.*, 1991; Usdowski and Hoefs, 1993; Spero *et al.*, 1997; Zeebe, 1999; Beck *et al.*, 2005).

This effect is almost always negligible compared to the effect of changes in lake water composition and temperature, but it may play a role in non-equilibrium precipitation of carbonate (cf. section 2.2.3) (Beck *et al.*, 2005).

The mineralogy of carbonate that precipitates from lake water has a significant effect on its $\delta^{18}O$ value, as carbonate ions have different vibrational frequencies in different minerals, and this affects the isotope fractionation between the mineral and water. The $\delta^{18}O$ of aragonite is ~0.6‰ higher than calcite that precipitates from the same water at 25°C (Tarutani *et al.*, 1969; Grossman and Ku, 1986; Kim and O'Neil, 2005). Similarly, the $\delta^{18}O$ of Mg-calcite is ~0.06‰ higher than calcite for every mol% $MgCO_3$ at 25°C (Tarutani *et al.*, 1969), and possibly three times higher than this when the mol% $MgCO_3$ is greater than 10 (Jiménez-López *et al.*, 2004).

2.2.3 $\delta^{13}C$ of endogenic carbonate

The $\delta^{13}C$ of carbonate that precipitates in equilibrium with lake water is determined by the $\delta^{13}C$ of the DIC from which it precipitates, and by water temperature. The temperature dependence of the fractionation factor between DIC and carbonate is almost negligible for carbon isotopes (+0.0355‰/°C), however. Consequently, the $\delta^{13}C$ of calcite that precipitates from bicarbonate is ~1-2‰ higher than the $\delta^{13}C$ of the bicarbonate at the range of temperatures experienced in the natural environment (Turner, 1982; Salomons and Mook, 1986). Different carbonate species have different $\delta^{13}C$ values, however, and the $\delta^{13}C$ of carbonate will therefore partly depend on the pH of lake water (section 2.1.3). The mineralogy of the carbonate also affects its $\delta^{13}C$ value, with the $\delta^{13}C$ of aragonite ~1.4‰ higher than that of calcite that precipitates in equilibrium from the same source of DIC (Turner, 1982), and the $\delta^{13}C$ of Mg-calcite ~0.024 ± 0.011‰ higher than calcite for every mol% $MgCO_3$ incorporated into the crystal at 25°C (Jiménez-López *et al.*, 2006).

It cannot, however, be assumed that carbonates always precipitate in equilibrium with DIC. Non-equilibrium precipitation produces carbonates with lower $\delta^{18}O$ and $\delta^{13}C$ values than those that precipitate at equilibrium, and appears to be the result of kinetic fractionation effects and/or changes in pH that alter the relative abundance of different inorganic carbon species (cf. sections 2.1.3 and 2.2.2) (McCrea, 1950; Turner, 1982; McConnaughey, 1989; Fronval *et al.*, 1995; Teranes *et al.*, 1999; Zeebe, 1999; Beck

et al., 2005). In lacustrine environments, non-equilibrium precipitation seems to occur when carbonates precipitate rapidly (*e.g.* Fronval *et al.*, 1995; Teranes *et al.*, 1999), although this effect has not been observed in laboratory experiments (*e.g.* Jiménez-López *et al.*, 2004, 2006).

2.2.4 Correlation of $\delta^{18}O$ and $\delta^{13}C$ of endogenic carbonate

The degree of correlation between the $\delta^{18}O$ and $\delta^{13}C$ of endogenic carbonate can provide information about the hydrological characteristics of the lake in which the carbonate precipitated. A high correlation coefficient between $\delta^{18}O$ and $\delta^{13}C$ records ($r \geq 7$) is most common in hydrologically closed lakes, where changes in the I/E ratio affect both the $\delta^{18}O$ of lake water and $\delta^{13}C_{DIC}$ (Talbot, 1990). The influence of the I/E ratio on the $\delta^{18}O$ of lake water is well understood. Evaporation increases the $\delta^{18}O$ of water through equilibrium and kinetic fractionation effects, while freshwater inputs dilute the isotopically-heavy lake water, and thus decrease its $\delta^{18}O$ value (section 2.1.2). If lake levels remain constant, the $\delta^{18}O$ of lake water reaches a steady-state value, but changes in the rate of input or evaporative output from the lake disrupt this equilibrium (section 2.1.2) (cf. Li *et al.*, 1997).

The I/E ratio also affects $\delta^{13}C_{DIC}$, but the mechanisms involved are not as well-understood. If lake levels remain stable, DIC may equilibrate with atmospheric CO_2, such that $\delta^{13}C_{DIC}$ reaches a steady-state value (section 2.1.3) (Li and Ku, 1997). Changes in the I/E ratio may disrupt this steady-state by affecting the extent to which lake water equilibrates with atmospheric CO_2, and thus cause changes in $\delta^{13}C_{DIC}$. In particular, evaporative concentration of lake water increases pCO_2, which causes outgassing of isotopically-light CO_2, and thus increases $\delta^{13}C_{DIC}$, particularly if the outgassing leads to non-equilibrium isotope fractionation (section 2.1.3) (Stiller *et al.*, 1985; Talbot and Kelts, 1990; Cole *et al.*, 1994; Mees *et al.*, 1998). This effect is accentuated by the decreasing solubility of CO_2 with increasing temperature and salinity (section 2.1.3) (Eugster and Jones, 1979). Increases in temperature, nutrient concentration, and the frequency of lake overturn associated with evaporative concentration may also increase $\delta^{13}C_{DIC}$ by increasing within-lake productivity (section 2.1.4.1) (McKenzie, 1985; Li and Ku, 1997). Increased inflow may also decrease $\delta^{13}C_{DIC}$ of lake water, because inflow contains isotopically-light carbon produced by plant-root respiration and the decay of organic material, which dilutes

^{13}C in the lake (section 2.1.3) (Li and Ku, 1997).

The degree of co-variance of the $\delta^{18}O$ of lake water and $\delta^{13}C_{DIC}$ can vary over time, even if the lake remains hydrologically closed. If lake levels are stable and both the $\delta^{18}O$ of lake water and the $\delta^{13}C$ of DIC reach a state of isotopic equilibrium, the $\delta^{18}O$ and $\delta^{13}C$ values of carbonates will change very little, and the degree of co-variance between them may therefore be low, despite the hydrologically-closed status of the lake (Li and Ku, 1997). Co-variance of $\delta^{18}O$ and $\delta^{13}C$ values can also be low in hydrologically closed lakes if water entering a lake contains significantly less DIC than the lake itself, because the dilution of ^{13}C by inflow will be less significant than the dilution of ^{18}O (Li and Ku, 1997).

2.2.5 $\delta^{18}O$ and $\delta^{13}C$ of authigenic carbonate

The isotope composition of authigenic carbonate is usually different from that of endogenic carbonate, and isotope records from such material should therefore be interpreted with caution. If authigenic carbonate precipitates in response to anaerobic decomposition of organic material, its $\delta^{13}C$ usually reflects the $\delta^{13}C$ of DIC generated by this process, which is often significantly different from the $\delta^{13}C$ of lake water (cf. section 2.1.3) (*e.g.* Nissenbaum *et al.*, 1988; Talbot and Kelts, 1990). The $\delta^{18}O$ of authigenic carbonate reflects the $\delta^{18}O$ and temperature of pore water. If the carbonate precipitates soon after sediment deposition (*i.e.* close to the sediment surface), these values may reflect the $\delta^{18}O$ and temperature of water in the hypolimnion, and the $\delta^{18}O$ of authigenic carbonate may therefore preserve a record of lake-water composition (Talbot and Kelts, 1986).

2.3 Organic matter in lacustrine sediments

The factors that influence the amount of organic material in lacustrine sediments and the $\delta^{13}C$ and C/N ratios of this material are outlined in this section to provide the background necessary to interpret records of %LOI 550°C and the $\delta^{13}C$ and C/N ratios of bulk organic matter.

2.3.1 Organic matter abundance

The amount of organic matter in lacustrine sediments is influenced by the amount of

organic material carried into the water body from the catchment and by production of organic material within the lake. The amount of material carried into a lake depends on the size of the lake catchment, the amount of runoff, and the type and amount of vegetation present (only a small proportion of organic material carried into lakes is derived from animals) (cf. Meyers and Lallier-Vergès, 1999). Most organic material produced within lakes is also derived from plants, although cyanobacteria can form a significant proportion of aquatic biomass. The amount of organic material produced within lakes depends on factors such as nutrient and oxygen status, temperature, mixing regime, and the depth of the photic zone.

The decomposition of organic material within the water column and/or sediments also influences the amount of organic matter present in lacustrine sediments. The amount removed by aerobic processes is influenced by the availability of oxygen in the water column and sediments, which depends on factors such as the lake's mixing regime and the rate of organic matter burial. If a lake is stratified and the hypolimnion becomes anoxic, most decomposition will occur through anaerobic processes, in which case the rate of decomposition depends on the availability of reducing agents. Aerobic decomposition is usually faster than anaerobic decay, and a higher proportion of organic material therefore tends to be preserved under anaerobic conditions (cf. Harvey *et al.*, 1995; Lehmann *et al.*, 2002).

Changes in the amount of organic material present may also be determined by changes in the deposition rate of other materials, unless meaningful accumulation rates can be calculated using an age-depth model. Rowan *et al.* (1992) demonstrated, for example, that the amount of organic matter present in the surface sediments of temperate lakes was determined by the rate of inorganic matter deposition and was unrelated to the trophic status of the lakes. Within-lake processes such as sediment focusing can also have a significant influence on organic matter concentration, and may be particularly difficult to detect (*e.g.* Verschuren, 1999a).

2.3.2 $\delta^{13}C$ and C/N ratios of bulk organic matter

The $\delta^{13}C$ of bulk organic material in lake sediments ($\delta^{13}C_{organic}$) and the C/N ratios of this material are determined by the $\delta^{13}C$ and C/N ratios of material deposited in the lake, by the relative proportions of these inputs, and by any changes in $\delta^{13}C$ and C/N

ratios that occur during decomposition. The factors that influence the $\delta^{13}C$ and C/N ratios of organic material were discussed in section 2.1.4, and the factors that influence the input of organic matter to lacustrine sediments were discussed in section 2.3.1. These controls will not, therefore, be outlined here. It is worth noting, however, that the C/N ratios of bulk organic matter may be reduced if clay forms a significant component of the sediment, as clays can contribute inorganic N to the sample and are not removed before analysis (cf. Meyers and Teranes, 2001).

2.4 $\delta^{18}O$ of diatom silica

Diatom valves are composed of biogenic silica ($SiO_2 \cdot nH_2O$). It is thought that the outer-most part of the valve is porous and hydrated and contains hydroxyl groups that can undergo isotopic exchange with water in the environment (Juillet, 1980a,b; Labeyrie and Juillet, 1982). The inner part of the valve is denser, less hydrated, and contains oxygen atoms that are unable to undergo isotopic exchange because they are strongly bonded to silicon atoms (Labeyrie and Juillet, 1982). If the biogenic silica in diatom valves forms in thermodynamic equilibrium with water, the oxygen isotope composition of the inner part of the valve should therefore reflect the isotope composition and temperature of the water from which it formed (Juillet-Leclerc and Labeyrie, 1987).

Juillet-Leclerc and Labeyrie (1987) proposed that the $\delta^{18}O$ of diatom silica ($\delta^{18}O_{diatom}$) decreases by 0.29‰ for every 1°C increase in water temperature (−0.29‰/°C). The validity of this value is uncertain, however, because it was determined using $\delta^{18}O_{diatom}$ values from marine core-tops and estimates of ocean temperature and isotope composition. Shemesh *et al.* (1992) used the composition of diatoms and planktonic foraminifera that precipitated from the same water to determine the temperature dependence of $\delta^{18}O_{diatom}$, and proposed a value of −0.49‰/°C at low temperatures. Brandriss *et al.* (1998) improved on these studies by using cultured diatoms, and proposed that the temperature dependence of fractionation is −0.19‰/°C. Moschen *et al.* (2005) found a similar temperature dependence (−0.2 ± 0.05‰/°C), based on the $\delta^{18}O_{diatom}$ of live planktonic diatoms from a closely monitored lake, and proposed that $\delta^{18}O_{diatom}$ is related to the temperature and isotope composition of lake water by the following relationship:

$$T(°C) = 190.07 - 5.05\ (\delta^{18}O_{diatom} - \delta^{18}O_{water}) \quad (2.6)$$

where T is the temperature at which the biogenic silica formed in degrees Celsius, and $\delta^{18}O_{diatom}$ and $\delta^{18}O_{water}$ are the isotope compositions of the silica and the water from which the silica formed, respectively.

If the $\delta^{18}O$ of lake water reflects the $\delta^{18}O$ of precipitation in the basin, the relationship between the $\delta^{18}O$ of precipitation and surface temperature therefore potentially allows temperature change to be reconstructed using $\delta^{18}O_{diatom}$ (where $\delta^{18}O_{diatom}$ increases by ~0.4‰/°C) (*e.g.* Hu and Shemesh, 2003). In the tropics, the $\delta^{18}O$ of precipitation is often determined by the amount of precipitation rather than temperature, however, and $\delta^{18}O_{diatom}$ may therefore record changes in this variable (section 2.1.1) (*e.g.* Barker *et al.*, 2001). In addition, the $\delta^{18}O$ of lake water in lakes with long residence times is often determined by the I/E ratio, as opposed to the $\delta^{18}O$ of precipitation, and $\delta^{18}O_{diatom}$ may therefore reflect changes in this ratio (section 2.1.2) (*e.g.* Lamb *et al.*, 2005).

The use of $\delta^{18}O_{diatom}$ to reconstruct environmental conditions is complicated by a number of factors. In particular, the effect of diagenesis on the isotope composition of diatom valves remains uncertain. Schmidt *et al.* (1997, 2001) proposed that $\delta^{18}O_{diatom}$ of fossil marine diatoms might be determined by isotope exchange associated with the condensation of hydroxyl groups in the outer layer of fresh valves during diagenesis. Moschen *et al.* (2005) suggested that shallower water depths and faster burial might limit the effect of this process in lacustrine environments, however, and this proposal is supported by the simultaneous changes in $\delta^{18}O_{diatom}$ and $\delta^{18}O_{calcite}$ observed in a single lake core by Lamb *et al.* (2005). It also remains uncertain whether individual diatom species fractionate oxygen isotopes differently due to disequilibrium (or "vital") effects. The weight of evidence currently suggests that such effects are insignificant, at least compared to the analytical errors associated with $\delta^{18}O_{diatom}$ analysis (*e.g.* Juillet-Leclerc and Labeyrie, 1987; Shemesh *et al.*, 1995; Brandriss *et al.*, 1998; Schmidt *et al.*, 2001; Moschen *et al.*, 2005), but these studies are based on limited data and further work is necessary to confirm this proposal.

The use of $\delta^{18}O_{diatom}$ for environmental reconstruction in lacustrine settings is complicated by the fact that diatom productivity usually varies seasonally, in response to factors such as the lake's mixing regime, nutrient input, temperature variations, and ice cover (*e.g.* Lewis, 1996). $\delta^{18}O_{diatom}$ will therefore tend to reflect the $\delta^{18}O$ and temperature of lake water at the time of maximum productivity, and any change in this time may influence $\delta^{18}O_{diatom}$ independently of changes in the average $\delta^{18}O$ and temperature of the lake. If enough is known about the modern lacustrine setting and diatom ecology, $\delta^{18}O_{diatom}$ records can provide valuable palaeoenvironmental information, however, particularly if complimentary palaeoenvironmental records are available (*e.g.* Barker *et al.*, 2001; Leng *et al.*, 2001; Shemesh *et al.*, 2001).

The measurement errors associated with $\delta^{18}O_{diatom}$ values are relatively high, but the most significant source of error in $\delta^{18}O_{diatom}$ analysis is usually the presence of impurities in the samples analysed (cf. Leng and Barker, 2006). The presence of detritus such as mineral grains, tephra, and organic material introduces significant error because the methods of $\delta^{18}O_{diatom}$ analysis release oxygen from these materials, as well as from diatom valves (cf. Morley *et al.*, 2004; Lamb *et al.*, 2005). In many cases, samples can be cleaned using procedures such as acid treatment, sieving, and settling (Juillet-Leclerc, 1984; Morley *et al.*, 2004), or gravitational split-flow lateral-transport thin (SPLITT) techniques (Giddings, 1985), but the method used must be tailored to the material analysed in order to produce pure samples (cf. Morley *et al.*, 2004; Lamb *et al.*, 2005).

Chapter 3: The modern environment at Tswaing crater lake

3.1 Introduction

The accurate interpretation of proxy records from lacustrine sediments is often dependent on an understanding of the processes that operate in the modern environment (cf. Leng and Marshall, 2004). This thesis attempts to reconstruct aspects of palaeoenvironmental change at Tswaing crater lake using records of $\delta^{18}O_{calcite}$, $\delta^{13}C_{calcite}$, $\delta^{13}C_{organic}$, and C/N ratios from sediments deposited in the lake (chapter 5), and this chapter aims to provide an understanding of the processes that operate at the site today in order to allow these records to be interpreted accurately. Human activity and sedimentary infilling of the basin have altered some features of the lake since its formation, but most characteristics of the site remain the same, and information about processes that operate in the modern environment should therefore shed light on processes that have operated over much of the lake's history (cf. Levin, 1991; Partridge *et al.*, 1991).

The $\delta^{18}O$ and $\delta^{2}H$ values of water samples from the lake and its vicinity are used, in conjunction with geochemical data, to provide information about the hydrological regime of the water body, and to thereby reveal the factors that control its isotope composition (cf. Dinçer, 1968; Gat, 1971). Similarly, $\delta^{13}C_{DIC}$ values of water samples are used to shed light on the factors that control the isotope composition of DIC in the lake. This information is essential for the accurate interpretation of $\delta^{18}O_{calcite}$ and $\delta^{13}C_{calcite}$ records, as these proxies are influenced by the isotope composition of the water and DIC from which the calcite precipitates (section 2.2) (cf. Leng and Marshall, 2004). In addition, the $\delta^{13}C$ values and C/N ratios of organic material from within and around the lake are used to shed light on the composition of potential sources of organic material to the lake sediments, in order to increase the certainty with which records of $\delta^{13}C_{organic}$ and C/N ratios from the sediments can be interpreted (section 2.3) (cf. Meyers and Teranes, 2001).

McCaffrey and Harris (1996) also explored the modern environment at Tswaing crater lake using stable isotope analysis. Their study attempted to reconstruct the hydrological setting of the lake using the $\delta^{18}O$ and $\delta^{2}H$ values and geochemical composition (major anion and cation concentrations, pH, and alkalinity) of six water samples from the vicinity of the lake, and two samples from a control area (McCaffrey and Harris, 1996). The study concluded that there is probably significant seepage of saline water from the lake into regional groundwater, but it failed to account for discrepancies between the isotopic and geochemical results. Further analysis is therefore required to fully understand the hydrological setting of the water body.

3.2 Setting

3.2.1 Regional climatology

Southern Africa can be divided into three climatic zones, defined by the seasonality of rainfall (Fig. 3.1). Most of the region lies in the summer rainfall zone, which receives more than 50% of its annual rainfall between October and March, but the proportion of precipitation received in this season decreases from more than 90% in the northeast of the zone, to less than 60% in the southwest (Schulze, 1984). In contrast, the western coastal region south of ~26°S receives most of its rainfall in winter, with more than 80% of rainfall in the southwestern Cape falling between April and September. Only the southern Cape coastal region and a narrow region east of the winter rainfall zone receive precipitation throughout the year.

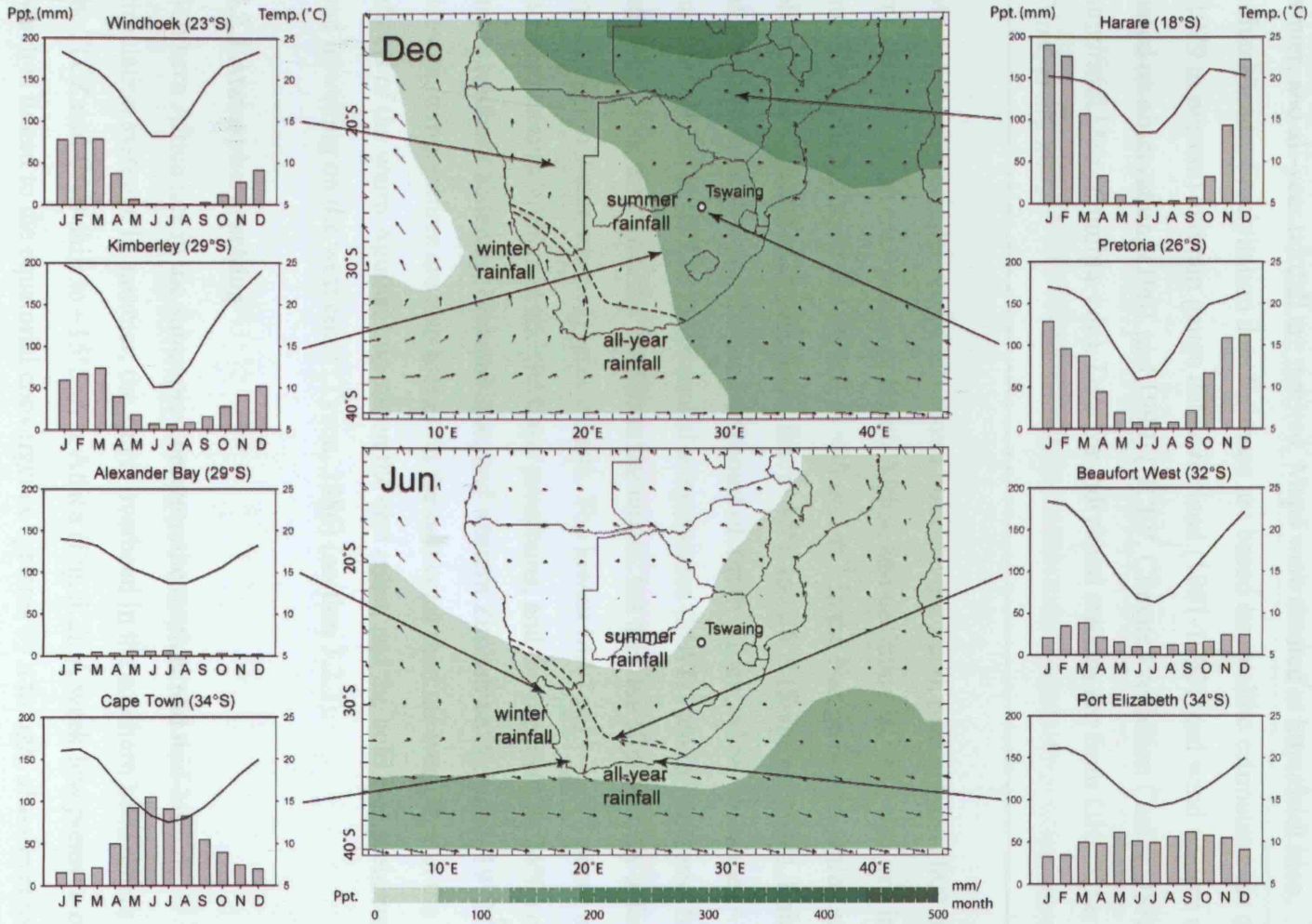

Figure 3.1: See following page for caption

Figure 3.1: Climate of southern Africa, showing precipitation and climatological wind vectors for the 925 hPa pressure level (arrows indicate direction and speed is proportional to arrow length) in December and June, as well as monthly averages of temperature (line) and precipitation (bars) at individual stations. Zones of summer, winter, and all-year rainfall are marked. Maps were created at http://iridl.ldeo. columbia.edu. Precipitation data for maps are based on satellite estimates over oceans (1979 to present) and rain gauge data over land (1961-1990), and wind vectors are based on observations (1961 and 1990) (NCEP, Climate Prediction Center USA, from http://iridl.ldeo.columbia. edu). Data for individual stations are from GHCN ver. 1 (Vose *et al.*, 2002).

Mean annual precipitation (MAP) shows an east-west trend, peaking at ~1000 mm yr^{-1} on the eastern escarpment of South Africa, and declining to ~125 mm yr^{-1} in the interior of the Kalahari desert, and to <20 mm yr^{-1} in the Namib desert, which extends along the west coast of the continent from ~15°S to ~26°S (Schulze, 1984). Rainfall is also relatively high along the southern coast of South Africa, where it reaches ~750 mm yr^{-1} (Schulze, 1972). Mean annual temperatures (MATs) tend to decrease from north to south, and from the interior to the coasts, but they are significantly affected by topographic and oceanographic effects. The lowest MATs (11-12°C) occur in the elevated eastern highlands and the Cape mountains, and the highest (20-24°C) occur in the southern Kalahari, Mozambique, and western Zimbabwe (Schulze, 1972). On average, temperatures are also higher on the east coast than the west, due to the effects of the warm Agulhas current on the east coast, and the cold Benguela current and upwelling on the west coast (Tyson, 1986) (section 3.2.3).

3.2.2 Atmospheric setting

Southern Africa lies in the subtropics, between the tropical and mid-latitude circulation systems. In summer, the sun is overhead in the southern hemisphere and the ITCZ and CAB shift to ~15°S over Africa (Fig. 3.2). A weak low pressure cell, which is linked to the equatorial convergence systems by a trough, also develops over the interior of South Africa due to heating of the atmosphere (Tyson, 1986). These convective systems draw warm, moist air onto the continent from the Indian Ocean, bringing precipitation to the summer and all-year rainfall zones (Taljaard, 1981). The

significance of these systems, which manifest themselves as disturbances in the tropical easterlies on synoptic timescales, is demonstrated by the observation that the wettest years on record are associated with anomalously low pressure over the interior of southern Africa (Tyson and Preston-Whyte, 2000).

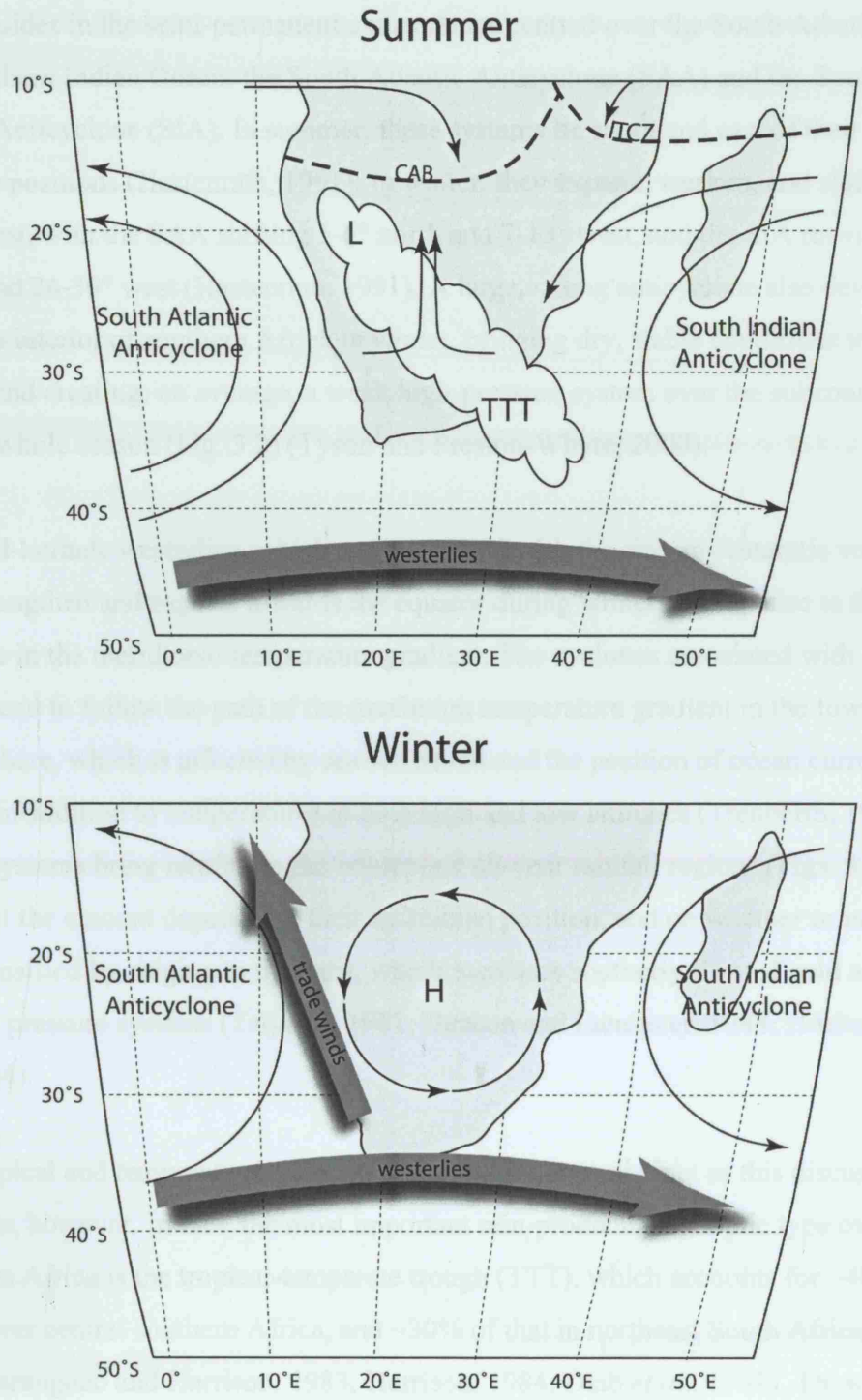

Figure 3.2: Schematic illustration of the primary controls on climate in southern Africa during austral summer and winter, showing the southerly location of the ITCZ and CAB in summer, and the equator-ward shift of the mid-latitude westerlies in winter. H indicates area of high pressure, L indicates area of low pressure, TTT indicates tropical-temperate trough, arrows indicate direction of prevailing winds.

The air that converges at the ITCZ and ascends in the southern hemisphere Hadley cell subsides in the semi-permanent anticyclones centred over the South Atlantic and the southern Indian Ocean: the South Atlantic Anticyclone (SAA) and the South Indian Anticyclone (SIA). In summer, these systems lie south and east of their average positions (Hastenrath, 1991). In winter, they expand, weaken, and shift to the northwest, with the SAA shifting 5-6° north and 7-13° west, and the SIA moving 5-6° north and 24-30° west (Hastenrath, 1991). A large, strong anticyclone also develops over the interior of southern Africa in winter, bringing dry, stable conditions to the region and creating, on average, a weak high-pressure system over the subcontinent for the whole season (Fig. 3.2) (Tyson and Preston-Whyte, 2000).

The mid-latitude westerlies, which are associated with the circum-Antarctic vortex, also strengthen and expand towards the equator during winter, in response to the increase in the meridional temperature gradient. The cyclones associated with these winds tend to follow the path of the maximum temperature gradient in the lower troposphere, which is affected by sea-ice extent and the position of ocean currents and fronts, in addition to temperatures at both high and low latitudes (Trenberth, 1991). These systems bring rainfall to the winter and all-year rainfall regions (Figs. 3.1 and 3.2), but the amount depends on their latitudinal position, and on whether or not they are intensified by ridging to the west, which increases southerly flow of cold air into the low pressure systems (Taljaard, 1981; Deacon and Lancaster, 1988; Hoelzmann *et al.*, 2004).

The tropical and temperate circulation systems are not as distinct as this discussion suggests, however. In fact, the most important rain-producing synoptic type over southern Africa is the tropical-temperate trough (TTT), which accounts for ~40% of MAP over central southern Africa, and ~30% of that in northeast South Africa (Fig. 3.2) (Harangozo and Harrison, 1983; Harrison, 1984; Diab *et al.*, 1991). These features develop over southern Africa when lows in the tropical easterlies at the southern limit of the tropical convergence zones in western Africa (over southeast Angola or southwest Zambia) link with disturbances in the mid-latitude westerlies (Jury and Pathack, 1993). This results in the formation of a NW-SE zone of convergence that extends from Namibia, across South Africa, to the southern ocean, along the western edge of the SIA (Todd and Washington, 1998; Todd and

Washington, 1999). Air from the tropical and temperate lows and the SIA converges at this zone, and thus generates high levels of precipitation over the summer rainfall region of southern Africa (Cook, 2000).

The locations at which TTTs tend to form are determined by the position of the long waves in the high-tropospheric (500-200 hPa) mid-latitude westerlies, because the low-pressure systems that develop in the pole-ward flowing arms of these waves tend to link with lows in the tropical easterlies to form TTTs (Tyson and Preston-Whyte, 2000). The semi-stationary position of the long waves, which is determined by orographic features and by latent heat release in the tropics, thus means that TTTs frequently form in the same locations. The three most important of these locations are: the South Atlantic Convergence Zone (SACZ), the South Pacific Convergence Zone (SPCZ), and the South Indian Convergence Zone (SICZ) over South Africa and the southern Indian Ocean. These zones are evident in long-term precipitation averages, but the SICZ is predominantly an austral summer phenomenon, due to the strong subsidence over southern Africa in winter (Cook, 2000) (Fig. 3.3).

December

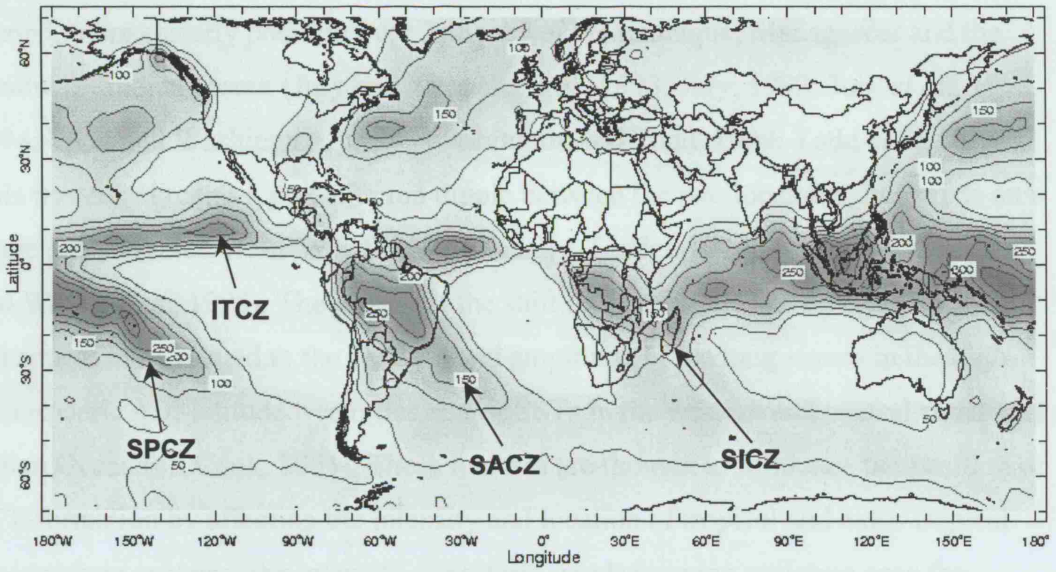

June

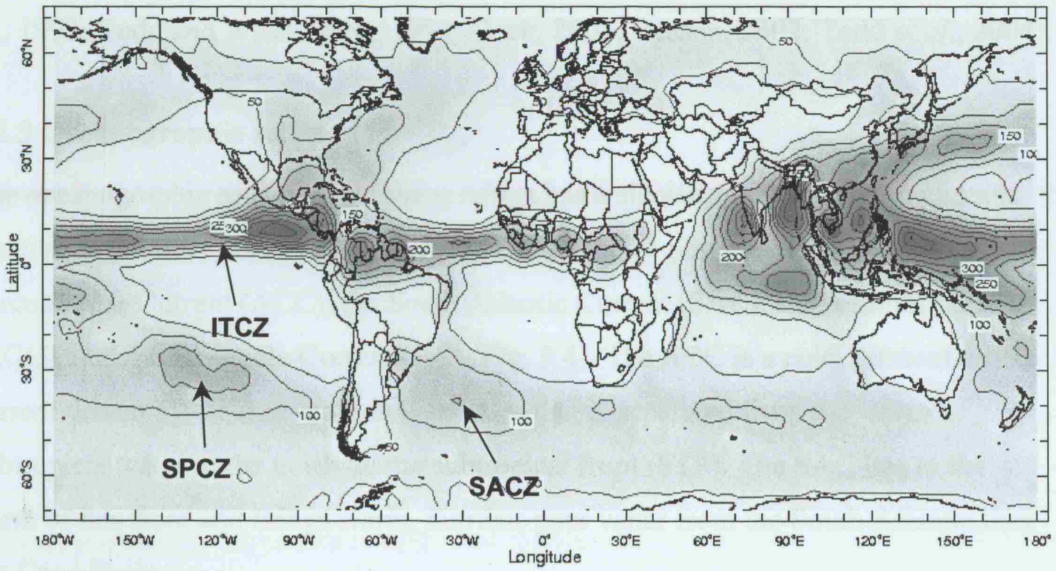

Figure 3.3: Maps of mean monthly precipitation in December and June showing the latitudinal migration of the ITCZ, particularly over land, and the three major southern hemisphere convergence zones: the South Pacific Convergence Zone (SPCZ), the South Atlantic Convergence Zone (SACZ), and the South Indian Convergence Zone (SICZ). Counters are 50 mm/month. Maps were created at http://iridl.ldeo.columbia.edu. Precipitation data are based on satellite precipitation estimates over oceans (1979 to present) and rain gauge data over land (1961-1990) (NCEP, Climate Prediction Center USA, from http://iridl.ldeo.columbia.edu).

Unlike the SACZ and SPCZ, the SICZ has a tendency to shift between two locations: the location over South Africa and the South Indian Ocean described above, and a second, more easterly position over Zimbabwe, Mozambique, Madagascar and the Southwest Indian Ocean (Jury and Pathack, 1991, 1993; Jury, 1992; Jury *et al.*, 1992, 1994; Todd and Washington, 1998; Washington and Todd, 1999; Todd *et al.*, 2004). This tendency creates a precipitation dipole between the two locations that exists on a range of timescales, from daily to inter-annually (Lindesay, 1988; Jury, 1992; Todd and Washington, 1998). The causes of the shift in location are not fully understood, but appear to be related to the position and amplitude of the long waves in the high-tropospheric mid-latitude westerlies and/or SSTs in the western and central equatorial Indian Ocean (cf. Cook, 2001). These features are thought to influence the position of TTT-formation by affecting the intensity and location of tropical and extra-tropical low pressure systems, the intensity of easterly winds carrying moisture onto the continent from the Indian Ocean, and/or the intensity and location of the SIA (Jury *et al.*, 1992; Todd and Washington, 1999; Cook, 2001; Reason, 2002; Todd *et al.*, 2004).

3.2.3 Oceanographic setting

The oceanographic setting of southern Africa has a significant influence on climatic conditions (cf. Jury, 1995). The main currents in this region are: the Antarctic Circumpolar Current (ACC), the South Atlantic Current (SAC), the Agulhas current (AGC), and the Benguela Current (BC) (Fig. 3.4). The ACC is a cold, nutrient-rich current driven by the mid-latitude westerlies that is separated from the warmer, subtropical water to the north by the subtropical front (STF). The SAC lies to the north of this front and brings warm, nutrient-poor water from the South Atlantic into the Cape Basin.

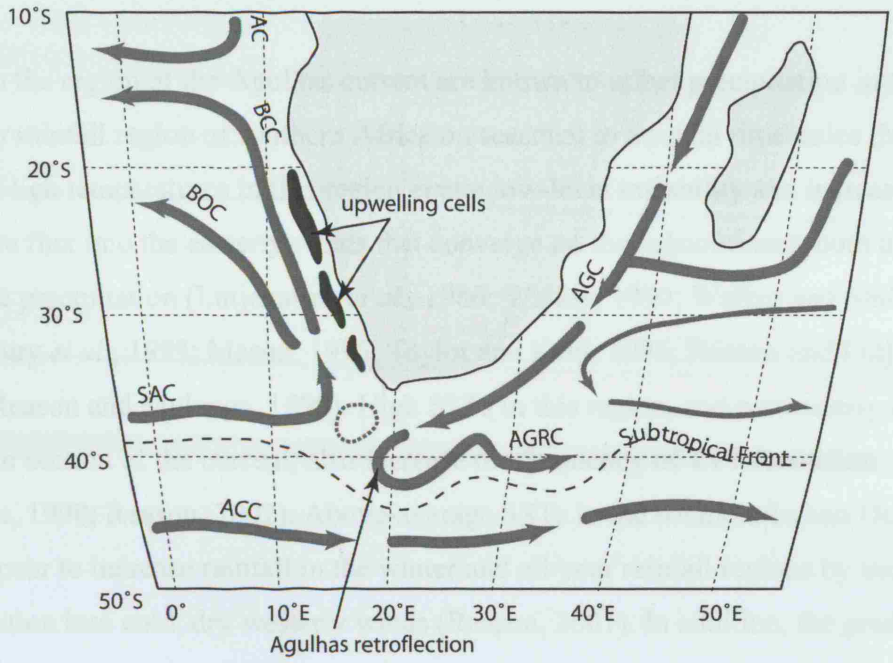

Figure 3.4: Schematic illustration of ocean currents in the vicinity of southern Africa, showing the Antarctic Circumpolar Current (ACC), the Agulhas Current (AGC), the Agulhas Return Current (AGRC), the South Atlantic Current (SAC), the Benguela Ocean Current (BOC), the Benguela Coastal Current (BCC), and the Angola Current (AC). The Agulhas retroflection and upwelling cells driven by the south-easterly trade winds are also shown.

The AGC flows southwards along the east coast of South Africa, bringing warm, saline water towards the STF from the southwest Indian Ocean subgyre (Fig. 3.4) (Stramma and Lutjeharms, 1997). Most of the water in this current is redirected into the Indian Ocean as the Agulhas Return Current (AGRC) when it reaches the STF, forming the Agulhas retroflection off the south coast of South Africa (Lutjeharms and van Ballegooyen, 1988). A small amount enters the South Atlantic Ocean as anticyclonic eddies or thin filaments, and joins the SAC to form the northward flowing BC (Lutjeharms and van Ballegooyen, 1988). The amount of water that enters the South Atlantic Ocean in this way is determined by the position of the STF and the volume transport of the AGC (which is determined by the strength and position of the SIA); with a more northerly location of the STF and increased volume transport of the AGC both reducing influx into the Atlantic Ocean (Lutjeharms and van Ballegooyen,

1984; Reason *et al.*, 1996; Matano *et al.*, 2002).

SSTs in the region of the Agulhas current are known to affect precipitation in the summer rainfall region of southern Africa on seasonal to decadal timescales (Mason, 1995). High temperatures in this region create low-level instability and increase moisture flux into the easterly winds that converge on the subcontinent, both of which increase precipitation (Lutjeharms *et al.*, 1986; Walker, 1990; Walker and Shillington, 1990; Jury *et al.*, 1993; Mason, 1995; Taylor and Kent, 1996; Reason and Lutjeharms, 1998; Reason and Mulenga, 1999). High SSTs in this region, and particularly the southern section of the current, also increase the frequency of TTT formation (Walker, 1990; Reason, 2002). Above-average SSTs in the southern Indian Ocean also appear to increase rainfall in the winter and all-year rainfall regions by increasing evaporation into cold, dry westerly winds (Reason, 2001). In addition, the gradient of SSTs in the southern Indian Ocean influences precipitation in the winter rainfall zone by affecting the frequency and intensity of cyclogenesis (Sanders and Gyakum, 1980; Walker and Lindesay, 1989; Crimp *et al.*, 1998; Reason, 2001).

The BC flows northwards, driven by the SAA, until it diverges into the Benguela Ocean Current (BOC) and the Benguela Coastal Current (BCC) at ~30°S (Fig. 3.4). The BCC hugs the coast of southern Africa until it converges with the southward flowing Angola Current (AC) at the Angola-Benguela Front, which lies at ~15°-17°S (Shannon *et al.*, 1987; Peterson and Stramma, 1991). The prevailing south-easterly trade winds, which form the eastern arm of the SAA, drive upwelling off the coast of southwest Africa between ~15°S and ~34°S, bringing cold, nutrient-rich water to the surface (Shannon, 1985). This zone of cold water increases subsidence over the west coast of southern Africa and, together with the cold water of the BCC and the strong, stable nature of the SAA, is responsible for the arid conditions in this region (section 3.2.1).

Oceanographic conditions in a number of other regions also affect climatic conditions in southern Africa. Above-average SSTs in the western and central equatorial Indian Ocean are associated with below-average precipitation in the summer rainfall region (Walker and Lindesay, 1989; Mason, 1990, 1995, 1998; Walker, 1990; Jury and Pathack, 1991; Mason *et al.*, 1994; Makarau and Jury, 1997; Mason and Jury, 1997;

Rocha and Simmonds, 1997a; Landman and Mason, 1999; Mason and Tyson, 2000). This negative relationship appears to be caused by increased convergence over the SST anomaly, which induces anomalous cyclonic circulation off southeast Africa, and thereby reduces the strength of the SIA and the moisture-bearing easterly winds associated with this system (Rocha and Simmonds, 1997a,b; Goddard and Graham, 1999). On synoptic scales, these changes are believed to cause TTTs to form in the more easterly of their two preferred locations, which significantly reduces summer rainfall over South Africa (Jury and Pathack, 1991; Tennant, 1996).

The El-Niño Southern Oscillation (ENSO) also affects climatic conditions in southern Africa. El Niño events are associated with dry conditions over the summer rainfall region, but the causes of this relationship are not fully understood (Lindesay *et al.*, 1986; Nicholson and Entekhabi, 1986; Lindesay, 1988; van Heerden *et al.*, 1988; Lindesay and Vogel, 1990; Mason and Jury, 1997; Nicholson and Kim, 1997; Camberlin *et al.*, 2001; Curtis *et al.*, 2001). SSTs in the western Indian Ocean tend to be above-average during El Niño events, and the mechanism outlined above may therefore be one of the causes of the teleconnection (Goddard and Graham, 1999), although it has also been suggested that atmospheric forcing causes both above-average SSTs in the Indian Ocean and below-average precipitation in the summer rainfall region (Cook, 2001). It is also worth noting that, in general, SST anomalies that occur independently of ENSO-related phenomena have a greater effect on precipitation in southern Africa than ENSO-related changes (Mason, 1995; Goddard and Graham, 1999; Tyson and Preston-Whyte, 2000).

3.2.4 Local climatology

Tswaing crater is positioned in the summer rainfall zone of southern Africa, where the ITCZ and CAB generate convectional precipitation in austral summer, and a high pressure cell that develops over South Africa creates dry, stable conditions in winter (Schulze, 1965). Summers are therefore hot and wet, while winters are cool and dry. Mean monthly temperatures reach a maximum of ~22°C in December and January and fall to ~11°C in June and July, while precipitation peaks at ~130 mm month^{-1} in December and January, and falls to less than 10 mm month^{-1} between June and August (Ashton, 1999 using data from Roodeplaat Horticultural Research Station 1975-1980).

The isotope composition of precipitation in the region is determined by the amount effect, which describes the observation that precipitation that falls during heavy rainfall events is isotopically lighter than precipitation that falls during light events (section 2.1.1) (Dansgaard, 1964; Araguás-Araguás *et al.*, 1998, 2000). Thus, precipitation that falls in the heavy convectional thunderstorms that bring rainfall to southern Africa during austral summer in association with the tropical convergence zones has lower $\delta^{18}O$ and $\delta^{2}H$ values than precipitation that falls during light showers in austral winter, despite higher surface temperatures during summer (Figs. 3.5 and 3.6) (IAEA/WMO, 2001).

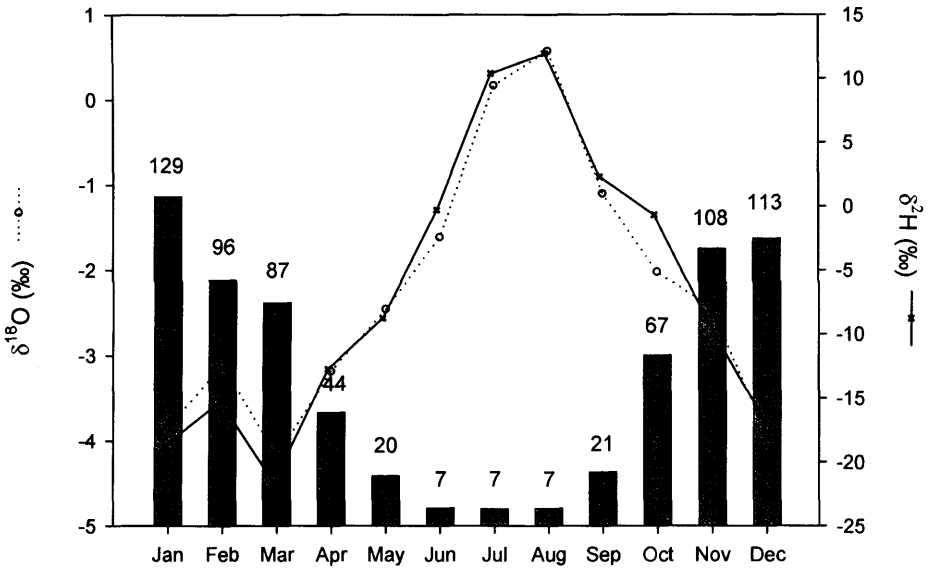

Figure 3.5: Mean monthly $\delta^{18}O$ and $\delta^{2}H$ values of precipitation (expressed as deviations from VSMOW) collected between 1958 and 2001 (lines) (IAEA/WMO, 2001) and mean monthly rainfall between 1910 and 1990 in mm (bars and numbers above bars) (Vose *et al.*, 2002) at Pretoria, ~40 km southeast of Tswaing crater lake.

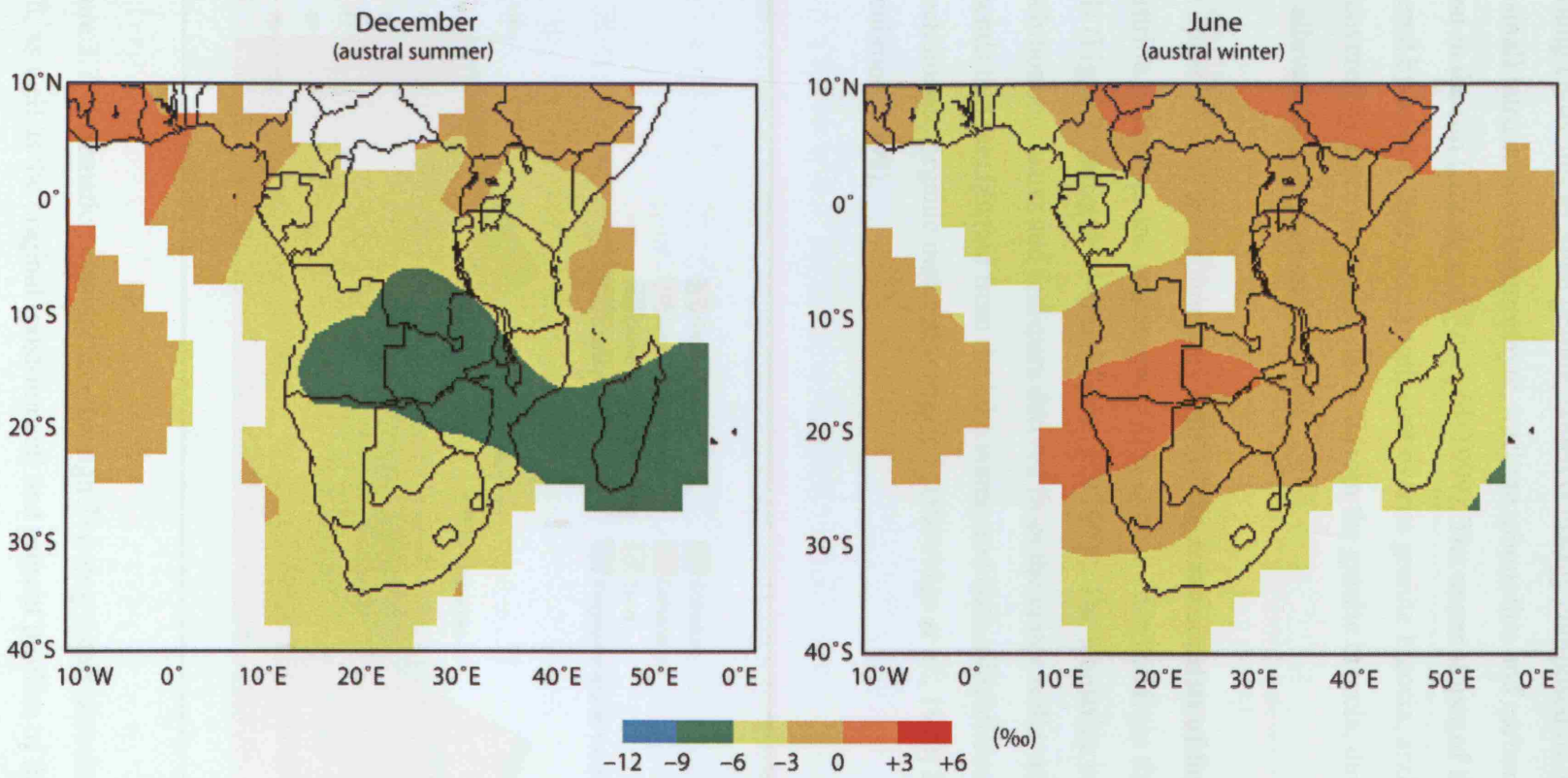

Figure 3.6: Amount-weighted monthly mean $\delta^{18}O$ values of precipitation over southern Africa in December and June, expressed as per mil deviations from VSMOW (IAEA, 2001). The GNIP database used to construct the maps spans 1961-1999, but data for many stations is only available for part of this period (IAEA, 2001).

3.2.5 Geology

Tswaing crater lies in Nebo granite, which is mainly composed of orthoclase granites, but small intrusions of lamprophyre, trachyte, phonolite, and carbonatite are also found in the rim (Brandt and Reimold, 1999). The upper slopes of the inner crater are covered by coarse sandy-loam soils that overlie granite breccia, and the lower slopes are covered by scree and sands derived from the granite breccia, dark organic clays, and alluvial fans (Brandt and Reimold, 1999).

The upper 90 m of the sedimentary infill of the crater consists of fine-grained lacustrine sediments and coarse mass-flow deposits derived from the granitic crater walls (Fig. 3.7) (chapter 1) (Partridge *et al.*, 1991). The lacustrine sediments consist of allochthonous quartz and feldspars derived from the crater walls, autochthonous minerals that precipitated from the lake water, and both allochthonous and autochthonous organic material (chapter 5) (Partridge *et al.*, 1993; Bühmann and Elsenbroek, 1999).

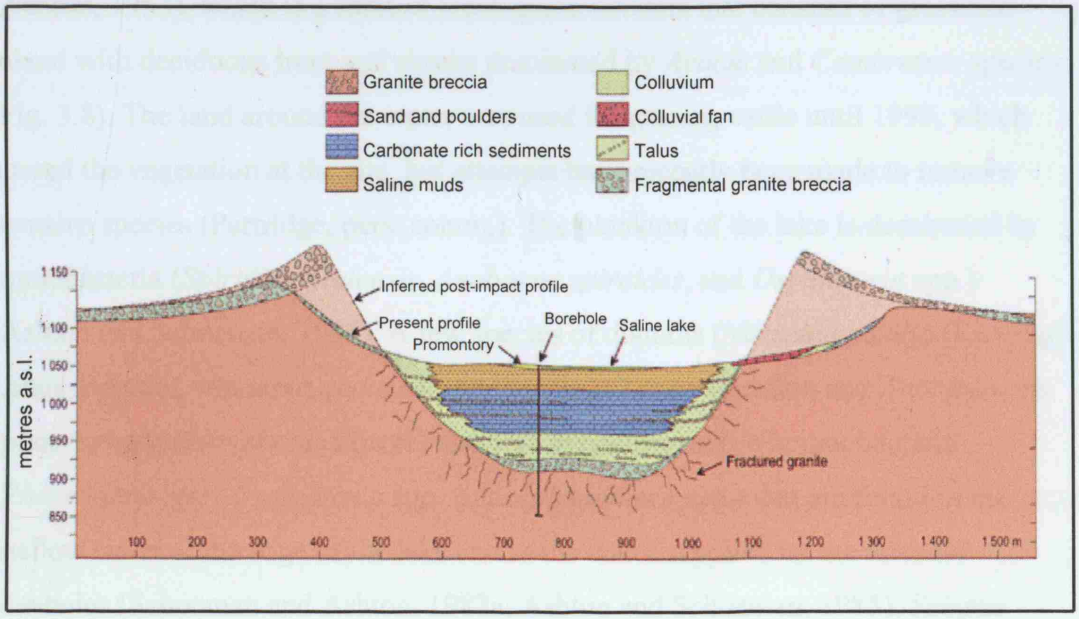

Figure 3.7: Schematic cross-section through Tswaing crater showing the sedimentary infill, as well as the original (post-impact) and present profiles of the crater. The location of the borehole made in 1988/89 is shown. Modified from Partridge *et al.* (1991) and Brandt and Reimold (1999).

The composition of the autochthonous minerals in the sediments changes from the base to the top of the sequence (cf. Figure A2, Appendix A). Calcite is the most abundant mineral below ~33 m, but halite is most abundant above this depth. In addition, trona is present above ~25 m, fluorite occurs above ~17 m, and gaylussite is present above ~13 m (uncorrected depths) (Partridge *et al.*, 1993; Bühmann and Elsenbroek, 1999). This sequence appears to reflect the evaporative concentration of water with a $HCO_3^-/Ca^{2+}+ Mg^{2+}$ ratio greater than 1, suggesting that the autochthonous minerals in the sediments precipitated in response to progressive concentration of the lake water by evaporation (Eugster and Hardie, 1978; Bühmann and Elsenbroek, 1999). It is worth noting that some of the calcite in the sediments may be derived from the small igneous intrusions in the crater rim, but calcite is a minor component of these outcrops, and any contribution from this source is therefore likely to be negligible relative to the amount produced within the lake (chapter 5) (Brandt and Reimold, 1999; Bühmann and Elsenbroek, 1999).

3.2.6 Vegetation

The vegetation around the crater is classified as mixed- and sourish-mixed bushveld (Acocks, 1953), which is a form of brush-grass savanna that consists of grassland mixed with deciduous trees and shrubs dominated by *Acacia* and *Combretum* species (Fig. 3.8). The land around the crater was used for grazing cattle until 1999, which altered the vegetation at the site, but attempts have recently been made to remove invasive species (Partridge, pers. comm.). The plankton of the lake is dominated by cyanobacteria (*Spirulina platensis*, *Anabaena spiroides*, and *Oscillatoria* spp.) (Ashton and Schoeman, 1985). A few species of diatoms (*Nitzschia pusilla* (Kützing) Lange-Bertalot, *Nitzschia quadrangula* (Kützing) Lange-Bertalot, and *Anomoeoneis sphaerophora* (Ehrenberg) Pfitzer) also live in benthic mats of cyanobacteria (*Phormidium* spp., *Oscillatoria* spp., and *Aphanothece* spp.) that are found in the shallow water at the edge of the lake and in the water supplied by the artesian boreholes (Schoeman and Ashton, 1982a; Ashton and Schoeman, 1985). *Scirpus maritima*, a salt-tolerant sedge, also lives in the water supplied by the artesian boreholes, but no macrophytes live in the lake itself (Ashton, 1999).

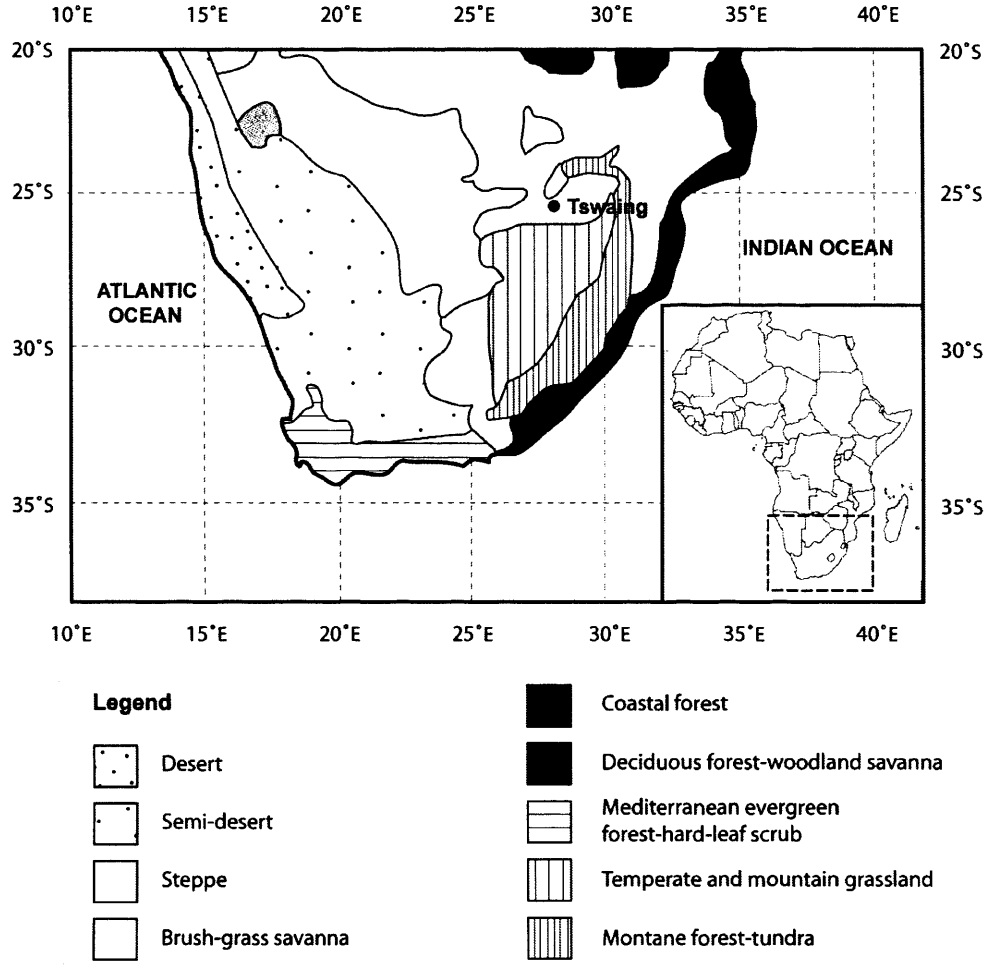

Figure 3.8: Map showing the location of Tswaing crater lake and the natural vegetation of southern Africa. After map 800630 from the Perry-Castañeda Library Map Collection.

3.2.7 Limnology

The lake that currently exists in Tswaing crater is ~300 m in diameter (Ashton and Schoeman, 1983). Its floor slopes gradually from the water's edge to a depth of 0.5 m, but then falls steeply to a maximum depth of 2.85 m due to the removal of sediments from the crater by commercial salt-production companies during the first half of the twentieth century (Ashton and Schoeman, 1983; Levin, 1991). The lake receives inputs from direct precipitation and runoff, as well as from springs in the crater wall and from a number of artesian boreholes sunk into the lake sediments by mining companies and scientific expeditions since 1973 (Ashton and Schoeman, 1983;

Partridge *et al.*, 1993). The water supplied by the artesian boreholes, and the lowering of the lake floor by salt-production companies are thought to account for the persistence of the modern lake, as the water body appears to have dried out in winter before commercial activities began (Ashton and Schoeman, 1983; Levin, 1991). There is no surface outflow from the lake, but McCaffrey and Harris (1996) proposed that some water is lost through groundwater seepage.

The lake water is hypersaline (salinity ~70-250 g l^{-1}, conductivity 60,000-200,000 μS/cm) and alkaline (400-2,000 meq l^{-1}), and is characterised by Na^+, CO_3^{2-}, and Cl^- ions (Ashton and Schoeman, 1983). The composition of the lake varies significantly with depth, with salinity increasing from ~70 g l^{-1} at the surface to ~250 g l^{-1} at a depth of 2.5 m (Ashton and Schoeman, 1983). This salinity gradient, combined with the unusual bathymetry of the lake and the low wind speeds in the crater, increase the stability of the water column, and Ashton and Schoeman (1983) found that the lake was meromictic, with a well-mixed mixolimnion in the upper 25-50 cm of the lake, and a saline, permanently stratified monimolimnion below (Ashton and Schoeman, 1983).

3.3 Methods

3.3.1 Water samples

Water samples for $\delta^{18}O$ and $\delta^{2}H$ analysis were collected using 100 ml leak-proof acid-washed polyethylene bottles. The bottles were rinsed several times in the water to be collected before being filled completely and sealed with insulation tape. Samples for $\delta^{13}C_{DIC}$ analysis were collected in the same way, but the water was filtered before being poured into the bottles to exclude any particulate carbonates or organic matter, and 15 ml of the sample was replaced with saturated NaOH-$BaCl_2$ solution to precipitate DIC before the bottle was capped, shaken, and sealed.

The locations at which water samples were taken in this study, and in other studies mentioned in this chapter, are shown in Figure 3.9, and details of the samples collected in this study are given in Table 3.1. Unfortunately, it was not possible to take samples from boreholes 1, 3, or 4 in this study because they were blocked or

inaccessible. In addition, only two of the artesian boreholes in the lake were sampled, to avoid extraneous repetition. Where possible, the height of the water table was measured in the boreholes sampled, using a dip-meter and a GPS.

Table 3.1: Details of the water samples collected in this study.

Site Description	Sample name	Grid reference	Date and time	Comment	Sample for $\delta^{18}O$ & $\delta^{2}H$	Sample for $\delta^{13}C_{DIC}$
Lake surface	Lake surface 1	25°24'30.7"S 28°04'53.4"E	26/02/2005 15.35	Turbid	X	X
Lake surface	Lake surface 2	25°24'33.7"S 28°04'55.3"E	27/02/2005 15.35	Turbid	X	X
Lake surface near borehole discharge	Lake surface near boreholes	25°24'28.8"S 28°04'56.3"E	26/02/2005 16.05	Turbid	X	X
Lake at 0.5 m deep	Lake at 0.5 m	25°24'33.7"S 28°04'56.0"E	27/02/2005 15.55	Turbid	X	X
Artesian borehole (1988/89)	Artesian borehole 2	25°24'28.8"S 28°04'56.1"E	26/02/2005 15.55	From tap; very clear	X	X
Artesian borehole (2001/02)	Artesian borehole 3	25°24'30.4"S 28°04'56.2"E	26/02/2005 16.00	Pool at borehole; turbid	X	X
Natural spring at lake edge	Spring	25°24'24.9"S 28°04'55.1"E	26/02/2005 16.20	Fairly turbid	X	X
Stream east of crater	Stream	25°24'48.9"S 28°04'55.1"E	27/02/2005 10.05	Polluted by settlement?	X	
Borehole at recep. south of crater	Borehole 5	25°25'21.4"S 28°04'46.4"E	27/02/2005 10.55	Stored in sealed tank	X	X
Borehole at Ismail's Store	Borehole 2	25°24'31.7"S 28°05'59.8"E	27/02/2005 17.00	Stored in tank	X	X

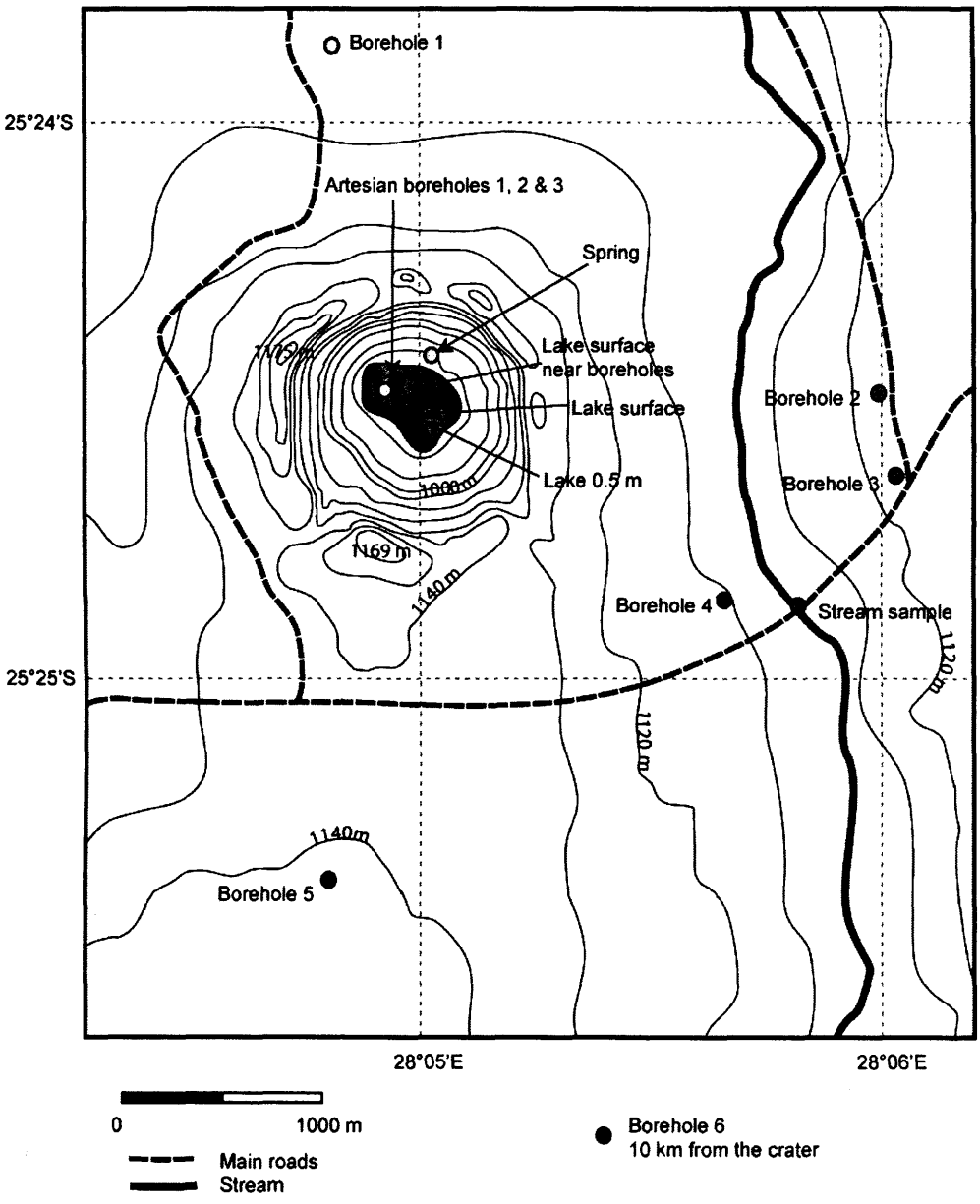

Figure 3.9: Map showing the sites at which water samples were taken in this study, and in other studies mentioned in the text. Borehole 6 is shown separately because it is 10 km away from the crater. Contour intervals are 10 m.

In order to measure the $\delta^{18}O$ value of samples, 2 ml of untreated water was equilibrated with CO_2 by shaking for six hours at 23°C, and the oxygen isotope composition of the gas was then measured using mass spectrometry (Epstein *et al.*, 1953). To measure the $\delta^{2}H$ value of the sample, 5 µl of sample water was reacted with

100 mg of zinc turnings at 500°C (Heaton, 1992), and the hydrogen gas liberated was collected and analysed using a VG SIRA 10, split-flight mass spectrometer. Isotope values ($\delta^{18}O$ and $\delta^{2}H$) are reported as per mil deviations from VSMOW. Analysis of laboratory standards showed that analytical reproducibility was ±0.05‰ for $\delta^{18}O$ values, and ±2.0‰ for $\delta^{2}H$ values (1 s.d.). The isotope analysis of the samples was carried out by C. Arrowsmith at the NERC Isotope Geosciences Laboratory (NIGL).

In order to measure the $\delta^{13}C$ value of DIC, the $BaCO_3$ precipitate was separated from the water sample by filtering under a flow of N_2. If the colour of the precipitate indicated that organic matter could be present (yellowy-brown instead of bright white), the samples were reacted with ~100 ml of 5% sodium hypochlorite for twelve hours before being rinsed three times with deionised distilled water under a flow of N_2. The samples were then dried at 40°C and ground to a fine power, and 10 mg of this powder was reacted with anhydrous phosphoric acid *in vacuo* overnight at 25°C (McCrea, 1950). The CO_2 produced was separated from water vapour using liquid nitrogen traps, and analysed using a VG Optima mass spectrometer. Isotope values were calculated relative to VPDB, based on the calibration of laboratory standards against NBS-19, and analysis of laboratory standards showed that analytical reproducibility was ±<0.05‰ (1 s.d.). The samples were prepared by the author, but mass-spectrometry was carried out by J. Greene (NIGL).

3.3.2 Organic samples

Forty-eight samples of plants and sediment were taken from within and around the lake for $\delta^{13}C$ and C/N analysis. These included twenty-nine samples of vegetation collected along a transect from the crater-rim to the lake-edge to ensure that all major vegetation types (which show an altitudinal gradient due to changing moisture availability (Partridge, pers. comm.)) were sampled. As much material as possible was collected from each plant, including leaves, twigs, and bark from trees and shrubs, and whole plants, including roots, from grasses. Reeds growing in a pool formed by the discharge of an artesian borehole before it entered the lake (cf. Figure 4.2), and in a spring supplying the lake were also sampled. Where possible, the vegetation sampled was identified to species level with the help of Prof. T. C. Partridge (Climatology Research Unit, University of the Witwatersrand). Seven soil samples and one sample of leaf litter were also collected along the transect from the

crater-rim to the lake-edge. Samples of organic mats, which consist of cyanobacteria and small numbers of diatoms (Schoeman and Ashton, 1982a; Ashton and Schoeman, 1985), growing in shallow, marginal areas of the lake and in a pool created by artesian borehole discharge were also obtained. Finally, surface-sediment samples were taken from within the lake, at depths of ~0.1 and ~0.5 m, and from the lake margin.

Vegetation samples were dried at 40°C and ground to a fine powder by freeze-milling. Samples of organic mats, soil, and lake sediments were left in ~100 ml of 5% HCl for 12 hours to remove any carbonates, rinsed three times with 200 ml of deionised distilled water, dried at 40°C, and ground to a fine powder. $\delta^{13}C$ values and percentage carbon and nitrogen content were analysed during combustion in a Carlo Erba 1500 elemental analyser coupled on-line to a VG TripleTrap and dual-inlet mass spectrometer. $\delta^{13}C$ values were converted to the VPDB scale using a within-run laboratory standard calibrated against NBS-19 and NBS-22, and C/N ratios were calibrated against an acetanilide standard. Replicate analyses of sample material had a standard deviation of 0.1‰ for $\delta^{13}C$ values, and 0.2 for C/N measurements, while standards analysed had a standard deviation of 0.04‰ for $\delta^{13}C$ values, and 0.14 for C/N measurements. Again, the samples were prepared by the author, but mass-spectrometry was carried out by J. Greene (NIGL).

3.4 Results

3.4.1 $\delta^{18}O$ and $\delta^{2}H$ of water samples

The $\delta^{18}O$ and $\delta^{2}H$ values of water samples analysed in this study are listed in Table 3.2. These values are shown in Figure 3.10, together with the values of additional groundwater samples published by McCaffrey and Harris (1996) or provided by Prof. T. C. Partridge (pers. comm.). The samples analysed by McCaffrey and Harris (1996) were collected in June 1993 and June/July 1994, and the samples provided by Prof. T. C. Partridge were collected between January 1987 and May 1995 and analysed by S. Talma (CSIR, South Africa) and W. Wood (USGS). The $\delta^{18}O$ and $\delta^{2}H$ values of all the samples are also shown on a $\delta^{2}H$-$\delta^{18}O$ plot in Figure 3.11, together with: the GMWL, a LMWL produced from 169 samples of precipitation collected at Pretoria between 1958 and 2001 (IAEA/WMO, 2001), and a LEL fitted to the values of lake-

water samples. The mean annual $\delta^{18}O$ and $\delta^{2}H$ values of the precipitation collected at Pretoria, weighted for the average amount of precipitation that falls each month, are also plotted in this figure (IAEA/WMO, 2001; Vose *et al.*, 2002).

Table 3.2: $\delta^{18}O$, $\delta^{2}H$, and $\delta^{13}C_{DIC}$ of water samples collected.

Sample name	$\delta^{18}O$ (‰) VSMOW	$\delta^{2}H$ (‰) VSMOW	$\delta^{13}C_{DIC}$ (‰) VPDB
Lake surface 1	+2.5	–0.7	–1.8
Lake surface 2	+3.3	+4.2	–1.6
Lake surface near boreholes	+1.7	–2.8	–2.4
Lake at 0.5 m	+11.0	+37.2	+1.9
Artesian borehole 2	–4.3	–26.2	–4.2
Artesian borehole 3	–4.1	–24.3	+1.2
Spring	–4.4	–25.6	–6.5
Stream	–0.6	–5.1	N/A
Borehole 5	–4.9	–28.1	–10.8
Borehole 2	–3.6	–19.8	–13.0

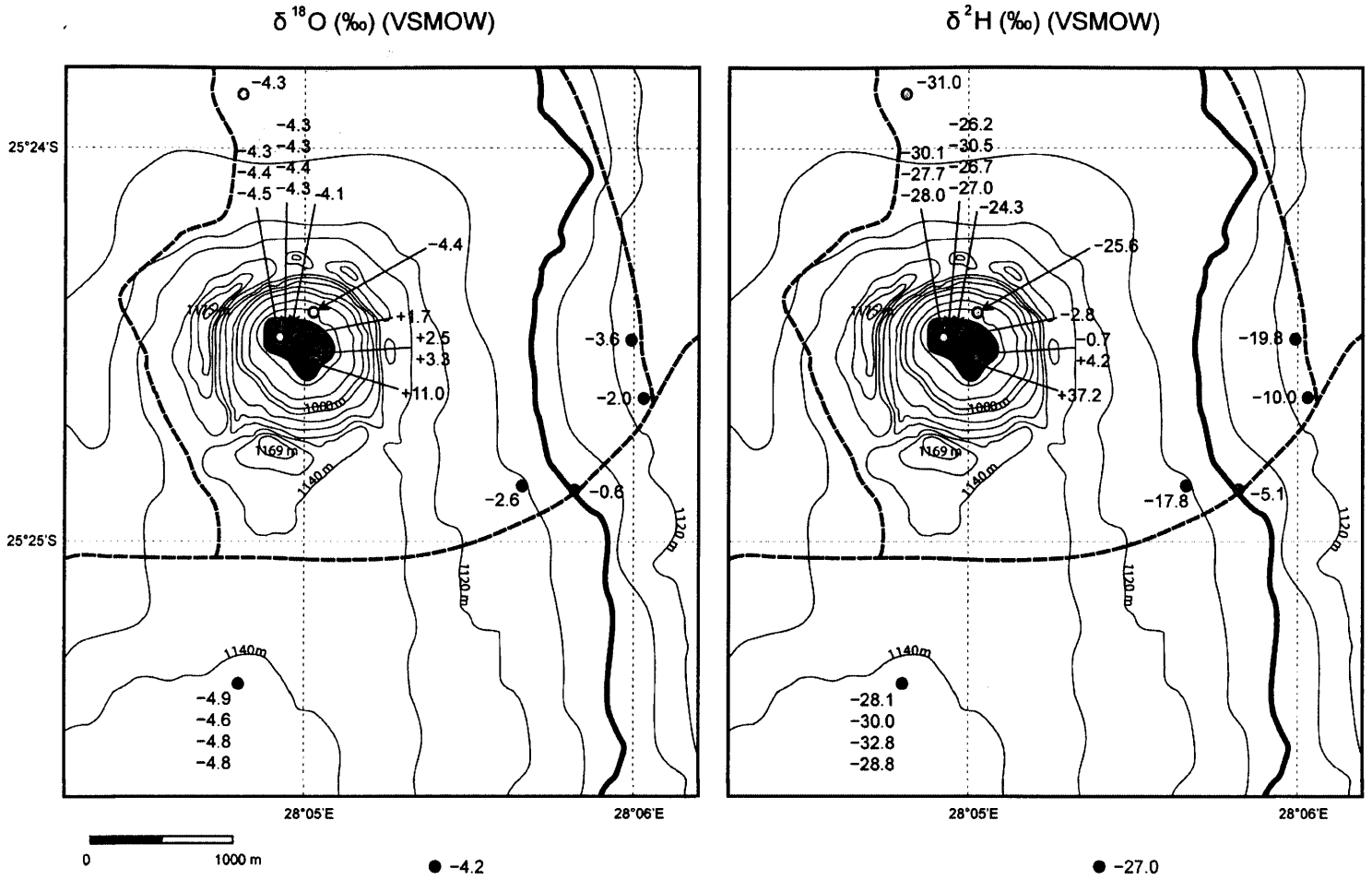

Figure 3.10: Location and $\delta^{18}O$ and $\delta^{2}H$ values of water samples from the vicinity of Tswaing crater lake. Samples were collected in this study, published by McCaffrey and Harris (1996), or provided by Prof. T. C. Partridge (pers. comm.). Legend as in Figure 3.9.

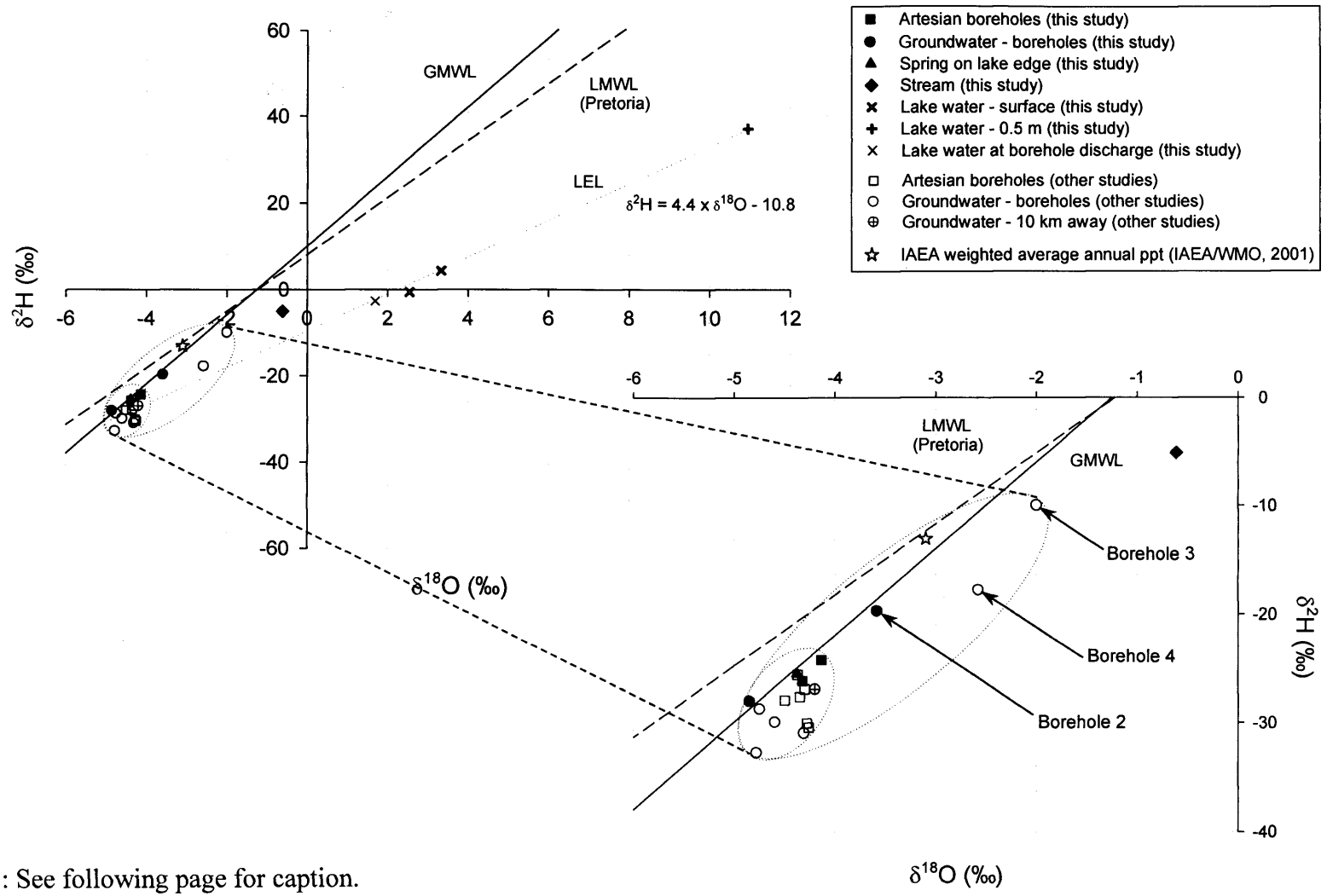

Figure 3.11: See following page for caption.

Figure 3.11: $\delta^{18}O$ and $\delta^{2}H$ values of water samples from the vicinity of Tswaing crater lake. Small oval encloses main cluster of groundwater samples, large oval encloses all groundwater samples. Lower graph shows groundwater samples in more detail. Filled symbols and crosses indicate data from this study. Open symbols indicate data published by McCaffrey and Harris (1996) or provided by Prof. T. C. Partridge (pers. comm.). Star indicates amount-weighted mean annual $\delta^{18}O$ and $\delta^{2}H$ values of precipitation collected at Pretoria between 1958 and 2001 (IAEA/WMO, 2001; Vose *et al.*, 2002)

It is evident from Figures 3.10 and 3.11 that water from the boreholes north and south of the crater, the artesian boreholes within the crater, and a spring on the lake's edge have similar $\delta^{18}O$ and $\delta^{2}H$ values. In Figure 3.11, these samples form a tight cluster that lies close to the GMWL, with $\delta^{18}O$ values between –4.1‰ and –4.9‰ (average = –4.4‰, s.d. = 0.2‰) and $\delta^{2}H$ values between –24.3‰ and –32.8‰ (average = –28.2‰, s.d. = 2.3‰). The $\delta^{18}O$ and $\delta^{2}H$ values of the samples from boreholes 2, 3 and 4, which lie east of the crater (Fig. 3.9), are higher than those of the other groundwater samples (Fig. 3.11). The samples from boreholes 3 and 4 also lie to the right of the GMWL, although they are not displaced significantly further from this line than other groundwater samples (Fig. 3.11).

The samples of lake water have significantly higher $\delta^{18}O$ and $\delta^{2}H$ values than all the groundwater samples, and define a LEL with a gradient of 4.4 (Fig. 3.11). The water sample from a depth of 0.5 m has the highest values, while the sample taken near the outflow of an artesian borehole has the lowest values. The LEL intercepts the GMWL at a $\delta^{18}O$ value of –5.8‰ and a $\delta^{2}H$ value of –36.2‰, close to the average values of the samples in the main cluster of groundwater samples. The sample from the stream that lies east of the crater also has higher $\delta^{18}O$ and $\delta^{2}H$ values than the groundwater samples, and lies to the right of the GMWL, but the values of this sample are not as high as the lake water samples, and do not lie on the LEL defined by them (Fig. 3.11).

3.4.2 Geochemistry of water samples

The geochemical composition of a number of water samples from the vicinity of Tswaing crater lake has been published by McCaffrey and Harris (1996) and Ashton

and Schoeman (1983). Prof. T. C. Partridge (pers. comm.) also provided unpublished geochemical data for a number of samples analysed by S. Talma (CSIR, South Africa) and W. Wood (USGS). All the samples were collected between February 1978 and May 1995. The ionic composition of these samples is shown in Figure 3.12, together with their conductivity values, where known. The samples from boreholes 3 and 4, which have higher isotope values than the other groundwater samples (Fig. 3.11), are labelled (the geochemical composition of the sample from borehole 2, which also has relatively high isotope values, was not determined).

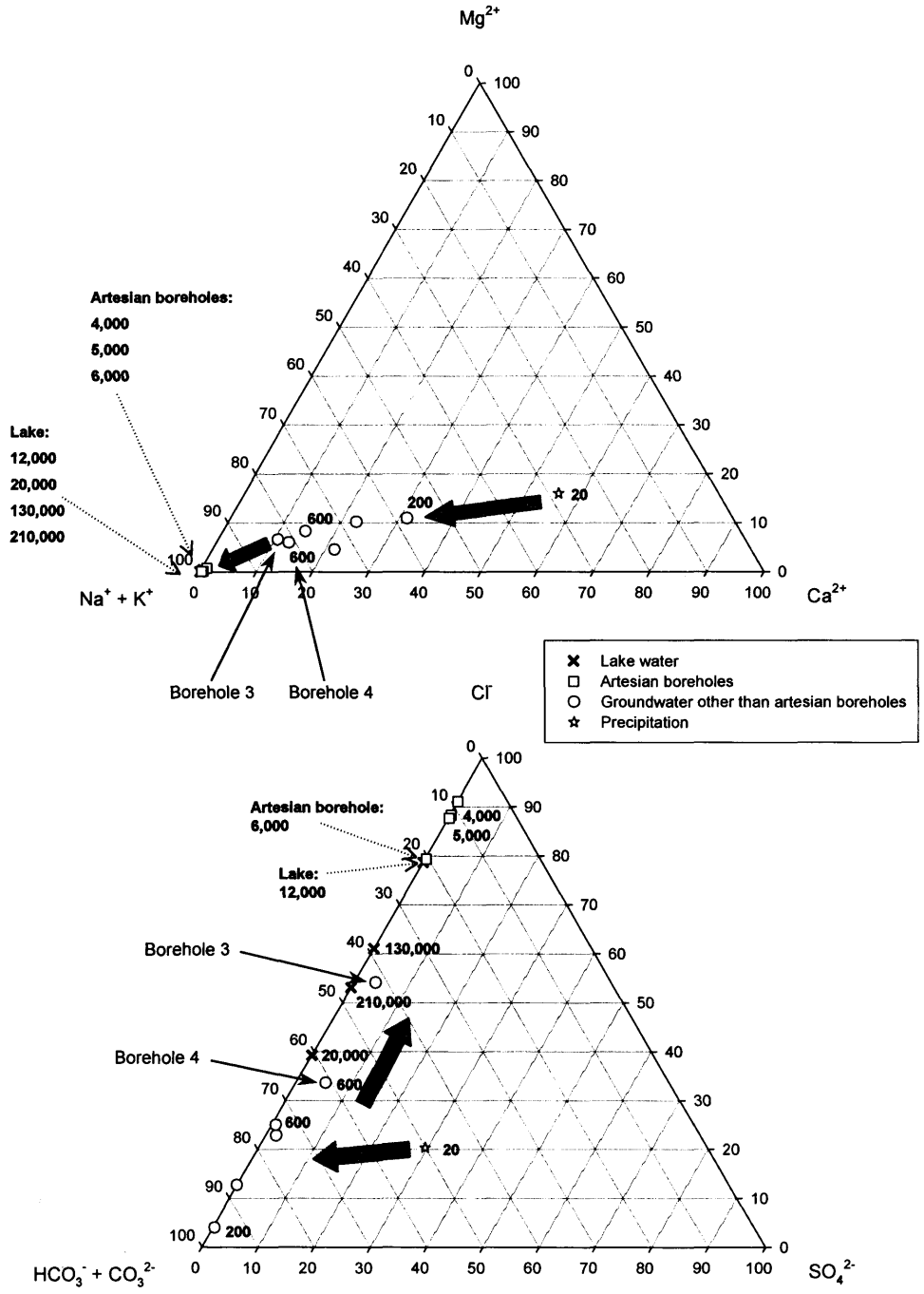

Figure 3.12: Ionic composition (mol%) of water samples from the vicinity of Tswaing crater lake. The data are either published (Ashton and Schoeman, 1983; McCaffrey and Harris, 1996), or were provided by Prof. T. C. Partridge (pers. comm.). Where available, conductivity values (μS/cm) are shown to the right of the sample or labelled using a dotted arrow. The groundwater samples with relatively high isotope values for which geochemical data are available (boreholes 3 and 4) are labelled using solid arrows. Large grey arrows indicate the progression from precipitation to groundwater (other than that from artesian boreholes) to lake water.

It is evident that samples from the same source (precipitation, groundwater from artesian boreholes, groundwater from other sources, and lake water) have similar ionic compositions and conductivities. It is particularly notable that the ionic compositions and conductivities of groundwater samples from the artesian boreholes in the lake are significantly different from those of groundwater samples from other sources. It is also notable that one lake water sample and the groundwater sample from borehole 3 have higher mol% Cl^- and lower mol% $HCO_3^- + CO_3^{2-}$ than other samples from the same sources.

3.4.3 $\delta^{13}C_{DIC}$ of water samples

The $\delta^{13}C_{DIC}$ of water samples analysed in this study are listed in Table 3.2 and plotted in Figures 3.13 and 3.9. The groundwater samples from boreholes outside the crater have the lowest $\delta^{13}C_{DIC}$ values (–13.0‰ and –10.8‰), while groundwater entering the crater at the spring line has a $\delta^{13}C_{DIC}$ of –6.5‰. The $\delta^{13}C_{DIC}$ of groundwater entering the lake through artesian boreholes is higher than that of other groundwater samples; a sample obtained from a borehole sealed by a tap has a value of –4.2‰, and a sample from a pool supplied by a different borehole has a value of +1.2‰. The values of samples from the lake surface range from –2.4‰ to –1.6‰, but the sample with a value of –2.4‰ was taken where the artesian boreholes discharge into the lake and may therefore be influenced by the composition of this water. The water sample from a depth of 0.5 m had the highest $\delta^{13}C_{DIC}$, with a value of +1.9‰.

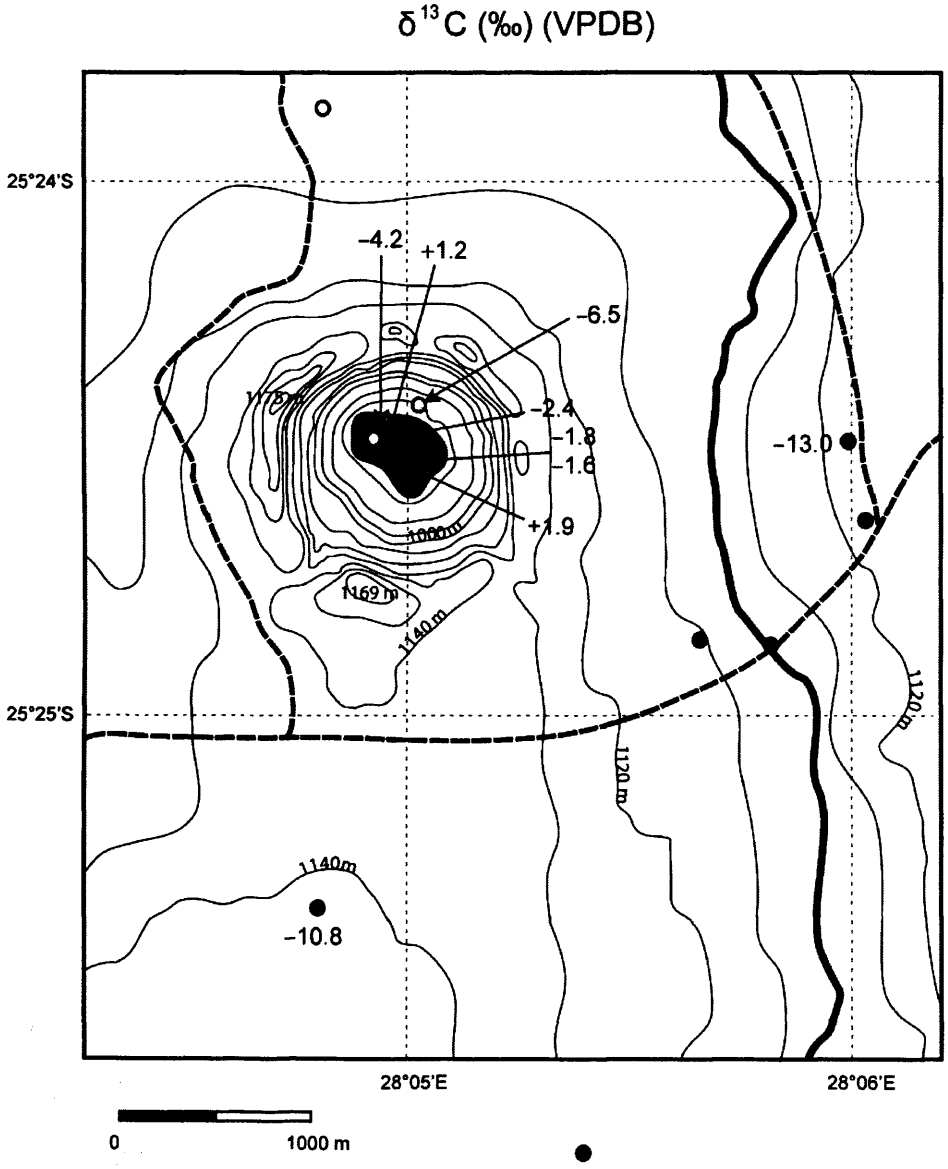

Figure 3.13: Location and $\delta^{13}C_{DIC}$ of water samples from the vicinity of Tswaing crater lake. Legend as in Figure 3.9.

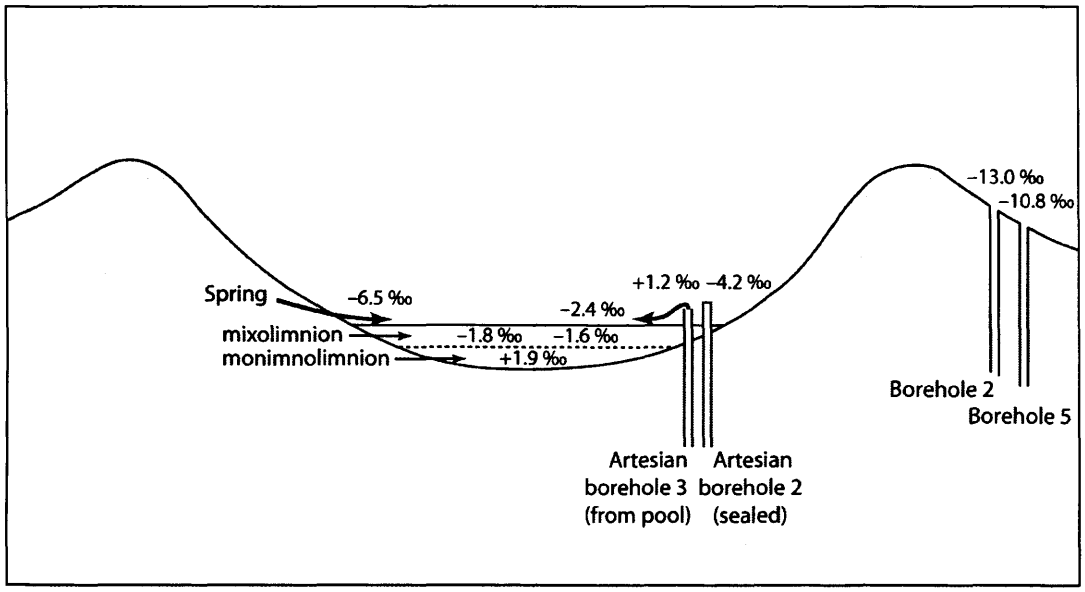

Figure 3.14: Schematic cross-section through Tswaing crater lake showing the $\delta^{13}C_{DIC}$ of water samples expressed as per mil deviations from VPDB.

3.4.4 $\delta^{13}C$ and C/N ratios of organic samples

The $\delta^{13}C$ and C/N ratios of organic material collected from within and around the lake, as well as the names of the terrestrial plants analysed, are listed in Tables 3.3 and 3.4. The values are also plotted in Figure 3.15, together with fields of $\delta^{13}C$ values and C/N ratios representative of C_3 and C_4 land plants and aquatic organisms (Tyson, 1995). The $\delta^{13}C$ values of the terrestrial and emergent plant samples fall into two groups (–23‰ to –31‰ and –11‰ to –14‰), which lie within the fields typical of terrestrial C_3 and C_4 plants (Tyson, 1995). The C/N ratios of these plants also lie within the ranges expected for terrestrial C_3 and C_4 plants, (Tyson, 1995). The sample of leaf litter has a $\delta^{13}C$ value of –25.1‰ and a C/N ratio of 32, and thus lies within the field considered representative of terrestrial C_3 plants. The soil samples lie in a separate group, with $\delta^{13}C$ values that either lie between the two groups of higher plants, or overlap with the values of plants in the group characteristic of C_3 plants (–18‰ to –24‰), and C/N ratios that are lower than all the higher plants (12 to 14).

Table 3.3: $\delta^{13}C$ and C/N ratios of higher plants sampled, ordered by increasing $\delta^{13}C$ values.

C_3/C_4	Name	Description	$\delta^{13}C$ (‰) VPDB	C/N ratio
$\delta^{13}C$ indicate C_4 plants	*Scirpus maritima*	Emergent - borehole	–11.9	47.2
	Sedge - unidentified	Emergent - spring	–12.4	96.2
	Grass - unidentified	Grass	–12.7	100.4
	Grass - *Digitaria erianthe*?	Grass	–12.9	37.6
	Grass - unidentified	Grass	–13.1	68.2
	Grass - unidentified	Grass	–13.3	57.6
	Grass - unidentified	Grass	–13.4	32.2
	Grass - unidentified	Grass	–13.5	47.8
	Grass - *Aristida junciformis*?	Grass	–13.5	41.9
	Grass - unidentified	Grass	–13.5	52.7
$\delta^{13}C$ indicate C_3 plants	*Ziziphus mucronata*	Tree	–23.9	29.2
	Combretum erythrophyllum	Tree	–24.7	26.9
	Combretum erythrophyllum	Tree	–25.0	28.7
	Peltophorum africanum	Tree	–25.0	23.5
	Combretum - unknown	Tree	–25.0	27.8
	Dichrostachys cinerea	Shrub	–25.5	27.2
	Peltophorum africanum	Tree	–25.6	27.6
	Grewia flavescens	Shrub	–26.3	23.5
	Acacia karroo	Tree	–26.4	27.3
	Pappea capensis	Tree	–26.5	38.2
	Typha angustifolia	Emergent - spring	–26.6	38.0
	Sclerocarya caffra	Tree	–26.9	45.7
	Acacia caffra	Tree	–27.1	27.7
	Combretum imberbe	Tree	–27.2	51.1
	Acacia tortilis	Tree	–27.3	28.9
	Dombeya discolour	Tree	–27.4	25.6
	Dombeya rotundifolia	Tree	–27.6	34.5
	Flowering plant - unidentified	Flowering plant	–30.7	102.0

Table 3.4: $\delta^{13}C$ and C/N ratios of organic samples, excluding higher plants.

Description	Grid reference	$\delta^{13}C$ (‰) VPDB	C/N ratio
Leaf litter	25°24'43.5"S, 28°05'07.5"E	–25.1	32.0
Soil 1	25°24'44.7"S, 28°05'13.7"E	–20.9	13.7
Soil 2	25°24'44.7"S, 28°05'13.7"E	–23.4	12.0
Soil 3	25°24'43.5"S, 28°05'07.5"E	–22.7	12.6
Soil 4	25°24'43.9"S, 28°05'01.6"E	–24.0	12.1
Soil 5	25°24'41.9"S, 28°04'56.6"E	–23.6	13.1
Soil 6	25°24'35.3"S, 28°04'53.1"E	–20.1	13.1
Soil 7	25°24'32.6"S, 28°04'52.5"E	–18.9	12.8
Sediment - lake margin	25°24'34.0"S, 28°04'55.1"E	–18.0	9.7
Lake surface sediment - 0.1 m	25°24'33.6"S, 28°04'55.3"E	–17.9	11.2
Lake surface sediment - 0.5 m	25°24'33.7"S, 28°04'56.0"E	–18.2	10.4
Algal/cyanobacterial mat - lake margin	25°24'33.4"S, 28°04'55.0"E	–17.5	0.0
Algal/cyanobacterial mat - lake margin	25°24'33.1"S, 28°04'55.2"E	–17.5	16.3
Algal/cyanobacterial mat - lake margin	25°24'30.7"S, 28°04'53.3"E	–16.5	4.7
Algal/cyanobacterial mat - borehole 3 pool	25°24'30.4"S, 28°04'56.2"E	–8.6	7.4

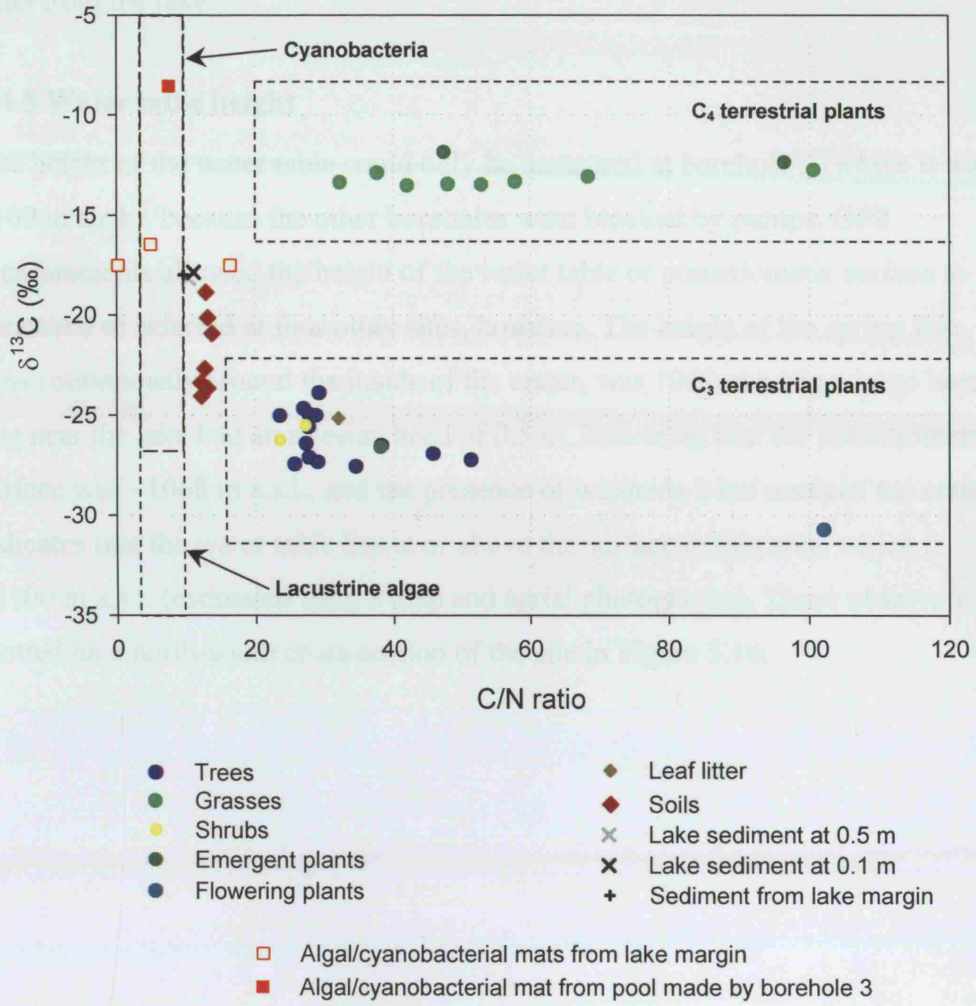

Figure 3.15: $\delta^{13}C$ values and C/N ratios of organic samples from Tswaing crater lake and its basin. Ranges of $\delta^{13}C$ values and C/N ratios representative of terrestrial C_3 and C_4 plants and aquatic organisms are shown as dashed rectangles (Tyson, 1995).

The samples of organic mats from marginal areas of the lake, which are composed of cyanobacteria and small quantities of diatoms (Schoeman and Ashton, 1982a; Ashton and Schoeman, 1985), have lower C/N ratios than the higher plants (0 to 16), and have $\delta^{13}C$ values that lie between those of the two groups of higher plants (–16.5‰ to –17.5‰). The organic mat from a pool fed by an artesian borehole has a C/N ratio of 7.4, which lies within the range of the other samples of aquatic material, but has a higher $\delta^{13}C$ value, of –8.6‰. Finally, the samples of sediment from the lake margin and from depths of 0.1 and 0.5 m within the lake have similar $\delta^{13}C$ values (–17.9‰ to

–18.2‰) and C/N ratios (9.7 to 11.2), which lie close to those of soils and the organic mats from the lake.

3.4.5 Water table height

The height of the water table could only be measured at borehole 5 (where it was 1109 m a.s.l.), because the other boreholes were blocked by pumps. GPS measurements allowed the height of the water table or potentiometic surface to be measured or inferred at four other sites, however. The height of the spring line, which runs continuously around the inside of the crater, was 1069 m a.s.l.; a large borehole dug near the lake had an artesian head of 0.5 m, indicating that the potentiometric surface was ~1068 m a.s.l.; and the presence of wetlands 2 km north of the crater indicates that the water table lies at or above the surface in this area, which is ~1100 m a.s.l. (estimated from a map and aerial photographs). These observations are plotted on a north-south cross-section of the site in Figure 3.16.

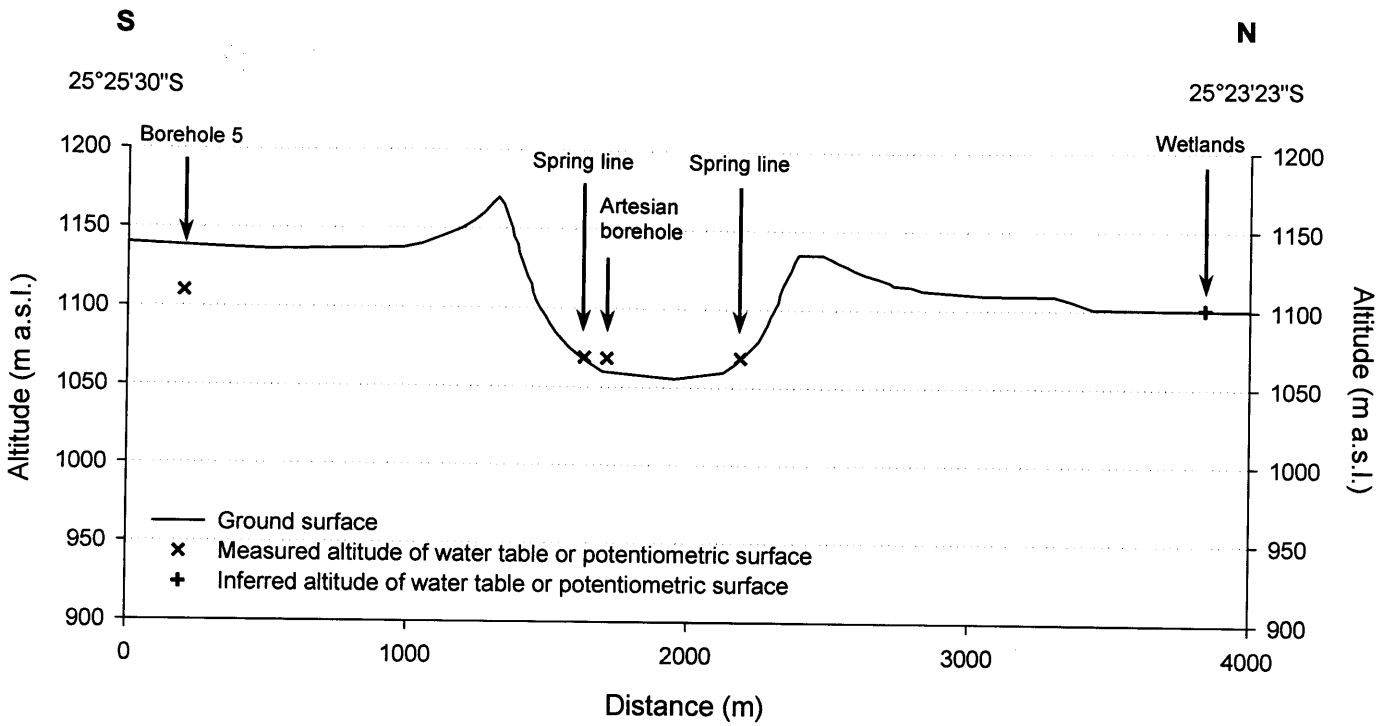

Figure 3.16: North-south cross-section through Tswaing crater (drawn using orthophoto map series number JR AC 17B), showing measured and inferred heights of the water table and potentiometic surface. Vertical exaggeration is 5.

3.5 Discussion

3.5.1 Hydrological setting

The $\delta^{18}O$ and $\delta^{2}H$ values of groundwater samples lie close to the GMWL, indicating that groundwater is recharged by meteoric water that has not been subject to significant evaporation (Fig. 3.11). The similarity of the isotope composition of these samples (except those from boreholes 2, 3 and 4) suggests that the meteoric water is well-mixed before it enters the groundwater system. It is therefore likely that the average $\delta^{18}O$ and $\delta^{2}H$ values of these samples ($\delta^{18}O = -4.4‰$, $\delta^{2}H = -28.2‰$) reflect the mean annual composition of precipitation that recharges groundwater, particularly as the samples were collected at different times of year over a period of eighteen years. These values are lower than the amount-weighted mean annual values of precipitation at Pretoria ($\delta^{18}O = -3.1‰$, $\delta^{2}H = -13.1‰$), which suggests that a disproportionately large amount of isotopically-light precipitation recharges local groundwater (IAEA/WMO, 2001; Vose *et al.*, 2002) (Fig. 3.11). This selective recharge probably occurs because a higher proportion of the rain that falls during heavy summer storms, which has lower average isotope values than rain that falls during light winter showers, enters the groundwater system before being evaporated (Figs. 3.5 and 3.6) (Vogel *et al.*, 1963).

It is notable that the groundwater samples lie closer to the GMWL than to the LMWL defined by precipitation at Pretoria (IAEA/WMO, 2001). Examination of the values used to construct the LMWL indicates that the gradient of this line is significantly affected by evaporation of precipitation that falls during light rainfall events (section 2.1.1). This effect decreases the gradient of the LMWL and thus decreases the fit of precipitation that is not subject to evaporation (such as the heavy rain that appears to recharge groundwater at Tswaing), which may explain the displacement of groundwater samples from this line (cf. Gat, 1996). It is also possible that the samples are displaced from both the GMWL and the LMWL because groundwater is recharged by a mixture of precipitation that is evaporated in the unsaturated zone and precipitation that enters the reservoir without evaporation, as this phenomenon

produces groundwater with values that are displaced from, but lie parallel to, MWLs (Allison *et al.*, 1983).

The samples of lake water lie to the right of the GMWL, on a LEL with a gradient of 4.4, demonstrating that the lake water is subject to evaporation. This line intercepts the GMWL at a $\delta^{18}O$ value of –5.8‰ and a $\delta^{2}H$ value of –36.2‰. These values are not significantly different from the average values of samples in the main cluster of groundwater samples ($\delta^{18}O$ = –4.4‰, $\delta^{2}H$ = –28.2‰), which suggests that the isotope composition of lake water reflects evaporation of groundwater. The high $\delta^{18}O$ and $\delta^{2}H$ values of the sample collected at a depth of 0.5 m relative to the samples of surface water demonstrates that the lake was stratified at the time of collection, and supports the proposal that stratification is due to evaporated, saline water forming a stable layer at depth, and less evaporated water forming a less dense layer at the surface (Ashton and Schoeman, 1983). The significant displacement of this sample along the LEL also suggests that water in the monimolimnion of the lake has been subject to evaporation without significant dilution for a long period of time, possibly since a permanent lake was re-established at the site in the second half of the twentieth century (section 3.2.7) (Ashton and Schoeman, 1983). The sample collected near the outlet of the artesian boreholes has the lowest isotope values of the lake water samples, suggesting that it represents a mixture of lake water and groundwater discharged from the boreholes.

The water sample from the stream to the east of the crater is also displaced to the right of the GMWL (although to a lesser extent than lake water), which indicates that it has also been affected by evaporation. The sample does not lie on the LEL defined by the lake water samples, however, which suggests that the stream is supplied by water with a different composition to that which supplies the lake and/or that it evaporates under different conditions (section 2.1.2) (Gat, 1971). It is difficult to explain the composition of a single sample with confidence, but it is likely that the composition of the stream partly reflects the composition of recent rainfall, rather than a long-term average (as is the case for the groundwater that supplies the lake) (cf. Darling *et al.*, 2006). Furthermore, stream water may have been subject to evaporation under conditions of lower relative humidity than lake water, due to higher wind speeds in the region surrounding the crater than in the crater itself (Ashton, 1999).

The samples of groundwater from the three boreholes to the east of the crater (boreholes 2, 3 and 4) have higher $\delta^{18}O$ and $\delta^{2}H$ values than the other groundwater samples, which suggests that the water supplying these boreholes may be different from that supplying the other sources of groundwater. A possible explanation for this difference is that that the boreholes east of the lake are shallower than the others sampled, and therefore reflect short-term fluctuations in the isotope composition of recharge water, rather than a long-term average (cf. Clark and Fritz, 1997). Alternatively, it is possible that the samples represent a mixture of the regional groundwater that supplies the other boreholes, and seepage from the stream east of the crater. This explanation is supported by the fact that all three boreholes lie close to this stream and by the observation that their isotope values lie close to the mixing line of stream water and the main cluster of groundwater samples (Figs. 3.10 and 3.11). McCaffrey and Harris (1996) proposed that lake-water seepage was responsible for the isotope composition of the sample from borehole 3, but this explanation is unlikely to be valid because the sample does not lie close to the LEL of lake water, and because water would have to leave the lake against groundwater flow into the crater, and without affecting the composition of water in artesian boreholes. Furthermore, the slope of the water table from south to north (Fig. 3.16) suggests that regional groundwater flow is northward, and it would therefore be unlikely for lake-water seepage to only affect groundwater composition to the east of the crater.

The geochemical analyses presented in Figure 3.12 also provide information about the hydrological setting at Tswaing. It is immediately evident that the groundwater supplied by the artesian boreholes has a significantly different geochemical composition to groundwater from other sources, as the samples from the artesian boreholes contain significantly higher mol% Na^{+} and Cl^{-}, and have higher conductivity values than the other groundwater samples (Fig. 3.12). This composition cannot result from the mixing of lake-water seepage and regional groundwater, because the mol% Cl^{-} of the water from the artesian boreholes is higher than that of both lake water and regional groundwater, and because the isotope analysis presented above demonstrates that water from the artesian boreholes is isotopically indistinguishable from regional groundwater. The chemical composition of water in the aquifer that supplies the artesian boreholes must, therefore, result from dissolution of local halite deposits, as suggested by Ashton and Schoeman (1983).

The geochemical composition of the samples also demonstrates that as rain water enters the regional groundwater system, it becomes enriched in HCO_3^- and CO_3^{2-} and Na^+ and K^+ ions, through processes such as absorption of CO_2 in the soil, weathering of silicate minerals, and the dissolution of small outcrops of carbonate minerals in the crater walls (Stumm and Morgan, 1970). The weathering of minerals also increases the conductivity of groundwater to ~200-600 µS/cm. The samples from boreholes 3 and 4 contain higher mol% Cl^- and, to a lesser extent, Na^+ than the other samples of regional groundwater, and their composition is thus more similar to lake water than the other samples. This finding was the basis of McCaffrey and Harris' (1996) proposal that water from boreholes east of the lake represents a mixture of regional groundwater and lake water seepage. As outlined above, this is unlikely to be the case, however, and it is therefore probable that the higher mol% Cl^- and Na^+ in these samples is due to mixing with stream water or the dissolution of halite deposits in the vicinity of the boreholes (cf. Eugster and Hardie, 1978).

The lake water is dominated by Na^+, Cl^-, and CO_3^{2-} ions, although one sample contains higher mol% Cl^- than the other samples (Fig. 3.12). The composition of the anomalous sample can probably be attributed to mixing of lake water with water from the artesian boreholes, as the ionic composition and the conductivity of this sample lie between those of the other lake water samples and samples from the artesian boreholes. The composition of the other lake water samples must be determined by the composition of inputs to the lake, and by within-lake processes that modify this composition (Eugster and Hardie, 1978). The principal inputs to the lake are regional groundwater (via springs) and the groundwater supplied by artesian boreholes, and this is reflected in the anionic composition of the lake water, which lies between the compositions of these sources (Fig. 3.12). In both these sources of water, the mol% of HCO_3^- and CO_3^{2-} is greater than the mol% of Ca^{2+} and Mg^{2+}. Evaporative concentration of water with this composition leads to the precipitation of alkaline earth carbonates, which removes Ca^{2+} and Mg^{2+} ions and increases the mol% of other cations (in this case Na^+) in the lake water (Eugster and Hardie, 1978). Further evaporation of water with this composition leads to the precipitation of minerals such as trona and halite (Eugster and Hardie, 1978). These minerals currently precipitate at the edge of Tswaing crater lake during the dry season (Ashton and Schoeman, 1983),

supporting the proposal that this pathway of mineral precipitation affected the composition of lake water in the past.

3.5.2 Inorganic carbon

The $\delta^{13}C_{DIC}$ of water from the vicinity of the lake provides information about the modern carbon cycle at the site. The low $\delta^{13}C_{DIC}$ of water from boreholes outside the crater (boreholes 2 and 5) is typical of groundwater, because isotopically-light CO_2 dissolves in groundwater as it passes through soils (section 2.1.3) (*e.g.* Andrews *et al.*, 1993, 1997). The $\delta^{13}C_{DIC}$ of groundwater entering the lake at the spring line and through artesian boreholes is between 5‰ and 13‰ higher than the samples from boreholes outside the crater (Fig. 3.14). The spring water and the sample from artesian borehole 3 may have relatively high $\delta^{13}C_{DIC}$ because they were collected from small pools, and exchange with atmospheric CO_2 and/or carbon fixation by algae and cyanobacteria in these pools may have increased $\delta^{13}C_{DIC}$ (section 2.1.3) (Park and Epstein, 1960; Mook *et al.*, 1974; Turner, 1982; McKenzie, 1985). These processes cannot explain the high $\delta^{13}C_{DIC}$ of the sample from artesian borehole 2, however, because this borehole is sealed from the atmosphere. The reaction of this water with lacustrine carbonates at depth may be responsible for its high $\delta^{13}C_{DIC}$, but it is not possible to confirm this hypothesis.

The $\delta^{13}C_{DIC}$ of lake surface water is higher than the $\delta^{13}C_{DIC}$ of all lake-water inputs, apart from artesian borehole 3. As with the pools of groundwater described above, the $\delta^{13}C_{DIC}$ of lake surface water may have increased due to exchange with atmospheric CO_2. The pH of the water is ~10.4, and most DIC must therefore be in the form of bicarbonate and carbonate (Ashton and Schoeman, 1983). At equilibrium with atmospheric CO_2, these forms of DIC would have $\delta^{13}C_{DIC}$ values of ~+0.5‰ (bicarbonate) and ~−1.5‰ (carbonate), which suggests that the lake surface water is close to isotope equilibrium, as the two samples of surface water have $\delta^{13}C_{DIC}$ values of −1.6‰ and −1.8‰ (section 2.1.3) (Mook *et al.*, 1974; Turner, 1982). It is also likely that photosynthesis has increased the $\delta^{13}C_{DIC}$ of lake water, because primary productivity in the lake is high, varying between 2 and 5 g C/m^2/day (Ashton and Schoeman, 1985; Ashton, 1999).

The $\delta^{13}C_{DIC}$ of the water sample from a depth of 0.5 m is ~3.6‰ higher than that of surface water. This situation is relatively unusual, because productivity usually increases $\delta^{13}C_{DIC}$ in the epilimnion, while decomposition of organic matter in the water column and sediments decreases $\delta^{13}C_{DIC}$ in the hypolimnion (section 2.1.3) (Park and Epstein, 1960; Williams and Gordon, 1970). The most likely explanation for high $\delta^{13}C_{DIC}$ at depth is the occurrence of methanogenesis in the organic-rich sediments (section 2.1.3) (Rosenfeld and Silverman, 1959; Stiller and Magaritz, 1974). Methanogenesis is most likely to occur in anaerobic environments when water temperatures and the supply of organic material are high, and sulphate concentrations are low (Talbot and Kelts, 1986; Ogrinc *et al.*, 2002, 2003). The high levels of productivity in the mixolimnion of Tswaing crater lake, combined with anoxic conditions, high temperatures, and low sulphate concentrations in the monimnolimnion, therefore mean that conditions in the lake sediments are suitable for methanogenesis, and that this process is likely to be responsible for the high $\delta^{13}C_{DIC}$ at depth (Ashton and Schoeman, 1983, 1985).

3.5.3 Organic carbon

The $\delta^{13}C$ values of terrestrial and emergent vegetation from the basin fall into the ranges characteristic of terrestrial C_3 and C_4 plants (Fig. 3.15) (Park and Epstein, 1960; Reibach and Benedict, 1977; O'Leary, 1981; Tyson, 1995; Meyers and Lallier-Vergès, 1999). It is unlikely that any of the plants use Crassulacean Acid Metabolism (CAM) to fix carbon, because none of them are succulents (section 2.1.4.1). All the grasses sampled lie in the range characteristic of C_4 plants, which are relatively abundant in the summer rainfall region of southern Africa due to the high growing season temperatures (section 2.1.4.1) (cf. Vogel, 1978). The C/N ratios of all the higher plants sampled are greater than 20, because they contain carbon-rich structural compounds such as cellulose and lignin (cf. Meyers, 1994; Raven *et al.*, 2004).

The $\delta^{13}C$ value and C/N ratio of the leaf litter sample lie within the range characteristic of terrestrial C_3 plants, suggesting that the sample was predominantly composed of material from C_3 vegetation. It is possible that the $\delta^{13}C$ value and C/N ratio of this sample were altered by the selective decay of organic compounds during decomposition, but it is unlikely that these changes were large enough to give a misleading picture of the sample's origin (section 2.1.4) (cf. Meyers, 1994, 1997).

The $\delta^{13}C$ values of the soil samples either lie within the range characteristic of terrestrial C_3 plants or between the ranges characteristic of C_3 and C_4 plants, indicating that soil in the catchment is derived from a mixture of C_3 and C_4 vegetation. Interestingly, the C/N ratios of all the soil samples are lower than those of the terrestrial plants that were sampled, suggesting that the C/N ratios of the soils do not reflect those of the vegetation from which they are derived. This offset may be due to carbon loss through respiration and leaching, combined with immobilisation of N-containing compounds during decomposition (*e.g.* Sollins *et al.*, 1984; Melillo *et al.*, 1989). It is also possible that the presence of microbial matter decreased the average C/N ratios of the soil samples analysed (Müller, 1977; Lehmann *et al.*, 2002).

The cyanobacteria and diatoms in the organic mats from the lake have $\delta^{13}C$ values between –16.5‰ and –17.5‰, and C/N ratios between 0 and 16. The low C/N ratios partly reflect the presence of nitrogen-rich compounds (such as petidoglycan in the case of cyanobacteria), and the lack of carbon-rich structural compounds such as lignin and cellulose in these organisms (cf. Meyers, 1994; Raven *et al.*, 2004). The extremely low values of some samples (<4) suggest that clays contributed inorganic nitrogen to the samples, however (section 2.3.2) (cf. Meyers and Teranes, 2001). The $\delta^{13}C$ of aquatic organisms reflects the $\delta^{13}C$ of their source of inorganic carbon, and isotope fractionation during photosynthesis (section 2.1.4.1). DIC in the lake surface water is in the form of bicarbonate and carbonate ions, and has an average $\delta^{13}C$ value of –1.7‰ (section 3.5.2), suggesting that aquatic organisms probably use bicarbonate ions with this composition as their source of inorganic carbon. The $\delta^{13}C$ of cyanobacteria using this source of inorganic carbon would be expected to lie between ~–18‰ and –24‰, while the $\delta^{13}C$ of diatoms would be expected to lie between –22‰ and –27‰ (section 2.1.4.1) (O'Leary, 1981; Guy *et al.*, 1993; Sakata *et al.*, 1997; Popp *et al.*, 1998). The $\delta^{13}C$ values of –16.5‰ to –17.5‰ for aquatic material from the lake are thus in fairly good agreement with the upper value expected for cyanobacteria, which is in accord with the observation that the biomass of the lake is dominated by these organisms (Ashton and Schoeman, 1985). The fact that the values observed are slightly higher than those expected might be because reduced fractionation against ^{13}C under conditions of carbon limitation (caused by low levels of DIC or by limited diffusion through organic mats or the boundary layer of organisms) also acted to increase the $\delta^{13}C$ of aquatic organisms (section 2.1.4.1).

The $\delta^{13}C$ of the organic mat from the pool supplied by an artesian borehole is 8-9‰ higher than the $\delta^{13}C$ of the organic mat samples from the lake. The $\delta^{13}C_{DIC}$ of the pool is ~3‰ higher than that of lake surface water, which accounts for some of the offset, but cannot explain it all. It is possible that the high $\delta^{13}C$ of this sample is caused by diffusion limitation of DIC. This process is known to occur in organic mats when photosynthesis is occurring rapidly, because the rate of photosynthesis is limited by the rate at which DIC diffuses into the mat, and it can also occur in benthic algae due to boundary layer effects (section 2.1.4.1). It leads to reduced discrimination against ^{13}C, and thus to higher $\delta^{13}C$ values of organic matter (cf. Schidlowski *et al.*, 1984; Des Marais and Canfield, 1994; Hecky and Hesslein, 1995; Lawson *et al.*, 2004).

The average $\delta^{13}C$ and C/N values of bulk organic matter in the samples of lake sediments from 0.1 and 0.5 m are –18.0‰ and 10.8, respectively. These values are similar to those of both organic mats in the lake and soils in the catchment, suggesting that organic material deposited in the lake is primarily derived from these sources (Fig. 3.15). The high rates of primary production in the lake suggest that, in fact, most material is probably derived from aquatic organisms, but it is not possible to exclude the possibility that soils in the catchment are also a significant source of organic material in the lake. The $\delta^{13}C$ and C/N ratios of organic matter in sediments from the lake margin are indistinguishable from those of organic matter in the lake sediments at greater depths, and are thus also similar to the values of organic mats in the lake and soils in the catchment. This finding provides support for the suggestion that sediments on the lake margin are dominated by the organic mats that grow in littoral areas of the lake (Ashton and Schoeman, 1985; Ashton, 1999), and thus hints that the organic material in sediments at greater depths is also dominated by aquatic organisms.

3.6 Conclusions

The $\delta^{18}O$ and $\delta^{2}H$ values of water samples from the vicinity of Tswaing crater lake, when considered in conjunction with geochemical data and information about the height of the water table, provide considerable information about the hydrological setting of this water body. The most significant sources of water to the lake are: springs in the crater wall, which are present because the floor of the crater lies below

the local water table; and boreholes drilled through the lake sediments, which supply water from an artesian aquifer below the floor of the lake. The $\delta^{18}O$ and $\delta^{2}H$ values of these sources indicate that they are both derived from local precipitation, with selective recharge by heavy summer storms, and that they are not subject to evaporative concentration. The water supplying the artesian boreholes is, however, enriched in Na^{+} and Cl^{-}, and has higher conductivity values than regional groundwater; characteristics that probably reflect dissolution of local halite deposits. After water enters the lake, it is subject to significant evaporative concentration, which increases its conductivity and changes its geochemical composition by causing minerals to precipitate (cf. Eugster and Hardie, 1978).

There is no surface outflow from the lake, but the nature of subsurface flow is less clear. Water from boreholes to the east of the crater have slightly higher $\delta^{18}O$ and $\delta^{2}H$ values than other groundwater samples, and also contain higher mol% Na^{+} and Cl^{-}, which could conceivably result from mixing of lake water seepage and groundwater (McCaffrey and Harris, 1996). This is unlikely, however, because the isotope values of the samples are not significantly displaced from the meteoric water line, and do not lie on the mixing line between lake water and regional groundwater. In addition, water leaving the lake would have to move against the flow of groundwater into the crater, as well as the north-south flow of regional groundwater. An alternative interpretation is that the composition of groundwater east of the crater is influenced by seepage from a stream in this area. Together, these results suggest that the lake is hydrologically closed, and effectively acts as an evaporating pan for regional groundwater.

These findings have implications for the interpretation of stable isotope records from the lacustrine sediments in the basin, as they indicate that the lake has a long residence time, and that the $\delta^{18}O$ and $\delta^{2}H$ values of lake water are primarily determined by the I/E ratio of the lake (section 2.1.2). It is therefore likely that the $\delta^{18}O_{calcite}$ record from the sedimentary sequence, which is determined by the isotope composition and temperature of lake water, provides a record of the I/E ratio in the basin, and that any variations caused by changes in the $\delta^{18}O$ of precipitation or the temperature of lake water were obscured by changes in this ratio (section 2.2.2) (cf. Leng and Marshall, 2004). Furthermore, it is notable that the steady-state isotope

composition of the lake water (and thus $\delta^{18}O_{calcite}$) will be independent of lake volume, as this value is determined by the I/E ratio, and this ratio is always 1 at steady-state in hydrologically closed basins (section 2.1.2) (Gat, 1995).

$\delta^{13}C_{DIC}$ of water samples from within and around the lake provide information about the carbon cycle at the site. The $\delta^{13}C_{DIC}$ of lake surface water is higher than the $\delta^{13}C_{DIC}$ of water inputs to the lake. This finding can be attributed to the high proportion of DIC in the lake in the form of bicarbonate and carbonate (as these species are enriched in ^{13}C relative to dissolved CO_2), equilibration of DIC in the surface water with atmospheric CO_2, and high rates of primary productivity in the mixolimnion. The $\delta^{13}C_{DIC}$ of water in the monimolimnion is higher than that in the mixolimnion, which is probably due to the release of isotopically-heavy carbon during methanogenesis in the warm, organic-rich, anoxic sediments.

These findings provide some indication of the factors that may have influenced the record of $\delta^{13}C_{calcite}$ from the sedimentary sequence, as this record reflects $\delta^{13}C_{DIC}$ (section 2.2.3). The long residence time of the lake indicates that $\delta^{13}C_{DIC}$ may tend towards equilibrium with atmospheric CO_2, and it is therefore possible that changes in the rate of water input or output that disturbed this equilibrium affected $\delta^{13}C_{calcite}$ (section 2.1.3). In particular, the importance of the I/E ratio in the hydrological balance of the lake suggests that evaporative concentration may have increased $\delta^{13}C_{DIC}$, and thus $\delta^{13}C_{calcite}$, while increased input of isotopically-light water may have decreased $\delta^{13}C_{DIC}$ and $\delta^{13}C_{calcite}$ (Talbot and Kelts, 1990; Cole *et al.*, 1994; Mees *et al.*, 1998). In addition, the suggestion that methanogenesis currently increases $\delta^{13}C_{DIC}$ in the monimolimnion of the lake indicates that this process may have influenced $\delta^{13}C_{calcite}$, particularly if it induced authigenic carbonate precipitation from isotopically-heavy pore water (sections 2.1.3 and 2.2.5) (Talbot and Kelts, 1986, 1990).

The $\delta^{13}C$ and C/N ratios of vegetation around the lake show that grasses and some emergent vegetation in the vicinity of the lake use the C_4 pathway of photosynthesis, but that all the trees, shrubs, and flowering plants sampled, which form the majority of the vegetation in the basin, use the C_3 pathway of photosynthesis. These plants decay to form soils that have relatively low C/N ratios, indicating that decomposition

leads to a greater loss of carbon than nitrogen. The $\delta^{13}C$ values of aquatic organisms are relatively high, which probably reflects the high $\delta^{13}C_{DIC}$ of lake surface water, the fact that most aquatic organisms probably use bicarbonate ions as their source of inorganic carbon, the relatively low fractionation against ^{13}C by cyanobacteria, and reduced fractionation against ^{13}C under conditions of carbon limitation. The $\delta^{13}C$ and C/N ratios of bulk organic matter in the lake sediments are similar to the values of aquatic organisms, suggesting that the majority of organic matter input to the lake sediments is autochthonous, although soil from the catchment may also contribute to this material.

These results indicate that the C/N ratios of bulk organic matter in the lake sediments probably provide an accurate indication of the proportion of organic material derived from terrestrial and emergent vegetation relative to that derived from aquatic organisms, as these sources have significantly different C/N ratios. In addition, the $\delta^{13}C$ of aquatic organisms is probably higher than the average $\delta^{13}C$ of terrestrial and emergent vegetation, which suggests that the record of $\delta^{13}C_{organic}$ from the lake sediments could also provide insights into the origin of organic matter deposited in the lake. Changes in the $\delta^{13}C$ of aquatic organisms and the relative proportions of C_3 and C_4 vegetation in the catchment in the past are likely to complicate this relationship, however.

The information presented in this chapter thus provides considerable insight into the processes that currently operate at Tswaing crater lake, and potentially provides an important basis from which to interpret records of palaeoenvironmental change from the basin.

Chapter 4: Age-depth model for sediments from Tswaing crater lake

4.1 Introduction

The sediments deposited in Tswaing crater lake currently provide the longest terrestrial records of palaeoclimatic change in southern Africa (Partridge *et al.*, 1999, and references therein). The reliability of these records is limited by poor chronological control beyond the limits of radiocarbon dating, however (chapter 1). Partridge *et al.* (1997) constructed an age-depth model for the sediments by removing mass-flow deposits from the sequence to correct the depth model, and then linearly interpolating between seven radiocarbon dates in the upper 18 m of the sequence and extrapolating the average sedimentation rate in this section to the rest of the sequence (Fig. 4.1). This model was then modified slightly below 18 m by tuning the record of MAP from the sediments to calculated values of January insolation at 30°S (Partridge *et al.*, 1997). The resulting model suggests that the base of the sequence was deposited 200 kyr B.P.; a finding that is in agreement with a fission-track date for crater formation of 220 ± 52 kyr B.P. (Fig. 4.1) (Storzer *et al.*, 1993, 1999; Koeberl *et al.*, 1994).

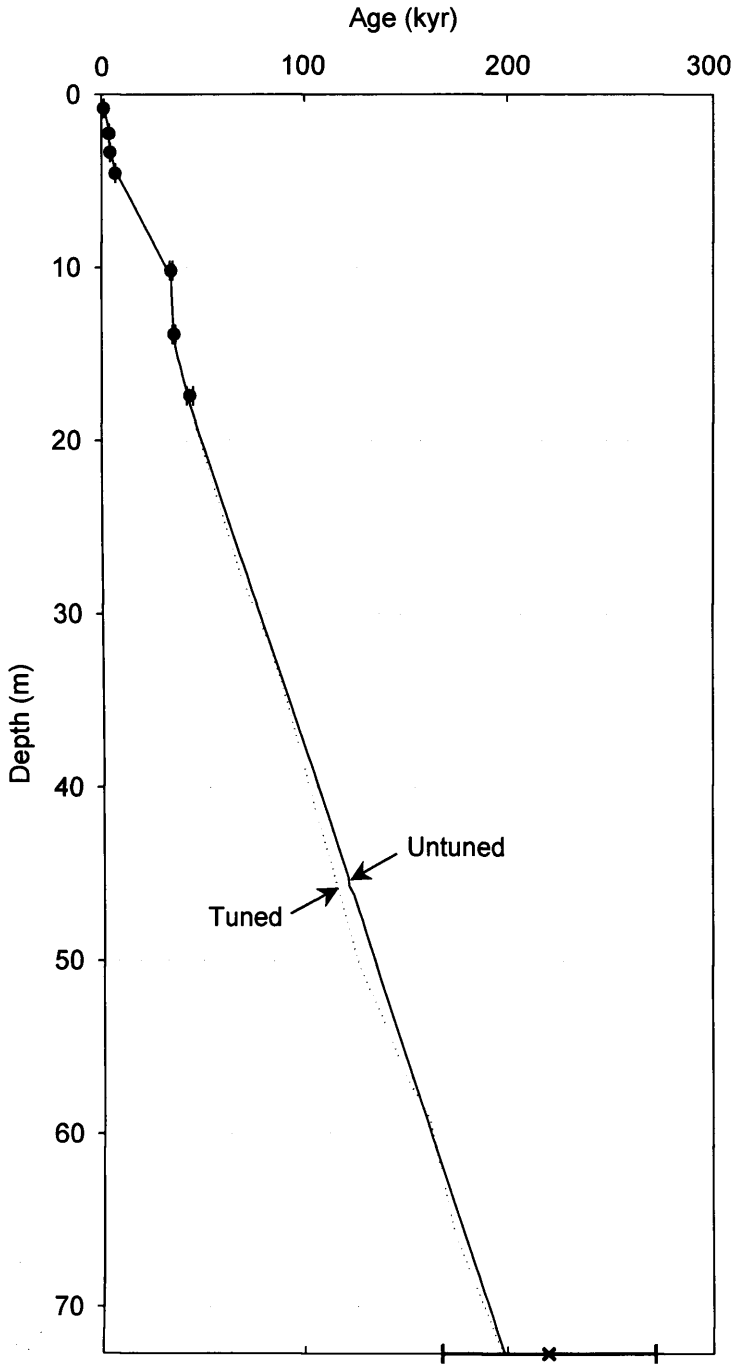

Figure 4.1: Age-depth model constructed for the sedimentary sequence from Tswaing crater lake by Partridge *et al.* (1997). Filled circles are radiocarbon dates on bulk organic matter (Partridge *et al.*, 1993, 1997), and the cross is a fission-track date for crater formation (Storzer *et al.*, 1993, 1999; Koeberl *et al.*, 1994) (errors are 1 s.d.). Solid line is the untuned model, and dotted line is the model constructed by tuning a record of MAP to January insolation at 30°S below 18 m.

$^{230}Th/^{234}U$ dating has the potential to improve this model by allowing absolute dates to be produced from the lower, previously undated section of the sediments. This method is based on the fact that minerals that precipitate from water contain significant quantities of uranium but negligible amounts of thorium, and that after a mineral precipitates, ^{234}U decays to form ^{230}Th until the isotopes reach secular equilibrium. Thus, as long as the mineral remains a closed system with respect to the isotopes in the decay chain, the extent of disequilibrium between ^{230}Th and ^{234}U can be used to determine the age of the mineral (Potratz *et al.*, 1955; Barnes *et al.*, 1956).

The dating of lacustrine sediments using this method is complicated by the fact that the minerals being dated cannot be separated from detrital material, which also contains uranium and thorium (cf. Schwarcz, 1989). Detritally-derived isotopes can, however, be corrected for by measuring the abundance of the long-lived nuclide ^{232}Th, which serves as a measure of detrital contamination. The most rigorous means of applying this correction is the total sample dissolution (TSD) isochron approach. This method involves analysing samples of the same age that contain different proportions of the mineral being dated and detrital material, and using these values to construct mixing lines between the two end-members (Osmond *et al.*, 1970; Rosholt, 1976; Bischoff and Fitzpatrick, 1991; Luo and Ku, 1991) (section 4.2.1).

This chapter presents five $^{230}Th/^{234}U$ dates on carbonates from new cores of the lacustrine sediments at Tswaing crater lake that were obtained using the TSD isochron approach. These dates are used, together with three radiocarbon dates on the new cores, seven radiocarbon dates on a previous core, and an estimated age for the top of the sediments, to construct a new age-depth model for the sediments. This model is significantly different from that presented by Partridge *et al.* (1997), because it suggests that the sequence covers ~320 kyr, rather than ~200 kyr. The new $^{230}Th/^{234}U$ dates appear to be reliable, but further dating is needed to confirm that this is the case. The new model is therefore presented as an alternative to, rather than a replacement of, the model presented by Partridge *et al.* (1997).

4.2 Theoretical background

4.2.1 $^{230}Th/^{234}U$ dating

Minerals that precipitate from water contain significant quantities of uranium but negligible amounts of thorium, because uranium is highly soluble in oxic water but thorium is insoluble (cf. Ivanovich and Harmon, 1992). After a mineral precipitates, the ^{234}U present decays to form ^{230}Th until the activity (disintegrations per unit time per unit weight of material) of the daughter isotope is equal to that of the parent, and the isotopes are said to be at secular equilibrium. If the mineral remains a closed system with respect to the isotopes in the decay chain, the time that has elapsed since the mineral precipitated can thus be determined from the extent of disequilibrium between ^{230}Th and ^{234}U (Potratz *et al.*, 1955; Barnes *et al.*, 1956). This relationship can be expressed as:

$$\frac{^{230}Th}{^{234}U} = 1 - e^{-\lambda_{230} t} \qquad (4.1)$$

where ^{230}Th and ^{234}U are the activities of these isotopes in the sample, λ_{230} is the decay constant of ^{230}Th, and t is the time that has elapsed since the mineral precipitated.

This relationship is dependent on ^{238}U, which decays to form ^{234}U, being in secular equilibrium with ^{234}U, because it assumes that the activity of ^{234}U is equal to the activity of ^{238}U. This is rarely the case in natural waters, and excess ^{234}U is consequently incorporated into most minerals when they precipitate (Cherdyntsev, 1955). This excess ^{234}U decays to form ^{230}Th and disrupts the relationship between $^{230}Th/^{234}U$ and time described in equation 4.1. The $^{234}U/^{238}U$ activity ratio of a sample must therefore be taken into account when dating minerals, according to the following equation:

$$\frac{^{230}Th}{^{234}U} = \frac{^{238}U}{^{234}U}\left(1 - e^{-\lambda_{230} t}\right) + \left(1 - \frac{^{238}U}{^{234}U}\right)\frac{\lambda_{230}}{\lambda_{230} - \lambda_{234}}\left(1 - e^{-(\lambda_{230} - \lambda_{234})t}\right) \qquad (4.2)$$

where ^{230}Th, ^{234}U, and ^{238}U are the activities of these isotopes in the sample, λ_{230} and λ_{234} are the decay constants of ^{230}Th and ^{234}U, respectively, and t is the time since the mineral precipitated (Kaufman and Broecker, 1965). This relationship is the basis of the $^{230}Th/^{234}U$ method of dating minerals that precipitate from natural waters (cf. Ivanovich and Harmon, 1992).

The use of this method to date carbonates is often complicated by the presence of detrital material that contains ^{238}U, ^{234}U and ^{230}Th, because the addition of these isotopes invalidates the use of equation 4.2 to determine the age of the sample (cf. Schwarcz, 1989). Detritus is usually inseparable from the carbonate being dated, and a correction must therefore be made for the isotopes contributed by the detritus. ^{232}Th is not part of the ^{238}U-^{206}Pb decay chain, and the amount of ^{232}Th present in a sample therefore reflects the amount of detrital contamination. Until recently, it was assumed that if the $^{230}Th/^{232}Th$ activity ratio of a sample was greater than 20 (as is often the case in speleothems and coral), contamination of the carbonate was negligible, and the sample's isotope ratios could therefore be used to determine the age of the carbonate without correction (Sutcliffe *et al.*, 1985; Schwarcz, 1989). Improved analytical precision means that this assumption should now only be made if the $^{230}Th/^{232}Th$ activity ratio of a sample is greater than ~100 (Gilmour, pers. com.).

The most rigorous way of correcting for the presence of isotopes derived from detritus is the isochron approach, which avoids the need to make assumptions about the isotope composition of detrital material (cf. Kaufman and Broecker, 1965; Osmond *et al.*, 1970). This method involves analysing samples of the same age that contain different proportions of detritus and carbonate. The activity ratios of the samples can then be plotted, and if the samples are actually mixtures of the two end members (carbonate that precipitated at a specific time and homogenous detritus), they will fall on a mixing line. When the samples are plotted on the axes: $^{230}Th/^{232}Th$ against $^{234}U/^{232}Th$, and $^{234}U/^{232}Th$ against $^{238}U/^{232}Th$, the gradients of the two mixing lines give the $^{230}Th/^{234}U$ and $^{234}U/^{238}U$ activity ratios of the carbonate in the sample, which can then be used to calculate its age using equation 4.2 (Rosholt, 1976).

In order to obtain samples of the same age but with different ratios of carbonate to detritus, early workers suggested that carbonate should be leached from a single

sample, and that various combinations of the bulk sample, leachates, and residue should be analysed and plotted on mixing lines (Szabo and Sterr, 1978; Szabo and Butzer, 1979; Schwarz and Latham, 1989). These approaches are based on one of the following assumptions: that isotopes do not undergo differential fractionation on leaching, that any differential fractionation that occurs is constant, or that the isotopes in the detritus are in secular equilibrium (cf. Bischoff and Fitzpatrick, 1991; Ivanovich and Harmon, 1992). These conditions are difficult to meet, and the reliability of this method is therefore questionable (Bischoff and Fitzpatrick, 1991; but see Pelegrina and Martínez-Aguirre (2005) for a successful application).

Bischoff and Fitzpatrick (1991) and Luo and Ku (1991) proposed that this problem can be overcome if samples that are effectively contemporaneous (*e.g.* samples from a short section of a lake core), but that contain varying proportions of detritus, are used to construct mixing lines after analysis by total sample dissolution (TSD). Theoretically, this method reduces the precision of the isochron approach because it assumes that carbonates from different samples are the same age, but if the samples chosen for each mixing line are close enough in age, this source of error is insignificant because it is less than the analytical error associated with isotope measurements. The limitation of this technique is that it is often difficult to select samples that have enough variation in the ratio of carbonate to detritus to construct reliable mixing lines.

A number of methods have been proposed to quantify the errors associated with dates obtained using mixing-line plots. The error associated with the activity ratio of isotopes is calculated by:

$$2\sigma_{(a/b)} = \frac{a}{b}\sqrt{\left(\frac{2\sigma_a}{y_a}\right)^2 + \left(\frac{2\sigma_b}{y_b}\right)^2} \qquad (4.3)$$

where $\sigma_{(a/b)}$ is the standard deviation of the activity ratio of two isotopes a and b, σ_a and σ_b are the standard deviations associated with the measured concentrations of isotopes a and b, and y_a and y_b are the absolute concentrations of isotopes a and b.

These errors can be plotted on mixing-line plots, but they should not be used to weight the mixing lines because samples that contain little detritus also contain little ^{232}Th and thus have large errors associated with their activity ratios, even though they provide the most accurate indication of the composition of the carbonate being dated (Schwarcz and Latham, 1989).

The scatter of points around the mixing lines is indicative of whether the carbonate has remained closed to the relevant isotopes since its formation and of whether the carbonate and detritus in the samples used for each mixing line are homogenous, as well as of analytical error. Luo and Ku (1991) proposed that this scatter, together with the errors associated with the activity ratios of $^{230}Th/^{234}U$, $^{232}Th/^{234}U$, and $^{234}U/^{238}U$ used to construct the mixing lines (equation 4.3), should therefore be used to assess the error associated with a date. For the mixing line used to obtain the $^{230}Th/^{234}U$ activity ratio of carbonate in a sample, the error associated with the slope of the line (U), and thus with the $^{230}Th/^{234}U$ ratio, is given by:

$$\sigma_U = \frac{\sqrt{\sum(\sigma_{ui}^2 + E^2\sigma_{vi}^2 + v_i^2\sigma_E^2)}}{n} \qquad (4.4)$$

where, σ_U is the standard deviation of the gradient of the line U, v_i is $^{232}Th/^{234}U$ for sample i, σ_{ui} and σ_{vi} are the standard deviations of $^{230}Th/^{234}U$ and $^{232}Th/^{234}U$ for sample i, E is the intercept of the mixing line, σ_E is the standard deviation of E, and n is the number of samples used to construct the mixing line. σ_E is given by:

$$\sigma_E^2 = \frac{U^2}{(n-2)} \frac{\sum v_i^{-2}}{n} \left(\frac{1-R^2}{R^2} \right) \qquad (4.5)$$

where R^2 is the coefficient of determination of the slope of the mixing line. In the case of the mixing line used to obtain the $^{234}U/^{238}U$ activity ratio of carbonate in a sample, the error of the slope of the mixing line (W) can be calculated using a modified version of equation 4.4, which often simplifies to:

$$\sigma_W = \frac{\sqrt{\sum \sigma_{wi}^2}}{n} \qquad (4.6)$$

where σ_{wi} is the standard deviation of $^{234}U/^{238}U$ for sample *i*. The errors generated by these equations are conservative, because they do not account for the error correlation that results from the common component of the activity ratios used to calculate them (Bischoff and Fitzpatrick, 1991). They are widely considered to give satisfactory results, however (Bischoff and Fitzpatrick, 1991; Luo and Ku, 1991; Ku *et al.*, 1998).

Ludwig and Titterington (1994) proposed that this approach is not a satisfactory method of deriving ages because the plots used to obtain the activity ratios of the mineral being dated have a common axis ($^{234}U/^{232}Th$), and consequently the slopes of the two mixing lines are not independent. They therefore advocated the construction of mixing lines in three-dimensional space using maximum-likelihood regression. They also proposed that the errors associated with dates should be calculated using maximum-likelihood estimation (MLE), in which the amount of scatter around mixing lines is described by the mean square of weighted deviates (MSWD). The errors derived using this approach are often significantly larger than those derived using equations 4.4 and 4.6 (Ludwig and Titterington, 1994). Ku *et al.* (1998) proposed that is because MLE requires a large number of data points to make error estimates on mixing lines meaningful, and that equations 4.4 and 4.6 are therefore most appropriate when a small number of samples (3-4) is used to construct mixing lines (cf. Bevington, 1969; Titterington and Halliday, 1979).

Until the 1980s, the isotope activities necessary to apply the $^{230}Th/^{234}U$ dating method could only be measured using alpha spectrometry, which involves counting the number of alpha particles emitted from a sample as a result of isotope decay. Today, thermal ionisation mass spectrometry (TIMS) is frequently used to measure the relevant activity ratios, because the measurements are more precise (±0.5% compared to ±5-10% by alpha spectrometry), more rapid, and require less material (Edwards *et al.*, 1987).

4.2.2 Age-depth models

The construction of accurate age-depth models is an essential component of palaeoenvironmental studies based on stratigraphic sequences. Unfortunately, this task is usually complicated by uncertainties associated with the sedimentary sequence and the available age-determinations. Furthermore, financial or methodological limitations often limit the number of age-determinations that can be obtained from a given sequence.

Various models can be used to fit age-depth relationships to the age-determinations that are available (cf. Bennett, 1994; Telford *et al.*, 2004b). In general, the optimum model for a given sedimentary sequence depends on the accuracy, number, and spacing of available age-determinations, and on the information available about changes in sedimentation rate over the sequence. Models that pass through every date, such as linear and spline interpolation, make the assumption that the age-determinations are "true", and that changes in sedimentation rate therefore occur at the depth of the age-determinations. These models have the advantage that the model cannot deviate too far from reality, but also incorporate noise associated with the age-determinations (Telford *et al.*, 2004b). Such models are therefore most appropriate where there are a large number of dates, or where changes in sedimentation rate have been identified and dated (Telford *et al.*, 2004b).

Where few age-determinations are available, polynomial models may be more appropriate because they increase the number of dates involved in the estimation of the age of sediment at any given depth, and thus reduce the dependence on individual dates (Bennett, 1994). These models make the important assumption that sedimentation rates change according to the order of the polynomial used to fit the model, which may not be the case. In addition, the use of low-order polynomials may introduce inaccuracies if age-determinations in one part of the sequence have a disproportionately high influence on the model in other parts of the sequence, while high-order polynomials may "over-fit" the data by fitting the model to noise associated with the age-depth determinations. Telford *et al.* (2004b) concluded that no model reliably performs well when there are few age-determinations available, and thus highlighted the importance of obtaining as many dates on a sequence as possible.

4.3 Methods

4.3.1 The sedimentary sequence

Two cores of the sediments deposited in Tswaing crater lake were obtained by Soiltech, a division of Franki Africa Ltd, between November 2001 and February 2002. The drilling was carried out through the end of a solid promontory that was built to facilitate salt-production at the crater (section 3.2.7) (Fig. 4.2). This site is located approximately half way between the centre of the lake and the shore, and is therefore unlikely to lie in the naturally deepest part of the lake (Figs. 1.5 and 3.7). It has probably remained in the zone of sediment accumulation throughout the lake's history, however, and was considered preferable to a site closer to the centre of the lake due to the ease of drilling through the promontory (Partridge, pers. comm.).

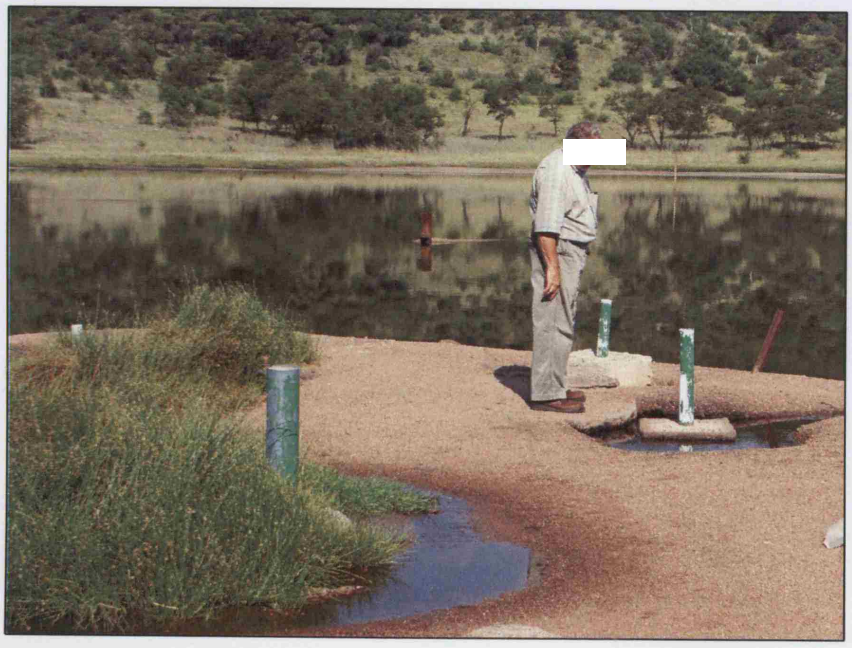

Figure 4.2: Photograph of the drill-site at Tswaing crater lake, which lies at the end of a promontory that extends into the lake (cf. Figure 1.5). The drill holes made during coring sessions in 1988/89 and 2001/02 are marked by green pipes. Photograph taken by the author in February 2005.

The upper part of the first core (TSW-1) was obtained using Shelby tube drilling, which provides good sediment recovery and little drilling disturbance, but drilling became too difficult to continue using this method at ~40 m. This core was therefore re-drilled from a depth of 30 m in a different drill-hole (TSW-1B) using wireline rotary core drilling with a triple-tube core barrel. This method provides less-complete sediment recovery and more drilling disturbance than Shelby tube drilling, but is able to penetrate the gravel layers present in the sediments (LeRoy and Colman, 2001). The second core (TSW-2) was collected from a single drill-hole using only wireline rotary core drilling. The core sections were transported to GFZ, Potsdam, where they are stored in refrigerated containers. The stratigraphy of the sediment cores is summarised in Figure 4.3 (as accurately as possible, given the resolution that can be achieved) (see Figure A1, Appendix A for the stratigraphy of the core obtained in 1988/89).

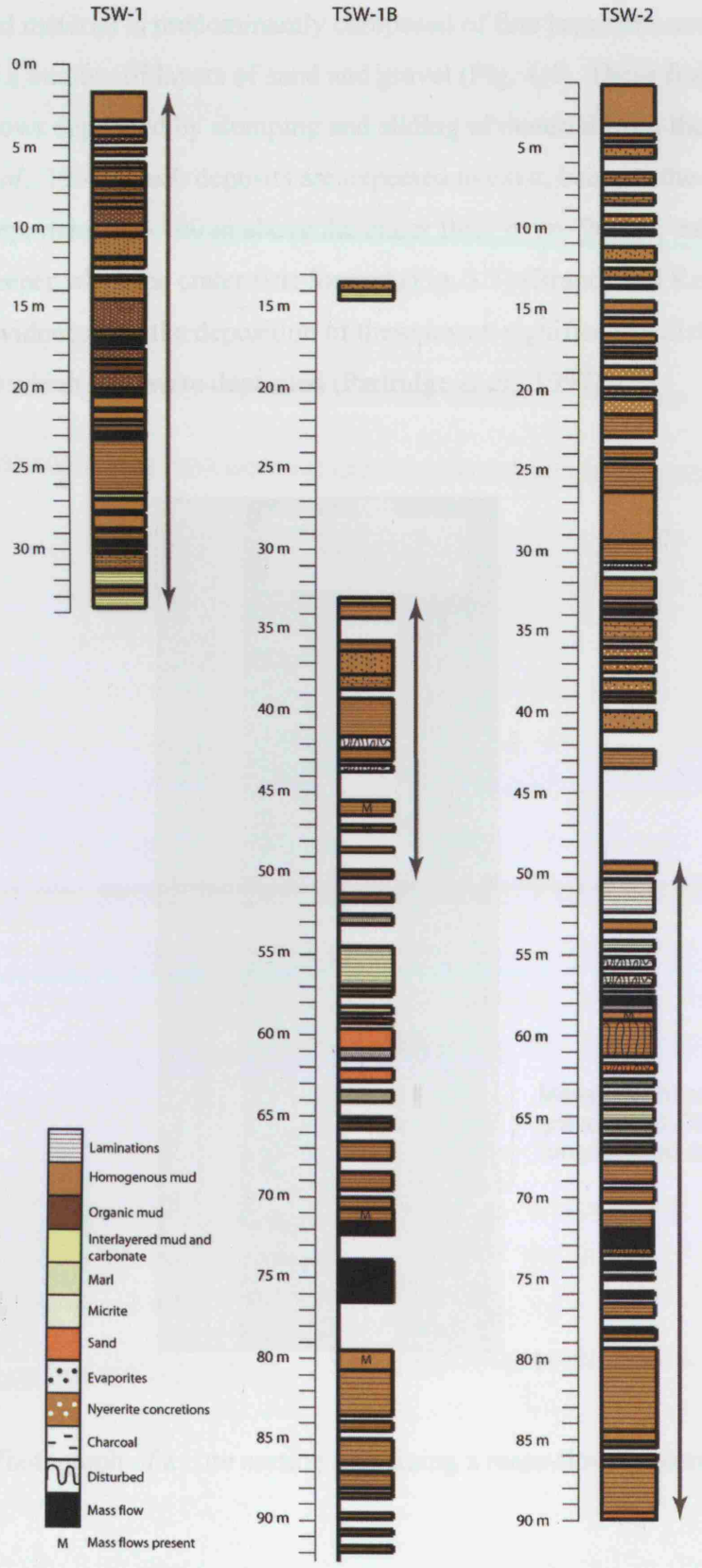

Figure 4.3: Stratigraphy of the sediment cores recovered from Tswaing crater lake (based on sedimentological descriptions by Prof. T.C. Partridge). Thick grey arrows indicate approximate sections of cores used to compile a single sedimentary sequence.

The recovered material is predominantly composed of fine lacustrine sediment, but also contains a number of layers of sand and gravel (Fig. 4.4). These features appear to be mass-flows deposited by slumping and sliding of material from the crater walls (Partridge *et al.*, 1993). Such deposits are expected to exist, because the walls of the crater are steep, rising to ~100 m above the crater floor over ~200 m, and would have been even steeper when the crater first formed (Fig. 3.7) (Brandt and Reimold, 1999). There is no evidence that the deposition of these layers significantly disturbed the sediments on which they were deposited (Partridge *et al.*, 1997).

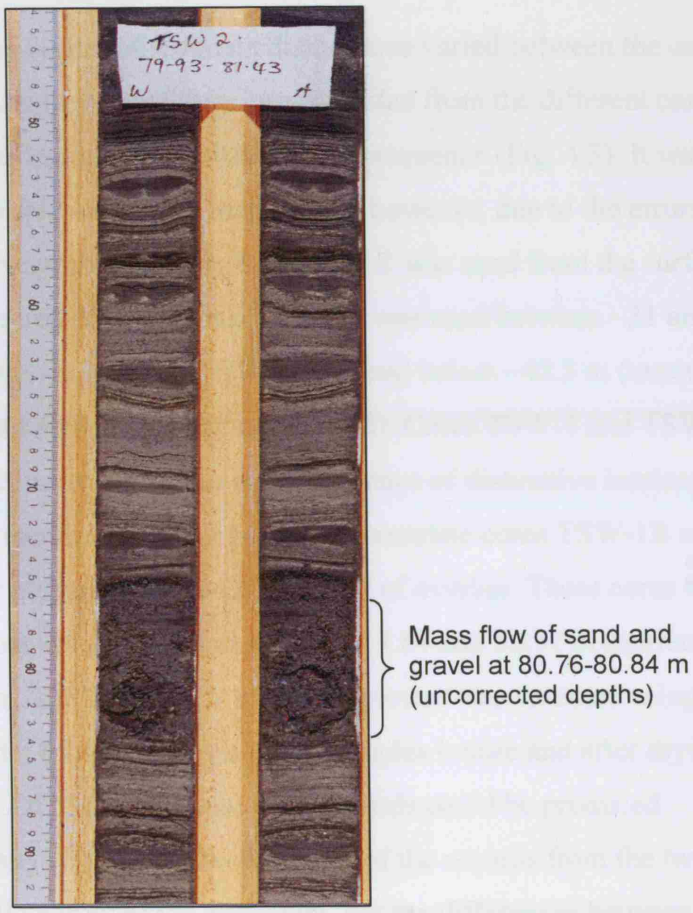

Figure 4.4: Photograph of a core section containing a mass-flow deposit of sand and gravel.

The mass-flow deposits were removed from the depth model of the sedimentary sequence to create a corrected depth scale because they represent instantaneous events, and are therefore unrepresentative of average sedimentation rates (cf.

Partridge *et al.*, 1997). In six instances, mass-flow deposits were found at the end of one core section and at the start of the subsequent section, and material was missing from the bottom of the upper core-liner. In these cases, it was assumed that the missing material was part of the mass flow, and that it was lost during core recovery due to its coarse texture. Other gaps in the sedimentary sequence caused by incomplete core recovery do not appear to be related to mass-flow deposits, however, and consequently were not used to adjust the depth scale. This correction procedure reduced the length of the sedimentary sequence from 89.97 m to 76.82 m. All depths quoted in this thesis are on this corrected depth scale, unless otherwise stated.

Sediment recovery and the degree of sediment disturbance varied between the cores, and a single sedimentary sequence was therefore compiled from the different cores to minimise the gaps and the degree of disturbance in the sequence (Fig. 4.3). It was considered undesirable to splice the cores many times, however, due to the errors that could be introduced when correlating them. Core TSW-1 was used from the surface to a depth of ~31 m (uncorrected depth ~34 m), TSW-1B was used between ~31 and ~42.5 m (uncorrected depth ~50 m), and TSW-2 was used below ~42.5 m (exact depths are not given because the cores were overlapped). Cores TSW-1 and TSW-1B could be correlated at millimetre scales due to the presence of distinctive laminations in the overlap zone. This method could not be used to correlate cores TSW-1B and TSW-2, however, as they are not laminated in the zone of overlap. These cores were therefore aligned using four visual tie-points between 54.84 and 55.37 m (corrected depths 46.94 and 47.47 m), and the validity of this alignment was assessed using records of percentage water (obtained by weighing samples before and after drying at 105°C overnight) and %LOI 550°C, because these records could be produced relatively quickly and easily (Fig. 4.5). The similarity of the records from the two cores confirms the overall validity of the alignment, but the differences between them also highlight a number of discrepancies. It is likely that these discrepancies are partly due to errors associated with the measurements of percentage water content and %LOI 550°C, but they may also be due to uncertainties associated with the depth models of the cores, including the elimination of mass flows and the causes of gaps in the sedimentary sequence.

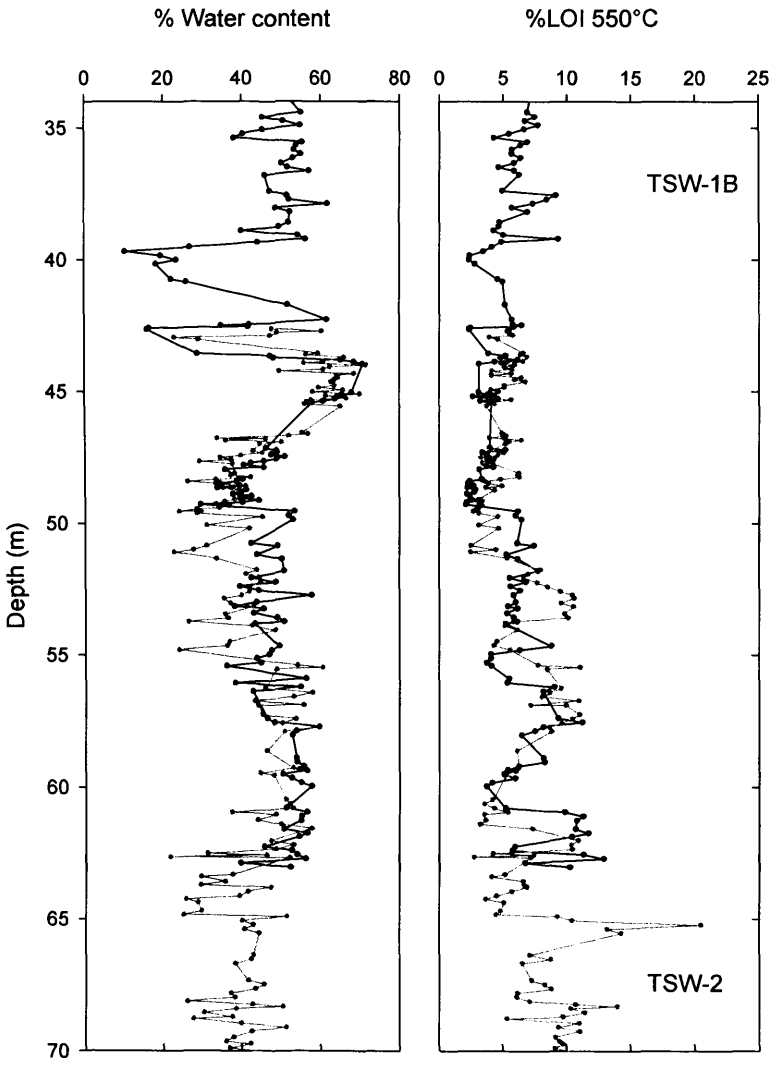

Figure 4.5: Records of percentage water content and %LOI 550°C from cores TSW-1B (black line) and TSW-2 (grey line) plotted on the corrected depth scale after correlation based on four visual tie-points.

4.3.2 $^{230}Th/^{234}U$ dating

Seven 25 cm-long sections of the sedimentary sequence were initially selected for dating. The material above ~33 m (uncorrected depth) was considered unsuitable for analysis because it contains significant quantities of autochthonous minerals other than calcite, some of which may have precipitated from pore water after the cores were collected (section 3.2.5; Partridge *et al.*, 1993; Bühmann and Elsenbroek, 1999), which could complicate the interpretation of its activity ratios (section 4.2.1). An

attempt to date material from a section centred on 33.38 m (uncorrected depth) proved unsuccessful for this reason.

Four samples were selected from each section with the aim of maximising the range of the ratio of carbonate to non-carbonate material sampled. An attempt to date material from a section centred on 81.03 m (uncorrected depth) proved unsuccessful because it was not possible to achieve a sufficiently large range (and the activity ratios of samples analysed from this section were thus too similar to allow reliable mixing lines to be produced), but a sufficient range was achieved in all other cases.

Samples were prepared and analysed by the author at the Open University Uranium Series Facility, with the help of Dr. Mabs Gilmour and Dr. Louise Thomas, using methods described by Chen *et al.* (1986) and Edwards *et al.* (1986). Each sample was dried and homogenised, and 0.2-0.5 g was weighed into a clean Savillex PFA beaker. The carbonate present was completely dissolved by drop-wise addition of concentrated TD 7M HNO_3. Any residue was separated from the acid by centrifugation and rinsed several times with HNO_3 to ensure complete removal of carbonate. The remaining material was dissolved in HF and, when organics were present, $HClO_4$, by heating overnight with each acid, and then evaporating the sample to dryness several times to ensure that all excess acid was removed. The sample was then re-dissolved in TD 6M HCl and spiked with a mixture containing known concentrations of ^{229}Th and ^{236}U. The carbonate leachate was added to this spiked solution and allowed to equilibrate, before evaporating to dryness and re-dissolving in TD 7M HNO_3.

The uranium and thorium fractions in this solution were separated on 2 ml anion exchange columns using standard techniques, in which U and Th fractions are dissolved in HBr and HCl solutions respectively. These solutions were evaporated to dryness and loaded onto graphite-coated rhenium filaments using 2 µl of 0.1 M HNO_3, which were then heated in a Finnigan MAT 262 mass spectrometer equipped with a retarding potential quadrapole and secondary electron multiplier (described by van Calsteren and Schwieters, 1995). A dynamic peak-switching routine was employed to measure $^{234}U/^{236}U$ and $^{235}U/^{236}U$ (where ^{235}U is a proxy for ^{238}U,

assuming a natural $^{238}U/^{235}U$ ratio of 137.88), and $^{230}Th/^{229}Th$ and $^{232}Th/^{229}Th$ activity ratios.

In some cases, analysis of samples had to be repeated due to high errors associated with the activity ratios measured (this was the case for samples from 46.11, 64.34, and 88.70 m - uncorrected depths). In these cases, the analyses with the lowest errors associated with the $^{230}Th/^{229}Th$ activity ratio measured (the ratio with the highest errors, due to the relatively small amounts of ^{230}Th present) were used to construct mixing lines (repeat analyses of the same samples should not be used to construct such lines). All samples used to construct mixing lines had $^{230}Th/^{229}Th$ activity ratio errors less than analytical error (5‰), except those from 46.35 m (uncorrected depth) (5.7‰) and 54.81 m (uncorrected depth) (7.4‰).

One total procedure blank was run in parallel with every five samples to assess sample contamination. These blanks represented less than 0.1% of the sample measurements for ^{238}U and ^{230}Th (assuming a silicate ratio of ~5 x 10^{-6} for the $^{230}Th/^{232}Th$ ratio), and were therefore assumed to have had negligible effects on the measured activity ratios. Three in-house standards were also analysed to assess external reproducibilities: a natural uranium standard spiked with ^{236}U single spike (U456 std3), which had a reproducibility of ±0.1% for $^{235}U/^{236}U$ measurements and ±0.4% for $^{234}U/^{236}U$ measurements over the period of analysis (1 s.d.); a thorium standard (CP230/229) that is a mixture of ^{230}Th and ^{229}Th spiked with a $^{230}Th/^{229}Th$ ratio that mimics that of a young carbonate sample, which had a reproducibility of ±0.3% over the period of analysis (1 s.d.); and a young speleothem standard, which had a reproducibility of ±0.8% for $^{234}U/^{238}U$ measurements, and ±1.8% for $^{230}Th/^{234}U$ measurements over the period of analysis (1 s.d.).

The activity ratios measured were used to construct mixing lines on plots of $^{234}U/^{232}Th$ against $^{238}U/^{232}Th$, and $^{230}Th/^{232}Th$ against $^{234}U/^{232}Th$, using linear least-squares regression. The errors associated with these measurements (which were propagated from the in-run precision errors, weighing errors, and uncertainties in spike concentrations and isotope compositions) were noted, but not used to weight the regression lines (section 4.2.1) (Schwarcz and Latham, 1989). The gradients of these mixing lines were used to determine the $^{234}U/^{238}U$ and $^{230}Th/^{234}U$ activity ratios of the

carbonate analysed. The errors associated with these ratios were calculated using equations 4.4 and 4.6, which take into account the errors associated with the measured activity ratios and the scatter of the data points around the mixing line (section 4.2.1) (Luo and Ku, 1991). The calculated $^{234}U/^{238}U$ and $^{230}Th/^{234}U$ activity ratios and errors were then used to calculate the age of the carbonate in the samples and the errors associated with this age using equation 4.2, the decay constants given by Cheng *et al.* (2000), and standard propagation of errors.

4.3.3 Age-depth models

Age-depth models for the sedimentary sequence were constructed using: the $^{230}Th/^{234}U$ dates presented in this chapter; three calibrated radiocarbon dates on charcoal obtained by I. Kristen (GFZ, Potsdam); seven calibrated radiocarbon dates on bulk organic matter from the core obtained from the lake in 1988/89 (Partridge *et al.*, 1993, 1997); and an estimated date of 93 years B.P. for the top of the lacustrine sediments. The estimated date of 93 years B.P. for the top of the sequence (where present is taken to be 2005, because this is when most of the $^{230}Th/^{234}U$ measurements were made) is based on the observation that the promontory through which the cores were taken was built on top of the lake sediments in, or soon after, 1912 (Ashton and Schoeman, 1983; Levin, 1991). This "date" was assigned an error of ±50 years so that the estimate was not given an unrealistically high weight in age-depth models (cf. Bennett, 1994).

The radiocarbon dates from the new cores were obtained by accelerator mass spectrometry (AMS) of charcoal picked from horizons between 3 and 9 cm thick (I. Kristen, pers. comm.). The depths of the radiocarbon dates on bulk organic matter from the core obtained in 1988/89 were transferred to the new cores by correlating a record of percentage organic carbon from the 1988/89 core with a record of %LOI 550°C from the current sedimentary sequence (Fig. 4.6). The maximum offset between the two records is 0.29 m, which is less than the 0.5 m-interval between samples on the 1988/89 core, and the depths of the dates were therefore transferred directly to the new sequence. A lake-reservoir correction of 1.15 kyr was applied to the radiocarbon dates from the core obtained in 1988/89 due to the presence of "old" carbon in the lake water (Partridge *et al.*, 1997), but this correction was not necessary for the new dates because charcoal is derived from the terrestrial environment.

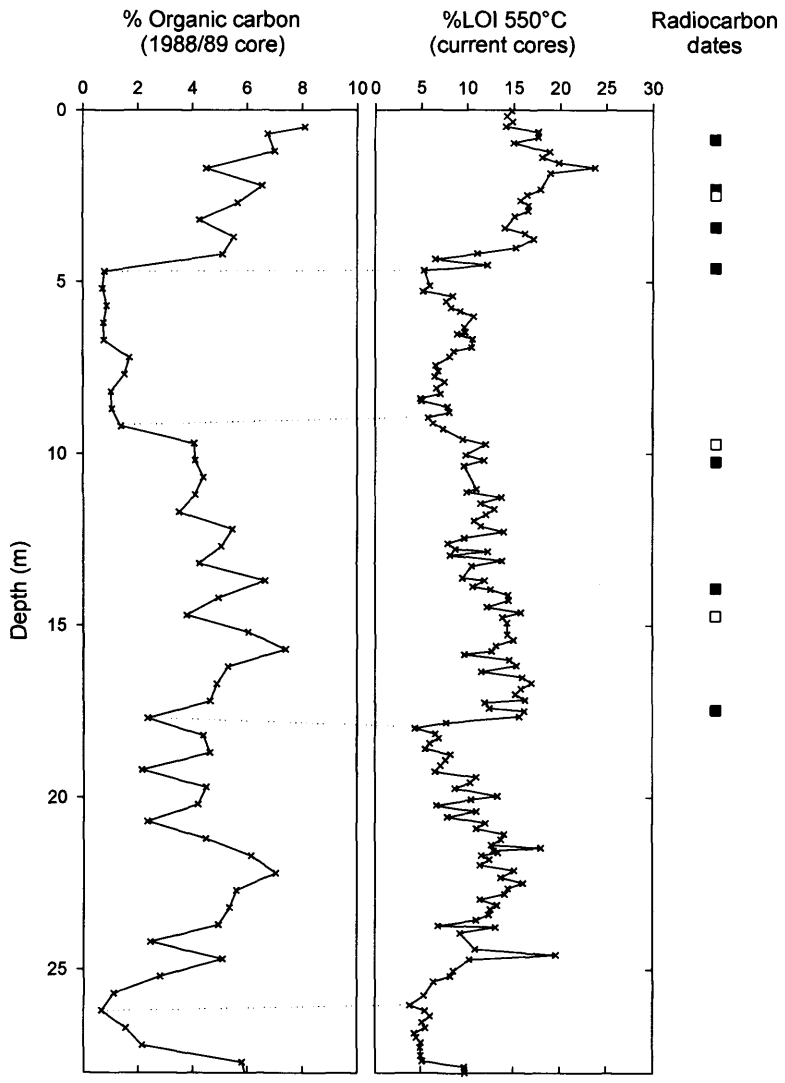

Figure 4.6: Records of percentage organic carbon from the core obtained in 1988/89 (Partridge *et al.*, 1993) and %LOI 550°C from the current cores (chapter 5) plotted on corrected depth scales, with proposed tie-lines. Closed squares represent depths of radiocarbon dates on 1988/89 core (Partridge *et al.*, 1993, 1997), open symbols represent depths of radiocarbon dates on current cores (provided by I. Kristen (GFZ, Potsdam)).

Four types of age-depth model were fitted to these age-determinations using the statistical program R (Ihaka and Gentleman, 1996): linear interpolation, cubic spline interpolation, least-squares polynomial line fitting, and weighted least-squares polynomial line fitting. In the case of weighted polynomial line fitting, the dates were weighted according to the inverse of their variances. Where the "plus" and "minus"

errors were not equal, the average was used. Fitted polynomial lines were extrapolated to the base of the sediment, which is not desirable but was considered acceptable because the end of the sedimentary sequence is only 84 cm below the mid-point of the last $^{230}Th/^{234}U$ date.

4.4 Results

4.4.1 $^{230}Th/^{234}U$ dates

The concentration of ^{238}U and the $^{234}U/^{238}U$, $^{230}Th/^{234}U$, and $^{230}Th/^{232}Th$ activity ratios of the four samples from each section with the lowest errors associated with their $^{230}Th/^{229}Th$ activity ratios, and the errors associated with these measurements, are given in Table 4.1. Measurements from the sections centred on 33.38 and 81.03 m (uncorrected depths) are not shown, as attempts to date these sections were unsuccessful for the reasons outlined in section 4.3.2. The concentrations of ^{238}U range from 10 to 27 ppm. These values are high relative to most terrestrial carbonates, which allowed isotopes in the ^{238}U-^{206}Pb decay chain to be measured with a high degree of accuracy (cf. Gascoyne, 1992; Lin *et al.*, 1996). The mixing lines constructed using these measurements are shown in Figures 4.7 and 4.8. The range of values used to construct the lines is large, which increases the likelihood that they are reliable.

Table 4.1: ^{238}U concentration and $^{234}U/^{238}U$, $^{230}Th/^{234}U$, and $^{230}Th/^{232}Th$ activity ratios of samples used to construct mixing lines (errors are 1 s.d.). Each group of four samples was used to construct mixing lines for a section of sediment. Both uncorrected and corrected depths are given for each sample.

Uncorrected sample depth (m)	Corrected sample depth (m)	^{238}U (ppm)	$^{234}U/^{238}U$	$^{230}Th/^{234}U$	$^{230}Th/^{232}Th$
46.11	39.93	22.39 ± 0.06	2.164 ± 0.0097	0.905 ± 0.0054	18.30 ± 0.18
46.21	40.03	18.39 ± 0.05	2.135 ± 0.0094	0.926 ± 0.0057	14.26 ± 0.14
46.27	40.09	17.32 ± 0.02	2.112 ± 0.0066	0.944 ± 0.0055	13.48 ± 0.13
46.35	40.17	13.32 ± 0.03	2.085 ± 0.0092	0.924 ± 0.0072	10.63 ± 0.12
54.58	47.52	21.67± 0.03	1.981 ± 0.0060	0.980 ± 0.0057	3.49 ± 0.04
54.64	47.58	20.19 ± 0.03	1.991 ± 0.0063	1.012 ± 0.0065	21.00 ± 0.22
54.73	47.67	19.30 ± 0.06	2.011 ± 0.0078	0.948 ± 0.0070	9.08 ± 0.47
54.81	47.75	18.02 ± 0.07	2.027 ± 0.0124	0.927 ± 0.0084	8.79 ± 0.11
64.22	56.79	18.77 ± 0.04	1.789 ± 0.0068	0.955 ± 0.0066	10.59 ± 0.11
64.26	56.83	13.11 ± 0.02	2.016 ± 0.0060	0.687 ± 0.0041	7.86 ± 0.08
64.28	56.85	17.90 ± 0.02	1.784 ± 0.0054	0.975 ± 0.0071	22.11 ± 0.25
64.34	56.91	10.32 ± 0.01	1.821 ± 0.0054	0.924 ± 0.0060	4.83 ± 0.05
71.66	63.87	23.39 ± 0.06	1.698 ± 0.0057	1.146 ± 0.0083	16.68 ± 0.86
71.74	63.95	23.47 ± 0.04	1.690 ± 0.0056	1.172 ± 0.0065	18.16 ± 0.17
71.82	64.03	19.61 ± 0.04	1.689 ± 0.0061	1.189 ± 0.0068	14.52 ± 0.14
71.90	64.11	26.77 ± 0.05	1.680 ± 0.0057	1.115 ± 0.0068	29.31 ± 0.30
88.54	76.31	21.65 ± 0.03	1.904 ± 0.0062	1.234 ± 0.0077	15.36 ± 0.16
88.62	76.36	25.34 ± 0.05	1.9023 ± 0.0072	1.148 ± 0.0079	18.16 ± 0.19
88.70	76.44	23.32 ± 0.04	1.913 ± 0.0062	1.224 ± 0.0069	20.52 ± 0.21
88.78	76.52	22.55 ± 0.04	1.895 ± 0.0063	1.245 ± 0.0081	13.07 ± 0.14

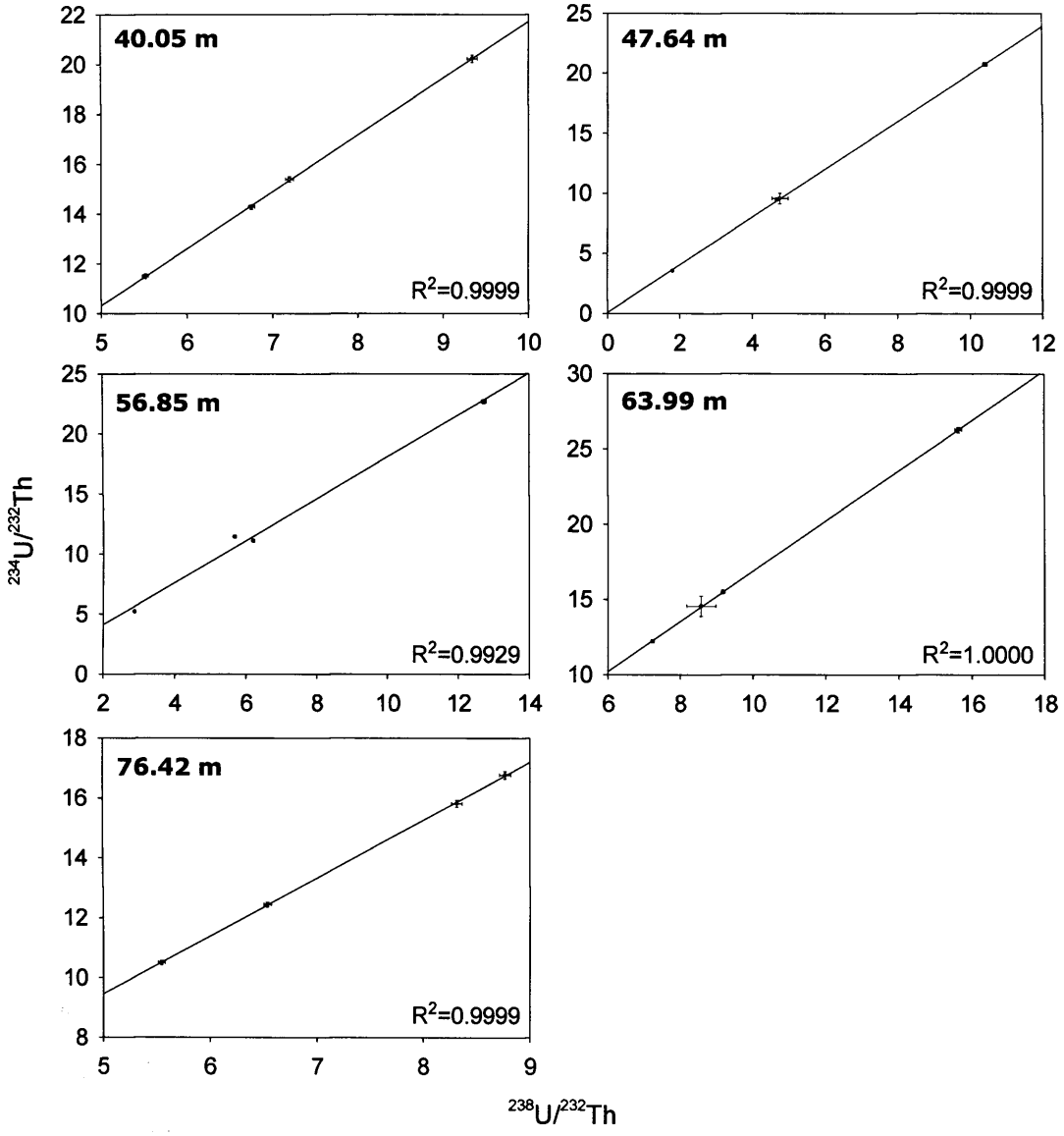

Figure 4.7: Mixing lines constructed using $^{234}U/^{232}Th$ and $^{238}U/^{232}Th$ activity ratios of the samples from each sediment section. Lines were fitted using linear least-squares regression. Each plot displays the mid-point of the section sampled (corrected depth), the coefficient of determination (R^2), and measurement errors (1 s.d.).

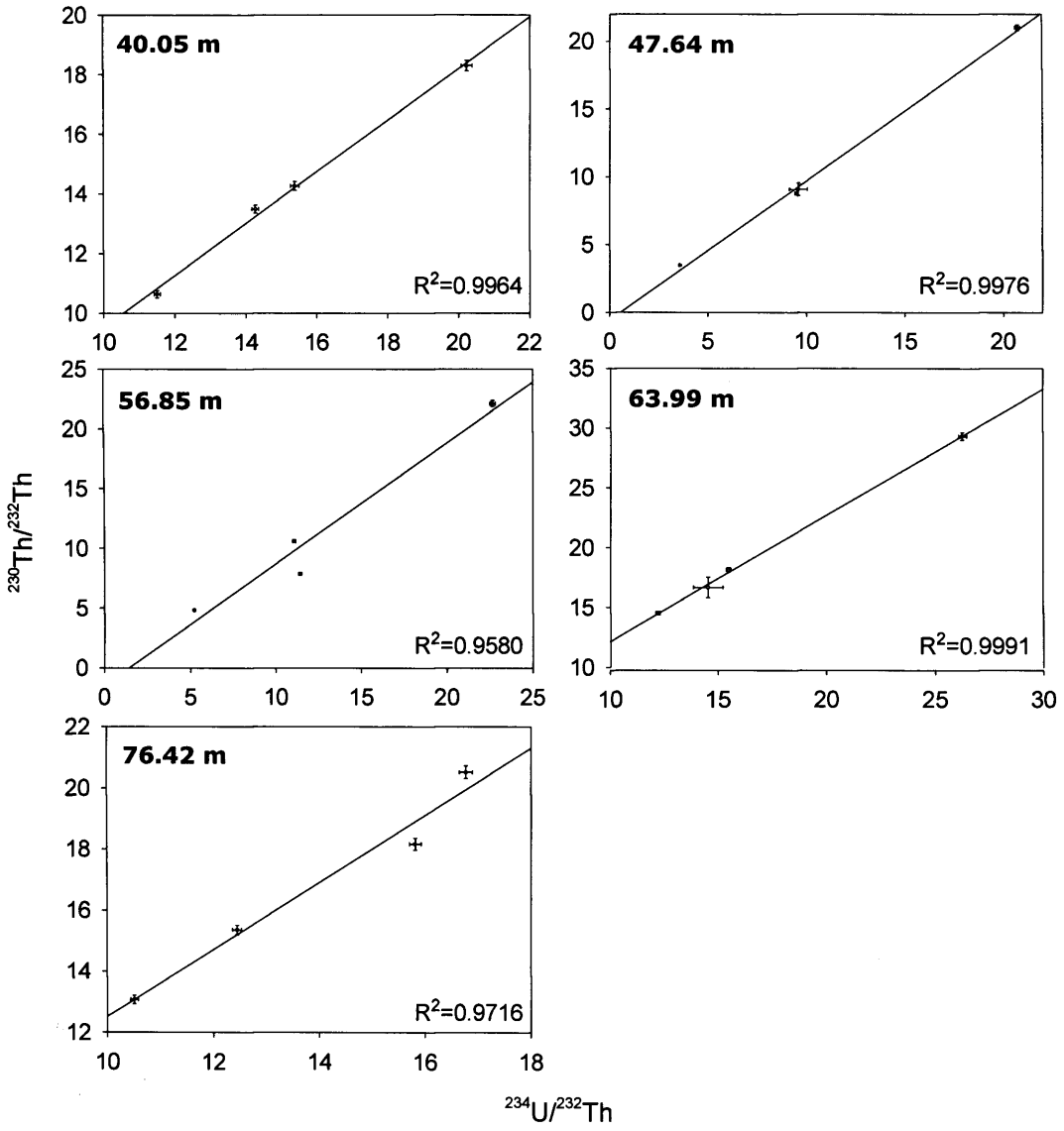

Figure 4.8: Mixing lines constructed using $^{230}Th/^{232}Th$ and $^{234}U/^{232}Th$ activity ratios of the samples from each sediment section. Lines were fitted using linear least-squares regression. Each plot displays the mid-point of the section sampled (corrected depth), the coefficient of determination (R^2), and measurement errors (1 s.d.).

The activity ratios calculated from the gradient of each mixing line and the associated errors are given in Table 4.2, together with the dates and errors calculated from these values. The errors associated with the dates are highly variable, ranging from ±3 kyr (1 s.d.) for the well-defined mixing line at 40.05 m, to errors an order of magnitude larger for the less well-defined mixing lines at 56.85 and 76.42 m. The dates are in stratigraphic order, but those from 47.64 and 56.85 m are only separated by 1 kyr, which is probably due to the large errors associated with these age-determinations.

Table 4.2: $^{234}U/^{238}U$ and $^{230}Th/^{234}U$ activity ratios and associated errors (1 s.d.) of carbonate in the samples from each sediment section, and the dates and errors (1 s.d.) calculated from these ratios.

Corrected mid-point of section sampled (m)	$^{234}U/^{238}U$	$^{230}Th/^{234}U$	Date (kyr B.P.)
40.05	2.2819 ± 0.00440	0.8679 ± 0.00775	165 ± 3
47.64	1.9880 ± 0.00426	1.0295 ± 0.03152	255 +25/−22
56.85	1.7458 ± 0.00297	1.0128 ± 0.04776	256 +44/−33
63.99	1.6677 ± 0.00288	1.0559 ± 0.00742	302 +9/−8
76.42	1.9322 ± 0.00323	1.0974 ± 0.03780	322 +56/−40

4.4.2 Age-depth models

The age-determinations used to construct age-depth models for the sedimentary sequence are summarised in Table 4.3, and plotted against the corrected depth model for the sequence in Figure 4.9. The new radiocarbon dates produced by I. Kristen (GFZ, Potsdam) are in good agreement with the radiocarbon dates presented by Partridge *et al.* (1993, 1997), allowing considerable confidence to be placed in their accuracy. The only discrepancy evident between the new radiocarbon dates and those from the core obtained in 1988/89 is that the new date from 2.44 m is older than the previously-published date from 3.36 m. This stratigraphic inconsistency could be due to an error in the depth assigned to the date from the previous core when transferring it to the new sedimentary sequence. It could also result from an error in the lake-reservoir correction applied to the radiocarbon dates from the core obtained in 1988/89 (section 4.3.3) (Partridge *et al.*, 1997). The reservoir effect can change through time due to changes in the surface-area to volume ratio and mixing regime of a lake, and as both these characteristics have changed at Tswaing crater lake (chapter

5), the value of 1.15 kyr determined from modern samples may not be applicable throughout the sequence (Geyh *et al.*, 1998).

Table 4.3: Age-determinations from the sedimentary sequence at Tswaing crater lake used to construct age-depth models. Radiocarbon dates on charcoal were provided by I. Kristen (GFZ, Potsdam). Radiocarbon dates on bulk organic material from the core obtained in 1988/89 are from Partridge *et al.* (1993, 1997).

Corrected depth of dated section (m)	Corrected mid-point of dated section (m)	Date type	Material dated	Date (kyr B.P.) and 1 s.d. error
0.00	0.00	Estimate	N/A	0.093 ± 0.05
0.77-0.85	0.81	^{14}C (calibrated)	Bulk organic - 1988/89 core	1.18 ± 0.05
2.22-2.28	2.25	^{14}C (calibrated)	Bulk organic - 1988/89 core	3.73 ± 0.05
2.41–2.47	2.44	^{14}C (calibrated)	Charcoal	4.86 ± 0.019
3.32-3.40	3.36	^{14}C (calibrated)	Bulk organic - 1988/89 core	4.14 ± 0.06
4.52-4.58	4.55	^{14}C (calibrated)	Bulk organic - 1988/89 core	6.78 ± 0.08
9.62-9.71	9.66	^{14}C (calibrated)	Charcoal	33.27 ± 1.03
10.15-10.22	10.19	^{14}C (calibrated)	Bulk organic - 1988/89 core	34.35 ± 0.7
13.82-13.92	13.87	^{14}C (calibrated)	Bulk organic - 1988/89 core	35.65 ± 0.75
14.66-14.69	14.68	^{14}C (calibrated)	Charcoal	37.37± 1.03
17.37-17.45	17.41	^{14}C (calibrated)	Bulk organic - 1988/89 core	43.35 ± 1.6
39.93-40.17	40.05	^{230}Th/^{234}U	Carbonate	165 ± 3
47.52-47.75	47.64	^{230}Th/^{234}U	Carbonate	255 +25/−22
56.79-56.91	56.85	^{230}Th/^{234}U	Carbonate	256 +44/−33
63.87-64.11	63.99	^{230}Th/^{234}U	Carbonate	302 +9/−8
76.31-76.52	76.42	^{230}Th/^{234}U	Carbonate	322 +56/−40

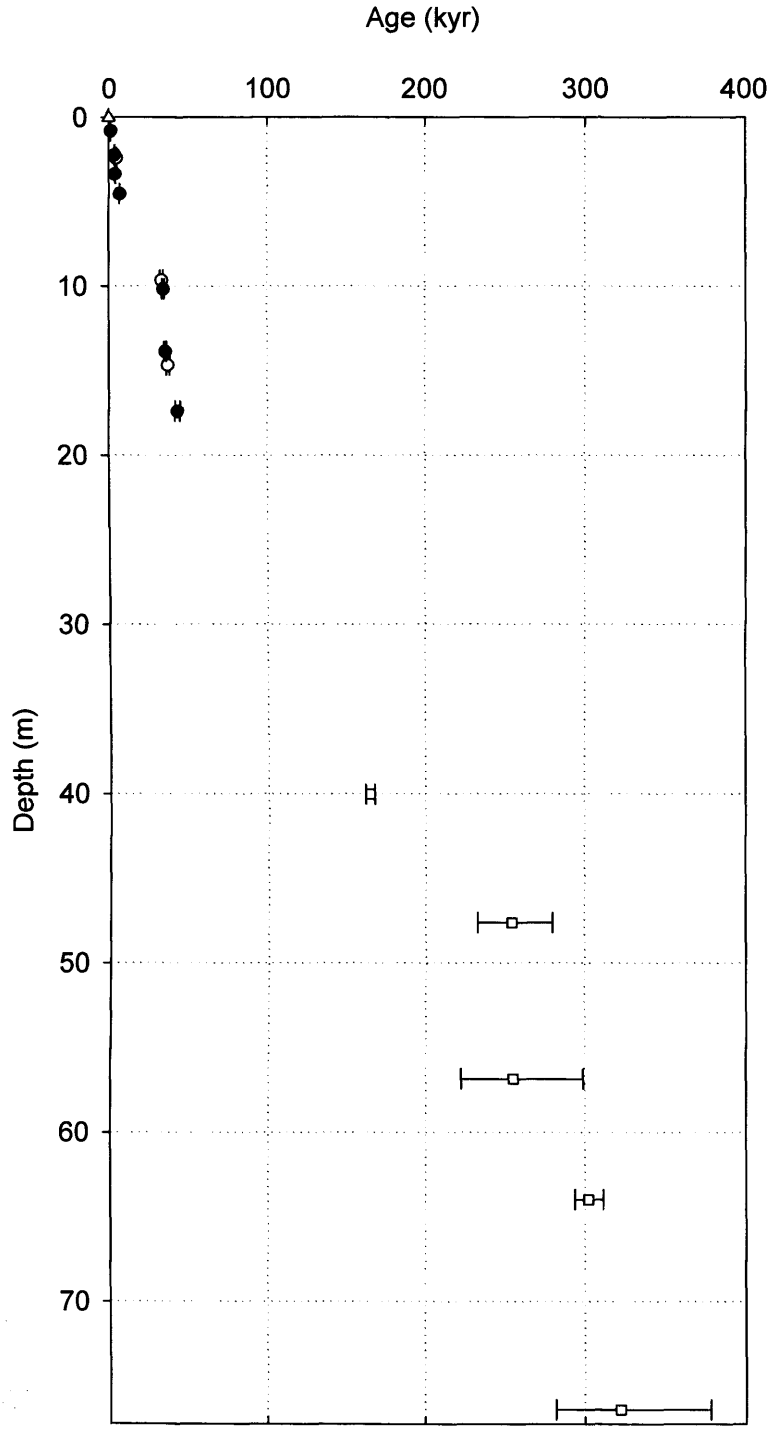

Figure 4.9: Age-determinations from sediments in Tswaing crater lake plotted against the corrected depth model. Triangle is estimated date for top of sedimentary sequence (Ashton and Schoeman, 1983; Levin, 1991), filled circles are calibrated radiocarbon dates on bulk organic material from the core obtained in 1988/89 (Partridge *et al.*, 1993, 1997), open circles are calibrated radiocarbon dates on charcoal from current cores (I. Kristen, pers. comm.), squares are $^{230}Th/^{234}U$ dates on carbonate from current cores. Errors are 1 s.d.

The age-depth models constructed using these age-determinations and the corrected depth model for the sedimentary sequence are shown in Figures 4.10, 4.11, and 4.12. The models constructed using linear and cubic-spline interpolation are shown in Figure 4.10, while the linear, quadratic, and cubic polynomial models fitted using weighted and non-weighted least-squares regression are shown in Figures 4.11 and 4.12, respectively. The equations of the polynomial models are given in Table 4.4.

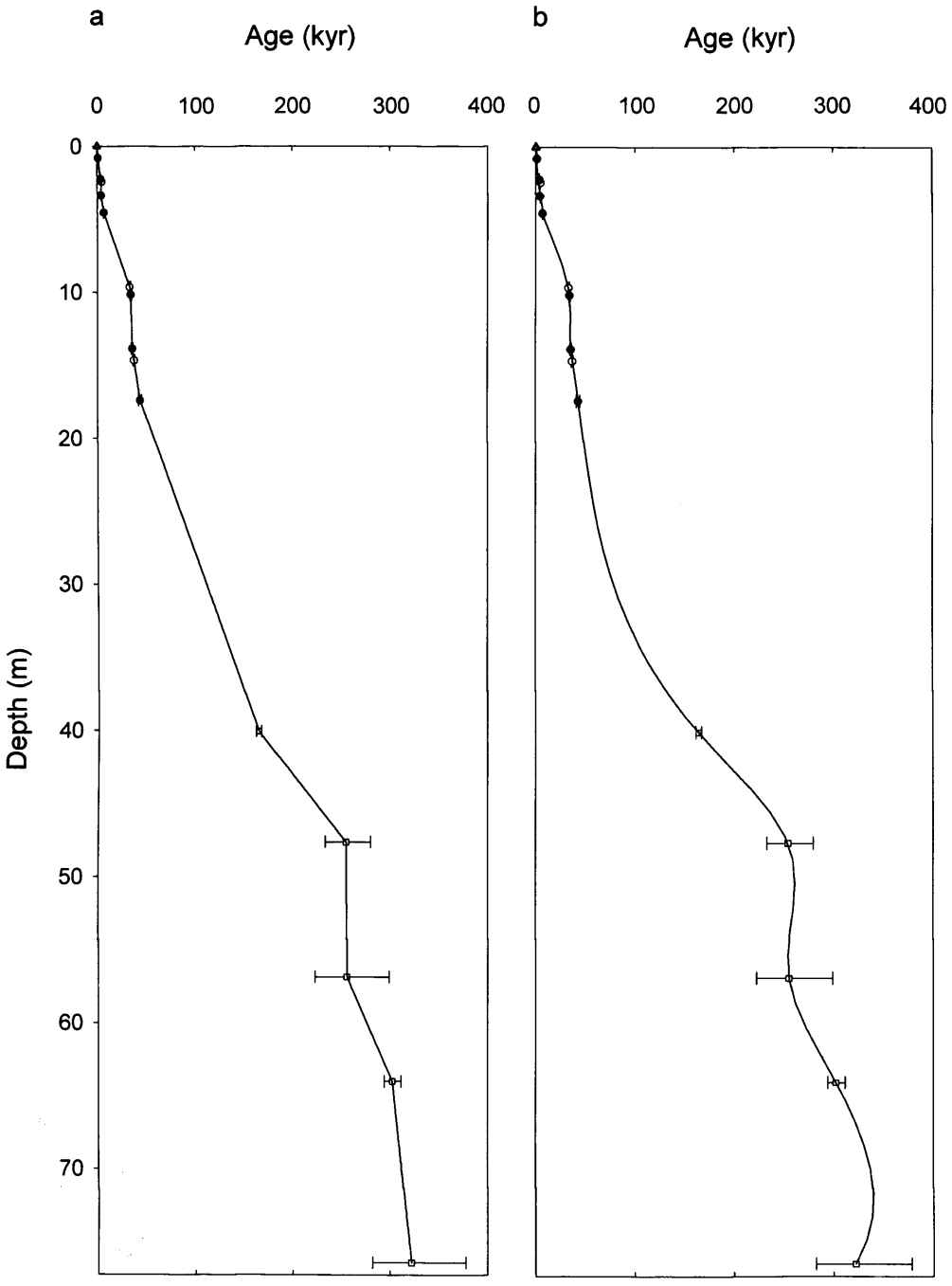

Figure 4.10: Age-depth models fitted to the age-determinations presented in Table 4.3 using (a) linear interpolation (b) cubic spline interpolation. Symbols are as in Figure 4.9.

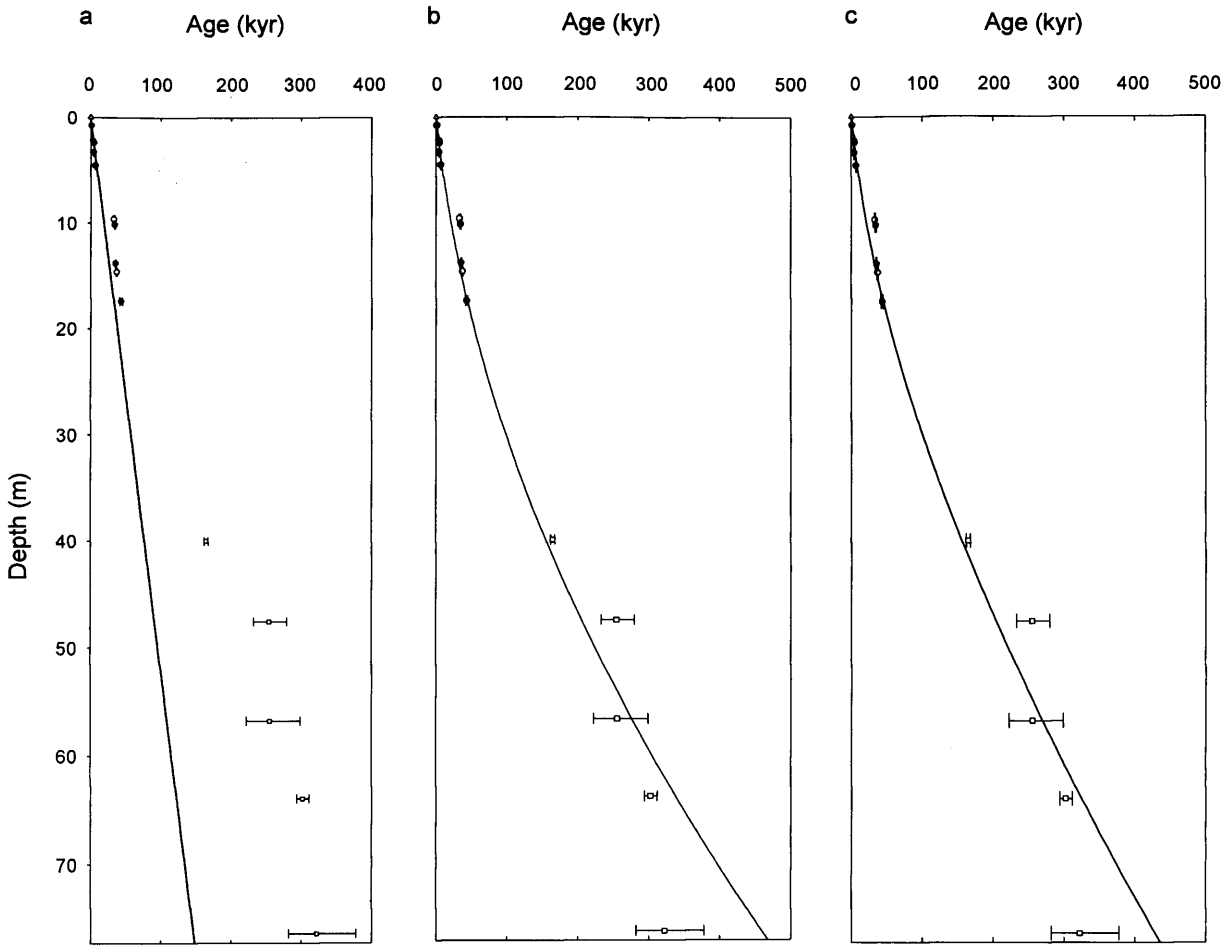

Figure 4.11: Age-depth models fitted to the age-determinations presented in Table 4.3 by weighted least-squares regression: (a) linear model, (b) quadratic model, (c) cubic model. The quadratic model is statistically most significant. Symbols are as in Figure 4.9.

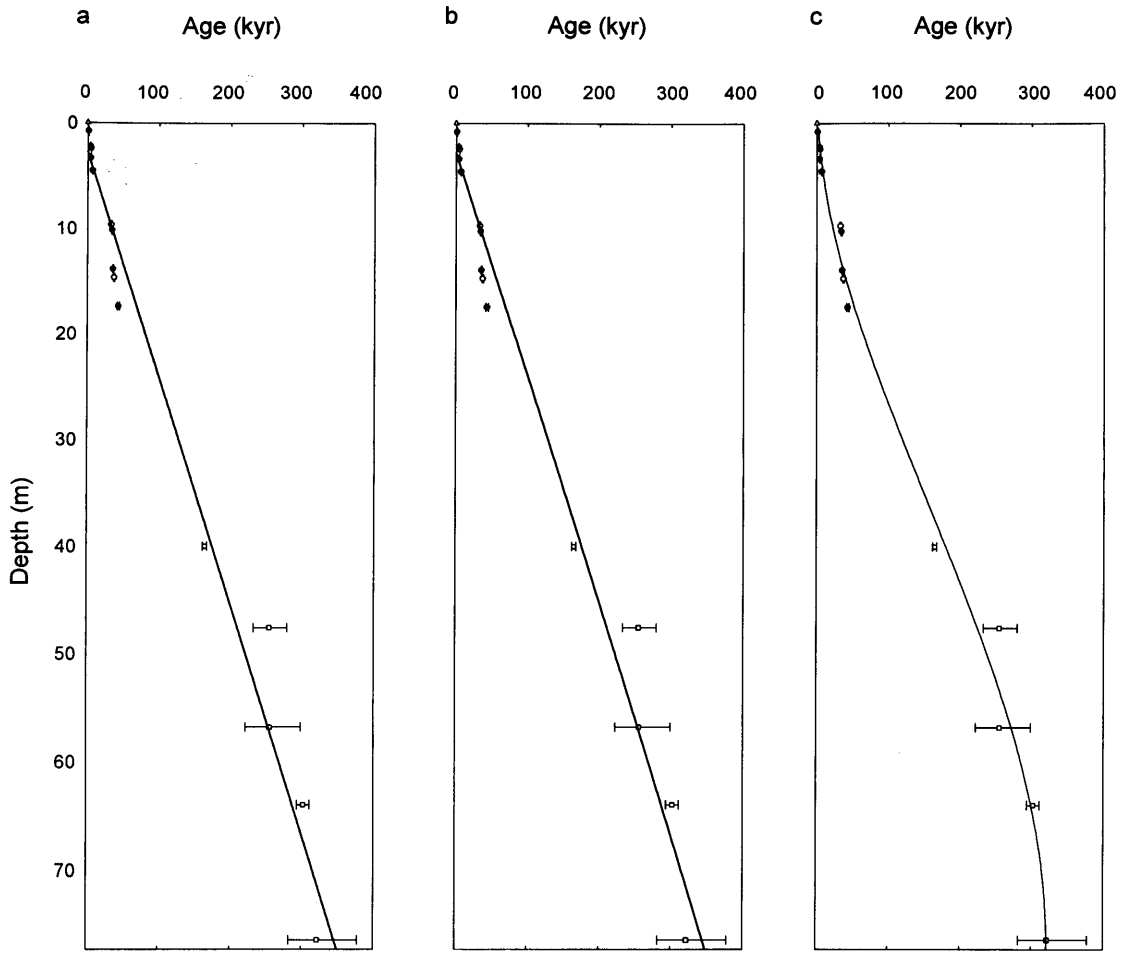

Figure 4.12: Age-depth models fitted to the age-determinations presented in Table 4.3 by non-weighted least-squares regression: (a) linear model, (b) quadratic model, (c) cubic model. The cubic model is statistically most significant. Symbols are as in Figure 4.9.

Table 4.4: Equations, adjusted R^2 values, and F-test results (comparing two models by ANOVA) for the polynomial models fitted by non-weighted least-squares regression and weighted least-squares regression (non-weighted model with 5 terms is shown for comparison with non-weighted model with 4 terms).

Method	Number of parameters	Adjusted R^2	F-test statistic & p-value for ANOVA comparing 2 models	Equation
Weighted	2	0.7877	F = 8.3766, p = 0.0126	Age = −179.0 + (1927.8 x Depth)
Weighted	3*	0.8609		Age = 419.9 + (1495.5 x Depth) + (59.0 x $Depth^2$)
Weighted	4	0.8497	F = 0.0248, p = 0.8775	Age = 454.0 + (1458.5 x Depth) + (67.5 x $Depth^2$) + (−0.2 x $Depth^3$)
Non-weighted	2	0.9781	F = 0.0123, p = 0.9133	Age = −12761 + (4692 x Depth)
Non-weighted	3	0.9765		Age = −13285.8 + (4773.4 x Depth) + (−1.2 x $Depth^2$)
Non-weighted	4*	0.9899	F = 18.18, p = 0.0011	Age = 1769.9 + (863.4 x Depth) + (141.1 x $Depth^2$) + (−1.3 x $Depth^3$)
Non-weighted	5	0.9890	F = 0.0285, p = 0.869	Age = 1248.0 + (1116.0 x Depth) + (121.0 x $Depth^2$) + (−0.8 x $Depth^3$) + (−0.003 x $Depth^4$)

* indicates that this is the most statistically significant model for a given method (based on whether the p-value associated with the F-test statistic of the ANOVA comparing two models is <0.05, and thus whether the addition of an extra term significantly increases the fit of the model, given the decrease in the number of degrees of freedom).

The model constructed using linear interpolation contains a number of abrupt changes in sedimentation rate (Fig. 4.10a), while the model constructed using cubic spline interpolation contains two age reversals (Fig. 4.10b). The polynomial models assume gradual changes in sedimentation rate and do not contain any age reversals, but they are highly variable in their fit to the age-determinations. The quadratic (3 terms) model is the most statistically significant model fitted by weighted least-squares regression, but it is evident that this model does not provide a good fit to the age-determinations in the lower section of the sequence (Fig. 4.11b). In contrast, the models fitted by non-weighted least-squares regression appear to fit the available age-determinations relatively well (Fig. 4.12). The cubic (4 terms) model is the most

statistically significant of the models fitted using this method, and has a good fit to the available dates (Fig. 4.12c).

4.5 Discussion

The $^{230}Th/^{234}U$ dates presented in this chapter provide the first absolute age-determinations from the lower part (below 18 m) of the sedimentary sequence from Tswaing crater lake, and should therefore improve the chronological control of palaeoclimatic records from this site. This information, in turn, has the potential to improve our understanding of the nature and causes of climatic change in southern Africa. The reliability of these dates is, however, dependent on whether the assumptions associated with the $^{230}Th/^{234}U$ method of dating and the TSD isochron method of correcting for the presence of detritus are met (section 4.2.1). The validity of these assumptions is therefore assessed in the following section. In order to assess the accuracy of the age-depth models constructed for the sequence, it is also necessary to consider the nature of the sedimentary sequence, and this is discussed in section 4.5.2. Finally, the applicability of the various age-depth models is assessed, and the implications of these findings for records of palaeoclimatic change from Tswaing crater lake are outlined in section 4.5.3.

4.5.1 Reliability of the $^{230}Th/^{234}U$ dates

The most important assumption of the $^{230}Th/^{234}U$ dating method is that the minerals dated have acted as a closed system since they precipitated. The most significant causes of open-system behaviour in lacustrine sediments are groundwater flow and diagenesis, which can preferentially remove uranium isotopes, particularly ^{234}U, and thus produce artificially old dates (*e.g.* Lao and Benson, 1988). Tswaing crater lake does not appear to lose water through groundwater seepage, but groundwater flow into the artesian aquifer below the lake floor may have leached uranium from the sediments (chapter 3). In addition, there is evidence that methanogenesis caused authigenic carbonate precipitation from pore water above ~41.5 m (chapter 5), and this process is sometimes associated with carbonate diagenesis (section 2.2.1) (cf. Talbot and Kelts, 1990). It is therefore possible that carbonate diagenesis affected the date at 40.05 m.

Leaching of uranium through groundwater movement and diagenesis tends to decrease the concentration of uranium in sediments, and to produce either highly variable or homogenous isotopic ratios, which in turn result in dates that are not in stratigraphic order (Lao and Benson, 1988; Geyh, 2001). The fact that the concentration of uranium in the samples is high and does not show any trend with sediment depth (Table 4.1), and that the dates produced are in stratigraphic order (Table 4.2), therefore suggests that groundwater movement and diagenesis have not significantly affected the isotope composition of the sediments.

The TSD isochron approach depends on the assumption that the samples used to construct mixing lines are composed of two homogenous end members: contemporaneous carbonate, and detritus with a uniform $^{230}Th/^{232}Th$ activity ratio. The scatter of data points around mixing lines provides an indirect indication of the extent to which this assumption is met (Bischoff and Fitzpatrick, 1991; Luo and Ku, 1991). The scatter of data points around the mixing lines presented in this chapter is extremely low in all cases, apart from those constructed using the $^{230}Th/^{232}Th$ and $^{234}U/^{232}Th$ activity ratios of samples from 56.85 and 76.42 m, which suggests that the samples from these sections may not be composed of two homogenous end members, or that the samples were subject to analytical error.

The carbonate in the samples from each section is almost certainly contemporaneous, because the dated sections are short relative to the age of the sequence, and because there are negligible amounts of carbonate in the catchment (Brandt and Reimold, 1999). As mentioned above, authigenic carbonates may have precipitated from pore water above 41.5 m, but the presence of this carbonate is unlikely to have affected the accuracy of the date at 40.05 m because stable-isotope evidence suggests that authigenic carbonate precipitation took place soon after burial (chapter 5). Authigenic carbonates are therefore likely to be indistinguishable from endogenic carbonates in terms of initial isotope composition and age (particularly given the use of samples from a 25 cm-long section of sediment for a single date). In addition, the scatter of data points around the mixing lines from 40.05 m is extremely low, which indicates that the assumptions of the TSD isochron method are met ($R^2 = 0.9999$, and $R^2 = 0.9964$).

It is also likely that the aluminosilicate component of the samples from each section is homogenous and has a uniform $^{230}Th/^{232}Th$ activity ratio, because it originates from the granite of the crater walls. It is possible, however, that organic material in the samples has a different isotope composition to both the carbonate and the aluminosilicate detritus, and therefore acts as a third end-member in the mixtures analysed, violating the assumptions of the TSD isochron method (cf. Garnett *et al.*, 2004). The organic content of the samples from the section centred on 56.85 m is higher (~10%) than that of the other samples analysed (~5%), which suggests that this explanation could account for the scatter of data points around the mixing line from this section. The organic content of samples from the section centred on 76.42 m is low (~3%), however, suggesting that this explanation is unlikely to account for the scatter of data points in this section, and that analytical error may therefore be responsible. Despite the relatively high scatter of data points around the mixing lines from these sections, the lines are still well-defined ($R^2 > 0.95$), and it is therefore likely that the dates from these sections are reliable, even though the errors associated with them are large. It therefore appears that the $^{230}Th/^{234}U$ dates presented in this chapter should provide an accurate, though sometimes imprecise, indication of the age of the sediments from Tswaing crater lake.

4.5.2 Sedimentary sequence

In order to assess the validity of the age-depth models constructed using the age-determinations from the sedimentary sequence at Tswaing, it is necessary to consider the nature of sediment deposition at the site. In particular, it is important to determine whether there were significant changes in the rate of sediment deposition during the lake's history. It is unlikely that there are hiatuses in the sedimentary sequence, because there is no evidence of subaerial exposure of the sediments (but this possibility cannot be ruled out). It is possible that there were significant changes in sedimentation rate, however. Records from the sedimentary sequence indicate that the lake became shallower and semi-permanently stratified above 41.5 m (chapter 6), and it is possible that these changes in lake status were accompanied by changes in within-lake productivity, autochthonous mineral precipitation, and/or sediment redistribution. The overall composition of the lake sediments does not change abruptly at this level, however, suggesting that any change in sedimentation rate was probably gradual rather than abrupt (chapter 5). In addition, the organic content of the sediments is, on

average, higher above 31 m than below this depth, which may be indicative of a change in the average rate of sediment deposition (chapter 5). Unfortunately, $^{230}Th/^{234}U$ dating could not be used to quantify these changes because: sediments in the upper section of the sequence are unsuitable for dating using this method (section 4.3.2); use of the $^{230}Th/^{234}U$ method is restricted to sediments that contain significant quantities of carbonate; the errors associated with $^{230}Th/^{234}U$ dates are often high; and insufficient funds were available to produce the number of dates that would be needed to quantify such changes. Further work is therefore required to determine whether there were changes in sedimentation rate at these depths.

4.5.3 Age-depth models

The most appropriate age-depth model for the sedimentary sequence can be assessed using the information presented in the previous sections. The models constructed using linear and cubic spline interpolation are considered inappropriate because the model based on linear interpolation suggests implausible changes in sedimentation rate, and the model constructed using cubic spline interpolation contains two age reversals (Fig. 4.10). These features result from the fact that these models assume that age-determinations are "true"; an assumption that is not appropriate when dates have large errors, as is the case for the $^{230}Th/^{234}U$ dates presented in this chapter.

The polynomial models have the advantage of involving a larger number of age-determinations in the estimation of the age of sediment at any given depth, and thus reducing the dependence of the model on individual dates (cf. Bennett, 1994). This feature is particularly advantageous when few age-determinations are available, and those that are available have large errors, as is the case for the sediments from Tswaing. These models are based on the assumption that the rate of sediment deposition changes gradually, which may not be the case, but the lack of information about sedimentation rates during the lake's history means that this assumption cannot be avoided in this case (section 4.5.2).

Despite the advantages of polynomial models, the models fitted by weighted least-squares regression do not provide a good fit to the available age-determinations (Fig. 4.11). This is because the weights assigned to the radiocarbon dates and the estimated age of the top of the sedimentary sequence are three orders of magnitude greater than

those assigned to the $^{230}Th/^{234}U$ dates. This difference is partly attributable to the different methods used to determine the dates and their errors, and thus results in disproportionately low weights being assigned to $^{230}Th/^{234}U$ dates (Birks, pers. comm.).

In contrast, the polynomial models fitted by non-weighted least-squares regression fit the available age-determinations relatively well (Fig. 4.12). These models therefore appear to be the most appropriate age-depth models for the sedimentary sequence, given the available data. The cubic model is the most statistically significant model fitted using this method and therefore appears to provide the most reliable age-depth model. The disadvantage of this relatively high-order polynomial model is that it may "over-fit" the data by fitting the model to noise associated with the age-depth determinations, and thus make incorrect assumptions about changes in sedimentation rate (section 4.2.2). Comparison of palaeoclimatic records from the sedimentary sequence at Tswaing crater lake with records of atmospheric temperature from the Vostok ice core (Petit *et al.*, 1999) suggests that this may, in fact, be the case, and this possibility is discussed further in chapter 5. The linear age-depth model is not subject to this form of error, as it assumes that sedimentation rates remained constant throughout the sequence, but this model does not fit the radiocarbon dates in the upper part of the sequence as well as the cubic model. Thus, based on the available age-determinations alone, the cubic age-depth model appears to provide the most reliable indication of the age of sediments in Tswaing crater lake.

This model suggests that sedimentation rates were high (~10 mm yr^{-1}) at the base of the sequence, but decreased to ~1 mm yr^{-1} at ~73 m, and decreased further (to 0.16 mm yr^{-1}) at ~37 m, before increasing to ~1 mm yr^{-1} at the top of the sequence. Sedimentation rates are determined by a range of factors, including basin morphology, catchment processes, lake-floor bathymetry, and lake mixing and productivity (cf. Sly, 1978). Many of these factors change during lake ontogeny, with concomitant effects on sedimentation rates, and such changes could account for the changes in sedimentation rate apparent in the cubic age-depth model for sediments at Tswaing.

In the early part of the lake's history, the average gradient of the basin would have been steeper than it is today, which may have resulted in higher rates of sediment input to the lake from the crater walls, and higher rates of sediment focusing in the lake itself (Fig. 3.7) (Hilton, 1985). Over time, erosion would have reduced the gradient of the crater walls, which may have decreased the input of allochthonous material to the lake. In addition, the accumulation of sediments in the basin would have reduced the average gradient of the lake floor, which may have decreased the rate of sediment focusing and increased the size of the sediment-accumulation zone, both of which would have reduced the rate of sediment deposition in the deepest part of the lake (Håkanson, 1977; Hilton, 1985; Blais and Kalff, 1995; Dearing, 1997). The possible causes of the apparent increase in sedimentation rate in the upper part of the sequence are less clear. It may have been caused by an increase in autochthonous mineral precipitation as the lake became more concentrated, or by a decrease in the rate of organic material decomposition related to the onset of anoxic conditions in the hypolimnion (chapter 5).

The cubic age-depth model for the sediments from Tswaing crater lake presented in this chapter differs significantly from that presented by Partridge *et al.* (1997) (Fig. 4.1). In the upper ~18 m of the sedimentary sequence, the two models are fairly similar, because both are based on the seven radiocarbon dates from the core collected in 1988/89, and the three new radiocarbon dates from this section are in agreement with these dates (Partridge *et al.*, 1993, 1997) (Fig. 4.13). The models diverge significantly below ~18 m, in the previously undated section of the sequence, however. The cubic age-depth model presented here suggests that the base of the sedimentary record was deposited at ~320 kyr B.P., while Partridge *et al.* (1997) proposed that sedimentation began ~200 kyr B.P. (based on extrapolation of the average sedimentation rate in the radiocarbon-dated section of the sequence to the base of the sediments and the agreement of this date with a fission-track date of 220 ± 52 kyr B.P. for crater formation) (section 4.1). The reason for the disagreement between the fission-track date for crater formation and the basal age suggested by the cubic age-depth model is not known. The use of the fission-track method to date impact glass from the crater was complicated by heterogeneous distribution of uranium, both within and between individual grains of glass (Storzer *et al.*, 1999). This complication reduced the precision of the date, with age-determinations

calculated from seven separate grain mounts ranging from 107 ± 76 kyr B.P. to 361 ± 161 kyr B.P. (Storzer *et al.*, 1999). There is no explicit reason to suggest that the final date calculated from these mounts is inaccurate, however (Storzer *et al.*, 1993, 1999; Koeberl *et al.*, 1994).

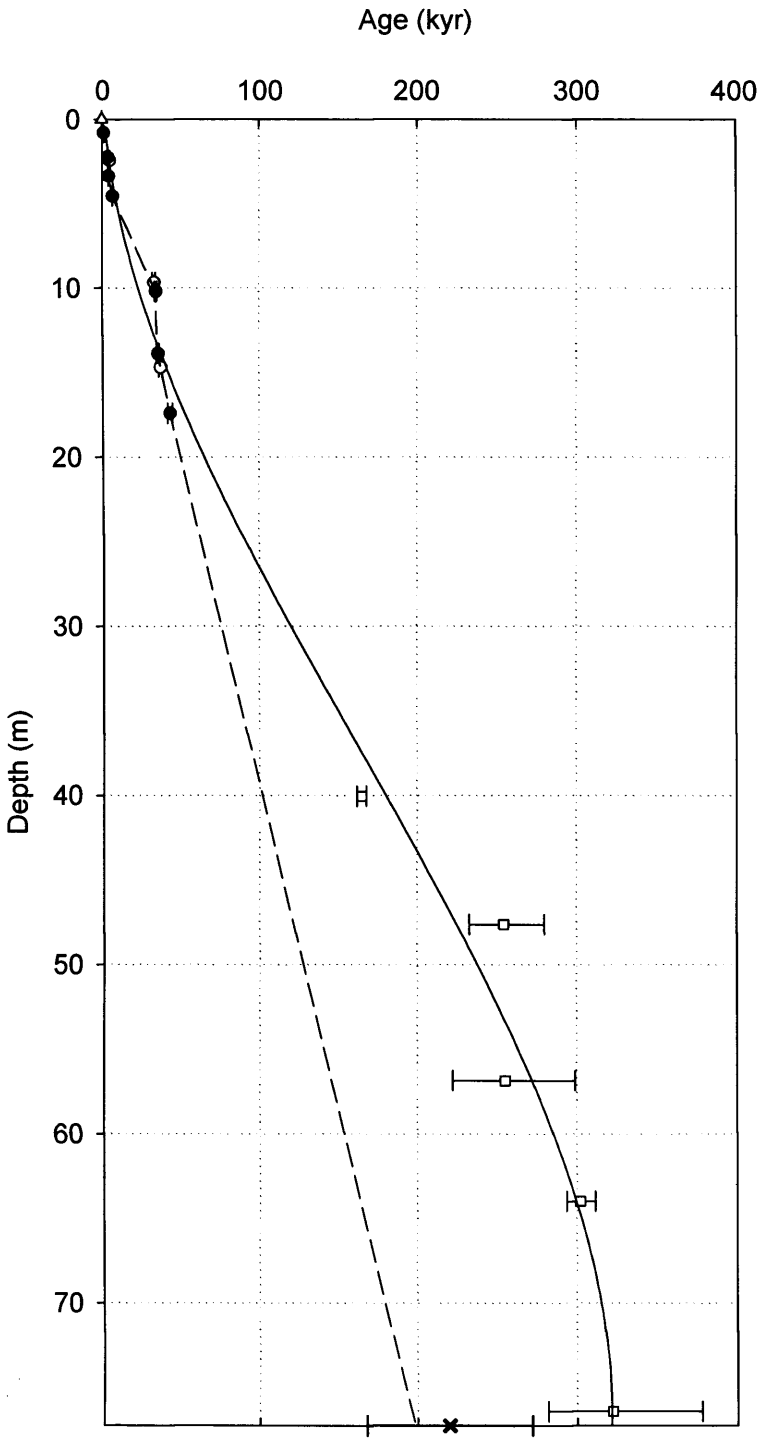

Figure 4.13: The cubic age-depth model fitted by non-weighted least-squares regression in this chapter (solid line), and the age-depth model constructed by Partridge *et al.* (1997) (dashed line) (altered slightly to fit corrected depth model presented in this chapter) for the sedimentary sequence from Tswaing crater lake. Symbols are as in Figure 4.9 and the cross is the fission-track date for crater formation (Storzer *et al.*, 1993, 1999; Koeberl *et al.*, 1994).

Further dating of the sequence, using different methods, is therefore required to determine which of the two models presented in Figure 4.13 is most accurate. $^{40}Ar/^{39}Ar$ analysis of the impact glass at the base of the sequence offers a promising means of re-assessing the date of crater formation, and the possibility of applying this method is currently being explored by Prof. T. C. Partridge (pers. comm.) (cf. McDougall and Harrison, 1999). Unfortunately, few methods are suitable for dating the lacustrine sediments from the crater. Attempts to date single quartz grains by optically-stimulated luminescence (OSL) were unsuccessful due to low quartz yields, anticipated saturation of the OSL signal due to high dose rates, and a small OSL signal dominated by an unsuitable OSL component (S. Woodbourne, pers. comm.). Moreover, materials that might be suitable for electron spin resonance (ESR) or amino acid racemisation (AAR) dating, such as molluscs or diatom valves, are not present in the sediments, or cannot be isolated in sufficient quantities to date (cf. Blackwell, 2001a,b).

If the cubic age-depth model presented in this chapter proves to be accurate, it will have significant consequences for the interpretation of palaeoclimatic records from the sedimentary sequence at Tswaing, and will therefore influence our understanding of palaeoclimatic change in southern Africa. The most significant implication of the new model is that cycles in the carbonate content and grain-size of the sediments that have a period of ~23 kyr according to the age-depth model presented by Partridge *et al.* (1997) have a significantly longer period according to the new model (chapter 5). This finding brings into question the proposal that precessionally-driven changes in insolation controlled precipitation in southern Africa during the late Quaternary (Partridge *et al.*, 1997, 1999). The new age-depth model also indicates that the sedimentary sequence from Tswaing covers the period since MIS 9, rather than the end of MIS 7, as the previous model suggests. Records from the site could therefore provide a unique opportunity to increase our understanding of the causes of climatic change in southern Africa over the last three glacial-interglacial cycles. These implications are discussed further in chapter 5, in the context of new palaeoclimatic records from the site.

4.6 Conclusions

Five new dates have been produced from the lower, previously undated section of the sedimentary sequence from Tswaing crater lake using the $^{230}Th/^{234}U$ method of dating carbonates, and the TSD isochron method for correcting for the presence of detritus. The dates appear to be reliable, but their precision is variable. Three new radiocarbon dates on charcoal have also been produced from the upper 18 m of the sequence by I. Kristen (GFZ, Potsdam). These dates, together with seven radiocarbon dates on bulk organic material from a core collected in 1988/89, and an estimated age for the top of the sequence, allow several age-depth models to be constructed for the sediments.

The polynomial models fitted by non-weighted least-squares regression provide the best fit to the available age-determinations, and the cubic model appears to be the most accurate of these alternatives. The changes in sedimentation rate implied by this model can be accounted for by changes in the average gradient of the basin, and by changes in autochthonous sediment influx. It is not possible to determine with certainty whether this model is an accurate reflection of reality, however. In particular, it remains uncertain whether there were abrupt changes in the rate of sediment deposition during the lake's history.

The cubic age-depth model is significantly different from that proposed by Partridge *et al.* (1997), because it suggests that the lacustrine sediments were deposited over the last ~320 kyr, as opposed to the last ~200 kyr (Partridge *et al.*, 1997). This difference has significant implications for the timing and frequency of palaeoclimatic changes recorded in the lake sediments (Partridge *et al.*, 1999). This information could, in turn, affect our understanding of the nature and causes of palaeoclimatic change in the summer rainfall region of South Africa, as Tswaing is the only site that provides a long, continuous record of palaeoclimatic change in this region (chapter 5). It is not currently possible to assess whether the new model is more reliable than that proposed by Partridge *et al.* (1997) because, although the $^{230}Th/^{234}U$ dates presented in this chapter appear to be accurate, the model presented by Partridge *et al.* (1997) is in better agreement with the fission-track date for crater formation (Storzer *et al.*, 1993, 1999; Koeberl *et al.*, 1994).

Further dating is therefore needed to assess the accuracy of the different age-depth models for the sedimentary sequence from Tswaing crater lake, as well as to improve these models. Further $^{230}Th/^{234}U$ analysis may go some way towards this aim. Analysis of additional samples could be used to further constrain the mixing lines presented in this chapter, and to thereby increase the certainty associated with the $^{230}Th/^{234}U$ dates calculated from them. The production of additional $^{230}Th/^{234}U$ dates from different sections of sediment could also improve the age-depth model for the sequence. Ideally, additional dates should also be produced using different methods, in order to independently assess the accuracy of the $^{230}Th/^{234}U$ dates. Unfortunately, relatively few techniques are suitable for dating the sediments from Tswaing, due to their age and composition. The most promising method currently available is $^{40}Ar/^{39}Ar$ dating, which could be used to date impact glass at the base of the sequence, and thereby yield a new date for crater formation (McDougall and Harrison, 1999).

Chapter 5: Records of late Quaternary climatic change at Tswaing crater lake on orbital timescales

5.1 Introduction

The relative influence of precessionally-driven changes in insolation and changes in global boundary conditions associated with glacial-interglacial cycles on climatic conditions at low latitudes remains uncertain, particularly in Africa (chapter 1). Records from the northern tropics and subtropics of the continent demonstrate that direct insolation has affected precipitation in these areas, but also suggest that global boundary conditions have influenced climatic conditions (cf. Gasse, 2000). Records from equatorial Africa also provide strong evidence for the influence of both direct insolation and global boundary conditions on precipitation during the late Quaternary (*e.g.* Trauth *et al.*, 2003). In contrast, records from the southern African tropics and subtropics suggest that global boundary conditions have determined climatic conditions since the LGM (cf. Gasse, 2000; Barker and Gasse, 2003), but that precessionally-driven changes in insolation may have been the primary control on precipitation before this period (Partridge *et al.*, 1997, 1999; Gasse and van Campo, 2001).

Palaeoclimatic records from Tswaing crater lake have made a significant contribution to our understanding of climatic change in southern Africa, due to their unique length and location (chapter 1) (Partridge *et al.*, 1997, 1999). The record of MAP from the site indicates that rainfall was determined by precessionally-driven changes in insolation between ~50 and 200 kyr B.P., in line with models of precipitation in regions affected by monsoonal circulation (*e.g.* Kutzbach, 1981; Kutzbach and Otto-Bliesner, 1982; Kutzbach and Street-Perrott, 1985). After ~50 kyr B.P., this relationship breaks down, and regional or global boundary conditions appear to have become the primary influence on climatic conditions at the site (Partridge *et al.*, 1997, 1999). The certainty associated with these findings is limited by the poor chronological control of the sedimentary sequence (chapter 4), and the fact that the

record of MAP is based on low resolution records of the grain-size and carbonate content of the sediments, both of which can be controlled by a number of different processes (chapter 1).

New cores from the lake provide the opportunity to increase the certainty associated with palaeoclimatic reconstructions from the site by producing additional, higher-resolution records of palaeoenvironmental change. This chapter therefore presents new, high-resolution records of the amount of organic material and carbonate in the sediments (based on %LOI 550°C and %LOI 950°C), the oxygen- and carbon-isotope composition of calcite ($\delta^{18}O_{calcite}$ and $\delta^{13}C_{calcite}$), and the carbon isotope composition ($\delta^{13}C_{organic}$) and C/N ratios of bulk organic matter from the newly-extracted sediment cores. These records are used to reconstruct palaeoenvironmental conditions at the site over the entire sedimentary sequence, with support from records of diatom assemblage composition and siliceous microfossil concentrations from the section of the sequence between 34.40 and 54.80 m (chapter 6). The implications of these reconstructions for our understanding of the nature and causes of palaeoclimatic change at Tswaing are then discussed in light of the new age-depth model for the sedimentary sequence presented in chapter 4. These findings are significantly different from those of Partridge *et al.* (1997, 1999), and the implications of these differences are addressed in the final section of the chapter.

5.2 Previous palaeoclimatic records from Tswaing crater lake

As mentioned in chapter 1, a core of lacustrine sediments was obtained from Tswaing crater lake in 1988/89 by a team led by Prof. T. C. Partridge (Climatology Research Unit, University of the Witwatersrand), and a number of palaeoenvironmental records were produced from this material. The most informative of these records are summarised briefly in this section, as background to the new records presented in this chapter. All depths are based on the corrected depth scale constructed by eliminating mass-flow deposits from the sequence (Partridge *et al.*, 1997).

The record of MAP at the site produced by Partridge *et al.* (1997) is based on the percentage carbonate in the sediments and the proportion of clastic material with a grain size <20 μm (Fig. 5.1). The authors proposed that the amount of carbonate in

the sediment reflects the evaporative concentration of lake water, and that the grain size of clastic material was determined by moisture availability (through its influence on chemical weathering of the granitic crater walls and on pedogenesis in the basin). Low carbonate-content and a high proportion of clastic material <20 μm in diameter were therefore considered to indicate high precipitation. The record was calibrated using grain-size analysis of sixteen soil samples from different regions in South Africa, allowing the authors to reconstruct MAP at the site.

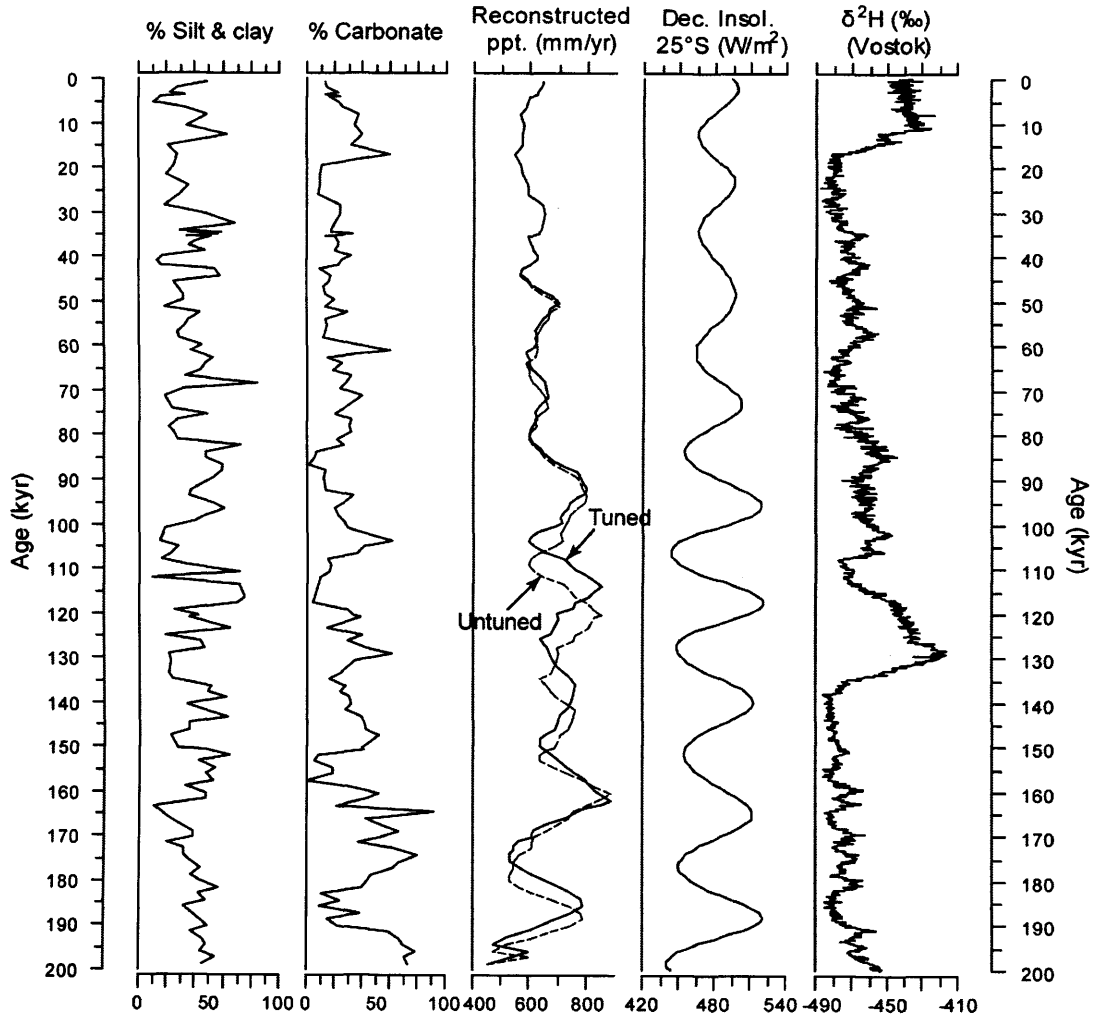

Figure 5.1: Records of the proportion of clastic material <20μm in diameter (% silt and clay) and the percentage carbonate content of sediments from Tswaing crater lake produced from the core obtained in 1988/89, and the record of MAP produced from these proxies (Partridge *et al.*, 1997, 1999). Records are plotted against the tuned age-depth model for the sequence, but the rainfall record is also plotted against the untuned model for comparison (grey dashed line) (chapter 4) (Partridge *et al.*, 1997). Mean daily insolation at 25°S between the 21st of November and the 20th of December (Laskar *et al.*, 2004), and the deuterium record from Vostok (Petit *et al.*, 1999) are also shown.

Pollen and spores are only preserved in short sections of the sediments, and are almost completely absent from the section between ~31.0 and 60.5 m (Scott, 1999) (cf. Figure A3, Appendix A). The poor preservation could be due to decomposition of organic matter under well-mixed, oxic conditions, or possibly due to subaerial

exposure of the lake sediments (Scott, 1999). Analysis of samples in which pollen is preserved suggests that climatic conditions fluctuated between warm, dry phases characterised by open grassland savanna, and cool, moist phases characterised by grassland, fynbos and *Podocarpus* forest, but gaps in the record make it difficult to compare these fluctuations with the record of MAP from the core (Scott, 1999). Metcalfe (1993, 1999) examined diatom assemblage composition at 0.5 m intervals above 17.0 m, and at 1.0 m intervals between 17.0 m and the base of the core (cf. Figure A4, Appendix A). The record shows that the lake was relatively fresh (~500 $\mu S\ cm^{-1}$) below 33.5 m, with the exception of a short-lived shift to higher conductivities (~6,000 $\mu S\ cm^{-1}$) at 46-49 m. A shift in assemblage composition and an increase in the number of sections in which diatoms are not preserved indicate that the lake was significantly more saline and alkaline above 33.5 m. Reconstructed conductivity values increase to ~15,000 $\mu S\ cm^{-1}$ at this depth, and remain high until the top of the record, with the exception of a decrease to ~2,000 $\mu S\ cm^{-1}$ at ~22 m. Again, the poor preservation of diatom valves in some sections of the core makes it difficult to compare these findings with the record of MAP produced by Partridge *et al.* (1997).

5.3 Methods

5.3.1 %LOI at 550°C and 950°C

Samples for %LOI measurements were taken at 16 cm intervals throughout the sedimentary sequence, except where there are gaps or the sediments are disturbed, and were processed using standard procedures (Dean, 1974; Heiri *et al.*, 2001). 1-2 g of sediment was heated to 105°C for 12 hours, allowed to cool to room temperature in a desiccator, and weighed. The samples were then heated to 550°C for 2 hours, cooled in a desiccator, and reweighed in order to calculate %LOI 550°C. Finally, the samples were heated to 950°C for 4 hours, cooled, and reweighed. The weight loss at 950°C was multiplied by 1.36 to allow the percent carbonate content of the dry samples to be calculated (since the molar mass of CO_3 is 1.36 times the molar mass of CO_2) (Bengtsson & Enell, 1986). Care was taken to ensure that sample weight, exposure time, and ignition temperatures were constant, in order to reduce errors associated with variation in these parameters (Heiri *et al.*, 2001).

5.3.2 $\delta^{18}O_{calcite}$ and $\delta^{13}C_{calcite}$

Samples were taken at 4 to 8 cm intervals between 34.40 and 54.80 m, and at 16 cm intervals between 12.80 and 34.40 m and between 54.80 m and the base of the sequence. The section of the sequence above 12.80 m was not sampled because XRD analysis of the core taken in 1988/89 showed that almost all carbonate in this section is trona ($Na_3(CO_3)HCO_3.2H_2O$) or gaylussite ($Na_2Ca(CO_3)_2.5H_2O$) (Bühmann and Elsenbroek, 1999), and the factors that control the isotope composition of these minerals have not been fully investigated (cf. Smith *et al.*, 1987; Li *et al.*, 1997; Mees *et al.*, 1998). The sediment above 22.00 m contains both calcite and trona (Bühmann and Elsenbroek, 1999), and samples between 12.80 and 22.00 m were therefore heated to 50°C in 50 ml of deionised distilled water for 30 minutes and rinsed three times before further treatment, to remove trona (which is readily soluble).

To prepare the samples for analysis, ~1-2 cm^3 of each sample was reacted with 100 ml of 5% sodium hypochlorite for 12 hours to oxidise organic matter, and then sieved at 80 μm to remove coarse biogenic carbonates (although none proved to be present). The <80 μm fraction was rinsed three times, dried overnight at 40°C, and ground to a fine power. The $\delta^{18}O$ and $\delta^{13}C$ values of the samples were determined by reacting 10 mg of the sample with anhydrous phosphoric acid *in vacuo* overnight at 25°C (McCrea, 1950), separating the carbon dioxide produced during this reaction from water vapour using liquid nitrogen traps, and then analysing the dry gas in a VG Optima mass spectrometer. Results were calculated relative to VPDB, based on the calibration of laboratory standards against NBS-19. Analysis of laboratory standards showed that analytical reproducibility was ±0.1‰ (1 s.d.). All samples were prepared by the author, but mass spectrometry was carried out by J. Greene (NIGL).

5.3.3 $\delta^{13}C_{organic}$ and C/N ratios

Samples for $\delta^{13}C$ and C/N analysis of bulk organic matter were taken at 8 cm intervals between 34.40 and 54.80 m, and at 16 cm intervals in the rest of the sequence. Each sample was reacted with ~100 ml of 5% HCl for 12 hours to remove carbonates, rinsed three times, dried overnight at 40°C, and then ground to a fine powder. $\delta^{13}C$, percentage carbon, and percentage nitrogen were analysed during combustion in a Carlo Erba 1500 elemental analyser coupled on-line to a VG TripleTrap and dual-inlet

mass spectrometer (section 3.3.2). $\delta^{13}C$ values were converted to the VPDB scale using a within-run laboratory standard calibrated against NBS-19 and NBS-22, and C/N ratios were calibrated against an acetanilide standard. Analysis of laboratory standards showed that analytical reproducibility was ±0.1‰ for $\delta^{13}C$ and ±0.3 for C/N measurements (1 s.d.). Again, samples were prepared by the author, but mass spectrometry was carried out by J. Greene (NIGL).

5.4 Results

The records produced from the sedimentary sequence are shown in Figure 5.2, together with major (>40 cm) zones of laminated sediments (smaller sections of laminated sediments are not shown because they are not easily resolved in the figure). The records were used to divide the sequence into eleven stratigraphic zones, which are also shown in Figure 5.2. As in other sections of this thesis, all depths quoted in this chapter are on the corrected depth scale constructed by elimination of mass-flow deposits from the sedimentary sequence (chapter 4).

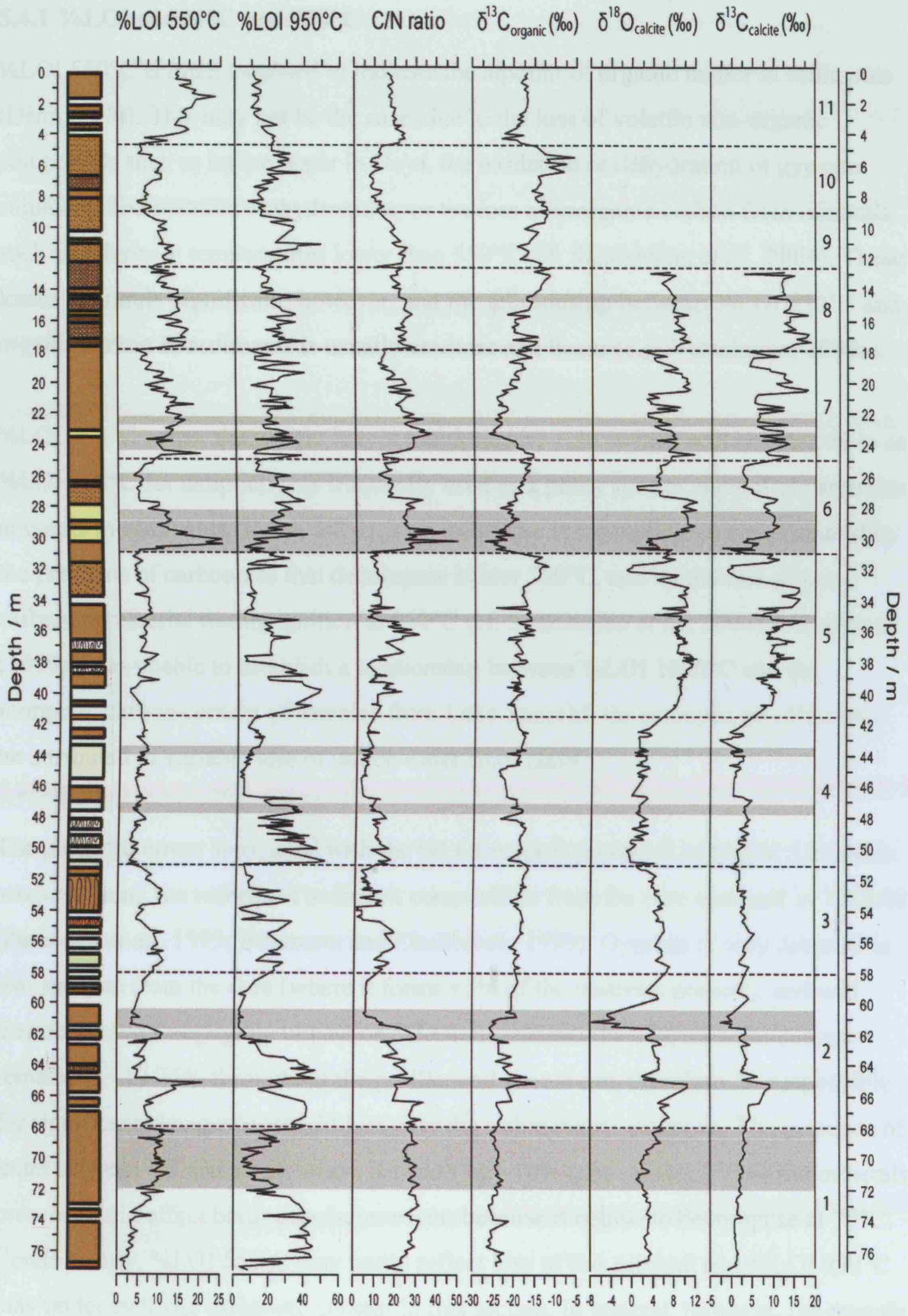

Figure 5.2: Records of %LOI 550°C, %LOI 950°C, C/N ratios and $\delta^{13}C_{organic}$ of bulk organic matter, $\delta^{18}O_{calcite}$, and $\delta^{13}C_{calcite}$ from the sedimentary sequence plotted against the corrected depth scale described in chapter 4. Stratigraphic zones defined by the records are shown by dotted lines. Grey bars indicate zones of laminated sediments >40 cm in width. A summary stratigraphic log is also shown (see Figure 4.3 for key).

5.4.1 %LOI at 550°C and 950°C

%LOI 550°C is often assumed to indicate the amount of organic matter in sediments (Dean, 1974). This may not be the case, due to the loss of volatile non-organic compounds such as lattice water in clays, the oxidation or dehydration of gypsum, sulphides, and metallic oxihydroxides, or the loss of inorganic carbon from minerals such as siderite at temperatures lower than 550°C (cf. Santisteban *et al.*, 2004). These losses are rarely significant, however, and the relationship between %LOI 550°C and organic carbon in sediments is usually constant and linear (*e.g.* Verschuren, 1999a).

%LOI 950°C where the weight loss is multiplied by 1.36 (which will be referred to as %LOI 950°C for simplicity) is frequently used as a proxy for the amount of carbonate minerals in sediments (Dean, 1974). This technique is susceptible to errors caused by the presence of carbonates that decompose below 550°C, and by the loss of non-carbonate material during ignition at 950°C (cf. Santisteban *et al.*, 2004). Verschuren (1999a) was unable to establish a relationship between %LOI 1000°C and the inorganic carbon content of samples from Lake Sonachi, for example; an effect that he attributed to variable loss of lattice water from clays.

The potential errors associated with the %LOI records presented in Figure 5.2 can be assessed using the records of sediment composition from the core obtained in 1988/89 (Partridge *et al.*, 1993; Bühmann and Elsenbroek, 1999). Gypsum is only detected in two samples from the core (where it forms <5% of the minerals present), and will therefore have a negligible impact on %LOI measurements. Clay mineral content remains at ~10-15% throughout the profile, and should not, therefore, be responsible for significant changes in weight loss over the sedimentary sequence. The presence of trona between 4.5 and 22 m, where it makes up ~10% (and up to 22%) of the minerals present, could affect both records, however, because it begins to decompose at 70°C. Consequently, %LOI 550°C may partly reflect loss of this mineral and %LOI 950°C may under-estimate carbonate content in this section. In general, however, the records should provide an accurate indication (though not quantitative records) of the organic matter and carbonate content of the sediments. This finding is confirmed for %LOI 550°C by the similarity of changes in this record with variations in percent organic carbon determined during C/N analysis.

%LOI 550°C fluctuates between 1% and 25% of the dry weight of the sediment over the course of the record. The record increases from less than 1% at the base of the sequence to 14% at the top of zone 1 (68.00 m), and then fluctuates between ~5% and ~20% until the top of zone 3 (51.10 m), peaking at approximately 65.2, 62, 56, and 53 m. The record then decreases and remains at ~5% until the top of zone 5 (31.00 m). In zones 6 to 11 (31.00 m to the top of the sequence), the record fluctuates significantly, increasing from minima of ~5% to maxima of between 11% and 25% in each zone.

%LOI 950°C indicates that the carbonate content of the sediment fluctuates between 2% and 51% of dry weight over the sedimentary sequence. In zones 1 to 5 (base of the sequence to 31.00 m), the record fluctuates between ~2% and ~45%, peaking once in zones 1 and 4, and twice in zones 2, 3, and 5. In zones 6 to 11 (31.00 m to the top of the sequence), the record fluctuates around 20%, but is highly variable, with sudden shifts of ~15%. Some trends are discernible in this section, however, with the record peaking in the middle of zone 6, the lower part of zone 8, the middle of zone 9, and at the top of zone 10.

5.4.2 $\delta^{18}O_{calcite}$ and $\delta^{13}C_{calcite}$

The stable isotope composition of the carbonates analysed should primarily reflect the composition of calcite, because trona is the only other form of carbonate present in significant quantities below 12.80 m, and this mineral was removed before analysis (Bühmann and Elsenbroeck, 1999). It should be noted, however, that XRD analysis of the core obtained in 1988/89 showed that dolomite was present at ~25 and ~64 m, and that aragonite and Mg-calcite were present at ~61-63 m (Bühmann and Elsenbroeck, 1999). In addition, XRD analysis of twenty-three samples between 34.00 and 56.00 m in this study revealed the presence of dolomite at 44.84 and 54.39 m, although this mineral made up less than 2% of the calcium carbonate present. This analysis also revealed the presence of Mg-calcite, which contained an average of 7 mol% $MgCO_3$, in half the samples analysed.

The use of off-line extraction during stable isotope analysis minimises the influence of dolomite, which has a much longer reaction time than calcite, but the presence of aragonite and Mg-calcite may increase the isotope values of these samples relative to those that only contain calcite (sections 2.2.2 and 2.2.3) (Tarutani *et al.*, 1969; Turner,

1982; Grossman and Ku, 1986; Jiménez-López *et al.*, 2004, 2006; Kim and O'Neil, 2005). Mg-calcite that contains 7 mol% $MgCO_3$ would theoretically have a $\delta^{18}O$ value ~0.42‰ higher, and a $\delta^{13}C$ value ~0.17‰ higher than calcite (Tarutani *et al.*, 1969; Jiménez-López *et al.*, 2006). These shifts are small compared to the fluctuations in the $\delta^{18}O_{calcite}$ and $\delta^{13}C_{calcite}$ records, and should consequently have a negligible impact on their interpretation.

SEM analysis carried out in this study also indicates that the dominant form of carbonate in the samples is probably calcite, because most of the grains observed were rhombohedral (Fig. 5.3). Calcite and dolomite are both based on rhombohedral unit cells, and thus form rhombohedral crystals, although they can also precipitate as polyhedral crystals (probably due to the rate of crystallisation or the chemical composition of lake water) (Kelts and Hsü, 1978). Aragonite, in contrast, is based on an orthorhombic unit cell and thus produces orthorhombic crystals (Tucker and Wright, 1990).

It is likely that the samples contain negligible quantities of detrital carbonate, because the only sources of carbonate in the lake basin are the small outcrops of intrusive rocks exposed on the crater walls (section 3.2.5) (Brandt and Reimold, 1999). The regular form of most crystals observed using SEM confirms this suggestion, as detrital carbonates usually have irregular anhedral to subhedral grains that are rounded or flaky (cf. Kelts, 1998). Some of the carbonate grains observed did have an irregular structure, however. Given that it is unlikely that detrital grains are present, this morphology could indicate authigenic carbonate precipitation or carbonate diagenesis, as both these processes can produce irregularly-shaped grains (Fig. 5.4) (cf. Talbot and Kelts, 1986, 1990). This is not necessarily the case, however, as authigenic calcite grains can be regularly shaped if they grow slowly within lacustrine sediments (Street-Perrott, pers. comm.).

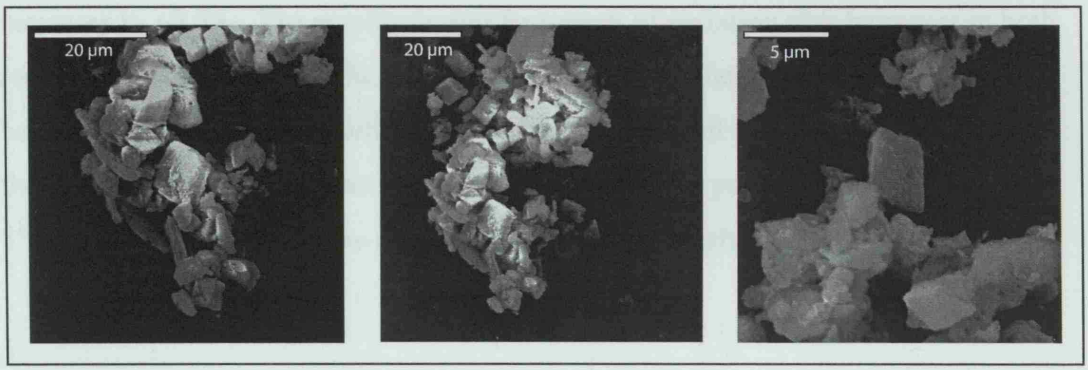

Figure 5.3: SEM images of carbonates from the sediments showing the rhombohedral structure of endogenic calcite grains.

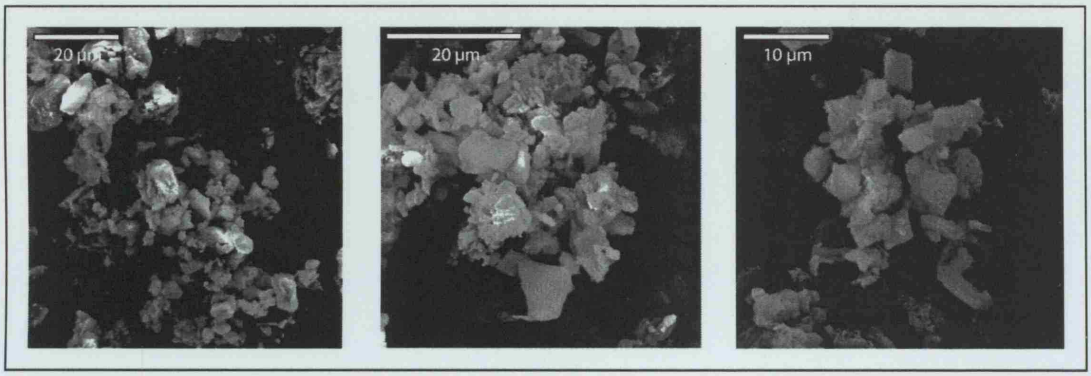

Figure 5.4: SEM images of carbonates from the sediments showing irregular grains that may indicate authigenic carbonate precipitation or carbonate diagenesis.

$\delta^{18}O_{calcite}$ values from the sedimentary sequence range from −7.7‰ to +12.0‰, and $\delta^{13}C_{calcite}$ values vary between −2.7‰ and +18.6‰ (Fig. 5.2). Both these ranges are unusually large for carbonates from lacustrine sediments (cf. Leng and Marshall, 2004). The $\delta^{13}C_{calcite}$ values are particularly unusual, as the maximum value is one of highest observed in lacustrine carbonates (cf. Valero-Garcés, 1999). It is also notable that the records are positively correlated, with an r value of 0.8 ($p = <0.001$) (Fig. 5.5a). The most significant feature of the records is the increase in both $\delta^{18}O_{calcite}$ and $\delta^{13}C_{calcite}$ between zones 4 and 5 (41.50 m), where $\delta^{18}O_{calcite}$ increases from +3.1‰ to +8.1‰, and $\delta^{13}C_{calcite}$ increases from +1.5‰ to +8.2‰. Below this shift (zones 1 to 4), the average $\delta^{18}O_{calcite}$ and $\delta^{13}C_{calcite}$ values are +3.0‰ and +2.5‰, respectively, and the records show relatively little variation ($\delta^{18}O_{calcite}$ s.d. = 2.5‰, $\delta^{13}C_{calcite}$ s.d. = 1.6‰), although $\delta^{18}O_{calcite}$ decreases markedly at ~61 m. Above the shift (zones 5 to 8), the average $\delta^{18}O_{calcite}$ value increases to +7.8‰, and the average $\delta^{13}C_{calcite}$ value

increases to +9.5‰. The amplitude and frequency of variation also increases in both records ($\delta^{18}O_{calcite}$ s.d. = 2.7‰, $\delta^{13}C_{calcite}$ s.d. = 4.0‰). The degree of correlation between the records is the same above and below the shift ($r = 0.7$, $p = <0.001$), but the relationship between them is different (Fig. 5.5b). In particular, changes in $\delta^{13}C_{calcite}$ are accompanied by smaller shifts in $\delta^{18}O_{calcite}$ above 41.50 m (Fig. 5.5b).

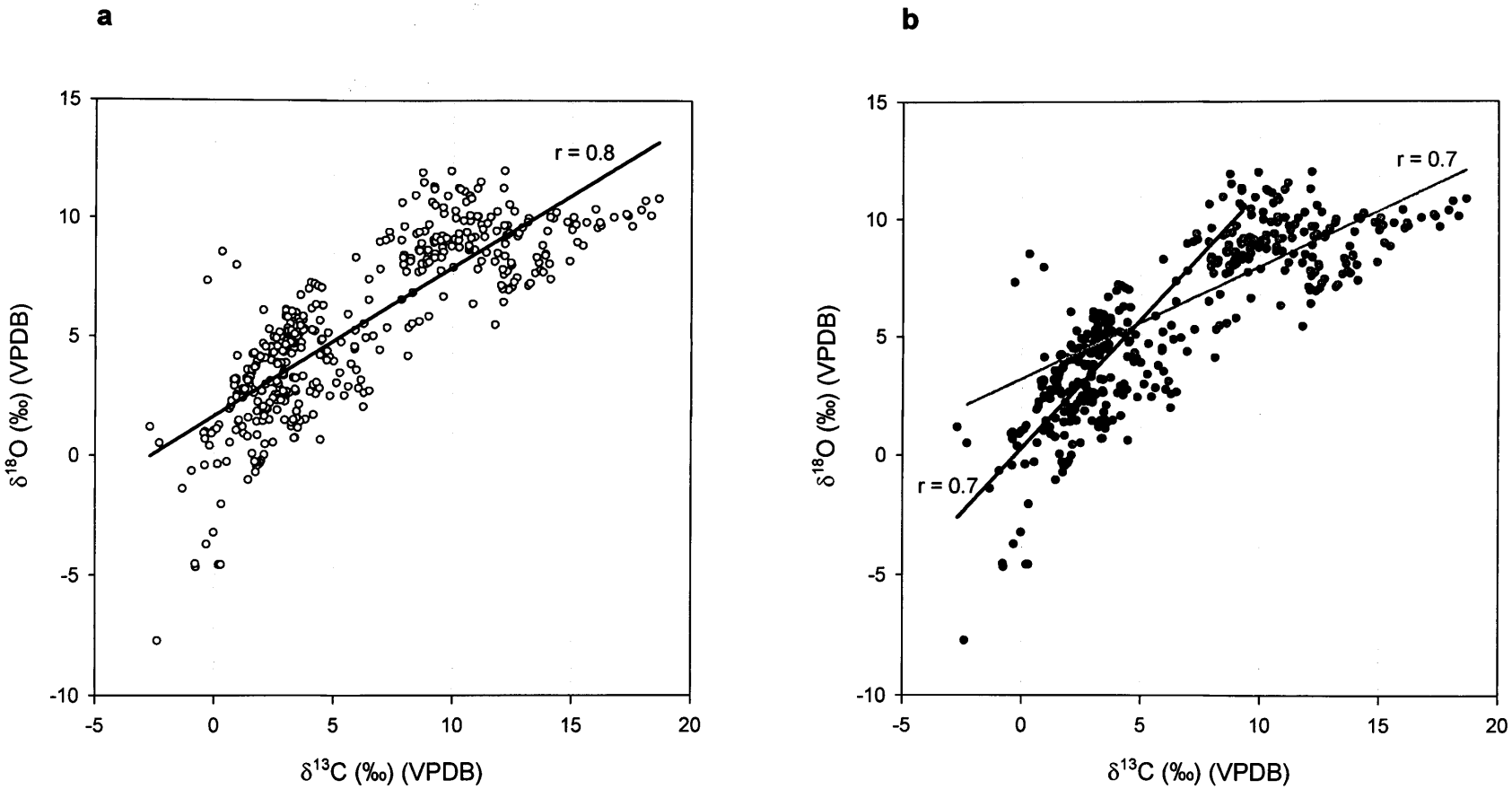

Figure 5.5: Correlation of $\delta^{18}O_{calcite}$ and $\delta^{13}C_{calcite}$ values of samples from (a) the entire sedimentary sequence, (b) above 41.50 m (grey circles and regression line) and below 41.50 m (black circles and regression line).

5.4.3 $\delta^{13}C_{organic}$ and C/N ratios

$\delta^{13}C_{organic}$ varies between −5.7‰ and −27.5‰, and C/N ratios range from 0.7 to 49 over the sequence. Below 62.0 m (bottom of the sequence to the middle of zone 2), $\delta^{13}C_{organic}$ fluctuates around −24‰, and C/N ratios remain close to 25, but between 62.00 m and 31.00 m (middle of zone 2 to zone 5), $\delta^{13}C_{organic}$ increases to ~−19‰, and C/N ratios decrease to ~10. Above 31.00 m (zones 6 to 11), the records are more variable. $\delta^{13}C_{organic}$ increases gradually in a series of steps, reaching successively higher maxima and minima in zones 6 to 10, before decreasing to −22‰ in zone 11, and finally increasing to −17‰ at the top of the record. C/N ratios decrease in a step-wise manner in this section of the record, reaching maxima at approximately the same depths as minima in $\delta^{13}C_{organic}$. The two records are significantly anti-correlated throughout the record ($r = -0.5$, $p = <0.001$) (Fig. 5.6a), but the degree is slightly higher above 31.00 m ($r = -0.7$, $p = <0.001$) than below this level ($r = -0.6$, $p = <0.001$) (Fig. 5.6b).

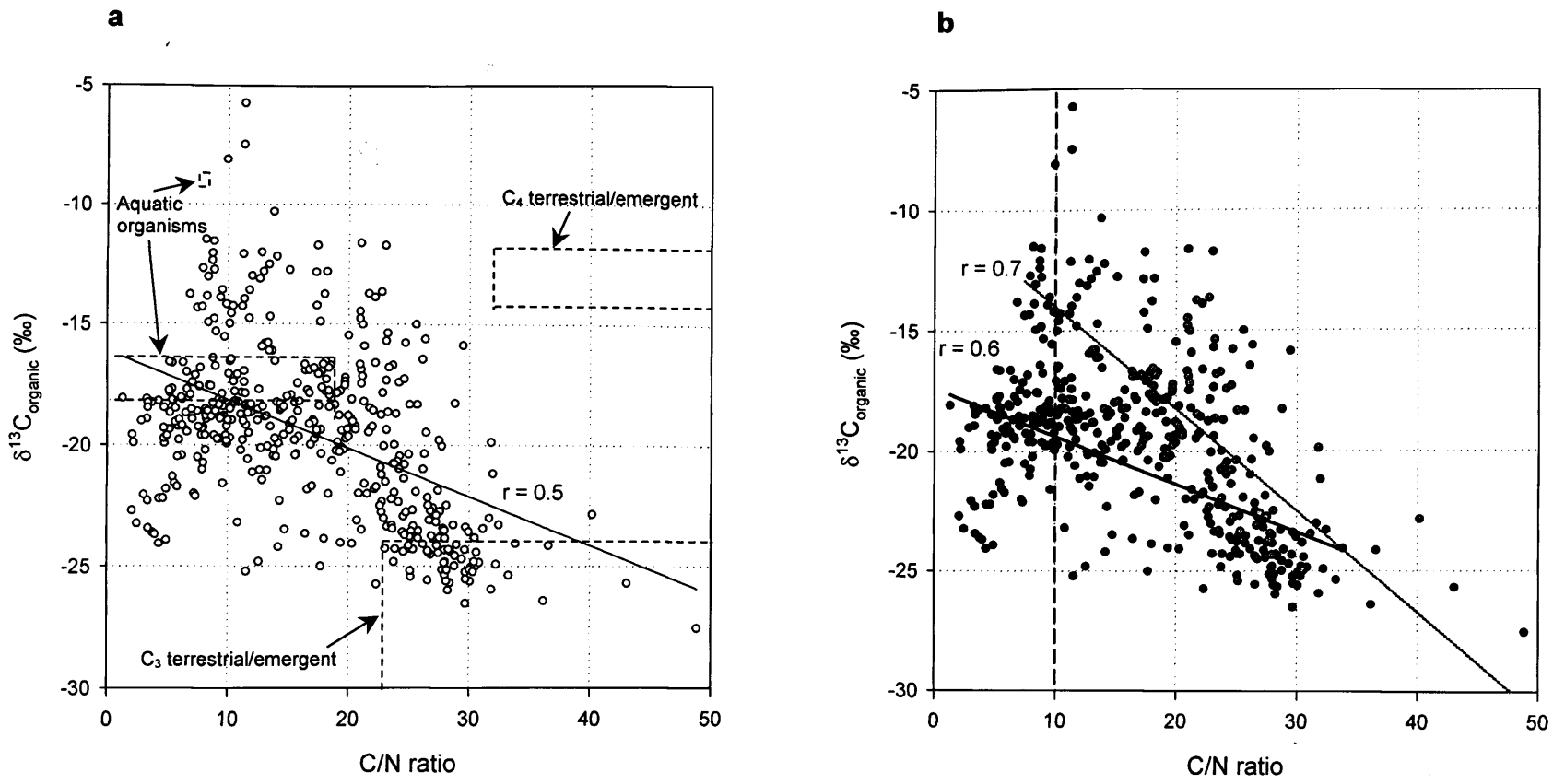

Figure 5.6: Correlation of $\delta^{13}C_{organic}$ and C/N ratios of samples from (a) the entire sedimentary sequence, (b) above 31.00 m (grey circles and regression line) and below 31.00 m (black circles and regression line). The ranges of $\delta^{13}C_{organic}$ and C/N ratios associated with organic matter from the modern environment are also shown in plot (a) (chapter 3). C/N ratio of 10 is shown as a black dashed line in (b) to highlight the different $\delta^{13}C_{organic}$ values of samples with C/N ratios <10 above and below 31.00 m.

5.5 Interpretation

In the following sections, the records of $\delta^{18}O_{calcite}$ and $\delta^{13}C_{calcite}$, and of $\delta^{13}C_{organic}$ and C/N ratios of bulk organic material from the sedimentary sequence are used to reconstruct palaeoenvironmental conditions at the site, in light of the records of %LOI 550°C and %LOI 950°C.

5.5.1 $\delta^{18}O_{calcite}$ and $\delta^{13}C_{calcite}$

The correlation between $\delta^{18}O_{calcite}$ and $\delta^{13}C_{calcite}$ ($r = 0.8$, $p = <0.001$), and the large range of values in both records ($\delta^{18}O_{calcite} = 19.7‰$, $\delta^{13}C_{calcite} = 21.3‰$), suggest that the lake has been hydrologically closed since its formation (section 2.2.4) (Talbot, 1990). This proposal is supported by the finding that the lake is almost certainly hydrologically closed today (chapter 3), and by the lack of evidence for surface outflow from the crater in the past. In hydrologically closed basins, the $\delta^{18}O$ and $\delta^{13}C_{DIC}$ of lake water are usually determined by the I/E ratio of the lake, and it is therefore likely that the records of $\delta^{18}O_{calcite}$ and $\delta^{13}C_{calcite}$ reflect changes in this ratio (section 2.2.4) (cf. Leng and Marshall, 2004).

The response of $\delta^{18}O_{calcite}$ and $\delta^{13}C_{calcite}$ to changes in the I/E ratio depends on the residence time of the lake. In the early part of its history, the lake may have been relatively deep, with a small surface-area to volume ratio, because the crater floor would have been up to 90 m below the local water table (if the height of the water table was similar to that at the site today) (chapter 3). Consequently, the $\delta^{18}O$ and $\delta^{13}C_{DIC}$ of lake water may have been relatively insensitive to changes in the I/E ratio of the lake, and may have remained at isotopic steady-state for significant periods of time (sections 2.1.2 and 2.1.3). It is also worth noting that the steady-state values of $\delta^{18}O_{lakewater}$ and $\delta^{13}C_{DIC}$ may be independent of lake volume in hydrologically closed lakes, because the I/E ratio (which determines $\delta^{18}O_{lakewater}$) is 1 at hydrological steady-state, regardless of lake volume, and the $\delta^{13}C$ of atmospheric CO_2 (which often determines $\delta^{13}C_{DIC}$ at steady-state) is constant (sections 2.1.2 and 2.1.3) (cf. Gat, 1995; Li and Ku, 1997). The records of $\delta^{18}O_{calcite}$ and $\delta^{13}C_{calcite}$ may therefore tend to revert to steady-state values if lake levels stabilised after a change in I/E ratio, irrespective of changes in lake volume (cf. Ricketts and Johnson, 1996).

The relatively low variability of $\delta^{18}O_{calcite}$ and $\delta^{13}C_{calcite}$ below 41.50 m (zones 1 to 4) suggests that the lake may have been close to isotopic steady-state for much of this section. The average $\delta^{13}C_{calcite}$ value below 41.50 m is +2.5‰, which supports this suggestion, as carbonates precipitating from bicarbonate in equilibrium with atmospheric CO_2 have $\delta^{13}C_{calcite}$ values of ~+3‰ (assuming a $\delta^{13}C$ of –6.7‰ for atmospheric CO_2 (measured in 1956 by Keeling *et al.* (1979)) (sections 2.1.3 and 2.2.3) (Turner, 1982; Salomons and Mook, 1986). The average $\delta^{18}O_{calcite}$ value below 41.50 m is +3.0‰, which indicates that the $\delta^{18}O$ of lake water was ~+4.7‰ (if the temperature of water in the epilimnion is assumed to have been 22°C when carbonates precipitated, as it is today (Ashton and Schoeman, 1983)) (section 2.2.2) (Kim and O'Neil, 1997). This value suggests that the lake was enriched in heavy isotopes at steady-state (due to evaporative concentration), if it is assumed that the average $\delta^{18}O$ of lake-water inputs, which is currently ~–4.4‰, was similar in the past (chapter 3).

In the lower part of zone 1 (base of the sequence to 72.00 m), $\delta^{18}O_{calcite}$ increases rapidly from −4.6‰ to +3.7‰ and then remains at this level, while $\delta^{13}C_{calcite}$ initially increases slightly from −0.8‰ to +1.7‰ and then remains relatively constant (Fig. 5.2). The $\delta^{18}O_{calcite}$ value of −4.6‰ at the base of the sequence is similar to the $\delta^{18}O_{calcite}$ value of −6.1‰ that would be expected if the $\delta^{18}O$ of lake water was the same as that of water that currently supplies the lake (assuming a lake-water temperature of 22°C) (Kim and O'Neil, 1997). It is therefore possible that the crater initially filled with water that had a similar $\delta^{18}O$ value to that feeding the lake today. The increase in $\delta^{18}O_{calcite}$ by 8.3‰ immediately above the base of the sequence suggests that evaporative concentration rapidly increased the $\delta^{18}O$ of lake water, however. %LOI 950°C also increases significantly at the base of the sequence, indicating that evaporative concentration of the lake water caused endogenic carbonate to precipitate from the water column (section 2.2.1). This relationship is not unexpected, as the sequence of autochthonous minerals in the sediments suggests that carbonates precipitated in response to evaporative concentration (section 3.2.5) (Partridge *et al.*, 1993; Bühmann and Elsenbroek, 1999).

In the upper part of zone 1 (72.00 to 68.00 m), $\delta^{18}O_{calcite}$ decreases slightly to +0.8‰ before increasing to +5.8‰ at the top of the zone, while $\delta^{13}C_{calcite}$ increases gradually to +3.7‰. The slight decrease and subsequent increase in $\delta^{18}O_{calcite}$ in this section is

accompanied by a similar change in %LOI 950°C, which falls from over 40% to 5%, before returning to 40%. These shifts indicate that the I/E ratio of the lake increased temporarily in this part of the sequence. Moreover, the laminated and organic-rich nature of the sediments between 72 and 68 m suggests that this shift increased the depth of the lake, and thereby prevented wind-induced turn-over, allowing anoxia to develop in the hypolimnion. $\delta^{13}C_{calcite}$ does not decrease in this section, but there are a number of reasons why $\delta^{13}C_{DIC}$ would not respond to an increase in the I/E ratio. It is possible that DIC remained in equilibrium with atmospheric CO_2 because the change in I/E ratio was slow. Alternatively, increased preservation of organic matter in the hypolimnion may have increased $\delta^{13}C_{DIC}$, and thus countered any decrease caused by the increase in I/E ratio. Finally, any decrease in $\delta^{13}C_{DIC}$ caused by the increase in I/E ratio may have been muted because the concentration of DIC in groundwater was low compared to that in the lake (section 2.2.4) (Li and Ku, 1997).

In zone 2 (68.00 to 58.00 m), $\delta^{18}O_{calcite}$ increases to +11‰ and $\delta^{13}C_{calcite}$ increases to +9‰ at 65 m. Both records then decrease to values similar to those at the base of the sequence at 61 m, before returning to their former values at the top of the zone. The positive excursion in the records at 65 m suggests that the I/E ratio decreased at this depth. %LOI 950°C decreases from 40% to 20% at this level, however, which is the opposite shift to that expected if the amount of carbonate in the sediment was determined by the concentration of the lake water. The diatom record from the core obtained in 1988/89 indicates that the lake decreased in depth and increased in conductivity at this level, and thus supports the proposal that the I/E ratio decreased at this time (subzone Ic in Figure 3.1 in Metcalfe, 1999). It is therefore likely that the decrease in %LOI 950°C was caused by the increase in the proportion of organic matter in the sediments at this depth (%LOI 550°C increases from 8% to 20%), which may have decreased the relative abundance of carbonate in the sediments. Furthermore, the laminated nature of the sediments between 65.5 and 65.0 m suggests that the increase in the abundance of organic matter was caused by a return to stratified conditions, presumably due to an increase in the salinity-induced stability of the lake. This mixing regime may have further decreased %LOI 950°C by increasing carbonate dissolution in the sediments, as sulphate reduction and acetate fermentation in anoxic environments can decrease the pH of pore water (section 2.2.1).

The marked negative excursion in $\delta^{18}O_{calcite}$ and the smaller excursion in $\delta^{13}C_{calcite}$ centred on 61 m suggest that there was a significant increase in the I/E ratio of the lake at this depth. This interpretation is supported by an increase in the relative abundance of arboreal pollen at this level (zone Z4 in Figure 4 in Scott, 1999) (cf. Figure A3, Appendix A). %LOI 950°C is also low at this depth, supporting the proposal that the I/E ratio of the lake was high, although the decrease in this record is longer and more gradual than that in the isotope records, extending from 63.5 to 58.0 m. Close examination of the $\delta^{18}O_{calcite}$ and $\delta^{13}C_{calcite}$ records shows that these proxies also decrease between 63.5 and 58.0 m, but that the gradual shifts in this section are partly obscured by the much sharper event centred on 61 m. The different responses of %LOI 950°C and the isotope records to the increase in I/E ratio may therefore reflect saturation of the %LOI 950°C record, or a threshold response in the isotope records. It is also notable that the sections of laminated sediments between 62.5 and 60.5 m suggest that the increase in lake depth that accompanied the increase in I/E ratio once again prevented wind-induced turn-over of the lake.

Many of the changes in $\delta^{18}O_{calcite}$ and $\delta^{13}C_{calcite}$ in zones 3 to 5 (58.00 to 31.00 m) are interpreted in chapter 6, because the diatom assemblage record presented in this chapter provides important information about the factors that control these records in this section of the sequence. Only a brief summary of these findings is therefore presented in this chapter. On average, $\delta^{18}O_{calcite}$ and $\delta^{13}C_{calcite}$ decrease slightly over zone 3 (58.00 to 51.10 m), suggesting that the I/E ratio increased; a finding that is supported by the overall decrease in %LOI 950°C in this zone. In zone 4 (51.10 to 41.50 m), %LOI 950°C suggests that the I/E ratio decreased rapidly and remained low until 46.8 m, when it increased and remained high for the rest of the zone. $\delta^{18}O_{calcite}$ and $\delta^{13}C_{calcite}$ do not reflect these changes, but the records of C/N ratios and diatom assemblage composition suggest that this interpretation is correct, and thus imply that other factors influenced $\delta^{18}O_{calcite}$ and $\delta^{13}C_{calcite}$ at this time (chapter 6).

Between zones 4 and 5 (41.50 m), there is a significant increase in the average values and the variability of the $\delta^{18}O_{calcite}$ and $\delta^{13}C_{calcite}$ records, as well as a change in the relationship between them, indicating that there was a significant shift in palaeohydrological conditions at this depth (Figs. 5.2 and 5.5b). The most likely explanation for these changes is an increase in the surface-area to volume ratio of the

lake, which would have decreased its I/E ratio and increased the sensitivity of $\delta^{18}O_{lakewater}$ and $\delta^{13}C_{DIC}$ to changes in lake-water input and evaporation. Sedimentary infilling of the basin may have caused this change, because the slope of the crater walls and the decrease in lake volume as the lake floor approached the water table (chapter 3) would have increased the surface-area to volume ratio of the lake as the basin filled with sediments. The reason that the transition between these states took place suddenly at 41.50 m is not known, but the presence of a 1.4 m-thick mass flow at this depth suggests that this deposit may have forced the lake across a hydrological threshold by rapidly increasing its surface-area to volume ratio (chapter 6). Alternatively, a permanent decrease in lake level at this depth could have increased the surface-area to volume ratio of the lake, and also triggered the mass-flow.

The average $\delta^{18}O_{calcite}$ value above this shift is +7.8‰, which suggests that carbonates precipitated from water with a $\delta^{18}O$ value of ~+9.5‰, assuming that carbonates precipitated at 22°C (section 2.2.2) (Kim and O'Neil, 1997). This value is unusually high, and suggests that the water from which carbonates precipitated was subject to a similar degree of evaporative concentration as water in the hypolimnion of the modern lake, which has a $\delta^{18}O$ value of +11.0‰ (chapter 3). The average $\delta^{13}C_{calcite}$ value in this section (+9.5‰) indicates that calcite precipitated from DIC with a $\delta^{13}C$ value of ~+7.5‰, which is also unusually high (section 2.2.3) (Turner, 1982; Salomons and Mook, 1986). A number of factors can increase $\delta^{13}C_{DIC}$ during evaporative concentration: increased pCO_2, salinity, and temperature can lead to outgassing of isotopically-light CO_2; increasing nutrient concentration, frequency of lake turn-over, or lake-water temperature can increase productivity; and any increase in pH will increase the proportion of inorganic carbon species in the form of bicarbonate and carbonate ions, which have higher $\delta^{13}C$ than dissolved CO_2 (although the increase in the proportion of carbonate ions relative to bicarbonate ions at very high pH will act to decrease $\delta^{13}C$ slightly) (sections 2.1.3 and 2.2.4). These processes are unlikely to account for the magnitude of the increase in $\delta^{13}C_{calcite}$ at 41.50 m (cf. Valero-Garcés, 1999), although Stiller *et al.* (1985) observed that non-equilibrium outgassing of CO_2 led to $\delta^{13}C_{DIC}$ values of up to +16.5‰, so this explanation cannot be ruled out completely.

The most common cause of elevated $\delta^{13}C_{calcite}$ values in lake sediments is authigenic

carbonate precipitation from pore water with high $\delta^{13}C_{DIC}$ in response to methanogenesis (sections 2.1.3, 2.2.1, and 2.2.5) (Talbot and Kelts, 1986, 1990; Nissenbaum *et al.*, 1988). It is not possible to determine definitively whether methanogenesis was taking place in the lake sediments above 41.50 m, but the irregular shape of some carbonate grains suggests that authigenic carbonates may have precipitated in this section (Fig. 5.4). Furthermore, methanogenesis almost certainly occurs in the anoxic hypolimnion of the modern lake (chapter 3), and the increase in the abundance of organic matter above 31.00 m (indicated by the increase in %LOI 550°C) suggests that the hypolimnion of the lake was anoxic, at least periodically, above this depth (Fig. 5.2). The highly variable $\delta^{13}C_{calcite}$ values in the lower half of zone 7 also suggest that methanogenesis affected the isotope composition of calcite, as changes in the mixing regime of the lake, and the resulting changes in oxygenation of the lake sediments, are most likely to account for such sudden and significant shifts in $\delta^{13}C_{calcite}$ through their influence on the occurrence of methanogenesis (Fig. 5.2) (cf. Lamb *et al.*, 2000). This interpretation is supported by the sporadic occurrence of laminated sediments in zone 7, which suggests that the lake was intermittently stratified in this section. Furthermore, the decrease in $\delta^{13}C_{organic}$ at 41.50 m indicates that the $\delta^{13}C_{DIC}$ of the epilimnion did not increase significantly at this time (section 5.5.2), and that $\delta^{13}C_{calcite}$ probably, therefore, reflects the $\delta^{13}C_{DIC}$ of pore water. Finally, the absence of significant quantities of pyrite or gypsum in the lake sediments suggests that if methanogenesis took place, it occurred in preference to sulphate reduction (Bühmann and Elsenbroek, 1999).

The precipitation of authigenic carbonates from pore water could also explain the increase in $\delta^{18}O_{calcite}$ at 41.50 m, because the $\delta^{18}O$ of pore water in the upper-most section of lake sediments reflects the $\delta^{18}O$ of water in the overlying hypolimnion, and this value may be unusually high if the lake is stratified due to its high salinity, as is the case in Tswaing crater lake today (chapter 3) (Talbot and Kelts, 1986). This suggestion is supported, to some extent, by the agreement between the average $\delta^{18}O_{calcite}$ value above 41.5 m (+7.8‰) and the $\delta^{18}O_{calcite}$ value expected if carbonates precipitated from water in the hypolimnion of the modern lake (+9.3‰) (Kim and O'Neil, 1997) (see above).

Authigenic calcite precipitation may thus be responsible for the increase in both

$\delta^{18}O_{calcite}$ and $\delta^{13}C_{calcite}$ above 41.50 m. If this is the case, the correlation of the records in this section requires explanation (Fig. 5.5b). Co-variance of the records during the largest shifts in $\delta^{18}O_{calcite}$ and $\delta^{13}C_{calcite}$ is almost certainly due to changes in the lake's mixing regime, such that the records reflect changes in the ratio of endogenic carbonate (low $\delta^{18}O_{calcite}$ and $\delta^{13}C_{calcite}$) to authigenic carbonate (high $\delta^{18}O_{calcite}$ and $\delta^{13}C_{calcite}$) in the lake sediments (cf. Lamb *et al.*, 2000). These changes could, in turn, be determined by the I/E ratio, as this ratio influences the salinity-induced stability of the lake. It is more difficult to explain the correlation of the records during the smaller, more gradual changes in $\delta^{18}O_{calcite}$ and $\delta^{13}C_{calcite}$, however (Fig. 5.2). If the amount of authigenic calcite precipitating from pore water remained relatively constant, the changes in $\delta^{18}O_{calcite}$ and $\delta^{13}C_{calcite}$ could reflect changes in the isotope composition of endogenic carbonates, which in turn reflect the I/E ratio of the lake. Alternatively, it is possible that the correlation reflects changes in the ratio of endogenic to authigenic carbonate in the sediments caused by gradual changes in the frequency of lake turnover. It is not possible to determine which, if either, of these hypotheses is correct, but both suggest that the low-amplitude shifts in $\delta^{18}O_{calcite}$ and $\delta^{13}C_{calcite}$ continue to reflect changes in the I/E ratio of the lake in this section of the sequence.

In zone 5 (41.50 to 31.00 m), $\delta^{18}O_{calcite}$ and $\delta^{13}C_{calcite}$ remain high, fluctuating around +9‰ and +11‰ respectively, until both records exhibit a significant negative excursion between 33.2 and 31.4 m. The lake therefore appears to have remained stratified for much of the time between 41.5 and 33.2 m, allowing significant amounts of authigenic carbonate to precipitate from pore water. The fluctuations in $\delta^{13}C_{calcite}$ in this section may reflect short-lived changes in the lake's mixing regime (possibly from seasonal stratification to permanent stratification), to which $\delta^{18}O_{calcite}$ was relatively insensitive; a scenario that is explored further in chapter 6. The negative excursions of $\delta^{18}O_{calcite}$ and $\delta^{13}C_{calcite}$ between 33.2 and 31.4 m probably indicate that the lake was well-mixed in this section, possibly due to an increase in the I/E ratio of the lake, and that authigenic carbonate precipitation was therefore minimal.

In zones 6 to 8 (31.00 m to the top of the records), $\delta^{18}O_{calcite}$ and $\delta^{13}C_{calcite}$ decrease gradually to minima at ~30.5, ~26, ~21, ~18 and ~13 m, and increase abruptly after each minimum, although there are also significant fluctuations in both records

between 25 and 21 m (the lower half of zone 7). These changes suggest that the I/E ratio of the lake increased gradually in each cycle and then decreased rapidly, causing the lake to become permanently stratified through an increase in salinity-induced stability, and thereby increasing the amount of authigenic carbonate precipitation from pore water. The minimum $\delta^{18}O_{calcite}$ and $\delta^{13}C_{calcite}$ values reached in each cycle increase gradually over this section; a trend that probably reflects the progressive enrichment of the lake water in heavy isotopes as a result of evaporative concentration. This trend is also observed in the successive precipitation of increasingly soluble minerals from the lake water in this section of the sequence (Eugster and Hardie, 1978; Bühmann and Elsenbroek, 1999).

In summary, the records of $\delta^{18}O_{calcite}$ and $\delta^{13}C_{calcite}$ from Tswaing crater lake appear to reflect changes in the hydrological balance of the lake in most parts of the sequence. The records may, however, have been affected by factors other than the I/E ratio of the lake in zone 4 (chapter 6). In addition, it is likely that the lake became semi-permanently stratified in response to a decrease in I/E ratio at ~41.5 m, and that this change in mixing regime led to the precipitation of authigenic carbonates with high $\delta^{18}O$ and $\delta^{13}C$ values in response to methanogenesis in the anoxic lake sediments. Consequently, $\delta^{18}O_{calcite}$ and $\delta^{13}C_{calcite}$ are high and sensitive to changes in the lake's mixing regime above 41.50 m, but the trends in both records appear to continue to reflect the hydrological balance of the lake.

5.5.2 $\delta^{13}C_{organic}$ and C/N ratios

The records of $\delta^{13}C_{organic}$ and C/N ratios can be interpreted in light of the $\delta^{13}C$ and C/N ratios of modern organic material from the site, as well as other records from the sedimentary sequence. In the modern environment, the C/N ratios of terrestrial and emergent vegetation are higher than those of aquatic organisms (cyanobacteria and diatoms), while the $\delta^{13}C$ values of aquatic organisms are, on average, higher than those of terrestrial and emergent vegetation (chapter 3). The high $\delta^{13}C$ of aquatic material appears to result from: the high $\delta^{13}C_{DIC}$ of lake water; the use of bicarbonate as a source of inorganic carbon by aquatic organisms; the abundance of cyanobacteria in the lake; and the effects of carbon limitation (chapter 3). It is therefore possible that the anti-correlation of $\delta^{13}C_{organic}$ and C/N ratios throughout the sequence ($r = -0.5$, $p = <0.001$), and particularly above 31.00 m ($r = -0.7$, $p = <0.001$), reflects changes in the

ratio of organic material derived from aquatic organisms and terrestrial and emergent vegetation (Fig. 5.6).

It is possible, however, that the average $\delta^{13}C$ values and C/N ratios of terrestrial and emergent vegetation and aquatic organisms were significantly different in the past. The $\delta^{13}C$ values of terrestrial and emergent vegetation may have changed due to shifts in the distribution of C_3 and C_4 plants caused by changes in growing season temperature, moisture availability, or atmospheric carbon dioxide levels (section 2.1.4.1). It is unlikely that these changes disrupted the relationship described above, however, because it is thought that either the relative abundance of C_3 and C_4 plants remained constant in the summer rainfall region of southern Africa during the late Quaternary, or that C_3 plants became more common during glacial periods; a change that would have only increased the contrast between the $\delta^{13}C$ values of terrestrial and emergent vegetation and aquatic organisms (section 2.1.4.1; Scott, 2002). Changes in the $\delta^{13}C$ value of atmospheric CO_2 could have also affected the $\delta^{13}C$ values of both terrestrial and emergent vegetation and aquatic organisms during glacials, but these changes are small (~0.3‰) relative to those observed in the records from Tswaing (section 2.1.3). It is also possible that lower atmospheric pCO_2 increased the $\delta^{13}C$ values of aquatic organisms during glacials by increasing carbon limitation (section 2.1.4.1; cf. Street-Perrott *et al.*, 1997). Such a change would have only accentuated the difference between the $\delta^{13}C$ values of terrestrial and emergent vegetation and aquatic organisms, however, and thus would not disrupt the direction of the relationship described above.

Finally, it is possible that aquatic macrophytes or green algae were abundant in the lake in the past (Scott, 1999). These organisms often have relatively high C/N ratios (section 2.1.4.2). Their presence could thus account for the relatively high $\delta^{13}C$ values and C/N ratios of some of the samples from the sequence (Fig. 5.6), or even mean that samples with high C/N ratios and low $\delta^{13}C$ values represent aquatic vegetation, as opposed to terrestrial and emergent vegetation (as the relationship described above proposes). Evidence from other records presented in this chapter and from the diatom records presented in chapter 6 suggests that these organisms were not present in sufficient quantities to disrupt the overall relationship, but this possibility cannot be ruled out completely, and needs to be explored further using biomarker analysis.

In zone 1 (base of the sequence to 68.00 m), C/N ratios increase from 15 to 30 and then remain at this level for the rest of the zone, while $\delta^{13}C_{organic}$ fluctuates at ~−24‰ throughout. These values probably reflect the establishment of C_3 vegetation on the walls of the recently-formed crater, and the resulting increase in the input of this material to the lake, although they could also reflect an increase in the abundance of aquatic macrophytes or green algae with relatively high C/N ratios. Neither record responds to the increase in lake level recorded by $\delta^{18}O_{calcite}$, $\delta^{13}C_{calcite}$, and %LOI 950°C in the upper half of the zone.

In zone 2 (68.00 to 58.00 m), C/N ratios decrease from 30 to 5, with the exception of a brief positive excursion at 62.5-62.0 m. This trend indicates that there was a significant increase in the proportion of organic matter in the lake sediments derived from aquatic material with low C/N ratios in this zone. The records of $\delta^{18}O_{calcite}$, $\delta^{13}C_{calcite}$, and %LOI 950°C indicate that the depth of the lake increased above 63.5 m, and thus suggest that the decrease in C/N ratios was caused by an increase in the abundance of aquatic organisms as lake volume increased. The shift in C/N ratios may have been accentuated by a decrease in the input of terrestrial material to the lake caused by a decrease in the area of the basin exposed to colonisation by terrestrial vegetation as lake levels rose, and possibly by a decrease in the abundance of emergent vegetation in the lake as lake depth increased (although the gradient of the crater walls means that changes in the abundance of emergent vegetation are unlikely to have had a significant effect unless the lake was initially shallow enough to allow wide-spread colonisation by emergent vegetation) (cf. Lamb *et al.*, 2004; Leng *et al.*, 2005).

The shift to low C/N ratios above ~62 m, which indicates that aquatic material dominated organic matter in the lake sediments, is accompanied by an increase in $\delta^{13}C_{organic}$ to ~−19‰. This value is higher than the $\delta^{13}C$ values associated with aquatic organisms using dissolved CO_2 in equilibrium with atmospheric CO_2 as a source of inorganic carbon (section 2.1.4.1). $\delta^{13}C_{calcite}$ indicates that $\delta^{13}C_{DIC}$ was in equilibrium with atmospheric CO_2 at this time (section 5.5.1), and it is therefore likely that the elevated $\delta^{13}C$ of aquatic organisms was caused by their use of bicarbonate as a source of inorganic carbon, the presence of cyanobacteria in the lake, and/or reduced fractionation against ^{13}C during photosynthesis under conditions of carbon limitation

(chapter 3). It is also notable that $\delta^{13}C_{organic}$ increases to −15‰ at ~65 m in zone 2. This peak coincides with peaks in %LOI 550°C, $\delta^{13}C_{calcite}$, and $\delta^{18}O_{calcite}$, and with a zone of laminated sediments that were attributed to falling lake levels and the onset of lake stratification (section 5.5.1). The increase in $\delta^{13}C_{organic}$ could therefore reflect an increase in $\delta^{13}C_{DIC}$ caused by the decrease in I/E ratio and/or increased preservation of organic matter, or an increase in the abundance of C_4 grasses on the crater walls in response to increased aridity.

C/N ratios are lower (average 10) between 61.00 and 31.00 m (middle of zone 2 to the top of zone 5) than above (average 20) or below (average 25) this section, which suggests that the contribution of aquatic material to the sediments was relatively high. C/N ratios co-vary with %LOI 950°C, which reflects the degree of evaporative concentration of the lake water in this section, suggesting that C/N ratios reflect changes in lake level. As in zone 2, this relationship is likely to arise because changes in lake level influenced the amount of organic matter produced within the lake, the area of the basin exposed to colonisation by terrestrial vegetation, and/or the abundance of emergent plants in the lake. In zone 3, C/N ratios are also positively correlated with the amount of organic material in the sediments (as reflected by %LOI 550°C, which appears to provide an accurate indication of the organic matter content of the sediments due to the similarity of this record with variations in percent organic carbon determined during C/N analysis). This correlation indicates that changes in either the amount of terrestrial material entering the lake from the catchment or the abundance of emergent vegetation in the lake (as opposed to the amount of organic matter produced within the lake) determined the amount and the C/N ratio of organic material in the sediments. %LOI 550°C remains low (~5%) throughout zones 4 and 5 (51.00 to 31.00 m), however, possibly because most organic material was decomposed under well-mixed conditions before burial. Consequently, this record cannot provide further insight into the causes of fluctuations in C/N ratios in this section. Based on these interpretations, the fluctuations in C/N ratios and %LOI 950°C between 61.00 and 31.00 m suggest that lake levels decreased at 58-55 m and 54-53 m in zone 3, at 51-47 m in zone 4, and at 40-39 m and 38-35 m in zone 5 (Fig. 5.2). These reconstructions are supported by a diatom assemblage record from this section of the sequence (chapter 6).

In zones 6 to 11 (31.00 m to the top of the sequence), the $\delta^{13}C_{organic}$ and C/N ratios of organic material are highly negatively correlated ($r = -0.7$, $p = <0.001$), suggesting that they reflect changes in the proportion of organic material derived from terrestrial and emergent vegetation and aquatic organisms, as in other parts of the sequence (Fig. 5.6b). The relationship between $\delta^{13}C_{organic}$ and C/N ratios is stronger in this section than below 31.00 m ($r = -0.6$, $p = <0.001$), which appears to reflect higher $\delta^{13}C$ values of aquatic material above 31.00 m (samples with C/N ratios less than 10 have $\delta^{13}C_{organic}$ values between −8‰ and −15‰ above 31.00 m, and between −12‰ and −24‰ below 31.00 m) (Fig. 5.6b). The possible explanations for this increase in the $\delta^{13}C$ of aquatic material include: an increase in $\delta^{13}C_{DIC}$ (cf. section 5.5.1); a larger proportion of organisms using bicarbonate as their source of inorganic carbon; an increase in the abundance of cyanobacteria in the lake; and reduced fractionation against ^{13}C due to carbon limitation under conditions of high primary productivity. Unfortunately, it is not possible to assess the extent to which changes in $\delta^{13}C_{DIC}$ affected the $\delta^{13}C$ of aquatic material using the record of $\delta^{13}C_{calcite}$, because changes in the contribution of terrestrial organic material affect $\delta^{13}C_{organic}$, and because $\delta^{13}C_{calcite}$ partly reflects the $\delta^{13}C_{DIC}$ of pore water in this section of the record (section 5.5.1). It is notable, however, that the large shifts in $\delta^{13}C_{calcite}$ are not paralleled by changes in $\delta^{13}C_{organic}$, which provides further evidence that at least some of the calcite in the sediments probably formed from DIC in pore water, rather than the epilimnion (section 5.5.1).

The causes of the changes in the relative contributions of aquatic and terrestrial and emergent material to the lake sediments above 31.00 m can be explored using other records from the sequence. %LOI 950°C does not co-vary with C/N ratios above 31.00 m, which could suggest that the record of C/N ratios was no longer controlled by lake-level fluctuations. This lack of co-variance is almost certainly due to changes in the factors that control %LOI 950°C, however. Significant quantities of trona (which begins to decompose at 70°C) and halides are present in the sediments above ~30.5 m (Bühmann and Elsenbroek, 1999). These minerals precipitate in response to evaporative concentration (after the supply of Ca^{2+} and Mg^{2+} and/or HCO_3^- and CO_3^{2-} has been exhausted (Eugster and Hardie, 1978)), but are not reflected in %LOI 950°C. Consequently, %LOI 950°C cannot provide an accurate indication of changes in the evaporative concentration of lake water above ~30.5 m. It is also possible that

significant quantities of carbonate dissolved and/or precipitated in response to methanogenesis in this section of the record (section 5.5.1), which would further dissociate the abundance of carbonate in the sediments from the evaporative concentration of lake water.

Partridge *et al.* (1993) produced a low-resolution record of the abundance of carbonates and halite in the sedimentary sequence by removing soluble minerals from the sediments in distilled water and chemically analysing the resultant solutions (Fig. 5.7). In theory, this record should provide a more reliable indication of the evaporative concentration of lake water than %LOI 950°C, although it does not overcome the problems of carbonate dissolution and authigenic carbonate precipitation, or record the presence of halides such as fluorite. Furthermore, Partridge *et al.* (1993) proposed that almost all the halite and some of the carbonate in the sediments precipitated from pore water when the samples were dried.

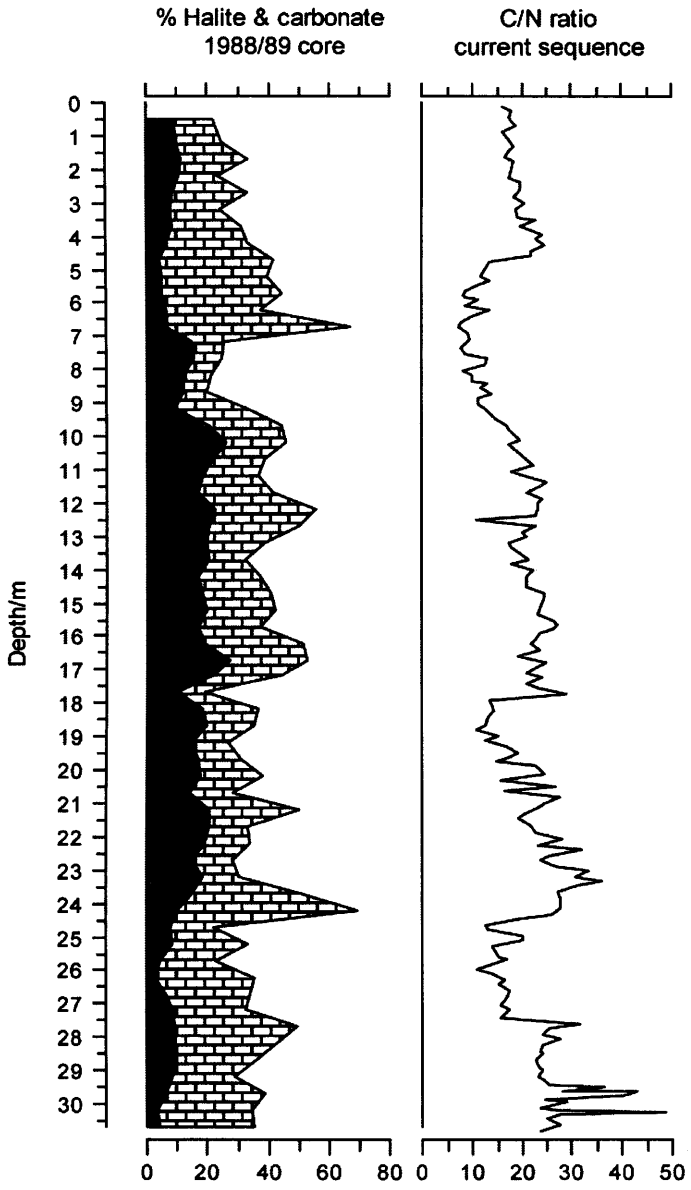

Figure 5.7: Record of the percentage halite (grey) and carbonate (brick pattern) above 30.5 m from the core obtained in 1988/89 (Partridge *et al.*, 1993) plotted against the corrected depth scale constructed by Partridge *et al.* (1997), and the record of C/N ratios of organic material produced in this study plotted against the corrected depth scale described in chapter 4.

As might be expected, the record of halite and carbonate abundance produced by Partridge *et al.* (1993) is not strongly correlated with the record of C/N ratios produced in this study (Fig. 5.7). There is, however, a weak positive relationship between the two records below ~7 m and above ~4.5 m, which hints that increasing

C/N ratios may have been associated with falling lake levels, as in lower parts of the sequence. In addition, $\delta^{18}O_{calcite}$ and $\delta^{13}C_{calcite}$ show some evidence of co-variance with C/N ratios in the section where $\delta^{18}O_{calcite}$ and $\delta^{13}C_{calcite}$ are available, which provides further support for the suggestion that C/N ratios reflect lake-level change (Fig. 5.2) (section 5.5.1). The co-variance of %LOI 550°C and C/N ratios in this section suggests that the amount of organic material in the lake sediments was determined by the amount of terrestrial or emergent vegetation entering the lake, although the amount of terrestrial material is most likely to have been responsible, because the lake was probably too saline to support emergent vegetation (as is the case today) (chapter 6, Metcalfe, 1999). It is therefore likely that C/N ratios, $\delta^{13}C_{organic}$, and %LOI 550°C were determined by variations in the area of the basin exposed to colonisation by terrestrial vegetation caused by changes in lake level in this section of the sequence.

There are two important exceptions to this interpretation, however. Between 31.0 and 30.0 m, C/N ratios increase and $\delta^{13}C_{organic}$ decreases, indicating that lake levels fell, but there are significant negative excursions in $\delta^{18}O_{calcite}$ and $\delta^{13}C_{calcite}$, which suggest that the I/E ratio of the lake increased. These shifts could be explained by increased in-wash of organic material from the basin during a period of high precipitation. This explanation is unlikely, however, because the sediments are laminated between 31.0 and 28.5 m, and it is improbable that meromixis persisted as the lake made the transition from a deep, fresh water body to a shallow, saline one after the period of high precipitation ended. In addition, halite is present in the sediments above 31 m, which indicates that lake levels were low in this section (Partridge *et al.*, 1993). It is therefore most likely that the shifts in $\delta^{18}O_{calcite}$ and $\delta^{13}C_{calcite}$ reflect changes in the ratio of authigenic to endogenic carbonate in the lake sediments caused by factors unrelated to lake depth.

Secondly, the C/N and $\delta^{13}C_{organic}$ records suggest that lake levels were high in zone 10 (9.00 to 4.70 m), but the record of carbonate abundance produced by Partridge *et al.* (1993) suggests that the I/E ratio decreased between ~7.0 and 4.5 m (Fig. 5.7). It is possible that a decrease in precipitation caused a decline in the amount of vegetation in the basin at this time, and thus countered the increase in terrestrial material input to the lake that would otherwise accompany a decrease in lake level. This hypothesis is

unlikely, however, because the amount of halite in the sediments is low between 7.0 and 4.5 m, and extreme evaporative enrichment would be expected to increase the abundance of this mineral (Fig. 5.7) (Eugster and Hardie, 1978). It is therefore possible that the increase in carbonate abundance between 7.0 and 4.5 m was caused by freshwater input to a highly alkaline water body, in which case, the relationship between carbonate abundance and the evaporative concentration of lake water would reverse (cf. Shapley *et al.*, 2005). This proposal is supported by the observation that the carbonates that increase in abundance at this depth are gaylussite and calcite (Bühmann and Elsenbroek, 1999), both of which contain Ca^{2+}, and both of which would therefore precipitate in response to freshwater input (section 2.2.1) (cf. Figure A2, Appendix A).

The pollen record cannot be used to test this hypothesis, because pollen is not preserved in this part of the sequence (Scott, 1999), but the diatom assemblage record does exhibit changes in this section, and can therefore be used to explore the causes of the increase in carbonate abundance (Metcalfe, 1999). There is a significant decrease in the proportion of *Nitzschia pusilla* and *Chaetoceros muelleri* valves, and an increase in the relative abundance of *C. muelleri* cysts (which may indicate conditions less favourable for this species) above 10 m (Metcalfe, 1999) (cf. Figure A4, Appendix A). Metcalfe (1999) suggested that this shift was caused by an increase in salinity, which supports the suggestion that the I/E ratio decreased between 7.0 and 4.5 m (Partridge *et al.*, 1993). It is possible, however, that the change in assemblage composition was caused by a shift from highly saline, Cl^--rich water to slightly less saline, HCO_3^--CO_3^{2-}-rich water, as both *C. muelleri* and *N. pusilla* are associated with highly saline conditions, and *C. muelleri* is also associated with Cl^--rich water (Gasse, 1987). In this case, the absence of diatom taxa other than *C. muelleri* cysts might be explained by the dominance of cyanobacteria at this time. In addition, diatom valves are completely absent from the lake sediments above 5 m, which suggests that increased lake-water salinity and/or alkalinity increased valve dissolution or prevented diatoms from living in this section (Metcalfe, 1999), and thus provides support for the proposal that lake levels decreased at this depth, as the records of C/N ratios and $\delta^{13}C_{organic}$ suggest.

The weight of evidence therefore suggests that the records of C/N ratios and $\delta^{13}C_{organic}$

reflect lake-level change above 31.00 m. The maxima in C/N ratios and minima in $\delta^{13}C_{organic}$ at 31-27.5, 23.5, 12, and 4.5 m therefore indicate low lake levels and increased exposure of the crater walls for colonisation by terrestrial plants. It is likely, however, that the long-term trends in these records above 31.00 m reflect factors other than lake-level change. The magnitude of peaks in the record of C/N ratios decreases over this section, and the maxima and minima reached by the $\delta^{13}C_{organic}$ record both increase, apart from in zone 11. These changes probably reflect infilling of the basin, which would have reduced the area of the catchment, and therefore reduced the relative input of terrestrial vegetation to the lake, independently of external climate change. In addition, sedimentary infilling probably increased the surface-area to volume ratio of the lake, and thereby decreased its I/E ratio (section 5.5.1), which may have increased the $\delta^{13}C$ of aquatic organisms (see above).

The only points at which the relationship between C/N ratios and $\delta^{13}C_{organic}$ breaks down are at ~27.5 m, ~18.0 m, and in zone 10 (9.00 to 4.70 m). At 27.5 m, $\delta^{13}C_{organic}$ does not increase as rapidly as the record of C/N ratios decreases. This discrepancy could be due to an increase in the amount of C_3 vegetation in the catchment as lake levels increased, as this would have modulated the increase in $\delta^{13}C_{organic}$ associated with the increase in lake volume. Similarly, the rapid increase in C/N ratios at ~18.0 m is not accompanied by a decrease in $\delta^{13}C_{organic}$, which could be due to an increase in the abundance of C_4 vegetation in the basin as conditions became more arid, or due to an increase in the abundance of aquatic macrophytes or green algae with high C/N ratios. Unfortunately, it is not possible to assess these hypotheses using the records of pollen and algae from the sequence, due to their low resolution (Scott, 1999). Finally, C/N ratios remain at ~9 in zone 10, suggesting that lake levels were high and stable, but $\delta^{13}C_{organic}$ decreases slightly in the lower half of this zone, and increases to −6‰ in the upper half. The amount of organic matter in the sediment also increases in the upper part of this zone (%LOI 550°C increases by ~4%). The most likely explanation for these shifts is that aquatic productivity was low in the first half of the zone, and increased in the second half, perhaps in response to the increase in water input at ~7.0-4.5 m described above. Alternatively, it is possible that the increase in $\delta^{13}C_{organic}$ and %LOI 550°C in the upper part of the zone reflects the onset of lake stratification, which could have increased the preservation of organic matter in the lake sediments, and thereby decreased the release of isotopically-light carbon into

the lake water, increasing $\delta^{13}C_{DIC}$. There is no evidence for such a change in mixing regime in the degree of lamination of the lake sediments, however.

5.6 Discussion

The timing of the palaeohydrological changes recorded in the sedimentary sequence can be estimated using the age-depth model presented in chapter 4. This information, in turn, allows the causes of these changes to be explored. The records are plotted according to this age-depth model in Figure 5.8, together with the deuterium record from the Vostok ice core, which is a proxy for atmospheric temperature (Petit *et al.*, 1999), the record of mean daily insolation at 25°S between the 21st of November and the 20th of December, which indicates the intensity of summer insolation at the site (Laskar *et al.*, 2004), and marine isotope stages (Imbrie *et al.*, 1984). The discussion of these records will be divided into two sections: before 150 kyr B.P., which corresponds to the section of the sequence below 35 m (zone 1 to the middle of zone 5); and after 150 kyr B.P., which corresponds to the section above 35 m (the middle of zone 5 to zone 11). This distinction is made because different factors appear to have influenced palaeohydrological conditions during these periods.

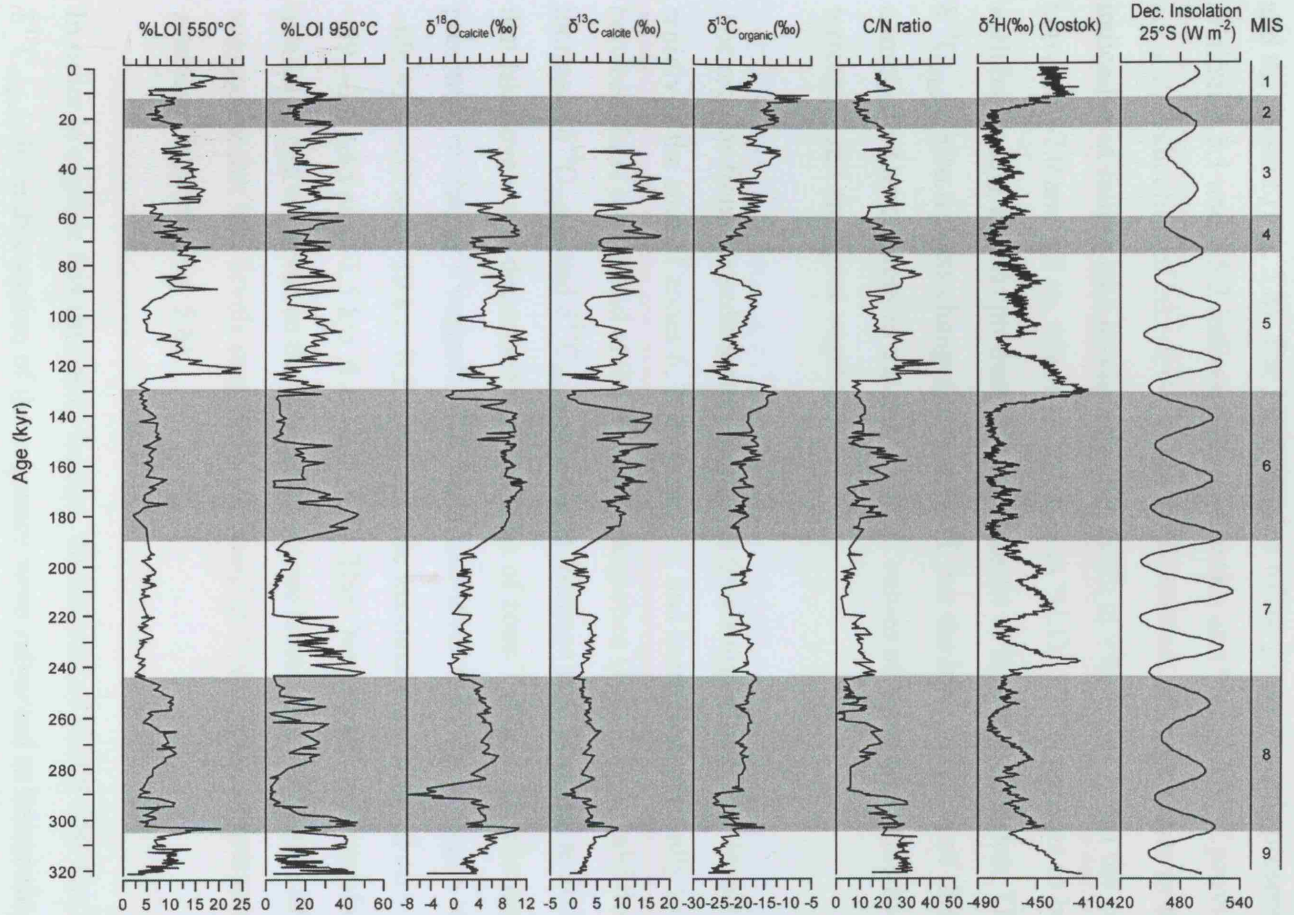

Figure 5.8: Records from the sedimentary sequence plotted against the cubic age-depth model (chapter 4), with the deuterium record from the Vostok ice core (Petit *et al.*, 1999) and mean daily insolation at 25°S between 21st of Nov. and 20th of Dec. (Laskar *et al.*, 2004). MISs shown as grey and white bars (Imbrie *et al.*, 1984).

5.6.1 150 kyr B.P. to the present

5.6.1.1 Timing of palaeohydrological change

According to the age-depth model presented in chapter 4, the section of the sedimentary sequence above 35 m corresponds to the period between 150 kyr B.P. and the present (Fig. 5.8). The interpretation of the proxy records presented in sections 5.5.1 and 5.5.2 indicates that C/N ratios and %LOI 550°C provide the most accurate indication of lake-level status in this section, with increases in these proxies indicative of falling lake levels. The only depth at which this is not the case is between ~7.0 and 4.5 m, where an increase in %LOI 550°C appears to be associated with increasing aquatic productivity or the onset of lake stratification. The record of $\delta^{13}C_{organic}$ also reflects changes in lake level, but the interpretation of this record is complicated by changes in the average $\delta^{13}C$ values of aquatic organisms and terrestrial and emergent vegetation.

The records from the sedimentary sequence thus suggest that lake levels decreased rapidly at the start of zones 6, 7, 8, 9, and 11, and increased gradually to maxima between these events and at the top of the sequence (Fig. 5.2). In addition, the increases $\delta^{18}O_{calcite,}$ and $\delta^{13}C_{calcite}$ and slight increase in C/N ratios at 20.8 m suggest that lake levels also decreased in the middle of zone 7 (Fig. 5.2). The age-depth model presented in chapter 4 suggests that these lake-level regressions began at ~126, ~90, ~69, ~56, ~32 and ~10 kyr B.P., and that the maxima were centred on ~132, ~97, ~71, ~59, ~34, ~16 and ~1.5 kyr B.P. (Fig. 5.8). This "saw-tooth" pattern of change is similar to that observed in the deuterium record from Vostok (Petit *et al.*, 1999), suggesting that lake levels may have increased at Tswaing as temperatures fell at high southern latitudes (Fig. 5.8).

In order to explore this similarity further, the records of %LOI 550°C, C/N ratios, and $\delta^{13}C_{organic}$ from this section of the sequence were subjected to harmonic analysis using the program SPECTRUM (Schulz and Stattegger, 1997). The $\delta^{18}O_{calcite}$ and $\delta^{13}C_{calcite}$ records were not analysed because they only cover part of the section, and because they are influenced by authigenic calcite precipitation in this part of the sequence (section 5.5.1). Similarly, the record of %LOI 950°C was not analysed because it does

not reflect palaeohydrological conditions in this section (section 5.5.2). Harmonic analysis is designed to detect periodic signal components in the presence of background noise, which could obscure periodic components in other forms of spectral analysis (Schulz and Stattegger, 1997). The method used by the program SPECTRUM assumes that the background noise in the dataset is white noise (random noise that has a uniform power spectral density at every frequency in the range of interest), but it appears to perform well if the data contain red noise (noise with energy that decreases monotonically as the frequency increases), which is the typical background noise in palaeoclimatic datasets (Schulz and Stattegger, 1997).

The analysis indicates that the records of %LOI 550°C, C/N ratios, and $\delta^{13}C_{organic}$ contain periodic signals with frequencies of ~41 kyr and ~23 kyr, and that the records of C/N ratios and $\delta^{13}C_{organic}$ also contain a signal with a frequency of ~19 kyr (Fig. 5.9). These frequencies are the same as those of variations in the obliquity of the earth's axis and the precession of the equinoxes, which suggests that these factors influenced palaeohydrological conditions at Tswaing between 150 kyr B.P. and the present. The obliquity of the earth's axis has a negligible influence on seasonal insolation at 25°S (Berger and Loutre, 1991), and the presence of a periodic signal with a frequency of ~41 kyr therefore suggests that climatic change at higher latitudes influenced palaeohydrological conditions at Tswaing during this period (chapter 1).

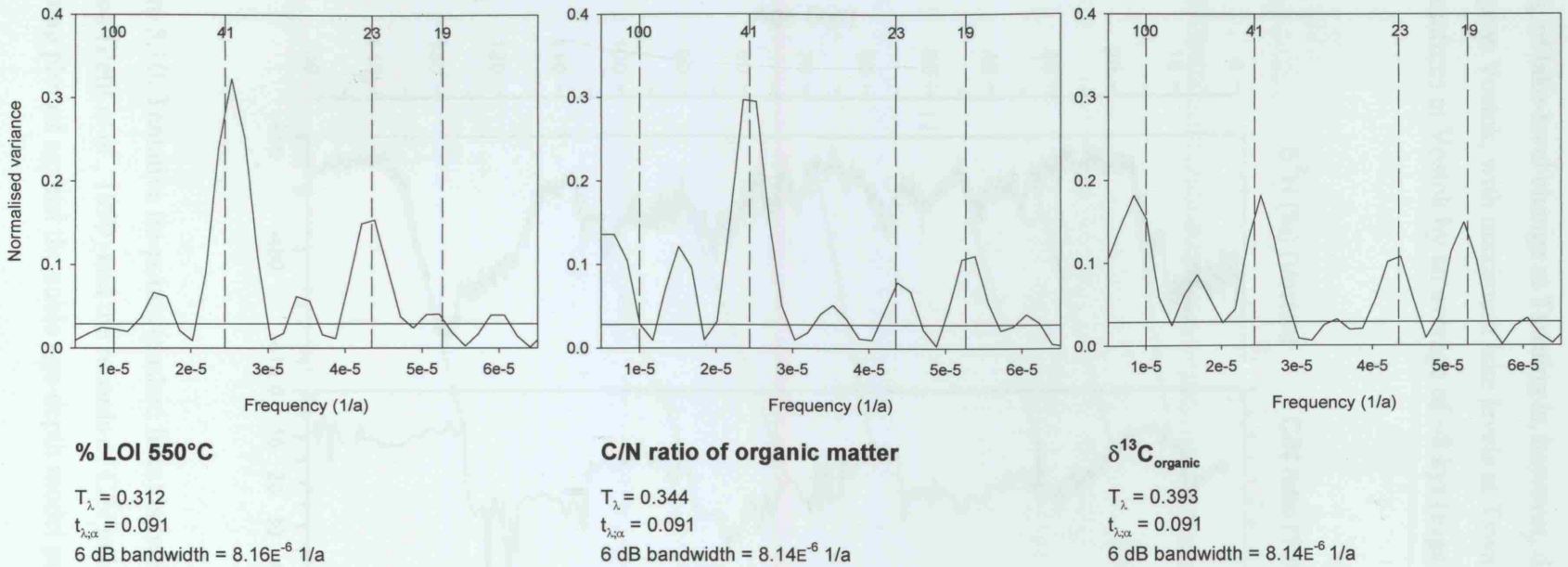

Figure 5.9: Periodograms showing the results of harmonic analysis of the records of %LOI 550°C, C/N ratios, and $\delta^{13}C_{organic}$ between 150 kyr B.P. and the present, according to the cubic age-depth model presented in chapter 4. Analysis performed using SPECTRUM (Schultz and Stattegger, 1997). T_λ (test statistic) > $t_{\lambda,\alpha}$ (critical value) for Siegel's test in all cases, and the null hypothesis that the signal is white noise can therefore be rejected (Siegel, 1980).

Both the pattern and frequency of lake-level change at Tswaing between 150 kyr B.P. and the present therefore show similarities to climatic change at high latitudes. The timing of lake-level change at Tswaing is, however, different from that of temperature change at Vostok, with maximum lake levels at Tswaing apparently lagging minimum temperatures at Vostok by an average of ~8 kyr (Figs. 5.10) (Petit *et al.*, 1999).

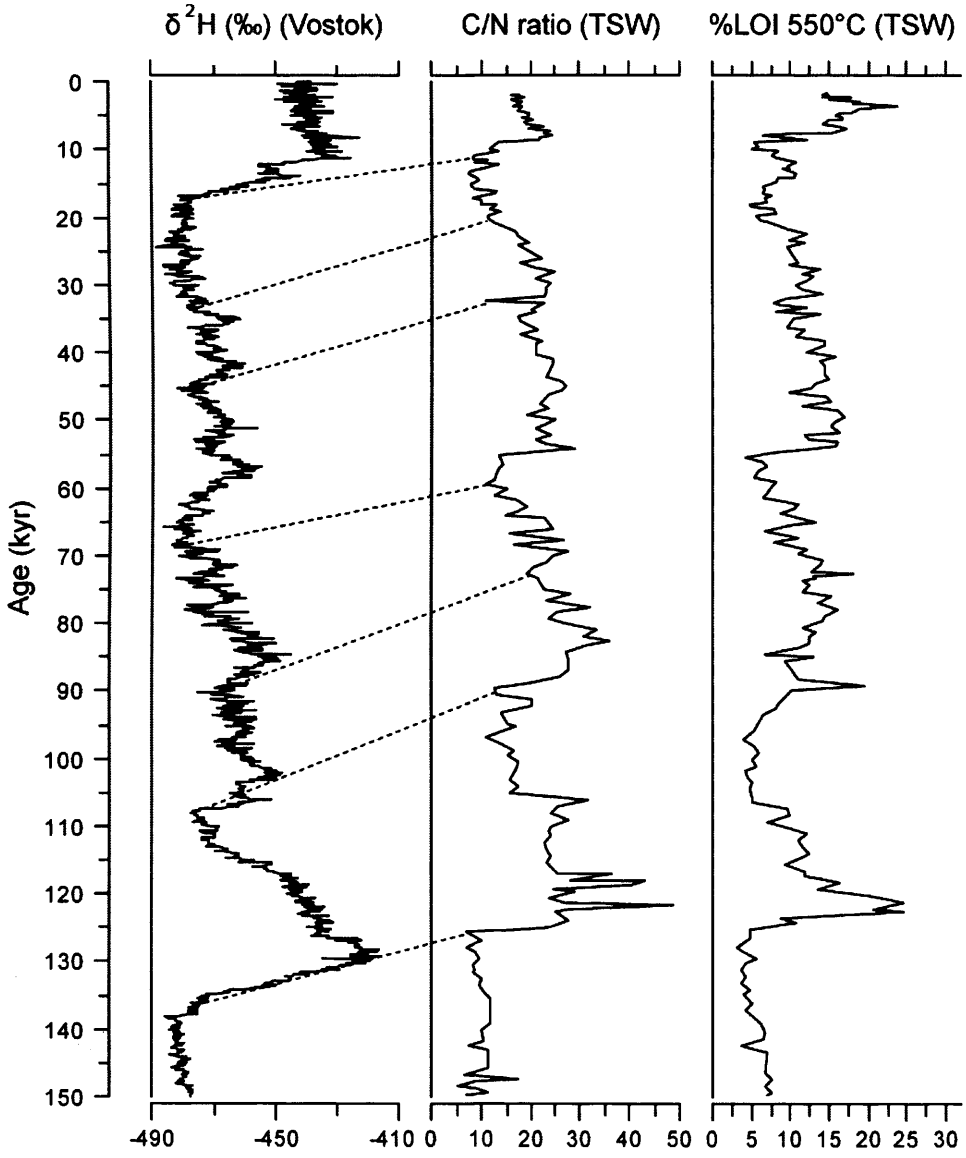

Figure 5.10: Tentative tie-points (dashed lines) between the deuterium record from Vostok (Petit *et al.*, 1999) and the records of C/N ratios and %LOI 550°C from Tswaing plotted against the cubic age-depth model presented in chapter 4.

The deuterium record from Vostok is plotted against the GT4 age-depth model developed by Petit *et al.* (1999), which was derived by ice flow modelling. This chronology is thought to have errors less than ±5 kyr over the last 110 kyr, and less than ±10 kyr for most of the rest of the record (Petit *et al.*, 1999). Alternative chronologies have been developed for the ice core using glaciological modeling (*e.g.* Parrenin *et al.*, 2004), orbital tuning (*e.g.* Waelbroeck *et al.*, 1995; Shackleton, 2000), and correlation with other records (*e.g.* Landwehr and Winograd, 2001), but the different models are generally in good agreement for the period between the present and ~180 kyr B.P. (differences between the models are less than 4 kyr during this period) (Parrenin *et al.*, 2004).

Given the low errors associated with the chronology of the Vostok ice core compared to the high degree of uncertainty associated with the age-depth model of the sediments from Tswaing (chapter 4), it is likely that the apparent offset between the timing of lake-level change at Tswaing and temperature change at Vostok is due to errors in the chronology of the lake-level records, and that lake-level change at Tswaing was actually simultaneous with temperature change at Vostok, at least within the resolution of the records presented here (chapter 4). In this respect, it is interesting to note that the ages of the tie-point events in Figure 5.10 inferred from the chronology of the Vostok record lie extremely close to those suggested by the linear age-depth model constructed using non-weighted least-squares regression in chapter 4 (hereafter referred to as the linear age-depth model). This model is shown, together with the cubic age-depth model and the ages of the tie-point events suggested by the deuterium record from Vostok, in Figure 5.11.

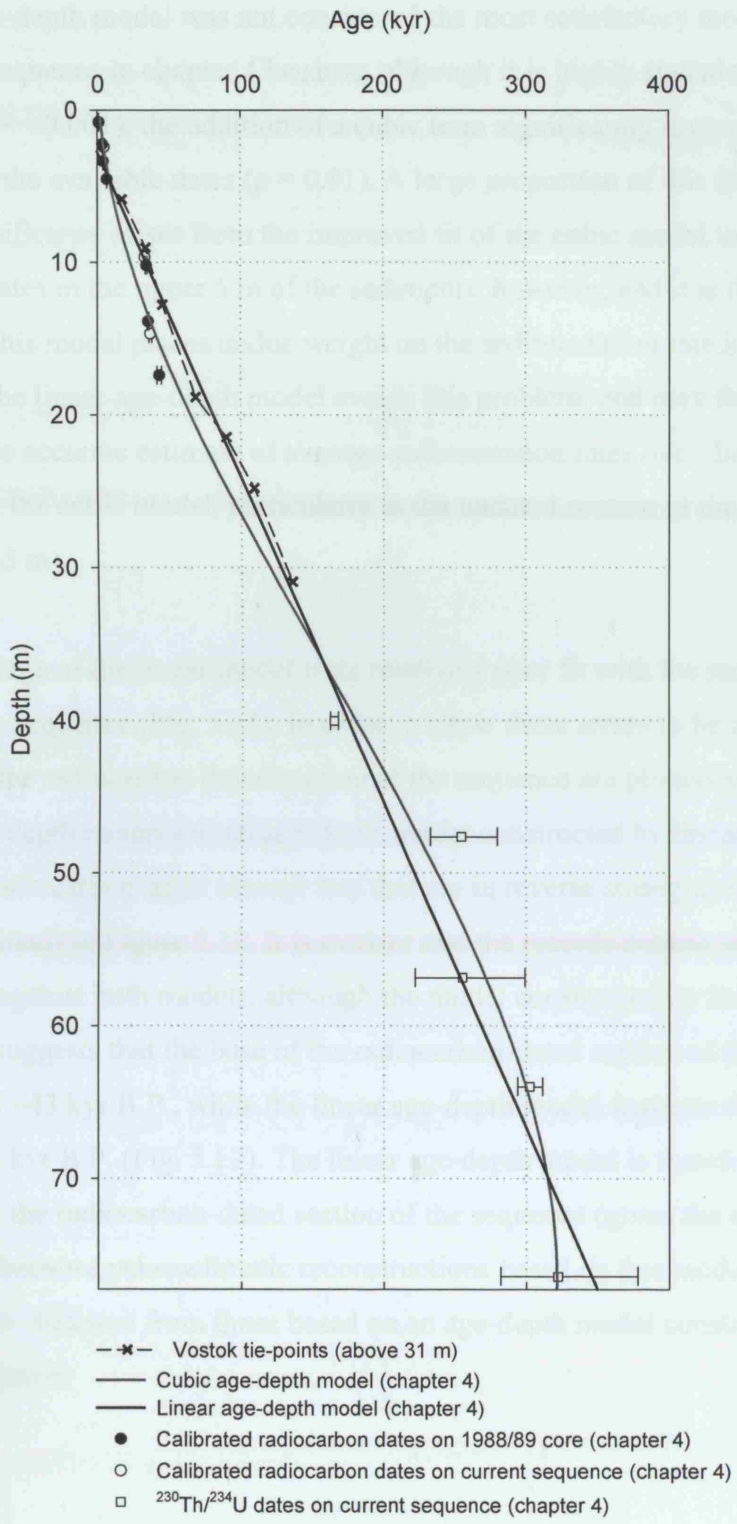

Figure 5.11: Age-depth diagram showing the ages of the tie-points between the deuterium record from Vostok (Petit *et al.*, 1999) and the records of C/N ratios and %LOI 550°C from Tswaing inferred from the Vostok record (cf. Figure 5.10) (crosses joined by dashed line), together with the cubic age-depth model (grey line) and the linear age-depth model (black line) for the sediments from Tswaing (chapter 4).

The linear age-depth model was not considered the most satisfactory model for the sedimentary sequence in chapter 4 because, although it is highly statistically significant ($p = <0.001$), the addition of a cubic term significantly improves the model's fit to the available dates ($p = 0.01$). A large proportion of this increase in statistical significance arises from the improved fit of the cubic model to the five radiocarbon dates in the upper 5 m of the sediments, however, and it is therefore possible that this model places undue weight on the sedimentation rate inferred from these dates. The linear age-depth model avoids this problem, and may therefore provide a more accurate estimate of average sedimentation rates over the whole sequence than the cubic model, particularly in the undated section of the sediments (17.41 to 40.05 m).

The disadvantage of the linear model is its relatively poor fit with the radiocarbon dates from the sequence (Fig. 5.11). In order to allow these errors to be assessed, the records from the radiocarbon-dated section of the sequence are plotted against both the linear age-depth model and an age-depth model constructed by linear interpolation between the radiocarbon dates (except two that are in reverse stratigraphic order, which are omitted) in Figure 5.12. It is evident that the records exhibit similar trends when plotted against both models, although the model constructed by linear interpolation suggests that the base of the radiocarbon-dated section of the sequence was deposited ~43 kyr B.P., while the linear age-depth model suggests that it was deposited ~68 kyr B.P. (Fig. 5.12). The linear age-depth model is therefore considered satisfactory in the radiocarbon-dated section of the sequence (given the available information), because palaeoclimatic reconstructions based on this model would not be significantly different from those based on an age-depth model constructed by linear interpolation.

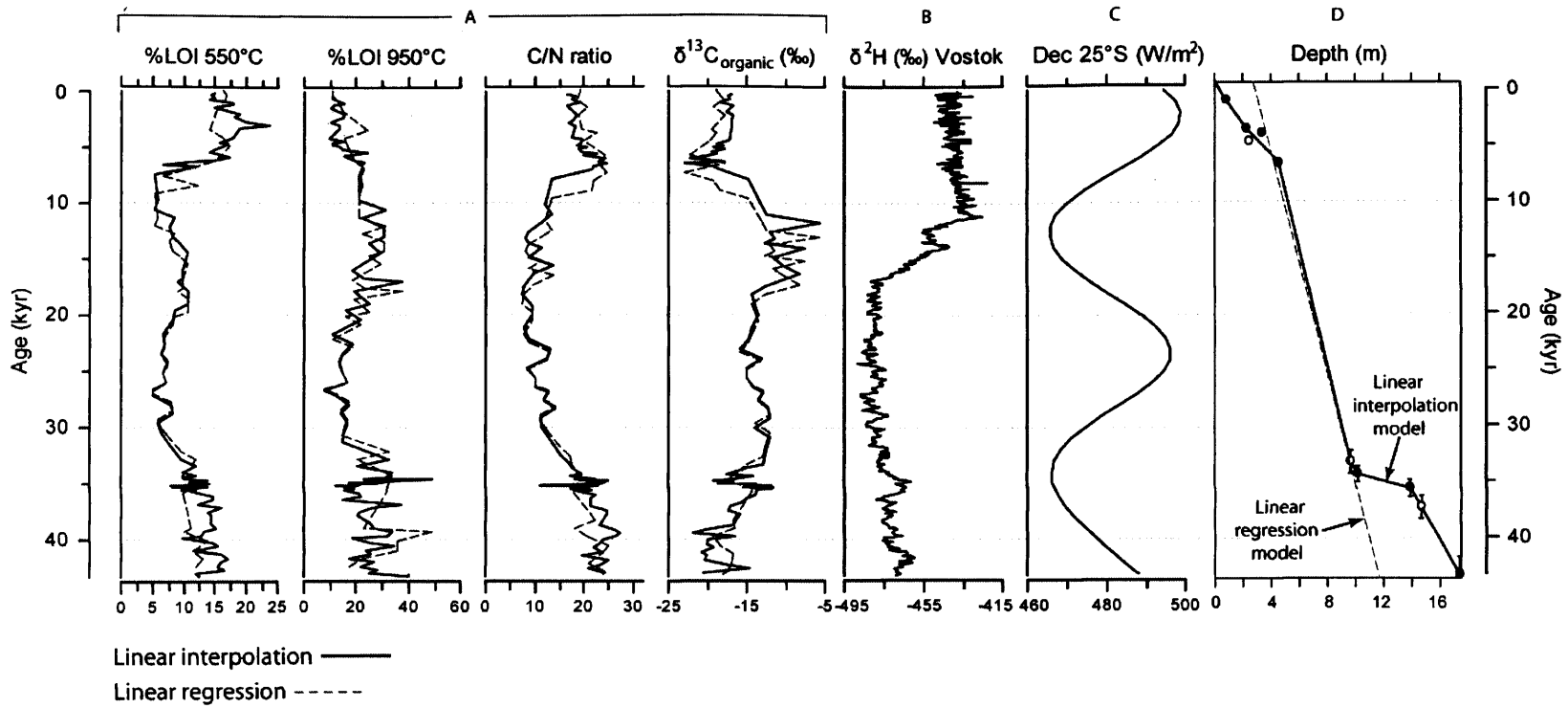

Figure 5.12: Records of %LOI 550°C, %LOI 950°C, C/N ratios, and $\delta^{13}C_{organic}$ from the radiocarbon-dated section of the sedimentary sequence plotted according to an age-depth model constructed by linear interpolation between the radiocarbon dates (black line) and the linear age-depth model constructed by non-weighted least-squares regression through all the dates in the sequence (grey dashed line) (A), together with the deuterium record from Vostok (Petit *et al.*, 1999) (B), and mean daily insolation at 25°S between the 21st of November and the 20th of December (Laskar *et al.*, 2004) (C). The two age-depth models are shown in (D), where radiocarbon dates on the 1988/89 core are closed circles (Partridge *et al.*, 1993) and radiocarbon dates on the most recent cores are open circles (chapter 4). Errors are 1 s.d. (where large enough to be shown).

It is not possible to determine with certainty which age-depth model for the sedimentary sequence is closest to reality, but the correspondence of the records from Tswaing with the deuterium record from Vostok when the records from Tswaing are plotted according to the linear age-depth model suggests that this model may be the most accurate of those that are currently available. This correspondence is obviously not the ideal way of assessing the accuracy of the different age-depth models for the sediments from Tswaing, because it is based on the assumption that the similarity between the records indicates that lake-level change at Tswaing occurred at the same time as temperature change at Vostok (which leads to a degree of circularity when discussing the causes of lake-level change). Given the uncertainty associated with all the age-depth models for the sediments from Tswaing, however, it is considered a valid indication that the linear age-depth model may be the most accurate of those that are currently available (although further dating is required to confirm whether or not this is the case). The records from the sequence are therefore plotted according to the linear age-depth model in Figure 5.13, and this model is used to assess the timing of lake-level change at Tswaing in the following discussion.

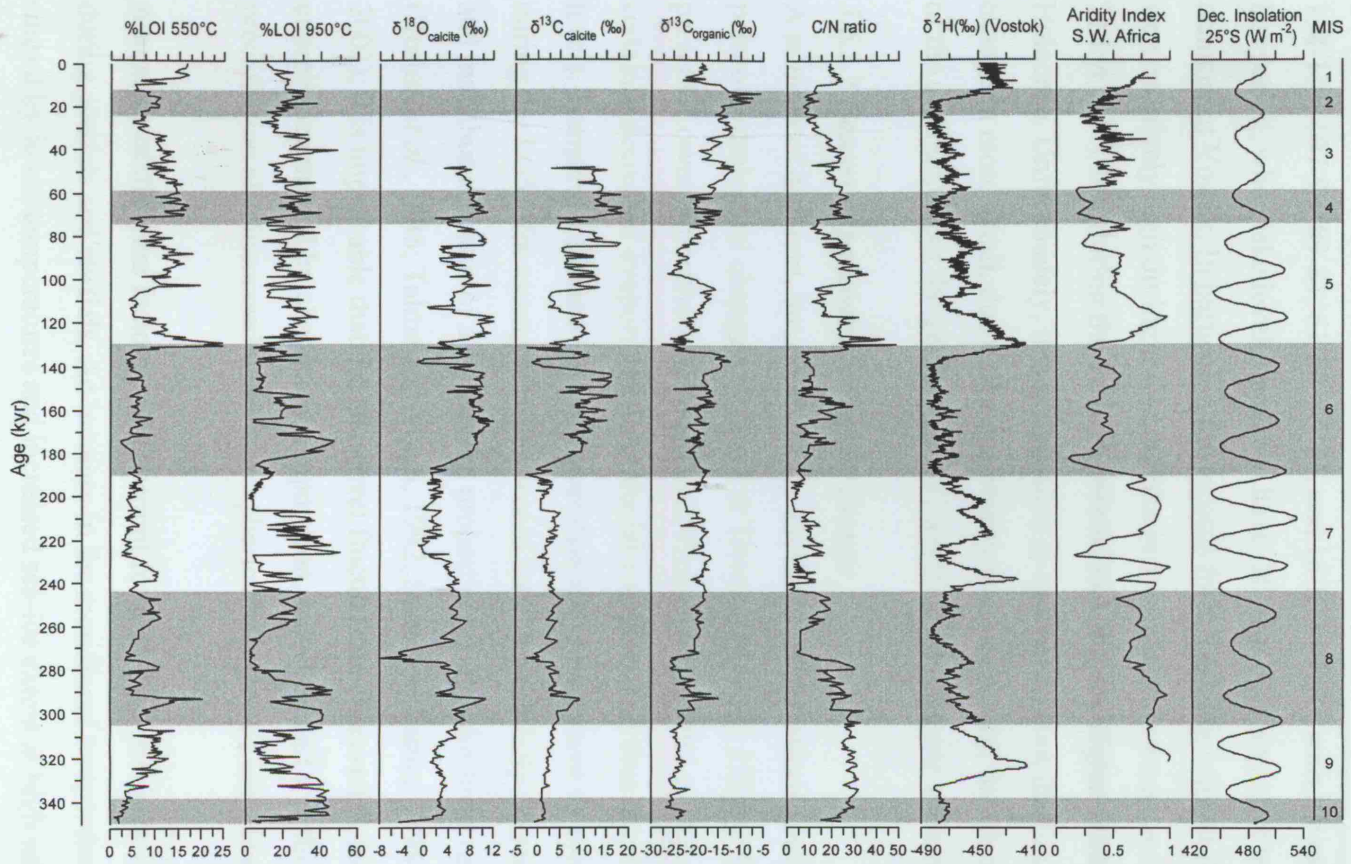

Figure 5.13: Records from the sequence plotted according to the linear age-depth model, together with the deuterium record from Vostok (Petit *et al.*, 1999), an index of aridity in southern Africa (~24°S to ~32°S) from a marine core off S.W. Africa (19°6'S, 9°2'E) (scale reversed from original so 1 = maximum aridity) (Stuut *et al.*, 2002), and mean daily insolation at 25°S from 21st Nov. to 20th Dec. (Laskar *et al.*, 2004). MISs are shown as grey and white bars (Imbrie *et al.*, 1984).

The linear age-depth model indicates that lake levels were low 132-116, 102-89, 87-80, 70-48, 46-32, and 9.5-4.5 kyr B.P., and higher in the intervening periods (although the increase in lake level after 4.5 kyr B.P. is smaller than the others). As expected from the previous discussion, the timing of these periods of low lake level is in fairly good agreement with the timing of periods of increased temperature at Vostok at: 134-116, 107-93, 89-81, 61-50, 45-34, and 16-8 kyr B.P., with the exception of the last period, when lake levels appear to have fallen at Tswaing after temperatures changed at Vostok. In particular, the records from Tswaing suggest that lake levels were relatively high during the LGM (the period of maximum ice volume centred on 21 kyr B.P.), low during the early Holocene, and slightly higher during the late Holocene. Unfortunately, it is not possible to speculate about the timing of lake-level change in more detail, due to the uncertainty associated with the chronological control of the sediments, but the general trends identified here appear to be robust.

5.6.1.2 Causes of palaeohydrological change

A number of different, but not mutually exclusive, explanations could account for the palaeo-hydrological changes observed at Tswaing between 150 kyr B.P. and the present. Lower atmospheric temperatures during glacials and stadials would have certainly decreased evaporation from the lake surface, and thus acted to increase lake levels. Temperatures were ~5-6°C lower than today over most of southern Africa during the LGM, for example, which would have substantially decreased evaporation, and may thus account for a significant proportion of the lake-level rise at this time (Heaton *et al.*, 1986; Talma and Vogel, 1992; Stute and Talma, 1998; Holmgren *et al.*, 2003). It is improbable that the lake-level fluctuations observed at the site were entirely determined by changes in evaporation, however, and it is therefore likely that precipitation also increased when atmospheric temperatures were low.

A number of different factors could account for increased precipitation at Tswaing during glacials and stadials. An increase in the meridional temperature gradient caused by lower temperatures and increased sea-ice extent at high southern latitudes may have increased precipitation by causing an equator-ward expansion and intensification of the circum-polar vortex and the associated mid-latitude westerlies (chapter 1) (Van Zinderen Bakker, 1967, 1976). It remains uncertain, however, how far the westerlies would have shifted, and whether such a shift would have increased

annual precipitation (as opposed to only altering the seasonality of rainfall) in areas north of the current winter rainfall belt. It is also possible that precipitation increased in the southern tropics during glacials and stadials because the increase in northern-hemisphere ice volume and changes in ocean circulation reduced the hemispheric disparity of the meridional temperature gradient, and thereby displaced the average position of the ITCZ to the south (chapter 1) (Flohn, 1967; van Zinderen Bakker, 1967; Ganopolski *et al.*, 1998; Chiang *et al.*, 2003; Clement *et al.*, 2004; Ivanochko *et al.*, 2005). This shift may have increased the strength of the low pressure system over southern Africa in summer, and thus increased precipitation in the summer rainfall region (van Zinderen-Bakker, 1967, 1976; Butzer *et al.*, 1973, 1978; Lancaster, 1979). It is also possible that changes in SSTs influenced precipitation at the site (cf. Mason, 1995). Finally, TTTs account for a significant proportion of precipitation in northeast South Africa today (section 3.2.2), and it is therefore possible that changes in the intensity, frequency, or location of these features influenced precipitation at Tswaing in the past (cf. Tyson, 1986; Cockroft *et al.*, 1987).

In order to determine which, if any, of these mechanisms affected precipitation at Tswaing, the records must be considered in the context of other records from southern Africa. The relevant evidence is considered in the following sections. The locations of the sites mentioned in the text are shown in Figure 5.14. All radiocarbon dates have been converted to calibrated calendar years (using Calib version 5.0.1 (Stuiver and Reimer, 1993) where necessary), unless otherwise stated.

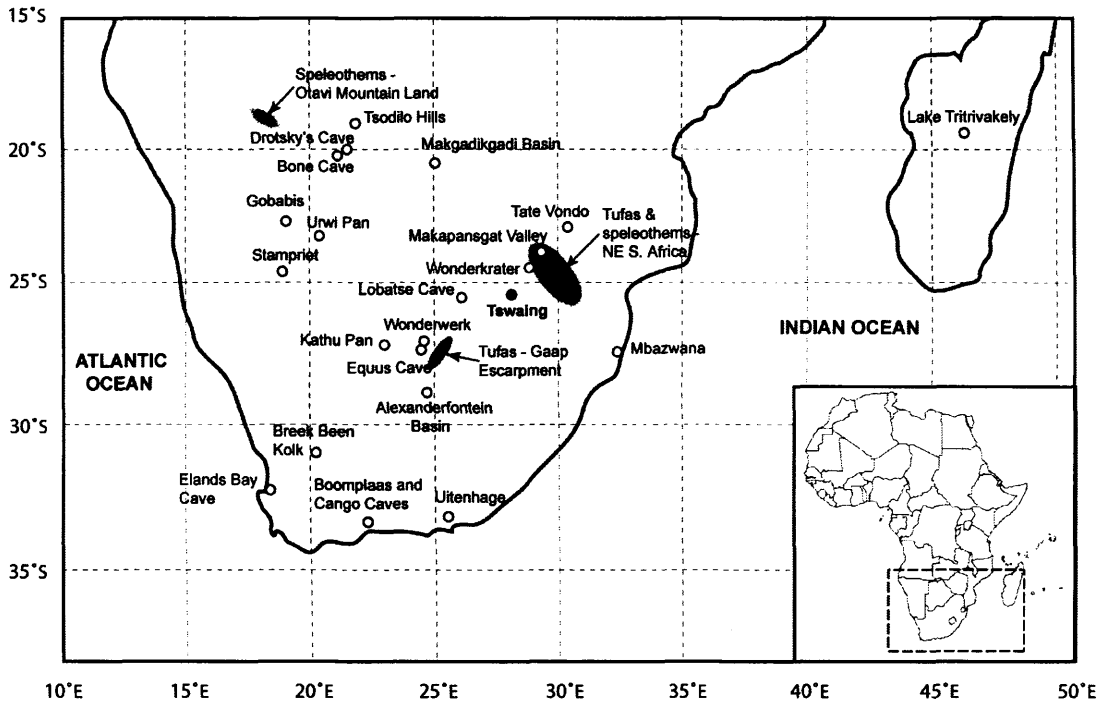

Figure 5.14: Map showing the location of Tswaing crater lake and sites mentioned in this chapter.

Location and intensity of the mid-latitude westerlies

If the location and intensity of the mid-latitude westerlies determined climatic conditions at Tswaing, moisture availability would have probably varied in a similar manner to that observed at Tswaing in areas south of the site over the last 150 kyr (cf. Figure 3.2). Unfortunately, there are few long records from this region, and it is therefore difficult to test this hypothesis. The longest terrestrial record currently available is that of tufa formation at the Gaap Escarpment (~27°S) (Fig. 5.14). This record indicates that moisture availability was often higher than at present between 45 and 9 kyr B.P. and between 3.6 and 0.5 kyr B.P., and thus suggests that conditions were wetter during the last glacial and the late Holocene than during the early Holocene (Butzer *et al.*, 1978; Beaumont and Vogel, 1993; Brook *et al.*, 1998). This pattern is similar to that observed at Tswaing, where relatively low C/N ratios and high $\delta^{13}C_{organic}$ values indicate high lake levels during the last glacial and the late Holocene, and the reverse situation indicates low lake levels during the early Holocene (Fig. 5.13). It is therefore possible that the location and intensity of the mid-latitude westerlies influenced climatic conditions at both sites over the last ~50 kyr.

A number of shorter records from the area south of Tswaing cover the period since the LGM. Some syntheses of these records have concluded that moisture availability was low throughout southern Africa during the LGM, and that it was spatially and temporally variable during the Holocene (*e.g.* Tyson *et al.*, 2001; Partridge *et al.*, 2004). If correct, this reconstruction would indicate that the mid-latitude westerlies did not drive the changes in moisture availability observed at Tswaing. The reconstruction is based on rather equivocal evidence, however, and some studies question its validity in both the summer rainfall zone and the winter and all-year rainfall zones of South Africa (*e.g.* Meadows and Baxter, 1999).

Evidence from the winter and all-year rainfall zones strongly suggests that moisture availability was higher than today during the LGM, and that precipitation may have also been higher during the late Holocene than during the early Holocene (cf. Meadows and Baxter, 1999); a pattern that is in line with the changes observed at Tswaing (Fig. 5.13). In particular, evidence from Elands Bay Cave and the surrounding region, on the southwest coast of South Africa (32°S), indicates that conditions were wetter during the LGM than during the Holocene, and that moisture availability increased during the late Holocene (Klein, 1991; Cowling *et al.*, 1999; Meadows and Baxter, 1999; Parkington *et al.*, 2000). Examination of the micro-mammalian and charcoal records from Boomplaas Cave (33°S), on the south coast of Africa, shows that moisture availability was higher than at present ~24 kyr B.P., and thus that conditions were relatively wet for at least part of the last glacial (Avery, 1982; Deacon *et al.*, 1984). Evidence from this site also suggests that effective moisture probably increased during the late Holocene (Deacon *et al.*, 1984). In addition, lake levels at Breek Been Kolk (31°S), in the all-year rainfall zone, appear to have been higher during the LGM than during the Holocene (Beaumont, 1986). The dates on freshwater shells from lacustrine deposits at this site may be subject to error, but the range of dates (14-28 ^{14}C kyr B.P.) suggests that the deposits probably cover the LGM. The similarity of changes in moisture availability in the winter and all-year rainfall zones of southern Africa to those observed at Tswaing crater lake since the LGM therefore suggests that changes in the location and intensity of the mid-latitude westerlies could have caused the lake-level changes observed at Tswaing.

It is important to note, however, that the δ^{13}C record from a stalagmite in Cango Cave

(33°S), which lies in the all-year rainfall zone of South Africa, indicates that C_4 grasses expanded at this site after ~6 kyr B.P. (Talma and Vogel, 1992; Lee-Thorp and Talma, 2000). This shift has been interpreted as indicating either an increase in aridity (Scott and Lee-Thorp, 2004), or an increase in the proportion of summer rainfall at the site (Talma and Vogel, 1992). Both these interpretations counter the hypothesis that moisture availability increased at Tswaing during the late Holocene due to an expansion and/or an increase in the intensity of the mid-latitude westerlies.

In the summer rainfall region, the Alexandersfontein Pan (29°S), which now holds an ephemeral pool, was thought to have held a 19 m-deep lake at ~17 kyr B.P. (Butzer *et al.*, 1973; Butzer, 1984), although the date of this highstand has been disputed (Partridge and Scott, 2000). Lacustrine deposits at Mbazwana (27°S), on the eastern coastal plain of South Africa, indicate that large, freshwater lakes were present in this region between 36 and 23 kyr B.P., supporting the proposal that effective moisture was high during the last glacial (although diatom-inferred lake levels indicate that moisture availability decreased towards 23 kyr B.P.) (Maud *et al.*, 1993). Records from Kathu Pan (27°S) also suggest that moisture availability was higher during the LGM than during the early Holocene, as water levels remained stable during the LGM and fell between 13 and 8 kyr B.P. (Beaumont *et al.*, 1984; Butzer, 1984). Furthermore, the $\delta^{18}O$ composition of groundwater from the Stampriet basin (24°S) indicates that these increases in moisture availability may have been caused by an equator-ward shift of the mid-latitude westerlies, because precipitation at this site appears to have originated from the Atlantic Ocean during the LGM, rather than the Indian Ocean, as it does today (Stute and Talma, 1998).

Evidence from the summer rainfall zone south of Tswaing thus suggests that moisture availability may have been higher in this region during parts of the last glacial and/or the LGM than during the Holocene, and thus that a northward shift of the mid-latitude westerlies could have conceivably caused the rise in lake level at Tswaing between ~32 and ~9.5 kyr B.P. recorded by low C/N ratios and %LOI 550°C and high $\delta^{13}C_{organic}$ values (Fig. 5.13). It is important to note, however, that a record of the nitrogen isotope composition of ostrich egg shells from Equus Cave (~28°S) indicates that precipitation was lower in central South Africa at 17 kyr B.P. than during the late Holocene (Johnson *et al.*, 1997), which, if true, would suggest that a northward shift

of the westerlies was not responsible for high levels of precipitation at Tswaing during the late glacial.

Some records of climatic change from this part of the summer rainfall zone also indicate that moisture availability increased during the mid- to late-Holocene, in line with the increase in lake levels at ~4.5 kyr B.P. recorded by a slight decrease in C/N ratios and increase in $\delta^{13}C_{organic}$ at Tswaing crater lake (Fig. 5.13). Records of small mammal assemblages and nitrogen isotopes in teeth from Wonderwerk Cave (27°S) suggest that conditions were relatively arid during the early Holocene but that moisture availability increased after 6 kyr B.P., for example (Avery, 1981; Thackeray, 1987; Thackeray and Lee-Thorp, 1992). Similarly, evidence from the Kathu Pan (27°S) suggests that lake levels increased after ~8 kyr B.P. (Beaumont *et al.*, 1984; Butzer, 1984). Once again, the similarity of these changes in moisture availability to those observed at Tswaing crater lake suggests that the location and intensity of the mid-latitude westerlies could have affected precipitation at Tswaing during the Holocene.

Changes in the location of the mid-latitude westerlies can also be assessed using marine records. Pollen records from the southeast Atlantic indicate that vegetation associated with a winter rainfall regime grew as far north as 19°S in southern Africa during the LGM (at least on the west coast), but that conditions were generally more arid, and therefore suggest that the mid-latitude westerlies shifted northwards during the LGM, but that they did not increase MAP in southwest Africa (Shi *et al.*, 1998, 2000; Dupont and Wyputta, 2003). Conversely, Stuut *et al.* (2002) reconstructed continental aridity over southern Africa between 24°S and 32°S using grain-size analysis of a core from the Walvis Ridge (19°6'S, 9°2'E), and concluded that an equator-ward shift of the westerlies increased moisture availability in southwestern Africa during glacial periods (Fig. 5.13).

The position of the STF and the extent of Antarctic sea ice also provide information about the position of the mid-latitude westerlies, as these winds are associated with the zone of greatest baroclinicity (section 3.2.2). The STF currently lies at 40°-42°S in the vicinity of South Africa, but studies indicate that it shifted 2°-5° further north during glacials, and ~2° further south during the early part of MIS 5e and during the

early Holocene (Prell *et al.*, 1979; Howard and Prell, 1992; Brathauer and Abelmann, 1999). The extent of Antarctic sea-ice appears to have followed a similar pattern, increasing gradually during glacials and retracting rapidly at glacial-interglacial transitions (Crosta, 2004). Gersonde *et al.* (2003) produced a detailed reconstruction of SST and sea-ice extent south of Africa at the LGM. They showed that the sub-Antarctic front and the maximum extent of sea-ice lay ~5° further north than today, but that the STF only lay ~2° further north, which increased the meridional temperature gradient at ~40°S and probably, therefore, increased the intensity of atmospheric circulation at this latitude. After the LGM, sea-ice extent decreased to a minimum as Antarctic temperatures increased to a maximum between 11 and 9 kyr B.P., while neoglacial conditions developed after ~6 kyr B.P. (Steig *et al.*, 1998; Masson *et al.*, 2000; Hodell *et al.*, 2001). The timing and direction of these changes fits well with the changes in moisture availability recorded at Tswaing (Fig. 5.13). The magnitude of the shifts in the location of the STF and in sea-ice extent are small, however, and it therefore appears unlikely that changes in the strength and location of the mid-latitude westerlies were large enough to cause the changes in precipitation observed at the site.

Overall, these studies suggest that the westerlies probably lay further north over southern Africa during glacial periods, and that they were probably more intense, bringing increased winter rainfall to sites that currently lie in, and immediately north of, the winter rainfall region, particularly in western parts of the subcontinent. This scenario also appears to apply to the late Holocene, when the westerlies may have intensified in response to lower temperatures and increased sea-ice extent in Antarctica. Marine records indicate, however, that the STF only moved ~2° further north during glacials, and it is therefore unlikely that a change in the location and intensity of the mid-latitude westerlies can explain increased rainfall at sites as far north as Tswaing.

Location of the ITCZ

If latitudinal shifts in the location of the ITCZ determined precipitation at Tswaing between 150 kyr B.P. and the present, moisture availability in the region between ~15°S (the southern limit of the ITCZ and the CAB) and 25°S would have probably varied in phase with that at Tswaing (cf. Figure 3.2). The distinction between a

southward shift of the ITCZ and an increase in the intensity of convection at this convergence zone should be noted, however, because a southward shift of the ITCZ could potentially increase precipitation in southern Africa even if convection at the ITCZ were weaker and sites that are currently affected by the ITCZ were consequently drier (cf. Ivanochko *et al.*, 2005). This distinction is important because parts of the southern African tropics were drier than at present during the LGM, when moisture availability was high at Tswaing (chapter 1) (cf. Gasse, 2000).

The longest continuous record of palaeoclimatic change in the region between 15°S and 25°S is from Lake Tritrivakely in Madagascar (19°S) (Gasse and van Campo, 2001). This record covers the last ~150 kyr, but it not directly dated beyond 41 kyr B.P. The longest and most extreme highstands of the lake appear to correspond with phases of high insolation during austral summer, suggesting that direct insolation affected precipitation at this site (chapter 1). At certain times, including the LGM, this relationship breaks down, however, possibly because increased evaporation during summer and low rainfall during winter out-weighed the increase in precipitation caused by high summer insolation (Gasse and van Campo, 2001). Climatic conditions at Lake Tritrivakely therefore appear to have been different from those at Tswaing, with precipitation responding to changes in summer insolation rather than glacial-interglacial cycles, and moisture availability remaining low rather than increasing during the LGM. These differences are not particularly surprising, however, because the ITCZ currently lies over northern Madagascar during summer (Fig. 3.2), and climatic conditions at Lake Tritrivakely may therefore be less sensitive to poleward shifts, and more sensitive to changes in the intensity of this system than climatic conditions at Tswaing.

The only other long terrestrial records of palaeoclimatic change from the area to the north of Tswaing are the records of speleothem and tufa growth from northeast South Africa (~25°S), Lobatse I and II Caves (25°S), and Drotsky's and Bone Caves (20°S) (summarised by Brook *et al.*, 1998) (Fig. 5.15). The extent to which these records can be used to infer climatic change is limited by sample availability, but they suggest that conditions were relatively wet during parts of the last glacial and the late Holocene, and relatively dry during the last interglacial and the early Holocene (Fig. 5.15). Furthermore, speleothems in the Otavi Mountain Land (~19°S) (Fig. 5.14) show that

conditions were extremely arid in northern Namibia between 130 and 111 kyr B.P., which hints that moisture availability may have decreased throughout the region between 15°S and 25°S during the last interglacial (Brook *et al.*, 1998). These patterns are similar to those observed at Tswaing, where high C/N ratios and %LOI 550°C and low $\delta^{13}C_{organic}$ values indicate that lake levels were low during interglacials and interstadials over the last 150 kyr (Figs. 5.13 and 5.15). The records of speleothem and tufa growth therefore provide some support for the suggestion that a southward shift of the ITCZ during glacials, and a northward retreat of this zone during interglacials, influenced precipitation at Tswaing crater lake.

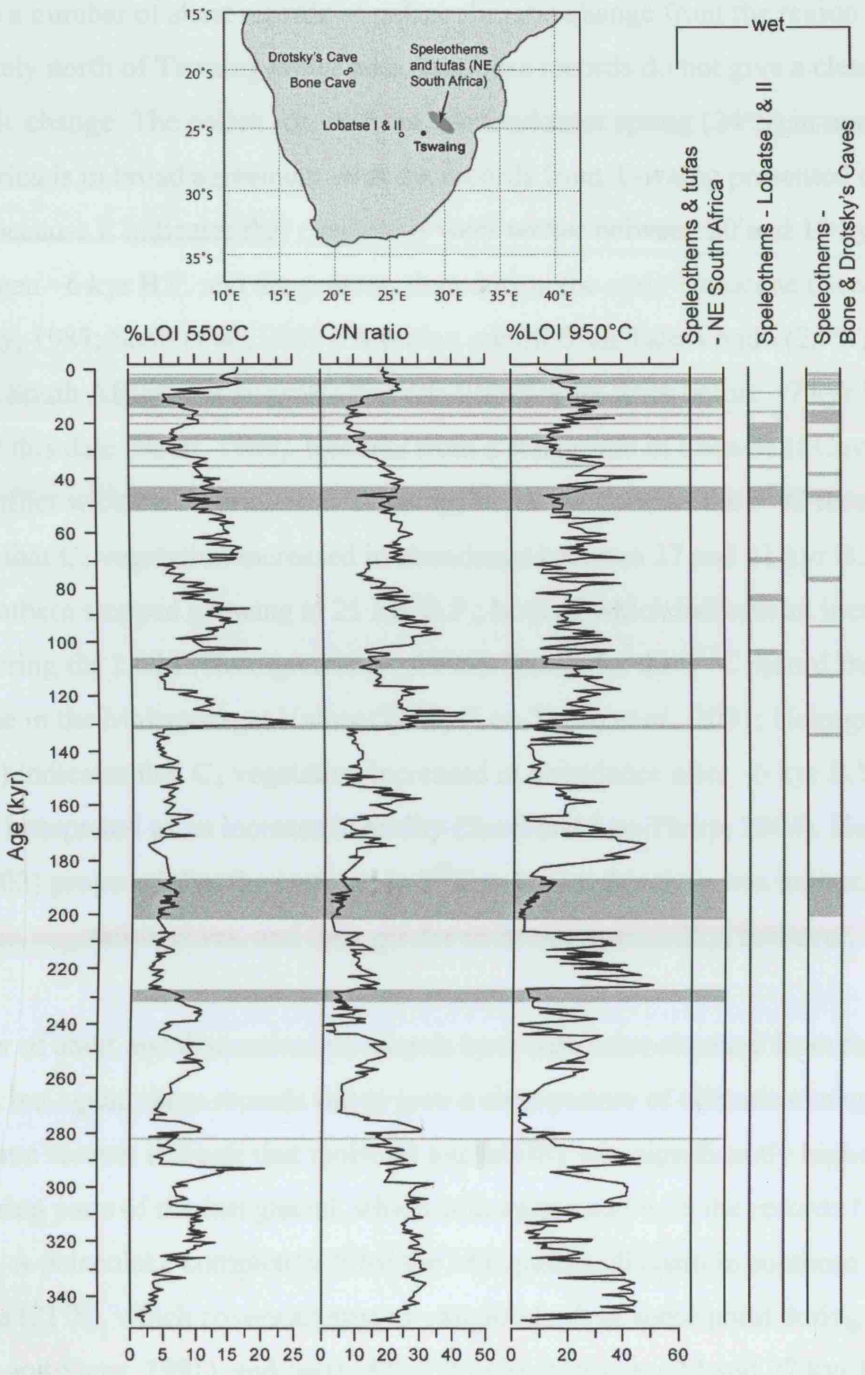

Figure 5.15: Periods of increased moisture availability (grey bars) recorded by speleothem and tufa growth in northeast South Africa, Lobatse I and II Caves, and Bone and Drotsky's Caves (Brook *et al.*, 1998), shown with the C/N ratio, %LOI 550°C, and %LOI 950°C records from Tswaing (plotted according to the linear age-depth model). Periods of increased moisture availability recorded by speleothem and tufa growth in northeast South Africa are extended over the records from Tswaing to allow easy comparison between these records. Map shows the location of the relevant sites.

There are a number of short records of palaeoclimatic change from the region immediately north of Tswaing crater lake, but these records do not give a clear picture of climatic change. The pollen record from Wonderkrater spring (24°S) in northeast South Africa is in broad agreement with the records from Tswaing presented in this chapter, because it indicates that conditions were wetter between 20 and 10 kyr B.P., and between ~6 kyr B.P. and the present, than during the early Holocene (Scott and Thackeray, 1987; Scott *et al.*, 2003). A pollen record from Tate Vondo (23°S) in northeast South Africa also suggests that conditions were drier before ~7 kyr B.P. than after this date (Scott, 1989). Records from a stalagmite in Lobatse II Cave (25°S) are in conflict with the records from Tswaing, however, because the $\delta^{13}C$ record indicates that C_4 vegetation increased in abundance between 27 and 21 kyr B.P., and the speleothem stopped growing at 21 kyr B.P.; both of which indicate an increase in aridity during the LGM (Holmgren *et al.*, 1995). Similarly, the $\delta^{13}C$ record from a stalagmite in the Makapansgat Valley (24°S) (Lee-Thorp *et al.*, 2001; Holmgren *et al.*, 2003) indicates that C_4 vegetation increased in abundance after ~6 kyr B.P., which has been interpreted as an increase in aridity (Scott and Lee-Thorp, 2004). Holmgren *et al.* (2003) proposed that the increase in $\delta^{13}C$ values at this time was indicative of an increase in vegetation cover, and thus greater moisture availability, however.

A number of short and discontinuous records have also been obtained from the Kalahari, but again, these records fail to give a clear picture of climatic change (Fig. 5.14). Some records indicate that moisture availability was significantly higher than today during parts of the last glacial, which is in agreement with the records from Tswaing. A palaeolake completely filled the Makgadikgadi basin in southern Botswana (21°S), which covers an area of ~80,000 km^2, at some point during MIS 3 (Thomas and Shaw, 1991), and partly filled it twice between ~32 and 27 kyr B.P. (Shaw *et al.*, 1997), for example. A record of lake level and dune construction in the Tsodilo Hills, Botswana (19°S), suggests that moisture availability was high 27-22 and 19-12 kyr B.P. (Brook *et al.*, 1992; Thomas *et al.*, 2003). This proposal is supported by evidence of high lake levels in pans such as Urwi (23°S), and of spring tufa deposition at sites such as Gobabis (22.5°S), which indicates that moisture availability was high in the Kalahari before ~25 kyr B.P. and between ~20 and ~12.5 kyr B.P. (Lancaster, 1979; Lancaster, 1989), although Partridge and Scott (2000) suggested that these dates should be regarded as minimum ages. These records are

thus in broad agreement with those from Tswaing, although they suggest that moisture availability may have decreased between ~25 and ~20 kyr B.P., which does not appear to have occurred at Tswaing, as C/N ratios remain low during this period, indicating high lake levels (Fig. 5.13).

Other records from the Kalahari indicate that moisture availability was lower than today during much of the last glacial, however. Optically-dated sand dunes in the southern Kalahari (~26°S) indicate that there were major phases of dune building in areas that are currently inactive at 30-23 and 16-10 kyr B.P., with only localised dune activation during the Holocene, for example (Stokes *et al.*, 1997a,b; Thomas *et al.*, 1997). Further north, there appear to have been significant phases of dune building at 26-20 kyr B.P. in western Zimbabwe (~19°S) (Stokes *et al.*, 1997a, 1998), at 32-27, 16-13, and 10-8 kyr B.P. in southwestern Zambia (~16°S) (O'Connor and Thomas, 1999), and at 36-29 and 23-21 kyr B.P. in northern Namibia (~18°S) (Thomas *et al.*, 2000). The discontinuous nature and the variability of these records makes it difficult to generalise about climatic change in the Kalahari, but Munyikwa (2005) suggested that, on average, conditions were drier between ~35 and 8 kyr B.P., than after 8 kyr B.P., which contrasts with the observation that moisture availability was higher during most parts of the last glacial than during the Holocene at Tswaing crater lake.

Some of the discrepancies between palaeoclimatic records from the region between 15°S and 25°S may be due to the different climatic settings of western and eastern parts of southern Africa (section 3.2.1). Southwestern Africa is currently arid, because the strong, stable SAA and the oceanic gyre it creates bring cold, dry, subsiding air to coastal regions (sections 3.2.2 and 3.2.3). In addition, the south-easterly trade winds generate upwelling off the southwest coast of Africa, which further increases the stability of the atmosphere over western regions (van Zinderen Bakker, 1976). In contrast, the SIA is weaker and lies further from the coast of Africa than the SAA. Furthermore, the south-easterly trades associated with this system bring moist air onto the continent and thus generate precipitation in eastern areas. Increases in trade-wind strength may have therefore decreased precipitation in western Africa by increasing the stability of the atmosphere in this region (through an increase in the strength of the SAA), by reducing the lateral transport of moisture onto the continent, and by increasing the strength of upwelling off the southwest coast (*e.g.* Little *et al.*, 1997;

Schefuβ *et al.*, 2005). In eastern areas, in contrast, stronger trade winds may have increased precipitation by enhancing lateral transport of moisture onto the continent.

Marine records indicate that the trade winds were strongest and most zonal during glacials, particularly MIS 3, but that the strength and zonality of the winds associated with the SAA were also influenced by precessionally-driven changes in the strength of the North African monsoon (Schneider *et al.*, 1995; Summerhayes *et al.*, 1995; Little *et al.*, 1997; Giraudeau *et al.*, 2001; Shi *et al.*, 2001; West *et al.*, 2004). It is therefore possible that precipitation increased in southeastern Africa during glacials due to a southward shift of the ITCZ combined with an increase in the strength of the trade winds, but that the increase in trade-wind strength acted to decrease precipitation in southwestern Africa. Furthermore, variations in the strength of the winds associated with the SAA driven by changes in the intensity of the North African monsoon may have caused additional variations in precipitation in southwestern Africa. This scenario may explain some of the differences between palaeoclimatic records from between 15°S and 25°S in southern Africa.

Records from South America also provide information about the location of the ITCZ during the late Quaternary but, as mentioned in chapter 1, these findings may not be directly applicable to Africa. Most records from the tropics and subtropics of South America indicate that the average location of the ITCZ is primarily determined by precessionally-driven changes in insolation, which does not fit the pattern of change observed at Tswaing. The peak in boreal summer insolation during the early Holocene appears to have caused the average position of the ITCZ to move further north, for example, increasing runoff into the Cariaco Basin (~10°N) and decreasing precipitation in the Bolivian Altiplano (Martin *et al.*, 1997; Haug *et al.*, 2001; Tapia *et al.*, 2003). Moreover, a peak in austral summer insolation during the late Holocene appears to have caused the ITCZ to move to the south, stimulating a southward expansion of the Amazon rainforest, an increase in the level of Lake Titicaca (17°S), and a decrease in runoff into the Cariaco basin (Mayle *et al.*, 2000; Haug *et al.*, 2001; Tapia *et al.*, 2003). A series of speleothem and travertine deposits from northeast Brazil (10°S) that cover the last 210 kyr also indicate that precipitation increased when the ITCZ shifted southwards in response to precessionally-driven changes in insolation (Wang *et al.*, 2004). It remains difficult, however, to separate the influences

of changes in the location of the ITCZ from changes in the intensity of tropical convection on these records, because they are from areas that are close to the current location of the ITCZ.

Some evidence from South America suggests that changes in ice-sheet volume and/or the strength of the thermohaline circulation affected the location of the ITCZ in South America, and therefore provides support for the suggestion that shifts in the ITCZ could have been responsible for the lake-level changes observed at Tswaing. A record of changes in the seasonality and the amount of precipitation over the last 116 kyr from a speleothem in southern Brazil (27°S), which lies south of the southern limit of the ITCZ, suggests that precipitation increased during glacials due to a southward shift of the ITCZ, for example, although precessionally-driven increases in austral summer insolation are the primary influence on precipitation at the site (Cruz *et al.*, 2005). Moreover, a pollen record from Panama (7°N), at the northern limit of the ITCZ, suggests such a southward shift of the ITCZ decreased precipitation in this region during glacials (Bush, 2002). These suggestions are supported by the record of millennial-scale productivity in the Cariaco basin, which suggests that colder temperatures in the North Atlantic were associated with a southward shift of the ITCZ over Venezuela (Peterson *et al.*, 2000).

In summary, the evidence available from southern Africa suggests that a southward shift of the ITCZ, combined with an increase in trade-wind strength, could have increased precipitation at Tswaing crater lake during glacials, as the records of %LOI 550°C, C/N ratios, and $\delta^{13}C_{organic}$ from the site suggest (Fig. 5.13). This hypothesis appears to be in conflict with evidence that conditions were arid in parts of the Kalahari basin during much of the last glacial (cf. Munyikwa, 2005), but it is possible that increased trade-wind strength acted to suppress precipitation in the Kalahari by increasing atmospheric stability, reducing lateral transport of moisture onto the continent, and increasing upwelling at this time. Records from South America counter these proposals, however, as they suggest that the position of the ITCZ is primarily influenced by precessionally-driven changes in insolation, rather than changes in ice-volume or the strength of the thermohaline circulation.

Sea-surface temperatures

It is possible that changes in SST influenced moisture availability at Tswaing, because SSTs currently have a significant influence on precipitation in southern Africa (section 3.2.3) (*e.g.* Walker, 1990; Jury *et al.*, 1993; Mason, 1995; Jury, 1995, 1996; Mason and Jury, 1997; Reason and Lutjeharms, 1998; Reason, 2001; Rouault *et al.*, 2002). SSTs in the southwest Indian Ocean are positively correlated with precipitation in southern Africa (Mason, 1995), but SSTs decreased by up to 3°C in this region during glacials and would not, therefore, have increased precipitation at Tswaing (Bard *et al.*, 1997; Sonzogni *et al.*, 1998). It is possible, however, that higher SSTs at the Agulhas retroflection increased precipitation in southern Africa during glacials, because SSTs in this region may have been influenced by the amount of water that flows around the tip of South Africa through the "Cape valve" (section 3.2.3). Marine records indicate that "Agulhas leakage" continued throughout the last ~500 kyr, but that the amount reached maxima at glacial terminations and remained high during interglacials due a more southerly location of the STF and a decrease in volume transport of the AGC caused by a decrease in the strength of the SIA (Prell *et al.*, 1980; Pether, 1994; Flores *et al.*, 1999; Giraudeau *et al.*, 2001; Chen *et al.*, 2002; Rau *et al.*, 2002; Esper *et al.*, 2004; Peeters *et al.*, 2004). It is therefore plausible that an accumulation of warm water at the Agulhas retroflection during glacials, caused by reduced Agulhas leakage, increased precipitation in southern Africa (Reason *et al.*, 1996, Reason, 2001).

SSTs in the western and central equatorial Indian Ocean are negatively correlated with precipitation in the summer rainfall region of southern Africa (Mason, 1995) (section 3.2.3). SSTs in this region varied with glacial-interglacial cycles and may, therefore, have increased precipitation at Tswaing during glacials and stadials (Rostek *et al.*, 1993; Bard *et al.*, 1997; Sonzogni *et al.*, 1998). The potential influence of tropical SSTs on precipitation in southern Africa is highlighted by the differences between PMIP simulations of climatic conditions during the LGM that use prescribed (CLIMAP) SSTs, and those that use calculated SSTs (cf. Barker and Gasse, 2003). Models that use the CLIMAP estimates of tropical SSTs tend to simulate decreased precipitation over southern Africa, and increased precipitation in East Africa (Pinot *et al.*, 1999). In contrast, simulations that use calculated SSTs, which are ~2°C colder than the CLIMAP estimates in the western and central equatorial Indian Ocean and

appear to be more accurate than the CLIMAP estimates (*e.g.* Rostek *et al.*, 1993; Bard *et al.*, 1997; Sonzogni *et al.*, 1998), indicate that precipitation decreased in tropical Africa but increased in eastern South Africa (Pinot *et al.*, 1999); a finding that is in close agreement with the palaeoclimatic records from both Tswaing crater lake and East Africa (cf. Barker and Gasse, 2003). It seems unlikely that variations in SST were the only cause of increased precipitation at Tswaing during glacials and stadials, but it is certainly plausible that changes in SSTs in the equatorial Indian Ocean, and possibly the southwest Indian Ocean, enhanced changes caused by atmospheric circulation.

Location and intensity of tropical-temperate troughs (TTTs)

A significant proportion of rainfall in the summer rainfall region of South Africa is generated by the TTTs that form between tropical lows and low-pressure systems associated with the semi-stationary long waves in the mid-latitude westerlies (section 3.2.2). Any change in the intensity, frequency, or location of these features would therefore have a significant effect on precipitation at Tswaing (cf. Tyson, 1986; Cockroft *et al.*, 1987). Today, the intensity and frequency of TTT-formation are influenced by the strength and frequency of disturbances in both the tropical easterlies and the extra-tropical westerlies (Walker, 1990; Mason, 1995; Cook, 2000). It is therefore possible that a southward shift of the ITCZ, combined with an increase in the strength and a northward shift of the mid-latitude westerlies (see above), increased the intensity and frequency of TTT-formation during glacials (cf. Tyson, 1986). Furthermore, high SSTs at the Agulhas retroflection and increased trade-wind strength during glacials may have accentuated these changes by increasing cyclogenesis at the STF, and increasing convergence at TTTs, respectively (Walker, 1990; Walker and Shillington, 1990; Crimp *et al.*, 1998; Reason, 2002).

The amount of precipitation generated by TTTs in southern Africa is also influenced by their longitudinal position, which alternates between a location over southern Africa and a location over Madagascar and the southern Indian Ocean (section 3.2.2). An increase in the strength of the SIA (Rind, 2000), as well as a possible shift of this system to the west (as occurs in winter today), and low SSTs in the western and central equatorial Indian Ocean (Rostok *et al.*, 1993, 1997), would have all increased the tendency of TTTs to form over southern Africa during glacials, and may have thus

increased precipitation in this region (cf. Jury and Pathack, 1991, 1993; Jury, 1992; Jury *et al.*, 1992, 1994; Todd and Washington, 1998; Washington and Todd, 1999; Todd *et al.*, 2004).

The validity of these suggestions relies on the assumption that the position of the southern-hemisphere standing waves was not significantly different during glacials (section 3.2.2). It is likely that this assumption is valid, because the position of these waves is partly controlled by topography and land/ocean contrast. A simulation of conditions during the LGM broadly confirms this suggestion, but shows that standing wave 3 shifted ~20° west, and that the current wave structure was amplified by the increase in the meridional temperature gradient (Rind, 1998). This shift in standing wave 3 would have probably increased the proportion of TTTs that formed over southern Africa, and the amplification of waves may have increased the frequency of TTT-formation by increasing the likelihood of links between tropical and extra-tropical disturbances (Tyson, 1986). These changes may, therefore, have contributed to the increase in the frequency of TTT-formation over southern Africa during glacials proposed above.

The hypothesis that increases in the intensity and frequency of TTT-formation over southern Africa increased precipitation at Tswaing during glacials and stadials is line with many of the palaeoclimatic records from southern Africa described above. An increase in the frequency of TTT-formation over southern Africa relative to the frequency of their formation over Madagascar and the southern Indian Ocean could partly account for the differences in moisture availability at Lake Tritrivakely and Tswaing during the LGM (Gasse and van Campo, 2001). The hypothesis is also in line with the observation that moisture availability was low in parts of the Kalahari during the last glacial (cf. Munyikwa, 2005), as TTTs do not generate precipitation in western areas of southern Africa (Fig. 3.2). Finally, the suggestion that an increase in TTT-formation increased precipitation at Tswaing during glacials fits with the observation that conditions were relatively dry in tropical East Africa during the LGM (Barker and Gasse, 2003), because TTT-formation is thought to be partly responsible for the anti-correlation of precipitation in these areas on annual timescales today (Goddard and Graham, 1999).

5.6.2 150-350 kyr B.P.

5.6.2.1 Timing of palaeohydrological change

According to the linear age-depth model, the section of the sedimentary sequence below 35 m corresponds to the period between 150 and 350 kyr B.P. The interpretation of the proxy records presented in sections 5.5.1 and 5.5.2 indicates that lake-level changes are recorded most accurately by %LOI 950°C in this section. The only depth at which this proxy does not reflect lake-level change is ~65 m, where an increase in the organic content of the sediment appears to have reduced %LOI 950°C. $\delta^{18}O_{calcite}$ and $\delta^{13}C_{calcite}$ also reflect palaeohydrological change in most parts of this section, although these records may have been influenced by factors other than the hydrological balance of the lake between 41.50 and 51.10 m (zone 4), and by authigenic calcite precipitation above 41.50 m (zones 5 to 8) (chapter 6). C/N ratios respond to lake-level change above ~62 m, but $\delta^{13}C_{organic}$ and %LOI 550°C are relatively insensitive to palaeohydrological change throughout this section.

Based on these interpretations, the records from this section of the sequence indicate that lake levels decreased in the lower parts of zones 1 to 5, as well as at ~53 m in the upper part of zone 3, and at 37.5-35.0 m in the middle of zone 5 (Fig. 5.2). The linear age-depth model suggests that these low-stands took place at 346-326, 307-285, 262-243, ~238, 227-207, 183-166, and 165-152 kyr B.P. (Fig. 5.13). Unlike the lake-level changes between 150 kyr B.P. and the present, the timing of these fluctuations does not appear to correspond with the timing of changes in atmospheric temperature at Vostok (Petit *et al.*, 1999) (Fig. 5.13). It is conceivable that the low-stands at ~238 and 227-207 kyr B.P. correspond with the periods of high temperature at Vostok during MISs 7e (240-235 kyr B.P.) and 7a-c (220-200 kyr B.P.), in which case the relationship between lake levels and global boundary conditions outlined for the period between 150 kyr B.P. and the present (section 5.6.1.1) would appear to hold before 150 kyr B.P. The validity of this suggestion is questionable, however, because the correspondence between the records is weak, and because the proxies from Tswaing do not reflect any other temperature changes at Vostok in this section. This apparent lack of response to changes in global boundary conditions could be because the proxy records were insensitive to climatic change at these times, but the magnitude of the fluctuations in %LOI 950°C and C/N ratios suggests that this is

unlikely. It is also possible that the lack of any relationship between the records results from errors in the age-depth model for the sediments from Tswaing, but it is likely that such errors would be obvious if the association between palaeohydrological conditions at Tswaing and atmospheric temperature at Vostok remained strong. Given these considerations, the records from Tswaing suggest that the causes of lake-level change may have been different before and after ~150 kyr B.P.

The records of %LOI 950°C, $\delta^{18}O_{calcite}$, and $\delta^{13}C_{calcite}$ from this section of the sequence were subjected to harmonic analysis (section 5.6.1.1) to determine the frequency of their periodic components (Fig. 5.16). The results of the analysis of the records of $\delta^{18}O_{calcite}$ and $\delta^{13}C_{calcite}$ should be regarded with caution, however, because these records were influenced by factors other than the hydrological status of the lake in parts of this section (section 5.5.1). The records of C/N ratios, $\delta^{13}C_{organic,}$ and %LOI 550°C were not analysed, due to their insensitivity to lake-level change in all, or parts, of this section (section 5.5.2). The periodogram for the record of %LOI 950°C shows a highly significant peak at 41 kyr, and the records of $\delta^{18}O_{calcite}$ and $\delta^{13}C_{calite}$ also exhibit significant, but smaller, peaks at frequencies close to 41 kyr. All three records also show significant peaks at frequencies greater than 60 kyr, but these peaks should be regarded with caution due to the relatively short period of time covered by the section analysed. The prominence of periodic components with frequencies close to 41 kyr suggests that the obliquity of the earth's axis had a significant effect on lake levels during this period, and comparison of the record of %LOI 950°C with a record of the earth's obliquity indicates that increases in obliquity were associated with decreases in lake depth (Fig. 5.17).

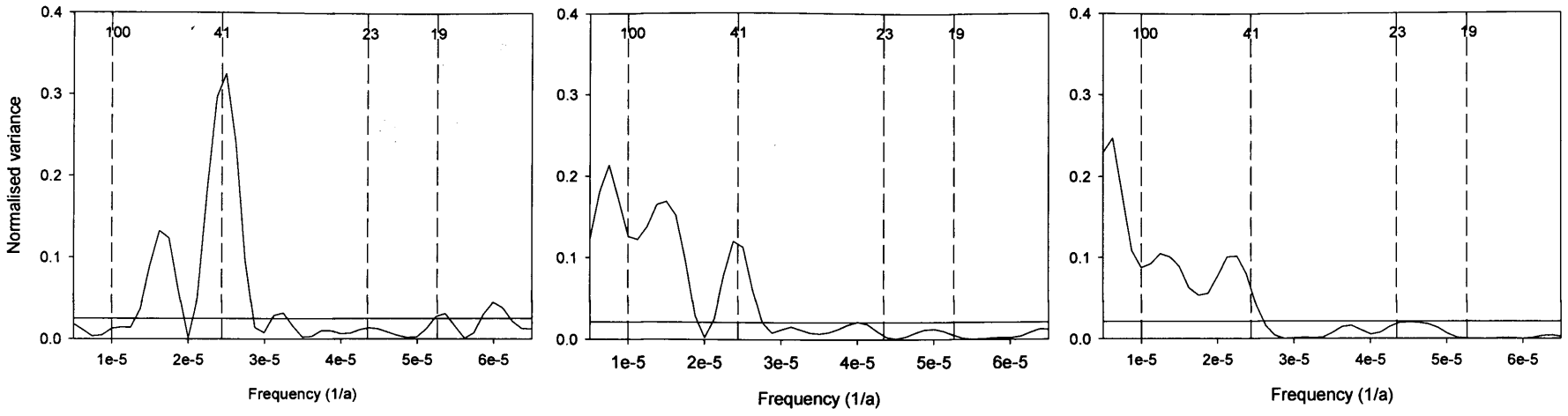

Figure 5.16: Periodograms showing the results of harmonic analysis of the records of %LOI 950°C, $\delta^{18}O_{calcite}$, and $\delta^{13}C_{calcite}$ between 150 and 350 kyr B.P., according to the linear age-depth model. Analysis performed using SPECTRUM (Schultz and Stattegger, 1997). T_λ (test statistic) > $t_{\lambda,\alpha}$ (critical value) for Siegel's test in all cases, and the null hypothesis that the signal is white noise can therefore be rejected (Siegel, 1980).

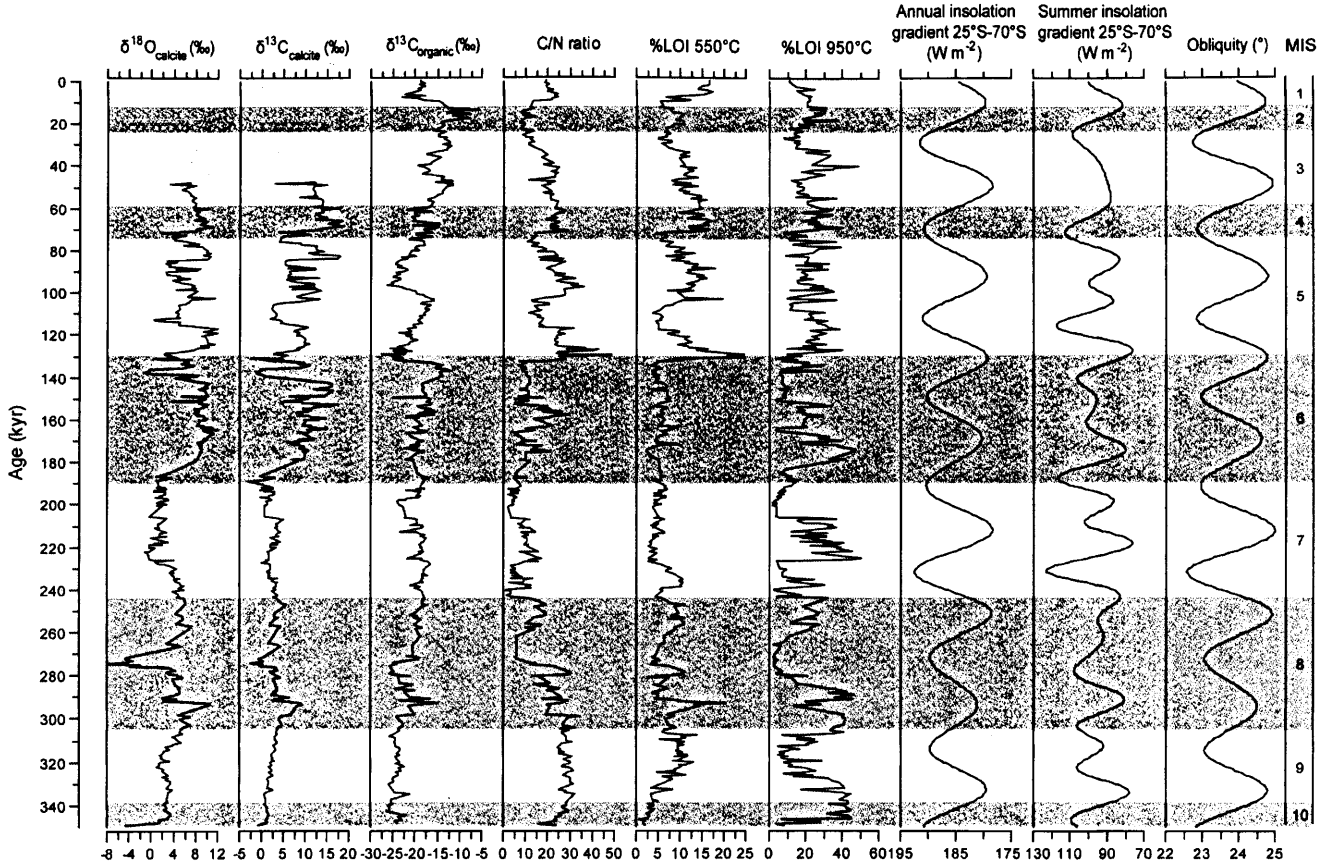

Figure 5.17: Proxy records from Tswaing plotted according to the linear age-depth model, with records of the mean daily insolation gradient 25°-70°S over a year, the mean daily insolation gradient 25°-70°S for the summer half year (21st Sept. to 20th March) (calculated using InsolA, Laskar *et al.*, 2004), and the obliquity of the earth's axis (Berger and Loutre, 1991). Note that the scales for insolation gradients are reversed. MISs shown as grey and white bars (Imbrie *et al.*, 1984).

5.6.2.2 Causes of palaeohydrological change

The obliquity of the earth's axis has a significant effect on both the seasonality and the total amount of insolation received at high latitudes, particularly over landmasses, but has a negligible effect on seasonality at low latitudes (Berger, 1978; Short *et al.*, 1991). Obliquity does, however, determine the annual insolation received at low latitudes, and this variable could conceivably influence SSTs, because the world's oceans have long response times to changes in insolation (Berger, 1978; Loutre *et al.*, 2004). It is unlikely that this effect had a significant influence on climatic conditions at Tswaing, however, because annual insolation at 25°S changed by <1% over the period covered by the records (Laskar *et al.*, 2004), and because records of SST in areas that currently affect precipitation in South Africa are not dominated by the obliquity signal at this time (*e.g.* Rostek *et al.*, 1997; Schneider *et al.*, 1999).

Obliquity can also influence low-latitude climate via teleconnections with mid- and high-latitude climate systems (cf. Clemens and Prell, 2003; Tuenter *et al.*, 2003; Liu and Herbert, 2004). If such teleconnections operated through the influence of obliquity on factors that influence, or are influenced by, global ice volume, a strong glacial-interglacial signal would be expected in the records from Tswaing, but this is not the case (Fig. 5.17). Similarly, if a teleconnection operated through the direct effect of high-latitude insolation on factors such as ocean- or atmospheric-circulation, the record from Tswaing would be expected to vary at frequencies associated with both precession and obliquity, in common with seasonal insolation at high latitudes (Berger and Loutre, 1991). Frequencies associated with precession are not evident in the records in this section, however, and it is therefore unlikely that teleconnections from high latitudes caused lake-level change at Tswaing during this period (Figs. 5.16 and 5.17).

The most likely explanation for the influence of the obliquity of the earth's axis on climate at Tswaing is therefore its influence on the insolation gradient between low and high latitudes. In winter, this effect is negligible, because insolation at high latitudes is so low that the gradient between low and high latitudes is determined by the precessionally-driven changes in insolation at low latitudes. In summer, a larger proportion of the difference between insolation at high and low latitudes is determined

by obliquity, due to higher insolation at high latitudes (Fig. 5.17) (Raymo and Nisancioglu, 2003). The most significant effect of obliquity on the insolation gradient is, however, over the course of a year, as obliquity produces opposing changes in annual insolation at latitudes above and below ~45° (cf. Loutre *et al.*, 2004) (Fig. 5.17).

Changes in the latitudinal gradient of insolation have a significant effect on the meridional temperature gradient, which in turn affects the strength of atmospheric circulation, particularly when combined with feedbacks in sea-ice extent (Gallimore and Kutzbach, 1995; Rind, 1998, 2000; Jackson and Broccoli, 2003; Raymo and Nisancioglu, 2003; Liu and Herbert, 2004; Loutre *et al.*, 2004). It is therefore possible that lower obliquity increased the annual meridional temperature gradient, which increased the intensity of atmospheric circulation, and thereby increased precipitation at Tswaing (as recorded by low %LOI 950°C, $\delta^{18}O_{calcite}$, and $\delta^{13}C_{calcite}$ values) (Fig. 5.17). As outlined in section 5.6.1.2, an increase in the meridional temperature gradient could have increased precipitation at Tswaing by causing the mid-latitude westerlies to intensify and shift towards the equator, or by increasing the intensity of tropical circulation, including the moisture-bearing trade winds. It is even possible that these changes combined to increase precipitation at Tswaing through their influence on the intensity, frequency, and location of TTT-formation (section 5.6.1.2).

This hypothesis suggests that the obliquity of the earth's axis had a greater effect on palaeohydrological conditions at Tswaing before ~150 kyr B.P. than after this date. This transition does not necessarily indicate that the factors controlling climatic conditions changed at this time, however, as it may simply reflect a change in the sensitivity of palaeohydrological conditions at the site to different climatic variables. The lake was, on average, deeper, with a lower surface-area to volume ratio, before 150 kyr B.P. than between 150 kyr B.P. and the present (section 5.5), and it is therefore likely that its water balance was less sensitive to changes in evaporation before 150 kyr B.P. than after this date. Consequently, the close relationship between lake levels at Tswaing and atmospheric temperatures at Vostok after 150 kyr B.P. may primarily reflect the sensitivity of the lake's water balance to changes in atmospheric temperature, while the relationship between lake levels and the earth's obliquity before 150 kyr B.P. may be more closely related to changes in precipitation.

It is also possible that the transition in the records at ~150 kyr B.P. reflects a "real" change in the factors that influenced climatic conditions in southern Africa at this time, however. This suggestion is not completely unprecedented, as palaeoceanographic records from areas influenced by the Benguela current and the Agulhas retroflection indicate that ocean circulation in the vicinity of southern Africa was linearly related to precession and obliquity before 150-200 kyr B.P., but closely linked to glacial-interglacial cycles after this date (Giraudeau *et al.*, 2001; Rau *et al.*, 2002; West *et al.*, 2004). This transition is thought to have been caused by a southward shift of the STF and the mid-latitude westerlies after ~150-200 kyr B.P. (Rau *et al.*, 2002; West *et al.*, 2004). When the STF was located close to southern Africa, before 150-200 kyr B.P., oceanic conditions were sensitive to changes in its location driven by obliquity and precession. After the front shifted to the south, there was greater leakage of the Agulhas current through the Cape valve, and surface-water conditions were only sensitive to the relatively large shifts in the location of the STF associated with glacial-interglacial cycles (Rau *et al.*, 2002; West *et al.*, 2004).

A recent record of oceanic conditions from this region does not highlight this shift (Peeters *et al.*, 2004), but it does demonstrate that the relationship between Agulhas leakage and glacial-interglacial cycles was weaker between 180 and 320 kyr B.P. than between 180 kyr B.P. and the present, which suggests that different factors may have influenced the location of the STF or volume transport of the Agulhas current during these periods (section 3.2.3). In addition, a short record of SST in the Cape Basin suggests that obliquity controlled SST in this area between ~25 and 41 kyr B.P. (Sachs *et al.*, 2001); a period when the STF lay relatively close to southern Africa (Giraudeau *et al.*, 2001). It is therefore plausible that the more northerly location of the STF before 150-200 kyr B.P. increased the sensitivity of climatic conditions in southern Africa to changes in obliquity, due to the influence of this front on both oceanic conditions and the location of the mid-latitude westerlies (section 3.2.3).

Unfortunately, only two other records of climatic change in southern Africa are long enough to compare with this section of the record. The 300-kyr record of aridity in southern Africa produced by Stuut *et al.* (2002) suggests that aridity was high during MISs 7a-c and 7e-9, and lower during MISs 6 and 7d, and does not exhibit a strong obliquity signal during this period (Fig. 5.13). This record does not, therefore, support

the hypothesis that obliquity affected climatic conditions in southern Africa before 150 kyr B.P., although it is notable that the record is less sensitive to changes in glacial-interglacial conditions before ~180 kyr B.P. than after this date (Fig. 5.13). The records of speleothem and tufa growth from northeast South Africa also cover parts of this period, but their discontinuous nature makes it difficult to compare them with the records from Tswaing (Brook *et al.*, 1998). Despite this limitation, periods of increased moisture availability coincide with periods of high lake level at Tswaing (as indicated by lower %LOI 950°C), and these records thus provide some support for the proposed pattern of climatic change (Fig. 5.15) (Brook *et al.*, 1998).

Evidence that the obliquity of the earth's axis has affected climatic conditions at low latitudes is limited, but two records suggest that this may have been the case. Calvo *et al.* (2001) demonstrated that SSTs in the tropical Pacific (17°S) varied in phase with obliquity, but only when the eccentricity of the earth's orbit was low (termination I and MIS 9-11). In contrast, the deuterium excess parameter from the Vostok ice core suggests that obliquity may have affected atmospheric and/or oceanic conditions at low latitudes in the southern hemisphere throughout the late Quaternary (Vimeux *et al.*, 1999, 2002). This parameter reflects SSTs in the source area of precipitation at Vostok and varies in phase with obliquity, indicating that the obliquity of the earth's axis influenced the strength of atmospheric and/or ocean circulation between low and high latitudes (and thus the location of the "average" source of precipitation at Vostok) through its influence on the mean annual insolation gradient (Vimeux *et al.*, 1999, 2002). This finding hints that obliquity could have influenced climatic conditions at Tswaing by affecting the meridional temperature gradient, and thus provides some support for this proposal. Additional records of climatic change at low latitudes in the southern hemisphere are required to test this hypothesis, however.

5.6.3 Comparison with previous records from Tswaing crater lake

The findings presented in this chapter are significantly different from the conclusions reached by Partridge *et al.* (1997, 1999) (section 5.2) (Fig. 5.1). These differences are primarily attributable to the age-depth models used in the two studies (cf. chapter 4), and the records presented in this chapter are therefore plotted against the age-depth model proposed by Partridge *et al.* (1997) in Appendix B, for comparison. It is notable, however, that the lake-level changes reconstructed in this study also differ

from those presented by Partridge *et al.* (1997, 1999) due to the different proxy records used to reconstruct lake-level change, and to the different ways in which some proxy records are interpreted. The palaeo-rainfall record produced by Partridge *et al.* (1997) was principally based on the amount of carbonate in the sediments, which was considered to reflect the evaporative concentration of lake water. In this study, it is proposed that the record of carbonate abundance is probably insensitive to changes in evaporative concentration above ~31 m, however, because halides precipitated in response to evaporative concentration and carbonates may have dissolved and/or precipitated in the lake sediments in response to methanogenesis in this part of the sequence (section 5.5). Consequently, it is suggested that records of %LOI 550°C, $\delta^{13}C_{organic}$, and C/N ratios provide a more accurate indication of lake-level change in this section of the sequence. According to the age-depth model proposed by Partridge *et al.* (1997), this change in the sensitivity of the record of carbonate abundance took place at ~68 kyr B.P., and could therefore explain the apparent change in the forces driving climatic change observed by the authors at ~50 kyr B.P. (Fig. 5.1).

The suggestion that lake-level changes at Tswaing were related to changes in global boundary conditions associated with glacial-interglacial cycles after ~150 kyr B.P., and with changes in the obliquity of the earth's axis before this date, as proposed in this chapter, counters the proposal made by Partridge *et al.* (1997, 1999) that precipitation at the site was controlled by precessionally-driven changes in insolation between ~50 and 200 kyr B.P. The proposal that changes in direct insolation caused lake-level change at the site is in closer agreement with our current understanding of the factors that drive climatic change at low latitudes than the proposal that forcing-factors originating at high latitudes caused palaeohydrological change (chapter 1), which provides indirect support for the validity of the age-depth model for the sedimentary sequence proposed by Partridge *et al.* (1997). There is no reason to believe that the $^{230}Th/^{234}U$ age determinations presented in this study are inaccurate, however (chapter 4), and the interpretations presented in this chapter may therefore be correct, despite their relative novelty. Further dating of the sequence is, however, required to confirm this proposal.

5.7 Conclusions

Tswaing crater lake is currently the only terrestrial site in southern Africa that has provided a continuous record of palaeoclimatic change that extends significantly beyond the LGM, and is thus of considerable importance to our understanding of climatic change in the southern hemisphere. Records of sediment composition and the isotope composition of calcite and organic material from the sediments, supported by a short record of diatom assemblage composition (chapter 6), have provided new evidence of palaeohydrological change at the site. These records are broadly in agreement with the pollen and diatom assemblage records from a previous sediment core (Scott, 1999; Metcalfe, 1999), but the low resolution of the older records, combined with the intermittent preservation of the microfossils, prevents detailed comparisons. The palaeohydrological reconstructions presented in this study differ from those based on the carbonate content and grain-size of sediments from the previous core, however, because the carbonate content of the sediment is interpreted differently in the two studies, and because the new records provide additional insights into palaeohydrological change at the site (Partridge *et al.*, 1997, 1999).

The cubic age-depth model for the sedimentary sequence presented in chapter 4 allows the timing of palaeohydrological change at the site to be estimated. This model suggests that, over the last 150 kyr, the timing and pattern of lake-level change at Tswaing was similar to that of temperature change at high southern latitudes (Petit *et al.*, 1999), with low lake levels associated with high atmospheric temperatures. It is therefore proposed that global boundary conditions associated with glacial-interglacial cycles determined palaeoclimatic conditions at the site during this period. If this proposal is valid, the linear age-depth model constructed using non-weighted least-squares regression (chapter 4) appears to provide the most accurate estimate of sediment age, and this model is therefore used to determine the timing of lake-level change at the site.

The mechanisms by which global boundary conditions affected palaeohydrological conditions at Tswaing cannot be established with certainty, but there are several possibilities. Decreasing atmospheric temperatures would have reduced evaporation from the lake surface, increasing lake levels, but it is likely that changes in

precipitation accentuated this effect. Precipitation may have increased at the site during glacials and stadials in response to an equator-ward shift and increase in the intensity of the circum-polar westerlies caused by an increase in the meridional temperature gradient (van Zinderen Bakker, 1967; 1976). This proposal is countered by the limited latitudinal movement of the STF during glacials, however (*e.g.* Brathauer and Abelmann, 1999). Precipitation could have also increased during glacials because the ITCZ shifted southward in response to the increase in the meridional temperature gradient in the northern hemisphere (van Zinderen-Bakker, 1967, 1976; Butzer *et al.*, 1973, 1978; Lancaster, 1979). This explanation is countered by the observation that the location of the ITCZ is primarily controlled by the intensity of direct insolation in South America, however (*e.g.* Haug *et al.*, 2001; Cruz *et al.*, 2005).

It is therefore suggested that changes in the intensity and frequency of TTT-formation over South Africa may account for the changes in precipitation at the site (cf. Tyson, 1986; Cockroft *et al.*, 1987). The intensity and frequency of TTT-formation may have increased in this region during glacials in response to the convergence of the mid-latitude westerlies and tropical easterlies over the subcontinent, an increase in the strength of the SIA, and decreasing SSTs in the equatorial Indian Ocean. This proposal has the advantage of explaining low precipitation in parts of the Kalahari and in Madagascar during the LGM (Gasse and van Campo, 2001; Munyikwa, 2005). It is also in line with the observation that conditions were relatively dry in tropical East Africa during the LGM (Barker and Gasse, 2003), as the formation of TTTs is thought to be partly responsible for the anti-correlation of precipitation in these areas today (Goddard and Graham, 1999). Unfortunately, however, it is not possible to determine with certainty whether this hypothesis is correct using the palaeoclimatic evidence currently available from southern Africa.

Between 150 and 350 kyr B.P., the records from Tswaing indicate that palaeohydrological conditions were determined by changes in the meridional temperature gradient caused by changes in the obliquity of the earth's axis. This gradient could have affected precipitation at the site by affecting the location and intensity of the mid-latitude westerlies or the intensity of the easterly winds that bring summer precipitation to the region (cf. Rind, 1998, 2000). This factor may have only

had a significant influence on palaeohydrological conditions at Tswaing before 150 kyr B.P. because atmospheric temperatures dominated the hydrological balance of the lake after 150 kyr B.P., or because the STF was located further north before ~150-200 kyr B.P. and terrestrial conditions were therefore more sensitive to changes in the location of the mid-latitude westerlies at this time (Rau *et al.*, 2002; West *et al.*, 2004). This hypothesis remains highly speculative, however, and few records are available to assess its validity.

These findings have significant implications for our understanding of climatic change in tropical and subtropical Africa. Records from the southern tropics of Africa indicate that global boundary conditions have had a more significant influence on climatic conditions than precessionally-driven changes in insolation since the LGM (cf. Gasse, 2000; Barker and Gasse, 2003). The records of precipitation at Tswaing produced by Partridge *et al.* (1997, 1999) suggest that this situation has only existed over the last ~50 kyr, and that precipitation was tightly coupled with summer insolation before this period. The records presented in this chapter suggest that this suggestion may not be valid (at least based on the evidence from Tswaing), however, because they indicate that climatic conditions at Tswaing were determined by processes originating at high latitudes, and that records from this site cannot, therefore, be used to assess the causes of climatic change in areas closer to the equator.

Unfortunately, the uncertainty associated with the chronology of the sedimentary sequence from Tswaing (chapter 4) means that some of the findings presented in this chapter, particularly those related to climatic change before 150 kyr B.P., remain tentative. Further work is therefore required to improve the chronological control of the sedimentary sequence, and to thereby determine whether the age-depth model presented here is more accurate than that presented by Partridge *et al.* (1997) (chapter 4) (cf. Appendix B). Further analysis of the sedimentary sequence might also clarify the nature and causes of the palaeohydrological changes identified in this chapter. Some of the inconsistencies between the sedimentological and geochemical records from the sequence are addressed in chapter 6, using records of diatom assemblage composition and siliceous microfossil concentrations, but additional analysis could provide further insights into palaeohydrological change at the site. High-resolution

studies of the structure of laminations in the sediments might provide information about the seasonality of precipitation, which could potentially show whether changes in the mid-latitude westerlies, which bring rainfall to the site in winter, or in the ITCZ and TTTs, which bring precipitation in summer, were responsible for changes in moisture availability. Biomarkers could also be used to shed further light on whether organic material is derived from autochthonous or allochthonous sources, and to identify times at which cyanobacteria, green algae, and aquatic macrophytes formed a significant proportion of aquatic biomass (cf. Summons *et al.*, 1999; Leavitt and Hodgson, 2001; Rosell-Melé, 2003). In addition, compound-specific isotope analysis might allow changes in the abundance of C_3 and C_4 vegetation to be explored, and could thereby resolve some of the uncertainties associated with the record of $\delta^{13}C_{organic}$ (cf. Huang *et al.*, 1999; Rosell-Melé, 2003).

Chapter 6: Records of palaeohydrological change at Tswaing crater lake from siliceous microfossils

6.1 Introduction

The sedimentological and geochemical proxies from the lacustrine sediments at Tswaing crater lake provide consistent records of palaeohydrological change in most parts of the sedimentary sequence (chapter 5). There are a number of uncertainties associated with these proxies in the central section of the sequence, however. In particular, the reconstructions of palaeohydrological conditions based on $\delta^{18}O_{calcite}$ and $\delta^{13}C_{calcite}$ are not consistent with those based on the records of %LOI 950°C and C/N ratios between ~42.5 and 51.0 m (chapter 5) (Fig. 6.1). In addition, a significant change in palaeohydrological conditions recorded by %LOI 950°C, $\delta^{18}O_{calcite}$, and $\delta^{13}C_{calcite}$ at 41.5 m, which may be related to the onset of authigenic carbonate precipitation from pore water, is not recorded by other proxies from the sequence (chapter 5) (Fig. 6.1). Finally, the effects of authigenic carbonate precipitation on $\delta^{18}O_{calcite}$ and $\delta^{13}C_{calcite}$ in the upper part of the sequence, and particularly between 33.2 and 41.5 m, remain uncertain (chapter 5) (Fig. 6.1).

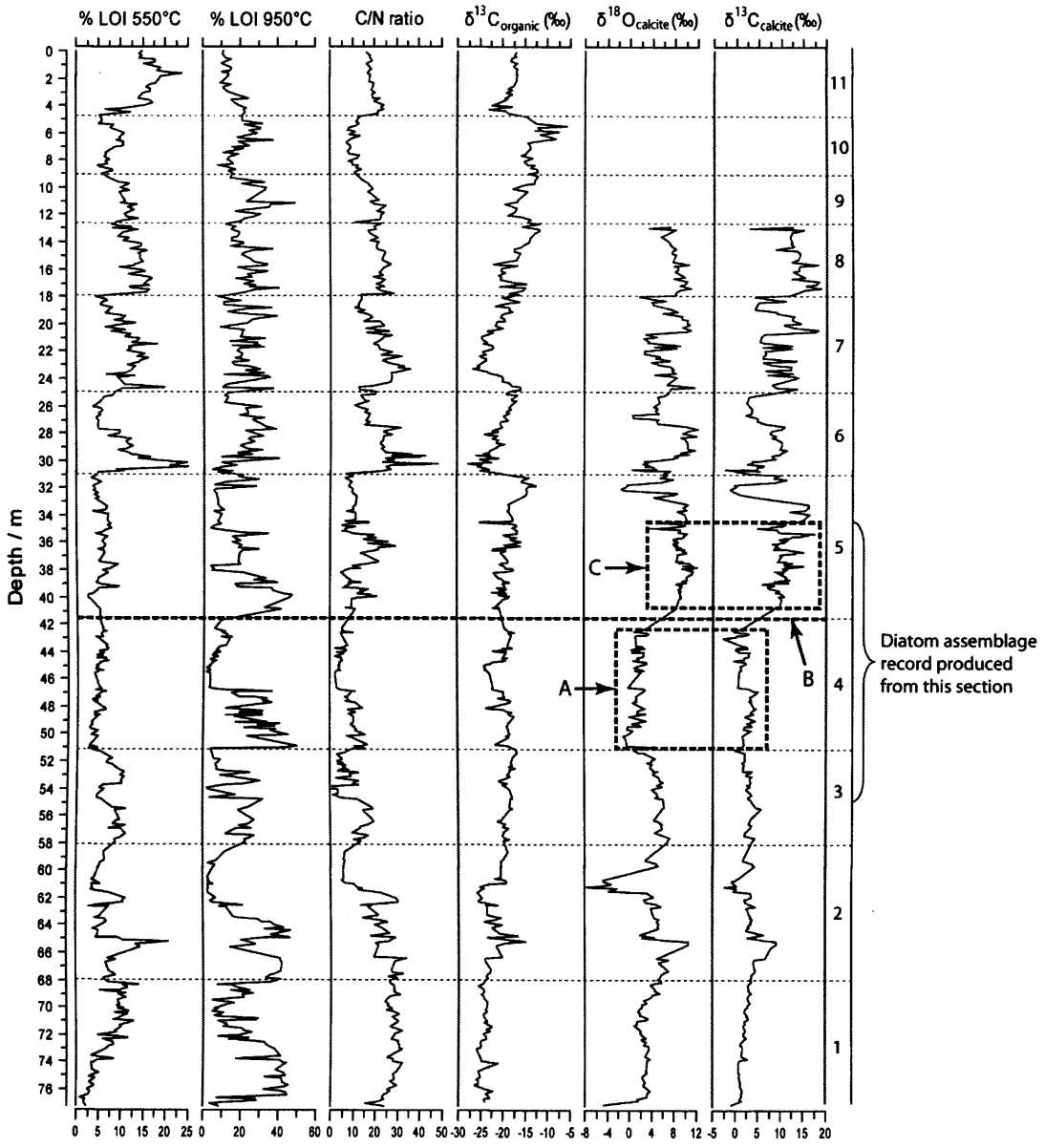

Figure 6.1: Sedimentological and geochemical records from Tswaing crater lake presented in chapter 5, showing the section from which a diatom assemblage record was produced, and three points at which the interpretation of the sedimentological and geochemical records remains uncertain: (A) indicates the section in which $\delta^{18}O_{calcite}$ and $\delta^{13}C_{calcite}$ show anomalous changes, (B) indicates the increase in %LOI 950°C, $\delta^{18}O_{calcite}$, and $\delta^{13}C_{calcite}$ that is not reflected in the other records, and (C) indicates the lower-most part of the section in which authigenic carbonate precipitation may have affected $\delta^{18}O_{calcite}$ and $\delta^{13}C_{calcite}$.

Diatom assemblage analysis potentially offers a means of producing highly sensitive, quantitative records of palaeohydrological change that could resolve these uncertainties and increase our understanding of palaeohydrological change at Tswaing crater lake (cf. Battarbee *et al.*, 2001). Metcalfe (1993, 1999) produced a record of diatom assemblage composition from the core of lacustrine sediments obtained from Tswaing in 1988/89, but the low resolution of this record (samples were analysed every 1 m in the section considered here) means that it is unable to provide the information needed to supplement the high-resolution records presented in chapter 5 (cf. Figure A4, Appendix A). This chapter therefore presents a higher resolution (8 cm) record of diatom assemblage composition from the central section of the sedimentary sequence (34.40 to 54.80 m), as well as a number of records of the concentration of siliceous microfossils, in order to resolve the uncertainties associated with the sedimentological and geochemical records in this section.

This multi-proxy approach increases the confidence associated with the palaeohydrological reconstructions from the site, and thereby increases the certainty associated with the palaeoclimatic reconstructions based on these findings (chapter 5). Multi-proxy records of this kind are rare in southern Africa due to the lack of lacustrine archives in this region, and the records presented in this chapter therefore represent a significant improvement in the confidence that can be afforded to reconstructions of palaeoclimatic change in this region. The insights into the nature of palaeoclimatic change at Tswaing that these records provide were discussed in chapter 5, and are not repeated here, but the evidence on which these insights were based is explored in some detail.

The section between 34.40 and 54.80 m was originally chosen for diatom assemblage analysis because the chronology of the sediments presented by Partridge *et al.* (1997) suggests that it covers MIS 5e, and records of palaeoclimatic change during this period would provide an opportunity to test the proposal that precessionally-driven changes in insolation determined climatic change in southern Africa at this time, as well as making an interesting comparison with the records from the CKR presented in chapter 7. In addition, the diatom record produced by Metcalfe (1993, 1999) indicates that diatom valves are relatively well preserved, and that diatom assemblage composition exhibits a number of fluctuations in this section (unlike the section

above, where valves are highly dissolved, and the section below, where *Pseudostaurosira brevistriata* and *Cyclotella stelligera* dominate the assemblage) (cf. Figure A4, Appendix A). In fact, the chronology of the sediments developed in chapters 4 and 5 suggests that this part of the sequence covers the period between ~150 and ~250 kyr B.P. (MISs 6 and 7), and thus does not include MIS 5e, but the diatom assemblage records from this section nevertheless provide a unique opportunity to increase our understanding of palaeohydrological and palaeoclimatic change at the site.

6.2 Theoretical background

The theoretical basis of diatom assemblage analysis and the background necessary to interpret records of siliceous microfossil concentration are outlined in this section. The principles behind the use of the other proxies discussed in this chapter (LOI 550°C, LOI 950°C, $\delta^{18}O_{calcite}$, $\delta^{13}C_{calcite}$, $\delta^{13}C_{organic}$, and C/N ratios of bulk organic matter) were presented in chapter 2.

6.2.1 Diatom assemblage composition

Diatoms are unicellular, eukaryotic algae that are classified as Protista, division Heterokontophyta, class Bacillariophyceae. They have a siliceous cell wall (frustule) consisting of two valves that allows individuals to be identified to species level. Diatom valves are often preserved in sediments, and can therefore be used to reconstruct the composition of diatom assemblages in the past (cf. Battarbee, 1986). Diatom assemblage composition is usually determined by environmental characteristics, because the ability of diatom species to grow and reproduce is influenced by factors such as the existence of a suitable substrate, light intensity, temperature, water movement, pH, ionic composition, electrical conductivity, and the availability of oxygen and dissolved inorganic nutrients (including carbon) (Battarbee *et al.*, 2001). Biological factors such as grazing intensity and competition can also influence assemblage composition, but the effects of these factors are often difficult to identify.

If the environmental preferences of diatom species or assemblages are known, the composition of fossil assemblages can be used to reconstruct environmental

conditions in the past. If the relationship between the taxa and their environment is complex, the data may only provide qualitative information about environmental conditions, but if an environmental variable exerts a strong influence on diatom assemblage composition, it may be possible to reconstruct this variable quantitatively, using transfer functions (Battarbee *et al.*, 2001). These functions are derived by quantifying the relationships between diatom species or assemblages and environmental variables in the modern environment, and are applied to fossil assemblages to produce quantitative estimates of environmental variables when the assemblages were living (*e.g.* Juggins, 1992a; Gasse *et al.*, 1995).

These methods of environmental reconstruction are based on the assumption that the relationships between diatom taxa and the environment have not changed over time (*i.e.* uniformitarianism) (cf. Birks and Birks, 1980). This proposal appears to hold during the Holocene, but could conceivably be invalid on longer timescales, such as those considered in this study. Environmental reconstruction based on diatom assemblage composition also assumes that taphonomic processes have not significantly altered the composition of diatom assemblages, and that fossil assemblages therefore reflect the composition of the living assemblages from which they are derived. This assumption does not hold if diatom valves are added to the fossil assemblage through processes such as lake-water inflow or resuspension of older sediment, or if valves are removed from the assemblage by processes such as lake-water outflow (*e.g.* Battarbee and Flower, 1984). Dissolution of diatom valves in the water column or lake sediments may also alter the composition of diatom assemblages. In extreme cases, dissolution may remove all diatom valves, but in other cases, certain taxa may dissolve more easily than others, which can lead to significant errors in environmental reconstructions (*e.g.* Mackay *et al.*, 2005).

Tswaing crater lake only receives lake-water inputs from surface runoff and groundwater, and has no surface outflow (chapter 3), so input of allochthonous valves and removal of autochthonous valves are unlikely to have affected diatom assemblage composition. The possibility that within-lake processes such as sediment focusing or redistribution have affected assemblage composition cannot be excluded, but the potential effects of these processes were minimised by only sampling sections that showed no evidence of disturbance. Dissolution may have had a significant effect on

diatom assemblage composition at the site, however. Metcalfe (1993, 1997) noted that diatom valves are increasingly dissolved towards the top of the sequence, particularly above ~34 m, where dissolution may have removed all diatom valves in some sections. The potential effects of dissolution on diatom assemblage composition are therefore considered in more detail below.

The degree of diatom valve dissolution is influenced by the temperature, pH, silica content, salinity, alkalinity, and ionic composition of the lake and pore water, as well as by the depth of the lake (Lewin, 1961; Hurd *et al.*, 1972; Barker 1992; Flower, 1993; Barker *et al.*, 1994; Battarbee *et al.*, 2001). The most common cause of dissolution in lacustrine environments is high pH because, in the absence of other influences, the rate of silica dissolution increases exponentially above pH 9 due to the dissociation of silicic acid (Stumm and Morgan, 1970). Dissolution of diatom valves may also be significant if the saturation of lake water with respect to silica is low due to low rates of silica input to the lake (cf. Barker, 1992). In carbonate-dominated systems, the rate of dissolution is also influenced by the activity of the dominant metal species; dissolution is greatest in sodium-dominated water, slightly less in magnesium-dominated water, and least in calcium-dominated water (Flower, 1993). Biological and physical processes can also influence the degree of diatom valve dissolution because processes such as grazing, sediment resuspension, bioturbation, and subaerial exposure often increase valve breakage, which can increase the susceptibility of valves to dissolution (cf. Hurd, 1972; Flower, 1993; Fritz *et al.*, 1993; Reed, 1998). Finally, the presence of organic compounds and metal cations, which can stabilise the amorphous silica in diatom valves, may reduce the rate of valve dissolution (Lewin, 1961; Hecky and Kilham, 1973).

The susceptibility of the valves of individual taxa to dissolution depends on their specific surface-area, sculpturing, silification, and composition (Hurd *et al.*, 1972; Barker, 1992; Barker *et al.*, 1994; Battarbee *et al.*, 2001; Ryves *et al.*, 2001). Usually, the valves of well-silicified taxa with a small surface-area to volume ratio, such as *Cyclotella meneghiniana* and *Rhopalodia gibberula*, are preferentially preserved, while less robust species with a large surface-area to volume ratio, such as *Nitzschia paleacea*, are selectively dissolved (Barker, 1992; Fritz *et al.*, 1993).

The extent of diatom valve dissolution can be assessed using dissolution indices. These indices are based on features such as the size of areolae, which are enlarged by dissolution, and the presence or absence of weakly silicified features such as the valve margins of some species in the genus *Cyclotella* (Barker, 1992). Experimental dissolution has helped clarify morphological changes in certain taxa during dissolution, and has thereby provided a secure basis for the application of dissolution indices (*e.g.* Barker, 1992; Flower, 1993; Barker *et al.*, 1994; Mikkelsen, 1997; Ryves *et al.*, 2001). The use of these indices may be subject to errors caused by changes in the resistance of valves of individual taxa to dissolution over time (due to changes in their surface-area to volume ratio, for example), but generally provides a useful means of assessing whether an assemblage has been affected by dissolution (cf. Ryves *et al.*, 2001). Dissolution may also lead to the diagenetic alteration of amorphous silica in diatom valves to authigenic silicates such as zeolites and potassium feldspars, and the presence of these minerals can therefore indicate significant dissolution of diatom valves (Utada, 1966).

6.2.2 Diatom valve concentration

The concentration of diatom valves in sediments can be calculated by spiking samples of known weight with a known number of plastic microspheres, and counting the microspheres at the same time as diatom valves (Battarbee and Kneen, 1982). This information can then be used, together with knowledge of the average size and shape of diatom taxa in the samples, to determine diatom biovolume (cf. Hillebrand *et al.*, 1999). If the rate of sediment deposition is known, these values can then be used to calculate the accumulation rate of diatom valves or biovolume. It should be noted, however, that the use of a spike to assess valve concentration is subject to experimental and analytical errors (cf. Woolfe, 1997), and that the assessment of diatom biovolume is subject to difficulties associated with assessing the average size and shape of diatom taxa in individual samples (as well as uncertainty in the relationship between frustule volume and cytoplasm volume) (cf. Hillebrand *et al.*, 1999). Undue confidence should not, therefore, be attributed to values calculated using these methods.

The concentration of diatom valves in lake sediments is influenced by diatom productivity, taphonomy, and changes in the accumulation rate of non-diatom

material. It is frequently difficult to distinguish between these controls when interpreting records of diatom valve concentration. If dissolution has a significant effect on valve concentration, there may be a relationship between this record and the level of valve dissolution (cf. Ryves *et al.*, 2001). If the accumulation rate of non-diatom material determines diatom valve concentration, the concentration of diatom valves will be anti-correlated with sediment accumulation rate, and the sedimentological composition of sediments may change at the same depths as the record of diatom valve concentration (*e.g.* Battarbee and Flower, 1984; Straub, 1993). Finally, if productivity has a significant influence on valve concentration, proxies such as $\delta^{13}C_{organic}$ may be correlated with this record (*e.g.* Johnson *et al.*, 1998). It is not straightforward to construct a record of diatom productivity from a record of diatom valve concentration, however, due to the potential effects of dissolution and sediment accumulation rate on valve concentration, and the fact that valve concentration does not necessarily indicate biovolume (if the assemblage is dominated by large species, diatom biovolume may be high, even though the concentration of diatom valves is low, for example) (cf. Anderson, 1989).

6.2.3 Phytolith, sponge spicule, and chrysophyte cyst concentrations

The concentration of phytoliths, sponge spicules, and chrysophyte cysts in lacustrine sediments can all provide useful information about palaeolimnological conditions (cf. Smol *et al.*, 2001). If these microfossils are counted at the same time as diatom valves, their concentrations can usually only be estimated, as they tend to occur at significantly lower concentrations than diatom valves. Such semi-quantitative estimates of concentration may still provide useful information, however (*e.g.* Stager, 1988).

Phytoliths are hydrated silica structures that are deposited in the inter-cellular spaces, cell walls, and lumina of plant organs (Piperno, 2001). They are resistant to degradation, and when a plant dies they can therefore be washed into lakes and deposited in sediments. Many phytoliths can be identified to genus level, but this was not attempted in this study. Phytoliths are particularly abundant in grasses, and the concentration of phytoliths in lake sediments can therefore indicate the abundance of grasses in the lake basin, or the proximity of grasses to the site of sediment deposition, but may also reflect the amount of in-wash into the lake (Piperno, 2001).

The concentration of sponge spicules, which form the internal skeletons of species in the phylum Porifera, may reflect the abundance of freshwater sponges in the lake (Frost, 2001). Sponges usually inhabit shallow environments, and changes in the concentration of sponge spicules can therefore indicate changes in lake depth. Sponges also require high concentrations of silica (>0.5 mg/l), and their growth may be restricted by the supply of this mineral (Jewell, 1935). In addition, many species are unable to tolerate high levels of total dissolved solids, and a decrease in sponge spicule concentration may therefore reflect an increase in lake-water salinity (Cumming *et al.*, 1993; Frost, 2001).

Chrysophyte cysts are the siliceous stomatocysts produced by species of algae in the classes Chrysophyceae and Synurophyceae. Most species in these classes are euplanktonic, and many are effective competitors in low-temperature, -nutrient, and -light environments. Chrysophyte cysts therefore tend to be most abundant in the sediments of fresh, acidic, and oligotrophic lakes, and less abundant in the sediments of saline, alkaline, and eutrophic water bodies (Cumming *et al.*, 1993; Zeeb and Smol, 2001).

6.3 Methods

Samples were taken for diatom assemblage analysis at 8 cm intervals between 34.40 and 54.80 m, except where there are gaps in the sequence or the sediments are disturbed. Diatom slides were prepared by reacting a known weight of sediment with hydrogen peroxide at 70°C to oxidise organic material, adding hydrochloric acid to remove carbonates, and rinsing the samples several times in distilled water (with a few drops of 1% ammonia in the final wash, to disaggregate clays) (Battarbee, 1986). The supernatant liquid was then siphoned off and a known weight of a solution of divinylbenzene (DVB) microspheres (of known concentration) was added to the sample, with the aim of producing a 1:1 ratio of diatom valves to microspheres (cf. Woolfe, 1997).

The samples were mounted onto slides using Naphrax, and between 300 and 400 valves were counted on each slide using a Leitz Laborlux S microscope at x1000 magnification. The number of phytoliths, sponge spicule tips, and chrysophyte cysts

were also noted as the valves were counted. Diatoms were identified using the taxonomic descriptions of diatoms from southern Africa by Archibald (1966, 1982, 1983), Schoeman and Archibald (1976-1980, 1988), Schoeman and Ashton (1982a,b, 1983), Archibald and Schoeman (1984), and Schoeman *et al.* (1984), as well as the flora of East Africa (Gasse, 1986) and the freshwater floras of Krammer and Lange-Bertalot (1991a,b, 1997a,b). Identifications were confirmed using SEM analysis where possible. Counts were then converted to percentage abundance and concentration per gram of dry sediment. The record of diatom assemblage composition was divided into stratigraphic zones using the split information method (SPLITINF), which uses binary division based on information statistic criteria. This classification was implemented on untransformed percentage data using the program ZONE (Juggins, 1992b).

Some of the samples contained fragmented and dissolved valves. To overcome the problem of fragmentation, either the ends or the central areas of valves were counted, and the total counts were adjusted accordingly. In order to account for the problem of dissolution, it was planned to categorise each valve according to its degree of dissolution, and to use the number of valves in each category to calculate a dissolution index for each sample. Unfortunately, this method was not satisfactory because there are significant shifts in assemblage composition over the record and it was difficult to standardise the dissolution categories of different taxa. In an attempt to overcome this problem, dissolution indices were calculated using only the categories assigned to *C. meneghiniana* and *C. stelligera* valves, because these taxa are present in most parts of the sequence and the categories used to assess their dissolution are robust and objective. Dissolution categories were assigned as follows: "stage 1" was assigned to valves apparently unaffected by dissolution ("pristine" valves), "stage 2" to valves with evidence of dissolution in marginal areas but with striae still extending to their full length, "stage 3" to those with evidence of partial dissolution of the outer ring of striae, and "stage 4" to those that had almost or completely lost this ring, leaving just the central area (cf. Barker, 1992) (Fig. 6.2). A dissolution index was then calculated for each taxon by taking the weighted average of the dissolution stages assigned (as long as five or more valves were assessed). The indices for the two taxa were not combined to avoid the problem that the dissolution stages for the two taxa may not be equivalent. This method is obviously not ideal, particularly as *C. meneghiniana* and

C. stelligera are not present, or are only present at low percentage frequencies, in some parts of the record, but it was considered the most objective way of assessing dissolution in the samples analysed.

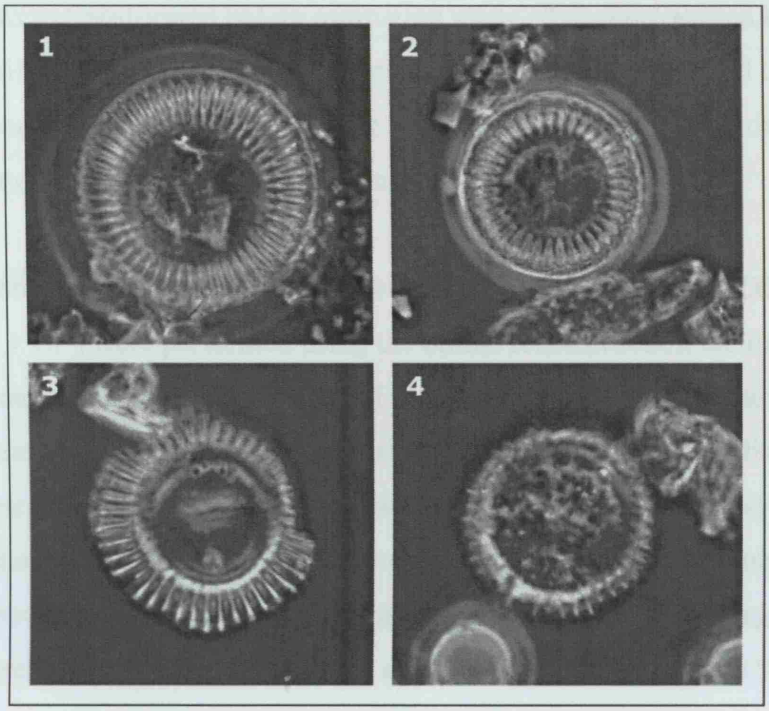

Figure 6.2: Photographs of *C. meneghiniana* valves categorised as dissolution stages 1 to 4, taken using a light microscope.

The diatom data were summarised by ordination, which was carried out using the program CANOCO for windows 4.5 (ter Braak and Šmilauer, 2002). Correspondence analysis (CA) and detrended correspondence analysis (DCA) both suffer from the problem that, because they are based on chi-squared distance, rare species may have a disproportionately large influence on the outcome of the ordination (Legendre and Legendre, 1998). The down-weighting of rare species implemented by CANOCO is not considered a satisfactory answer to this problem (Legendre and Gallagher, 2001). Principal components analysis (PCA) does not experience this problem because it is based on Euclidian distance, but this method is not suitable for datasets that cover long environmental gradients (Legendre and Legendre, 1998). Rao (1995) proposed that this problem can be overcome by transforming species data so that the Euclidean distance between samples after transformation is equal to the Hellinger distance

before transformation, and then ordinating the transformed data using PCA. This method was adopted in this study, because DCA demonstrated that the length of the longest DCA axis is 3.7 standard deviations, which indicates that the data should be ordinated using unimodal methods (Legendre and Legendre, 1998). The percentage species data were transformed before ordination using a program written by Pierre Legendre available from http://www.fas.umontreal.ca/biol/legendre, and then ordinated using CANOCO, without further transformation. The species data were centered but not standardised during this analysis.

Reconstructions of lake-water conductivity (µS/cm) and anion ratio (HCO_3^- + CO_3^{2-}/SO_4^{2-} + Cl^-) were performed using the online reconstruction facility of the European Diatom Database (EDDI) (EDDI participants, 2001). These variables were chosen because the closed nature of the basin (chapter 3) and previous diatom analysis (Metcalfe, 1993, 1999) suggest that they were probably the most important controls on diatom assemblage composition. The combined salinity training set was used for the reconstructions because this training set contained, on average, 92% of the species present (more than the training set from the region closest to South Africa, the East African training set (Gasse *et al.*, 1983)). The reconstructions were performed using locally-weighted weighted averaging (LWWA), because the errors associated with this method were indistinguishable from those associated with reconstructions based on weighted averaging (WA), and the EDDI participants (2001) found that LWWA outperforms WA for merged datasets such as the combined salinity dataset used here.

6.4 Results

6.4.1 Diatom taxonomy

The taxonomy of the assemblages is relatively straightforward, but some taxonomic issues remain unresolved, including the identification of two unknown taxa. The first of these is a small *Fragilaria*-type that is ~6-15 µm long and ~2-6 µm wide, with fine (~28/10 µm) transapical striae, and a rectangular shape in girdle view. The valves of this type were tentatively divided into two groups based on their shape: a group with linear- to linear-lanceolate-shaped valves, and a group with a distinct central bilateral

inflation. Specimens in the first group are similar to *Fragilaria exiguissima* Archibald 1966, which was found in Lake Sibayi in northeastern Natal (Archibald, 1966). Specimens in the second group are similar to specimens of *Fragilaria sundayensis* Archibald 1982, which was found in the brackish waters of the estuary and the lower course of the Sundays River (Archibald, 1982). The names *F.* cf. *exiguissima* and *F.* cf. *sundayensis* are therefore adopted in this chapter, but further work is needed to clarify the taxonomy of these specimens. The second unknown taxon is a small *Achnanthes*-type, which is referred to as "unknown *Achnanthes* species". Specimens of this taxon are elliptical, ~9 μm long, and ~5 μm wide, and appear transparent under the light microscope, possibly because they are highly dissolved.

The samples in which these taxa occurred were highly friable and therefore difficult to coat with gold, which limited the quality of photographs that could be taken using SEM (cf. Metcalfe, 1999). In addition, many of the valves in the samples were affected by dissolution, which limited the taxonomic information that could be obtained from the photographs. Low-quality photographs of *F.* cf. *exiguissima* are, however, shown in Figure 6.3. Unfortunately, no photographs of *F.* cf. *sundayensis* or the unknown *Achnanthes* species could be taken under SEM because specimens of these taxa could not be found on the stubs, despite several attempts to do so. Moreover, it was not possible to take useful photographs of these taxa under the light microscope due to their small size and, in the case of the unknown *Achnanthes* species, transparent appearance.

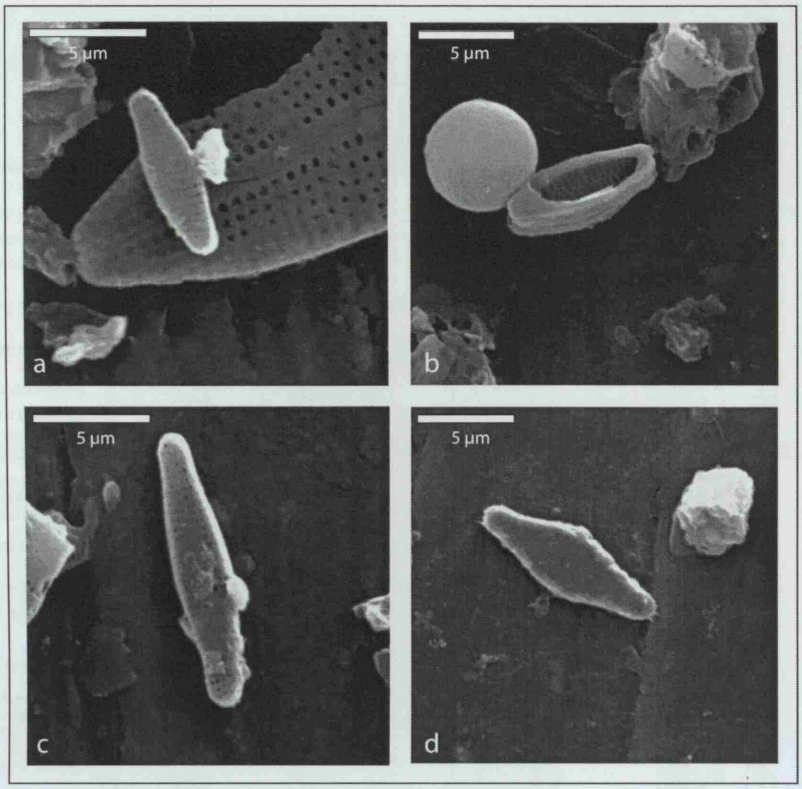

Figure 6.3: Photographs of specimens of *F.* cf. *exiguissima* taken using SEM.

Finally, *P. brevistriata* displayed a high degree of variability in the samples. Two varieties were tentatively identified, in addition to the nominate species. Specimens with a distinct central inflation were labelled *P. brevistriata* var. *inflata* (Pant.) Hartley *et al.* 1996, and linear-elliptical shaped specimens with broadly rounded poles were labelled *P. brevistriata* var. *elliptica* (formerly *Fragilaria brevistriata* var. *elliptica* Héribaud 1903) (cf. Schoeman and Archibald, 1988). The taxonomy of these varieties remains uncertain, and even less is known about their autecologies, but they were distinguished in order to avoid the loss of taxonomic information.

6.4.2 Diatom assemblages

The record of diatom assemblage composition from the sedimentary sequence is shown in Figure 6.4, together with the percentage of euplanktonic diatoms and the zones defined by SPLITINF. The sections of the sequence in which the concentration of diatom valves is too low to allow reliable counts to be made are also shown (the other gaps in the record are due to gaps or disturbances in the sedimentary sequence).

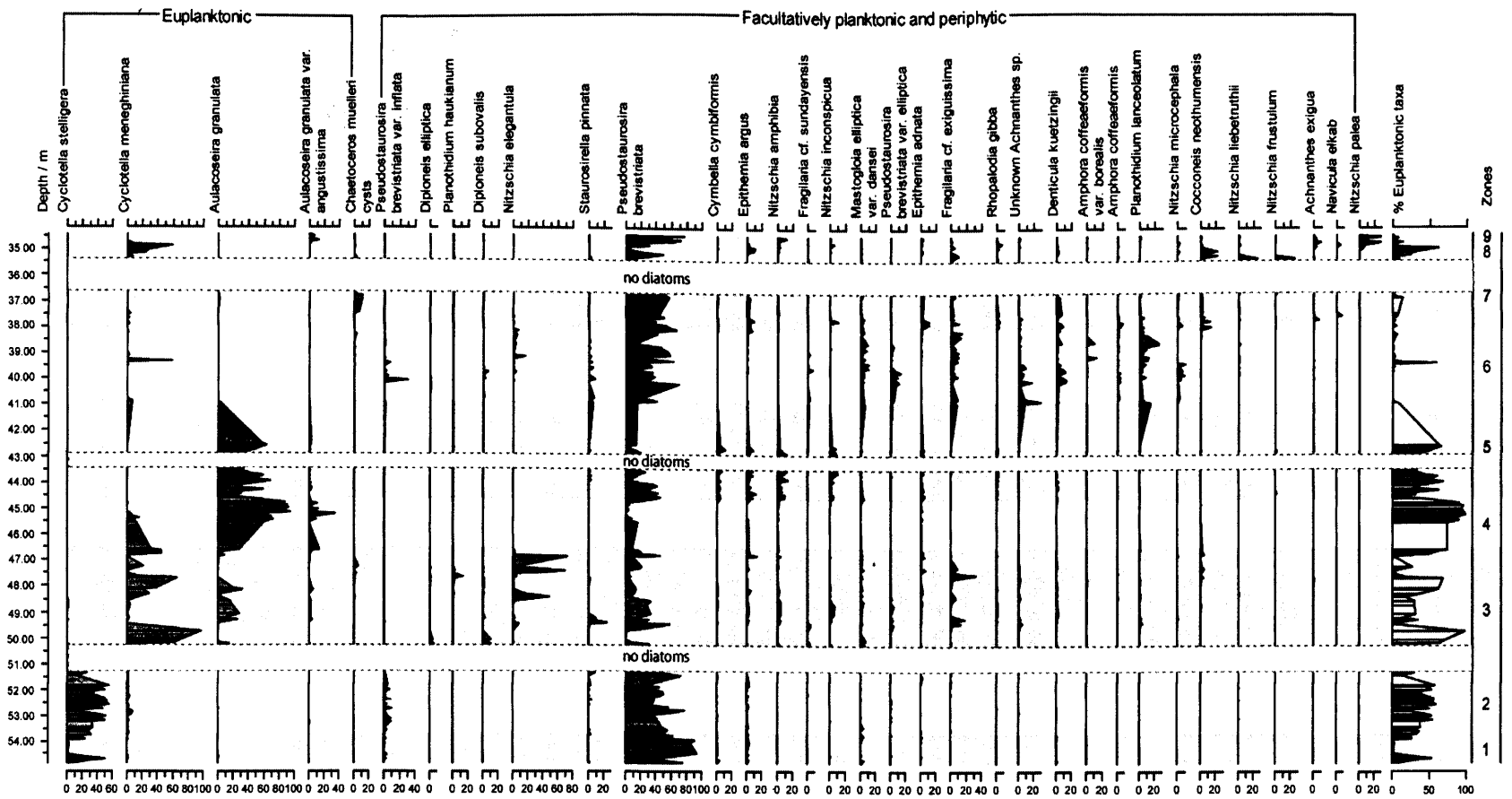

Figure 6.4: Percentage abundance of diatom taxa with a maximum abundance ≥5% from the section of the sedimentary sequence between 34.40 and 54.80 m. Taxa are ordered firstly by habitat, and secondly by the weighted average of their occurrence with depth. The percentage of euplanktonic diatoms is also shown. Zones defined by SPLITINF are shown by grey and white bars. Sections where no diatom valves are preserved are indicated; other gaps are gaps or disturbances in the sedimentary sequence.

Zone 1, which covers the section from 54.80 to 53.69 m, is dominated by *Pseudostaurosira brevistriata* (Grunow in Van Heurck) Williams and Round 1987, and *Cyclotella stelligera* Cleve and Grunow in Van Heurck 1882. The proportion of *C. stelligera* decreases to less than 5% in the middle of the zone, between 54.47 and 53.93 m, which significantly reduces the percentage of planktonic diatoms present. *C. stelligera* dominates the assemblage in zone 2 (53.69 to 51.34 m), forming approximately 50% of the diatoms present, but *Cyclotella meneghiniana* Kützing 1844 is also present at low frequencies. In zone 3 (51.34 to 46.58 m), the abundance of *C. meneghiniana* increases significantly above a gap in the diatom record, together with the abundances of *Nitzschia elegantula* Grunow in Van Heurck 1881 and *Fragilaria* cf. *exiguissima*. Between the peaks in these species, the proportions of *Aulacoseira granulata* (Ehrenberg) Simonsen 1979 and, to a lesser extent, *Nitzschia amphibia* Grunow 1862 and *Nitzschia inconspicua* Grunow 1862 increase. The percentage of planktonic diatoms remains above 25% in most parts of this zone due to the presence of *C. meneghiniana* and *A. granulata*, but it decreases to less than 5% at ~49.4, ~47.5, and ~46.9 m.

The abundance of the planktonic taxa *A. granulata* and *A. granulata* var. *angustissima* (O. Müller) Simonsen 1979 increases significantly in zone 4 (46.58 to 44.62 m). Together, these taxa account for up to 95% of the diatoms present, and the percentage of planktonic diatoms consequently increases to its highest level in this zone. The taxonomic status of *A. granulata* var. *angustissima* remains uncertain, because valves of this type may represent one extreme of the morphological variation in *A. granulata* (Kilham and Kilham, 1975; Turkia and Lepisto, 1999). Nevertheless, the two forms are distinguished here because they appear to be associated with different environmental conditions (Gasse, 1986; Turkia and Lepisto, 1999; Metcalfe, pers. comm.). *A. granulata* remains the dominant species in zone 5 (44.62 to 40.89 m), but its relative abundance decreases to approximately 60%, and *A. granulata* var. *angustissima* is only present at low frequencies (<5%). In contrast, the relative abundance of periphytic taxa such as *Cymbella cymbiformis* Agardh 1830, *Epithemia argus* (Ehrenberg) Kützing 1844, *N. amphibia*, and *N. inconspicua* increases slightly in this zone, reducing the percentage of planktonic diatoms.

Diatom assemblage composition changes significantly in zone 6 (40.89 to 38.06 m). *A. granulata* is no longer present, and *C. meneghiniana* only occurs sporadically, at low frequencies (<3%). In contrast, the proportions of *Planothidium lanceolatum* (Brébisson) Lange-Bertalot 1999, *F.* cf. *exiguissima*, *Mastogloia elliptica* var. *dansei* (Thwaites) Cleve 1895, *N. elegantula, P. brevistriata* var. *elliptica,* the unknown *Achnanthes* species, *Denticula kuetzingii* Grunow 1862, *Amphora coffeaeformis* (Agardh) Kützing 1844, and *Nitzschia microcephala* Grunow in Cleve et Moller 1878 all increase. The assemblage changes again in zone 7 (38.06 to 35.31 m), where the frequencies of *Chaetoceros muelleri* Lemmermann 1898 cysts, *E. argus, E. adnata* (Kützing) Brébisson 1838, and *Cocconeis neothumensis* Krammer 1991 increase slightly. *P. brevistriata* is the dominant taxon in both zones 6 and 7, however. The proportion of planktonic diatoms is less than 5% throughout this section of the record, with the exception of a peak at 39.34 m that is associated with an increase in the abundance of *C. meneghiniana*, and a slight increase centred on 37 m that is associated with an increase in the abundance of *C. muelleri* cysts.

There is a gap in the record at the top of zone 7, from 36.75 m to 35.31 m, but there are two further zones above this gap. *C. meneghiniana, C. neothumensis, F.* cf. *exiguissima*, *Nitzschia liebetruthii* Rabenhorst 1864, and *Nitzschia frustulum* (Kützing) Grunow in Cleve et Grunow 1880 dominate the assemblage in zone 8 (35.31 to 34.74 m). The increase in the abundance of *C. meneghiniana* in this zone increases the percentage of planktonic diatoms to over 60%. In zone 9 (34.74 to 34.40 m), *A. granulata* var. *angustissima, N. amphibia, N. inconspicua*, and *Nitzscia palea* (Kützing) W. Smith 1856 all increase in abundance. *P. brevistriata* dominates the assemblage, however, and the percentage of planktonic species therefore decreases to less than 15% in this section.

6.4.3 Concentration and dissolution of diatom valves

The concentration of diatom valves in the sediments is shown in Figure 6.5, together with the dissolution indices based on *C. meneghiniana* and *C. stelligera* valves. Diatom valve concentration changes significantly over the section, varying between ~10,000 and ~5 million valves per gram of dry sediment. The concentration is, on average, relatively high in zones 1 and 2 (~0.5 million valves per gram), and in zones 4 and 5 and the upper part of zone 6 (~1 million valves per gram). Conversely,

concentrations are low in zone 3, the lower part of zone 6, and in zones 7 to 9, where they fluctuate between 100,000 and 300,000 valves per gram of dry sediment, with the exception of brief peaks at 49.73 and 49.08 m in zone 3, at 35.14 m in zone 8, and at 34.42 m in zone 9.

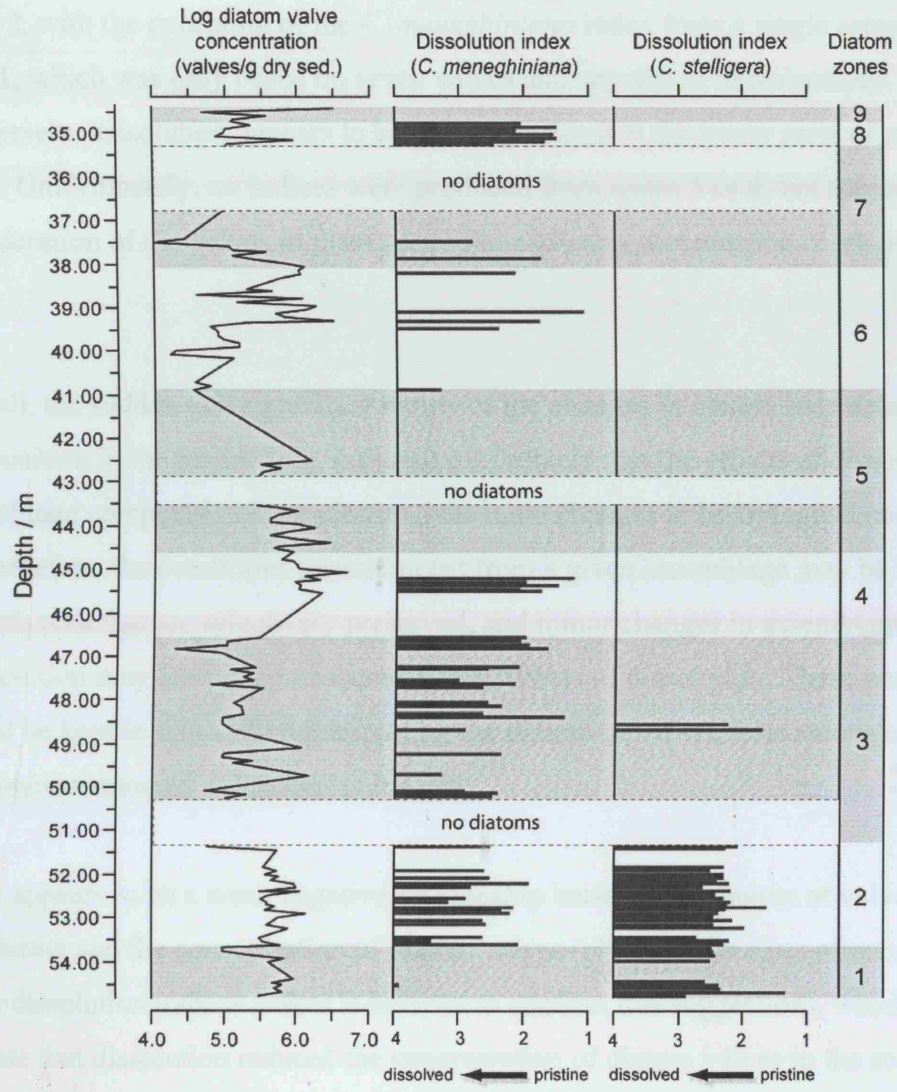

Figure 6.5: Concentration of diatom valves in the sediment (log base 10), and dissolution indices based on 5 or more *C. meneghiniana* or *C. stelligera* valves, where 1 = pristine and 4 = extremely dissolved (note reversed scale for easy comparison with the record of valve concentration). Diatom zones defined by SPLITINF are also shown.

The dissolution indices based on *C. meneghiniana* and *C. stelligera* valves are greater than 1 throughout the record, indicating that dissolution has affected the preservation of most diatom valves (Fig. 6.5). It is therefore possible that robust taxa such as *C. meneghiniana* and *R. gibberula* are over-represented in some of the assemblages (cf. Barker, 1992). The indices suggest that preservation is best in the upper parts of zones 3 and 6, and in zones 4 and 8. Preservation also appears to be relatively good in zones 1 and 2, with the exception of the *C. meneghiniana* index from a single sample in zone 1, which was only based on seven valves and appears to be anomalous. Conversely, dissolution appears to be most significant in the lower parts of zones 3 and 6. Unfortunately, no indices were produced from zones 5 or 9, but subjective consideration of the valves in these zones indicates that preservation is relatively good.

Overall, the sudden and significant nature of the changes in diatom assemblage composition in the record (Fig. 6.4) make it unlikely that the effects of dissolution on assemblage composition have obscured the main changes in hydrological conditions. Nevertheless, the conditions reconstructed from a given assemblage may be biased towards taxa that are selectively preserved, and minor changes in assemblage composition may have been obscured by the effects of dissolution. These possibilities should be kept in mind when interpreting the diatom-based reconstructions of palaeoenvironmental conditions at the site.

There appears to be a weak negative relationship between the degree of valve dissolution and the concentration of diatom valves (although the discontinuous nature of the dissolution indices makes it difficult to confirm this suggestion), which could indicate that dissolution reduced the concentration of diatom valves in the sediments (Fig. 6.5). The magnitude of the changes in diatom valve concentration relative to the changes in the dissolution indices suggests, however, that any such relationship was probably caused by a factor that affected both parameters independently. Increasing salinity may have increased the dissolution of diatom valves while simultaneously reducing diatom productivity, for example.

6.4.4 Reconstructions of lake-water conductivity and anion ratio

The lake-water conductivity values and anion ratios reconstructed using the diatom assemblage data are shown in Figure 6.6. The reconstructed conductivity values have a RMSE of prediction of 0.46 (log μS/cm), and the reconstructed anion ratios have a RMSE of prediction of 0.53 (log); both of which were calculated by jack-knifing (EDDI participants, 2001). The major shifts in both records are greater than these errors, as well as the sample-specific standard errors estimated by Monte-Carlo simulation (EDDI participants, 2001), and can thus be considered statistically significant (Fig. 6.6). The two reconstructions are anti-correlated throughout the section, which is probably because increased endogenic carbonate precipitation during phases of high conductivity reduced the concentration of bicarbonate and carbonate ions relative to the concentration of sulphate and chloride ions (chapter 5) (cf. Talling and Talling, 1965; Stumm and Morgan, 1970; Eugster and Hardie, 1978).

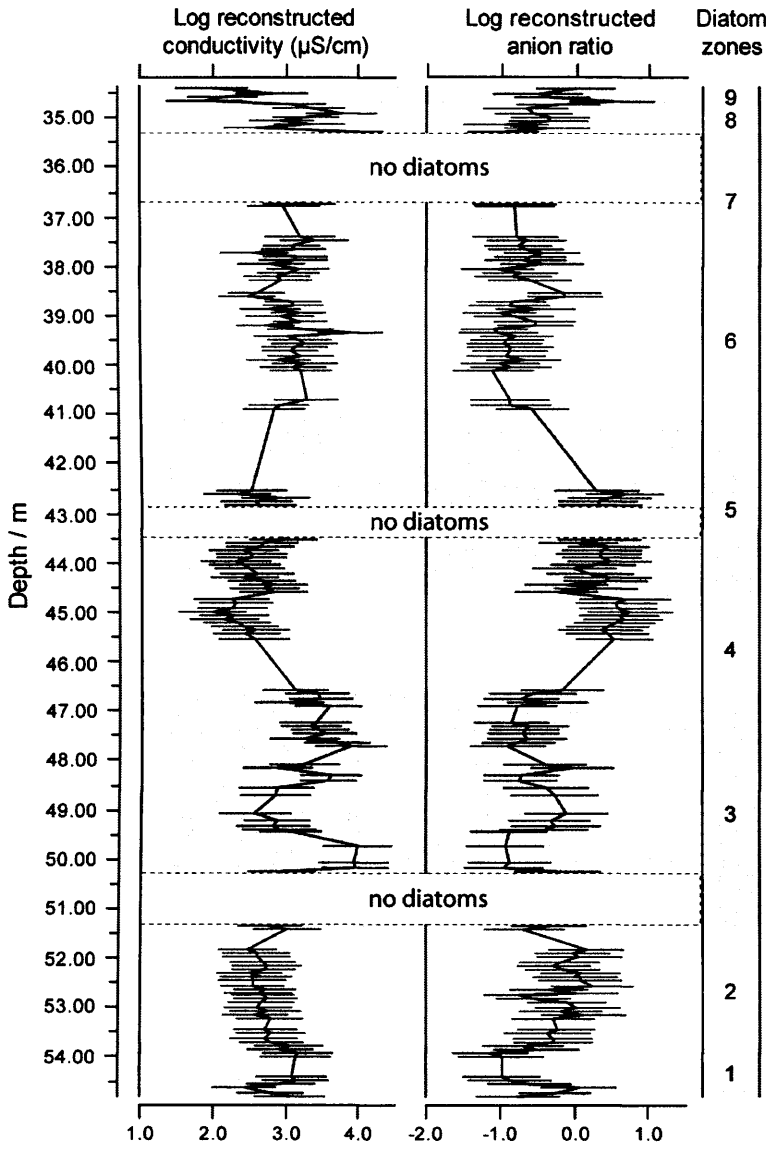

Figure 6.6: Diatom-inferred records of lake-water conductivity and anion ratio ($HCO_3^- + CO_3^{2-}/SO_4^{2-} + Cl^-$) (log base 10) reconstructed using LWWA. Error bars indicate sample-specific standard errors estimated by Monte-Carlo simulation (EDDI participants, 2001). Diatom zones defined by SPLITINF are also shown.

According to the reconstructions, lake-water conductivity fluctuates around 3 log µS/cm (1,000 µS/cm) and anion ratios remain low, at −0.8 log (0.2), in most of zone 1 and in zones 6-7. Conductivity decreases to ~2.7 log µS/cm (500 µS/cm) in zone 2 (where anion ratios increase to 0 log (1)), and in zones 4-5 (where anion ratios reach their highest values of the record (~0.5 log, ~3)). Conductivity values are highest in zone 3, where they reach 4 log µS/cm (10,000 µS/cm), and in zone 8, where they

reach 3.9 log µS/cm (8,000 µS/cm), but they fluctuate significantly in these sections. Reconstructed anion ratios remain low, at ~−0.5 log (0.3), in both these zones. Reconstructed conductivity values are also low (~2.2 log µS/cm, ~150 µS/cm) in zone 9, but the anion ratio fluctuates between −0.5 and 0.5 log (0.3 and 3) in this section.

These reconstructions should be regarded with a degree of caution, because although the fluctuations are greater than the RMSE of prediction for both variables, the RMSE of prediction does not account for errors introduced by selective dissolution and/or the omission of unknown taxa. As outlined above, dissolution is unlikely to have obscured the major fluctuations in reconstructed variables, but it may have affected the accuracy of the reconstructed values. In addition, the omission of the three unknown taxa (*F.* cf. *exiguissima*, *F.* cf. *sundayensis*, and the unknown *Achnanthes* species) could be a significant source of error in zones 3 and 6, where these taxa are most abundant.

6.4.5 Ordination of diatom assemblages

A PCA biplot of the diatom assemblage data (ordinated after Hellinger transformation) is shown in Figure 6.7. The eigenvalues associated with the first four axes of this ordination indicate that the axes explain 30%, 18%, 13%, and 7% of the variance in the data, respectively (Table 6.1). Comparison of these eigenvalues with eigenvalues generated using the broken-stick model suggests that each of the axes explains a significant proportion of the variance in the data, but only the first two axes are considered here, for clarity (Table 6.1) (cf. Jackson, 1993).

Table 6.1: Eigenvalues and cumulative percentage variance of the species data explained by the first four axes of the PCA of Hellinger-transformed data, and eigenvalues expected under the broken-stick model.

Ordination Axis	1	2	3	4
Eigenvalue (λ)	0.298	0.182	0.126	0.067
Cumulative percentage variance of species data	29.8	48.0	60.6	67.3
Eigenvalue expected under broken-stick model	0.042	0.034	0.030	0.028

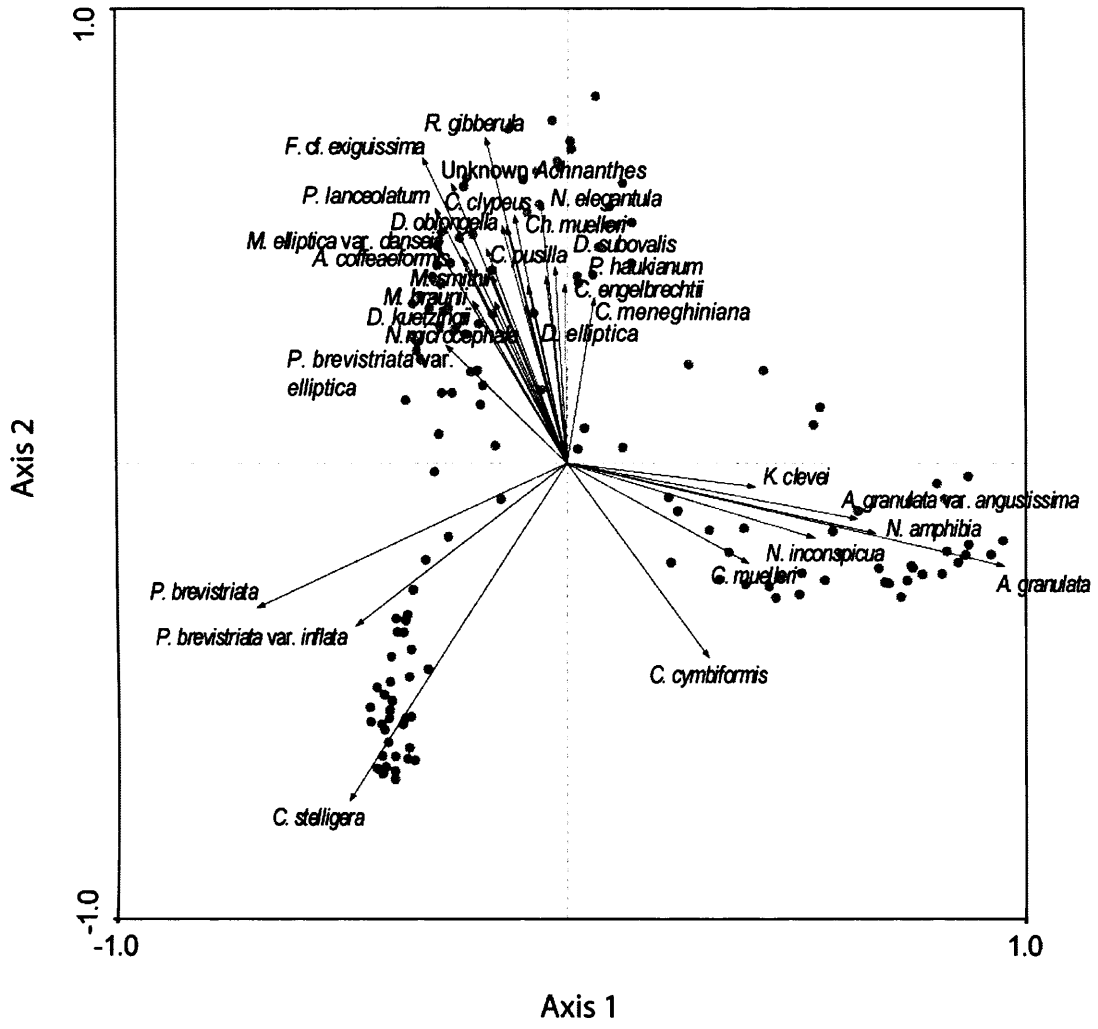

Figure 6.7: PCA biplot showing species loadings (vectors) and sample scores (circles) on axes 1 ($\lambda = 0.298$) and 2 ($\lambda = 0.182$) (species with species fit ≥12% are shown).

The sample scores on the first two PCA axes are plotted against depth in Figure 6.8, together with the diatom-inferred records of lake-water conductivity and anion ratio (section 6.4.4). Comparison of these records shows that there is a strong positive relationship between the sample scores on PCA axis 2 and reconstructed conductivity values, and a strong negative relationship between the sample scores on this axis and reconstructed anion ratios. The variability summarised by PCA axis 2 therefore appears to be related to changes in these lake-water characteristics, such that high sample scores on this axis are indicative of increased lake-water conductivity and low anion ratios. It is evident from Figure 6.7 that high sample scores on this axis are associated with increased abundance of taxa such as *R. gibberula*, *F.* cf. *exiguissima*,

the unknown *Achnanthes* species, *N. elegantula*, *C. muelleri* cysts, and *M. elliptica* var. *dansei*, while low values are most significantly related to increased abundance of *C. stelligera* and *C. cymbiformis*.

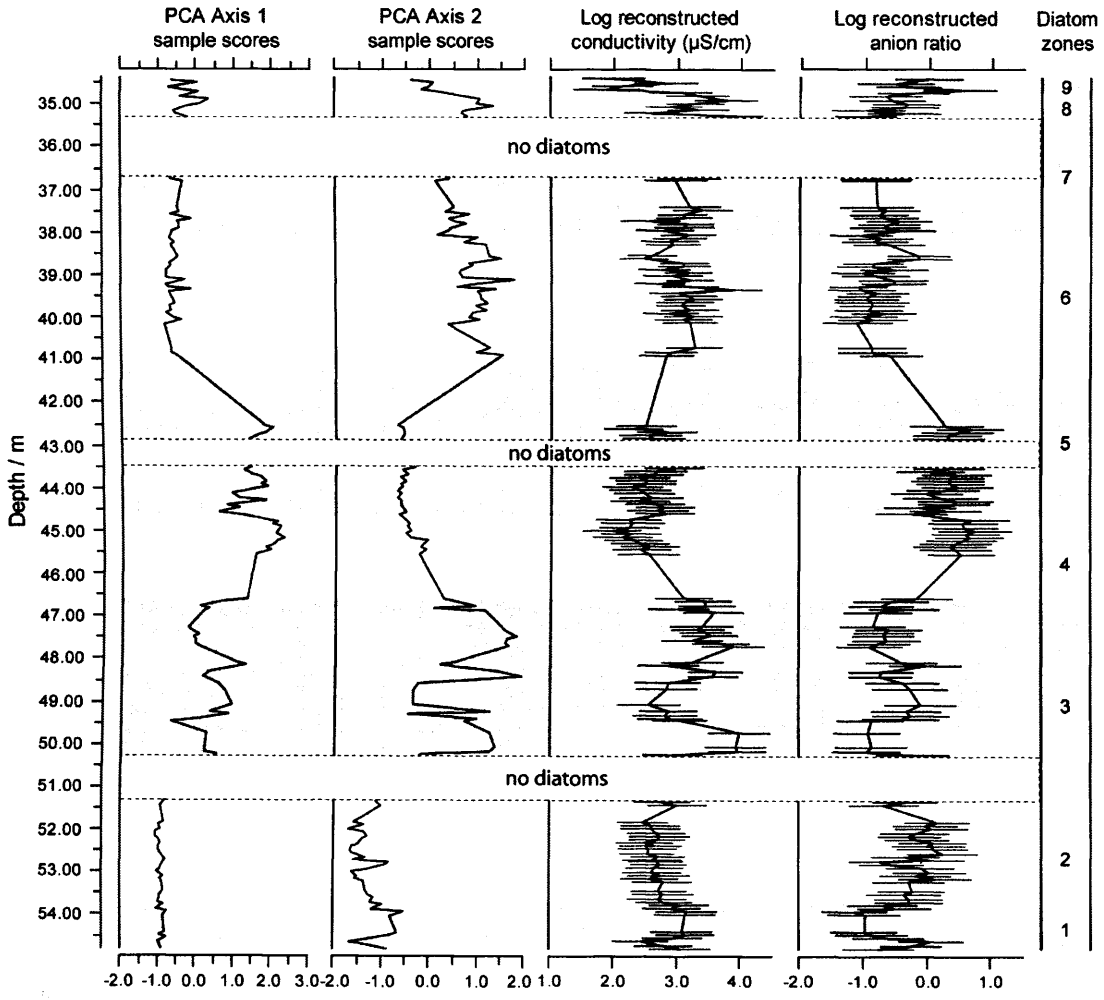

Figure 6.8: Sample scores on PCA axes 1 and 2, shown with the diatom-inferred records of lake-water conductivity and anion ratio (log base 10). Diatom zones defined by SPLITINF are shown.

In zones 3-7, sample scores on PCA axis 1 are, to a certain extent, positively related to the reconstructed anion ratios, and negatively related to the reconstructed conductivity values, but they appear to be unrelated to these variables in zones 1-2 and 8-9 (Fig. 6.8). It is evident from Figure 6.7 that high sample scores on this axis are associated with increased abundance of *A. granulata*, *A. granulata* var. *angustissima*, *N. amphibia*, and *N. inconspicua*, while low sample scores are

associated with high proportions of *P. brevistriata*. These relationships suggest that sample scores on PCA axis 1 could be related to changes in lake depth, as *A. granulata* and *A. granulata* var. *angustissima* are euplanktonic taxa, while *P. brevistriata* is either considered facultatively planktonic or periphytic (cf. Kilham and Kilham, 1975; Gasse, 1986; Bradbury, 1989; Wilson *et al.*, 1997). The fact that *A. granulata* and *A. granulata* var. *angustissima* are frequently found in shallow water means that any differentiation by lake depth would have to be slight, however (cf. Brugam, 1983; Stoermer, 1993; Metcalfe, pers. comm.). The association of *N. inconspicua* with high sample scores on PCA axis 1 is also puzzling, because *N. inconspicua* is usually associated with saline water (Fritz *et al.*, 1993; Gasse *et al.*, 1995). The taxonomy of *N. inconspicua* is highly variable, however, and it is possible that this taxon has been incorrectly identified, or that the specimens identified in this study have different environmental preferences to those identified in other studies (cf. Krammer and Lange-Bertalot, 1997b).

6.4.6 Concentration of phytoliths, sponge spicules, and chrysophyte cysts

The records of phytolith, sponge spicule, and chrysophyte cyst concentration are shown in Figure 6.9, together with the records of diatom valve concentration and reconstructed lake-water conductivity values and anion ratios. The records are semi-quantitative, because insufficient numbers of the microfossils were counted to allow accurate values to be determined, but they exhibit changes that could have palaeohydrological significance, and are therefore described briefly here. Phytoliths are present throughout the record, but there are several peaks in their concentration. The concentration of chrysophyte cysts is highest, and their presence most persistent, in zones 3-5. Few sponge spicules were counted in each sample, and no significance should therefore be placed on the apparent changes in their absolute concentration, but it is worth noting that no spicules are present in zone 1 or zones 6-9. The similarities between the record of phytolith concentration and the record of diatom valve concentration suggest that the concentration of siliceous microfossils may be determined by changes in the sedimentation rate of the lake sediments (Fig. 6.9), but it is possible that some of the changes in these records are directly related to environmental conditions.

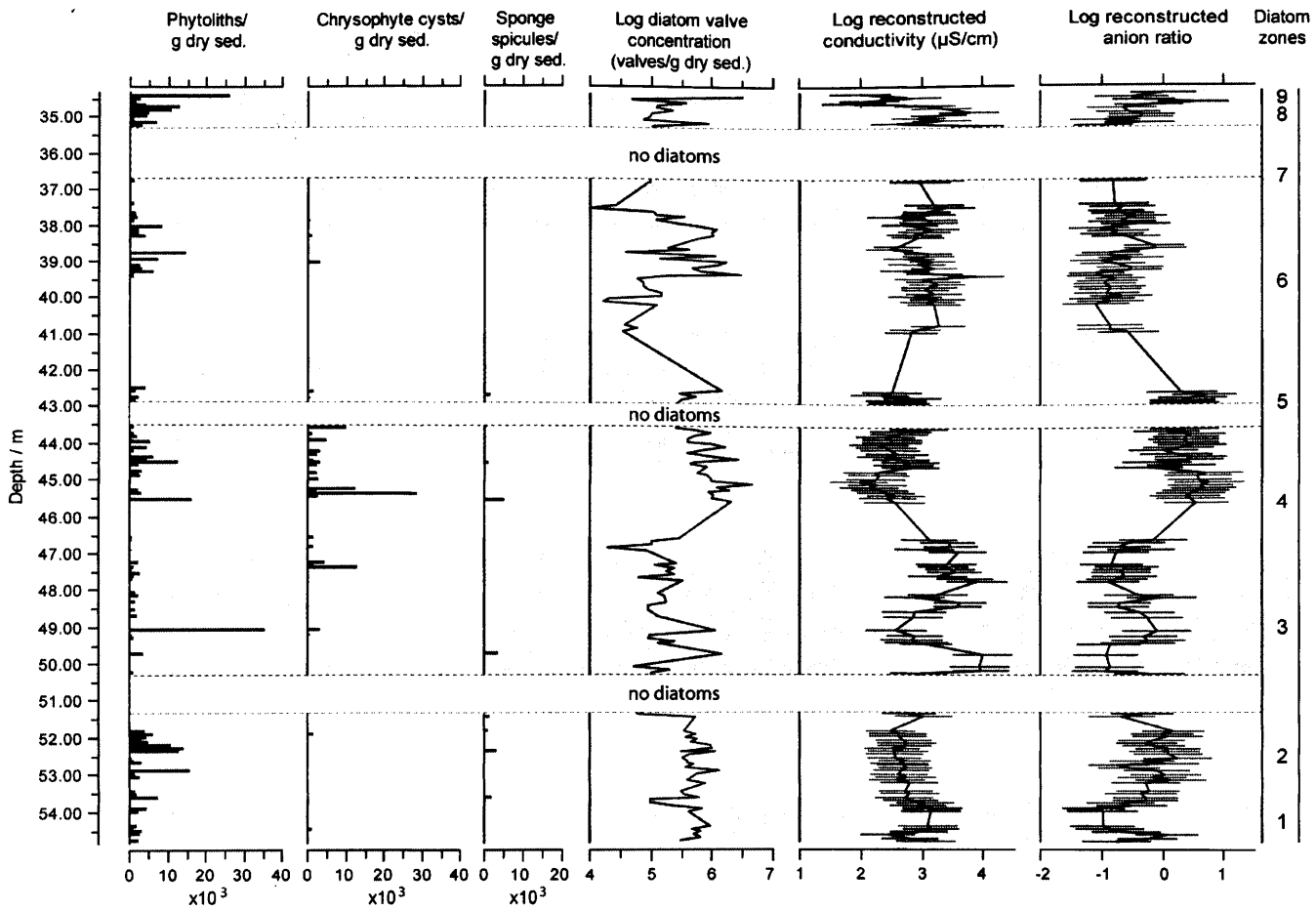

Figure 6.9: Approximate concentrations of phytoliths, chrysophyte cysts, and sponge spicules per gram of dry sediment (scales are values $x10^{-3}$), shown with the record of diatom valve concentration and diatom-inferred records of lake-water conductivity and anion ratio (log base 10). Diatom zones defined by SPLITINF are also shown.

6.5 Discussion

6.5.1 Diatom-inferred palaeohydrological reconstructions

The records of diatom assemblage composition and siliceous microfossil concentrations from between 34.40 and 54.80 m indicate that there were significant changes in palaeohydrological conditions during the period covered by this section of the sedimentary sequence (~150-250 kyr B.P. according to the chronology developed in chapters 4 and 5). The autecologies of the diatom taxa present, combined with the insights provided by ordination of the diatom assemblage data, the diatom-inferred records of lake-water conductivity and anion ratio, and the records of siliceous microfossil concentrations, have the potential to provide considerable information about the nature of these changes.

C. stelligera is associated with fresh, oligotrophic lake water with relatively low alkalinity and pH (Gasse *et al.*, 1983; Hall and Smol, 1992; Poulièková; 1993; Fallu *et al.*, 2002; Tapia *et al.*, 2003). The abundance of this species in the upper- and lower-most parts of zone 1 and throughout zone 2 thus suggests that the lake was fresh, oligotrophic, and moderately deep in these sections. These preferences are reflected in the low reconstructed conductivity values (~500 µS/cm) at these depths. The decrease in the abundance of *C. stelligera* and the concomitant increase in the abundance of *P. brevistriata* in the central part of zone 1 is likely to reflect a decrease in lake level and an increase in lake-water alkalinity at this depth, as *P. brevistriata* is usually found in shallow, moderately alkaline waterbodies (Bradbury, 1989; Gasse *et al.*, 1995; Wilson *et al.*, 1997; Fallu *et al.*, 2002). The environmental preferences of *P. brevistriata* are reflected in the increase in reconstructed conductivity values to ~1,500 µS/cm at this level, although the decrease in reconstructed anion ratios from 1 to 0.1 indicates that carbonate precipitation reduced the anion ratio of lake water at this depth, irrespective of any increase in alkalinity (section 6.4.4).

In zone 3, the peaks in *C. meneghiniana*, *N. elegantula*, and *A. granulata* indicate significant shifts in lake-water composition. *C. meneghiniana* is a planktonic species that is often associated with shallow, eutrophic, and brackish conditions, although it can tolerate a wide range of salinities (Hecky and Kilham, 1973; Tuchman *et al.*,

1984; Gasse, 1986; Fritz *et al.*, 1993; Wilson *et al.*, 1997; Gasse *et al.*, 1995; Håkansson and Chepurnov, 1999; Metcalfe, pers. comm.), while *N. elegantula* is exclusively associated with high lake-water conductivity (Gasse *et al.*, 1995). *A. granulata*, in contrast, is associated with low lake-water conductivity, although, in common with *C. meneghiniana*, it is a planktonic species that is often associated with shallow, eutrophic conditions (Hutchinson, 1967; Kilham and Kilham, 1975; Hancok, 1979; Brugam, 1983; Kilham *et al.*, 1986; Davey, 1987; Wood and Talling, 1988; Bradbury, 1989; Blinn, 1993; Fritz *et al.*, 1993; Stoermer, 1993; Metcalfe, pers. comm.). The autecological preferences of these taxa are reflected in the reconstructed values of lake-water conductivity in this zone, which increase to between 3,000 and 10,000 µS/cm when the abundance of *C. meneghiniana* or *N. elegantula* increases, and decrease to less than 400 µS/cm when *A. granulata* is abundant. Reconstructed anion ratios remain low (0.1 to 1) throughout this zone, suggesting that, as in zone 1, endogenic carbonate precipitation induced by high lake-water conductivity reduced the concentration of carbonate and bicarbonate ions relative to the concentration of sulphate and chloride ions.

It is worth noting that *C. meneghiniana* and *A. granulata* have different nutrient requirements: *C. meneghiniana* is an efficient competitor for Si, while *A. granulata* requires high levels of both P and Si (Kilham *et al.*, 1986; Kilham and Kilham, 1990; Interlandi and Kilham, 2001). It is therefore possible that increases in the abundance of *A. granulata* relative to *C. meneghiniana* were caused by increased input of Si to the lake. The strong relationship between the abundances of *C. meneghiniana* and *N. elegantula* and PCA axis 2, and between sample scores on PCA axis 2 and reconstructed values of lake-water conductivity and anion ratio suggest, however, that lake-water conductivity and/or anion ratio determined the abundance of these taxa (Figs. 6.7 and 6.8).

The dominance of *A. granulata* in zones 4 and 5 suggests that the lake was fresh and well-mixed in this section of the sequence. This is reflected in the low reconstructed conductivity values (100-900 µS/cm) in this section. Anion ratios reach their highest values (up to 5.75) in zone 4, and remain high (~2.5) in zone 5, which presumably reflects a significant decrease in the amount of carbonate precipitating from the lake water, caused by a decrease in lake-water conductivity. It is also notable that

A. granulata var. *angustissima,* which is usually associated with slightly higher conductivity, pH, and light levels than the nominate variety, is more abundant in zone 4 than in zone 5 (Talling and Talling, 1965; Hancok, 1979; Kilham, 1990; Gasse *et al.*, 1995; Turkia and Lepisto, 1999; Metcalfe, pers. comm.). The reason that this taxon is more abundant in zone 4 remains unclear, but the possibility that the higher frequency simply reflects the greater abundance of *A. granulata* should not be excluded, as *A. granulata* var. *angustissima* may represent one extreme of the morphological variation in this species (section 6.4.2) (Kilham and Kilham, 1975).

In zone 6, the increase in the abundance of periphytic species such as *P. brevistriata, P. lanceolatum*, *M. elliptica* var. *dansei*, and *N. elegantula* at the expense of *A. granulata* suggests that lake levels may have decreased, as *A. granulata* is a planktonic species and therefore requires deeper water than periphytic taxa. It should be noted that *A. granulata* is often associated with shallow water, however, and that the decrease in lake level may not, therefore, have been large (cf. Brugam, 1983; Stoermer, 1993; Metcalfe, pers. comm.). The low concentration of chrysophyte cysts in zones 6-9 compared to zones 3-5 provides some support for the suggestion that lake levels fell, as most species of algae in the classes Chrysophyceae and Synurophyceae are planktonic (Fig. 6.9) (section 6.2.3) (Zeeb and Smol, 2001). Reconstructed lake-water conductivity values also increase from ~300 to ~1,200 µS/cm between zones 5 and 6, and reconstructed anion ratios decrease from 2 to ~0.1, suggesting that carbonate precipitation increased in response to higher lake-water conductivity. The absence of sponge spicules in zone 6 may be attributable to this increase in lake-water conductivity, as freshwater sponges cannot tolerate high levels of dissolved solids (Fig. 6.9) (section 6.2.3) (Cumming *et al.*, 1993; Frost, 2001).

It is important to note, however, that the reconstructed values of lake-water conductivity and anion ratio may be subject to errors in zone 6 because *F.* cf. *exiguissima* and the unknown *Achnanthes* species, which could not be included in the environmental reconstructions, are relatively abundant. The co-occurrence of these taxa with *C. meneghiniana* and *N. elegantula* in lower sections of the sequence (Fig. 6.4), and their association with high sample scores on PCA axis 2 (Figs. 6.7 and 6.8), suggest that they may be associated with high lake-water conductivity, and their omission may have therefore led to the under-estimation of lake-water conductivity in

this zone. In addition, the abundance of *P. brevistriata* and *P. lanceolatum* in this section of the record may reduce the precision of the reconstructions, because these species are associated with a range of lake-water compositions (Krammer and Lange-Bertalot, 1991b; Gasse *et al.*, 1995).

The increase in the abundance of *C. muelleri* cysts, *E. argus, E. adnata,* and *C. neothumensis* at the bottom of zone 7 suggests that environmental conditions changed slightly in this zone, although reconstructed conductivity values and anion ratios remain approximately the same. The presence of *C. muelleri* cysts could be indicative of a slight increase in lake depth, because this species is planktonic, but this is unlikely to be the case, because *C. muelleri* is often associated with shallow conditions, and because the absence of valves of this species (as opposed to cysts) suggests that conditions were not ideal for its reproduction. The cause of the change in diatom assemblage composition in zone 7 therefore remains uncertain.

In zone 8, the increased abundance of *C. meneghiniana, C. neothumensis, F.* cf. *exiguissima, N. liebetruthii,* and *N. frustulum* is associated with an increase in reconstructed lake-water conductivity, which peaks at 6,000 µS/cm but fluctuates significantly in this section. Reconstructed anion ratios remain similar to those in zone 7, which suggests that the increase in conductivity did not increase carbonate precipitation significantly at this time. The abundance of *C. meneghiniana* also indicates that the lake remained deep enough to support planktonic diatoms, although this taxon is frequently found in shallow water, and does not, therefore, indicate a significant increase in lake depth (Metcalfe, pers. comm.). Finally, the increase in the percentage abundance of *A. granulata* var. *angustissima, N. amphibia,* and *N. palea* in zone 9 suggests that the conductivity of lake water was lower in this zone than in most parts of zones 6-8. Reconstructed conductivity values decrease to ~500 µS/cm in this section, supporting this proposal. The anion ratio also increases, on average, in this zone, indicating that decreased carbonate precipitation may have increased the concentration of carbonate and bicarbonate ions relative to the concentration of sulphate and chloride ions. The dominance of *P. brevistriata* in the assemblage indicates that the depth of the water body did not increase significantly in this section, however.

6.5.2 Multi-proxy-inferred palaeohydrological reconstructions

The extent to which the palaeohydrological reconstructions outlined above agree with the reconstructions based on the sedimentological and geochemical records from this section of the sedimentary sequence has the potential to resolve some of the uncertainties associated with the latter, and to provide insights into the nature of palaeohydrological change at this time. The principal diatom-derived records are therefore shown with the sedimentological and geochemical records from this section in Figure 6.10. The relationships between these records were explored by passively projecting the sedimentary and geochemical records and the records of siliceous microfossil concentrations into the ordination space of the diatom assemblages. This was performed by multiple regression of the sample scores on the first and second PCA axes of the diatom assemblage data on the other records, using CANOCO (ter Braak and Šmilauer, 2002). The results of this analysis are shown in Figure 6.11.

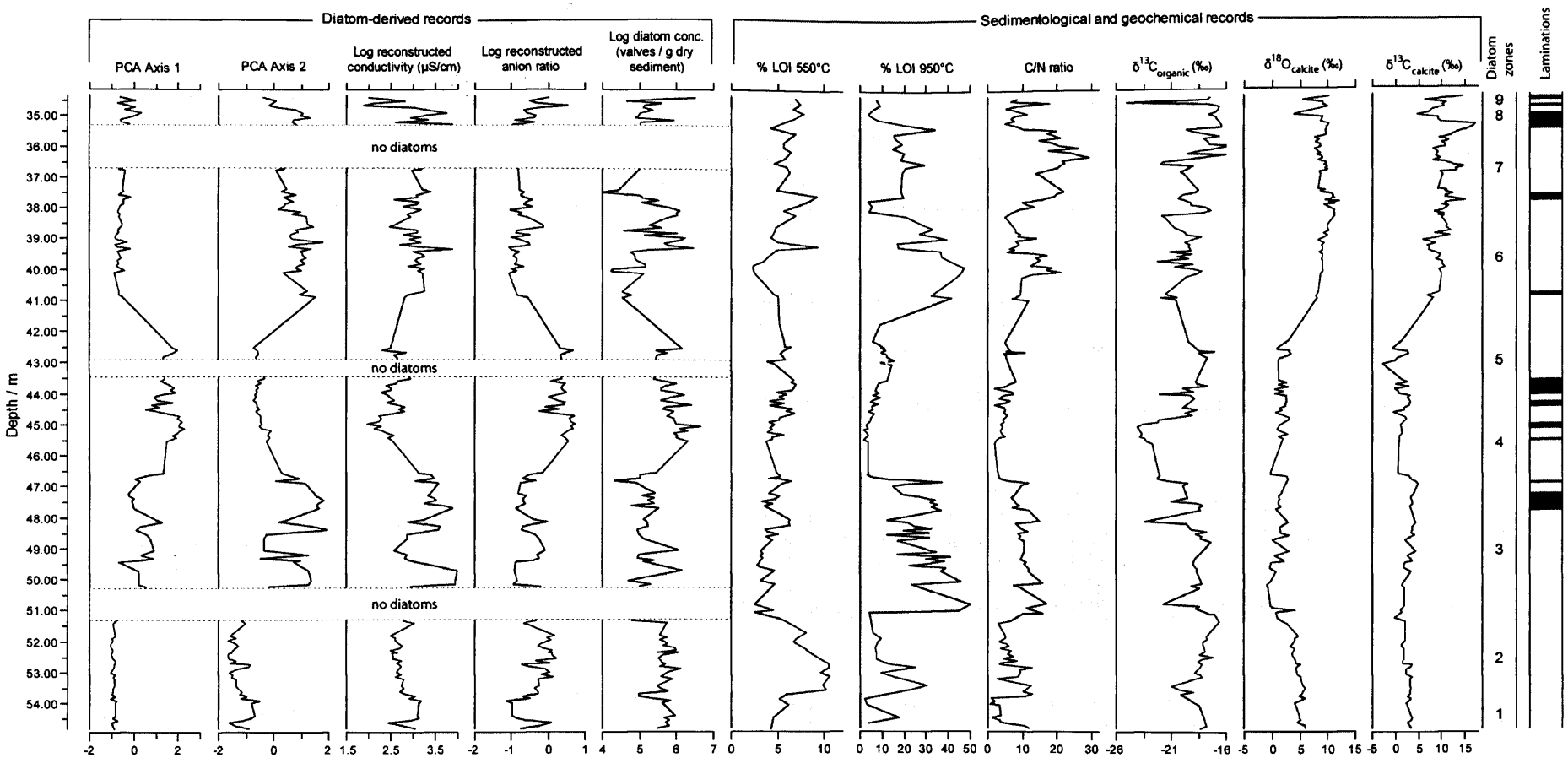

Figure 6.10: Principal diatom-derived records presented in this chapter, plotted with the sedimentological and geochemical records presented in chapter 5 and the depths of laminated sediments. Diatom zones defined by SPLITINF are shown as grey and white bars.

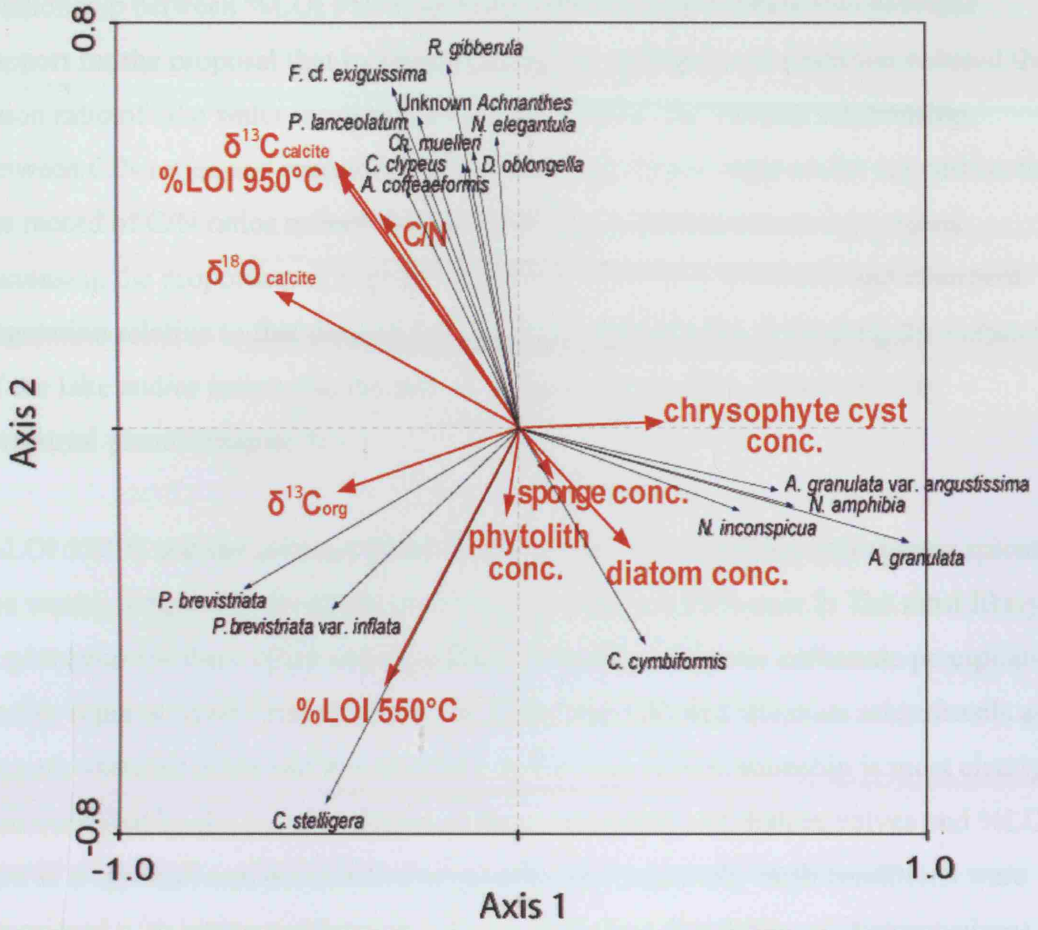

Figure 6.11: Plot showing sedimentological, geochemical, and siliceous-microfossil concentration records (red vectors) passively projected into the ordination space defined by diatom assemblage data. Species loadings on PCA axes 1 and 2 are shown as thin black vectors (species with species fit >26% are shown).

It is evident from Figures 6.10 and 6.11 that the %LOI 950°C, $\delta^{13}C_{calcite}$, and C/N records are positively correlated with sample scores on PCA axis 2 and, to a lesser extent, negatively correlated with sample scores on PCA axis 1. As described above, sample scores on PCA axis 2 are positively correlated with reconstructed conductivity values and negatively correlated with reconstructed anion ratios (section 6.4.5). Thus, it appears that increasing %LOI 950°C, $\delta^{13}C_{calcite}$, and C/N ratios are all associated with increasing lake-water conductivity and decreasing anion ratios. This finding is in excellent agreement with the proposal that decreases in the I/E ratio of the lake increased $\delta^{13}C_{calcite}$ and lake-water conductivity, and that increasing lake-water

conductivity induced endogenic carbonate precipitation (chapter 5). The negative relationship between %LOI 950°C and reconstructed anion ratios also provides support for the proposal that increased endogenic carbonate precipitation reduced the anion ratio of lake water (section 6.4.4). Furthermore, the positive relationship between C/N ratios and reconstructed conductivity values supports the suggestion that the record of C/N ratios reflects lake-level change, with lake-level regressions increasing the proportion of organic material derived from terrestrial and emergent vegetation relative to that derived from aquatic organisms by decreasing the volume of the lake and/or increasing the area of the basin exposed to colonisation by terrestrial plants (chapter 5).

%LOI 550°C and the concentrations of diatom valves, phytoliths, and sponge spicules are weakly negatively correlated with sample scores on PCA axis 2. The most likely explanation for these relationships is that increasing endogenic carbonate precipitation and/or input of clastic material from the crater walls diluted siliceous microfossils and organic material in the sediments as lake levels fell. This relationship is most clearly demonstrated by the anti-correlation of the concentration of diatom valves and %LOI 950°C (Figs. 6.10 and 6.11). It is also possible that relatively fresh conditions were associated with higher productivity (and possibly less dissolution of diatom valves), which increased the concentration of diatom valves and organic material in the sediments. Low lake-water conductivity may have also allowed freshwater sponges to grow, explaining the presence of sponge spicules (Frost, 2001). It is difficult to imagine why phytolith concentrations would have increased under such conditions, however, as C/N ratios indicate that input of organic material from the basin decreased when lake levels were high. It is therefore most likely that the concentrations of siliceous microfossils and organic matter in the sediments were primarily determined by the sedimentation rate of endogenic carbonates, or possibly clastic material, in this section of the sequence.

$\delta^{18}O_{calcite}$ is negatively correlated with sample scores on PCA axis 1, while the concentration of chrysophyte cysts is weakly positively correlated with sample scores on this axis. High sample scores on PCA axis 1 are associated with increased abundance of *A. granulata*, *A. granulata* var. *angustissima,* and *N. amphibia*; an assemblage that is associated with relatively fresh, well-mixed, and possibly slightly

deeper conditions (section 6.4.5). These relationships are in good agreement with the suggestion that low $\delta^{18}O_{calcite}$ values are associated with high I/E ratios (chapter 5), and with the planktonic nature of species that produce chrysophyte cysts (Zeeb and Smol, 2001). The relationships between $\delta^{18}O_{calcite}$ and the other records remain puzzling, however, because $\delta^{18}O_{calcite}$ is usually closely related to lake-water conductivity and $\delta^{13}C_{calcite}$ in hydrologically closed basins, and this is not the case in this section of the sequence (section 2.2) (Talbot, 1990). It is therefore possible that factors other than the I/E ratio influenced $\delta^{18}O_{calcite}$ in this part of the sequence.

The negative correlation between $\delta^{13}C_{organic}$ and sample scores on PCA axis 1 is also difficult to explain. As described in chapters 2 and 5, $\delta^{13}C_{organic}$ is determined by the $\delta^{13}C$ values of aquatic, terrestrial, and emergent vegetation, and by the proportion of organic material derived from these sources; all of which can change simultaneously. It is therefore likely that the factors that influenced $\delta^{13}C_{organic}$ were complex, and cannot be determined from the relationships of this record with other proxies from this section of the sequence.

The records of diatom assemblage composition and siliceous microfossil concentrations therefore provide considerable support for the interpretations of the sedimentological and geochemical records proposed in chapter 5. There are, however, some inconsistencies between these records. In particular, $\delta^{18}O_{calcite}$ is not as closely related to $\delta^{13}C_{calcite}$ and lake-water conductivity as might be expected in a hydrologically closed basin, and there are a number of points at which the relationships between the proxies diverge from those evident in Figure 6.11. These discrepancies will be briefly addressed in the following section, in order to provide a full understanding of the nature of palaeohydrological change at the site.

In zone 1, the relatively low %LOI 950°C and C/N ratios suggest that the lake was deep and dilute, which is in agreement with the reconstructed conductivity values of ~1,000 µS/cm. C/N ratios and, to a lesser extent, $\delta^{18}O_{calcite}$ decrease in the central part of this zone, however, indicating that lake levels increased, while the shift from an assemblage dominated by *C. stelligera* to one dominated by *P. brevistriata* suggests that lake levels decreased and lake-water conductivity increased (Fig. 6.10). It is possible that this discrepancy is due to the influence of a factor other than lake depth

or conductivity on diatom assemblage composition. *C. stelligera* is an oligotrophic species, and it is therefore possible that it was replaced by *P. brevistriata* because in-wash from the crater walls increased nutrient availability as lake levels rose (Hall and Smol, 1992). Unfortunately, it is not possible to confirm this hypothesis, however.

$\delta^{18}O_{calcite}$, %LOI 950°C, and C/N ratios decrease gradually over zone 2, indicating an increase in lake level in this section of the sequence (Fig. 6.10). The diatom assemblage appears to be insensitive to this change, however, as it is dominated by the freshwater, oligotrophic species *C. stelligera* throughout. As in zone 1, it is possible that the abundance of this taxon was determined by nutrient availability. High %LOI 550°C in this zone suggests that the release of nutrients from the sediments may have been slow at this time, possibly due to anoxia in the hypolimnion, and this may have allowed *C. stelligera* to dominate the assemblage. This explanation is supported by the strong relationship between %LOI 550°C and the species loading of *C. stelligera* in Figure 6.11, although this correlation obviously does not indicate causation. $\delta^{13}C_{calcite}$ is also insensitive to lake-level change in this section, which is probably because DIC remained in equilibrium with atmospheric CO_2 at this time, or possibly because changes in freshwater input had little effect on $\delta^{13}C_{DIC}$ due to the high concentration of DIC in the lake relative to that in the input water (chapters 2 and 5) (Li and Ku, 1997).

In zone 3, %LOI 950°C and C/N ratios are high, but decrease gradually, indicating that lake levels were low, but increased slightly, in this section of the record. This reconstruction is in good agreement with the diatom-inferred records of lake-water conductivity and anion ratio, which indicate that lake-water conductivity was high but decreased over time, and that the precipitation of endogenic carbonates maintained low anion ratios throughout. The gap in the diatom record at the start of this zone corresponds with high %LOI 950°C values, suggesting that increased endogenic carbonate precipitation diluted diatom valves, or that diatom valves dissolved in the relatively concentrated lake water.

The records of $\delta^{18}O_{calcite}$ and $\delta^{13}C_{calcite}$ are at odds with these interpretations of lake-level change, however. This is particularly evident in Figure 6.12, where these records are shown on different scales above and below 41 m to highlight low-amplitude

fluctuations. On average, $\delta^{13}C_{calcite}$ is higher in zone 3 than in zones 1 and 2, which supports the finding that the I/E ratio of the lake decreased in zone 3, but it does not respond to the significant decrease in lake level at the start of this zone indicated by the increase in %LOI 950°C and C/N ratios (Fig. 6.12). Moreover, $\delta^{18}O_{calcite}$ does not appear to respond to the changes in lake level at all, as this record is lower in zone 3 than in zones 1 and 2, which suggests that the I/E ratio increased in this section (Fig. 6.12). The most likely explanation for these anomalous values is non-equilibrium precipitation of calcite. This process produces carbonates with lower $\delta^{18}O$ and $\delta^{13}C$ values than carbonates that precipitate in equilibrium, either through kinetic fractionation or the effect of high pH, and could thus explain the anomalously low $\delta^{18}O_{calcite}$ and $\delta^{13}C_{calcite}$ values in this section of the record (section 2.2.3) (McCrea, 1950; Turner, 1982; McConnaughey, 1989; Fronval *et al.*, 1995; Teranes *et al.*, 1999; Zeebe, 1999; Beck *et al.*, 2005). The high %LOI 950°C in zone 3, combined with the evidence that an increase in the rate of carbonate precipitation decreased the concentration of siliceous microfossils in this zone, supports this explanation, as non-equilibrium precipitation often occurs when the rate of carbonate precipitation is high (Fig. 6.10) (*e.g.* Turner, 1982; Fronval *et al.*, 1995; Teranes *et al.*, 1999).

It is unlikely that the anomalous $\delta^{18}O_{calcite}$ and $\delta^{13}C_{calcite}$ values were caused by changes in the mineralogy of the carbonates analysed, because XRD analysis of twenty-three samples between 34.00 and 56.00 m demonstrated that the carbonate present was entirely composed of calcite, except in two cases (44.84 and 54.39 m), where dolomite made up less than 2% of the carbonate analysed (chapter 5). This analysis also revealed the presence of Mg-calcite (average 7 mol% $MgCO_3$) in half the samples analysed. As outlined in chapter 5, Mg-calcite with this composition would be expected to have $\delta^{18}O_{calcite}$ values ~0.42‰ higher and $\delta^{13}C_{calcite}$ values ~0.17‰ higher than calcite, and the presence of this mineral cannot, therefore, account for the anomalous values observed (sections 2.2.2 and 2.2.3) (Tarutani *et al.*, 1969; Jiménez-López *et al.*, 2006).

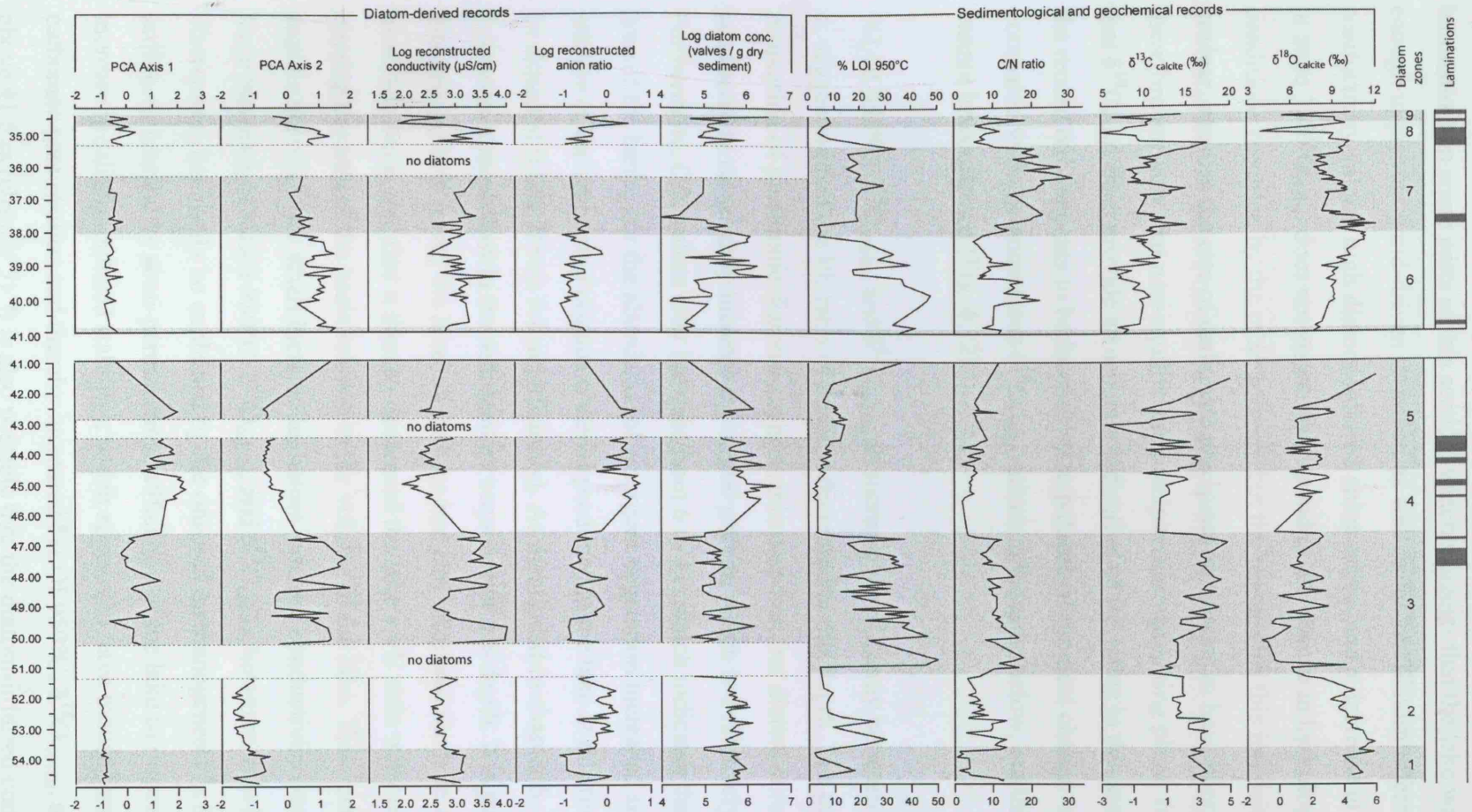

Figure 6.12: Principal diatom-derived, sedimentological, and geochemical records from the section of the sequence between 34.40 and 54.80 m, as in Figure 6.10, but with different scales for the records of $\delta^{13}C_{calcite}$ and $\delta^{18}O_{calcite}$ above and below 41 m to highlight low-amplitude fluctuations in these records.

In zones 4 and 5, %LOI 950°C and C/N ratios remain low, indicating that the lake was relatively deep and dilute. This interpretation is supported by the occurrence of laminations in some parts of this section, which suggests that the lake was deep enough to prevent wind-driven turnover, as well as by low diatom-inferred conductivity values, high diatom-inferred anion ratios, and a decrease in $\delta^{13}C_{calcite}$. As in zone 3, $\delta^{18}O_{calcite}$ does not appear to respond to the change in hydrological conditions recorded by the other proxies, but the reasons for this insensitivity are unclear, because the rate of carbonate precipitation appears to have been low, and it is therefore unlikely that non-equilibrium precipitation was taking place. It is possible that $\delta^{18}O_{calcite}$ does provide an accurate indication of I/E ratios in this section, and that the record only appears to be insensitive to palaeohydrological change when compared with the anomalous $\delta^{18}O_{calcite}$ values in the zone below, but this hypothesis cannot be confirmed (Fig. 6.12).

%LOI 950°C, $\delta^{18}O_{calcite}$, and $\delta^{13}C_{calcite}$ all increase significantly between zones 5 and 6, suggesting that the I/E ratio of the lake decreased at this depth. The decrease in the proportion of planktonic diatoms supports this proposal, but diatom-inferred conductivity values only increase by ~1,000 µS/cm, which is a relatively small shift. Furthermore, C/N values only increase from 6 to 11, which indicates that neither the area of the basin, nor the abundance of emergent vegetation increased significantly relative to the amount of organic material produced in the lake at this time (as would be expected if lake levels fell significantly). As mentioned in chapter 5, there is a 1.4 m-thick mass-flow in the sedimentary sequence at this depth. It is possible that this deposit both raised the level of the lake-bed and increased the lake's surface-area to volume ratio, and that it thereby decreased the lake's I/E ratio without significantly altering the area of the basin relative to the volume of the lake. This scenario does not explain the relatively small increase in diatom-inferred conductivity compared to the large increases in %LOI 950°C, $\delta^{18}O_{calcite}$, and $\delta^{13}C_{calcite}$, however. It is likely that this discrepancy can partly be explained by the onset of methanogenesis in the lake sediments (caused by semi-permanent stratification of the lake in response to an increase in salinity-induced stability), which appears to have induced authigenic carbonate precipitation and thereby increased %LOI 950°C, $\delta^{18}O_{calcite}$, and $\delta^{13}C_{calcite}$ above 41.5 m (chapter 5). It is also possible that the diatom-inferred conductivity values underestimate the increase in lake-water conductivity at this depth due to errors

in the reconstructions in zone 6 (section 6.5.1). Irrespective of the precise controls on the different proxies, it is notable that the decrease in lake level at this depth was probably smaller than the records of %LOI 950°C, $\delta^{18}O_{calcite}$, and $\delta^{13}C_{calcite}$ suggest, and that it may have been independent of climatic change.

In zones 6 and 7, there are peaks in both %LOI 950°C and C/N ratios centred on ~39.7, 38.9, and 36.5 m, indicating significant lake-level regressions at these depths. $\delta^{18}O_{calcite}$ and $\delta^{13}C_{calcite}$ do not appear to reflect these changes, however. As outlined above, authigenic carbonates may have precipitated from pore water in this section of the sequence, which would have reduced the sensitivity of $\delta^{18}O_{calcite}$ and $\delta^{13}C_{calcite}$ to changes in the I/E ratio of the lake (chapter 5). If this was the case, $\delta^{18}O_{calcite}$ and $\delta^{13}C_{calcite}$ are likely to have been influenced by changes in the lake's mixing regime, as the amount of authigenic carbonate precipitation was probably controlled by the rate of methanogenesis, which would have been affected by the degree of anoxia in the lake sediments (chapter 5). This suggestion is supported by the correlation of two peaks in $\delta^{13}C_{calcite}$ with sections of laminated sediment, as this suggests that authigenic carbonate precipitation was greatest when the lake was stratified for long enough to prevent bioturbation of the sediments (Fig. 6.12). The fact that $\delta^{18}O_{calcite}$ and $\delta^{13}C_{calcite}$ remain high in zones 6 and 7 indicates that authigenic carbonates precipitated throughout this section, however, and thus suggests that the lake was at least seasonally stratified for most of this period. Changes in $\delta^{18}O_{calcite}$ and $\delta^{13}C_{calcite}$ in this section may therefore reflect shifts from seasonal to permanent stratification. It is also notable that the large shifts in $\delta^{13}C_{calcite}$ in this section of the sequence (up to 7‰) are accompanied by relatively small shifts in $\delta^{18}O_{calcite}$ (up to 2‰). This apparent insensitivity of $\delta^{18}O_{calcite}$ to changes in the lake's mixing regime may reflect the fact that the $\delta^{18}O$ of pore water (which appears to have been determined by the $\delta^{18}O$ of the hypolimnion) was similar to the $\delta^{18}O$ of water in the epilimnion. If this was the case, the I/E ratio of the lake must have been particularly high at this time. It is also possible that the $\delta^{13}C_{DIC}$ of pore water increased if the lake was stratified for long periods, due to the progressive enrichment of DIC in ^{13}C as a result of carbon dioxide reduction, and that the fluctuations in this record therefore reflect changes in the permanence of lake stratification, as opposed to changes in the ratio of endogenic to authigenic carbonate in the sediments. Finally, it is notable that diatom assemblage composition also appears to have been insensitive to the lake-level changes recorded

by %LOI 950°C and C/N ratios in zones 6 and 7, possibly due to selective dissolution of diatom valves or because the shifts were not large enough to initiate changes in the flora.

It is difficult to compare the different proxies in the two small zones at the top of the sequence (zones 8 and 9), but some general points can be made. %LOI 950°C and C/N ratios decrease and remain low in this section (apart from a single-point increase in C/N ratios), suggesting that lake levels increased at this time. $\delta^{18}O_{calcite}$ and $\delta^{13}C_{calcite}$ fluctuate in this section, however, decreasing significantly at 35.0 and 34.5 m. These shifts were almost certainly caused by the break-down of lake stratification, as described in chapter 5, because laminations disappear when $\delta^{18}O_{calcite}$ and $\delta^{13}C_{calcite}$ decrease (Fig. 6.12). These fluctuations show some agreement with the diatom-inferred records of lake-water conductivity, which suggests that the decrease in lake-water density that accompanies a decrease in lake-water conductivity may have induced the break-down of meromixis, although it is also possible that the change in mixing regime influenced diatom assemblage composition. The records of $\delta^{18}O_{calcite}$ and $\delta^{13}C_{calcite}$, and possibly diatom assemblage composition, therefore appear to be sensitive indictors of changes in the lake's mixing regime in this section.

6.6 Conclusions

Records of diatom assemblage composition and siliceous microfossil concentrations from the section of the sediments at Tswaing crater lake between 34.40 and 54.80 m provide significant insights into the nature of palaeohydrological change at this time. Overall, they provide considerable support for the palaeohydrological reconstructions based on sedimentological and geochemical proxies presented in chapter 5. In particular, they confirm the proposal that %LOI 950°C reflects the concentration of lake water, and that C/N ratios increase as lake levels fall (chapter 5). The records also confirm that $\delta^{18}O_{calcite}$ and $\delta^{13}C_{calcite}$ reflect the I/E ratio of the lake in certain parts of the sequence (chapter 5).

There are, however, a number of sections in which these relationships do not hold. Some of these inconsistencies are caused by anomalies in the sedimentological and geochemical records. $\delta^{18}O_{calcite}$ and $\delta^{13}C_{calcite}$ do not reflect the I/E ratio of the lake

between ~46.5 and 51 m, for example, possibly due to non-equilibrium precipitation of endogenic carbonates. In addition, $\delta^{18}O_{calcite}$ and $\delta^{13}C_{calcite}$ are probably influenced by authigenic carbonate precipitation above 41.5 m (chapter 5). This process reduces the sensitivity of these records to changes in the I/E ratio, but accentuates their sensitivity to changes in the mixing regime of the lake. In other sections, the record of diatom assemblage composition appears to be insensitive to changes in palaeohydrological conditions recorded by the other proxies. In zones 1 and 2, diatom assemblage composition may have been determined by nutrient availability, and may not, therefore, provide a reliable record of changes in lake-water conductivity and anion ratio. Diatom assemblage composition also appears to be insensitive to changes in palaeohydrological conditions in zones 6 and 7, possibly due to selective dissolution of diatom valves, or because the palaeohydrological changes were too small to initiate a significant response in diatom assemblage composition.

The consideration of diatom assemblage, sedimentological, and geochemical records has thus allowed palaeohydrological conditions to be reconstructed with some confidence, but further work could resolve some of the remaining uncertainties. Detailed SEM analysis might reveal whether authigenic carbonate precipitation is responsible for the different $\delta^{18}O_{calcite}$ and $\delta^{13}C_{calcite}$ values above and below 41.5 m, because secondary carbonates are often spheroidal or irregularly shaped (chapter 5). This analysis would also reveal whether calcite grains are larger in zone 3 than in other parts of the record, which would support the suggestion that non-equilibrium precipitation was responsible for the anomalous $\delta^{18}O_{calcite}$ and $\delta^{13}C_{calcite}$ values in this section, because large grains can be associated with high rates of carbonate precipitation (cf. Teranes *et al.*, 1999). In addition, biomarker analysis might identify sections of the record in which cyanobacteria formed a significant proportion of the biomass in the lake, which would allow changes in diatom assemblage composition or valve concentration that might have been caused by competition with these organisms to be identified (cf. Summons *et al.*, 1999; Leavitt and Hodgson, 2001; Rosell-Melé, 2003). Further work is also required to identify and establish the autecologies of the three unknown taxa and the varieties of *P. brevistriata* found in the samples. Finally, high-resolution diatom assemblage records could be produced from the sections of the sedimentary sequence above 34.40 m and below 54.80 m to supplement the sedimentary and geochemical records from these sections. These records would

probably provide relatively little information, however, because the diatom assemblages are dominated by *P. brevistriata* and *C. stelligera* below 54.80 m, and diatom valves are highly dissolved, or not preserved, above 34.40 m (Metcalfe, 1999).

In summary, the records of diatom assemblage composition and siliceous microfossil concentrations presented in this chapter provide considerable information about palaeohydrological conditions at Tswaing crater lake. They broadly confirm the interpretations of the sedimentological and geochemical records presented in chapter 5, and thus increase the confidence with which these records can be used to reconstruct palaeohydrological conditions at the site. They also resolve a number of inconsistencies between the reconstructions based on sedimentological and geochemical proxies, and provide quantitative reconstructions of variables that can only be considered in relative terms using these records. It is also evident, however, that diatom-based records are not always sensitive to changes in hydrological conditions that are recorded by other proxies. Wherever possible, palaeohydrological reconstructions should therefore be based on records of both diatom assemblage composition and the sedimentological and geochemical properties of sediments.

Chapter 7: Palaeohydrological change during a late Pleistocene lake-level highstand in the Central Kenya Rift

7.1 Introduction

Lacustrine deposits from the Naivasha and Nakuru-Elmenteita basins in the CKR provide some of the longest and most accurately dated records of lake-level change in equatorial Africa. Long-term records of palaeohydrological change from sediments deposited in the Naivasha basin during the late Quaternary indicate that orbitally-driven changes in insolation at the equator are the primary influence on precipitation in equatorial East Africa, but that changes in tropical SSTs also affect climatic conditions in this region (chapter 1) (Trauth *et al.*, 2003; Bergner and Trauth, 2004).

Sediments deposited in the CKR also offer the opportunity to reconstruct hydrological conditions on sub-orbital timescales. Richardson and Dussinger (1986) and Verschuren (2001) used sediment cores from Lakes Naivasha, Nakuru, and Elmenteita to produce detailed records of palaeoclimatic conditions over the last 15 kyr, but relatively little is known about climatic change on sub-orbital timescales before this period. Diatomite beds deposited in lakes in the Rift and subsequently exposed by faulting offer an opportunity to reduce this gap in our knowledge by allowing the production of high-resolution records of hydrological change during lake-level highstands.

Trauth *et al.* (2001, 2003) and Bergner and Trauth (2004) used sedimentological, authigenic mineral, and diatom assemblage analysis of diatomite beds deposited in Lake Naivasha and exposed in the Ol Njorowa Gorge to reconstruct palaeohydrological conditions in the Naivasha basin during lake-level highstands between 60 and 175 kyr B.P., but the records they produced were low resolution and did not always concur. The regional extent of the changes they identified also remains uncertain, because there are few comparable records from East Africa (cf. Hillaire-Marcel *et al.*, 1986; Casanova and Hillaire-Marcel, 1992; Sturchio *et al.*, 1993).

This chapter presents a high-resolution record of $\delta^{18}O_{diatom}$ from a diatomite bed deposited in the Naivasha basin during a lake-level highstand centred on ~135 kyr B.P., and compares this to a $\delta^{18}O_{diatom}$ record from a newly investigated, $^{40}Ar/^{39}Ar$-dated diatomite bed from the neighbouring Nakuru-Elmenteita basin. The $\delta^{18}O$ of diatom silica reflects the isotope composition and temperature of the water from which the valves formed (Juillet-Leclerc and Labeyrie, 1987; Schmidt *et al.*, 1997; Brandriss *et al.*, 1998; Moschen *et al.*, 2005), and the isotope composition of lake water is determined by the $\delta^{18}O$ of lake-water inputs and any subsequent changes caused by evaporation (cf. Leng and Marshall, 2004) (chapter 2). The $\delta^{18}O_{diatom}$ records can therefore be used to reconstruct palaeohydrological conditions in the two basins (section 2.4). Sedimentological and diatom assemblage records produced from the beds by A. Bergner (University of Potsdam) are used to support these interpretations, but the $\delta^{18}O_{diatom}$ records form the basis of the discussion, as these records were obtained by the author. The palaeohydrological reconstructions based on these records provide valuable insights into the nature and causes of palaeoclimatic change in the CKR during the late Pleistocene.

7.2 Setting

7.2.1 Climate

The CKR is part of the East African Rift System, which extends over more than 5,000 km, from the Gulf of Aden to Mozambique. The Naivasha and Nakuru-Elmenteita basins lie in the most elevated section of the CKR (~1,800 m), between the Mau Escarpment (3,080 m) to the west, and the Aberdare volcanic complex (4,000 m a.s.l.) and the Kinangop Plateau (2,400 m a.s.l.) to the east (Fig. 7.1).

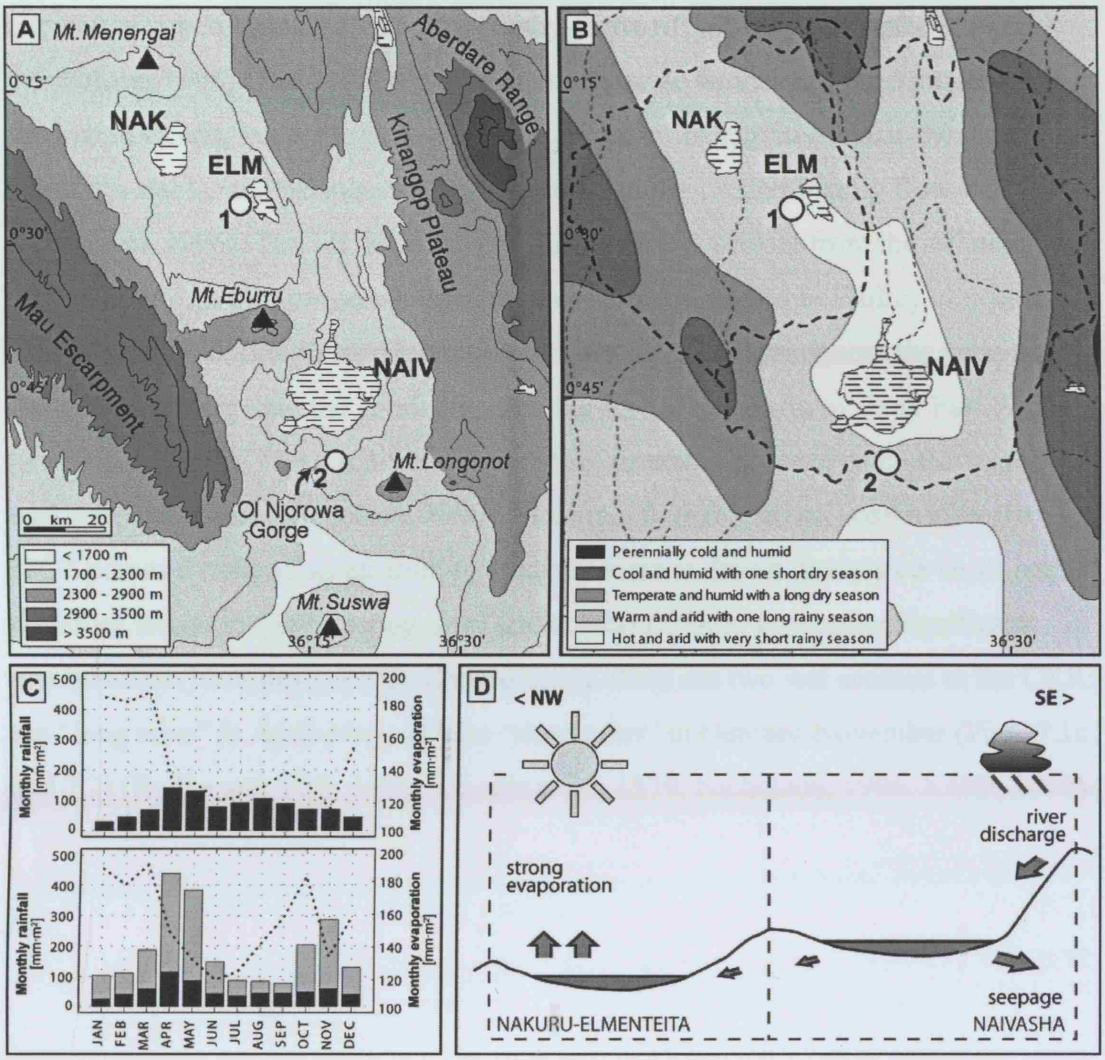

Figure 7.1: Topographical and hydrological setting of lakes in the CKR. (A) Map showing regional topography, location of modern lakes Nakuru, Elmenteita and Naivasha, and location of surface outcrops analysed in this study at (1) Soysambu in the Nakuru-Elmenteita basin and (2) the Ol Njorowa Gorge in the Naivasha basin. (B) Present-day climatic zones (patterns) over the lake catchments (dashed line). (C) Climatic charts from Nakuru (top) and Naivasha (bottom), with rainfall from a station in the Aberdare Range shown as light bars in the Naivasha chart to demonstrate the high levels of precipitation in elevated sections of the Naivasha basin. (D) Schematic profile along the rift floor, indicating the hydrological setting of the basins, with precipitation input from elevated sections of the rift valley, strong evaporative stress over the lakes, and groundwater seepage from Lake Naivasha. Modified from a figure created by A. Bergner (University of Potsdam).

The climate of the CKR is determined by the effects of large-scale atmospheric circulation superimposed on the topography of the rift (Fig. 7.2) (chapter 1) (Nicholson, 1996). The ITCZ draws the easterly trade winds onto the continent from the Indian Ocean, but these winds bring little rain to the region because they are thermally stable, and because the north-easterly trades predominantly flow over land (Nicholson, 1996). The ITCZ also draws air onto the continent from the Atlantic Ocean, in a form of monsoonal circulation not directly related to Hadley circulation. This air is humid, bringing precipitation to western Africa throughout the year, and can penetrate deep into the continent, crossing the Congo Basin to reach East Africa (Nicholson, 1996). The CAB forms where this air mass converges with the trade winds from the east (Nicholson, 1996). Most rain falls four to six weeks after the ITCZ passes overhead, as air from the Indian Ocean is drawn directly on-shore and is therefore forced to rise by topography and coastal friction, generating significant precipitation (Nicholson, 1996). Consequently, there are two wet seasons in the CKR: the "long rains" in April-May, and the "short rains" in October-November (Figs. 7.1c and 7.2) (Rodhe and Virji, 1976; Vincent *et al.*, 1979; Nicholson, 1996; KMD, 2000).

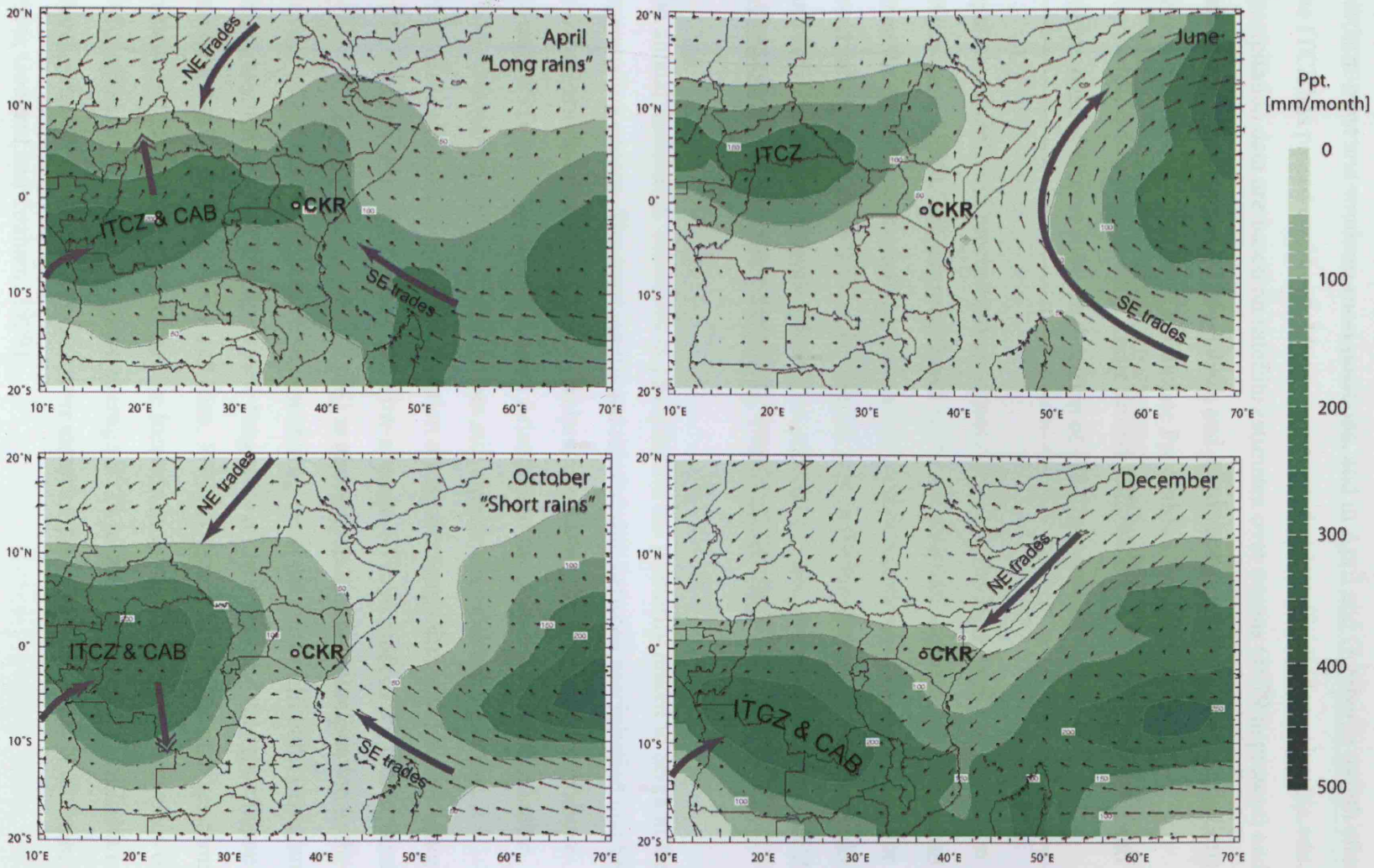

Figure 7.2: See following page for caption.

Figure 7.2: Climate of eastern Africa, showing precipitation and climatological wind vectors for the 925 hPa pressure level in June and December, when the ITCZ is at its northern-most and southern-most positions, and in April and October, a month after the ITCZ has passed overhead. Maps were created at http://iridl.ldeo.columbia.edu. Precipitation data are based on satellite estimates over oceans (1979 to present) and rain gauge data over land (1961-1990), and wind vectors are based on observations between 1961 and 1990 (NCEP, Climate Prediction Center USA, from http://iridl.ldeo.columbia.edu). Large arrows indicate prevailing air movement and double-headed arrows indicate direction of ITCZ movement.

Spatial variability in precipitation is closely linked to the topography of the region (Nicholson, 1996). The exposed flanks of the rift generate orographic precipitation from the easterly trade winds, and therefore receive high levels of precipitation for much of the year. The rift floor, in contrast, lies in the lee of the eastern rift shoulder, and only receives precipitation from convectional storms generated when the ITCZ is overhead (Hastenrath, 1991; Nicholson, 1996; Leroux, 2001) (Fig. 7.1c).

On annual timescales, variations in precipitation are primarily linked to SSTs in the surrounding oceans. The most significant relationship between precipitation and SSTs is the association of above-average precipitation during the short rains with above-average SSTs in the eastern equatorial Atlantic and the central and western Indian Ocean (Nicholson, 1996). A weaker, but still significant, relationship is the association of above-average precipitation during the long rains with above-average SSTs in the equatorial Atlantic and below-average SSTs in most of the Indian Ocean north of 35°S (Nicholson, 1996). ENSO is also known to affect precipitation in the region, with above-average precipitation during the short rains of El Niño years, and below-average precipitation during the long rains of the following year (Nicholson and Entekhabi, 1987; Nicholson and Kim, 1997). The causes of these changes remain unclear, but modelling suggests that the increase in rainfall during the short rains of El Niño years may be related to above-average SSTs in the western equatorial Indian Ocean, which increase convergence over eastern Africa (Ogallo, 1988; Nicholson, 1996; Goddard and Graham, 1999).

7.2.2 Sites

As a consequence of the climatic setting of the CKR, the floor of the rift valley is characterised by a highly negative water budget, with precipitation averaging 650-750 mm yr^{-1} and potential evapotranspiration averaging 1800-1900 mm yr^{-1} (Allen *et al.*, 1989; Bergner *et al.*, 2003). The persistence of intra-rift lakes therefore depends on the supply of water from the elevated parts of their basins (Milbrink, 1977; Gaudet and Melack, 1981).

Lake Naivasha (0°55'S 36°20'E, 1890 m a.s.l.) is the highest lake in the CKR and has a drainage area of ~3,200 km^2 (Fig. 7.1). Its basin includes highly elevated sections of the rift, such as the Aberdare Range (~4,000 m a.s.l), which provide the lake with a perennial source of water via the Malewa and Gilgil Rivers (Fig. 7.1). The basin is topographically closed, but a significant amount of water leaves the lake through seepage. Most of this water flows to the south, but a small amount flows north towards the Nakuru-Elmenteita basin (Fig. 7.1d) (Gaudet and Melack, 1981; Barton *et al.*, 1987; Darling *et al.*, 1990; Ojiambo and Lyons, 1996). As a consequence of this topographical and hydrological setting, Lake Naivasha is relatively large (~170 km^2 in area and up to ~8 m deep), fresh (250-500 µS cm^{-1}), and has a pH of ~8 (Melack and Kilham, 1974; Gasse *et al.*, 1983; Verschuren, 1999b).

The Nakuru-Elmenteita basin is smaller (~2,400 km^2) and lies at a lower elevation (1,760 to 3,080 m a.s.l.) than the Naivasha basin (Fig. 7.1). Lakes Nakuru (0°22'S 36°05'E, 1758 m a.s.l.) and Elmenteita (0°20'S 36°10'E, 1776 m a.s.l.), which occupy the basin today, therefore receive little freshwater input. The two lakes also appear to be hydrologically closed (cf. Vareschi, 1982; Gasse *et al.*, 1983; Allen *et al.*, 1989). Consequently, both lakes are small (40 and 24 km^2 in area and less than 3 m deep), saline (conductivity >10,000 µS cm^{-1}), and alkaline (alkalinity 100-300 meq l^{-1}, pH ~10.5) (Hecky and Kilham, 1973; Melack and Kilham, 1974; Milbrink, 1977; Vareschi, 1982; Gasse *et al.*, 1983). As mentioned in chapter 1, exposed lake sediments and strandlines show that Lakes Nakuru and Elmenteita joined to form a single lake, known as Palaeolake Nakuru-Elmenteita, during the early Holocene and the late Pleistocene (Washbourn, 1967; Washbourn-Kamau, 1970, 1971; Dühnforth *et al.*, in prep.).

7.3 Methods

In order to reconstruct palaeohydrological conditions in the Naivasha and Nakuru-Elmenteita basins during the late Pleistocene, records were produced from the largest late Pleistocene diatomite beds in each basin. These beds were deposited in Lake Naivasha and Palaeolake Nakuru-Elmenteita during lake-level highstands, and are now exposed as surface outcrops. Both profiles were sampled by A. Bergner and M. Trauth (University of Potsdam).

In the Naivasha basin, a 340 cm-thick deposit exposed in the Ol Njorowa Gorge, south of modern Lake Naivasha, was sampled at continuous 2.5 cm intervals between the base of the profile and 300 cm above the base, excluding tephra layers, for $\delta^{18}O_{diatom}$ analysis (Figs. 1.6a and 7.1). The material between 300 and 340 cm was not sampled because it contains significant amounts of clay, and is therefore unsuitable for $\delta^{18}O_{diatom}$ measurements (section 2.4). This bed has been investigated previously, using sedimentological and diatom assemblage analysis, by Trauth *et al.* (2001, 2003) and Bergner and Trauth (2004). Trauth *et al.* (2003) dated a tuff layer below the deposit to 146 ± 2 kyr B.P. using $^{40}Ar/^{39}Ar$-dating, providing a maximum age for the start of diatomite deposition. A tuff between 80 and 100 cm above the base was also dated to 141 ± 3 kyr B.P. (Trauth *et al.*, 2003).

In the Nakuru-Elmenteita basin, a 410 cm-thick bed of diatomite deposited in Palaeolake Nakuru-Elmenteita and exposed at Soysambu, two kilometres west of present-day Lake Elmenteita, was sampled every 20 cm for $\delta^{18}O_{diatom}$ analysis (Figs. 1.6b and 7.1). An intercalated tuff layer 270 cm above the base of this profile has been dated to 114 ± 2 kyr B.P. using the single-crystal laser-fusion (SCLF) $^{40}Ar/^{39}Ar$ method, by A. Deino (Berkeley Geochronology Center). A. Bergner (University of Potsdam) has also produced a record of diatom assemblage composition and a semi-quantitative record of the abundance of clastic material from this profile. The diatom assemblage analysis was carried out using standard procedures (chapter 6), and diatom identification followed the principles of Hustedt (1949), Gasse (1986), and Krammer and Lange-Bertalot (1991a,b, 1997a,b) (A. Bergner, pers. comm.). These data are unpublished, and are therefore reproduced and briefly discussed in this thesis (with the permission of A. Deino and A. Bergner).

For $\delta^{18}O_{diatom}$ analysis, 3-4 cm^3 of each sample was cleaned using a modified version of the method described by Morley *et al.* (2004). The samples were treated with H_2O_2 and HCl, rinsed in deionised water, and wet-sieved at 10 and 75 μm. The 10-75 μm fraction was left to settle, and the uppermost layer was siphoned off and centrifuged with sodium polytungstate (SPT) (density 2.1 g cm^{-3}). Material with a density less than 2.1 g cm^{-3} was rinsed in deionised water, boiled with 5% sodium hexametaphosphate to disaggregate clays, rinsed again, and sieved at 10 μm, before drying overnight at 40°C. Analysis of pure diatom samples before and after treatment with sodium hexametaphosphate demonstrated that this step had no effect on $\delta^{18}O_{diatom}$.

The oxygen isotope composition of the samples was measured by step-wise fluorination (Haimson and Knauth, 1983; Leng and Barker, 2006). The samples were outgassed in nickel reaction tubes and firstly reacted with a stoichiometric deficiency of bromine pentafluoride (BrF_5) at 250°C as a prefluorination clean-up step to remove the outer hydrous layer of the diatom valves (section 2.4). They were then reacted overnight at 450°C with a stoichiometric excess of BrF_5 to liberate the tetrahedrally-bonded oxygen in the valves. The oxygen released during this reaction was converted to carbon dioxide using the procedure outlined by Clayton and Mayeda (1963), and the $\delta^{18}O$ of this gas was measured on a dual inlet mass spectrometer. Standard laboratory quartz and diatomite samples were analysed to assess measurement errors. The values obtained were normalised using an international standard quartz (NBS 28). The values are presented in δ form, as per mil deviations from VSMOW. The internal laboratory standard diatomite (BFC) had a reproducibility of ±0.3‰ (1 s.d.). The samples were prepared by the author, but were analysed by H. Sloane (NIGL).

Although diatom valves made up, on average, 94% (±4%, 1 s.d.) of each sample analysed, the $\delta^{18}O_{diatom}$ values were corrected using a mass-balance equation to ensure that oxygen from contaminants (which were predominantly clay particles) did not bias the records (cf. Morley *et al.*, 2004; Leng and Barker, 2006). The amount of contaminant in each sample was determined by mounting a sub-sample on a slide and counting the percentage cover of different components in a 100 μm x 100 μm grid, until at least 200,000 μm^2 had been assessed. The average $\delta^{18}O$ of contaminants

($\delta^{18}O_{detritus}$) was determined by pre-treating eight samples as described above, and then heating them with 2M KOH at 70°C to dissolve diatom valves before determining their oxygen isotope composition.

In order to ensure that alkali digestion did not affect $\delta^{18}O_{detritus}$, the $\delta^{18}O$ values of contaminants in two of the samples were also determined using a mixing-line approach, in which each sample was divided into four fractions of varying purity by settling after chemical treatment but prior to analysis. The $\delta^{18}O$ values of these sub-samples were then used to construct mixing lines of the two end members: diatom valves and contaminants (Fig. 7.3). The $\delta^{18}O_{detritus}$ values determined using alkali digestion are in good agreement with those inferred using the mixing-line approach (+17.5‰ and +18.3‰ in one sample, and +21.1‰ and +20.8‰ in the other) (Fig. 7.3), and the average $\delta^{18}O_{detritus}$ values determined using alkali digestion (+19.3‰ for the profile from the Naivasha basin and +17.7‰ for the profile from the Nakuru-Elmenteita basin) were therefore used to correct $\delta^{18}O_{diatom}$ values. This correction increased $\delta^{18}O_{diatom}$ by an average of 0.7‰ (±0.6‰, 1 s.d.).

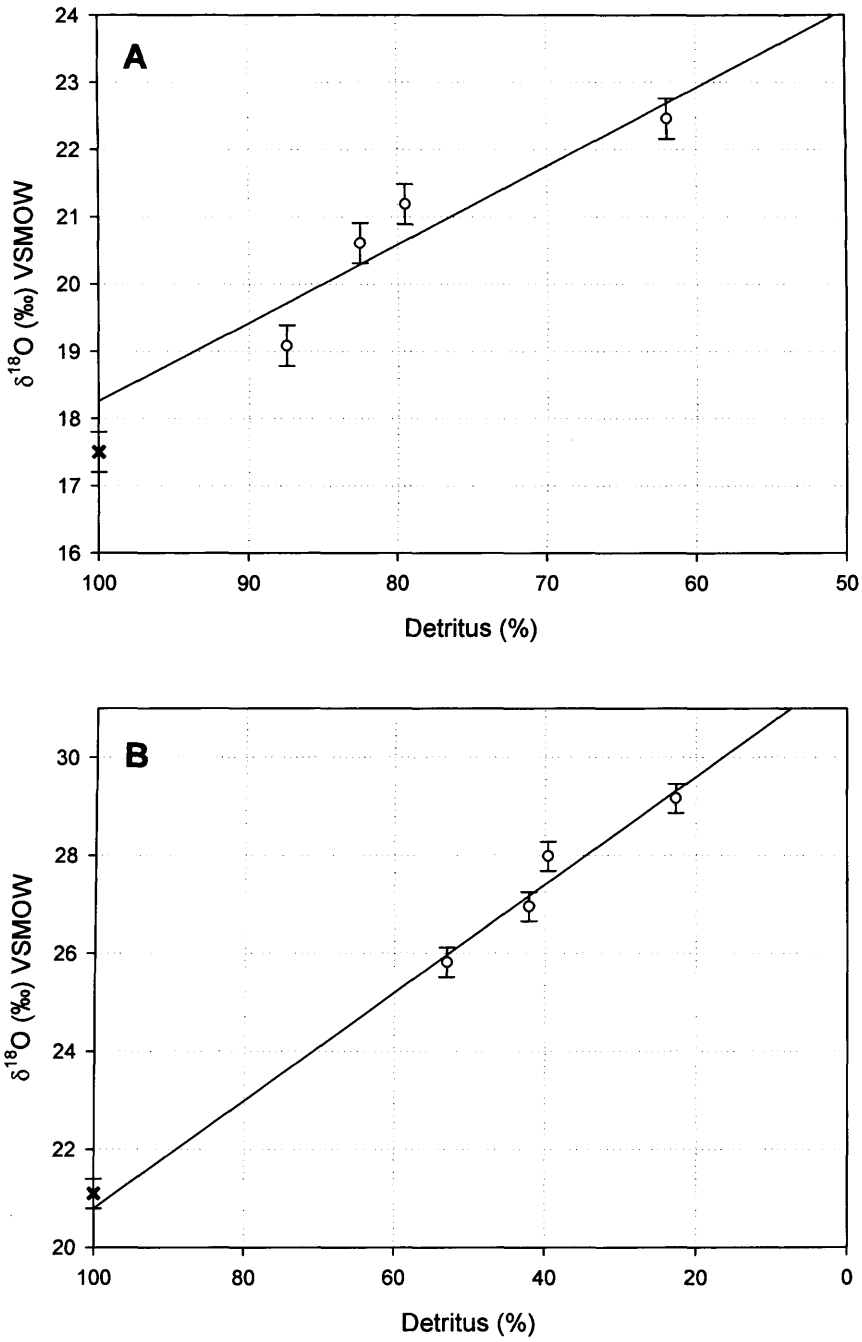

Figure 7.3: Mixing lines used to assess the validity of the alkali-digestion method for determining $\delta^{18}O_{detritus}$. $\delta^{18}O$ values of sub-samples with varying proportions of detritus are shown as circles, and the $\delta^{18}O_{detritus}$ value of the same sample determined using alkali-digestion is shown as a cross. Mixing lines were constructed using linear least-squares regression of the sub-sample values. Samples are from (A) 292.5 cm and (B) 155.0 cm above the base of the profile in the Naivasha basin. Error bars are 1 s.d. Note reversed scale on the x-axis.

It should be noted that small quantities (<1%) of phytoliths and sponge spicules remained in the samples after cleaning, and that the procedure outlined above does not correct for the presence of these microfossils. In addition, the mass-balance method may be subject to errors caused by the different oxygen contents of diatom valves and contaminants (Leng and Barker, 2006). The high diatom content of the samples analysed means that these sources of error are unlikely to mask changes in the oxygen isotope composition of diatom valves, however.

To aid the interpretation of the $\delta^{18}O_{diatom}$ records, modern water samples were obtained from Lakes Naivasha, Nakuru, and Elmenteita, an ephemeral stream entering Lake Nakuru, runoff in the Ol Njorowa Gorge, and precipitation at Lake Nakuru, in August 2003 (by the author) and August 2005 (by M. Trauth (University of Potsdam)). The samples were collected and their isotope values ($\delta^{18}O$ and $\delta^{2}H$) were determined using standard methods, which are described in section 3.3.1. The values obtained are reported as per mil deviations from VSMOW, and analytical precision was ±0.05‰ for $\delta^{18}O$ and ±2.0‰ for $\delta^{2}H$. The analysis of these samples was carried out by C. Arrowsmith (NIGL).

7.4 Results

7.4.1 Modern hydrological setting

The $\delta^{18}O$ and $\delta^{2}H$ values of the modern water samples are shown in Figure 7.4, together with the GMWL, and a LMWL and amount-weighted mean annual isotope values of precipitation calculated using the $\delta^{18}O$ and $\delta^{2}H$ values of 38 precipitation samples collected at Kericho (0°22'S 35° 21'E) and Muguga (1° 13'S 36° 37'E) between 1967 and 1971 (IAEA/WMO, 2001; Vose *et al.*, 2002).

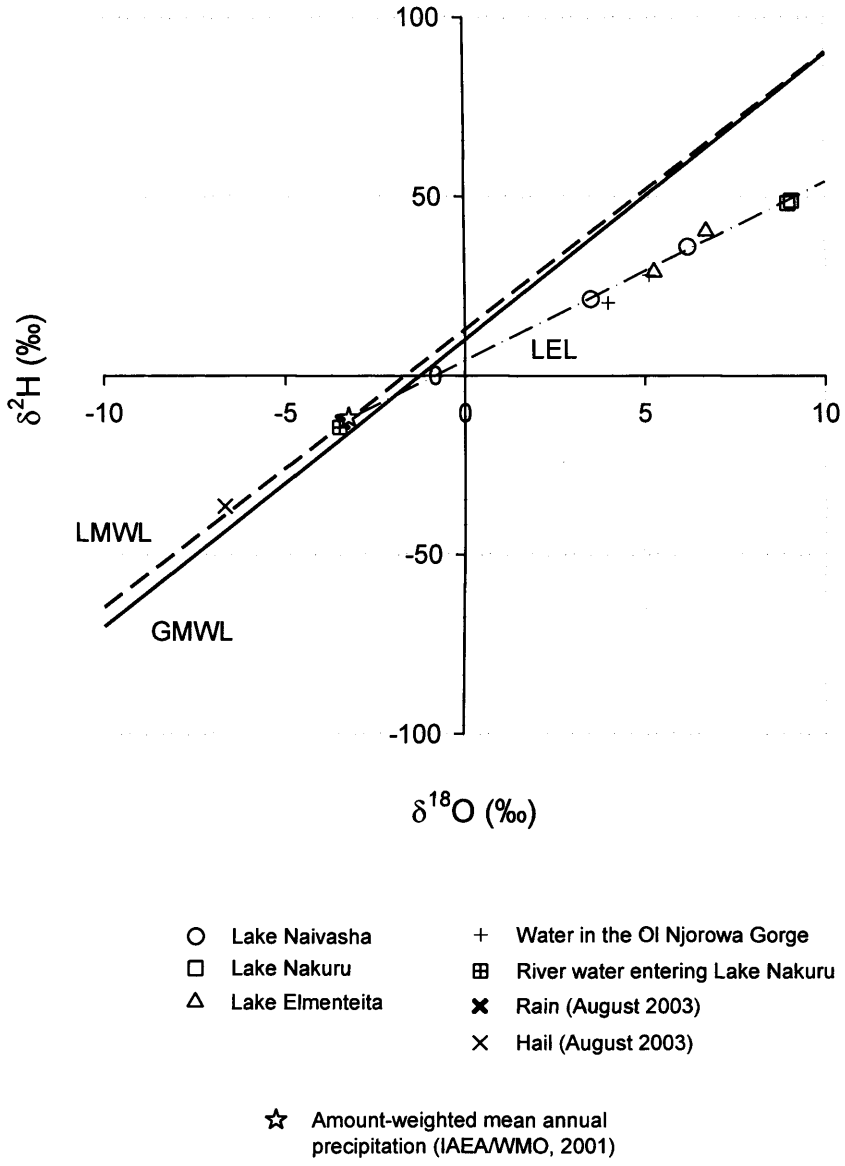

Figure 7.4: $\delta^{18}O$ and $\delta^{2}H$ values of modern water samples collected in the CKR, together with the GMWL (Craig, 1961), and a LMWL and amount-weighted mean annual isotope values of precipitation calculated using samples collected at Kericho and Muguga between 1967 and 1971 (IAEA/WMO, 2001; Vose *et al.*, 2002). The LEL is based on the composition of the lake water samples.

As expected, the spot samples of rain and hail lie close to the LMWL (Fig. 7.4) (section 2.1.1). The sample of river water entering Lake Nakuru also lies on the LMWL, indicating that the river is fed by local precipitation and is not subject to evaporation. The spot samples from Lakes Naivasha, Elmenteita, and Nakuru lie on a LEL, which demonstrates that evaporation has increased the $\delta^{18}O$ and $\delta^{2}H$ values of

these water bodies. The LEL intercepts the LMWL at the amount-weighted mean annual $\delta^{18}O$ and $\delta^{2}H$ values of precipitation, showing that the lakes are fed by local precipitation, and that rainfall is not "lost" or subject to evaporation before it enters the lake (section 2.1.2). The samples from Lake Nakuru have the highest isotope values, which indicates that the fraction of lake-water inputs lost through evaporation is highest in this lake (section 2.1.2). Finally, the samples from the Ol Njorowa Gorge lie close to the LEL, confirming that they are predominantly composed of groundwater seeping southward from Lake Naivasha (Barton *et al.*, 1987; Allen *et al.*, 1989; Darling *et al.*, 1990).

The fact that the lakes are isotopically enriched relative to meteoric water indicates that the ratio of water input to evaporative output (I/E ratio) is the dominant control on their isotope composition, and that changes in this ratio probably obscure any variations in the $\delta^{18}O$ of lake-water inputs (section 2.1.2) (cf. Leng and Marshall, 2004). This suggestion is supported by the observation that the lakes fluctuate significantly in response to seasonal changes in rainfall (Vincent *et al*; 1979; Åse *et al.*, 1986; Verschuren, 1996). There is no reason to believe that this hydrological regime was different during the late Pleistocene, as the hydrological setting of the basins has not changed since this time (Bergner *et al.*, 2003; Dühnforth *et al.*, in prep.). It is therefore likely that the $\delta^{18}O_{diatom}$ records from the Naivasha and Nakuru-Elmenteita basins reflect the I/E ratios of the lakes in which the diatom valves formed (section 2.4).

7.4.2 Palaeohydrological records

The diatomite bed in the Naivasha basin that was sampled in this study consists almost entirely of diatom valves, with minor amounts of siliciclastic material, phytoliths, and sponge spicules. The $\delta^{18}O_{diatom}$ record from this profile is presented in Figure 7.5a, together with the principal sedimentary records produced by Bergner and Trauth (2004). The record of diatom assemblage composition produced by Bergner and Trauth (2004) is also reproduced in Figure 7.6, for comparison.

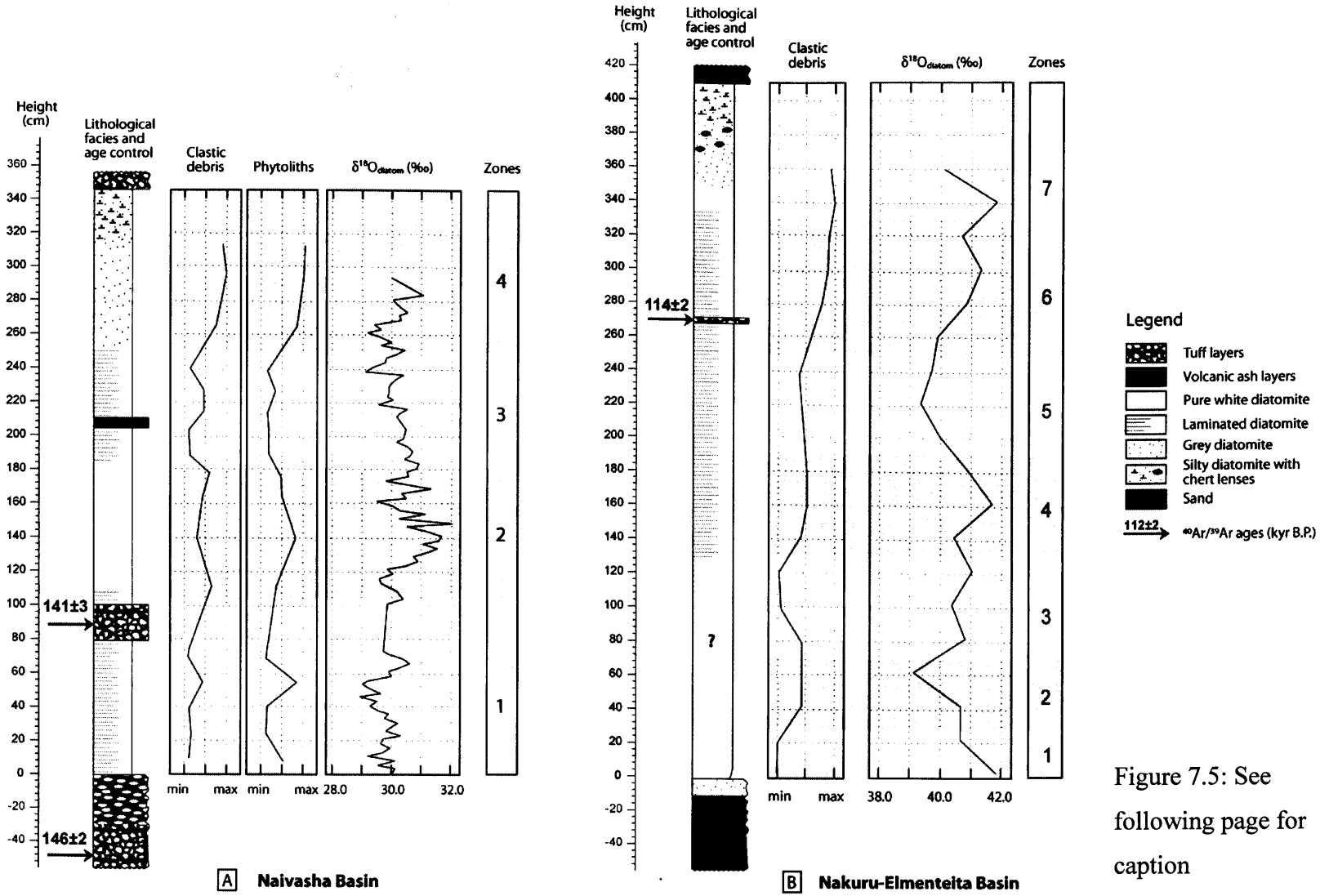

Figure 7.5: See following page for caption

Figure 7.5: Lithological facies, $\delta^{18}O_{diatom}$ records, and semi-quantitative records of clastic debris and phytolith abundance from the diatomite beds exposed in (A) the Naivasha basin and (B) the Nakuru-Elmenteita basin. Stratigraphic zones defined by the lithological facies and records from the profiles are shown as grey and white bars. Age control is provided by $^{40}Ar/^{39}Ar$ dating of volcanic tuffs. With the exception of the $\delta^{18}O_{diatom}$ record, the data relating to the profile in the Naivasha basin are from Trauth *et al.* (2003) and Bergner and Trauth (2004). The lithological information and the record of clastic debris abundance from the profile in the Nakuru-Elmenteita basin were provided by A. Bergner (pers. comm.), and the $^{40}Ar/^{39}Ar$ date from this profile was provided by A. Deino (pers. comm.).

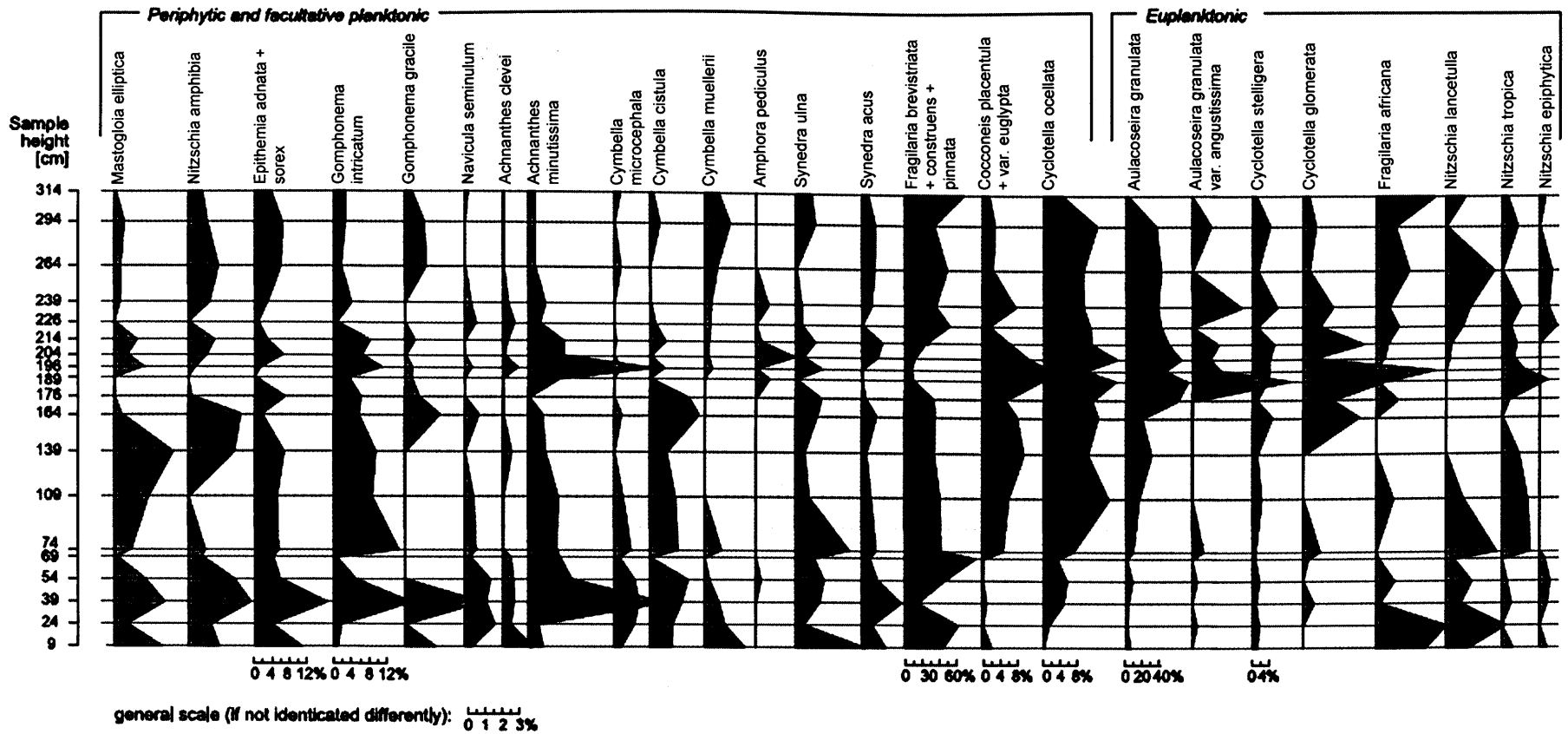

Figure 7.6: Relative abundance of selected diatom taxa from the diatomite bed in the Naivasha basin. Stratigraphic zones, which are based on the lithological facies and sedimentological records from the bed (cf. Figure 7.5a), are shown as grey and white bars. Note altered scales, particularly for *P. brevistriata* (labelled *Fragilaria brevistriata*) and *A. granulata*. Reproduced from Figure 4a in Bergner and Trauth (2004).

The oxygen isotope record from the diatomite bed in the Naivasha basin is at a higher resolution than the previous records from the profile, but it exhibits comparable trends, and can therefore be discussed in the context of the stratigraphic zones defined by these records (Bergner and Trauth, 2004). In zone 1 (base of the sequence to 105 cm), $\delta^{18}O_{diatom}$ fluctuates around +30‰, decreasing to +28.9‰, the lowest value in the record, at 45 cm. In zone 2 (105 to 180 cm), the record increases by 2.4‰, reaching +32‰ at 147.5 cm, before decreasing rapidly to +29.5‰ at 160 cm, and then peaking briefly for a second time at 167.5 cm. The record then decreases in a step-wise manner in zone 3 (180 to 250 cm), reaching +29.1‰ at 237.5 cm. In zone 4 (250 cm to the top of the sequence), the record initially decreases to +29.2‰ at 260 cm, but subsequently shows a trend towards higher values, reaching +30.0‰ at 292.5 cm above the base of the profile.

The $\delta^{18}O_{diatom}$ record from the newly investigated diatomite bed in the Nakuru-Elmenteita basin is shown in Figure 7.5b, together with the lithological facies and sedimentological characteristics of the profile identified by A. Bergner (pers. comm.). The diatom assemblage data from this deposit, which were also produced by A. Bergner (University of Potsdam), are plotted in Figure 7.7. The diatomite bed is underlain by a layer of brown sand, which rapidly grades into grey-coloured diatomite with a relatively high clastic component. The bed itself is pure, white diatomite, containing over 95% diatom valves, but the amount of clastic debris present increases from the base to the top of the deposit. A tuff layer up to 3 cm thick intercalates the diatomite 270 cm above the base of the bed. The deposit is laminated above ~130 cm but, unfortunately, commercial activity at the site prevented detailed stratigraphic analysis of the section below this level. From ~360 cm above the base of the bed, the diatomite grades into diatomaceous silt, and this layer, in turn, is overlain by massive pyroclastic deposits.

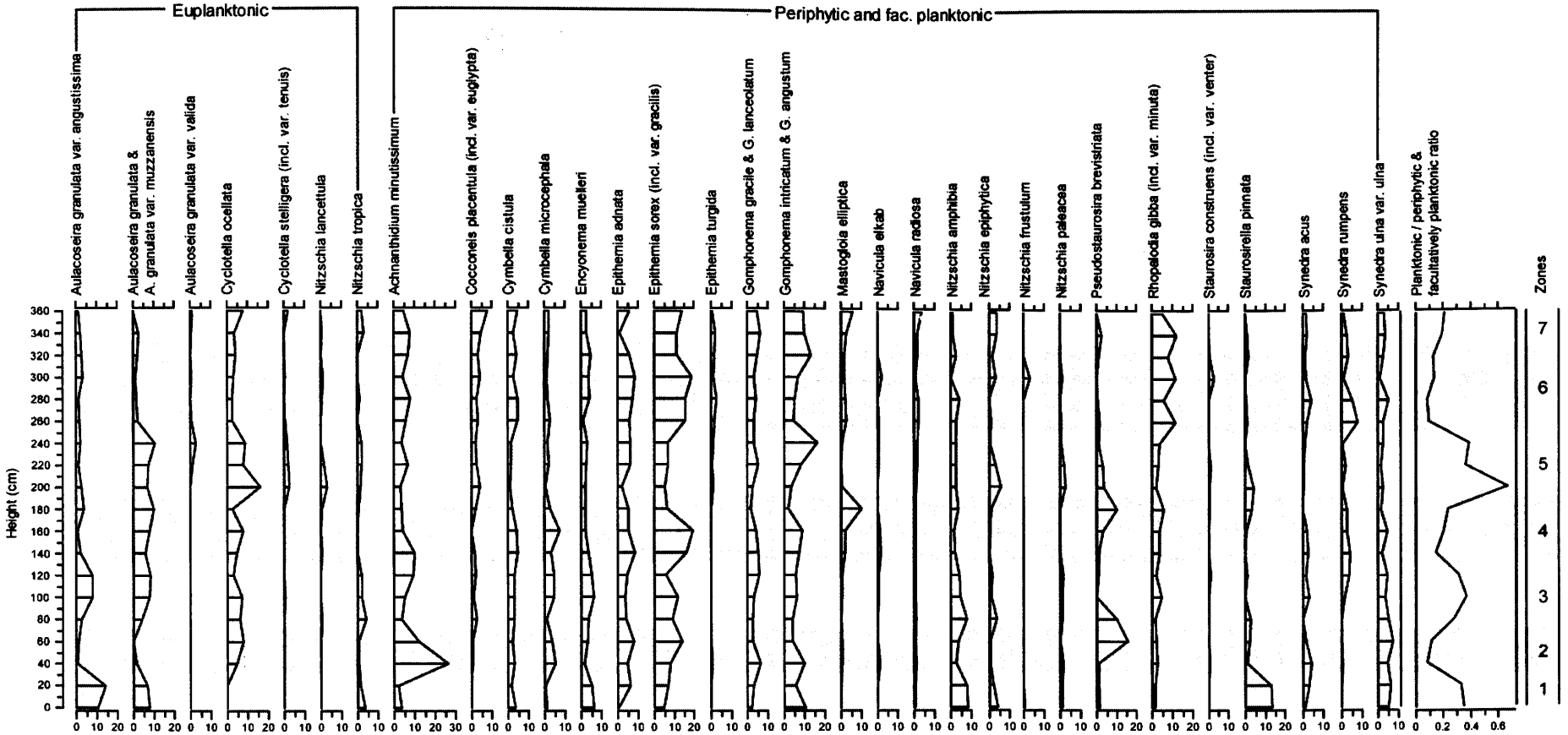

Figure 7.7: Records of the percentage frequency of diatom taxa with a maximum occurrence >2%, and the ratio of planktonic to facultatively planktonic and periphytic taxa from the profile exposed in the Nakuru-Elmenteita basin. Data provided by A. Bergner (University of Potsdam).

The $\delta^{18}O_{diatom}$, sedimentological, and diatom assemblage records from the profile allow seven stratigraphic zones to be defined (Figs. 7.5b and 7.7). Zone 1 (base to 30 cm) contains a relatively high proportion of the planktonic diatoms *Aulacoseira granulata*, *A. granulata* var. *muzzanensis*, and *A. granulata* var. *angustissima*, but a number of facultatively planktonic and periphytic taxa, including *Staurosirella pinnata* and *Nitzschia amphibia*, are also abundant. The amount of clastic material is low in this zone, and $\delta^{18}O_{diatom}$ decreases from +41.8‰ to +40.6‰. In zone 2 (30 to 70 cm), the relative abundance of *A. granulata* and its varieties decreases, while the frequencies of the periphytic taxa *Achnanthidium minutissimum*, *Cymbella microcephala*, and *Epithemia sorex*, the facultatively planktonic species *Pseudostaurosira brevistriata*, and the planktonic species *Cyclotella ocellata* all increase. *Mastogloia elliptica* and *Navicula elkab,* which are associated with brackish water, also appear in this zone, but $\delta^{18}O_{diatom}$ continues to decrease, reaching +39.2‰, the lowest value in the record, at 60 cm.

In zone 3 of the profile (70 to 130 cm), the proportion of the planktonic taxa *A. granulata* and its varieties and *Nitzschia tropica* increases, while the relative abundance of *A. minutissimum* and *P. brevistriata* decreases, raising the ratio of planktonic to periphytic and facultatively planktonic diatoms. $\delta^{18}O_{diatom}$ remains at about +41.0‰ in this section of the profile, before rising to +41.7‰ at 160 cm in zone 4 (130 to 190 cm). The proportion of periphytic taxa such as *E. sorex* and *M. elliptica* increases in this zone, while the abundance of the planktonic taxa *N. tropica* and *A. granulata* var. *angustissima* decreases, reducing the ratio of planktonic to periphytic and facultatively planktonic diatoms. In zone 5 (190 to 250 cm), the relative abundance of planktonic *Nitzschia* spp., *C. ocellata*, and *Cyclotella stelligera* all increase, significantly increasing the ratio of planktonic to periphytic and facultatively planktonic species. $\delta^{18}O_{diatom}$ decreases by almost 2‰ in this zone, reaching +39.4‰ at 220 cm.

The proportion of planktonic species decreases in zone 6 (250 to 330 cm), as the relative abundance of periphytic diatoms such as *Cymbella cistula* and *E. sorex* increases. In particular, the fraction of periphytic diatoms associated with brackish water, such as *M. elliptica*, *Nitzschia frustulum,* and *Rhopalodia gibba*, increases in this zone. $\delta^{18}O_{diatom}$ also increases in this section of the profile, reaching +41.3‰ at

300 cm, and clastic material becomes more abundant. At the top of the sequence, in zone 7 (330 to 360 cm), the proportion of planktonic species such as *C. ocellata* and *N. tropica* increases slightly, and $\delta^{18}O_{diatom}$ decreases to +40.1‰. Unfortunately, the increasing abundance of clastic material prevents biological and isotopic analysis above this level.

7.5 Discussion

7.5.1 Lake-level reconstructions

The diatomite beds described in this study document a period in which deep, extensive lakes occupied the Naivasha and Nakuru-Elmenteita basins; a situation that contrasts with the presence of relatively small and shallow lakes in these basins today (cf. Trauth *et al.*, 2003; Bergner and Trauth, 2004). The thickness and purity of the beds make them unique amongst the late Pleistocene sediments in the two basins, and suggest that they were deposited during the longest and deepest late Pleistocene highstands of Lakes Naivasha and Nakuru-Elmenteita (cf. Trauth *et al.*, 2003). The $^{40}Ar/^{39}Ar$-age determinations from the profiles indicate that both highstands occurred close to the time of the last interglacial, which, combined with the striking similarity of the deposits in terms of their thickness and purity, suggests that the highstands documented by the two beds were contemporaneous. The records from the profiles thus allow the reconstruction of palaeohydrological conditions in the CKR during a period of unusually high lake levels.

The modern isotope hydrology of the lakes suggests that low $\delta^{18}O_{diatom}$ values are associated with high I/E ratios (section 7.4.1). The low $\delta^{18}O_{diatom}$ values in zones 1 and 3 of the profile from the Naivasha basin therefore indicate that the ratio of input to evaporative loss from Lake Naivasha was high at these times (Fig. 7.5a). This finding is supported by the presence of laminations and by the low concentrations of clastic particles, phytoliths, and sponge spicules in the sediments in these sections, as these features suggest that the sediments were deposited in a calm, deep-water environment (Bergner and Trauth, 2004). In zone 2, the peak in $\delta^{18}O_{diatom}$ (+32.0‰) at 147.5 cm indicates a decrease in the I/E ratio, which would have led to a significant, but temporary, shrinking of the lake. Similarly, the trend towards higher $\delta^{18}O_{diatom}$

values in zone 4 indicates that the I/E ratio decreased at this time; a shift that probably reflects a decrease in lake depth at the end of the highstand. The lack of laminations and the greater abundance of clastic debris, phytoliths, and sponge spicules in zones 2 and 4 also indicate that lake levels fell in these sections, as they suggest that deposition occurred in a shallow, near-shore environment (Bergner and Trauth, 2004).

The isotopic and sedimentological records from the profile thus give a coherent picture of palaeohydrological change during the lake-level highstand. There are, however, discrepancies between the lake levels reconstructed from these proxies and those inferred from the record of diatom assemblage composition (cf. Figure 7.6) (Bergner and Trauth, 2004). It is possible that these inconsistencies are due to changes in the lake's mixing regime, which can have a significant effect on diatom assemblage composition (*e.g.* Stager *et al.*, 1997). In zone 1, the isotope and sedimentological records suggest that the lake was deep and dilute, while the presence of taxa usually associated with shallow water, such as *A. minutissimum* (labelled *Achnanthes minutissima* in Figure 7.6), and high lake-water conductivity, such as *M. elliptica*, suggests that lake levels were low (Figs. 7.5a and 7.6) (Bergner and Trauth, 2004). The presence of laminations in this section indicates that the lake was stratified at this time, and it is possible that the low turbulence and epilimnetic nutrient depletion associated with this mixing regime prevented the growth of planktonic diatoms that are associated with low lake-water conductivity, such as *A. granulata* (Talling, 1966; Kilham *et al.*, 1986; Stager *et al.*, 1997). This scenario could lead to erroneously high diatom-inferred conductivity values, and might therefore explain the difference between the two reconstructions. Similarly, low diatom-inferred conductivity values in zone 4 contrast with the low lake levels inferred from the isotope and sedimentological records, but it is possible that holomixis of the lake allowed planktonic diatoms such as *A. granulata* to thrive, despite slightly higher lake-water conductivity at this time.

The records from the diatomite bed in the Nakuru-Elmenteita basin allow palaeohydrological conditions to be reconstructed in this basin (Figs. 7.5b and 7.7). The decrease in $\delta^{18}O_{diatom}$ in zone 1 suggests that lake levels increased at this time, which is in agreement with the relatively high ratio of planktonic to periphytic and

facultatively planktonic diatoms, good diatom preservation, and the rare occurrence of clastic particles. The most abundant diatom taxa in this zone are varieties of *A. granulata*, which require turbulent conditions and are often found in shallow, alkaline, eutrophic lakes, and *S. pinnata*, which is often associated with shallow water and the colonisation of new habitats (*e.g.* Brugam, 1983; Stoermer, 1993; Schmidt *et al.*, 2004; Metcalfe, pers. comm.). It is therefore likely that the diatom assemblage in this zone reflects the transgression of the lake over the site and is indicative of well-mixed, but fairly shallow conditions.

The low $\delta^{18}O_{diatom}$ values in zone 2 indicate that the I/E ratio was high at this time, but the ratio of planktonic to periphytic and facultatively planktonic diatoms decreases in this zone, suggesting that lake levels decreased. The change in this ratio is driven by an increase in the relative abundance of *A. minutissimum* and *P. brevistriata*, and by a decrease in the relative abundance of *A. granulata* and its varieties, but is also accompanied by a decrease in the percentage frequency of *S. pinnata* and an increase in the proportion of *C. ocellata*. These changes hint that lake levels may have increased slightly in this zone, because *C. ocellata* is often associated with deeper water than *A. granulata* and its varieties, and *P. brevistriata* may reflect deeper water than *S. pinnata* (cf. Brugam, 1983; Stoermer, 1993; Schmidt *et al.*, 2004). The increase in the frequency of the periphytic species *A. minutissimum* may thus reflect an increase in the abundance of macrophytes as the lake expanded across the flat graben floor, rather than a decrease in lake depth.

Above 70 cm (zones 3-7), the lake-level changes inferred from the $\delta^{18}O_{diatom}$, diatom assemblage, and sedimentological records are in close agreement. In zone 3, $\delta^{18}O_{diatom}$ remains around +40.5‰, indicating a fairly high I/E ratio, and thus relatively high lake levels, and this interpretation is supported by an increase in the ratio of planktonic to periphytic and facultatively planktonic diatoms. In zone 4, $\delta^{18}O_{diatom}$ increases to +41.7‰ at 160 cm, suggesting that lake levels fell. This finding is supported by an increase in the proportion of periphytic diatoms, and by an increase in the abundance of species associated with brackish conditions, such as *M. elliptica* and *N. elkab*. In zone 5, the decrease in $\delta^{18}O_{diatom}$ and the significant increase in the ratio of planktonic to periphytic and facultatively planktonic diatoms suggest that lake levels increased in this section. In zone 6, $\delta^{18}O_{diatom}$ increases and the ratio of

planktonic to periphytic and facultatively planktonic diatoms decreases, suggesting a significant regression of the lake. These changes are accompanied by an increase in the abundance of *R. gibba, E. sorex*, and *N. elkab*, which are indicative of brackish and alkaline conditions. There is also an increase in the amount of clastic debris in the sediments, which suggests that the diatomite was probably deposited in a near-shore environment. Finally, $\delta^{18}O_{diatom}$ decreases by almost 2‰, and the ratio of planktonic to periphytic and facultatively planktonic diatoms increases slightly in zone 7, suggesting that there was a small rise in lake level. The amount of clastic debris in the samples remains high and diatom preservation is poor in this part of the profile, however, indicating that the sediments were deposited close to the shore of the lake, and thus that the transgression was less significant than those in zones 2-3 and zone 5.

The timing of these lake-level fluctuations can be estimated using the $^{40}Ar/^{39}Ar$-age determinations from the two profiles. In the profile from the Naivasha basin, the average sedimentation rate between the two dated horizons is 0.16 mm yr^{-1} (Fig. 7.5a) (Bergner and Trauth, 2004). This rate is similar to rates of diatomite deposition observed in other lakes (cf. Einsele, 2000), and a tentative chronology for the bed was therefore constructed by extrapolating this rate to the rest of the profile (dark grey line in Fig. 7.8). According to this model, the peaks in lake level at ~50 and ~230 cm (zones 1 and 3) were centred on ~143 and ~133 kyr B.P., the decrease in lake level at ~150 cm (zone 2) was centred on ~138 kyr B.P., and the lake-level highstand ended at ~126 kyr B.P. (Fig. 7.8).

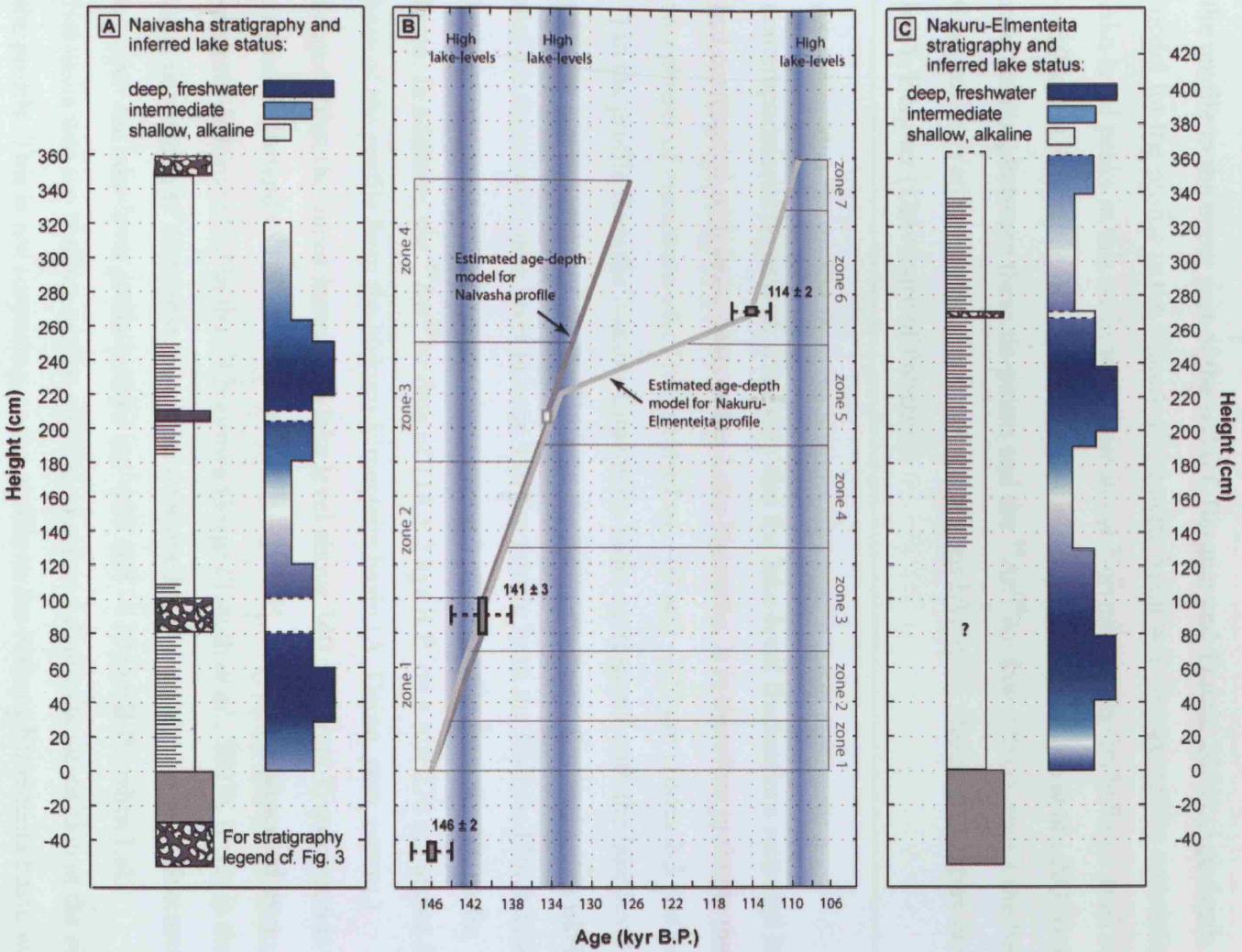

Figure 7.8: See following page for caption.

Figure 7.8: Tentative age-depth models for the diatomite beds, showing lithological facies and schematic lake-level reconstructions from (A) the Naivasha and (C) the Nakuru-Elmenteita basins, as well as estimated age-depth models for both profiles (B). Age-depth model for the profile in the Naivasha basin was constructed by extrapolating the rate of sediment deposition between the $^{40}Ar/^{39}Ar$ ages at the base of the profile to the upper part of the bed (cf. Bergner and Trauth, 2004). Age-depth model for the profile in the Nakuru-Elmenteita basin was constructed by correlating lake-level peaks in this basin with those in the Naivasha basin (including a peak at ~110 kyr B.P. documented by a different diatomite bed (cf. Trauth *et al.*, 2003)), and interpolating between these tie-points and the $^{40}Ar/^{39}Ar$ date 270 cm above the base of this profile. Vertical bars indicate periods of high lake level. Based on a figure created by A. Bergner (University of Potsdam).

Assuming that the profile from the Nakuru-Elmenteita basin represents a contemporaneous highstand, it is likely that the lake-level fluctuations recorded in this bed correspond with those observed in Lake Naivasha. It is therefore probable that the two phases of maximum lake level centred on ~60 and ~220 cm (zones 2-3 and zone 5) in the profile from the Nakuru-Elmenteita basin correspond with the lake-level peaks in zones 1 and 3 of the profile from the Naivasha basin. Similarly, it is likely that the decrease in lake level in zone 4 of the profile from the Nakuru-Elmenteita basin corresponds with the regression in zone 2 of the profile from the Naivasha basin. In addition, the $^{40}Ar/^{39}Ar$ date of 114 ± 2 kyr B.P. on a tuff 270 cm above the base of the profile from the Nakuru-Elmenteita basin (A. Deino, pers. comm.) suggests that the minor increase in lake level above 340 cm (zone 7) corresponds with a minor highstand of Lake Naivasha at ~110 kyr B.P., which is represented by a separate diatomite bed in the Ol Njorowa Gorge (Trauth *et al.*, 2003). If this is the case, deposition of diatomite must have continued in Palaeolake Nakuru-Elmenteita between the lake-level peaks centred on ~133 and ~110 kyr B.P., when Lake Naivasha was too shallow and/or alkaline to support diatomite deposition at the site of the profile. This is not surprising, as the profile in the Nakuru-Elmenteita basin was deposited close to the centre of the palaeo-lake, while the profile from the Naivasha basin was deposited at the edge of Lake Naivasha (Fig. 7.1).

It is therefore likely that the peaks in the level of Palaeolake Nakuru-Elmenteita at ~60, ~220 and ~350 cm correspond with the peaks in the level of Lake Naivasha at ~143, ~133 and ~110 kyr B.P., and a tentative age-depth model can thus be constructed for the profile from the Nakuru-Elmenteita basin by interpolating between these tie-points and the $^{40}Ar/^{39}Ar$ date of 114 ± 2 kyr B.P. (light grey line in Fig. 7.8). This model suggests that the sedimentation rate in the Nakuru-Elmenteita basin was similar to that in the Naivasha basin in the lower part of the profile, but that it changed significantly in the upper part (Fig. 7.8). Such changes in sedimentation rate are not implausible, given the changes in lake depth in this part of the record, and the fact that sedimentation rates often vary substantially in diatomite beds (cf. Smol *et al.*, 2001). It is unlikely that the changes in deposition rate occurred exactly at the depths marked in Figure 7.8, however, and further age-determinations are therefore required to improve this age-depth model.

It should be noted that these interpretations are subject to a number of assumptions. In particular, it is possible that dissolution and/or diagenesis altered diatom assemblage composition and/or $\delta^{18}O_{diatom}$ values, either during deposition of the diatom valves, or after subaerial exposure of the profiles (sections 2.4 and 6.2). This is a particularly important consideration in this study because diatom valves may have been exposed to percolating groundwater and, in the case of the profile from the Ol Njorowa Gorge, to hydrothermal groundwater (cf. Darling *et al.*, 1990, 1996). It is unlikely that these factors are significant sources of error, however, because the diatom valves are generally well-preserved (Bergner, pers. comm.), and because diagenesis during subaerial exposure might be expected to homogenise the isotope signal from the profiles, which does not appear to have occurred. The possibility that these processes affected diatom assemblage composition and/or $\delta^{18}O_{diatom}$ values cannot, however, be ruled out.

It is also possible that the $\delta^{18}O_{diatom}$ records were influenced by changes in the season of maximum diatom productivity, as changes in the time of year at which most diatom valves form may influence $\delta^{18}O_{diatom}$ independently of changes in the average $\delta^{18}O$ and temperature of lake water (section 2.4). Seasonality usually plays a relatively minor role in diatom growth in low-latitude lakes, because high temperatures and nutrient availability often encourage growth throughout the year (Lewis, 1996). This

is likely to be the case in Lakes Naivasha, Nakuru, and Elmenteita today, as the lakes are polymictic, circulating completely when wind speeds increase in the afternoon (Melack and Kilham 1974; Melack, 1979; Vareschi, 1982; Verschuren, 1999b; Hubble and Harper, 2002). The lakes may have been up to ~150 m deep during the highstand considered here, however, and it is therefore likely that they were either permanently stratified, or mono- or dimictic at this time (Talling, 1986; Lewis, 1996; Bergner and Trauth, 2004). This proposal is supported by the presence of laminations in sections of the sediments (Fig. 7.5). If the lakes were mono- or dimictic, diatom productivity may have peaked during overturn, when nutrients are brought into the photic zone. The $\delta^{18}O_{diatom}$ records may therefore be biased towards the $\delta^{18}O$ and temperature of lake water during the drier months of the year, when deep tropical lakes tend to experience overturn (Lewis, 1996). This bias would only introduce error into the $\delta^{18}O_{diatom}$ records if the season of maximum productivity changed over the course of the profiles, and if the effects of such changes out-weighted the effects of variations in the I/E ratio of the lake. This scenario seems unlikely, particularly as any change in mixing regime is likely to have been stimulated by a change in I/E ratio.

Finally, tephra deposition may have influenced diatom assemblage composition and/or $\delta^{18}O_{diatom}$ values independently of palaeohydrological change. Deposition of tephra can influence diatom assemblage composition by changing the nutrient balance of the lake (by reducing the release of P from lake sediments or increasing Si concentration in the lake water), changing habitat availability (by altering basin bathymetry, increasing surface availability for epipelic or episammic diatoms, or killing macrophytes), reducing light availability, or altering lake-water pH (cf. Telford *et al.*, 2004a). These effects can be particularly important in small lakes, where nutrient cycling is dominated by within-lake processes (Barker *et al.*, 2000). The diatom records from the profiles do not show any evidence of changes in assemblage composition after tephra deposition, however, which is probably because the lakes were large, and the addition of tephra therefore had negligible effects on lake-water chemistry and habitat availability (Figs. 7.6 and 7.7). Furthermore, any changes that did occur were probably too short-lived to be detected in the records presented here, as most tephra-deposition events only affect diatom assemblage composition for decades to centuries (cf. Barker *et al.*, 2000; Telford *et al.*, 2004a). Theoretically, dissolution of tephra deposited in lakes can also affect $\delta^{18}O_{diatom}$ values, because the

$\delta^{18}O$ of orthosilicic acid released from the tephra affects the $\delta^{18}O$ of the orthosilicic acid reservoir in the lake. This effect is probably negligible, however, because there is rapid isotope exchange between aqueous orthosilicic acid and water, and the majority of oxygen atoms in the orthosilicic acid-water system are from water molecules (Felipe *et al.*, 2004). This proposal is supported by the fact that the $\delta^{18}O_{diatom}$ records do not appear to change in response to tephra deposition (Fig. 7.5).

7.5.2 Palaeohydrological and palaeoclimatic interpretations

Comparison of the diatomite profiles from the Naivasha and Nakuru-Elmenteita basins provides a regional picture of palaeohydrological conditions in the CKR, from which it is possible to infer palaeoclimatic conditions during the late Pleistocene. The $\delta^{18}O_{diatom}$ values from the two profiles are significantly different, with values from Palaeolake Nakuru-Elmenteita, on average, 10‰ higher than those from Lake Naivasha. The fact that the diatom taxa in the two profiles are similar precludes the possibility that this offset is caused by species-specific fractionation, and it must therefore reflect differences in the $\delta^{18}O$ values of the two lakes, which are currently determined by their I/E ratios. An offset of this magnitude is certainly plausible, given that the spot samples of modern water analysed in this study indicate that the $\delta^{18}O$ of Lake Nakuru is up to 5.5‰ higher than that of Lake Naivasha, and that Allen *et al.* (1989) found an offset of 10‰ between the $\delta^{18}O$ values of these lakes in the late 1980s (Fig. 7.4).

The magnitude of the difference in the $\delta^{18}O$ composition of the two lakes during the late Pleistocene demonstrates that seepage of groundwater from Lake Naivasha into the Nakuru-Elmenteita basin was not large enough to cause a significant decrease in the $\delta^{18}O$ of Palaeolake Nakuru-Elmenteita (cf. Figure 7.1d). This finding counters the suggestion that subsurface flow from Lake Naivasha significantly increased the depth of Palaeolake Nakuru-Elmenteita during an early-Holocene highstand of the two lakes (Hastenrath and Kutzbach, 1983; Dühnforth *et al.*, in prep.). Furthermore, the finding that the two basins were not linked by large volumes of subsurface flow also indicates that the lakes would have responded to palaeoclimatic change independently of one another, and thus allows lake-level fluctuations in the two basins to be interpreted in terms of regional climatic change.

Assuming that the chronologies of the two profiles are relatively accurate, it is possible to speculate about the causes of the lake-level changes observed. The timing of the lake-level peaks suggests that they correspond with peaks in insolation received on the equator during March and September at ~144, ~133, and ~110 kyr B.P. (Fig. 7.9). This correspondence provides support for the proposal that precessionally-driven changes in insolation affect the amount of precipitation in the CKR by influencing the intensity of convection at the ITCZ (Trauth *et al.*, 2001; Trauth *et al.*, 2003) (chapter 1). A peak in September insolation at ~121 kyr B.P. does not appear to be accompanied by an increase in lake level in either basin, however, and this discrepancy must be explained before the proposal that precessionally-driven changes in insolation affect precipitation in the CKR can be fully accepted.

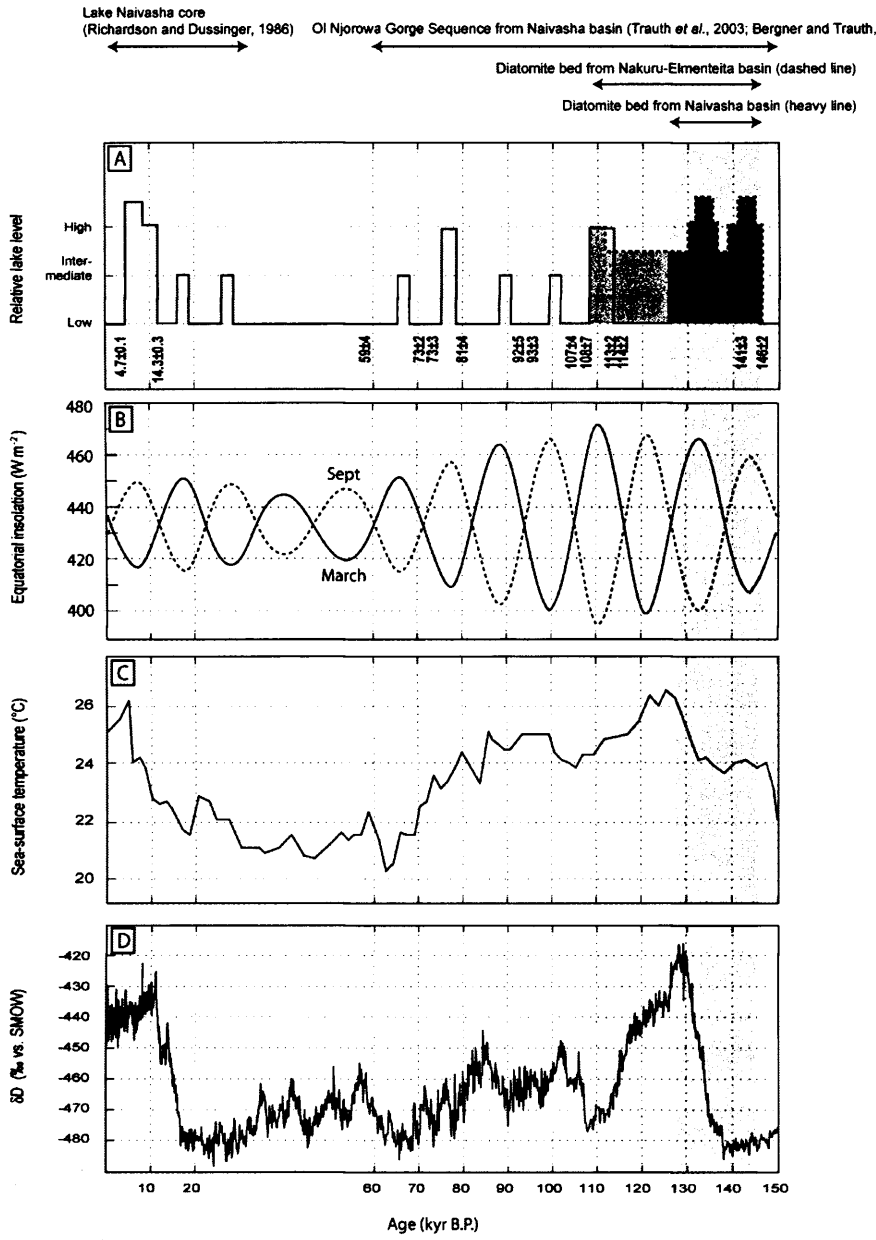

Figure 7.9: Lake-level change in the CKR compared to changes in insolation at the equator and global boundary conditions, showing (A) lake-level change in the Naivasha (heavy line) and Nakuru-Elmenteita (dashed line) basins reconstructed in this study (also marked by vertical grey bars), and lake-level changes in the Naivasha basin over the last 150 kyr reconstructed by Richardson and Dussinger (1986), Trauth *et al.* (2003), and Bergner and Trauth (2004), (B) insolation on the equator during March and September (Berger and Loutre, 1991), (C) SSTs in the eastern tropical Atlantic Ocean reconstructed using alkenones from marine core GeoB 1016-3 (Müller *et al.*, 1994), and (D) deuterium value of ice from Vostok, Antarctica, as a proxy for atmospheric temperature (Petit *et al.*, 1999). Based on Figure 8 in Bergner and Trauth (2004).

The observation that lakes in the CKR were probably deeper and more dilute during the period covered by the diatomite beds analysed in this study than at any other time during the last 150 kyr apart from the early Holocene also provides support for the proposal that high SSTs during the last interglacial increased precipitation in the CKR by enhancing lateral transport of moisture into East Africa (Fig. 7.9) (Trauth *et al.*, 2003). Feedbacks caused by changes in soil moisture and vegetation may have also helped to maintain high lake levels during this highstand (cf. Kutzbach *et al.*, 1996; Bergner *et al.*, 2003). Uncertainties remain in the exact timing of the lake-level fluctuations, but it is notable that the proposed increase in lake levels at ~146 kyr B.P. is several thousand years earlier than the transition from MIS 6 to MIS 5e (*e.g.* Martinson *et al.*, 1987; Henderson and Slowey, 2000). This date corresponds with the time at which alkenone-derived estimates of SST indicate that temperatures began to rise in the equatorial Atlantic Ocean and the Arabian Sea, however, suggesting that these changes may have contributed to the substantial increase in lake levels in the CKR at this time (Fig. 7.9) (Müller *et al.*, 1994; Schneider *et al.*, 1996, 1999; Rostek *et al.*, 1997). Furthermore, it is possible that the low SSTs in the equatorial Atlantic Ocean and southeast Arabian Sea between ~30 and 60 kyr B.P., combined with the low amplitude of peaks in insolation, account for the absence of evidence of lake-level highstands in the CKR at this time (Fig. 7.9) (Müller *et al.*, 1994; Rostek *et al.*, 1997).

7.6 Conclusions

Diatomite beds deposited in the Naivasha and Nakuru-Elmenteita basins between ~110 and ~146 kyr B.P. document a period in which deep, dilute lakes existed in the CKR. Lakes of comparable extent existed in the two basins during the early Holocene, but these highstands are otherwise unparalleled over the last 150 kyr (Richardson and Dussinger, 1986; Trauth *et al.*, 2003). The records of lake-level change from the profiles thus provide insights into palaeohydrological and palaeoclimatic conditions in the CKR during a period of unusually high lake levels.

A significant offset in the $\delta^{18}O_{diatom}$ values from the two profiles indicates that Palaeolake Nakuru-Elmenteita was subject to greater evaporative enrichment than Lake Naivasha during the highstand. This situation also exists today, and can be

explained by the fact that the Nakuru-Elmenteita basin is smaller and lower than the Naivasha basin, and does not lose water through groundwater seepage. The magnitude of the offset demonstrates that the lakes were not linked by significant volumes of sub-surface flow at this time, and it is therefore likely that they responded independently to climatic forcing. The lake-level fluctuations recorded in the two diatomite beds can therefore be interpreted in terms of regional palaeoclimatic change.

Age-depth models for the two profiles constructed using the $^{40}Ar/^{39}Ar$ dates from the beds and by correlating lake-level maxima in the two basins suggest that lake levels peaked in the CKR at ~143, ~133, and ~110 kyr B.P. These increases correspond with peaks in March and September insolation on the equator, and thus provide support for the proposal that precessionally-driven changes in insolation influenced precipitation in East Africa by affecting the intensity of convection at the ITCZ (Kutzbach, 1981; Kutzbach and Street-Perrott, 1985), although the observation that lake levels did not increase during a peak in September insolation ~121 kyr B.P. requires further explanation. The unusual length and magnitude of the reconstructed highstand also supports the suggestion that high tropical SSTs during the last interglacial increased precipitation in East Africa by enhancing lateral transport of moisture into the region (Trauth *et al.*, 2003).

The records presented in this chapter therefore support the suggestion that changes in both insolation at the equator and global boundary conditions associated with glacial-interglacial cycles affected precipitation in the CKR during the late Pleistocene (Trauth *et al.*, 2003). Further work is needed to resolve the uncertainties associated with these records, however. $\delta^{18}O_{diatom}$ analysis of the diatomite bed deposited in the Naivasha basin at ~110 kyr B.P. might confirm whether this deposit corresponds with the upper part of the bed deposited in the Nakuru-Elmenteita basin, and could provide further information about the nature and causes of palaeoclimatic change in the CKR at this time. $\delta^{18}O_{diatom}$ analysis of modern diatoms from Lakes Naivasha, Nakuru, and Elmenteita, and of diatom valves from the surface sediments of these lakes could also provide information about the factors that influence $\delta^{18}O_{diatom}$, and thus allow the $\delta^{18}O_{diatom}$ records to be interpreted with greater certainty. It might also be possible to produce pure diatom samples using SPLITT techniques, which would eliminate errors

associated with the use of a mass-balance approach to correct for the presence of contaminants, and thus improve the accuracy of the $\delta^{18}O_{diatom}$ records (Giddings, 1985; Leng and Barker, 2006). Finally, it might be possible to improve the chronological control of the diatomite beds using techniques such as electron-spin resonance dating, which theoretically allow diatom valves to be dated (cf. Blackwell, 2001b).

Chapter 8: Summary and conclusions

This thesis has presented new records of palaeoclimatic change from Tswaing crater lake in South Africa and from the Naivasha and Nakuru-Elmenteita basins in the CKR, as well as information about the modern environment necessary to interpret these records. This chapter summarises the findings from each site (sections 8.1 and 8.2), and then explores the implications of these results for our understanding of palaeoclimatic change in equatorial and southern Africa by placing them in the context of other palaeoclimatic records from these regions (section 8.3). Finally, this discussion is used to draw tentative conclusions about the factors that may have influenced climatic conditions south of the equator in Africa during the late Quaternary (section 8.4).

8.1 Tswaing crater lake

Tswaing crater lake currently provides the longest continuous terrestrial records of palaeoclimatic change in southern Africa. The record of MAP produced from the site by Partridge *et al.* (1997) indicates that precipitation varied in phase with precessionally-driven changes in summer insolation between ~50 and 200 kyr B.P., but that this relationship broke down after ~50 kyr B.P. due to the increasing dominance of regional or global influences (Fig. 5.1). The unique length and location of this record means that it has formed the basis of many reconstructions of palaeoclimatic change in southern Africa, despite its chronological uncertainty (*e.g.* Tyson *et al.*, 2001; Partridge *et al.*, 2004). This study aimed to improve the chronological control of the sedimentary sequence from the lake, and to provide further insights into the nature and causes of climatic change at the site by producing higher-resolution, multi-proxy records from newly-extracted sediment cores.

In order to allow the new palaeoclimatic records from the sequence to be interpreted accurately, the modern environment at the site was explored using stable isotope analysis of water, DIC, and organic matter (chapter 3). The δ^2H and $\delta^{18}O$ values of water samples, interpreted in the light of geochemical data, show that groundwater inputs to the lake reflect selective recharge of regional precipitation, and that the lake is almost certainly hydrologically closed. It is therefore likely that the I/E ratio of the

lake is the primary control on its volume and isotope composition. Moreover, the small, well-defined nature of the lake catchment means that these variables may be highly sensitive to changes in this ratio.

Stable isotope analysis of DIC revealed that the surface water of the lake has higher $\delta^{13}C_{DIC}$ than groundwater inputs. This finding is attributed to equilibration of DIC with atmospheric CO_2, high productivity in the lake, and the high pH of lake water (as this means that most DIC is in the form of bicarbonate and carbonate ions, which have higher $\delta^{13}C$ than dissolved CO_2). In addition, $\delta^{13}C_{DIC}$ is higher in the hypolimnion than the epilimnion of the lake, which suggests that methanogenesis is taking place in the lake sediments. It is therefore possible that these processes affected $\delta^{13}C_{DIC}$ in the past (chapter 3).

The C/N ratios of organic material from the site show that terrestrial and emergent plants have significantly higher C/N ratios than aquatic material. The C/N ratio of bulk organic matter in the lake sediments should therefore provide a reliable indication of its origin, assuming that diagenesis has not significantly altered this value. Stable isotope analysis revealed that the $\delta^{13}C$ of aquatic organic matter is unusually high, which is attributed to the high $\delta^{13}C_{DIC}$ of lake water, the use of bicarbonate as a source of inorganic carbon by aquatic organisms, the abundance of cyanobacteria in the lake, and reduced fractionation against ^{13}C under conditions of carbon limitation. In fact, the $\delta^{13}C$ of aquatic material appears to be higher than the average $\delta^{13}C$ of terrestrial and emergent vegetation in the catchment, which suggests that $\delta^{13}C_{organic}$ of the lake sediments could be affected by the proportion of material derived from these sources, although the $\delta^{13}C$ of both sources is likely to have changed in the past. Finally, the $\delta^{13}C$ and C/N ratios of organic matter in the surface sediments of the lake indicate that aquatic material currently dominates the organic matter deposited in the water body. Together, these observations provide an important basis from which to interpret palaeoenvironmental records from the site (chapter 3).

Partridge *et al.* (1997) constructed an age-depth model for the sedimentary sequence at the site by interpolating between seven radiocarbon dates in the upper 18 m of the sediments and extrapolating the average sedimentation rate in this section to the base of the sequence (Fig. 4.1). This model suggests that the base of the sequence was

deposited ~200 kyr B.P., and is therefore in agreement with a fission-track date of 220 ± 52 kyr B.P. for crater formation (Storzer *et al.*, 1993, 1999; Koeberl *et al.*, 1994). The confidence that can be placed in this model is limited by the lack of dates between 18 m and the base of the sediments, however. Five $^{230}Th/^{234}U$ dates on carbonate were therefore produced from the undated section of the sequence in this study, using TIMS analysis and the TSD isochron approach for correcting for the presence of detritus (chapter 4).

The new $^{230}Th/^{234}U$ dates appear to provide accurate, if relatively imprecise, indications of the age of the sediments deposited in the lake. They are therefore used, together with three new radiocarbon dates obtained by I. Kristen (GFZ, Potsdam), seven radiocarbon dates from a previous core, and an estimate of the age of the top of the sequence, to construct new age-depth models for the sediments (chapter 4). A cubic polynomial model fitted by non-weighted least-squares regression provides the best fit to the available dates, but the similarity of records from the sedimentary sequence to the deuterium record from the Vostok ice core (Petit *et al.*, 1999) suggests that a linear model fitted by non-weighted least-squares regression may provide the most accurate indication of sediment age (chapter 5). The linear model is therefore used to estimate the timing of palaeoclimatic change at the site, although further dating is required to confirm its accuracy. This model suggests that the sediments were deposited over the last ~350 kyr, which is significantly longer than the period of ~200 kyr suggested by Partridge *et al.* (1997).

Records of %LOI 550°C, %LOI 950°C, $\delta^{18}O_{calcite}$, $\delta^{13}C_{calcite}$, $\delta^{13}C_{organic}$, and C/N ratios of bulk organic matter from the newly extracted sediment cores provide important insights into the nature of palaeoenvironmental change at the site (chapter 5). Below 31 m, %LOI 950°C reflects the carbonate content of the sediment, which is determined by evaporative concentration of the lake water and therefore provides an indication of lake volume. Above 31 m, the interpretation of this record is complicated by the presence of halides and trona, carbonate dissolution, and authigenic carbonate precipitation, however. %LOI 550°C reflects the organic content of the sediment. Above 31 m and below 51 m, this proxy is determined by the amount of terrestrial and emergent vegetation carried into the lake, but between these depths the organic content of the sediment remains low, possibly due to decomposition of

organic matter before burial. The C/N ratios of bulk organic matter reflect the proportion of organic material derived from aquatic sources relative to that derived from terrestrial and emergent vegetation. Over much of the sequence, this ratio provides an indication of lake-level change, because it is determined by the area of the basin exposed to colonisation by terrestrial vegetation and/or the volume of the lake. $\delta^{13}C_{organic}$ also reflects this ratio, particularly above 31 m, where the $\delta^{13}C$ of aquatic material is significantly higher than that of terrestrial and emergent vegetation.

$\delta^{18}O_{calcite}$ and $\delta^{13}C_{calcite}$ appear to reflect the I/E ratio of the lake in most parts of the sequence, although this relationship is complicated by authigenic carbonate precipitation above 41.5 m (chapters 5 and 6). It is likely that the lake became semi-permanently stratified in response to a decrease in the I/E ratio at this level, and that anoxia therefore developed in the lake sediments. These conditions appear to have led to the onset of methanogenesis, which in turn induced authigenic carbonate precipitation from pore water. The $\delta^{13}C$ and $\delta^{18}O$ values of the authigenic carbonates are probably higher than those of endogenic carbonates because methanogenesis increased the $\delta^{13}C_{DIC}$ of pore water, and because the $\delta^{18}O$ of pore water was determined by the $\delta^{18}O$ of the isotopically-enriched hypolimnion. $\delta^{13}C_{calcite}$ and $\delta^{18}O_{calcite}$ are consequently high (up to +18.6‰ and +12.0‰, respectively) and sensitive to changes in the lake's mixing regime in this section, although they continue to respond to changes in the I/E ratio of the lake (chapters 5 and 6).

Records of diatom assemblage composition and the concentration of various siliceous microfossils from the section of the sedimentary sequence between 34.40 and 54.80 m provide further insights into the nature of palaeohydrological change at the site (chapter 6). This part of the sequence was originally chosen for diatom assemblage analysis because it was thought to cover the last interglacial, and because diatom valves are well-preserved and responsive to palaeohydrological change in this section (Metcalfe, 1993, 1999). In fact, the new chronology suggests that the section analysed covers the period between ~150 and ~250 kyr B.P., but the records nevertheless provide useful insights into the nature of environmental change at this time and, in particular, resolve a number of inconsistencies between the sedimentological and geochemical records from this section of the sequence (chapter 6).

Overall, the records of diatom assemblage composition and siliceous microfossil concentrations provide strong support for the interpretations of the sedimentary and geochemical records outlined above. In particular, they confirm the proposals that %LOI 950°C reflects the concentration of lake water, that increasing C/N ratios indicate falling lake levels, and that $\delta^{18}O_{calcite}$ and $\delta^{13}C_{calcite}$ reflect the I/E ratio of the lake in some parts of the sequence. The records also indicate that rapid calcite precipitation probably caused non-equilibrium fractionation of oxygen and carbon isotopes between ~46.5 and 51.0 m, and support the suggestion that methanogenesis induced authigenic carbonate precipitation above 41.5 m, thereby explaining anomalous $\delta^{18}O_{calcite}$ and $\delta^{13}C_{calcite}$ values in these sections. In some parts of the sequence, the record of diatom assemblage composition appears to be insensitive to changes in palaeohydrological conditions, however, highlighting the importance of a multi-proxy approach to palaeoenvironmental reconstruction (chapter 6).

When interpreted in terms of the new chronology for the sedimentary sequence, the new records from Tswaing crater lake provide a number of insights into the nature and causes of palaeoclimatic change at the site (chapter 5). Over the last 150 kyr, the records indicate that palaeohydrological conditions were determined by global boundary conditions associated with glacial-interglacial cycles, with lake levels rising during glacials and stadials, and falling during interglacials and interstadials. In particular, the records indicate that lake levels were high during the LGM, fell significantly during the early Holocene, and rose slightly during the second half of the Holocene. Lake levels were also high during MISs 6 and 5d, but decreased significantly during MIS 5e.

It is likely that these lake-level fluctuations were partly driven by changes in evaporation associated with changes in atmospheric temperature, but it is improbable that evaporation alone was responsible for the fluctuations observed. It is therefore proposed that precipitation also varied in response to glacial-interglacial cycles. The most likely explanations for an increase in precipitation at the site during glacials and stadials are: an equator-ward shift and increase in the strength of the circum-polar westerlies in response to an increase in the meridional temperature gradient (Van Zinderen Bakker, 1967, 1976); a pole-ward shift of the ITCZ in response to a decrease in the hemispheric disparity of the meridional temperature gradient (van Zinderen-

Bakker, 1967, 1976; Butzer *et al.*, 1973, 1978; Lancaster, 1979); or an increase in the intensity and frequency of TTT-formation over southern Africa in response to an increase in the strength of, and latitudinal shifts in, the circum-polar westerlies and the tropical easterlies, an increase in the intensity of the SIA, and low SSTs in the equatorial Indian Ocean (cf. Tyson, 1986; Cockroft *et al.*, 1987) (chapter 5).

The suggestion that an equator-ward shift of the circum-polar westerlies increased precipitation at Tswaing during glacials is countered by records of the location of the STF (*e.g.* Howard and Prell, 1992; Brathauer and Abelmann, 1999), and by pollen-based records of moisture availability in southwest Africa (Shi and Dupont, 1997; Shi *et al.*, 1998, 2000; Dupont and Wyputta, 2003), which both indicate that the westerlies did not move as far north as Tswaing during glacials (section 5.6.1.2). Similarly, the proposal that a pole-ward shift of the ITCZ increased precipitation at Tswaing during glacials is countered by the observation that precipitation decreased at some sites north of Tswaing during the LGM (cf. Munyikwa, 2005), and by the fact that records from South America indicate that the position of the ITCZ is primarily determined by the strength of precessionally-driven changes in insolation (*e.g.* Haug *et al.*, 2001; Cruz *et al.*, 2005) (section 5.6.1.2).

In contrast, the proposal that changes in the intensity and frequency of TTT-formation over southern Africa were responsible for the changes in precipitation observed at Tswaing fits much of the available palaeoclimatic evidence. In particular, an increase in the frequency of TTT-formation over southern Africa during the LGM could explain low moisture availability in Madagascar (Gasse and van Campo, 1998, 2001) and spatial variation of moisture availability in southern Africa (*e.g.* Brook *et al.*, 1998; Munyikwa, 2005). This explanation is also consistent with the observation that conditions were dry in tropical East Africa during the LGM (Barker and Gasse, 2003), as TTTs are partly responsible for the anti-correlation of precipitation in these areas on annual timescales today (Goddard and Graham, 1999). It is therefore suggested that changes in the intensity and frequency of TTT-formation over southern Africa may have determined changes in precipitation at the site over the last ~150 kyr.

Before ~150 kyr B.P., the records from Tswaing suggest that precipitation was affected by changes in the obliquity of the earth's axis (chapter 5). This aspect of the

earth's orbital configuration is most likely to have affected precipitation at the site via its influence on the meridional temperature gradient, which may have affected the strength and location of the circum-polar westerlies (cf. Rind, 1998, 2000). If this was the case, the reason that the obliquity of the earth's axis directly influenced climatic conditions at the site before ~150 kyr B.P., but not between ~150 kyr B.P. and the present, needs to be determined. It is possible that changes in atmospheric temperature dominated the hydrological balance of the lake after 150 kyr B.P. because infilling of the basin increased the lake's surface-area to volume ratio and thereby made it more sensitive to changes in evaporation after this date. It is also possible that the more northerly location of the STF before ~150-200 kyr B.P. made climatic conditions at Tswaing more sensitive to changes in the position of the mid-latitude westerlies (Rau *et al.*, 2002; West *et al.*, 2004). The lack of long records of climatic change from ~25°S makes it difficult to assess the validity of these hypotheses, however, and the suggestion that the obliquity of the earth's axis influenced climatic conditions in southern Africa before 150 kyr B.P. therefore remains highly speculative.

The uncertainty associated with the chronology of the records from Tswaing crater lake means that many of the findings presented in this thesis, particularly those related to climatic change before 150 kyr B.P., remain tentative. This uncertainty is increased by the fact that the timing of lake-level changes at the site proposed by Partridge *et al.* (1997, 1999) supports the hypothesis that precipitation in tropical and subtropical regions is determined by direct insolation (Fig. 5.1) (Kutzbach, 1981; Kutzbach and Street-Perrott, 1985). Further work is therefore required to improve the chronological control of the sedimentary sequence, and to thereby determine whether the age-depth model presented in this thesis is more accurate than that presented by Partridge *et al.* (1997). In particular, $^{40}Ar/^{39}Ar$ dating of impact glass might provide a more accurate estimate of the date of crater formation, and thus provide a maximum age for sediments at the base of the sequence (cf. McDougall and Harrison, 1999).

8.2 Central Kenya Rift

Diatomite beds deposited in lakes in the CKR during lake-level highstands offer the opportunity to reconstruct palaeohydrological change in this region on sub-orbital timescales (cf. Bergner and Trauth, 2004). The number of palaeoenvironmental

proxies available from diatomite beds is limited, but the material is ideally suited for $\delta^{18}O_{diatom}$ analysis. $\delta^{18}O_{diatom}$ records were therefore produced from diatomite beds deposited in Lake Naivasha and Palaeolake Nakuru-Elmenteita during a lake-level highstand at the time of the last interglacial, with the aim of reconstructing palaeohydrological change at this time (chapter 7).

The $\delta^{2}H$ and $\delta^{18}O$ values of water samples from Lakes Naivasha, Nakuru, and Elmenteita demonstrate that the lakes are subject to significant evaporation, and thus suggest that the ratio of lake-water input to evaporative output is the dominant control on their isotope composition. A significant offset in the $\delta^{18}O_{diatom}$ values of the diatomite beds from the Naivasha and Nakuru-Elmenteita basins is therefore attributed to the different I/E ratios of Lakes Naivasha and Nakuru-Elmenteita, which were determined by their topographical and hydrological settings. The offset suggests that there was little subsurface flow between the lakes during the highstand, and thus allows records from the two basins to be interpreted independently, in terms of regional climatic change. This finding brings into question the proposal, based on palaeohydrological modelling, that there was significant sub-surface flow from Lake Naivasha into Lake Nakuru-Elmenteita during other lake-level highstands (Hastenrath and Kutzbach, 1983; Dühnforth *et al.*, in prep.).

The $\delta^{18}O_{diatom}$ records indicate that there were significant changes in the I/E ratios of Lakes Naivasha and Nakuru-Elmenteita during the period covered by the diatomite beds. These changes, when considered in conjunction with sedimentological and diatom assemblage records produced from the beds by A. Bergner (University of Potsdam), allow lake levels to be reconstructed in the two basins. The $^{40}Ar/^{39}Ar$ dates from the profiles suggest that high lake levels correspond with peaks in insolation on the equator in March and September. It is therefore proposed that precessionally-driven changes in insolation increased precipitation in the region by increasing the intensity of convection at the ITCZ, although it is notable that a peak in September insolation at ~121 kyr B.P. is not accompanied by an increase in reconstructed lake levels. The unusual magnitude and length of the reconstructed highstand also suggests that high tropical SSTs increased precipitation in East Africa during the last interglacial by enhancing lateral transport of moisture into the region (Trauth *et al.*, 2003). The records therefore suggest that both equatorial insolation and global

boundary conditions affected hydrological conditions in the CKR during the late Pleistocene (chapter 7).

The certainty of these conclusions is limited by the poor chronological control of the diatomite beds. $^{40}Ar/^{39}Ar$ dating can only be applied to the tephra deposits in the profiles, and methods for dating the diatomite directly, such as electron-spin resonance dating, therefore need to be explored (cf. Blackwell, 2001b). A $\delta^{18}O_{diatom}$ record should also be produced from the diatomite bed deposited in the Naivasha basin at ~110 kyr B.P., as this bed may correspond with the upper part of the bed deposited in the Nakuru-Elmenteita basin (chapter 7). In addition, $\delta^{18}O_{diatom}$ analysis of other diatomite beds in the CKR might provide further insights into late Quaternary climatic change in the region, although high levels of clastic detritus may make it difficult to obtain samples that are pure enough for analysis (cf. Bergner and Trauth, 2004).

8.3 Regional climatic change

In this section, the implications of the records presented in this thesis for our understanding of palaeoclimatic change in equatorial and southern Africa are explored by placing them in the context of other palaeoclimatic records from these regions.

8.3.1 Southern Africa

The records from Tswaing crater lake indicate that changes in boundary conditions associated with glacial-interglacial cycles were the primary influence on precipitation at this site between ~150 kyr B.P. and the present. The only other record from the summer rainfall region of southern Africa and the surrounding islands that covers this period is from Lake Tritrivakely in Madagascar (Gasse and van Campo, 1998, 2001). This record indicates that direct insolation determined precipitation in northern Madagascar over the last ~150 kyr (Gasse and van Campo, 1998, 2001). It is not implausible that different factors influenced climatic conditions at Lake Tritrivakely and Tswaing crater lake, however, because Lake Tritrivakely lies directly under the influence of the ITCZ (and is therefore likely to be sensitive to changes in its strength and location), while Tswaing lies south of the region that is directly influenced by the ITCZ (and might therefore be sensitive to changes in other features of the climate

system).

On shorter timescales, several records from the summer rainfall region of southern Africa (including those from Tswaing presented in this study) indicate that moisture availability was higher than today during the LGM (*e.g.* Shaw *et al.*, 1997; Brook *et al.*, 1998; Stuut *et al.*, 2002), but other records from this region indicate that moisture availability was lower than today during this period (*e.g.* Holmgren *et al.*, 1995; Shi *et al.*, 1998; Munyikwa, 2005). Thus, if boundary conditions associated with glacial-interglacial cycles determined climatic conditions in southern Africa at this time, as the records presented in this thesis suggest, their effects must have been spatially variable. The reasons for this variation remain uncertain, but it is possible that changes in trade-wind strength (which could potentially influence precipitation in eastern and western areas differently), ocean currents and upwelling (which currently act to increase precipitation in eastern areas and to decrease it in western areas), and TTT-formation (which affects precipitation in a NW-SE oriented band) were partly responsible.

In the winter and all-year rainfall zones of South Africa, precipitation appears to have been determined by changes in the strength of the circum-polar westerlies caused by variations in the meridional temperature gradient associated with glacial-interglacial cycles (*e.g.* Meadows and Baxter, 1999; Parkington *et al.*, 2000; Stuut *et al.*, 2002, 2004). Marine records suggest that these changes did not affect mean annual precipitation north of this area (*e.g.* Howard and Prell, 1992; Shi *et al.*, 1998, 2000), but the records from Tswaing hint that the westerlies may have influenced precipitation in the summer rainfall region before ~150 kyr B.P.

It therefore appears that, while precessionally-driven changes in insolation may have affected precipitation in regions under the direct influence of the ITCZ, forcing-factors originating at high latitudes may have had a more significant impact on climatic conditions in many parts of southern Africa during the late Quaternary. The proposal that precessionally-driven changes in insolation were the primary influence on climatic conditions in southern Africa over the last 200 kyr (cf. Partridge *et al.*, 2004) may therefore need to be revised in light of the new chronology and palaeoclimatic records from Tswaing crater lake presented in this thesis.

Unfortunately, the lack of records from southern Africa, and the chronological uncertainty of those that do exist (including those presented in this thesis), mean that it remains difficult to construct a definite picture of the nature and causes of climatic change in this region, however.

8.3.2 Equatorial Africa

The records from the CKR presented in this thesis indicate that both direct insolation and global boundary conditions affected precipitation in this region during the late Quaternary. This proposal is corroborated by a number of other records from equatorial East Africa. Long-term records from the Naivasha basin indicate that the level of Lake Naivasha increased in response to peaks in September and March insolation on the equator between 60 and 150 kyr B.P., and a ~110-kyr mineral magnetic record from Sacred Lake in Kenya varies with a periodicity of ~11.5 kyr, which also points to forcing by equatorial insolation (Olago *et al.*, 2000; Trauth *et al.*, 2001, 2003). The influence of global boundary conditions is demonstrated by the evidence of extreme lake-level highstands in the East African Rift Valley during the last interglacial and the early Holocene (*e.g.* Butzer *et al.*, 1969; Hillaire-Marcel *et al.*, 1986; Richardson and Dussinger, 1986; Sturchio *et al.*, 1993; Trauth *et al.*, 2001, 2003). In addition, the similar patterns of climatic change in equatorial, northern, and southern East Africa since the LGM suggest that global boundary conditions determined climate in East Africa at this time, as forcing by direct insolation would have produced different patterns of climatic change in these regions (cf. Barker and Gasse, 2003).

It is unlikely that these findings can be extended to western and central parts of equatorial Africa, because different factors appear to influence climatic conditions in these regions. In particular, precipitation in the Congo Basin appears to have been influenced by the strength of the trade winds, which affect the intensity of on-shore monsoonal circulation in this region (Schefuβ *et al.*, 2005). The strength of the trade winds appears, in turn, to have been determined by the SST gradient between the tropical and subtropical South Atlantic, and it is therefore likely that changes in direct insolation had a less significant influence on precipitation in this region than in equatorial East Africa (Schefuβ *et al.*, 2005).

8.4 Synthesis

When viewed in the context of other palaeoclimatic records, the records presented in this thesis allow some tentative conclusions to be drawn about the factors that may have influenced climatic conditions south of the equator in Africa during the late Quaternary.

It is evident that precessionally-driven changes in insolation have influenced precipitation in equatorial East Africa (chapter 7) (Olago *et al.*, 2000; Trauth *et al.*, 2001, 2003). Direct insolation may have also affected climate in southern East Africa, as records from Kashiru swamp (4°S) and Lake Massoko (9°S) indicate that moisture availability was high close to the time of a peak in austral summer insolation at ~47 kyr B.P. (Bonnefille *et al.*, 1990; Bonnefille and Chalié, 2000; Barker *et al.*, 2003). The possibility that this increase in moisture availability was caused by changes in boundary conditions during MIS 3 cannot be ruled out, however. An increase in the level of Lake Malawi after ~4.5 kyr B.P. might also indicate that direct insolation affected climatic conditions in southern East Africa, as austral summer insolation was increasing at this time (Gasse *et al.*, 2002; Johnson *et al.*, 2004). Further south, precessionally-driven changes in insolation also appear to have determined precipitation at Lake Tritrivakely in Madagascar (Gasse and van Campo, 1998, 2001).

Changes in boundary conditions associated with glacial-interglacial cycles, which are thought to originate at high latitudes, have also influenced climatic conditions south of the equator in Africa. In East Africa, changes in boundary conditions appear to have reduced precipitation during glacials and increased precipitation during interglacials (chapter 7) (*e.g.* Hillaire-Marcel *et al.*, 1986; Barker and Gasse, 2003; Trauth *et al.*, 2003). The records from the CKR presented in this thesis indicate that these changes were superimposed on those caused by direct insolation during the last interglacial (chapter 7), but records of climatic change since the LGM suggest that changes in moisture availability were largely driven by global boundary conditions during this period (cf. Barker and Gasse, 2003). It is therefore possible that the effects of high-latitude forcing overwhelm changes driven by direct insolation if changes in boundary conditions are particularly large and changes in insolation are small, as has

been the case since the LGM (Fig. 1.3) (cf. Prell and Kutzbach, 1987; deMenocal *et al.*, 1993).

Records from regions further south of the equator indicate that high-latitude forcing has dominated climatic change during the late Quaternary. A 190-kyr marine pollen record that reflects conditions in West Africa south of ~6°S indicates that conditions were cold and dry during glacials and warm and wet during interglacials (although there is also evidence that precessionally-driven changes in northern hemisphere insolation influenced climatic conditions during MIS 5) (Schneider *et al.*, 1995, 1996; Jahns, 1996). As outlined above, the records from Tswaing crater lake presented in this thesis indicate that high-latitude forcing also dominated climatic change in southern Africa, but that moisture availability was higher during glacials than interglacials in this region. Most other records from southern Africa are too short or discontinuous to provide insights into the causes of climatic change in this area, but they do show that moisture availability varied significantly during the LGM, and thus suggest that high-latitude forcing had spatially-variable effects (*e.g.* Holmgren *et al.*, 1995; Shaw *et al.*, 1997; Brook *et al.*, 1998; Shi *et al.*, 1998; Munyikwa, 2005).

This picture contrasts with that of climatic change at low latitudes in South America, where variations in direct insolation appear to have been the primary influence on climatic conditions (*e.g.* Hodell *et al.*, 1991; Haug *et al.*, 2001; Bush *et al.*, 2002; Hillesheim *et al.*, 2005 from the northern hemisphere, and Martin *et al.*, 1997; Baker *et al.*, 2001a,b; Cruz *et al.*, 2005 from the southern hemisphere). The reasons for this difference remain unclear, but they are probably related to the different climatic settings of the two continents (cf. Baker, 2002). The north-easterly trade winds bring significant quantities of moisture to South America but are relatively dry over Africa, and precipitation in Africa may therefore be relatively insensitive to changes in the intensity of the northern hemisphere Hadley cell, for example (Barker and Gasse, 2003). This insensitivity might, in turn, increase the relative influence of SSTs on precipitation in Africa. It is also possible that the different configurations of the two continents led to different shifts in the position of the ITCZ during the late Quaternary, producing different patterns of climatic change (cf. Philander *et al.*, 1996).

In summary, it appears that changes in boundary conditions associated with glacial-interglacial cycles have influenced climatic conditions in most parts of Africa south of the equator during the late Quaternary, but that the nature of this influence has varied significantly. The influence of precessionally-driven changes in summer insolation may, in contrast, have been confined to eastern areas north of Tswaing crater lake, and possibly to times at which the influence of global boundary conditions was relatively low. Together, these findings demonstrate that it is not possible to generalise about climatic change in Africa south of the equator in terms of changes in the intensity of atmospheric circulation or the location of climatic belts. Instead, it is likely that the interaction of many climatic systems, superimposed on the topographical features of the continent, produced spatially variable patterns of climatic change. In order to increase our understanding of these factors, it is necessary to improve the chronological control of palaeoclimatic records from this region, including those produced in this study, and to obtain new records of palaeoclimatic change. In particular, records that extend over more than one precessional cycle are required in order to distinguish between the effects of precessionally-driven changes in insolation and changes in boundary conditions associated with glacial-interglacial cycles.

Appendix A: Records from the core obtained from Tswaing crater lake in 1988/89

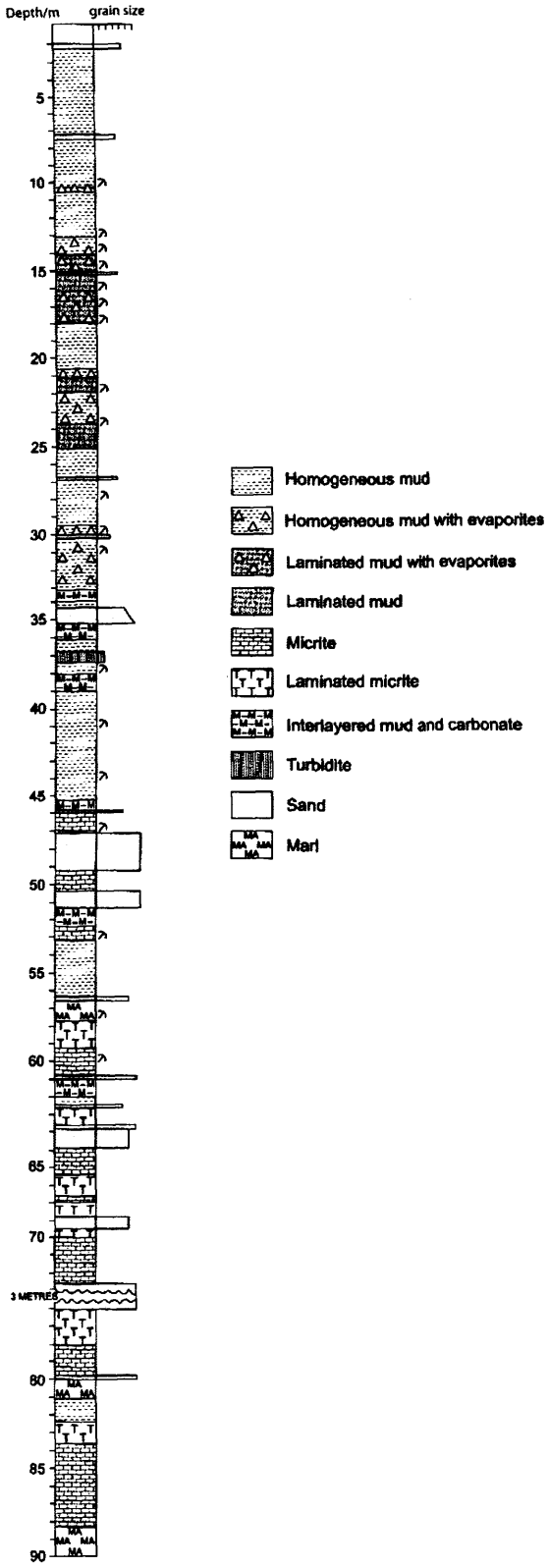

Figure A1: Sedimentological log of the lacustrine sediments obtained from Tswaing crater lake in 1988/89 (from Partridge *et al.*, 1993) (uncorrected depths).

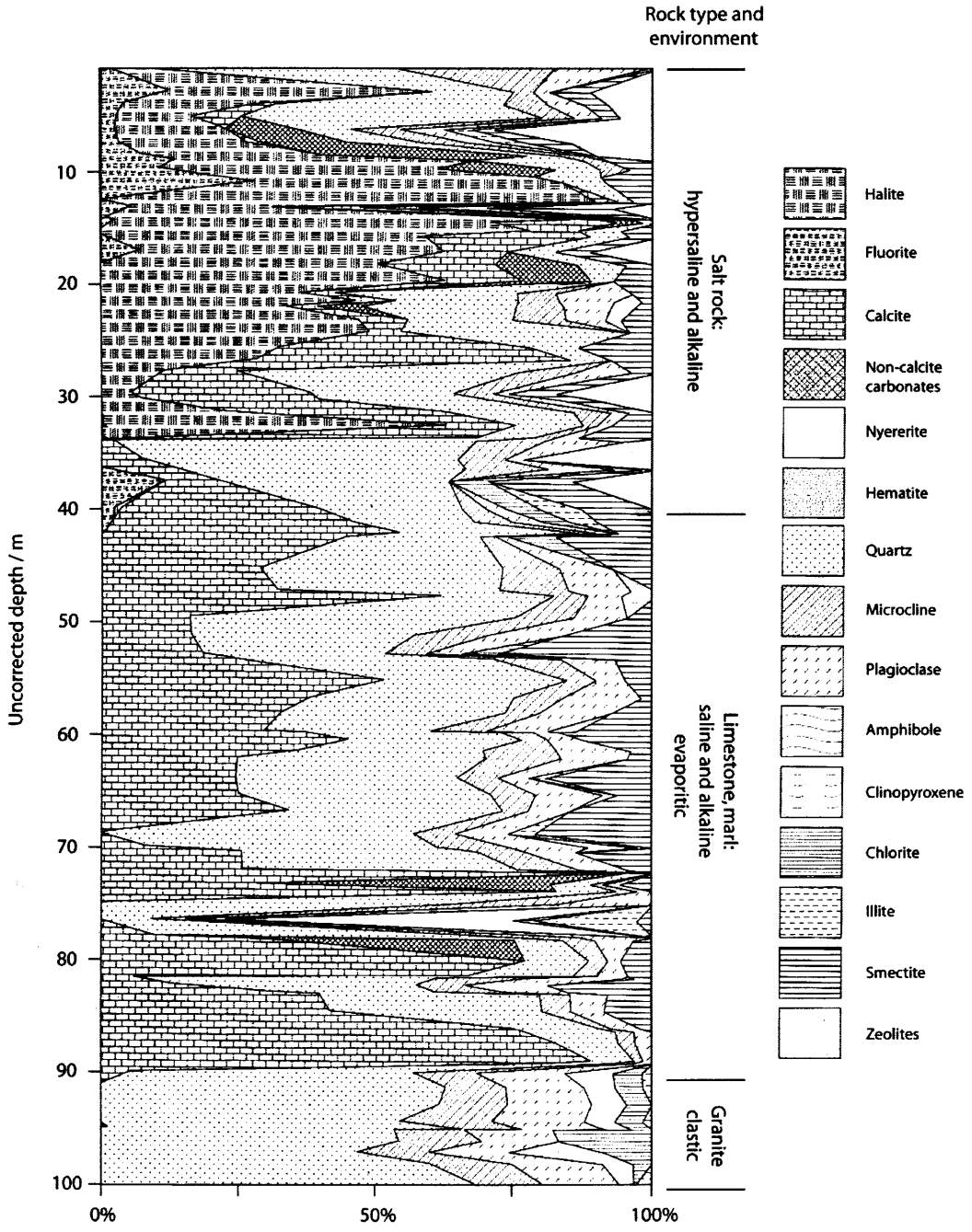

Figure A2: Mineralogical composition of the upper section (<100 m) of the sediments obtained from Tswaing crater lake in 1988/89 (from Bühmann and Elsenbroek, 1999) (uncorrected depths).

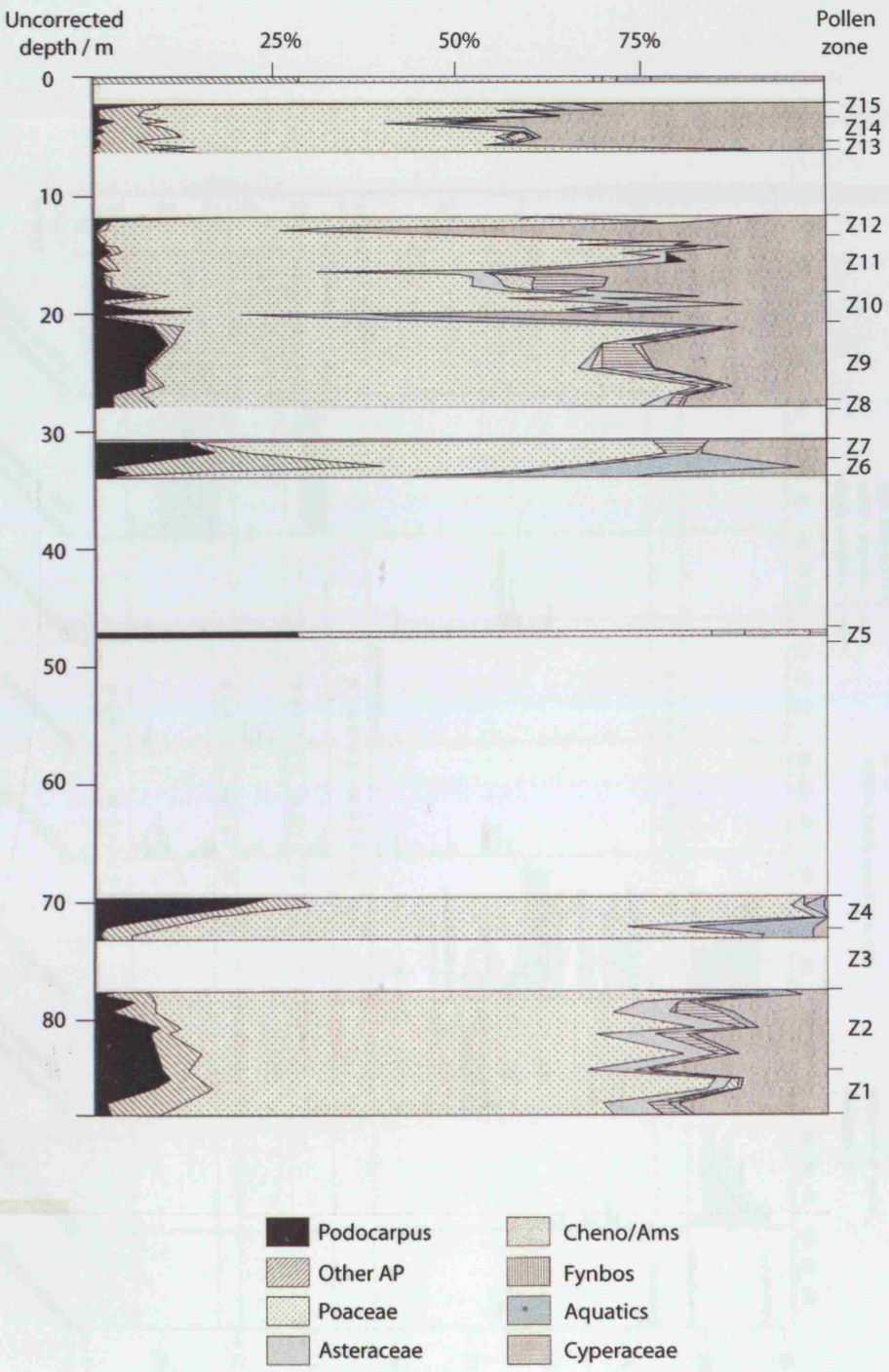

Figure A3: Summary pollen diagram for the core obtained from Tswaing crater lake in 1988/89, showing the total pollen and spore percentages (from Scott, 1999) (uncorrected depths).

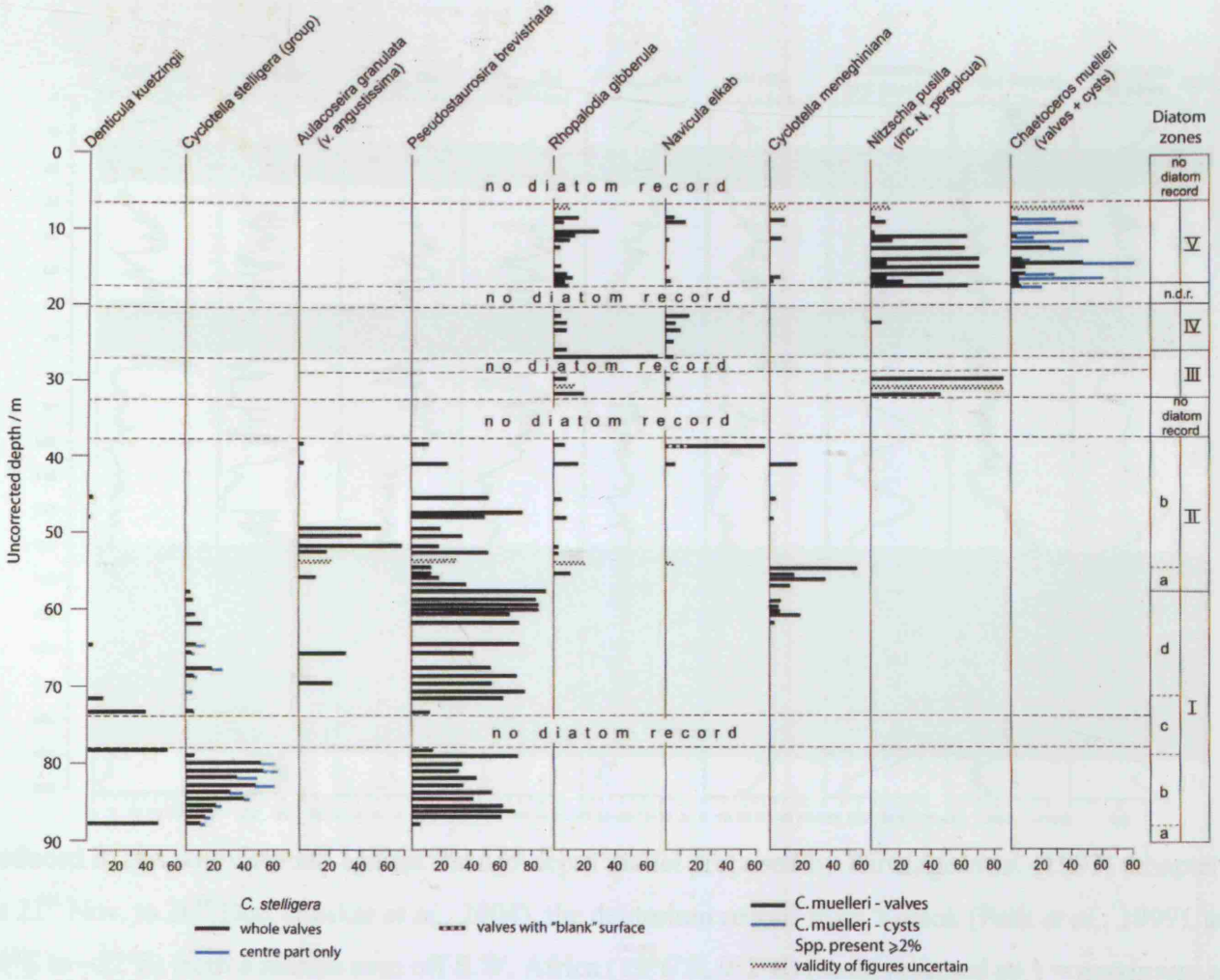

Figure A4: Summary diatom diagram for the core obtained from Tswaing crater lake in 1988/89 (from Metcalfe, 1999) (uncorrected depths).

Appendix B

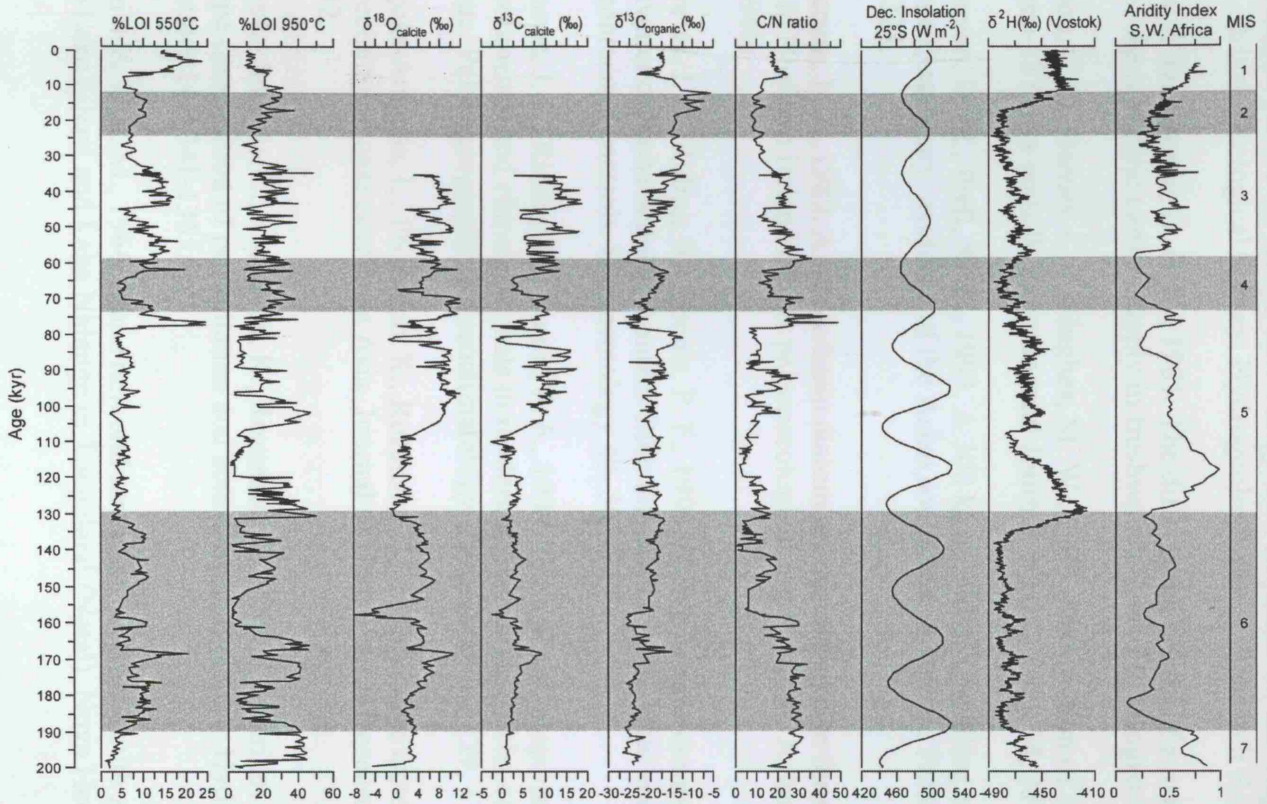

Figure B1: Records produced in this study plotted against the age-depth model proposed by Partridge *et al.* (1997) (chapter 4). Mean daily insolation at 25°S from 21st Nov. to 20th Dec. (Laskar *et al.*, 2004), the deuterium record from Vostok (Petit *et al.*, 1999), and the index of aridity in southern Africa (~24°S to ~32°S) from a marine core off S.W. Africa (19°6'S, 9°2'E) (scale reversed so 1 = maximum aridity) (Stuut *et al.*, 2002) are also shown. MISs shown as grey and white bars (Imbrie *et al.*, 1984).

Bibliography

Acocks, J. P. H., 1953. Veld types of South Africa. Government Printer, Pretoria, South Africa.

Allen, D. J., Darling, W. G., Burgess, W. G., 1989. Geothermics and hydrogeology of the southern part of the Kenya Rift Valley with emphasis on the Magadi-Nakuru Area. British Geological Survey, Hydrogeology Series, Research Report SD/89/1.

Allen, E. D., Spence, D. H. N., 1981. The differential ability of aquatic plants to utilize the inorganic carbon supply in freshwaters. New Phytologist 87, 269-283.

Allison, G. B., Barnes, C. J., Hughes, M. W., 1983. Distribution of deuterium and oxygen-18 in dry soils II. Experimental Journal of Hydrology 64, 377-397.

Anderson, D. M., Prell, W. L., 1993. A 300 ka record of upwelling off Oman during the late Quaternary: evidence of the Asian southwest monsoon. Paleoceanography 8, 193-208.

Anderson, N. J., 1989. A whole-basin diatom accumulation rate for a small eutrophic lake in Northern Ireland and its palaeoecological implications. Journal of Ecology 77, 926-946.

Andrews, J. E., Riding, R., Dennis, P. F., 1993. Stable isotope compositions of recent freshwater cyanobacterial carbonates from the British Isles: local and regional environmental controls. Sedimentology 40, 303-314.

Andrews, J. E., Riding, R., Dennis, P. F., 1997. The stable isotope record of environmental and climatic signals in modern terrestrial microbial carbonates from Europe. Palaeogeography, Palaeoclimatology, Palaeoecology 129, 171-189.

Araguás-Araguás, L., Froehlich, K., Rozanski, K., 1998. Stable isotope composition of precipitation over Southeast Asia. Journal of Geophysical Research 103, 28721-28742.

Araguás-Araguás, L., Froehlich, K., Rozanski, K., 2000. Deuterium and oxygen-18 isotope composition of precipitation and atmospheric moisture. Hydrological Processes 14, 1341-1355.

Archibald, R. E. M., 1966. Some new and rare diatoms from South Africa 2. Diatoms from Lake Sibayi and Lake Nhlange in Tongaland (Natal). Nova Hedwigia 12, 477-495.

Archibald, R. E. M., 1982. Diatoms of South Africa. 1. New species from the Sundays River (Eastern Cape Province). Bacillaria 5, 23-42.

Archibald, R. E. M., 1983. The diatoms of the Sundays and Great Fish Rivers in the eastern Cape Province of South Africa. Bibliotecha Diatomologica.

Archibald, R. E. M., Schoeman, F. R., 1984. *Amphora coffeaeformis* (Agardh) Kützing: a revision of the species under light and electron microscopy. South African Journal of Botany 3, 83-102.

Archibald, R. E. M., Schoeman, F. R., 1987. Taxonomic notes on diatoms (Bacillariophyceae) from the Great Usutu River in Swaziland. South African Journal of Botany 53, 75-92.

Åse, L. E., Sernbo, K., Syrén, P., 1986. Studies of Lake Naivasha, Kenya, and its drainage basin. Forskningsrapport fran Naturgeografiska Institutionen Stockholms Universitet 63, 1-75.

Ashton, P. J., 1985. Seasonality in Southern Hemisphere freshwater phytoplankton assemblages. Hydrobiologia 125, 179-190.

Ashton, P. J., 1999. Limnology of the Pretoria Saltpan Crater Lake. In: T. C. Partridge (Ed.), Tswaing: Investigations into the origin, age and palaeoenvironments of the Pretoria Saltpan. Geological Survey of South Africa, pp. 72-90.

Ashton, P. J., Schoeman, F. R., 1983. Limnological studies on the Pretoria Salt Pan, a hypersaline maar lake, I: Morphometric, physical and chemical features. Hydrobiologia 99, 61-73.

Ashton, P. J., Schoeman, F. R., 1985. The Pretoria Salt Pan, a unique southern African saline lake ecosystem. The Naturalist 29, 41-43.

Avery, D. M., 1981. Holocene micromammalian faunas from the Northern Cape, South Africa. South African Journal of Science 77, 265-273.

Avery, D. M., 1982. Micromammals as palaeoenvironmental indicators and as an interpretation of the late Quaternary in the southern Cape Province, South Africa. Annals of the South African Museum 85, 183-374.

Badger, M. R., 1985. The fluxes of inorganic carbon species during photosynthesis in cyanobacteria with particular reference to *Synechococcus* sp. In: W. J. Lucas, J. A. Berry (Eds.), Inorganic carbon uptake by aquatic photosynthetic organisms. American Society of Plant Physiologists, Rockville, MD, pp. 39-52.

Baker, P. A., Rigsby, C. A., Seltzer, G. O., Fritz, S. C., Lowenstein, T. K., Bacher, N. P., Veliz, C., 2001a. Tropical climate changes at millennial and orbital timescales on the Bolivian Altiplano. Nature 409, 698-701.

Baker, P. A., Seltzer, G. O., Fritz, S. C., Dunbar, R. B., Grove, M. J., Tapia, P. M., Cross, S. L., Rowe, H. D., Broda, J. P., 2001b. The history of South American tropical precipitation for the last 25,000 years. Science 291, 640-643.

Baker, P. A., 2002. Trans-Atlantic climate connections. Science 296, 67-68.

Bard, E., Rostek, F., Sonzogni, C., 1997. Interhemispheric synchrony of the last deglaciation inferred from alkenone palaeothermometry. Nature 385, 707-710.

Barkan, E., Luz, B., Lazar, B., 2001. Dynamics of the carbon dioxide system in the Dead Sea. Geochimica et Cosmochimica Acta 65, 355-368.

Barker, J. F., Fritz, P., 1981. Carbon isotope fractionation during microbial methane oxidation. Nature 293, 289-291.

Barker, P., 1992. Differential diatom dissolution in Late Quaternary sediments from Lake Manyara, Tanzania: an experimental approach. Journal of Paleolimnology 7, 235-251.

Barker, P., Gasse, F., 2003. New evidence for a reduced water balance in East Africa during the Last Glacial Maximum: implication for model-data comparison. Quaternary Science Reviews 22, 823-837.

Barker, P., Fontes, J.-C., Gasse, F., Druart, J.-C., 1994. Experimental dissolution of diatom silica in concentrated salt solutions and implications for paleoenvironmental reconstruction. Limnology and Oceanography 39, 99-110.

Barker, P., Telford, R., Merdaci, O., Williamson, D., Taieb, M., Vincens, A., Gibert, E., 2000. The sensitivity of a Tanzanian crater lake to catastrophic tephra input and four millennia of climate change. The Holocene 10, 303-310.

Barker, P. A., Street-Perrott, F. A., Leng, M. J., Greenwood, P. B., Swain, D. L., Perrott, R. A., Telford, R. J., Ficken, K. J., 2001. A 14,000-year oxygen isotope record from diatom silica in two alpine lakes on Mt. Kenya. Science 292, 2307-2310.

Barker, P., Telford, R. J., Gasse, F., Thevenon, F., 2002. Late Pleistocene and Holocene palaeohydrology of Lake Rukwa, Tanzania, inferred from diatom analysis. Palaeogeography, Palaeoclimatology, Palaeoecology 187, 295-305.

Barker, P., Williamson, D., Gasse, F., Gibert, E., 2003. Climatic and volcanic forcing revealed in a 50,000-year diatom record from Lake Massoko, Tanzania. Quaternary Research 60, 368-376.

Barnes, J. W., Lang, E. J., Potratz, H. A., 1956. Ratio of ionium to uranium in coral limestone. Science 124, 175-176.

Barnola, J. M., Raynaud, D., Korotkevich, Y. S., Lorius, C., 1987. Vostok ice core provides 160,000-year record of atmospheric CO_2. Nature 329, 408-414.

Barton, C. E., Solomon, D. K., Bowman, J. R., Cerling, T. E., Sayer, M. D., 1987. Chloride budgets in transient lakes: Lakes Baringo, Naivasha, and Turkana. Limnology and Oceanography 32, 745-751.

Battarbee, R. W., 1986. Diatom analysis. In: B. E. Berglund (Ed.), Handbook of Holocene Palaeoecology and Palaeohydrology. Wiley, Chichester, pp. 527-570.

Battarbee, R. W., Kneen, M. J., 1982. The use of electronically counted microspheres in absolute diatom analysis. Limnology and Oceanography 27, 184-188.

Battarbee, R. W., Flower, R. J., 1984. The inwash of catchment diatoms as a source of error in the sediment-based reconstruction of pH in an acid lake. Limnology and Oceanography 29, 1325-1329.

Battarbee, R., Jones, V. J., Flower, R. J., Cameron, N. G., Bennion, H., Carvalho, L., Juggins, S., 2001. Diatoms. In: J. P. Smol, H. J. B. Birks, W. M. Last (Eds.), Tracking Environmental Change using Lake Sediments. Volume 3: Terrestrial, Algal, and siliceous indicators. Kluwer Academic Publishers, Dordrecht, pp. 155-202.

Battarbee, R. W., Gasse, F., Stickley, C. E., 2004. Past climate variability through Europe and Africa. Springer, Dordrecht.

Beaumont, P. B., 1986. Where did all the young men go during O-18 stage 2? Palaeoecology of Africa 17, 79-86.

Beaumont, P. B., Vogel, J. C., 1993. What turned the young tufas at Gorrokop? South African Journal of Science 89, 196-198.

Beaumont, P. B., van Zinderen Bakker, E. M., Vogel, J. C., 1984. Environmental changes since 32,000 BP at Kathu Pan, northern Cape. In: J. C. Vogel (Ed.), Late Cainozoic Palaeoclimates of the Southern Hemisphere. Balkema, Rotterdam, pp. 329-338.

Beck, J. W., Récy, J., Taylor, F., Edwards, R. L., Cabioch, G., 1997. Abrupt changes in early Holocene tropical sea surface temperature derived from coral records. Nature 385, 705-707.

Beck, W. C., Grossman, E. L., Morse, J. W., 2005. Experimental studies of oxygen isotope fractionation in the carbonic acid system at 15°, 25°, and 40°C. Geochimica et Cosmochimica Acta 69, 3493-3503.

Bengtsson, L., Enell, M., 1986. Chemical analysis. In: B. E. Berglund (Ed.), Handbook of Holocene Paleoecology and Paleohydrology. Wiley, Chichester, pp. 423-451.

Benner, R., Fogel, M. L., Sprague, E. K., Hodson, R. E., 1987. Depletion of ^{13}C in lignin and its implications for stable isotope studies. Nature 329, 708-710.

Bennett, K. D., 1994. Confidence intervals for age estimates and deposition times in late-Quaternary sediment sequences. The Holocene 4, 337-348.

Berger, A. L., 1978. Long-term variations of caloric insolation resulting from the earth's orbital elements. Quaternary Research 9, 139-167.

Berger, A., Loutre, M.-F., 1991. Insolation values for the climate of the last 10 million years. Quaternary Science Reviews 10, 297-317.

Berger, A., Tricot, C., Gallée, H., Loutre, M. F., 1993. Water vapour, CO_2 and insolation over the last glacial-interglacial cycles. Philosophical Transactions of the Royal Society of London B 341, 253-261.

Bergner, A. G. N., Trauth, M. H., 2004. Comparison of the hydrological and hydrochemical evolution of Lake Naivasha (Kenya) during three highstands between 175 and 60 kyr BP. Palaeogeography, Palaeoclimatology, Palaeoecology 215, 17-36.

Bergner, A. G. N., Trauth, M. H., Bookhagen, B., 2003. Palaeoprecipitation estimates for the Lake Naivasha basin Kenya during the last 175 k.y. using a lake-balance model. Global and Planetary Change 36, 117-136.

Beuning, K. R. M., Talbot, M. R., Kelts, K., 1997. A revised 30000-year paleoclimatic and paleohydrologic history of Lake Albert, East Africa. Palaeogeography, Palaeoclimatology, Palaeoecology 136, 259-279.

Bevington, P. R., 1969. Data Reduction and Error Analysis for the Physical Sciences. MacGraw-Hill, New York.

Biasutti, M., Battisti, D. S., Sarachik, E. S., 2003. The annual cycle over the tropical Atlantic, South America, and Africa. Journal of Climate 16, 2491-2508.

Birks, H. J. B., Birks, H. H., 1980. Quaternary palaeoecology. Edward Arnold, London.

Bischoff, J. L., Fitzpatrick, J. A., 1991. U-series dating of impure carbonates: an isochron technique using total-sample dissolution. Geochimica et Cosmochimica Acta 55, 543-554.

Blackwell, B. A. B., 2001a. Amino acid racemization (AAR) dating and analysis in lacustrine environments. In: W. M. Last, J. P. Smol (Eds.), Tracking Environmental Change using lake sediments. Volume 1: Basin analysis, coring, and chronological techniques. Kluwer Academic Publishers, Dordrecht, pp. 391-450.

Blackwell, B. A. B., 2001b. Electron spin resonance (ESR) dating in lacustrine environments. In: W. M. Last, J. P. Smol (Eds.), Tracking Environmental Change using lake sediments. Volume 1: Basin analysis, coring, and chronological techniques. Kluwer Academic Publishers, Dordrecht, pp. 283-368.

Blais, J. M., Kalff, J., 1995. The influence of lake morphometry on sediment focusing. Limnology and Oceanography 40, 582-588.

Blinn, D. W., 1993. Diatom community structure along physicochemical gradients in saline lakes. Ecology 74, 1246-1263.

Bolin, B., 1959. On the use of tritium as a tracer for water in nature. In: Proceedings of the 2nd Conference on the Peaceful Uses of Atomic Energy, 18. United Nations, Geneva. pp. 336-344.

Bonnefille, R., Chalié, F., 2000. Pollen-inferred precipitation time-series from equatorial mountains, Africa, the last 40 kyr BP. Global and Planetary Change 26, 25-50.

Bonnefille, R., Roeland, J. C., Guiot, J., 1990. Temperature and rainfall estimates for the past 40,000 years in equatorial Africa. Nature 346, 347-349.

Bonnefille, R., Riollet, G., Buchet, G., Icole, M., LaFont, R., Arnold, M., Jolly, D., 1995. Glacial/interglacial record from intertropical Africa, high resolution pollen and carbon data at Rusaka, Burundi. Quaternary Science Reviews 14, 917-936.

Boom, A., Marchant, R., Hooghiemstra, H., Sinninghe Damsté, J.S., 2002. CO_2- and temperature-controlled altitudinal shifts of C_4- and C_3-dominated grasslands allow reconstruction of palaeoatmospheric pCO_2. Palaeogeography, Palaeoclimatology, Palaeoecology 177, 151-168.

Boston, H. L., Adams, M. S., Madsen, J. D., 1989. Photosynthetic strategies and productivity in Aquatic Systems. Aquatic botany 34, 27-57.

Bottinga, Y., 1968. Calculation of fractionation factors for carbon and oxygen isotopic exchange in the system calcite-carbon dioxide-water. The Journal of Physical Chemistry 72, 800-808.

Bottinga, Y., 1969. Calculated fractionation factors for carbon and hydrogen isotope exchange in the system calcite-carbon dioxide-graphite-methane-hydrogen-water vapor. Geochimica et Cosmochimica Acta 33, 49-64.

Boyle, E. A., Keigwin, L., 1987. North Atlantic thermohaline circulation during the past 20,000 years linked to high-latitude surface temperature. Nature 330, 35-40.

Braconnot, P., Joussaume, S., de Noblet, N., Ramstein, G., 2000. Mid-Holocene and last glacial maximum African monsoon changes as simulated within the Paleoclimate Modelling Intercomparison Project. Global and Planetary Change 26, 51-66.

Bradbury J.P., 1989. Late Quaternary lacustrine paleoenvironments in the Cuenca de México. Quaternary Science Reviews 8, 75-100.

Brandriss, M. E., O'Neil, J. R., Edlund, M. B., Stoermer, E. F., 1998. Oxygen isotope fractionation between diatomaceous silica and water. Geochimica et Cosmochimica Acta 62, 1119-1125.

Brandt, D., Reimold, W. U., 1999. The geology and geophysical signature of the Pretoria Saltpan (Tswaing) impact structure. In: T. C. Partridge (Ed.), Tswaing: Investigations into the origin, age and palaeoenvironments of the Pretoria Saltpan. Geological Survey of South Africa, pp. 6-34.

Brathauer, U., Abelmann, A., 1999. Late Quaternary variations in sea surface temperatures and their relationship to orbital forcing recorded in the Southern Ocean (Atlantic sector). Paleoceanography 14, 135-148.

Broccoli, A. J., 2000. Tropical Cooling at the Last Glacial Maximum: An Atmosphere-Mixed Layer Ocean Model Simulation. Journal of Climate 13, 951-976.

Broecker, W. S., Oversby, V. M., 1971. Chemical equilibria in the earth. McGraw-Hill, New York.

Brook, G. A., Haberyan, K. A., de Filippis, S., 1992. Evidence of a shallow lake at Tsodilo Hills, Botswana, 17500 to 15000 yr BP: Further confirmation of a widespread

late Pleistocene humid period in the Kalahari desert. Palaeoecology of Africa 23, 165-175.

Brook, G. A., Cowart, J. B., Brandt, S. A., 1998. Comparison of Quaternary environmental change in eastern and southern Africa using cave speleothem, tufa and rock shelter sediment data. In: A. Alsharan, K. W. Glennie, G. L. Wintle, C. G. St. C. Kendall (Eds.), Quaternary deserts and climate change. Balkema, Rotterdam, pp. 239-250.

Brooks, K., Scholz, C. A., King, J. W., Peck, J., Overpeck, J. T., Russell, J. M., Amoako, P. Y. O., 2005. Late-Quaternary lowstands of lake Bosumtwi, Ghana: evidence from high-resolution seismic-reflection and sediment-core data. Palaeogeography, Palaeoclimatology, Palaeoecology 216, 235-249.

Bröstrom, A., Coe, M., Harrison, S. P., Gallimore, R., Kutzbach, J. E., Foley, J., Prentice I.C., Behling P., 1998. Land-surface processes and paleomonsoons in northern Africa. Geophysical Research Letters 25, 3615-3618.

Brugam, R. B., 1983. The relationship between fossil diatom assemblages and limnological conditions. Hydrobiologia 98, 223-235.

Brunskill, J. E., 1969. Fayetteville Green Lake: II. Precipitation and sedimentation of calcite in a meromictic lake with laminated sediments. Limnology and Oceanography 14, 830-847.

Budziak, D., Schneider, R. R., Rostek, F., Müller, P. J., Bard, E., Wefer, G., 2000. Late Quaternary insolation forcing on total organic carbon and C_{37} alkenone variations in the Arabian Sea. Paleoceanography 15, 307-321.

Bühmann, D., Elsenbroek, J. H., 1999. Mineralogy and geochemistry of the Pretoria Saltpan borehole core. In: T. C. Partridge (Ed.), Tswaing: Investigations into the origin, age and palaeoenvironments of the Pretoria Saltpan. Geological Survey of South Africa, pp. 91-117.

Bush, A. G. B., Philander, S. G. H., 1998. The role of ocean-atmosphere interactions in tropical cooling during the Last Glacial Maximum. Science 279, 1341-1344.

Bush, M. B., 2002. On the interpretation of fossil Poaceae pollen in the lowland humid neotropics. Palaeogeography, Palaeoclimatology, Palaeoecology 177, 5-17.

Bush, M. B., Miller, M. C., De Oliveira, P. E., Colinvaux, P. A., 2002. Orbital forcing signal in sediments of two Amazonian lakes. Journal of Paleolimnology 27, 341-352.

Butzer, K. W., 1984. Late Quaternary environments in South Africa. In: J. C. Vogel (Ed.), Late Cainozoic Palaeoclimates of the Southern Hemisphere. Balkema, Rotterdam, pp. 235-264.

Butzer, K. W., Brown, F. H., Thurber, D. L., 1969. Horizontal sediments of the lower Omo valley: the Kibish formation. Quaternaria 11, 15-29.

Butzer, K. W., Isaac, G. L., Richardson, J. L., Washbourn-Kamau, C., 1972. Radiocarbon dating of East African lake levels: new observations provide fresh insights into late Quaternary paleoclimates. Science 175, 1069-1076.

Butzer, K. W., Fock, G. J., Stuckenrath, R., Zilch, A., 1973. Paleohydrology of late Pleistocene lake Alexandersfontein, Kimberley, South Africa. Nature 243, 328-330.

Butzer, K. W., Stuckenrath, R., Bruzewicz, A. J., Helgren, D. M., 1978. Late Cenozoic paleoclimates of the Gaap Escarpment, Kalahari margin, South Africa. Quaternary Research 10, 310-339.

Calvo, E., Pelejero, C., Herguera, J. C., Palanques, A., Grimalt, J. O., 2001. Insolation dependence of the southeastern Subtropical Pacific sea surface temperature over the last 400 kyrs. Geophysical Research Letters 28, 2481-2484.

Camberlin, P., Janicot, S., Poccard, I., 2001. Seasonality and atmospheric dynamics of the teleconnection between African rainfall and tropical sea-surface temperature: Atlantic vs. ENSO. International Journal of Climatology 21, 973-1005.

Casanova, J., Hillaire-Marcel, C., 1992. Chronology and paleohydrology of Late Quaternary high lake levels in the Manyara Basin (Tanzania) from isotopic data (^{18}O, ^{13}C, ^{14}C, Th/U) on fossil stromatolites. Quaternary Research 38, 205-226.

Chalié, F., Gasse, F., 2002. Late Glacial-Holocene diatom record of water chemistry and lake level change from the tropical East African Rift Lake Abiyata (Ethiopia). Palaeogeography, Palaeoclimatology, Palaeoecology 187, 259-283.

Chappellaz, J., Blunier, T., Raynaud, D., Raynaud, D., Schwander, J., Stauffer, B., 1993. Synchronous changes in atmospheric CH_4 and Greenland climate between 40 and 8 kyr BP. Nature 366, 443-445.

Chen, J. H., Edwards, R. L., Wasserburg, G. J., 1986. ^{238}U, ^{234}U, and ^{232}Th in seawater. Earth and Planetary Science Letters 80, 241-251.

Chen, M.-T., Chang, Y.-P., Chang, C.-C., Wang, L.-W., Wang, C.-H., Yu, E.-F., 2002. Late Quaternary sea-surface temperature variations in the southeast Atlantic; a planktic foraminifer faunal record of the past 600 000 yr (IMAGES II MD962085). Marine Geology 180, 163-181.

Cheng, H., Adkins, J., Edwards, R. L., Boyle, E. A., 2000. U-Th dating of deep-sea corals. Geochimica et Cosmochimica Acta 64, 2401-2416.

Cherdyntsev, V. V., 1955. Ob izotopnom sostave radio elementov-V privodnykh obyektakh V sviazi S voprosami geokhronologii. In: V. V. Cherdyntsev, P. I. Chalov, Z. Khaidarov (Eds.), Trudy III Sessii Komiss Opredeleniyu Absolyutnogo Yozrastu. Izd. Akad. Nauk SSSR, Moscow, pp. 175-233.

Chiang, J. C. H., Biasutti, M., Battisti, D. S., 2003. Sensitivity of the Atlantic Intertropical Convergence Zone to Last Glacial maximum boundary conditions. Paleoceanography 18, 1-18.

Clark, I. D., Fritz, P., 1997. Environmental Isotopes in Hydrogeology. CRC Press, Boca Raton.

Claussen M., Gayler, V., 1997. The greening of the Sahara during the mid-Holocene: results of an interactive atmosphere-biome model. Global Ecology and Biogeography Letters 6, 369-377.

Claussen, M., Kubatzki, C., Brovkin, V., Ganopolski, A., Hoelzmann, P., Pachur, H.-J., 1999. Simulation of an abrupt change in Saharan vegetation in the mid-Holocene. Geophysical Research Letters 26, 2037-2040.

Clayton, R. N., Mayeda, T. K., 1963. The use of bromine pentafluoride in the extraction of oxygen from oxide and silicates for isotopic analysis. Geochimica et Cosmochimica Acta 27, 43-52.

Clemens, S. C., Prell, W. L., 1990. Late Pleistocene variability of Arabian Sea summer monsoon winds and continental aridity: eolian records from the lithogenic component of deep-sea sediments. Paleoceanography 5, 109-145.

Clemens, S. C., Prell, W. L., 2003. A 350,000 year summer-monsoon multi-proxy stack from the Owen Ridge, Northern Arabian Sea. Marine Geology 201, 35-51.

Clement, A. C., Seager, R., Cane, M. A., 1999. Orbital controls on the El Niño/Southern Oscillation and the tropical climate. Paleoceanography 14, 441-456.

Clement, A. C., Hall, A., Broccoli, A. J., 2004. The importance of precessional signals in the tropical climate. Climate Dynamics 22, 327-341.

CLIMAP Project Members, 1981. Seasonal reconstruction of the earth's surface at the Last Glacial Maximum. Geological Society of America Map and Chart Series MC-36.

Cockcroft, M. J., Wilkinson, M. J., Tyson, P. D., 1987. The application of a present-day climatic model to the late Quaternary in Southern Africa. Climatic Change 10, 161-181.

Coe, M. T., Bonan, G. B., 1997. Feedbacks between climate and surface water in northern Africa during the middle Holocene. Journal of Geophysical Research - Atmospheres 102, 11087-11102.

COHMAP Members, 1988. Climatic changes of the last 18,000 years: observations and model simulations. Science 241, 1043-1052.

Cole, J. J., Caraco, N. F., Kling, G. W., Kratz, T. K., 1994. Carbon dioxide supersaturation in the surface waters of lakes. Science 265, 1568-1570.

Cook, K. H., 2000. The South Indian Convergence Zone and interannual rainfall variability over Southern Africa. Journal of Climate 13, 3789-3804.

Cook, K. H., 2001. A southern hemisphere wave response to ENSO with implications for Southern Africa precipitation. Journal of the Atmospheric Sciences 58, 2146-2162.

Cowling, R. M., Cartwright, C. R., Parkington, J. E., Allsopp, J. C., 1999. Fossil wood charcoal assemblages from Elands Bay Cave, South Africa: implications for Late Quaternary vegetation and climates in the winter-rainfall fynbos biome. Journal of Biogeography 26, 367-378.

Craig, H., 1961. Isotopic variations in meteoric waters. Science 133, 1702-1703.

Craig H., 1965. The measurement of oxygen isotope palaeotemperatures. In: E. Tongiorgi (Ed.), Stable isotopes in Oceanographic studies and Paleotemperatures. C.N.R., Laboratorio di Geologia Nucleare, Pisa, pp. 161–182.

Craig, H., Gordon, L. I., 1965. Deuterium and oxygen-18 variations in the ocean and the marine atmosphere. In: E. Tongiorgi (Ed.), Stable isotopes in Oceanographic studies and Paleotemperatures. C.N.R., Laboratorio di Geologia Nucleare, Pisa, pp. 9-130.

Craig, H., Gordon, L., Horibe, Y., 1963. Isotopic exchange effects in the evaporation of water, 1. Low-temperature experimental results. Journal of Geophysical Research 68, 5079-5087.

Crimp, S. J., Lutjeharms, J. R. E., Mason, S. J., 1998. Sensitivity of a tropical-temperate trough to sea-surface temperature anomalies in the Agulhas retroflection region. Water SA 24, 93-100.

Croll, J., 1890. Climate and time. Edward Stanford, London.

Cross, S. L., Baker, P. A., Seltzer, G. O., Fritz, S. C., Dunbar, R. B., 2000. A new estimate of the Holocene lowstand level of Lake Titicaca, central Andes, and implications for tropical palaeohydrology. The Holocene 10, 21-32.

Crosta, X., Sturm, A., Armand, L., Pichon, J.-J., 2004. Late Quaternary sea ice history in the Indian sector of the Southern Ocean as recorded by diatom assemblages. Marine Micropaleontology 50, 209-223.

Cruz, F. W., Burns, S. J., Karmann, I., Sharp, W. D., Vuille, M., Cardoso, A. O., Ferrari, J. A., Silva Dias, P. L., Viana, O., 2005. Insolation-driven changes in atmospheric circulation over the past 116,000 years in subtropical Brazil. Nature 434, 63-66.

Cumming, B. F., Wilson, S. E., Smol, J. P., 1993. Paleolimnological potential of chrysophyte cysts and scales and of sponge spicules as indicators of lake salinity. International Journal of Salt Lake Research 2, 87-92.

Curry, W. B., Oppo, D. W., 1997. Synchronous, high-frequency oscillations in tropical sea surface temperatures and North Atlantic Deep Water production during the last glacial cycle. Paleoceanography 12, 1-14.

Curtis, S., Adler, R., Huffman, G., Nelkin, E., Bolvin, D., 2001. Evolution of tropical and extratropical preciptation anaomalies during the 1997-1999 ENSO cycle. International Journal of Climatology 21, 961-971.

Dansgaard, W., 1954. The O^{18} abundance in fresh water. Geochimica et Cosmochimica Acta 6, 241-260.

Dansgaard, W., 1964. Stable isotopes in precipitation. Tellus 16, 436-468.

Darling, W. G., Allen, D. J., Armannsson, H., 1990. Indirect detection of subsurface outflow from a rift valley lake. Journal of Hydrology 113, 297-305.

Darling, W. G., Gizaw, B., Arusei, M. K., 1996. Lake-groundwater relationships and fluid-rock interaction in the East African Rift Valley: isotopic evidence. Journal of African Earth Sciences 22, 423-431.

Darling, W. G., Bath, A. H., Gibson, J. J., Rozanski, K., 2006. Isotopes in water. In: M. J. Leng (Ed.), Isotopes in Palaeoenvironmental Research. Springer, Dordrecht, pp. 1-66.

Davey, M. C., 1987. Seasonal variation in the filament morphology of the freshwater diatom *Melosira granulata* (Ehrenb.) Ralfs. Freshwater Biology 18, 5-16.

de Noblet, N., Braconnot, P., Joussaume, S., Masson, V., 1996. Sensitivity of simulated Asian and African summer monsoons to orbitally induced variations in insolation 126, 115, and 6 ka BP. Climate Dynamics 12, 589-603.

Deacon, H. J., Deacon, J., Scholtz, A., Thackeray, J. F., Brink, J. S., Vogel, J., 1984. Correlation of palaeoenvironmental data from the late Pleistocene and Holocene deposit at Boomplaas Cave, southern Cape. In: J. C. Vogel (Ed.), Late Cainozoic Palaeoclimates of the Southern Hemisphere. Balkema, Rotterdam, pp. 339-352.

Deacon, J., Lancaster, N., 1988. Late Quaternary Palaeoenvironments of Southern Africa. Oxford University Press, Oxford.

Dean, W. E. Jr., 1974. Determination of carbonate and organic matter in calcareous sediments and sedimentary rocks by loss on ignition: Comparison with other methods. Journal of Sedimentary Petrology 44, 242-248.

Dearing, J. A., 1997. Sedimentary indicators of lake-level change in the humid temperate zone: a critical review. Journal of Paleolimnology 18, 1-14.

Deines, P., 1980. The isotopic composition of reduced organic carbon. In: P. Fritz, J. Ch. Fontes (Eds.), Handbook of environmental isotope geochemistry. Volume 1. The terrestrial environment, A. Elsevier, Amsterdam, pp. 329-406.

Deines, P., Harmon, R. S., Langmuir, D., 1974. Stable carbon isotope ratios and the existence of a gas phase in the evolution of carbonate ground waters. Geochimica et Cosmochimica Acta 38, 1147-1164.

deMenocal, P., Rind, D., 1993. Sensitivity of Asian and African climate to variations in seasonal insolation, glacial ice cover, sea surface temperature, and Asian orography. Journal of Geophysical Research 98(D4), 7265-7287.

deMenocal, P. B., Ruddiman, W. F., Pokras, E. M., 1993. Influences of high- and low-latitude processes on African terrestrial climate: Pleistocene eolian records from equatorial Atlantic Ocean Drilling Program Site 663. Paleoceanography 8, 209-242.

deMenocal, P., Ortiz, J., Guilderson, T., Adkins, J., Sarnthein, M., Baker, L., Yarusinsky, M., 2000. Abrupt onset and termination of the African Humid Period: rapid responses to gradual insolation forcing. Quaternary Science Reviews 19, 347-361.

Des Marais, D. J., Canfield, D. E., 1994. The carbon isotope biogeochemistry of microbial mats. In: L.J. Stal, P. Caumette (Eds.), Microbial mats: structure, development, and environmental significance. Springer-Verlag, Berlin, pp. 289-298.

Devol, A. H., Anderson, J. J., Kuivila, K., Murray, J. W., 1984. A model for coupled sulfate reduction and methane oxidation in the sediments of Saanich Inlet. Geochimica et Cosmochimica Acta 48, 993-1004.

Diab, R. D., Preston-Whyte, R. A., Washington, R., 1991. Distribution of rainfall by synoptic type over Natal, South Africa. Journal of Climatology 11, 877-888.

Dinçer, T., 1968. The use of oxygen 18 and deuterium concentrations in the water balance of lakes. Water Resources Research 4, 1289-1306.

Doherty, R., Kutzbach, J., Foley, J., Pollard, D., 2000. Fully coupled/dynamical vegetation model simulations over Northern Africa during the mid-Holocene. Climate Dynamics 16, 561-573.

Drummond, C. N., Patterson, W. P., Walker, J. C. G., 1995. Climatic forcing of carbon-oxygen isotopic co-variance in temperature-region marl lakes. Geology 23, 1032-1034.

Dühnforth, M., Bergner, A. G. N., Trauth, M. H., Bookhagen, B., Strecker, M. R., in prep. The hydrological budget of the Nakuru-Elmenteita basin, Central Kenya Rift, during the Early Holocene wet period.

Dupont, L. M., 1993. Vegetation zones in NW Africa during the Brunhes chron reconstructed from marine palynological data. Quaternary Science Reviews 12, 189-202.

Dupont, L. M., Wyputta, U., 2003. Reconstructing pathways of aeolian transport to the marine sediments along the coastline of SW Africa. Quaternary Science Reviews 22, 157-174.

EDDI participants, 2001. The European Diatom Database User Guide Version 1.0.

Edmunds, W. M., Dodo, A., Djoret, D., Gasse, F., Gaye, C. B., Goni, I. B., 2004. Groundwater as an archive of climatic and environmental change: Europe to Africa. In: R. W. Battarbee, F. Gasse, C. E. Stickley (Eds.), Past climate variability through Europe and Africa. Springer, Dordrecht, pp. 279-306.

Edwards, R. L., Chen, J. H., Wasserburg, G. J., 1986. ^{238}U-^{234}U-^{230}Th-^{232}Th systematics and the precise measurement of time over the past 500,000 years. Earth and Planetary Science Letters 81, 192.

Edwards, R. L., Chen, J. H., Ku, T.-L., Wasserburg, G. J., 1987. The precise timing of the last interglacial period from mass spectrometric determination of ^{230}Th in corals. Science 236, 1547-1553.

Ehhalt, D., Knott, K., Nagel, J. F., Vogel, J. C., 1963. Deuterium and oxygen-18 in rain water. Journal of Geophysical Research 68, 3775-3780.

Einsele, G., 2000. Sedimentary basins: evolution, facies and sediment budget. Springer, Berlin.

Elenga, H., Schwartz, D., Vincens, A., 1994. Pollen evidence of late Quaternary vegetation and inferred climate changes in Congo. Palaeogeography, Palaeoclimatology, Palaeoecology 109, 345-356.

Emrich, K., Ehhalt, D. H., Vogel, J. C., 1970. Carbon isotope fractionation during the precipitation of calcium carbonate. Earth and Planetary Science Letters 20, 252-261.

EPICA community members, 2004. Eight glacial cycles from an Antarctic ice core. Nature 429, 623-628.

Epstein, S., Buchsbaum, R., Lowenstam, H. A., Urey, H. C., 1953. Revised carbonate-water isotopic temperature scale. Bulletin of the Geological Society of America 64, 1315-1326.

Esper, O., Versteegh, G. J. M., Zonneveld, K. A. F., Willems, H., 2004. A palynological reconstruction of the Agulhas Retroflection (South Atlantic Ocean) during the Late Quaternary. Global and Planetary Change 41, 31-62.

Eugster, H. P., Hardie, L. A., 1978. Saline Lakes. In: A. Lerman (Ed.), Lakes: Chemistry, Geology, Physics. Springer-Verlag, New York, pp. 237-293.

Eugster, H. P., Jones, B. F., 1979. Behaviour of major solutes during closed-basin brine evolution. American Journal of Science 279, 609-631.

Fallu, M.-A., Allaire, N., Pienitz, R., 2002. Distribution of freshwater diatoms in 64 Labrador (Canada) lakes: species-environment relationships along latitudinal gradients and reconstruction models for water color and alkalinity. Canadian Journal of Fisheries and Aquatic Sciences 59, 329-349.

Farrera, I., Harrison, S. P., Prentice, I. C., Ramstein, G., Guiot, J., Bartlein, P. J., Bonnefille, R., Bush, M., Cramer, W., von Grafenstein, U., Holmgren, K., Hooghiemstra, H., Hope, G., Jolly, D., Lauritzen, S. E., Ono, Y., Pinot, S., Stute, M., Yu, G., 1999. Tropical climates at the last glacial maximum: a new synthesis of terrestrial palaeoclimate data. I. Vegetation, lake levels and geochemistry. Climate Dynamics 15, 823-856.

Felipe, M. A., Kubicki J.D., Rye, D. M., 2004. Oxygen isotope exchange kinetics between H_2O and H_4SiO_4 from ab initio calculations. Geochimica et Cosmochimica Acta 68, 949-958.

Fenchel, T., King, G. M., Blackburn, T. H., 1998. Bacterial biogeochemistry: The ecophysiology of mineral cycling. Academic Press.

Filippi, M. L., Talbot , M. R., 2004. The palaeolimnology of northern Lake Malawi over the last 25 ka based upon the elemental and stable isotopic composition of sedimentary organic matter. Quaternary Science Reviews 24, 1303-1328.

Findlater, J., 1977. A numerical index to monitor the Afro-Asian monsoon during the Northern summer. Meterological Magazine 106, 170-180.

Finney, B. P., Johnson, T. C., 1991. Sedimentation in Lake Malawi (East Africa) during the past 10,000 years: a continuous paleoclimatic record from the southern tropics. Palaeogeography, Palaeoclimatology, Palaeoecology 85, 351-366.

Finney, B. P., Scholz, C. A., Johnson, T. C., Trumbore, S., 1996. Late Quaternary lake-level changes of Lake Malawi. In: T. C. Johnson, E. O. Odada (Eds.), The Limnology, Climatology and Paleoclimatology of the East African Lakes. Gordon and Breach, London, pp. 495-508.

Flohn, H., 1964. Grundfragen der Paläoklimatologie im Lichte einer theoretischen Klimatologie. Geol. Rdsch. 54, 504-515.

Flohn, H., 1967. Bemerkungen zur Asymmetrie der atmospharischen Zirkulation. Annalen der Meteorologie, Neue Folge 3, 76-80.

Flohn, H., 1978. Comparison of Antarctic and Arctic climate and its relevance to climatic evolution. In: E. M. van Zinderen Bakker (Ed.), Antarctic glacial history and world palaeoenvironments. A. A. Balkema, Rotterdam, pp. 3-13.

Flores, J.-A., Gersonde, R., Sierro, F. J., 1999. Pleistocene fluctuations in the Agulhas current retroflection based on the calcareous plankton record. Marine Micropaleontology 37, 1-22.

Flower, R. J., 1993. Diatom preservation: experiments and observations on dissolution and breakage in modern and fossil material. Hydrobiologia 269/270, 473-484.

Fontes, J. Ch., Gasse, F., 1991. PALHYDAF (Palaeohydrology in Africa) program: objectives, methods, major results. Palaeogeography, Palaeoclimatology, Palaeoecology 84, 191-215.

Friedman, I., 1953. Deuterium content of natural water and other substances. Geochimica et Cosmochimica Acta 4, 89-103.

Friedman, I., Machta, L., Soller, R., 1962. Water vapour exchange between a water droplet and its environment. Journal of Geophysical Research 67, 2761-2766.

Fritz, S. C., Juggins, S., Battarbee, R. W., 1993. Diatom assemblages and ionic characterization of freshwater and saline lakes of the Northern Great Plains, North America: a tool for reconstructing past salinity and climate fluctuations. Canadian Journal of Fisheries and Aquatic Sciences 50, 1844-1856.

Fritz, S., Baker, P. A., Lowenstein, T. K., Seltzer, G. O., Rigsby, C. A., Dwyer, G. S., Tapia.P.M., Arnold, K. K., Ku, T.-L., Luo, S., 2004. Hydrologic variation during the last 170,000 years in the southern hemisphere tropics of South America. Quaternary Research 61, 95-104.

Fronval, T., Jensen, N. B., Buchardt, B., 1995. Oxygen isotope disequilibrium precipitation of calcite in Lake Arresø, Denmark. Geology 23, 463-466.

Frost, T. M., 2001. Freshwater sponges. In: J. P. Smol, H. J. B. Birks, W. M. Last (Eds.), Tracking environmental change using lake sediments. Volume 3: Terrestrial, Algal, and Siliceous Indicators. Kluwer Academic Publishers, Dordrecht, pp. 253-263.

Gallimore, R. G., Kutzbach, J. E., 1995. Snow cover and sea ice sensitivity to generic changes in Earth orbital parameters. Journal of Geophysical Research 100, 1103-1120.

Ganopolski, A., Rahmstorf, S., Petoukhov, V., Claussen, M., 1998. Simulation of modern and glacial climates with a coupled global model of intermediate complexity. Nature 391, 351-356.

Garnett, E. R., Gilmour, M. A., Rowe, P. J., Andrews, J. E., Preece, R. C., 2004. $^{230}Th/^{234}U$ dating of Holocene tufas: possibilities and problems. Quaternary Science Reviews 23, 947-958.

Gascoyne, M., 1992. Geochemistry of the actinides amd their daughters. In: M. Ivanovich, R. S. Harmon (Eds.), Uranium series disequilibrium: applications to environmental problems. Oxford University press, Oxford.

Gasse, F., 1977. Evolution of Lake Abhé (Ethiopia and TFAI), from 70,000 b.p. Nature 265, 42-45.

Gasse, F., 1986. East African Diatoms: taxonomy, ecological distribution. Kramer, Berlin.

Gasse, F., 1987. Diatoms for reconstructing palaeoenvironments and paleohydrology in tropical semi-arid zones. Hydrobiologia 154, 127-163.

Gasse, F., 2000. Hydrological changes in the African tropics since the Last Glacial Maximum. Quaternary Science Reviews 19, 189-211.

Gasse, F., 2002. Diatom-inferred salinity and carbonate oxygen isotopes in Holocene waterbodies of the western Sahara and Sahel (Africa). Quaternary Science Reviews 21, 737-767.

Gasse, F., van Campo, E., 1998. A 40,000-yr pollen and diatom record from Lake Tritrivakely, Madagascar, in the Southern Tropics. Quaternary Research 49, 299-311.

Gasse, F., van Campo, E., 2001. Late Quaternary environmental change from a pollen and diatom record in the southern tropics (Lake Tritrivakely, Madagascar). Palaeogeography, Palaeoclimatology, Palaeoecology 167, 287-308.

Gasse, F., Rognon, P., Street, F. A., 1980. Quaternary history of the Afar and Ethiopian Rift lakes. In: M. A. J. Williams, H. Faure (Eds.), The Sahara and the Nile. A. A. Balkema, Rotterdam, pp. 361-400.

Gasse, F., Talling, J. F., Kilham, P., 1983. Diatom assemblages in East Africa: Classification, distribution and ecology. Revue Hydrobiologie tropicale 16, 3-34.

Gasse, F., Téhet, R., Durand, A., Gilbert, A., Fontes, J.-C., 1990. The arid-humid transition in the Sahara and the Sahel during the last deglaciation. Nature 346, 141-146.

Gasse, F., Juggins, S., Khelifa, L. B., 1995. Diatom-based transfer functions for inferring past hydrochemical characteristics of African lakes. Palaeogeography, Palaeoclimatology, Palaeoecology 117, 31-54.

Gasse, F., Barker, P., Johnson, T. C., 2002. A 24,600 yr diatom record from the northern basin of Lake Malawi. In: E. O. Odada, D. O. Olago (Eds.), The East African Great Lakes: Limnology, Palaeoclimatology and Biodiversity. Kluwer Academic Publishers, Dordrecht, pp. 393-414.

Gat, J. R., 1971. Comments on stable isotope method in regional groundwater investigations. Water Resources Research 7, 980-993.

Gat, J. R., 1980. The isotopes of hydrogen and oxygen in precipitation. In: P. Fritz, J. Ch. Fontes (Eds.), Handbook of environmental isotope geochemistry. Volume 1. The terrestrial environment, A. Elsevier, Amsterdam, pp. 21-47.

Gat, J. R., 1981. Isotopic fractionation. In: J. R. Gat, R. Gonfiantini (Eds.), Stable isotope hydrology: deuterium and oxygen-18 in the water cycle. IAEA Technical Report Series, No. 210. IAEA, Vienna, pp. 21-34.

Gat, J. R., 1995. Stable isotopes of fresh and saline lakes. In: A. Lerman, D. M. Imboden, J. R. Gat (Eds.), Physics and Chemistry of lakes. Springer Verlag, Berlin, pp. 139-165.

Gat, J. R., 1996. Oxygen and hydrogen isotopes in the hydrological cycle. Annual Reviews of Earth and Planetary Sciences 24, 225-262.

Gat, J. R., Tzur, Y., 1967. Modification of the isotopic composition of rainwater by processes which occur before groundwater recharge. In: Isotopes in Hydrology, IAEA, Vienna. pp. 49-60.

Gat, J. R., Carmi, I., 1970. Evolution of the isotopic composition of atmospheric waters in the Mediterranean Sea area. Journal of Geophysical Research 75, 3039-3048.

Gaudet, J. J., Melack, J. M., 1981. Major ion chemistry in a tropical African lake basin. Freshwater Biology 11, 309-333.

Gersonde, R., Abelmann, A., Brathauer, U., Becquey, S., Bianchi, C., Cortese, G., Grobe, H., Kuhn, G., Niebler, H.-S., Segl, M., Sieger, R., Zielinski, U., Fütterer, D. K., 2003. Last glacial sea surface temperatures and sea-ice extent in the Southern Ocean (Atlantic-Indian sector): A multiproxy approach. Paleoceanography 18, 6-1 - 6-18.

Geyh, M. A., 2001. Reflections on the ^{230}Th/U dating of dirty material. Geochronometria 20, 9-14.

Geyh, M. A., Schotterer, U., Grosjean, M., 1998. Temporal changes of the C-14 reservoir effect in lakes. Radiocarbon 40, 921-931.

Giddings, J. C., 1985. A system based on split-flow lateral-transport thin (SPLITT) separation cells for rapid and continuous particle fractionation. Separation Science and Technology 20, 749-768.

Gillespie, R., Street-Perrott, F. A., Switzur, R., 1983. Post-glacial arid episodes in Ethiopia have implications for climate prediction. Nature 306, 680-683.

Giraudeau, J., Pierre, C., Herve, L., 2001. A late Quaternary, high-resolution record of planktonic foraminiferal species distribution in the Southern Benguela region: site 1087. In: G. Wefer, W. H. Berger, C. Richter (Eds.), Proceedings of the Ocean Drilling Program, Scientific Results Volume 175. pp. 1-26.

Giresse, P., Maley, J., Kelts, K., 1991. Sedimentation and palaeoenvironment in crater lake Barombi Mbo, Cameroon, during the last 25,000 years. Sedimentary Geology 71, 151-175.

Goddard, L., Graham, N. E., 1999. Importance of the Indian Ocean for simulating rainfall anomalies over eastern and southern Africa. Journal of Geophysical Research 105, 19099-19166.

Gonfiantini, R., 1986. Environmental isotopes in lake studies. In: P. Fritz, J. Ch. Fontes (Eds.), Handbook of Environmental Isotope Geochemistry, Volume 2. The terrestrial environment, B. Elsevier, Amsterdam, pp. 113-168.

Grossman, E. L., Ku, T.-L., 1986. Oxygen and carbon isotope fractionation in biogenic aragonite: temperature effects. Chemical Geology 59, 59-74.

Guilderson, T. P., Fairbanks, R. G., Rubenstone, J. L., 1994. Tropical temperature variations since 20,000 years ago: modulating interhemispheric climate change. Science 263, 663-665.

Guy, R. D., Fogel, M. L., Berry, J. A., 1993. Photosynthetic fractionation of the stable isotopes of oxygen and carbon. Plant Physiology 101, 37-47.

Haberyan, K. A., Hecky, R. E., 1987. The late Pleistocene and Holocene stratigraphy and paleolimnology of Lakes Kivu and Tanganyika. Palaeogeography, Palaeoclimatology, Palaeoecology 61, 169-197.

Haimson, M., Knauth, L. P., 1983. Stepwise-fluorination - a useful approach for the isotopic analysis of hydrous minerals. Geochimica et Cosmochimica Acta 47, 1589-1595.

Håkanson, L., 1977. The influence of wind, fetch and water depth on the distribution of sediments in Lake Vänern, Sweden. Canadian Journal of Fisheries and Aquatic Sciences 14, 397-412.

Håkansson, H., Chepurnov, V., 1999. A study of variation in valve morphology of the diatom *Cyclotella meneghiniana* in monoclonal cultures: effect of auxospore formation and different salinity conditions. Diatom Research 14, 251-272.

Hall, R. I., Smol, J. P., 1992. A weighted-averaging regression and calibration model for inferring total phosphorous concentration from diatoms in British Columbian (Canada) lakes. Freshwater Biology 27, 417-434.

Hancok, F. D., 1979. Diatom associations and succession in Lake Kariba, South Central Africa. Hydrobiologia 67, 33-50.

Harangozo, S., Harrison, M. S. J., 1983. On the use of synoptic data indicating the presence of cloud bands over southern Africa. South African Journal of Science 79, 413-414.

Harrison, M. S. J., 1984. The annual rainfall cycle over the central interior of South Africa. South African Geographical Journal 66, 47-64.

Harvey, H. R., Tuttle, J. H., Bell, J. T., 1995. Kinetics of phytoplankton decay during simulated sedimentation: Changes in biochemical composition and microbial activity under oxic and anoxic conditions. Geochimica et Cosmochimica Acta 59, 3367-3377.

Hastenrath, S., 1991. Climate Dynamics of the Tropics. Kluwer Academic Publishing, Dordrecht.

Hastenrath, S., Kutzbach, J. E., 1983. Paleoclimatic estimates from water and energy budgets of East African Lakes. Quaternary Research 19, 141-153.

Haug, G. H., Hughen, K. A., Sigman, D. M., Peterson, L. C., Röhl, U., 2001. Southward migration of the Intertropical Convergence Zone through the Holocene. Science 293, 1304-1307.

Hays, J. D., Imbrie, J., Shackleton, N. J., 1976. Variations in the earth's orbit: pacemaker of the Ice Ages. Science 194, 1121-1132.

Heaton, T. H. E., 1992. Procedure and notes on zinc reduction of water for D/H analysis and aluminium-bronze hot-block. Unpublished report, Series number 43, NERC Isotope Geosciences Laboratory.

Heaton, T. H. E., Talma, A. S., Vogel, J. C., 1983. Origin and history of nitrate in confined groundwater in the western Kalahari. Journal of Hydrology 62, 243-262.

Heaton, T. H. E., Talma, A. S., Vogel, J. C., 1986. Dissolved gas palaeotemperatures and ^{18}O variations derived from groundwater near Uitenhage, South Africa. Quaternary Research 25, 79-88.

Hecky, R.E., Hesslein, R.H., 1995. Contributions of benthic algae to lake food webs as revealed by stable isotope analysis. Journal of the North American Benthological Society 14, 631-653.

Hecky, R. E., Kilham, P., 1973. Diatoms in alkaline, saline lakes: ecology and geochemical implications. Limnology and Oceanography 18, 53-71.

Heiri, O., Lotter, A. F., Lemcke, G., 2001. Loss on ignition as a method for estimating organic and carbonate content in sediments: reproducibility and comparability of results. Journal of Paleolimnology 25, 101-110.

Henderson, G. M., Slowey, N. C., 2000. Evidence from U-Th dating against Northern Hemisphere forcing of the penultimate deglaciation. Nature 404, 61-66.

Hess, S. L., 1959. Introduction to theoretical meteorology. Krieger Publishing Company, Malabar, Florida.

Hillaire-Marcel, C., Riser, C., Rognon, P., Petit-Maire, N., Rosso, J. C., Soulié-Märsche, I., 1983. Radiocarbon chronology of Holocene hydrologic changes in Northeastern Malawi. Quaternary Research 20, 145-164.

Hillaire-Marcel, C., Carro, O., Casanova, J., 1986. ^{14}C and Th/U dating of Pleistocene and Holocene Stromatolites from East African Paleolakes. Quaternary Research 25, 312-329.

Hillebrand, H., Dürselen, C.-D., Kirschtel, D., Pollingher, U., Zohary, T., 1999. Biovolume calculation for pelagic and benthic microalgae. Journal of Phycology 35, 403-424.

Hillesheim, M. B., Brenner, M., Curtis, J. H., Anselmetti, F. S., Ariztegui, D., Buck, D. G., Guilderson, T. P., Rosenmeier, M. F., Schnurrenberger, D. W., 2005. Climate change in lowland Central America during the late deglacial and early Holocene. Journal of Quaternary Science 20, 363-376.

Hilton, J., 1985. A conceptual framework for predicting the occurrence of sediment focusing and sediment redistribution in small lakes. Limnology and Oceanography 30, 1131-1143.

Hodell, D. A., Curtis, J. H., Jones, G. A., Higuera-Gundy, A., Brenner, M., Binford, M. W., Dorsey, K. T., 1991. Reconstruction of Caribbean climate change over the past 10,500 years. Nature 352, 790-793.

Hodell, D. A., Kanfoush, S. L., Shemesh, A., Crosta, X., Charles, C. D., Guilderson, T. P., 2001. Abrupt cooling of Antarctic surface waters and sea ice expansion in the South Atlantic sector of the Southern Ocean at 5000 cal yr B.P. Quaternary Research 56, 191-198.

Hoelzmann, P., Gasse, F., Dupont, L. M., Salzmann, U., Staubwasser, M., Leuschner, D. C., Sirocko, F., 2004. Palaeoenvironmental changes in the arid and sub arid belt (Sahara-Sahel-Arabian Peninsula) from 150 kyr to present. In: R. W. Battarbee, F. Gasse, C. E. Stickley (Eds.), Past climate variability through Europe and Africa. Springer, Dordrecht, pp. 219-256.

Hollander, D. J., MacKenzie, J. A., 1991. CO_2 control on carbon-isotope fractionation during aqueous photosynthesis: a paleo pCO_2 barometer. Geology 19, 929-932.

Holmes, J. A., Street-Perrott, F. A., Perrott, R. A., Stokes, S., Waller, M. P., Huang, Y., Eglington, G., Ivanovich, M., 1999. Holocene landscape evolution of the Manga grasslands, NE Nigeria: evidence from palaeolimnology and dune chronology. Journal of the Geological Society 156, 357-368.

Holmgren, K., Karlén, W., Shaw, P. A., 1995. Paleoclimatic significance of the stable isotopic composition and petrology of a late Pleistocene stalagmite from Botswana. Quaternary Research 43, 320-328.

Holmgren, K., Lee-Thorp, J. A., Cooper, G. R. J., Lundblad, K., Partridge, T. C., Scott, L., Sithaldeen, R., Talma, A. S., Tyson, P. D., 2003. Persistant millennial-scale climatic variability over the past 25,000 years in Southern Africa. Quaternary Science Reviews.

Hooghiemstra, H., Stalling, H., Agwu, C. O. C., Dupont, L. M., 1992. Vegetational and climatic changes at the northern fringe of the Sahara 250,000-5,000 years BP: evidence from 4 marine pollen records located between Portugal and the Canary Islands. Review of Palaeobotany and Palynology 74, 1-53.

Hostetler, S. W., Mix, A. C., 1999. Reassessment of ice-age cooling of the tropical ocean and atmosphere. Nature 399, 673-676.

Howard, W. R., Prell, W. L., 1992. Late Quaternary surface circulation of the Southern Indian Ocean and its relationship to orbital variations. Paleoceanography 7, 79-117.

Hu, F. S., Shemesh, A., 2003. A biogenic-silica $\delta^{18}O$ record of climatic change during the last glacial-interglacial transition in southwestern Alaska. Quaternary Research 59, 379-385.

Huang, Y., Freeman, K. H., Eglinton, T. I., Street-Perrott, F. A., 1999. $\delta^{13}C$ analyses of individual lignin phenols in Quaternary lake sediments: a novel proxy for deciphering past terrestrial vegetation changes. Geology 27, 471-474.

Hubble, D. S., Harper, D. M., 2002. Phytoplankton community structure and succession in the water column of Lake Naivasha, Kenya: a shallow tropical lake. Hydrobiologia 488, 89-98.

Hurd, D. C., 1972. Factors affecting solution rate of biogenic opal in seawater. Earth and Planetary Science Letters 15, 411-417.

Hustedt, F., 1949. Süßwasserdiatomeen aus dem Albert-Nationalpark in Belgisch Kongo. In: H. Damas (Ed.), Exploration du Parc National Albert (1935-1936). Hayez, Bruxelles.

Hutchinson, G. E., 1967. A treatise on limnology, volume 2. Wiley.

IAEA, 2001. GNIP Maps and Animations, International Atomic Energy Agency, Vienna. Accessible at http://isohis.iaea.org.

IAEA/WMO, 2001. Global Network of Isotopes in Precipitation. The GNIP Database. Accessible at: http://isohis.iaea.org

Ihaka, R., Gentleman, R., 1996. R: a language for data analysis and graphics. Journal of Computational and Graphical Statistics 5, 299-314.

Imbrie, J., Hays, J. D., Martinson, D. G., McIntyre, A., Mix, A. C., Morley, J. J., Pisias, N. G., Prell, W. L., Shackleton, N. J., 1984. The orbital theory of Pleistocene climate: support from a revised chronology of the marine ^{18}O record. In: A. L. Berger, J. Imbrie, J. Hays, G. Kukla, B. Saltzmann (Eds.), Milankovitch and Climate: understanding the response to astronomical forcing. Reidel, Dordrecht, pp. 269-305.

Interlandi, S. J., Kilham, S. S., 2001. Limiting resources and the regulation of diversity in phytoplankton communities. Ecology 82, 1270-1282.

Irwin, H., Curtis, C., Coleman, M., 1977. Isotopic evidence for source of diagenetic carbonates formed during burial of organic-rich sediments. Nature 269, 209-213.

Ito, E., 2001. Application of stable isotope techniques to inorganic and biogenic carbonates. In: W. M. Last, J. P. Smol (Eds.), Tracking Environmental Change Using Lake Sediments. Volume 2: Physical and geochemical methods. Kluwer Academic Publishers, Dordrecht, pp. 351-371.

Ivanochko, T. S., Ganeshram, R. S., Brummer, G.-J. A., Ganssen, G., Jung, S. J. A., Moreton, S. G., Kroon, D., 2005. Variations in tropical convection as an amplifier of global climate change at the millennial scale. Earth and Planetary Science Letters 235, 302-314.

Ivanovich, M., Harmon, R. S., 1992. Uranium series disequilibrium: applications to environmental problems. Clarendon Press, Oxford.

Iversen, J., 1929. Studien über die pH-Verhältnisse Dänischer Gewässer und ihren Einfluss auf die Hydrophyten Vegetation. Bot. Tidsskr. 40, 277-333.

Jackson, C. S., Broccoli, A. J., 2003. Orbital forcing of Arctic climate: mechanisms of climate response and implications for continental glaciation. Climate Dynamics 21, 539-557.

Jackson, D. A., 1993. Stopping rules in Principal Components Analysis: A comparison of heuristical and statistical approaches. Ecology 74, 2204-2214.

Jahns, S., 1996. Vegetation history and climate changes in West Equatorial Africa during the Late Pleistocene and Holocene, based on a marine pollen diagram from the Congo Fan. Vegetation History and Archaeobotany 5, 207-213.

Jewell, M. E., 1935. An ecological study of the freshwater sponges of northern Wisconsin. Ecological Monographs 5, 461-504.

Jiménez-López, C., Romanek, C. S., Huertas, F. J., Ohmoto, H., Caballero, E., 2004. Oxygen isotope fractionation in synthetic magnesian calcite. Geochimica et Cosmochimica Acta 68, 3367-3377.

Jiménez-López, C., Romanek, C. S., Caballero, E., 2006. Carbon isotope fractionation in synthetic magnesian calcite. Geochimica et Cosmochimica Acta 70, 1163-1171.

Johnson, B. J., Miller, G. H., Fogel, M. L., Beaumont, P. B., 1997. The determination of late Quaternary palaeoenvironments at Equus Cave, South Africa, using stable isotopes and amino acid racemization in ostrich egg shell. Palaeogeography, Palaeoclimatology, Palaeoecology 136, 121-137.

Johnson, T. C., 1996. Sedimentary processes and signals of past climatic change in the large lakes of the East African Rift valley. In: T. C. Johnson, E. O. Odada (Eds.), The limnology, climatology, and paleoclimatology of the East African Lakes. Gordon and Breach, Amsterdam, pp. 367-412.

Johnson, T. C., Chan, Y., Beuning, K. R. M., Kelts, K., Ngobi, G., Verschuren, D., 1998. Biogenic silica profiles in Holocene Cores from Lake Victoria: implications for lake level history and initiation of the Victoria Nile. In: J. T. Lehman (Ed.), Environmental change and response in East African Lakes. Kluwer, Dordrecht.

Johnson, T. C., Brown, E. T., McManus, J., Barry, S., Barker, P., Gasse, F., 2002. A high-resolution paleoclimate record spanning the past 25,000 years in southern East Africa. Science 296, 113-132.

Johnson, T. C., Brown, E. T., McManus, J., 2004. Diatom productivity in northern Lake Malawi during the past 25,000 years: implications for the position of the intertropical convergence zone at millennial and shorter timescales. In: R. W. Battarbee, F. Gasse, C. E. Stickley (Eds.), Past climate variability through Europe and Africa. Springer, Dordrecht, pp. 93-116.

Jones, B. F., Bowser, C. J., 1978. The mineralogy and related chemistry of lake sediments. In: A. Lerman (Ed.), Lakes: Chemistry, Geology, Physics. Springer-Verlag, New York, pp. 179-235.

Jouzel, J., Merlivat, L., 1984. Deuterium and oxygen-18 in precipitation, modelling of the isotope effect during snow formation. Journal of Geophysical Research 89D, 11749-11757.

Juggins, S., 1992a. Diatoms in the Thames Estuary, England: ecology, palaeoecology, and salinity transfer function. Bibliotheca Diatomologica. J. Cramer, Berlin, Stuttgart.

Juggins, S., 1992b. TRAN (version 1.8) and ZONE (version 1.2) User Manual.

Juillet, A., 1980a. Analyse isotopique de la silice des diatomees lacustres et marines: fractionnement des isotopes de l'oxygene en fonction de la temperature. Université Paris-Sud XI.

Juillet, A., 1980b. Structure de la silice biogènique: nouvelles donneés apportees par l'analyse isotopique de l'oxygène. CR Academy of Science, Paris 290, 1237-1239.

Juillet-Leclerc, A., 1984. Cleaning process for diatomaceous samples. 8th Diatom Symposium, pp. 733-736.

Juillet-Leclerc, A., Labeyrie, L., 1987. Temperature dependence of the oxygen isotope fractionation between diatom silica and water. Earth and Planetary Science Letters 84, 69-74.

Jury, M. R., 1992. A climatic dipole governing the interannual variability of convection over the SW Indian Ocean and SE Africa region. Trends in Geophysical Research 1, 165-172.

Jury, M. R., 1995. A review of research on ocean-atmosphere interactions and South African Climate variability. South African Journal of Science 91, 289-294.

Jury, M. R., 1996. Regional teleconnection patterns associated with summer rainfall over South Africa, Namibia and Zimbabwe. International Journal of Climatology 16, 135-153.

Jury, M. R., Pathack, B., 1991. A study of climate and weather variability over the tropical southwest Indian Ocean. Meteorology and Atmospheric Physics 47, 37-48.

Jury, M. R., Pathack, B. M. R., 1993. Composite climatic patterns associated with extreme modes of summer rainfall over southern Africa: 1975–1984. Theoretical and Applied Climatology 47, 137-145.

Jury, M. R., Pathack, B. M. R., Sohn, B. J., 1992. Spatial structure and interannual variability of summer convection over southern Africa and the SW Indian Ocean. South African Journal of Science 88, 275-280.

Jury, M. R., Valentine, H. R., Lutjeharms, J. R. E., 1993. Influence of the Agulhas Current on Summer Rainfall along the Southeast Coast of South Africa. Journal of Applied Meteorology 32, 1282-1287.

Jury, M. R., McQueen, C. A., Levey, K. M., 1994. SOI and QBO signals in the African region. Theoretical and Applied Climatology 50, 103-115.

Kaplan, A., Zenvirth, D., Reinhold, L., Berry, J. A., 1982. Involvement of a primary electrogenic pump in the mechanism for bicarbonate uptake by the cyanobacterium *Anabaena variabilis*. Plant Physiology 69, 978-982.

Kaufman, A., Broecker, W. S., 1965. Comparison of ^{230}Th and ^{14}C ages for carbonate materials from Lakes Lahontan and Bonneville. Journal of Geophysical Research 70, 4039-4054.

Keeling, C.D., Mook, W.G., Tans, P.P., 1979. Recent trends in the $^{13}C/^{12}C$ ratio of atmospheric carbon dioxide. Nature 277, 121-123.

Keeling, C. D., Whorf, T. P., Wahlen, M., van der Plicht, J., 1995. Interannual extremes in the rate of rise of atmospheric carbon dioxide since 1980. Nature 375, 666-670.

Keith, M. L., Weber, J. N., 1964. Isotopic composition and evironmental classification of selected limestones and fossils. Geochimica et Cosmochimica Acta 28, 1787-1816.

Kelts, K., 1998. Components in lake sediments: Smear slide identifications. http://lrc.geo.umn.edu/ smears/smsl.html.

Kelts, K., Hsü, K. J., 1978. Freshwater carbonate sedimentation. In: A. Lerman (Ed.), Lakes: chemistry, geology, physics. Springer-Verlag, New York, pp. 295-353.

Kilham, P., 1990. Ecology of *Melosira* Species in the Great Lakes of Africa. In: M. M. Tilzer, C. Serruya (Eds.), Large Lakes. Ecological structure and function. Springer-Verlag, Berlin, New York, pp. 414-427.

Kilham, P., Kilham, S. S., 1990. Endless summer: internal loading processes dominate nutrient cycling in tropical lakes. Freshwater Biology 23, 379-389.

Kilham, P., Kilham, S. S., Hecky, R. E., 1986. Hypothesized resource relationships among African planktonic diatoms. Limnology and Oceanography 31, 1169-1181.

Kilham, S. S., Kilham, P., 1975. *Melosira granulata* (Eh.) Ralfs: morphology and ecology of a cosmopolitan freshwater diatom. Verh. Internat. Verein. Limnol. 16, 2716-2721.

Kim, S.-J., Crowley, T. J., Stössel, A., 1998. Local orbital forcing of Antarctic climate change during the last interglacial. Science 280, 728-730.

Kim, S.-T., O'Neil, J. R., 1997. Equilibrium and non-equilibrium oxygen isotope effects in synthetic carbonates. Geochimica et Cosmochimica Acta 61, 3461-3475.

Kim, S.-T., O'Neil, J. R., 2005. Comment on "An experimental study of oxygen isotope fractionation between inorganically precipitated aragonite and water at low temperatures" by G.-T. Zhou and Y.-F. Zheng. Geochimica et Cosmochimica Acta 69, 3195-3197.

Kirst, G. J., Schneider, R. R., Müller, P. J., von Storch, I., Wefer, G., 1999. Late Quaternary temperature variability in the Benguela Current System derived from alkenones. Quaternary Research 52, 92-103.

Klass, D. L., 1984. Methane from anaerobic fermentation. Science 223, 1021-1028.

Klein, R. G., 1991. Size variation in the Capedune molerat (*Bathyergus suillus*) and late Quaternary climatic change in the southwestern Cape Province, South Africa. Quaternary Research 36, 243-256.

KMD (Kenya Meteorological Department), 2000. Unpublished synoptic rain station data. Ministry of Information, Transport and Communications, Nairobi, Kenya.

Koeberl, C., Storzer, D., Reimold, W. U., 1994. The age of the Saltpan impact crater, South Africa. Meteoritics 29, 374-379.

Köppen, W., Wegener, A., 1924. Die Klimate der Geologischen Vorzeit. Gebrüder Borntraeger, Berlin.

Krammer, K., Lange-Bertalot, H., 1991a. Bacillariophyceae-3. Teil: Centrales, Fragilariaceae, Eunotiaceae. In: Ettl, H., Gerloff, J., Heynig, H., and Mollenhauer, D. (Eds.), Süßwasserflora von Mitteleuropa vol. 2/3. Gustav Fischer Verlag, Stuttgart.

Krammer, K., Lange-Bertalot, H., 1991b. Bacillariophyceae-4. Teil: Achnanthaceae, kritische ergänzungen zu navicula (lineolatae) und gomphonema, gesamtliteraturverzeichnis teil 1-4. In: Ettl, H., Gerloff, J., Heynig, H., and Mollenhauer, D. (Eds.), Süßwasserflora von Mitteleuropa vol. 2/4. Gustav Fischer Verlag, Stuttgart.

Krammer, K., Lange-Bertalot, H., 1997a. Bacillariophyceae-1. Teil: Naviculaceae. In: Ettl, H., Gerloff, J., Heynig, H., and Mollenhauer, D. (Eds.), Süßwasserflora von Mitteleuropa vol. 2/1. Gustav Fischer Verlag, Stuttgart.

Krammer, K., Lange-Bertalot, H., 1997b. Bacillariophyceae-2. Teil: Bacillariaceae, Epithemiaceae, Surirellaceae. In: Ettl, H., Gerloff, J., Heynig, H., and Mollenhauer, D. (Eds.), Süßwasserflora von Mitteleuropa vol. 2/2. Gustav Fischer Verlag, Stuttgart.

Kraus, E. B., 1959. The evaporation-precipitation cycle of the trades. Tellus 11, 147-158.

Kraus, E. B., 1977. Subtropical droughts and cross-equatorial energy transports. Monthly Weather Review 105, 1009-1018.

Ku, T.-L., Luo, S., Lowenstein, T. K., Li, J., Spencer, R. J., 1998. U-series chronology of lacustrine deposits in Death Valley, California. Quaternary Research 50, 261-275.

Kuhn, G., Diekmann, B., 2002. Late Quaternary variability of ocean circulation in the southeastern South Atlantic inferred from the terrigenous sediment record of a drift deposit in the southern Cape Basin (OSP Site 1089). Palaeogeography, Palaeoclimatology, Palaeoecology 182, 287-303.

Kukla, G., Gavin, J., 2005. Did glacials start with global warming? Quaternary Science Reviews 24, 1547-1557.

Kutzbach, J. E., 1981. Monsoon climate of the early Holocene: climate experiment with the earth's orbital parameters for 9000 years ago. Science 214, 59-61.

Kutzbach, J. E., Otto-Bliesner, B. L., 1982. The sensitivity of the African-Asian monsoonal climate to orbital parameter changes for 9000 years B.P. in a low-resolution general circulation model. Journal of Atmospheric Science 39, 1177-1188.

Kutzbach, J. E., Guetter, P. J., 1984a. Sensitivity of late-glacial and Holocene climates to the combined effects of orbital parameter changes and lower boundary condition changes: "snapshot" simulations with a general circulation model for 18, 9 and 6 ka BP. Annals of Glaciology 5, 85-87.

Kutzbach, J. E., Guetter, P. J., 1984b. The sensitivity of monsoon climates to orbital parameter changes for 9000 years B.P.- experiments with the NCAR general circulation model. In: A. L. Berger, J. Imbrie, J. Hays, G. Kukla, B. Saltzman (Eds.), Milankovitch and Climate: understanding the response to astronomical forcing. Part 2. D. Reidel, Dordrecht, pp. 801-820.

Kutzbach, J. E., Guetter, P. J., 1986. The influence of changing orbital parameters and surface boundary conditions on climate simulations for the past 18,000 years. Journal of the Atmospheric Sciences 43, 1726-1759.

Kutzbach, J. E., Street-Perrott, F. A., 1985. Milankovitch forcing of fluctuations in the level of tropical lakes from 18 to 0 kyr BP. Nature 317, 130-134.

Kutzbach, J. E., Liu, Z., 1997. Response of the African monsoon to orbital forcing and ocean feedbacks in the Middle Holocene. Science 278, 440-443.

Kutzbach, J., Bonan, G., Foley, J., Harrison, S. P., 1996. Vegetation and soil feedbacks on the response of the African monsoon to orbital forcing in the early to middle Holocene. Nature 384, 623-626.

Labeyrie, L. D., Juillet, A., 1982. Oxygen isotopic exchangeability of diatom valve silica; interpretation and consequences for paleoclimatic studies. Geochimica et Cosmochimica Acta 46, 967-975.

Lamb, A. L., Leng, M. J., Lamb, H. F., Umer Mohammed, M., 2000. A 9000-year oxygen and carbon isotope record of hydrological change in a small Ethiopian crater lake. The Holocene 10, 167-177.

Lamb, A. L., Leng, M. J., Umer Mohammed, M., Lamb, H. F., 2004. Holocene climate and vegetation change in the Main Ethiopian Rift Valley, inferred from the composition (C/N and $\delta^{13}C$) of lacustrine organic matter. Quaternary Science Reviews 23, 881-891.

Lamb, A. L., Leng, M. J., Sloane, H. J., Telford, R. J., 2005. A comparison of the palaeoclimate signals from diatom oxygen isotope ratios and carbonate oxygen isotope ratios from a low latitude crater lake. Palaeogeography, Palaeoclimatology, Palaeoecology 223, 290-302.

Lancaster, N., 1979. Evidence for a widespread late Pleistocene humid period in the Kalahari. Nature 279, 145-146.

Lancaster, N., 1989. Late quaternary palaeoenvironments in the southwestern Kalahari. Palaeogeography, Palaeoclimatology, Palaeoecology 70, 267-276.

Landman, W. A., Mason, J. A., 1999. Change in the association between Indian Ocean sea-surface temperatures and summer rainfall over South Africa and Namibia. International Journal of Climatology 19, 1477-1492.

Landwehr, J.M., Winograd, I.J., 2001. Dating the Vostok ice core record by importing the Devils Hole chronology. Journal of Geophysical Research 106, 31853-31861.

Lao, Y., Benson, L., 1988. Uranium-series age estimates and palaeoclimatic significance of Pleistocene tufas from the Lahontan Basin, California and Nevada. Quaternary Research 30, 165-176.

Laskar, J., Robutel, P., Joutel, F., Gastineau, M., Correia, A. C. M., Levrard, B., 2004. A long-term numerical solution for the insolation quantities of the Earth. Astronomy and Astrophysics 428, 261-285.

Last, W. M., 2002. Geolimnology of salt lakes. Geosciences Journal 6, 347-369.

Lawrence, J. R., Taylor, H. P., 1971. Deuterium and oxygen-18 correlation: clay minerals and hydroxides in Quaternary soils compared to meteoric water. Geochimica et Cosmochimica Acta 35, 993-1003.

Laws, E. A., Popp, B. N., Bidigare, R. R., Kennicutt, M. C., Macko, S. A., 1995. Dependence of phytoplankton isotopic composition on growth rate and $[CO_2]_{aq}$: theoretical considerations and experimental results. Geochimica et Cosmochimica Acta 59, 1131-1138.

Lawson, J., Doran, P. T., Kenig, F., Des Marais, D. J., Prisc, J. C., 2004. Stable carbon and nitrogen isotopic composition of benthic and pelagic organic matter in lakes of the McMurdo dry valleys, Antarctica. Aquatic Geochemistry 10, 269-301.

Lea, D. W., Pak, D. K., Spero, H. J., 2000. Climate impact of late Quaternary equatorial Pacific sea surface temperature variations. Science 289, 1719-1724.

Leavitt, P. R., Hodgson, D. A., 2001. Sedimentary pigments. In: J. P. Smol, H. J. B. Birks, W. M. Last (Eds.), Tracking Environmental Change using Lake Sediments. Volume 3: Terrestrial, Algal, and siliceous indicators. Kluwer Academic Publishers, Dordrecht, pp. 295-325.

Ledru, M.-P., Rousseau, D.-D., Cruz, F. W., Riccomini, C., Karmann, I., Martin, L., 2005. Paleoclimate changes during the last 100,000 yr from a record in the Brazilian Atlantic rainforest region and interhemispheric comparison. Quaternary Research 64, 444-450.

Lee-Thorp, J. A., Talma, A. S., 2000. Stable light isotopes and past environments in the Southern African Quaternary. In: T. C. Partridge, R. R. Maud (Eds.), The Cenozoic of Southern Africa. Oxford University Press, New York, pp. 236-251.

Lee-Thorp, J. A., Holmgren, K., Lauritzen, S.-E., Linge, H., Moberg, A., Partridge, T. C., Stevenson, C., Tyson, P. D., 2001. Rapid climate shifts in the Southern African interior throughout the mid to late Holocene. Geophysical Research Letters 28, 4507-4510.

Legendre, P., Legendre, P., 1998. Numerical Ecology. Elsevier Science B.V., Amsterdam.

Legendre, P., Gallagher, E. D., 2001. Ecologically meaningful transformations for ordination of species data. Oecologia 129, 271-280.

Lehmann, M. F., Bernasconi, S. M., Barbieri, A., McKenzie, J. A., 2002. Preservation of organic matter and alteration of its carbon and nitrogen isotope composition during simulated and in situ early sedimentary diagenesis. Geochimica et Cosmochimica Acta 66, 3573-3584.

Leng, M. J., Marshall, J. D., 2004. Palaeoclimate interpretation of stable isotope data from lake sediment archives. Quaternary Science Reviews 23, 811-831.

Leng, M. J., Barker, P. A., 2006. A review of the oxygen isotope composition of lacustrine diatom silica for palaeoclimate reconstruction. Earth-Science Reviews 75, 5-27.

Leng, M., Barker, P., Greenwood, P., Roberts, N., Reed, J., 2001. Oxygen isotope analysis of diatom silica and authigenic calcite from Lake Pinarbasi, Turkey. Journal of Paleolimnology 25, 343-349.

Leng, M. J., Lamb, A. L., Heaton, T. H. E., Marshall, J. D., Wolfe, B. B., Jones, M. D., Holmes, J. A., Arrowsmith, C., 2006. Isotopes in lake sediments. In: M. J. Leng (Ed.), Isotopes in Palaeoenvironmental Research. Springer, Dordrecht, pp. 147-184.

Lerman, A., 1979. Geochemical processes: water and sediment environments. Wiley, New York.

Leroux, M., 2001. The meteorology and climate of tropical Africa. Springer-Praxis Publishing, London-Chichester.

LeRoy, S. A. G., Colman, S. M., 2001. Coring and drilling equipment and procedures for recovery of long lacustrine sequences. In: W. M. Last, J. P. Smol (Eds.), Tracking Environmental Change using lake sediments. Volume 1: Basin analysis, coring, and chronological techniques. Kluwer Academic Publishers, Dordrecht.

Leuenberger, M., Siegenthaler, U., Langway, C. C., 1992. Carbon isotope composition of atmospheric CO_2 during the last ice age from an Antarctic ice core. Nature 357, 488–490.

Leuschner, D. C., Sirocko, F., 2000. The low-latitude monsoon climate during Dansgaard-Oeschger cycles and Heinrich events. Quaternary Science Reviews 19, 243-254.

Leuschner, D. C., Sirocko, F., 2003. Orbital insolation forcing of the Indian Monsoon - a motor for global climate changes? Palaeogeography, Palaeoclimatology, Palaeoecology 197, 83-95.

Levin, G., 1991. The Pretoria Salt Pan: the historical aspects. Geobulletin 34, 13-16.

Lewin, J. C., 1961. The dissolution of silica from diatom walls. Geochimica et Cosmochimica Acta 21, 182-198.

Lewis, W. M. Jr., 1996. Tropical lakes: how latitude makes a difference. In: F. Schiemer, K. T. Boland (Eds.), Perspectives in Tropical Limnology. SPB Academic Publishing bv, Amsterdam, pp. 43-64.

Lézine, A.-M., 1991. West African Paleoclimates during the last climatic cycle inferred from an Atlantic Deep-Sea Pollen Record. Quaternary Research 35, 456-463.

Lézine, A.-M., Casanova, J., 1991. Correlated oceanic and continental records demonstrate past climate and hydrology of North Africa (0-140 ka). Geology 19, 307-310.

Lézine, A.-M., Cazet, J.-P., 2005. High-resolution pollen record from core KW31, Gulf of Guinea, documents the history of the lowland forests of West Equatorial Africa since 40,000 yr ago. Quaternary Research 64, 432-443.

Lézine, A.-M., Duplessy, J.-C., Cazet, J.-P., 2005. West African monsoon variability during the last deglaciation and the Holocene: Evidence from fresh water algae, pollen and isotope data from core KW31, Gulf of Guinea. Palaeogeography, Palaeoclimatology, Palaeoecology 219, 225-237.

Li, H.-C., Ku, T.-L., 1997. $\delta^{13}C$-$\delta^{18}O$ covariance as a paleohydrological indicator for closed-basin lakes. Palaeogeography, Palaeoclimatology, Palaeoecology 133, 69-80.

Li, H.-C., Ku, T.-L., Stott, L., Anderson, R. Y., 1997. Stable isotope studies on Mono Lake (California) 1. $\delta^{18}O$ in lake sediments as proxy for climatic change during the last 150 years. Limnology and Oceanography 42, 230-238.

Lin, J. C., Broecker, W. S., Anderson, R. F., Hemming, S., Rubenstone, J. L., Bonani, G., 1996. New $^{230}Th/U$ and ^{14}C ages from Lake Lahontan carbonates, Nevada, USA, and a discussion of the origin of initial thorium. Geochimica et Cosmochimica Acta 60, 2817-2832.

Lindesay, J. A., 1988. South African rainfall, the Southern Oscillation and a Southern hemisphere semi-annual cycle. Journal of Climatology 8, 17-30.

Lindesay, J. A., Vogel, C. H., 1990. Historical evidence for Southern Oscillation-South African rainfall relationships. International Journal of Climatology 10, 679-689.

Lindesay, J. A., Harrison, M. S. J., Haffner, M. P., 1986. The Southern Oscillation and South African rainfall. South African Journal of Science 82, 196-198.

Lindzen, R. S., Nigam, S., 1987. On the role of sea surface temperature gradients in forcing low-level winds and convergence in the tropics. Journal of the Atmospheric Sciences 44, 2418-2436.

Little, M. G., Schneider, R. R., Kroon, D., Price, B., Bickert, T., Wefer, G., 1997. Rapid paleoceanographic changes in the Benguela Upwelling System for the last 160,000 years as indicated by abundances of planktonic foraminifera. Palaeogeography, Palaeoclimatology, Palaeoecology 130, 135-161.

Liu, Z., Herbert, T. D., 2004. High-latitude influence on the eastern equatorial Pacific climate in the early Pleistocene epoch. Nature 427, 720-723.

Liu, Z., Otto-Bliesner, B., Kutzbach, J., Li, L., Shields, C., 2003. Coupled climate simulation of the evolution of global monsoons in the Holocene. Journal of Climate 16, 2472-2490.

Liu, Z., Harrison, S. P., Kutzbach, J., Otto-Bliesner, B., 2004. Global monsoons in the mid-Holocene and oceanic feedback. Climate Dynamics 22, 157-182.

Loutre, M.-F., Paillard, D., Vimeux, F., Cortijo, E., 2004. Does mean annual insolation have the potential to change the climate? Earth and Planetary Science Letters 221, 1-14.

Lovely, D. R., Klug, M. J., 1986. Model for the distribution of sulfate reduction and methanogenesis in fresh water sediments. Geochimica et Cosmochimica Acta 50, 11-18.

Lucas, W. J., 1983. Photosynthetic assimilation of exogenous HCO_3^- by aquatic plants. Annual Reviews of Plant Physiology and Plant Molecular Biology 34, 71-104.

Ludwig, K. R., Titterington, D. M., 1994. Calculation of $^{230}Th/U$ isochrons, ages, and errors. Geochimica et Cosmochimica Acta 58, 5031-5042.

Luo, S., Ku, T.-L., 1991. U-series isochron dating: a generalised method employing total-sample dissolution. Geochimica et Cosmochimica Acta 55, 555-564.

Lutjeharms, J. R. E., van Ballegooyen, R. C., 1984. Topographic control in the Agulhas current system. Deep-Sea Research 81, 1321-1337.

Lutjeharms, J. R. E., van Ballegooyen, R. C., 1988. The retroflection of the Agulhas current. Journal of Physical Oceanography 18, 1570-1583.

Lutjeharms, J. R. E., Mey, R. D., Hunter, I. T., 1986. Cloud lines over the Agulhas Current. South African Journal of Science 82, 635-640.

Maberly, S. C., Spence, D. H. N., 1983. Photosynthetic inorganic carbon use by freshwater plants. Journal of Ecology 71, 705-724.

Mackay, A. W., Ryves, D. B., Battarbee, R. W., Flower, R. J., Jewson, D., Rioual, P., Sturm, M., 2005. 1000 years of climate variability in central Asia: assessing the evidence using Lake Baikal (Russia) diatom assemblages and the application of a diatom-inferred model of snow cover on the lake. Global and Planetary Change 46, 281-297.

Makarau, A., Jury, M. R., 1997. Predictability of Zimbabwe summer rainfall. International Journal of Climatology 17, 1421-1432.

Maley, J., 1977. Palaeoclimates of central Sahara during the early Holocene. Nature 269, 573-577.

Maley, J., Brenac, P., 1998. Vegetation dynamics, palaeoenvironments and climatic changes in the forests of western Cameroon during the last 28,000 years BP. Review of Palaeobotany and Palynology 99, 157-187.

Martin, L., Bertaux, J., Corrège, T., Ledru, M.-P., Mourguiart, P., Sifeddine, A., Soubiès, F., Wirrmann, D., Suguio, K., Turcq, B., 1997. Astronomical forcing of contrasting rainfall changes in tropical South America between 12,400 and 8,800 cal yr B.P. Quaternary Research 47, 117-122.

Martinson, D. G., Pisias, N. G., Hays, J. D., Imbrie, J., Moore, T. C., Shackleton, N. J., 1987. Age dating and the orbital theory of the ice ages: Development of a high resolution 0 to 300000 year chronostratigraphy. Quaternary Research 27, 1-29.

Mason, S. J., 1990. Temporal variability of sea surface temperatures around Southern Africa: a possible forcing mechanism for the 18-year rainfall oscillation? South African Journal of Science 86, 243-252.

Mason, S. J., 1995. Sea-surface temperature - South African rainfall associations 1910-1989. International Journal of Climatology 19, 119-135.

Mason, S. J., 1998. Seasonal forecasting of South African rainfall using a non-linear discriminant analysis model. International Journal of Climatology 18, 147-164.

Mason, S. J., Jury, M. R., 1997. Climatic variability and change over southern Africa: a reflection on underlying processes. Progress in Physical Geography 21, 23-50.

Mason, S. J., Tyson, P. D., 2000. The occurrence and predictability of droughts over southern Africa. In: D. A. Wilhite (Ed.), Drought: A Global Assessment. Volume 1. Routledge, London, pp. 113-134.

Mason, S. J., Lindesay, J. A., Tyson, P. D., 1994. Simulating drought in southern Africa using sea-surface temperature variations. Water SA 20, 15-22.

Masson, V., Vimeux, F., Jouzel, J., Morgan, V., Delmotto, M., Ciais, P., Hammer, C., Johnsen, S., Lipenkov, V., Mosley-Thompson, E., Petit, J.-R., Steig, E. J., Stievenard, M., Vaikmae, R., 2000. Holocene climate variability in Antarctica based on 11 ice-core isotopic records. Quaternary Research 54, 348-358.

Matano, R. P., Beier, E. J., Strub, P. T., Tokmakian, R., 2002. Large-scale forcing of the Agulhas variability: the seasonal cycle. Journal of Physical Oceanography 32, 1228-1241.

Maud, R. R., Partridge, T. C., Alhonen, P., Donner, J., Vogel, J. C., 1993. A preliminary assessment of the environmental conditions represented by the Mbazwana diatomite (Zululand coast). 11th Conference of the South African Society for Quaternary Research, Kimberley, July 1993.

Mayle, F. E., Burbridge, R., Killeen, T. J., 2000. Millennial-scale dyamics of southern Amazonian Rain Forests. Science 290, 2291-2294.

McCaffrey, L. P., Harris, C., 1996. Hydrological impact of the Pretoria Saltpan crater, South Africa. Journal of African Earth Sciences 23, 205-212.

McConnaughey, T., 1989. ^{13}C and ^{18}O disequilibrium in biological carbonates: II. In vitro simulation of kinetic isotope effects. Geochimica et Cosmochimica Acta 53, 163-172.

McCrea, J. M., 1950. On the isotopic chemistry of carbonates and a paleotemperature scale. The Journal of Chemical Physics 18, 849-857.

McDougall, I., Harrison, T. M., 1999. Geochronology and thermochronology by the $^{40}Ar/^{39}Ar$ method. Oxford University Press, Oxford.

McIntyre, A., Molfino, B., 1996. Forcing of Atlantic Equatorial and Subpolar millennial cyles by precession. Science 274, 1867-1870.

McIntyre, A., Ruddiman, W. F., Karlin, K., Mix, A. C., 1989. Surface water response of the equatorial Atlantic Ocean to orbital forcing. Paleoceanography 4, 19-55.

McKenzie, J. A., 1985. Carbon isotopes and productivity in the lacustrine and marine environment. In: W. Stumm (Ed.), Chemical processes in lakes. Wiley, New York, pp. 99-118.

Meadows, M. E., Baxter, A. J., 1999. Late Quaternary palaeoenvironments of the southwestern Cape, South Africa: a regional synthesis. Quaternary International 57/58, 193-206.

Meehl, G. A., Washington, W. M., Wigley, T. M. L., Arblaster, J. M., Dai, A., 2003. Solar and greenhouse gas forcing and climate response in the 20th century. Journal of Climate 16, 426-444.

Mees, F., Reyes, E., Keppens, E., 1998. Stable isotope chemistry of gaylussite and nahcolite from the deposits of the crater lake at Malha, northern Sudan. Chemical Geology 146, 87-98.

Melack, J. M., 1979. Temporal variability of phytoplankton in tropical lakes. Oecologia 44, 1-7.

Melack, J. M., Kilham, P., 1974. Photosynthetic rates of phytoplankton in East African alkaline, saline lakes. Limnology and Oceanography 19, 743-755.

Melillo, J. M., Aber, J. D., Linkins, A. E., Ricca, A., Fry, B., Nadelhoffer, K. J., 1989. Carbon and nitrogen dynamics along the decay continuum: plant litter to soil organic matter. Plant and Soil 115, 189-198.

Mengard, R. O., 1968. Planktonic photosynthesis and the environment of carbonate deposition in lakes. 2. University of Minnesota LRC Interim Report.

Merlivat, L., 1978. Molecular diffusivities of water $H_2{}^{16}O$, $HD^{16}O$ and $H_2{}^{18}O$ in gases. The Journal of Chemical Physics 69, 2864-2871.

Metcalfe, S. E., 1993. Evolution of the Pretoria Saltpan - a diatom record spanning a full glacial-interglacial cycle. Hydrobiologia 269/270, 159-166.

Metcalfe, S. E., 1999. Diatoms from the Pretoria Saltpan – a record of lake evolution and environmental change. In: T. C. Partridge (Ed.), Tswaing: Investigations into the origin, age and palaeoenvironments of the Pretoria Saltpan. Geological Survey of South Africa, pp. 172-192.

Meyers, P. A., 1994. Preservation of elemental and isotopic source identification of sedimentary organic matter. Chemical Geology 144, 289-302.

Meyers, P. A., 1997. Organic geochemical proxies of paleoceanographic, paleolimnologic, and paleoclimatic processes. Organic Geochemistry 27, 213-250.

Meyers, P. A., Eadie, B. J., 1993. Sources, degradation and recycling of organic matter associated with sinking particles in Lake Michigan. Organic Geochemistry 20, 47-56.

Meyers, P. A., Lallier-Vergès, E., 1999. Lacustrine sedimentary organic matter records of Late Quaternary paleoclimates. Journal of Paleolimnology 21, 345-372.

Meyers, P. A., Teranes, J. L., 2001. Sediment Organic Matter. In: J. P. Smol, H. J. B. Birks, W. M. Last (Eds.), Tracking environmental change using lake sediments. Volume 3: Terrestrial, Algal, and Siliceous Indicators. Kluwer Academic Publishers, Dordrecht, pp. 239-269.

Mikkelsen, N., 1997. Silica dissolution and overgrowth of fossil diatoms. Micropaleontology 23, 223-226.

Milankovitch, M., 1920. Theorie mathematique des phenomenes thermiques produits par la radiation solaire. Acadamie Yougoslave des Sciences et des Artes de Zagreb, Gauthier-Villars.

Milankovitch, M., 1941. Canon of insolation and the ice-age problem.

Milbrink, G., 1977. On the limnology of two alkaline lakes (Nakuru and Naivasha) in the East Rift Valley System in Kenya. Internationale Revue der gesamten Hydrobiologie 62, 1-17.

Miller, A. G., Colman, B., 1980. Evidence for HCO_3^- transport by the blue-green alga (Cyanobacterium) *Coccochloris peniocystis*. Plant Physiology 65, 397-402.

Mix, A. C., Morey, A. E., Pisias, N. G., Houzel, J., 1999. Foraminiferal faunal estimates of palaeotemperature: Circumventing the no-analog problem yields cool ice age tropics. Paleoceanography 14, 350-359.

Mook, W. G., Brommerson, J. C., Staverman, W. H., 1974. Carbon isotope fractionation between dissolved bicarbonate and gaseous carbon dioxide. Earth and Planetary Science Letters 22, 169-176.

Morley, D. W., Leng, M. J., Mackay, A. W., Sloane, H. J., Rioual, P., Battarbee, R. W., 2004. Cleaning of lake sediment samples for diatom oxygen analysis. Journal of Paleolimnology 31, 391-401.

Morley, J. J., Heusser, L. E., 1997. Role of orbital forcing in east Asian monsoon climates during the last 350 kyr: Evidence from terrestrial and marine climate proxies from core RC14-99. Paleoceanography 12, 483-493.

Morse, J. W., Mackenzie, F. T., 1990. Geochemistry of sedimentary carbonates. In: Elsevier, Amsterdam.

Morse, J. W., Zullig, J. J., Berstein, L. D., Millero, F. J., Milne, P., Mucci, A., Choppin, G. R., 1985. Chemistry of calcium carbonate-rich shallow water sediments in the Bahamas. American Journal of Science 285, 147-185.

Moschen, R., Lücke, A., Schleser, G. H., 2005. Sensitivity of biogenic silica oxygen isotopes to changes in surface water temperature and palaeoclimatology. Geophysical Research Letters 32, 1-4.

Müller, G., Irion, G., Förstner, U., 1972. Formation and diagenesis of inorganic Ca-Mg carbonates in the lacustrine environment. Naturwissenschaften 59, 158-164.

Müller, P. J., 1977. C/N ratios in Pacific deep-sea sediments: effect of inorganic ammonium and organic nitrogen compounds sorbed by clays. Geochimica et Cosmochimica Acta 41, 549-553.

Müller, P. J., Schneider, R. R., Ruhland, G., 1994. Late Quaternary pCO_2 variations in the Angola Current: evidence from organic carbon $\delta^{13}C$ and alkenone temperatures. In: R. Zahn, M. A. Kaminski, L. Labeyrie, T. F. Pedersen (Eds.), Carbon cycling in the glacial ocean: constraints on the ocean's role in global change. Springer, Berlin, Heidelberg, New York, pp. 343-366.

Munyikwa, K., 2005. Synchrony of Southern Hemisphere Late Pleistocene arid episodes: A review of luminescence chronologies from arid aeolian landscapes south of the Equator. Quaternary Science Reviews 24, 2555-2583.

Newell, R. E., 1973. Climate and the Galapagos Islands. Nature 245, 91-92.

Nicholson, S. E., 1996. A review of climate dynamics and climate variability in Eastern Africa. In: T. C. Johnson, E. O. Odada (Eds.), The limnology, climatology, and paleoclimatology of the East African Lakes. Gordon and Breach, Amsterdam, pp. 25-56.

Nicholson, S. E., Flohn, H., 1980. African environmental and climatic changes and the general atmospheric circulation in late Pleistocene and Holocene. Climatic Change 2, 313-348.

Nicholson, S. E., Entekhabi, D., 1986. The quasi-periodic behavior of rainfall variability in Africa and its Relationship to the Southern Oscillation. Archives for Meteorology, Geophysics and Bioclimatology, Series A 34, 311-348.

Nicholson, S. E., Entekhabi, D., 1987. Rainfall variability in equatorial and southern Africa: Relationships with sea surface temperatures along the southwestern coast of Africa. Journal of Applied Meteorology and Climate 26, 561-578.

Nicholson, S. E., Kim, J., 1997. The relationship of the El Niño-Southern Oscillation to African rainfall. Journal of Climatology 17, 117-135.

Nissenbaum, A., Magaritz, M., Goldberg, M., 1988. ^{13}C enrichment in recent freshwater carbonate. Naturwissenschaften 75, 252-253.

O'Connor, P., Thomas, D. S. G., 1999. The timing and environmental significance of Late Quaternary linear dune development in western Zambia. Quaternary Research 52, 44-55.

O'Leary, M. H., 1981. Carbon isotope fractionation in plants. Phytochemistry 20, 553-567.

O'Leary, M. H., 1988. Carbon isotopes in photosynthesis. Bioscience 38, 328-336.

O'Neil, J. R., Clayton, R. N., Meyeda, T. K., 1969. Oxygen isotope fractionation in divalent metal carbonate. Journal of Chemistry and Physics 51, 5547-5558.

Ogallo, L. J., 1988. Relationships between seasonal rainfall in East Africa and the Southern Oscillation. Journal of Climatology 8, 31-43.

Ogrinc, N., Lojen, S., Faganeli, J., 2002. A mass balance of carbon stable isotopes in an organic-rich methane producing lacustrine sediment (Lake Bled, Slovenia). Global and Planetary Change 33, 57-72.

Ogrinc, N., Hintelmann, H., Eckley, C., Lojen, S., 2003. Biogeochemical influence on carbon isotope signature in boreal lake sediments. Hydrobiologia 494, 207-213.

Ojiambo, B. S., Lyons, W. B., 1996. Residence times of major ions in Lake Naivasha, Kenya, and their relationship to lake hydrology. In: T. C. Johnson, E. O. Odada (Eds.), The limnology, climatology, and paleoclimatology of the East African Lakes. Gordon and Breach, Amsterdam, pp. 267-278.

Olago, D. O., Street-Perrott, F. A., Perrott, R. A., Ivanovich, M., Harkness, D. D., Odada, E. O., 2000. Long-term temporal characteristics of palaeomonsoon dynamics in equatorial Africa. Global and Planetary Change 26, 159-171.

Osmond, J. K., May, J. P., Tanner, W. F., 1970. Age of the Cape Kennedy Barrier-and-Lagoon complex. Journal of Geophysical Research 75, 469-479.

Osmond C. B., Winter K., Zielger H., 1982. Functional significance of different pathways of CO_2 fixation in photosynthesis. In: O. L. Lange *et al.* (Eds.), Physiological Plant Ecology II. Water Relations and Carbon Assimilation. Springer-Verlag, Berlin, pp. 479–547.

Owen, R. B., Barthelme, J. W., Renaut, R. W., Vincens, A., 1982. Palaeolimnology and archaeology of Holocene deposits north-east of Lake Turkana, Kenya. Nature 298, 523-529.

Park, R., Epstein, S., 1960. Carbon isotope fractionation during photosynthesis. Geochimica et Cosmochimica Acta 21, 110-126.

Park, R., Epstein, S., 1961. Metabolic fractionation of C^{13} and C^{12} in plants. Plant Physiology 36, 133-138.

Parkington, J., Cartwright, C., Cowling, R. M., Baxter, A., Meadows, M., 2000. Palaeovegetation at the last glacial maximum in the western Cape, South Africa:

wood charcoal and pollen evidence from Elands Bay Cave. South African Journal of Science 96, 543-546.

Parrenin, F., Rémy, F., Ritz, C., Siegert, M. J., Jouzel, J., 2004. New modeling of the Vostok ice flow line and implication for the glaciological chronology of the Vostok ice core. Journal of Geophysical Research 109, D20102, doi:10.1029/2004JD004561.

Partridge, T. C., Scott, L., 2000. Lakes and Pans. In: T. C. Partridge, R. R. Maud (Eds.), The Cenozoic of Southern Africa. Oxford University Press, New York, pp. 145-161.

Partridge, T. C., Reimold, W. U., Kerr, S. J., Stanistreet, I. G., 1991. The Pretoria Saltpan - the scientific aspect. Geobulletin 34, 16-22.

Partridge, T. C., Kerr, S. J., Metcalfe, S. E., Scott, L., Talma, A. S., Vogel, J., 1993. The Pretoria Saltpan: a 200,000 year Southern African lacustrine sequence. Palaeogeography, Palaeoclimatology, Palaeoecology 101, 317-337.

Partridge, T. C., deMenocal, P. B., Lorentz, S. A., Paiker, M. J., Vogel, J. C., 1997. Orbital forcing of climate over South Africa: a 200,000-year rainfall record from the Pretoria Saltpan. Quaternary Science Reviews 16, 1125-1133.

Partridge, T. C. *et al.*, 1999. Tswaing: Investigations into the origin, age and palaeoenvironments of the Pretoria Saltpan. Geological Survey of South Africa.

Partridge, T. C., Scott, L., Schneider, R. R., 2004. Between Agulhas and Benguela: responses of Southern African climates of the late Pleistocene to current fluxes, orbital precession, and the extent of the circum-Antarctic vortex. In: R. W. Battarbee, F. Gasse, C. E. Stickley (Eds.), Past climate variability through Europe and Africa. Springer, Dordrecht, pp. 45-68.

Peeters, F. J. C., Acheson, R., Brummer, G.-J. A., de Ruijter, W. P. M., Schneider, R. R., Ganssen, G. M., Ufkes, E., Kroon, D., 2004. Vigorous exchange between the Indian and Atlantic oceans at the end of the past five glacial periods. Nature 430, 661-665.

Pelegrina, J. M. A., Martínez-Aguirre, A., 2005. Isotopic fractionation during leaching of impure carbonates and their effect on uranium series dating. Quaternary Science Reviews 24, 2584-2593.

Penck, A., 1914. The shifting of the climatic belts. Scottish Geographical Magazine 30, 281-293.

Peterson, L. C., Haug, G. H., Hughen, K. A., Röhl, U., 2000. Rapid changes in the hydrologic cycle of the tropical Atlantic during the last glacial. Science 290, 1947-1951.

Peterson, R. G., Stramma, L., 1991. Upper-level circulation in the South Atlantic Ocean. Progress in Oceanography 26, 1-73.

Pether, J., 1994. Molluscan evidence for enhanced deglacial advection of Agulhas water in the Benguela current, off southwestern Africa. Palaeogeography, Palaeoclimatology, Palaeoecology 111, 99-117.

Petit, J. R., Briat, M., Royer, A., 1981. Ice age aerosol content from East Antarctic ice core samples and past wind strength. Nature 293, 391-394.

Petit, J. R., Jouzel, J., Raynaud, D., Barkov, N. I., Barnola, J. M., Basile, I., Bender, M., Chappellaz, J., Davis, M., Delaygue, G., Delmotte, M., Kotlyakov, V. M., Legrand, M., Lipenkov, V. Y., Lorius, C., Pépin, L., Ritz, C., Saltzman, E., Stievenard, M., 1999. Climate and atmospheric history of the past 420,000 years from the Vostok ice core, Antarctica. Nature 399, 429-436.

Petit-Maire, N., Page, N., Marchand, J., 1993. The Sahara in the Holocene: Map 1/5,000,000. Marseille, France, Laboratoire de Géologie du Quaternaire CNRS.

Philander, S. G. H., Gu, D., Halpern, D., Lambert, G., Lau, N.-C., Li, T., Pacanowski, R. C., 1996. Why the ITCZ is mostly north of the equator? Journal of Climate 9, 2958-2972.

Pinot, S., Ramstein, G., Harrison, S. P., Prentice, I. C., Guiot, J., Stute, M., Joussaume, S., 1999. Tropical paleoclimates at the Last Glacial Maximum: comparison of Paleoclimate Modeling Intercomparison Project (PMIP) simulations and paleodata. Climate Dynamics 15, 857-874.

Piperno, D. R., 2001. Phytoliths. In: J. P. Smol, H. J. B. Birks, W. M. Last (Eds.), Tracking environmental change using lake sediments. Volume 3: Terrestrial, Algal, and Siliceous Indicators. Kluwer Academic Publishers, Dordrecht, pp. 235-251.

Pokras, E. M., Mix, A. C., 1985. Eolian evidence for spatial variability of late Quaternary climates in tropical Africa. Quaternary Research 24, 137-149.

Pokras, E. M., Mix, A. C., 1987. Earth's precession cycle and Quaternary climatic change in tropical Africa. Nature 326, 486-487.

Popp, B. N., Laws, E. A., Bidigare, R. R., Dore, J. E., Hanson, K. L., Wakeham, S. G., 1998. Effect of phytoplankton cell geometry on carbon isotopic fractionation. Geochimica et Cosmochimica Acta 62, 69-77.

Potratz, H. A., Barnes, J. W., Lang, E. J., 1955. A radiochemical procedure for thorium and its application to the determination of ionium in coral limestone. Los Alamos Scientific Laboratory Publication LA-1845.

Poulièková, A., 1993. Ecological study of seasonal maxima of centric diatoms. Archiv für Hydrobiologie 96, 85-106.

Prell, W. P., van Campo, E., 1986. Coherent response of Arabian Sea upwelling and pollen transport to late Quaternary monsoonal winds. Nature 323, 526-528.

Prell, W. L., Kutzbach, J. E., 1987. Monsoon variability over the past 150,000 years. Journal of Geophysical Research 94(D7), 8411-8425.

Prell, W. L., Hutson, W. H., Williams, D. F., 1979. The subtropical convergence and late Quaternary circulation in the southern Indian Ocean. Marine Micropaleontology 4, 225-234.

Prell, W. L., Hutson, W. H., Williams, D. F., Bé, A. W. H., Geitzenauer, K., Molfino, B., 1980. Surface circulation of the Indian Ocean during the last glacial maximum, approximately 18,000 yr B.P. Quaternary Research 14, 309-336.

Rao, C. R., 1995. A review of canonical coordinates and an alternative to correspondance analysis using Hellinger distance. Qûestiió 19, 23-63.

Rau, A. J., Rogers, J., Lutjeharms, J. R. E., Giraudeau, J., Lee-Thorp, J. A., Chen, M.-T., Waelbroeck, C., 2002. A 450-kyr record of hydrological conditions on the western Agulhas Bank Slope, south of Africa. Marine Geology 180, 183-201.

Raven, J. A., Handley, L. L., Andrews, M., 2004. Global aspects of C/N interactions determining plant-environment interactions. Journal of Experimental Botany 55, 11-25.

Raymo, M. E., Nisancioglu, K., 2003. The 41-kyr world: Milankovitch's other unsolved mystery. Paleoceanography 18, 1011-1016.

Reason, C. J. C., 2001. Evidence for the influence of the Agulhas current on regional atmospheric circulation patterns. Journal of Climate 14, 2769-2778.

Reason, C. J. C., 2002. Sensitivity of the southern African circulation to dipole sea-surface temperature patterns in the South Indian Ocean. International Journal of Climatology 22, 377-393.

Reason, C. J. C., Lutjeharms, J. R. E., 1998. Variability of the South Indian Ocean and implications for southern African rainfall. South African Journal of Science 94, 115-123.

Reason, C. J. C., Mulenga, H., 1999. Relationships between South African rainfall and SST anomalies in the southwest Indian Ocean. International Journal of Climatology 19, 1651-1673.

Reason, C. J. C., Allan, R. J., Lindesay, J. A., 1996. Dynamical response of the oceanic circulation and temperature to interdecadal variability in the surface winds over the Indian Ocean. Journal of Climate 9, 97-114.

Reed, J. M., 1998. Diatom preservation in the recent sediment record of Spanish saline lakes: implications for palaeoclimate study. Journal of Paleolimnology 19, 129-137.

Reibach, P. H., Benedict, C. R., 1977. Fractionation of stable carbon isotopes by phosphoenolpyruvate carboxylase from C_4 plants. Plant Physiology 59, 564-568.

Reimold, W. U., Koeberl, C., Kerr, S. J., Partridge, T. C., 1991. The Pretoria Saltpan - the first firm evidence for an origin by impact. Lunar and Planetary Science 22, 1117-1118.

Reimold, W. U., Koeberl, C., Partridge, T. C., Kerr, S. J., 1992. Pretoria Saltpan crater: Impact origin confirmed. Geology 20, 1079-1082.

Richardson, J. L., Richardson, J. B., 1972. History of an African Rift lake and its climatic implications. Ecological Monographs 42, 499-534.

Richardson, J. L., Dussinger, R. A., 1986. Paleolimnology of the mid-elevation lakes in the Kenya Rift Valley. Hydrobiologia 143, 167-174.

Ricketts, R. D., Johnson, T. C., 1996. Climate change in the Turkana basin as deduced from a 4000 year long $\delta^{18}O$ record. Earth and Planetary Science Letters 142, 7-17.

Rind, D., 1998. Latitudinal temperature gradients and climate change. Journal of Geophysical Research 103, 5943-5971.

Rind, D., 2000. Relating paleoclimate data and past temperature gradients: Some suggestive rules. Quaternary Science Reviews 19, 381-390.

Rind, D., Peteet, D., 1985. Terrestrial conditions at the last glacial maximum and CLIMAP sea-surface temperature estimates: are they consistent? Quaternary Research 24, 1-22.

Rocha, A., Simmonds, I., 1997a. Interannual variability of south-eastern African summer rainfall. Part 1: Relationships with air-sea interaction processes. International Journal of Climatology 17, 235-265.

Rocha, A., Simmonds, I., 1997b. Interannual variability of south-eastern African summer rainfall. Part II. Modelling the impact of sea-surface temperatures on rainfall and circulation. International Journal of Climatology 17, 267-290.

Rodhe, H., Virji, H., 1976. Trends and Periodicities in East African Rainfall Data. Monthly Weather Review 104, 307-315.

Romanek, C. S., Grossman, E. L., Morse, J. W., 1992. Carbon isotopic fractionation in synthetic aragonite and calcite: effects of temperature and precipitation rate. Geochimica et Cosmochimica Acta 56, 419-430.

Rosell-Melé, A., 2003. The use of biomarkers as climate proxies. In: A. W. Mackay, R. W. Battarbee, H. J. B. Birks, F. Oldfield (Eds.), Global Change in the Holocene. Arnold, London, pp. 358-372.

Rosenfeld, W. D., Silverman, S. R., 1959. Carbon isotope fractionation in bacterial production of methane. Science 130, 1658-1659.

Rosholt, J. N., 1976. $^{230}Th/^{234}U$ dating of travertine and caliche rinds. Geological Society of America Abstracts with Programs 8, 1076.

Rossignol-Strick, M., 1983. African monsoons, an immediate climatic response to orbital insolation. Nature 304, 46-49.

Rostek, F., Ruhland, G., Bassinot, F. C., Müller, P. J., Labeyrie, L. D., Lancelot, Y., Bard, E., 1993. Reconstructing sea surface temperature and salinity using $\delta^{18}O$ and alkenone records. Nature 364, 319-321.

Rostek, F., Bard, E., Beaufort, L., Sonzogni, C., Ganssen, G., 1997. Sea surface temperature and productivity records for the past 240 kyr in the Arabian Sea. Deep-Sea Research II 44, 1461-1480.

Rouault, M., White, S. A., Reason, C. J. C., Lutjeharms, J. R. E., Jobard, I., 2002. Ocean-Atmosphere Interaction in the Agulhas Current Region and a South African Extreme Weather Event. Weather and Forecasting 17, 655-669.

Rowan, D. J., Kalff, J., Rasmussen, J. B., 1992. Profundal sediment organic content and physical character do not reflect lake trophic status, but rather reflect inorganic sedimentation and exposure. Canadian Journal of Fisheries and Aquatic Sciences 49, 1431-1438.

Rozanski, K., Sonntag, C., Münnich, K. O., 1982. Factors controlling stable isotope composition of European precipitation. Tellus 34, 142-150.

Rozanski, K., Araguás-Araguás, L., Gonfiantini, R., 1992. Relation between long-term trends of oxygen-18 isotope composition of precipitation and climate. Science 258, 981-985.

Rozanski, K., Araguás-Araguás, L., Gonfiantini, R., 1993. Isotopic patterns in modern global precipitation. In: P. K. Swart, K. C. Lohmann, J. McKenzie, S. Savin (Eds.), Climate Change in Continental Isotopic Records. AGU Geophysical Monographs 78, pp. 1-37.

Ryves, D. B., Juggins, S., Fritz, S. C., Battarbee, R. W., 2001. Experimental diatom dissolution and the quantification of microfossil preservation in sediments. Palaeogeography, Palaeoclimatology, Palaeoecology 172, 99-113.

Sachs, J. P., Anderson, R. F., Lehman, S. J., 2001. Glacial surface temperatures of the southeast Atlantic Ocean. Science 293, 2077-2079.

Sakata, S., Hayes, J. M., McTaggart, A. R., Evans, R. A., Leckrone, K. J., Togasaki, R. K., 1997. Carbon isotopic fractionation associated with lipid biosynthesis by a cyanobacterium: relevance for interpretation of biomarker records. Geochimica et Cosmochimica Acta 61, 5379-5389.

Salomons, W., Mook, W. G., 1986. Isotope geochemistry of carbonates in the weathering zone. In: P. Fritz, J. Ch. Fontes (Eds.), Handbook of envrionmental isotope geochemistry. Volume 2. The terrestrial environment, A. Elsevier, Amsterdam, pp. 239-269.

Salzmann, U., Hoelzmann, P., Morcinek, I., 2002. Late Quaternary climate and vegetation of the sudanian zone of NE-Nigeria. Quaternary Research 58, 73-83.

Sanders, F., Gyakum, J. R., 1980. Synoptic-Dynamic Climatology of the "Bomb". Monthly Weather Review 108, 1589-1606.

Santisteban, J. I., Mediavilla, R., López-Pamo, E., Dabrio, C. J., Ruiz Zapata, M. B., Gil García, M. J., Castaño, S., Martínez-Alfaro, P. E., 2004. Loss on ignition: a qualitative or quantitative method for organic matter and carbonate mineral content in sediments? Journal of Paleolimnology 32, 287-299.

Savin, S. M., Epstein, S., 1970. The oxygen and hydrogen isotope geochemistry of clay minerals. Geochimica et Cosmochimica Acta 34, 25-42.

Schefuß, E., Schouten, S., Schneider, R. R., 2005. Climatic controls on central African hydrology during the past 20,000 years. Nature 437, 1003-1006.

Schidlowski, M., Matzigkeit, U., Krumbein, W. E., 1984. Superheavy organic carbon from hypersaline microbial mats. Naturwissenschaften 71, 303-308.

Schmidt, M., Botz, R., Stoffers, P., Anders, S., Bohrmann, G., 1997. Oxygen isotopes in marine diatoms: a comparative study of analytical techniques and new results on the isotopic composition of recent marine diatoms. Geochimica et Cosmochimica Acta 61, 2275-2280.

Schmidt, M., Botz, R., Rickert, D., Bohrmann, G., Hall, S. R., Mann, S., 2001. Oxygen isotopes of marine diatoms and relations to opal-A maturation. Geochimica et Cosmochimica Acta 65, 201-211.

Schmidt, R., Kamenik, C., Lange-Bertalot, H., Klee, R., 2004. *Fragilaria* and *Staurosira* (Bacillariophyceae) from sediment surfaces of 40 lakes in the Austrian Alps in relation to environmental variables, and their potential for palaeoclimatology. Journal of Limnology 63, 171-189.

Schneider, R. R., Müller, P. J., Ruhland, G., 1995. Late Quaternary surface circulation in the east equatorial South Atlantic: evidence from alkenone sea surface temperatures. Paleoceanography 10, 197-219.

Schneider, R. R., Müller, P. J., Ruhland, G., Meinecke, G., Schmidt, H., Wefer, G., 1996. Late Quaternary surface temperatures amd productivity in the east-equatorial South Atlantic: response to changes in trade/monsoon wind forcing and surface water advection. In: G. Wefer, W. H. Berger, G. Siedler, D. J. Webb (Eds.), The South Atlantic: present and past circulation. Springer-Verlag, Berlin Heidelberg, pp. 527-551.

Schneider, R. R., Price, B., Müller, P. J., Kroon, D., Alexander, I., 1997. Monsoon related variations in Zaire (Congo) sediment load and influence of fluvial silicate supply on marine productivity in the east equatorial Atlantic during the last 200,000 years. Paleoceanography 12, 463-481.

Schneider, R. R., Müller, P. J., Acheson, R., 1999. Atlantic alkenone sea-surface temperature records. In: F. Abrantes, A. Mix (Eds.), Reconstructing Ocean History: A window into the future. Kluwer Academic/Plenum, New York, pp. 33-55.

Schoeman, F. R., Archibald, R. E. M., 1976-1980. The diatom flora of Southern Africa. CSIR Special Report WAT 50, Pretoria.

Schoeman, F. R., Archibald, R. E. M., 1988. Taxonomic notes on the diatoms (Bacillariophyceae) of the Gross Barmen thermal springs in South West Africa/Namibia. South African Journal of Botany 54, 221-256.

Schoeman, F. R., Ashton, P. J., 1982a. The diatom flora of the Pretoria Salt Pan, Transvaal, Republic of South Africa. Bacillaria 5, 63-99.

Schoeman, F. R., Ashton, P. J., 1982b. The diatom flora in the vicinity of the Pretoria Salt Pan, Transvaal, Republic of South Africa I. Nova Hedwigia 73, 21-54.

Schoeman, F. R., Ashton, P. J., 1983. The diatom flora in the vicinity of the Pretoria Salt Pan, Transvaal, Republic of South Africa. Part II. South African Journal of Botany 2, 191-201.

Schoeman, F. R., Archibald, R. E. M., Ashton, P. J., 1984. The diatom flora in the vicinity of the Pretoria Salt Pan, Transvaal, Republic of South Africa. Part III (final). South African Journal of Botany 3, 191-207.

Scholz, C. A., King, J. W., Ellis, G. S., Swart, P. K., Stager, J. C., Colman, S. M., 2003. Paleolimnology of Lake Tanganyika, East Africa, over the past 100 k yr. Journal of Paleolimnology 30, 139-150.

Schulz, H., von Rad, U., Erlenkeuser, H., 1998. Correlation between Arabian Sea and Greenland climate oscillations of the past 110,000 years. Nature 393, 54-57.

Schulz, M., Stattegger, K., 1997. Spectrum: spectral analysis of unevenly spaced paleoclimatic timeseries. Computers and Geosciences 23, 929-945.

Schulze, B. R., 1965. Climate of South Africa. Part 8. General Survey. Government Printer, Pretoria.

Schulze, B. R., 1972. South Africa. In: J. F. Griffiths (Ed.), Climates of Africa. World Survey of Climatology, Volume 10. Elsevier, Amsterdam, pp. 501-566.

Schulze, B. R., 1984. Climate of South Africa: Part 8: General Survey. South African Weather Bureau. WB28.

Schwarcz, H. P., 1989. Uranium series dating of Quaternary deposits. Quaternary International 1, 7-17.

Schwarcz, H. P., Latham, A. G., 1989. Dirty calcites 1. Uranium series dating of contaminated calcite using leachates alone. Chemical Geology (Isotope Geoscience Section) 80, 35-43.

Scott, L., 1982. A late Quaternary pollem record from the Transvaal Bushveld. Quaternary Research 17, 339-370.

Scott, L., 1989. Climatic conditions in Southern Africa since the Last Glacial Maximum, inferred from pollen analysis. Palaeogeography, Palaeoclimatology, Palaeoecology 70, 345-353.

Scott, L., 1999. Palynological analysis of the Pretoria Saltpan (Tswaing Crater) sediments and vegetation history of the Bushveld savanna biome, South Africa. In: T. C. Partridge (Ed.), Tswaing: Investigations into the origin, age and palaeoenvironments of the Pretoria Saltpan. Geological Survey of South Africa, pp. 143-166.

Scott, L., 2002. Grassland development under glacial and interglacial conditions in southern Africa: review of pollen, phytolith and isotope evidence. Palaeogeography, Palaeoclimatology, Palaeoecology 177, 47-57.

Scott, L., Thackeray, J. F., 1987. Multivariate analysis of late Pleistocene and Holocene pollen spectra from Wonderkrater, Transvaal, South Africa. South African Journal of Science 83, 93-98.

Scott, L., Vogel, J. C., 2000. Evidence for environmental conditions during the last 20,000 years in Southern Africa from ^{13}C in fossil hyrax dung. Global and Planetary Change 26, 207-215.

Scott, L., Lee-Thorp, J. A., 2004. Holocene climatic trends and rhythms in southern Africa. In: R. W. Battarbee, F. Gasse, C. E. Stickley (Eds.), Past climate variability through Europe and Africa. Springer, Dordrecht, pp. 69-91.

Scott, L., Holmgren, K., Talma, A. S., Woodborne, S., Vogel, J. C., 2003. Age interpretation of the Wonderkrater spring sediments and vegetation change in the savanna biome, Limpopo province, South Africa. South African Journal of Science 99, 484-488.

Seltzer, G., Rodbell, D., Burns, S., 2000. Isotopic evidence for late Quaternary climatic change in tropical South America. Geology 28, 35-38.

Shackleton, N. J., 1987. Oxygen isotopes, ice volume and sea level. Quaternary Science Reviews 6, 183-190.

Shackleton, N. J., 2000. The 100,000-year ice-age cycle identified and found to lag temperature, carbon dioxide, and orbital eccentricity. Science 289, 1897–1902.

Shannon, L. V., 1985. The Benguela Ecosystem: Part I. The evolution of the Benguela, physical features and processes. Oceanography and Marine Biology Annual Review 23, 105-182.

Shannon, L. V., Agenbag, J. J., Buys, M. E. L., 1987. Large- and mesoscale features of the Angola-Benguela Front. South African Journal of Marine Science 5, 11-34.

Shapley, M. D., Ito, E., Donovan, J. J., 2005. Authigenic calcium carbonate flux in groundwater-controlled lakes: implications for lacustrine paleoclimate records. Geochimica et Cosmochimica Acta 69, 2517-2533.

Shaw, P. A., Stokes, S., Thomas, D. S. G., Davies, F. B. M., Holmgren, K., 1997. Palaeoecology and age of a late Quaternary high lake level in the Makgadikgadi Basin of the Middle Kalahari, Botswana. South African Journal of Science 93, 273-276.

Shemesh, A., Charles, C. D., Fairbanks, R. G., 1992. Oxygen isotopes in biogenic silica: global changes in ocean temperature and isotopic composition. Science 256, 1434-1436.

Shemesh, A., Burckle, L. H., Hays, J. D., 1995. Late Pleistocene oxygen isotope records of biogenic silica from the Atlantic sector of the Southern Ocean. Paleoceanography 10, 179-196.

Shemesh, A., Rosqvist, G., Rietti-Shati, M., Rubensdotter, L., Bigler, C., Yam, R., Karlén, W., 2001. Holocene climatic change in Swedish Lapland inferred from an oxygen-isotope record of lacustrine biogenic silica. The Holocene 11, 447-454.

Sherman, C. E., Glenn, C. R., Jones, A. T., Burnett, W. C., Schwarcz, H. P., 1993. New evidence for two highstands of the sea during the last interglacial, oxygen isotope substage 5e. Geology 21, 1079-1082.

Shi, N., Dupont, L. M., 1997. Vegetation and climatic history of southwest Africa: a marine palynological record of the last 300,000 years. Vegetation History and Archaeobotany 6, 117-131.

Shi, N., Dupont, L. M., Beug, H.-J., Schneider, R., 1998. Vegetation and climate changes during the last 21 kyrs in SW Africa based on a marine pollen record. Vegetation History and Archaeobotany 7, 127-140.

Shi, N., Dupont, L. M., Beug, H.-J., Schneider, R., 2000. Correlation between vegetation in southwestern Africa and oceanic upwelling in the past 21,000 years. Quaternary Research 54, 72-80.

Shi, N., Schneider, R., Beug, H.-J., Dupont, L. M., 2001. Southeast trade wind variations during the last 135 kyr: evidence from pollen spectra in eastern South Atlantic sediments. Earth and Planetary Science Letters 187, 311-321.

Shin, S.-I., Liu, Z., Otto-Bliesner, B., Brady, E. C., Kutzbach, J. E., Harrison, S. P., 2003. A simulation of the last glacial maximum climate using the NCAR-CCSM. Climate Dynamics 20, 127-151.

Short, D. A., Mengel, J. G., Crowley, T. J., Hyde, W. T., North, G. R., 1991. Filtering of Milankovitch cycles by Earth's geography. Quaternary Research 35, 157-173.

Siegel, A. F., 1980. Testing for periodicity in a time series. Journal of the American Statistical Association 75, 345-348.

Sirocko, F., Sarnthein, M., Erienkeuser, H., Lange, H., Arnold, M., Duplessy, J. C., 1993. Century-scale events in monsoonal climate over the past 24,000 years. Nature 364, 322-324.

Sirocko, F., Garbe-Schönberg, D., McIntyre, A., Molfino, B., 1996. Teleconnections between the subtropical monsoons and high-latitude climates during the last deglaciation. Science 272, 526-529.

Sly, P. G., 1978. Sedimentary processes in lakes. In: A. Lerman (Ed.), Lakes: chemistry, geology, physics. Springer-Verlag, New York, pp. 65-90.

Smith, F. A., Walker, N. A., 1980. Photosynthesis by aquatic plants: effects of unstirred layers in relation to assimilation of CO_2 and HCO_3^- and to carbon isotopic discrimination. New Phytologist 86, 245-259.

Smith, G. I., Friedman, I., McLaughlin, R. J., 1987. Studies of Quaternary saline lakes: III. Mineral, chemical, and isotopic evidence of salt solution and crystallization processes in Owens Lake, California, 1969-1971. Geochimica et Cosmochimica Acta 51, 811-827.

Smol, J. P., Birks, H. J. B., Last, W. M., 2001. Tracking Environmental Change using Lake Sediments. Volume 3: Terrestrial, algal, and siliceous indicators. Kluwer Academic Publishers, Dordrecht.

Smythe, F. W., Ruddiman, W. F., Lumslen, D. N., 1985. Ice-rafted evidence of long-term North Atlantic circulation. Marine Geology 64, 131-141.

Sollins, P., Spycher, G., Glassman, C. A., 1984. Net nitrogen mineralization from light- and heavy-fraction forest soil organic matter. Soil Biology and Biochemistry 16, 31-37.

Sonntag, C., Klitzsch, E., Lohnert, E. P., El Shazly, E. M., Munnich, K. O., Jumghans, Ch., Thorweihe, U., Weistroler, K., Swailem, F. M., 1978. Paleoclimatic information from deuterium and oxygen-18 in carbon-14-dated north Saharian groundwaters. Isotope Hydrology.International Atomic Energy Agency, Vienna 978, 569-580.

Sonntag, C., Münnich, K. O., Jacob, H., Rozanski, K., 1983. Variations of deuterium and oxygen-18 in continental precipitation and groundwater and their causes. In: A. Street-Perrott, M. Beran, R. Ratcliffe (Eds.), Variations in the Global Water Budget. D. Reidel Publishing Company, Dordrecht, pp. 107-124.

Sonzogni, C., Bard, E., Rostek, F., 1998. Tropical sea-surface temperatures during the last glacial period: a view based on alkenones in Indian Ocean sediments. Quaternary Science Reviews 17, 1185-1201.

Spero, H. J., Bijma, J., Lea, D. W., Bemis, B. E., 1997. Effect of seawater carbonate concentration on foraminiferal carbon and oxygen isotopes. Nature 390, 497-500.

Stager, J. C., 1988. Environmental changes at Lake Cheshi, Zambia since 40,000 years BP. Quaternary Research 29, 54-65.

Stager, J. C., Cumming, B., Meeker, L., 1997. A high-resolution 11,400-yr diatom record from Lake Victoria, East Africa. Quaternary Research 47, 81-89.

Stager, J. C., Mayewski, P. A., Meeker, L. D., 2002. Cooling cycles, Heinrich event I, and the desiccation of Lake Victoria. Palaeogeography, Palaeoclimatology, Palaeoecology 183, 169-178.

Steig, E. J., Brook, E. J., White, J. W. C., Sucher, C. M., Bender, M. L., Lehman, S. J., Morse, D. L., Waddington, E. D., Clow, G. D., 1998. Synchronous climate changes in Antarctica and the North Atlantic. Science 282, 92-95.

Stiller, M., Magaritz, M., 1974. Carbon-13 enriched carbonate in interstitial waters of Lake Kinneret sediments. Limnology and Oceanography 19, 849-853.

Stiller, M., Rounick, J. S., Shasha, S., 1985. Extreme carbon-isotope enrichments in evaporating brines. Nature 316, 434-435.

Stoermer, E. F., 1993. Evaluating diatom succession: some peculiarities of the Great Lakes case. Journal of Paleolimnology 8, 71-83.

Stokes, S., Thomas, D. S. G., Shaw, P. A., 1997a. New chronological evidence for the nature and timing of linear dune development in the southwest Kalahari. Geomorphology 20, 81-93.

Stokes, S., Thomas, D. S. G., Washington, R., 1997b. Multiple episodes of aridity in southern Africa since the last interglacial period. Nature 388, 154-158.

Stokes, S., Haynes, G., Thomas, D. S. G., Horrocks, J. L., Higginson, M., and Malifa, M., 1998. Punctuated aridity in southern Africa during the last glacial cycle: the chronology of linear dune construction in the northeastern Kalahari. Palaeogeography, Palaeoclimatology, Palaeoecology 137, 305-322.

Storzer, D., Koeberl, C., Reimold, W. U., 1993. The age of the Pretoria Saltpan crater, South Africa. Lunar and Planetary Science 24, 1365-1366.

Storzer, D., Reimold, W. U., Koeberl, C., 1999. Fission-track age of the Pretoria Saltpan impact crater. In: T. C. Partridge (Ed.), Tswaing: Investigations into the origin, age and palaeoenvironments of the Pretoria Saltpan. Geological Survey of South Africa, pp. 64-71.

Stramma, L., Lutjeharms, J. R. E., 1987. The flow field of the subtropical gyre of the South Indian Ocean. Journal of Geophysical Research 102, 5513-5530.

Straub, F., 1993. Diatoms and their preservation in the sediments of Lake Neuchâtel (Switzerland) as evidence of past hydrological changes. Hydrobiologia 269/270, 167-178.

Street, F. A., 1979. Late Quaternary precipitation estimates for the Ziway-Shala Basin, southern Ethiopia. Palaeoecology of Africa 11, 135–143.

Street, F. A., Grove, A. T., 1976. Environmental and climatic implications of late Quaternary lake-level fluctuations in Africa. Nature 261, 385-390.

Street-Perrott, F. A., 1993. Ancient tropical methane. Nature 366, 411-412.

Street-Perrott, F. A., Mitchell, J. F. B., Marchand, D. S., Brunner, J. S., 1990. Milankovitch and albedo forcing of the tropical monsoons: a comparison of geological evidence and numerical simulations for 9000 yr BP. Transactions of the Royal Society of Edinburgh 81, 407-427.

Stuiver, M., 1968. Oxygen-18 content of atmospheric precipitation during the last 11,000 years in the Great Lakes region. Science 162, 994-997.

Stuiver, M., 1970. Oxygen and carbon isotope ratios of fresh-water carbonates as climatic indictors. Journal of Geophysical Research 75, 5247-5257.

Stuiver, M., Reimer, P. J., 1993, Extended ^{14}C database and revised CALIB radiocarbon calibration program. Radiocarbon 35, 215-230.

Stumm, W., Morgan, J. J., 1970. Aquatic Chemistry. Wiley-Interscience.

Sturchio, N. C., Dunkley, P. N., Smith, M., 1993. Climate-driven variations in geothermal activity in the northern Kenya rift valley. Nature 362, 233-234.

Stute, M., Talma, A. S., 1998. Glacial temperatures and moisture transport regimes reconstructed from noble gas and $\delta^{18}O$, Stampriet aquifer, Namibia. Proceedings of the international symposium on isotope techniques in the study of past and current environmental changes in the hydrosphere and atmosphere, IAEA, Vienna, April 1997, SM-349/53, pp. 307-328.

Stuut, J.-B. W., Prins, M. A., Schneider, R. R., Weltje, G. J., Jansen, J. H. F., Postma, G., 2002. A 300-kyr record of aridity and wind strength in southwestern Africa: inferences from grain-size distributions of sediments on Walvis Ridge, SE Atlantic. Marine Geology 180, 221-233.

Stuut, J.-B. W., Crosta, Z., van der Borg, K., Schneider, R., 2004. Relationship between Antarctic sea ice and southwest African climate during the late Quaternary. Geology 32, 909-912.

Sultan, M., Stucchio, N., Hassan, F. A., Hamdan, M. A., Mahmoud, A. N., Alfy, Z., Stein, T., 1997. Precipitation source inferred from stable isotopic composition of Pleistocene groundwater and carbonate deposition in the Western desert. Quaternary Research 48, 29-37.

Summerhayes, C. P., Kroon, D., Rosell-Melé, A., Jordan, R. W., Schrader, H.-J., Hearn, R., Villanueva, J., Grimalt, J. O., Eglington, G., 1995. Variability in the Benguela current upwelling system over the past 70,000 years. Progress in Oceanography 35, 207-251.

Summons, R. E., Jahnke, L. L., Hope, J. M., Logan, G. A., 1999. 2-methylhopanoids as biomarkers for cyanobacterial oxygenic photosynthesis. Nature 400, 544-557.

Sutcliffe, A. J., Lord, T. C., Harmon, R. S., Ivanovich, M., Rae, A., Hess, J. W., 1985. Wolverine in northern England at about 83,000 yr B.P.: Faunal evidence for climatic change during isotope stage 5. Quaternary Research 24, 73-86.

Swezey, C., 2001. Eolian sediment responses to late Quaternary climate changes: temporal and spatial patterns in the Sahara. Palaeogeography, Palaeoclimatology, Palaeoecology 167, 119-155.

Szabo, B. J., Sterr, H., 1978. Dating caliches from southern Nevada by $^{230}Th/^{232}Th$ versus $^{234}U/^{232}Th$ and $^{234}U/^{232}Th$ versus $^{238}U/^{232}Th$ isochron-plot method. US Geological Survey open-file report 78-701.

Szabo, B. J., Butzer, K. W., 1979. Uranium-series dating of lacustrine limestones from pan deposits with final Acheulian assemblage at Rooidam, Kimberly district South Africa. Quaternary Research 11, 257-260.

Talbot, M. R., 1990. A review of the palaeohydrological interpretation of carbon and oxygen isotopic ratios in primary lacustrine carbonates. Chemical Geology 80, 261-279.

Talbot, M. R., Kelts, K., 1986. Primary and diagenetic carbonates in the anoxic sediments of Lake Bosumtwi, Ghana. Geology 14, 912-916.

Talbot, M. R., Kelts, K., 1990. Paleolimnological signatures from carbon and oxygen isotopic ratios in carbonates from organic carbon-rich sediments. In: B. J. Katz (Ed.), Lacustrine Basin Exploration: Case Studies and Modern Analogs. American Association of Petroleum Geologists. Memoir 50, pp. 99-112.

Talbot, M. R., Livingstone, D. A., 1989. Hydrogen index and carbon isotopes of lacustrine organic matter as lake level indicators. Palaeogeography, Palaeoclimatology, Palaeoecology 70, 121-137.

Talbot, M. R., Johannessen, T., 1992. A high resolution palaeoclimatic record for the last 27,500 years in tropical West Africa from the carbon and nitrogen isotopic composition of lacustrine organic matter. Earth and Planetary Science Letters 110, 23-37.

Talbot, M. R., Laerdal, T., 2000. The Late Pleistocene-Holocene palaeolimnology of Lake Victoria, East Africa, based upon elemental and isotopic analyses of sedimentary organic matter. Journal of Paleolimnology 23, 141-164.

Talbot, M. R., Livingstone, D. A., Palmer, P. G., Maley, J., Melack, J. M., Delibrias, G., Gulliksen, S., 1984. Preliminary results from sediment cores from Lake Bosumtwi, Ghana. Palaeoecology of Africa 16, 173-192.

Taljaard, J. J., 1981. Upper air circulation, temperature and humidity over southern Africa. South African Weather Bureau Technical Paper 9, 1-92.

Talling, J. F., 1966. The annual cycle of stratification and phytoplankton growth in Lake Victoria (East Africa). Internationale Revue der gesamten Hydrobiologie 51, 545-621.

Talling, J. F., 1986. The seasonality of phytoplankton in African lakes. Hydrobiologia 138, 139-160.

Talling, J. F., Talling, I. B., 1965. The chemical composition of African Lake Waters. Internationale Revue der gesamten Hydrobiologie 50, 421-463.

Talma, A. S., Vogel, J. C., 1992. Late Quaternary paleotemperatures derived from a speleothem from Cango Caves, Cape Province, South Africa. Quaternary Research 37, 203-213.

Tapia, P. M., Fritz, S. C., Baker, P. A., Seltzer, G. O., Dunbar, R. B., 2003. A late Quaternary diatom record of tropical climatic history from Lake Titicaca (Peru and Bolivia). Palaeogeography, Palaeoclimatology, Palaeoecology 194, 139-164.

Tarutani, T., Clayton, R. N., Mayeda, T., 1969. The effect of polymorphism and magnesium substitution on oxygen isotope fractionation between calcium carbonate and water. Geochimica et Cosmochimica Acta 33, 987-996.

Taylor, P. K., Kent, E. C., 1996. Estimates of air-sea fluxes from climatological data. In: R. T. Pollard, D. Smythe-Wright (Eds.), Understanding Ocean Circulation, UK WOCE - The first six years. Natural Environment Research Council, U.K., pp. 5-6.

Telford, R. J., Barker, P., Metcalfe, S., Newton, A., 2004a. Lacustrine responses to tephra deposition: examples from Mexico. Quaternary Science Reviews 23, 2337-2353.

Telford, R. J., Heegaard, E., Birks, H. J. B., 2004b. All age-depth models are wrong: but how badly? Quaternary Science Reviews 23, 1-5.

Tennant, W. J., 1996. Influence of Indian Ocean sea-surface temperature anomalies on the general circulation of Southern Africa. South African Journal of Science 92, 289-295.

ter Braak, C. J. F., Šmilauer, P., 2002. CANOCO reference manual and Canodraw for windows user's guide: software for canonical community ordination (version 4.5). Microcomputer power, Ithaca.

Teranes, J. L., McKenzie, J. A., Bernasconi, S. M., Lotter, A. F., Stute, M., 1999. A study of oxygen isotopic fractionation during bio-induced calcite precipitation in eutrophic Baldeggersee, Switzerland. Geochimica et Cosmochimica Acta 63, 1981-1989.

Texier, D., de Noblet, N., Harrison, S. P., Haxeltine, A., Jolly, D., Joussaume, S., Laarif, F., Prentice I.C., Tarasov, P., 1997. Quantifying the role of biosphere-atmosphere feedbacks in climate change: coupled model simulations for 6000 years BP and comparison with palaeodata for northern Eurasia and northern Africa. Climate Dynamics 13, 865-882.

Texier, D., de Noblet, N., Braconnot, P., 2000. Sensitivity of the African and Asian monsoons to mid-Holocene insolation and data-inferred surface changes. Journal of Climate 13, 164-181.

Thackeray, J. F., 1987. Late Quaternary environmental changes inferred from small mammalian fauna, southern Africa. Climatic Change 10, 1-21.

Thackeray, J. F., Lee-Thorp, J. A., 1992. Isotopic analysis of equid teeth from Wonderwerk Cave, northern Cape Province, South Africa. Palaeogeography, Palaeoclimatology, Palaeoecology 99, 141-150.

Thomas, D. S. G., Shaw, P. A., 1991. The Kalahari Environment. Cambridge University Press, Cambridge.

Thomas, D. S. G., Stokes, S., Shaw, P. A., 1997. Holocene aeolian activity in the southwestern Kalahari desert, southern Africa: significance and relationships to late-Pleistocene dune building events. The Holocene 7, 273-281.

Thomas, D. S. G., O'Connor, P. W., Bateman, M. D., Shaw, P. A., Stokes, S., Nash, D. J., 2000. Dune activity as a record of late Quaternary aridity in the northern Kalahari: new evidence from Northern Namibia interpreted in the context of regional arid and humid chronologies. Palaeogeography, Palaeoclimatology, Palaeoecology 156, 243-259.

Thomas, D. S. G., Brook, G., Shaw, P., Bateman, M., Haberyan, K., Appleton, C., Nash, D., McLaren, S., Davies, F., 2003. Late Pleistocene wetting and drying in the NW Kalahari: an integrated study from the Tsodilo Hills, Botswana. Quaternary International 104, 53-67.

Titterington, D. M., Halliday, A. N., 1979. On the fitting of parallel isochrons and the method of maximum likelihood. Chemical Geology 26, 183-195.

Todd, M., Washington, R., 1998. Extreme daily rainfall in southern African and southwest Indian Ocean tropical-temperate links. South African Journal of Science 94, 64-70.

Todd, M., Washington, R., 1999. Circulation anomalies associated with tropical-temperate troughs in southern Africa and the south west Indian Ocean. Climate Dynamics 15, 937-951.

Todd, M. C., Washington, R., Palmer, P. I., 2004. Water vapour transport associated with tropical-temperate trough systems over Southern Africa and the southwest Indian Ocean. International Journal of Climatology 24, 555-568.

Trauth, M. H., Deino, A., Strecker, M. F., 2001. Response of the East African climate to orbital forcing during the last interglacial and the early last glacial. Geology 29, 499-502.

Trauth, M. H., Deino, A. L., Bergner, G. N., Strecker, M. R., 2003. East African climate change and orbital forcing during the last 175 kyr BP. Earth and Planetary Science Letters 206, 297-313.

Trenberth, K. E., 1991. Storm tracks in the southern hemisphere. Journal of the Atmospheric Sciences 48, 2159-2178.

Tuchman, M. L., Theriot, E., Stoermer, E. F., 1984. Effects of low level salinity concentrations on the growth of *Cyclotella meneghiniana* Kütz. (Bacillariophyta). Archiv Für Protistenkunde 128, 319-326.

Tucker, M. E., Wright, V. P., 1990. Carbonate sedimentology. Blackwell, Oxford.

Tuenter, E., Weber, S. L., Hilgen, F. J., Lourens, L. J., 2003. The response of the African summer monsoon to remote and local forcing due to precession and obliquity. Global and Planetary Change 36, 219-235.

Turkia, J., Lepisto, L., 1999. Size variations of planktonic *Aulacoseira* Thwaites (Diatomae) in water and in sediment from Finnish lakes of varying trophic state. Journal of Plankton Research 21, 757-770.

Turner, J. V., 1982. Kinetic fractionation of carbon-13 during calcium carbonate precipitation. Geochimica et Cosmochimica Acta 1183-1191.

Tyson, P. D., 1986. Climatic change and variability in southern Africa. Oxford University press, Cape Town.

Tyson, P. D., Preston-Whyte, R. A., 2000. The weather and climate of southern Africa. Oxford University Press Southern Africa, Cape Town.

Tyson, P. D., Odada, E. O., Partridge, T. C., 2001. Late Quaternary environmental change in southern Africa. South African Journal of Science 97, 139-150.

Tyson, R. V., 1995. Sedimentary organic matter: organic facies and palynofacies. Chapman & Hall, London, New York.

Usdowski, E., Hoefs, J., 1993. Oxygen isotope exchange between carbonic acid, bicarbonate, carbonate and water: A re-examination of the data of McCrea (1950) and an expression for the overall partitioning of oxygen isotope between the carbonate species and water. Geochimica et Cosmochimica Acta 57, 3815-3818.

Usdowski, E., Michaelis, J., Böttcher, M. E., Hoefs, J., 1991. Factors for the oxygen isotope equilibrium fractionation between aqueous and gaseous CO_2, carbonic acid, bicarbonate, carbonate, and water (19°C). Zeitschrift für Physikalische Chemie 170, 237-249.

Utada, M., 1966. Zeolites in sedimentary rocks, with reference to the depositional environments and zonal distribution. Sedimentology 7, 237-257.

Valero-Garcés, B. L., Delgado-Huertas, A., Ratto, N., Navas, A., 1999. Large ^{13}C enrichment in primary carbonates from Andean Altiplano lakes, northwest Argentina. Earth and Planetary Science Letters 171, 253-266.

Van Calsteren, P., Schwieters, J. B., 1995. Performance of a thermal ionization mass-spectrometer with a deceleration lens system and post-deceleration detector selection. International Journal of Mass Spectrometry and Ion Processes 146, 119-129.

Van Heerden, J., Terblanche, D. E., Schulze, G. C., 1988. The Southern Oscillation and South African summer rainfall. Journal of Climatology 8, 577-597.

van Zinderen Bakker, E. M., 1967. Upper Pleistocene and Holocene stratigraphy and ecology on the basis of vegetation changes in sub-Saharan Africa. In: W. W. Bishop, J. D. Clark (Eds.), Background to Evolution in Africa. The University of Chicago Press, Chicago and London, pp. 125-147.

van Zinderen Bakker, E. M., 1976. The evolution of late Quaternary palaeoclimates of southern Africa. Palaeoecology of Africa 9, 160-202.

Vandergoes, M. J., Newnham, R. M., Preusser, F., Hendy, C. H., Lowell, T. V., Fitzsimons, S. J., Hogg, A. G., Kasper, H. U., Schlüchter, C., 2005. Regional insolation forcing of late Quaternary climate change in the Southern Hemisphere. Nature 436, 242-245.

Vareschi, E., 1982. The ecology of Lake Nakura (Kenya) III, abiotic factors and primary production. Oecologia 55, 81-101.

Verschuren, D., 1996. Comparative paleolimnology in a system of four shallow, climate-sensitive tropical lake basins. In: T. C. Johnson, E. Odada (Eds.), The Limnology, Climatology and Paleoclimatology of the East African Lakes. Gordon and Breach, New York, pp. 559-572.

Verschuren, D., 1999a. Influence of depth and mixing regime on sedimentation in a small, fluctuating tropical soda lake. Limnology and Oceanography 44, 1103-1113.

Verschuren, D., 1999b. Sedimentation controls on the preservation and time resolution of climate-proxy records from shallow fluctuating lakes. Quaternary Science Reviews 18, 821-837.

Verschuren, D., 2001. Reconstructing fluctuations of a shallow East African lake during the past 1800 years from sediment stratigraphy in a submerged crater basin. Journal of Paleolimnology 25, 297-311.

Vimeux, F., Masson, V., Jouzel, J., Stievenard, M., Petit, J. R., 1999. Glacial-interglacial changes in ocean surface conditions in the southern hemisphere . Nature 398, 410-413.

Vimeux, F., Cuffey, K. M., Jouzel, J., 2002. New insights into Southern Hemisphere temperature changes from Vostok ice cores using deuterium excess correction. Earth and Planetary Science Letters 203, 829-843.

Vincent, C. E., Davies, T. D., Beresford, A. K. C., 1979. Recent changes in the level of Lake Naivasha, Kenya, as an indicator of equatorial westerlies over East Africa. Climatic Change 2, 175-189.

Vogel, J. C., 1978. Isotopic assessment of dietary habits of ungulates. South African Journal of Science 74, 298-301.

Vogel, J. C., 1983. Isotopic evidence for the past climates and vegetation of southern Africa. Bothalia 14, 391-394.

Vogel, J. C., Ehhalt, D., Roether, W., 1963. A survey of the natural isotopes of water in South Africa. Radioisotopes in Hydrology, 407-415.

Vogel, J. C., Grootes, P. M., Mook, W. G., 1970. Isotopic fractionation between gaseous and dissolved carbon dioxide. Zeitschrift für Physik A 230, 225-238.

Vogel, J. C., Fuls, A., Ellis, R. P., 1978. The geographical distribution of Kranz grasses in South Africa. South African Journal of Science 74, 209-215.

Vogt, H. J., 1976. Isotopentrennung bei der Verdunstung von Wasser. University of Heidelberg.

Vose, R. S., Schmoyer, R. L., Steurer, P. M., Peterson, T. C., Heim, R., Karl, T. R., Eischeid, J. K., 2002. SAFARI 2000 Global Historical Climatology Network, Version 1, 1874-1990. Data set available on-line at http://www.daac.ornl.gov, from Oak Ridge National Laboratory Distributed Active Archive Center, Oak Ridge, Tennessee, U.S.A.

Waelbroeck, C., Jouzel, J., Labeyrie, L., Lorius, C., Labracherie, M., Stiévenard, M., Barkov, N. I., 1995. A comparison of the Vostok ice deuterium record and series from Southern Ocean core MD 88-770 over the last two glacial-interglacial cycles. Climate Dynamics 12, 113-123.

Walker, N. D., 1990. Links between South African summer rainfall and temperature variability of the Agulhas and Benguela current systems. Journal of Geophysical Research 95(C3), 3297-3319.

Walker, N. D., Lindesay, J. A., 1989. Preliminary observations of oceanic influences on the February-March 1988 floods in central South Africa. South African Journal of Science 85, 164-169.

Walker, N. D., Shillington, F. A., 1990. The effect of oceanographic variability on South African weather and climate. South African Journal of Science 86, 382-386.

Wang, X., Auler, A. S., Edwards, R. L., Cheng, H., Cristalli, P. S., Smart, P. L., Richards, D. A., Shen, C.-C., 2004. Wet periods in northeastern Brazil over the past 210 kyr linked to distant climate anomalies. Nature 432, 740-743.

Wang, Y. J., Cheng, H., Edwards, R. L., An, Z. S., Wu, J. Y., Shen, C.-C., Dorale, J. A., 2001. A high-resolution absolute-dated late Pleistocene monsoon record from Hulu Cave, China. Science 294, 2345-2348.

Wang, Y., Cheng, H., Edwards, R. L., He, Y., Kong, X., An, Z., Wu, J., Kelly, M. J., Dykoski, C. A., Li, X., 2005. The Holocene Asian Monsoon: links to solar changes and North Atlantic climate. Science 308, 854-857.

Washbourn, C., 1967. Lake levels and Quaternary climates in the eastern Rift Valley of Kenya. Nature 216, 672-673.

Washbourn-Kamau, C., 1970. Late Quaternary chronology of the Nakuru-Elmenteita Basin, Kenya. Nature 226, 253-254.

Washbourn-Kamau, C., 1971. Late Quaternary lakes in the Nakuru-Elmenteita Basin, Kenya. Geographical Journal 137, 522-535.

Washbourn-Kamau, C. K., 1977. The Ol Njorowa Gorge, Lake Naivasha Basin, Kenya. In: D. C. Greer (Ed.), Desertic and terminal lakes. Utah Water Research Laboratory, pp. 297-307.

Washington, R., Todd, M., 1999. Tropical-temperate links in southern African and Southwest Indian Ocean satellite-derived daily rainfall. International Journal of Climatology 19, 1601-1616.

West, S., Jansen, J. H. F., Stuut, J.-B., 2004. Surface water conditions in the Northern Benguela Region (SE Atlantic) during the last 450 kyr reconstructed from assemblages of planktonic foraminifera. Marine Micropaleontology 51, 321-344.

Whiticar, M. J., Faber, E., Schoell, M., 1986. Biogenic methane formation in marine and freshwater environments: CO_2 reduction vs. acetate fermentation - Isotopic evidence. Geochimica et Cosmochimica Acta 50, 693-709.

Williams, M. A. J., Adamson, D. A., Williams, F. M., Morton, W. H., Parry, D. E., 1980. Jebel Marra Volcano: a link between the Nile Valley, the Sahara and Central Africa. In: M. A. J. Williams, H. Faure (Eds.), The Sahara and the Nile. Balkema, Rotterdam, pp. 305-337.

Williams, P. M., Gordon, L. I., 1970. Carbon-13: carbon-12 ratios in dissolved and particulate organic matter in the sea. Deep-Sea Research 17, 19-27.

Wilson, S. E., Smol, J. P., Sauchyn, D. J., 1997. A Holocene paleosalinity diatom record from southwestern Saskatchewan, Canada: Harris Lake revisited. Journal of Paleolimnology 17, 23-31.

Woldstedt, P., 1965. Das Eiszeitalter. Vol. III. Ferdinand Enke, Stuttgart.

Wood, R. B., Talling, J. F., 1988. Chemical and algal relationships in a salinity series of Ethiopian inland waters. Hydrobiologia 158, 29-67.

Woolfe, A. P., 1997. On diatom concentrations in lake sediments: results from an inter-laboratory comparison and other tests performed on a uniform sample. Journal of Paleolimnology 18, 261-268.

Wooller, M. J., Street-Perrott, F. A., Agnew, A. D. Q., 2000. Late Quaternary fires and grassland palaeoecology of Mount Kenya, East Africa: evidence from charred grass cuticles in lake sediments. Palaeogeography, Palaeoclimatology, Palaeoecology 164, 207–230.

Yuan, D., Cheng, H., Edwards, R. L., Dykoski, C. A., Kelly, M. J., Zhang, M., Qing, J., Lin, Y., Wang, Y., Wu, J., Dorale, J. A., An, Z., Cai, Y., 2004. Timing, duration, and transitions of the last interglacial Asian monsoon. Science 304, 575-578.

Zeeb, B. A., Smol, J. P., 2001. Chrysophyte scales and cysts. In: J. P. Smol, H. J. B. Birks, W. M. Last (Eds.), Tracking environmental change using lake sediments. Volume 3: Terrestrial, Algal, and Siliceous Indicators. Kluwer Academic Publishers, Dordrecht, pp. 203-223.

Zeebe, R. E., 1999. An explanation of the effect of seawater carbonate concentration on foraminiferal oxygen isotopes. Geochimica et Cosmochimica Acta 63, 2001-2007.